U.S. DEPARTMENT OF COMMERCE
National Technical Information Service
PB-276 489

Filtration Model for Coal Fly Ash with Glass Fabrics

GCA Corp, Bedford, Mass GCA Technology Div

Prepared for

Industrial Environmental Research Lab, Research Triangle Park, N C

Aug 77

PB 276 489

EPA
U.S. Environmental Protection Agency
Office of Research and Development

Industrial Environmental Research
Laboratory
Research Triangle Park, North Carolina 27711

EPA-600/7-77-084
August 1977

FILTRATION MODEL FOR COAL FLY ASH WITH GLASS FABRICS

Interagency
Energy-Environment
Research and Development
Program Report

REPRODUCED BY
NATIONAL TECHNICAL
INFORMATION SERVICE
U. S. DEPARTMENT OF COMMERCE
SPRINGFIELD, VA. 22161

RESEARCH REPORTING SERIES

Research reports of the Office of Research and Development, U.S. Environmental Protection Agency, have been grouped into seven series. These seven broad categories were established to facilitate further development and application of environmental technology. Elimination of traditional grouping was consciously planned to foster technology transfer and a maximum interface in related fields. The seven series are:

1. Environmental Health Effects Research
2. Environmental Protection Technology
3. Ecological Research
4. Environmental Monitoring
5. Socioeconomic Environmental Studies
6. Scientific and Technical Assessment Reports (STAR)
7. Interagency Energy-Environment Research and Development

This report has been assigned to the INTERAGENCY ENERGY-ENVIRONMENT RESEARCH AND DEVELOPMENT series. Reports in this series result from the effort funded under the 17-agency Federal Energy/Environment Research and Development Program. These studies relate to EPA's mission to protect the public health and welfare from adverse effects of pollutants associated with energy systems. The goal of the Program is to assure the rapid development of domestic energy supplies in an environmentally--compatible manner by providing the necessary environmental data and control technology. Investigations include analyses of the transport of energy-related pollutants and their health and ecological effects; assessments of, and development of, control technologies for energy systems; and integrated assessments of a wide range of energy-related environmental issues.

REVIEW NOTICE

This report has been reviewed by the participating Federal Agencies, and approved for publication. Approval does not signify that the contents necessarily reflect the views and policies of the Government, nor does mention of trade names or commercial products constitute endorsement or recommendation for use.

This document is available to the public through the National Technical Information Service, Springfield, Virginia 22161.

TECHNICAL REPORT DATA
(Please read Instructions on the reverse before completing)

1. REPORT NO.
EPA-600/7-77-084

2.

3. RECIPIENT'S ACCESSION NO.
PB276489

4. TITLE AND SUBTITLE
Filtration Model for Coal Fly Ash with Glass Fabrics

5. REPORT DATE
August 1977

6. PERFORMING ORGANIZATION CODE

7. AUTHOR(S) Richard Dennis, R.W.Cass, D.W.Cooper, R.R.Hall, Vladimir Hampl, H.A.Klemm, J.E.Langley, and R.W.Stern

8. PERFORMING ORGANIZATION REPORT NO.
GCA-TR-75-17-G

9. PERFORMING ORGANIZATION NAME AND ADDRESS
GCA Corporation
GCA/Technology Division
Bedford, Massachusetts 01730

10. PROGRAM ELEMENT NO.
EHE624

11. CONTRACT/GRANT NO.
68-02-1438, Task 5

12. SPONSORING AGENCY NAME AND ADDRESS
EPA, Office of Research and Development
Industrial Environmental Research Laboratory
Research Triangle Park, NC 27711

13. TYPE OF REPORT AND PERIOD COVERED
Task Final; 6/74-6/77

14. SPONSORING AGENCY CODE
EPA/600/13

15. SUPPLEMENTARY NOTES IERL-RTP project officer for this report is James H. Turner, Mail Drop 61, 919/541-2925.

16. ABSTRACT The report describes a new mathematical model for predicting woven glass filter performance with coal fly ash aerosols from utility boilers. Its data base included: an extensive bench- and pilot-scale laboratory investigation of several dust/fabric combinations; field data from three prior GCA studies involving coal fly ash filtration with glass fabrics; past GCA studies of fabric filter cleaning mechanisms; and a broad based literature survey. Trial applications of the model to field filter systems at Sunbury (PA) and Nucla (CO) indicate excellent agreement between theory and practice for both penetration and resistance. The introduction and experimental confirmation of two basic concepts were instrumental in model design: one relates to the way dust dislodges from a fabric and its subsequent impact upon resistance and penetration in a multichambered system; the other, to the relatively large fly ash fractions that pass with minimal collection through temporarily or permanently unblocked pores or pinholes such that observed particle penetrations are essentially independent of size. Cleaning parameters were quantified, and estimates of specific resistance coefficient, K2, were improved.

17. KEY WORDS AND DOCUMENT ANALYSIS

a. DESCRIPTORS		b. IDENTIFIERS/OPEN ENDED TERMS	c. COSATI Field/Group	
Air Pollution	Woven Fabrics	Air Pollution Control	13B	11E
Mathematical Models	Glass Fibers	Stationary Sources	12A	11B
Filtration	Aerosols	Fabric Filters	07D	
Fly Ash	Dust	Particulate	21B	11G
Coal	Utilities		21D	
	Boilers			13A

18. DISTRIBUTION STATEMENT
Unlimited

19. SECURITY CLASS *(This Report)*
Unclassified

20. SECURITY CLASS *(This page)*
Unclassified

21. NO. OF PAGES
490

22. PRICE
PC A21 / MF A01

EPA Form 2220-1 (9-73)

EPA-600/7-77-084
August 1977

FILTRATION MODEL FOR COAL FLY ASH WITH GLASS FABRICS

by

Richard Dennis, R.W. Cass, D.W. Cooper, R.R. Hall,
Vladimir Hampl, H.A. Klemm, J.E. Langley, and R.W. Stern

GCA Corporation
GCA/Technology Division
Bedford, Massachusetts 01730

Contract No. 68-02-1438
Task No. 5
Program Element No. EHE624

EPA Project Officer: James H. Turner

Industrial Environmental Research Laboratory
Office of Energy, Minerals, and Industry
Research Triangle Park, N.C. 27711

Prepared for

U.S. ENVIRONMENTAL PROTECTION AGENCY
Office of Research and Development
Washington, D.C. 20460

ABSTRACT

A new mathematical model for predicting the performance of woven glass filters with coal fly ash aerosols from utility boilers is described in this report. The data base for this development included an extensive bench and pilot scale laboratory program in which several dust/fabric combinations were investigated; field data from three prior GCA studies involving coal fly ash filtration with glass fabrics; past GCA studies of fabric filter cleaning mechanisms and a broad-based literature survey. Trial applications of the modeling technique to field filter systems operating at Sunbury, Pennsylvania and Nucla, Colorado indicate excellent agreement between theory and practice for both penetration and resistance characteristics. The introduction and experimental confirmation of two basic concepts were instrumental in model design. The first relates to the manner in which dust dislodges from a fabric and its subsequent impact upon resistance and penetration in a multichambered system. The second concept is associated with the relatively large fractions of fly ash that pass with minimal collection through temporarily or permanently unblocked pores or pinholes such that observed particle penetrations are essentially independent of size. Additionally, the quantitation of the cleaning action with dust removal in terms of method, intensity and duration of cleaning was essential to the overall modeling process. The examination of specific resistance coefficient, K_2, for the dust layer in the light of polydispersed rather than monodispersed particle components provided improved estimates of K_2 although direct measurement of this parameter and other terms defining the filter resistance (or drag) versus fabric loading relationship is the recommended approach at this time.

CONTENTS

Page

Abstract iii

List of Figures xii

List of Tables xxii

Acknowledgments xxvii

Nomenclature xxviii

Special Nomenclature - English and Metric Equivalencies for Key Filtration Parameters xxxiv

Sections

I Summary 1

II Introduction 5

  Description of a Filtration System 7

  Objectives 7

  Outline of Model 9

  Summary of Methodology 10

  The Laboratory Program 12

III A Review of Fabric Filtration Models 14

  Predictive Models 14

    Robinson, Harrington and Spaite Model 14

    Solbach Model 18

    Dennis and Wilder Model 20

Preceding page blank

CONTENTS (Continued)

Sections Page

Noll, Davis and Shelton Model 22

Noll, Davis and LaRosa (1975) Model 23

Stinessen's Approach 24

Fraser and Foley Model 25

Leith and First Model 25

Conclusions 27

IV Laboratory Test Equipment and Measurement Procedures for Determination of Filter Performance 29

Bench Scale Filtration Equipment 29

Dust Generation Apparatus 35

Pilot Scale Filtration Equipment 35

Test Aerosols 42

Particulate Sampling and Assessment 45

Basic Sampling Equipment 45

Assessment and Interpretation of CNC and B&L Measurements 48

Tensile Properties 53

V Fabric Structure Studies 57

Introduction 57

Basic Manufacturer or User Specifications 58

Bag Resistance Versus Pore Velocity 61

Simplified Weave Representations 62

Pore Properties 65

Yarn Shape 71

CONTENTS (Continued)

Sections Page

Pore Type and Area 72

Air Flow Through Pores 76

Physical Properties of Fabrics 80

Tensile Modulus 83

Bag Tension and Permeability 87

Fabric Thickness 92

Initial Dust Deposition Characteristics 92

VI Analysis of Sunbury and Nucla Field Measurements 100

Fabric Dust Loadings 100

Bag Resistance 103

Collection Efficiency 109

Specific Resistance Coefficient 115

VII Bench Scale Laboratory Tests 117

Fabric Resistance Characteristics 117

Clean (Unused) Fabrics 117

Cleaned (Used) Fabrics 117

Resistance Versus Fabric Loading-Bench Scale Tests 126

Dust Deposition and Removal Characteristics 129

Deposition on Used Fabrics 129

Pinholes and Air Leakage 135

Fabric Appearance After Cleaning 144

Dust Release From Glass Fabrics 154

Filtration With Partially Cleaned Fabrics 157

CONTENTS (Continued)

Sections Page

Specific Resistance Coefficient 160

Effect of Velocity 160

Effect of Particle Size 163

Dacron Filtration Tests 164

Collection Efficiency and Penetration 167

Weight Collection Efficiency Measurements 167

Condensation Nuclei Measurements 174

Particle Size and Concentration by Optical Counter 186

Nuclei Versus Mass Concentrations 190

Effluent Concentrations Versus Face Velocity 198

Rating Fabrics With Atmospheric Dust 198

VIII Pilot Plant Tests 205

Introduction 205

Summary of Testing Procedures 205

General Comments 206

Dust Removal Versus Fabric Loading 208

Dust Removal With Successive Filtration and Cleaning Cycles 217

Dust Removal and Bag Tension 217

Resistance Versus Fabric Loading 219

Dust Penetration Measurements 219

Constant Velocity Tests 219

Penetration Versus Face Velocity 223

Rear Face Slough-Off 223

CONTENTS (Continued)

Sections Page

IX Prediction of Fabric Filter Drag 228

- Critique of Linear Drag Model 229
- Derivation of Nonlinear (Pore) Model 229
- Verification of Nonlinear Drag Model 239
- Empirical Correlations 241
  - Clean Fabric Drag, S_o 224
  - Effective Drag, S_E 244
  - Residual Drag, S_R 249
  - Initial Slope, K_R 249
  - Estimation of W* 251
- Theoretical Correlations 251
  - Clean Fabric Permeability 251
  - Specific Resistance Coefficient, K_2 252
    - K_2 Versus Face Velocity 254
    - K_2 Versus Specific Surface Parameter 260
    - K_2 Versus Dust Cake Porosity 261
    - Calculated and Observed K_2 Values, Field and Laboratory Tests 261
- Fabric Cleaning and Filter Performance 270
  - Resistance (Drag) Versus Dust Distribution on Fabric 271
  - Dust Removal Versus Cleaning Conditions 288
- Full Scale Applications - Modeling Concepts 306
- Pressure Controlled Cleaning 306

CONTENTS (Continued)

Sections | Page

Time Cycle Cleaning 311

X Prediction of Fabric Filter Penetration 315

Particle Capture by Unobstructed Pores 316

Particle Capture by Bulk Fiber Substrates 320

Particle Capture by Dust Cake (Granular Bed) 327

Fly Ash Penetration for Woven Glass Fabrics 333

Penetration Versus Pore Properties 333

Penetration and Inlet Concentration 336

Penetration Versus Face Velocity 337

Dust Penetration Model 341

XI Mathematical Model for a Fabric Filter System 347

Introduction 347

Principal Modeling Relationships 348

Designed Model Capability 352

Basic Modeling Process 353

Program Description 361

Computational Procedures 363

Drag Computation 363

Fabric Penetration 366

Program Input and Output 367

Predictive Validation 373

Introduction 373

System Parameters 374

CONTENTS (Continued)

Sections Page

Nucla Data Inputs 374

Sunbury Data Inputs 381

Nucla Plant - Model Validation 386

Predicted Versus Actual Resistance Characteristics 386

Predicted Velocity Relationships 390

Predicted Penetration 390

Sunbury Plant - Model Validation 394

Predicted Versus Actual Resistance Characteristics 394

Predicted Velocity Relationships 399

Predicted Penetration 402

Summary of Model Highlights and Direction for Future Work 406

References 409

APPENDIX

A Effect of Sequential Pore Closure on Shape of Resistance Versus Fabric Loading Curve 412

B Input Parameters For Estimating Fiber Efficiency in Substrate Layer 414

C Determination of Constants Used in Dust Penetration Model 416

D Baghouse Computer Program Description 423

LIST OF FIGURES

No.		Page
1	Schematic of n-Compartment Baghouse	8
2	Flow Chart for Baghouse Model	11
3	Three-Compartment Baghouse With Sequential Cleaning	15
4	Fabric Drag Versus Loading	17
5	Schematic of Filter Test Assembly With Exploded View of Fabric Sandwich	31
6	Bench Scale Filtration Apparatus Showing Inlet Manifold and Test Aerosol Loop	32
7	Bench Scale Filtration Apparatus	32
8	Size Distribution Measurements for GCA Fly Ash for Particle Density of 2 grams/cm^3	33
9	NBS Type Dust Generator	36
10	All Components of Bench Scale Filtration System	37
11	Schematic of Pilot Scale Fabric Filter System	39
12	Inlet and Outlet Fly Ash Size Distributions for a 10 ft x 4 in. Woven Glass Bag, Sunbury Fabric	41
13	Size Distribution for GCA Fly Ash Entering Bench Scale Filter System, Andersen In-Stack Impactor Measurements	43
14	Mass Distribution for Sunbury Inlet Aerosol, Field Measurements, Based Upon Aerodynamic Diameter. In-Stack Andersen Impactor	44
15	Size Properties for Coarse and Fine Rhyolite Dust	46
16	Particle Size Properties for Lignite Ash From Precipitator Hopper	47

LIST OF FIGURES (Continued)

No.		Page
17	Number Size Distributions for Background (Laboratory) Dust Based on B&L Counter Measurements	50
18	Relationship Between Nuclei Concentrations by CNC Measurements and Weight Concentrations Derived From B&L Data	51
19	Concurrent Measurements for Nuclei Concentrations (CNC) and Particle Concentrations by Bausch and Lomb Counter in Different Size Ranges	54
20	Test Apparatus for Measurement of Fabric Tensile Properties	55
21	Resistance Versus Face and Maximum Pore Velocity for Clean (Unused) Sunbury Glass Fabric	63
22	Textile Schematic Drawing of Sunbury Fabrics A. 1973 Bags, B. 1975 Bags. Circles on Diagonal, Warp Yarn Crossovers, Indicate Open Pore Locations	64
23	Schematic of Sunbury Fabric, Filtering Face, 3/1 Twill, Left-hand Diagonal Indicating Pore Locations and Average Dimensions. No Space Between Warp Yarns Except at Crossing Points	66
24	Warp and Fill Surfaces of Clean (Unused) Sunbury Fabric With Substage Illumination (20X Mag)	67
25	Warp and Fill Surfaces of Clean (Unused) Nucla Fabric With Substage Illumination (20X Mag)	68
26	Individual Sunbury Warp and Fill Yarns as Seen in Plane of Fabric Showing Maximum and Minimum Dimensions (20X Mag)	69
27	Individual Nucla Warp and Fill Yarns as Seen in Plane of Fabric Showing Maximum and Minimum Dimensions (20X Mag)	70
28	Schematic Drawing Showing Alignment, Approximate Form, and Spacing of Yarns and Pores in Sunbury Filter Bags (Menardi Southern Woven Glass Media)	73
29	Edge Views of Clean Sunbury Fabric (20X Mag)	74
30	Schematic Drawing Showing Idealized Alignment of Parallel Yarns and Maximum Pore Cross Section (Shaded Area)	75

LIST OF FIGURES (Continued)

No.		Page
31	Stress/Strain Relationship for Used Sunbury Media 7.6 cm x 45.7 cm (3 in. x 18 in.) Strip With Tension Applied in Warp Direction	84
32	Effect of Dust Loading on Tensile Properties of Woven Glass Bags	89
33	Effect of Bag Tension on Resistance to Airflow, With Conventional Bag Suspension	91
34	Fabric Thickness Versus Compressive Loading	93
35	Schematic of GCA Fly Ash Filtration at 2 ft/min. Dark Areas Show Dust Deposits. Light Areas Indicate Relatively Clean Warp Yarns Transmitting Light With Rear Face Illumination	94
36	Fly Ash Deposition on Monofilament Screen Versus Filtration Time, Surface Illumination	96
37	Fly Ash Deposition of Monofilament Screen Versus Filtration Time, Rear and Surface Illumination	97
38	Fly Ash Deposition on Monofilament Screen Versus Filtration Time, Rear and Surface Illumination	98
39	Residual Dust Loadings for Bags in 14-Compartment Sunbury Collector. Cycle Interrupted Between Cleaning of Compartments 12 and 13 for Removal and Replacement of All Bags	102
40	Average Filter Resistance for Sunbury Glass Bags, Normal Field Use After 2 Years Service	104
41	Filter Resistance and Outlet Concentration Versus Time for Glass Bag Filters at Sunbury, Pennsylvania Power Plant	105
42	Resistance Versus Time for Old and New Sunbury Bags	106
43	Filter Resistance Versus Time for Successive Filtering, Compartment Cleaning and Reverse Flow Manifold Flushing, Sunbury Field Test of February 14, 1975	108
44	Inlet and Outlet Dust Concentrations for Sunbury Field Tests	112
45	Inlet and Outlet Dust Concentrations for Nucla Field Tests	113

LIST OF FIGURES (Continued)

No.		Page
46	Field Measurements of Outlet Concentrations From New and Well-Used Sunbury Bags	114
47	Filtration Resistance for Unused Sunbury and Nucla Glass Bags, Laboratory Measurements	118
48	Resistance Characteristics of Used Sunbury Fabrics Cleaned in the Laboratory to Various Residual Dust Holdings, Tests 1 to 5	120
49	Resistance Characteristics of Used Sunbury Fabrics Cleaned in the Laboratory to Various Residual Dust Holdings, Tests 6 to 8	121
50	Resistance Characteristics of Used Nucla Fabrics Cleaned in the Laboratory to Various Residual Dust Holdings	122
51	Fabric Resistance Versus Residual Fabric Loading for Sunbury Bags at 0.61 m/min (2 ft/min) Filtration Velocity	124
52	Typical Resistance Versus Dust Loading Curves for Fly Ash Filtration With Staple and Multifilament Yarns	125
53	Resistance Versus Average Fabric Loading for Sunbury Fabric With GCA Fly Ash at 0.61 m/min Face Velocity	127
54	Resistance Versus Average Fabric Loading for Nucla Fabric With GCA Fly Ash at 0.61 m/min Face Velocity	129
55	Filtration of Granite Dust (Rhyolite) and Lignite Fly Ash With Sunbury Fabric at 0.61 m/min Face Velocity	130
56	GCA Fly Ash Filtration With Unused Sateen Weave Cotton (Unnapped) and Dacron (Crowfoot Weave) at 0.61 m/min Face Velocity	131
57	Fly Ash Dust Layer on Sunbury Fabric, Laboratory Tests Prior to Removal of 945 grams/m^2 Cloth Loading (20X Mag)	133
58	Photomicrograph of Sunbury Media Showing GCA Fly Ash Loading With Pinhole Leak and Cracks Induced by Flexure	134
59	GCA Fly Ash Deposit on Previously Used Sunbury Fabric Showing Crater and Pinholes, 430 grams/m^2 Cloth Loading	136

LIST OF FIGURES (Continued)

No.		Page
60	Pinhole Leak Structures, GCA Fly Ash Filtration on Sunbury Fabric	137
61	Estimation of Pinhole Velocities by Capillary (A) and Orifice (B) Theory for Fly Ash Loaded Sunbury Fabric	141
62	Checking or Cracking of Deposited Fly Ash Layer on Glass Fabric by Intentional Flexing (60X Mag). Test With Clean (Unused) Sunbury Fabric With Cloth Loading of 945 grams/m^2	145
63	Dust Cake as Seen in Sectional Views With GCA Fly Ash on Sunbury Fabrics (20X Mag)	146
64	Before and After Appearance of Dirty and Cleaned Sunbury Fabric With GCA Fly Ash Filtration	147
65	Pore Appearances for Clean and Dirty Faces of Cleaned Sunbury Fabric With GCA Fly Ash Filtration (60X Mag)	149
66	Appearance of Previously Used Nucla Fabric Before and After Cleaning. GCA Fly Ash Loading of 1200 grams/m^2 (20X Mag)	150
67	Appearance of Fill and Warp Faces of Nucla Fabrics After Removal of GCA Fly Ash Loading of Approximately 1000 grams/m^2, Previously Clean (Unused) Fabric (20X Mag)	151
68	Photograph Showing a Section of Nucla Test Panel From Which Dust has been Dislodged. Roughly 3/4 Actual Size	153
69	Fly Ash Filtration With Clean and Partially Cleaned Sateen Weave Cotton, Flat Panel and Bag Tests	158
70	Effect of Filtration Velocity (V) on Specific Resistance Coefficient (K_2). Sunbury Fabric With GCA Fly Ash	161
71	Effect of Face Velocity on K_2, Sunbury Fabric With GCA Fly Ash	162
72	Effluent Concentration Versus Fabric Loading For Unused Sunbury Media With GCA Fly Ash, Test 65	175
73	Effluent Concentration Versus Fabric Loading for Used Sunbury Fabric (Test 66) With GCA Fly Ash	177
74	Effluent Concentration Versus Fabric Loading for Used Sunbury Media With GCA Fly Ash, Test 67	178

LIST OF FIGURES (Continued)

No.		Page
75	Effluent Concentration Versus Fabric Loading for Unused Nucla (Test 68) Media With GCA Fly Ash	179
76	Effluent Concentration Versus Fabric Loading for Used Nucla Fabric (Test 69) With GCA Fly Ash	180
77	Effluent Concentration Versus Fabric Loading for Used Sunbury Fabric and GCA Fly Ash With Uniform (Test 71) and Nonuniform (Test 72) Dust Loading	181
78	Effluent Nuclei Concentration Versus Fabric Loading for Used Sunbury Fabric With Lignite, Test 83	183
79	Effluent Nuclei Concentration Versus Fabric Loading With Used Cotton Sateen and GCA Fly Ash, Test 84	184
80	Effluent of Filtration Velocity on Effluent Nuclei Concentration, GCA Fly Ash With New Sunbury Fabric	185
81	Effluent Concentration Versus Fabric Loading and Particle Size for Used Sunbury Media With GCA Fly Ash, Test 67	187
82	Effluent Concentration Versus Fabric Loading and Particle Size for Unused Nucla Fabric With GCA Fly Ash, Test 68	188
83	Effluent Concentration Versus Fabric Loading and Particle Size for Used Nucla Media With GCA Fly Ash, Test 69	189
84	Effluent Particle Concentration Versus Fabric Loading and Particle Size for Used Sunbury Fabric and Lignite, Test 83, B&L Measurements	191
85	Effluent Concentration Versus Fabric Loading for Unused Cotton Sateen With GCA Fly Ash, Test 84, B&L Measurements	192
86	Calibration Curve - Nuclei and Related Mass Concentrations for GCA Fly Ash	194
87	Outlet Concentration Versus Fabric Loading at 0.61 m/min (2 ft/min) Face Velocity. GCA Fly Ash With Sunbury and Nucla Fabrics. Loading Increase Referred to State of Filtering Cycle	199
88	Outlet Concentration Versus Fabric Loading for Three Face Velocities. GCA Fly Ash and Sunbury Fabric. Loading Increase Referred to Start of Filtering Cycle.	200

LIST OF FIGURES (Continued)

No. Page

89 Room Air Filtration With Clean (Unused) Woven Fabrics at 0.61 m/min Face Velocity, Inlet (x) and Outlet (o) Concentrations 204

90 Dust Removal Versus Fabric Loading and Estimated Distribution of Interfacial Adhesive Forces for GCA Fly Ash and Sunbury Type Fabric 212

91 Dust Removal Characteristics for Repetitive Cleaning Cycles, Sunbury Type Fabric With GCA Fly Ash 215

92 Performance of Sunbury Fabric With GCA Fly Ash With Repetitive Filtration and Cleaning Cycles 218

93 Successive Filtration and Cleaning Cycles for Sunbury Fabric With GCA Fly Ash Based on Data of Table 25 220

94 Single Bag (10 ft x 4 in.) Filtration of GCA Fly Ash With Sunbury Fabric - Three Cleaning Cycles With Variations in Residual Loading 221

95 Effect of Face Velocity on Outlet Concentration, GCA Fly Ash With 10 ft x 4 in. Woven Glass Bag (Sunbury Type Fabric) 222

96 Relationship Between Final and Average Outlet Concentration and Face Velocity for 10 ft x 4 in. Bag and Test Panel With GCA Fly Ash and Sunbury Type Fabric 225

97 Effluent Particle Size Parameters From GCA Fly Ash Loaded Sunbury Fabric When Filtering Atmospheric Dust 227

98 Typical Drag Versus Fabric Loading Curve for a Uniformly Distributed Dust Holding 230

99 Schematic, Dust Accumulation Below Surface of Fabric With Bulked Fiber or Staple Support 234

100 Comparison Between Experimental and Predicted Drag Properties 243

101 Relationship Between Effective (S_E) and Clean (S_0) or Residual (S_R) Drag 247

102 Effect of Previous Fabric Loading on Residual Drag for New and Well Used Fabric 250

LIST OF FIGURES (Continued)

No.		Page
103	Specific Resistance Coefficient (K_2) Versus Mass Median Diameter and Face Velocity. Data From Table 34	257
104	Estimated Effect of Face Velocity on K_2 Based Upon Literature Review, Table 6	259
105	Specific Resistance Coefficient Versus Specific Surface Parameter (S_o^2) for Various Dusts	269
106	Average Filter Drag With Various Degrees of Dust Removal - Fly Ash Filtration With Woven Glass Fabric	273
107	Effect of Cleaning Duration on Filter Capacity for Several Shaking Conditions	276
108	Effect of Shaker Acceleration on Filter Capacity	276
109	Typical Drag Versus Loading Curves for Filters With Different Degrees of Cleaning and a Maximum Allowable Level for Terminal Drag, S_T, and Terminal Fabric Loading, W_T	278
110	Appearance of Partially Cleaned Fabrics	281
111	Fly Ash Filtration With Completely and Partially Cleaned Woven Glass Fabric (Menardi Southern), Tests 71 and 72	284
112	Fly Ash Filtration With Completely and Partially Cleaned Woven Glass Fabric (Menardi Southern), Tests 96 and 97	285
113	Fly Ash Filtration With Completely and Partially Cleaned Sateen Weave Cotton, Unnapped (Albany International), Tests 84 and 85	286
114	Resistance Versus Fabric Loading for Partially-Loaded Fabric, Measured and Predicted (Using Linear and Bilinear Models), Test 72	289
115	Average Residual Fly Ash Loadings Versus Fabric Type and Number of Mechanical Shakes (8 cps at 1 in. Amplitude), Reference 10	293
116	Estimated Distribution of Adhesive Forces for Woven Glass Fabrics and One Dacron Fabric With Coal Fly Ash	298

LIST OF FIGURES (Continued)

No.		Page
117	Adhesion of Spherical Fe Particles of 4 μm Diameter to Fe Substrate at Room Temperature in Air as a Function of Applied Force (From Bohme, et al, Reference 36) and Reference 1	301
118	Effect of Particle Size and Relative Humidity on Adhesion for Various Materials (Reference 1)	302
119	Relationship Between Cleaned Area Fraction and Initial Fabric Loading. GCA Fly Ash and Woven Glass Fabric	305
120	Efficiency of Sampling an Aerosol From a Variable Velocity Flow Field at a Constant Sampling Velocity of 6 m/sec	318
121	Filtration Velocity Through Cleaned and Uncleaned Areas of Filter. GCA Fly Ash and Sunbury Fabric	340
122	Predicted and Observed Outlet Concentrations for Bench Scale Tests. GCA Fly Ash and Sunbury Fabric	345
123	Effect of Inlet Concentration on Predicted Outlet Concentrations at a Face Velocity of 0.61 m/min. GCA Fly Ash and Sunbury Fabric	346
124	System Breakdown for I Bags and J Areas per Bag	355
125	Schematic Representation of Approach to Steady State Cleaning and Fabric Loading Conditions for a Three-Compartment System With 50 Percent of Each Compartment Surface Cleaned	357
126	Baghouse Model Computational Procedure	360
127	Baghouse Simulation Program Flow Diagram	362
128	Pressure-Time Trace for Run Number 1, Nucla Generation Station (Reference 8)	387
129	Test Run No. 0422 Nucla Baghouse Simulation - Linear Pressure Versus Time Graph	388
130	Test Run No. 0422 Nucla Baghouse Simulation - Linear Flow Rate Versus Time Graph	391

LIST OF FIGURES (Continued)

No.		Page
131	Test Run No. 0422 Nucla Baghouse Simulation - Linear Individual Flow Rate Graph	392
132	Test Run No. 0422 Nucla Baghouse Simulation - Linear Penetration Versus Time Graph	393
133	Pressure Drop History of Sunbury Baghouse - Run No. 1 (Reference 9)	395
134	Test Run No. 0422 Sunbury Baghouse Simulation - Linear Pressure Versus Time Graph	397
135	Test Run No. 0422 Sunbury Baghouse Simulation - Nonlinear Pressure Versus Time Graph	398
136	Test Run No. 0422 Sunbury Baghous Simulation - Linear Individual Flow Rate Graph	400
137	Test Run No. 0422 Sunbury Baghouse Simulation - Nonlinear Individual Flow Rate Graph	401
138	Test Run No. 0422 Sunbury Baghouse Simulation - Linear Penetration Versus Time Graph	403
139	Test Run No. 0422 Sunbury Baghouse Simulation - Nonlinear Penetration Versus Time Graph	404
140	Estimation of Pore Cross Section in Fiber Substrate Region	415
141	Penetration Versus Loading for Bench Scale Tests	417
142	Steady State Penetration as a Function of Velocity	420
143	Initial Slope of Penetration Versus Loading Curve as a Function of Velocity	421

LIST OF TABLES

No.		Page
1	Some Permeabilities and Fabric Weights per Unit Area	23
2	Fabric Properties for Glass Bag Filters Used at Sunbury, Pennsylvania and Nucla, Colorado Coal-Burning Power Plants	59
3	Special Properties, Sunbury and Nucla Fabrics	60
4	Dacron and Cotton Properties for Fabric Test Panels Studied in Laboratory	62
5	Characteristic Pore Dimensions for Sunbury (Menardi Southern) and Nucla (Criswell) Glass Fabrics	77
6	Results of Physical Characterization Tests on Sunbury Fabric Filter Bags	81
7	Results of Physical Characterization Tests on a Nucla Fabric Filter Bag	82
8	Tensile Modulus Values for Glass Bags Used for Coal Fly Ash Filtration	86
9	Properties of Common Woven Fabrics Including Tensile Modulus	88
10	Residual Fabric Dust Loading for Sunbury Bags as Received From Field	101
11	Field Performance of Filter Systems with Glass Bags - Sunbury/Nucla Station	110
12	Measured K_2 Based on Field Tests at Nucla Generating Station	116
13	Fabric/Dust Combinations Studied in the Laboratory Program	129
14	Filtration Characteristics of New (Unused) Sunbury Fabric With GCA Fly Ash	140

LIST OF TABLES (Continued)

No.		Page
15	Fabric Resistance Before and After Cleaning by Flexure, 0.61 m/min Filtration Velocity	155
16	Weight Collection Efficiency for Sateen Weave Cotton With GCA Fly Ash	159
17	GCA Fly Ash Filtration With Crowfoot Dacron, Bench Scale Tests	165
18	Summary of Bench Scale Filtration Tests	168
19	Summary of Concentration, Efficiency and Penetration Measurements for GCA Fly Ash Filtration With Woven Glass Fabrics at 0.61 m/min Face Velocity	196
20	Initial and Average Outlet Concentrations and Related Penetration Data for Fly Ash/Woven Glass Fabric Filters	197
21	Change in Effluent Concentration With Increasing Fabric Loading for Fly Ash Filtration With Woven Glass Fabrics	201
22	Atmospheric Dust Penetration With Woven Glass and Cotton Fabrics	203
23	Effluent Concentration From New (Unused) and Partially Loaded Sunbury Type Fabric With GCA Fly Ash and Atmospheric Dust	207
24	Relationship Between Dust Removal and Previous Fabric Loading, GCA Fly Ash Filtration With 10 ft x 4 in. Woven Glass Bag (Sunbury Type) at 0.61 m/min Face Velocity	209
25	Repetitive Cleaning and Filtration Cycles With GCA Fly Ash and Woven Glass (Sunbury Type) Fabric at 0.61 m/min Face Velocity and 50 lbs Tension	210
26	Effect of Reduced Bag Tension, 15 lbs, on Dust Removal and Penetration GCA Fly Ash With 10 ft x 4 in. Bag, Sunbury Fabric, at 0.61 m/min Face Velocity	211
27	Effect of Several Successive Cleanings by Bag Collapse and Reverse Flow, GCA Fly Ash With Woven Glass Fabric (Sunbury Type)	214
28	Effect of Face Velocity on Outlet Concentration, GCA Fly Ash 10 ft x 4 in. Woven Glass Bag, Sunbury Fabric	224

LIST OF TABLES (Continued)

No.		Page
29	Physical Properties of Fabrics Involved in Model Testing	240
30	Summary of Measured Filtration Parameters for Model Testing	242
31	Clean (Unused) and Effective Drag Values for Commercial and Experimental Fabrics by Draemel With Resuspended Coal Fly Ash	245
32	Summary of Experimentally Derived Model Input Parameters Used to Predict Drag Versus Fabric Loading Relationship	248
33	Corrections Factors for K_2	255
34	Data Summaries for Estimating K_2 as a Function of Face Velocity and Particle Size	256
35	Porosity Function for Granular Porous Media	262
36	Measured and Calculated K_2 Values for Nucla Field Tests	263
37	Summary of Average K_2 Value From Nucla Field Studies	265
38	Calculated and Measured Values for Specific Resistance Coefficients for Various Dusts	266
39	Measured and Predicted K_2 Values	268
40	Relationship Between Cleaned Fabric Surface and Average Filter Drag - Coal Fly Ash Filtration With Woven Glass Fabric (Predicted)	274
41	Fraction of Filter Surface Cleaned Versus Dust Separation Force, GCA Fly Ash With Woven Glass Fabric (Sunbury Type)	291
42	Effect of Number of Mechanical Shakes on GCA Fly Ash Removal From Selected Fabrics	294
43	Physical Properties and Penetration Data for Woven Fabric Examined for Dust Cake Adhesion	296
44	Input Parameters for Estimating Bulk Fiber Efficiency	322
45	Collection Parameters and Initial Efficiency for Woven Fabric Filters for Fiber Phase Collection	323

LIST OF TABLES (Continued)

No.		Page
46	Filtration Parameters for Combined Fiber-Particle Collection	324
47	Penetration Estimates for a 2 μm Particle as a Function of Fabric Loading and Inlet Concentration at 0.61 m/min Face Velocity, Fiber Filtration Phase	325
48	Parameters for, and Estimation of, Overall Weight Collection for Fly Ash During Fiber Phase Filtration	326
49	Estimated Values for Diffusion, Interception and Impaction Parameters, Granular Bed Collection	330
50	Parameters Used to Compute Dust Cake Particle Collection Efficiency	331
51	Estimated Overall Weight Collection Efficiencies as a Function of Cake Thickness and Inlet Particle Size for Fly Ash	332
52	Comparative Penetration Characteristics for Uniformly Loaded and Partially Loaded Fabrics, GCA Fly Ash	339
53	Simulation Program Input Data	368
54	Sample Program Output With Supplementary Definition of Terms	372
55	Data Used for Model Trials With the Nucla and Sunbury Fabric Filter Systems	375
56	Normal Cleaning Sequence for Each Nucla Compartment	376
57	Simplified Cleaning Sequence per Nucla Compartment Used in Predictive Modeling	377
58	Test Run No. 0422 Nucla Baghouse Simulation - Linear Printout of Input Data for Baghouse Analysis	379
59	Normal Cleaning Sequence for Sunbury Compartment	382
60	Simplified Cleaning Sequence per Sunbury Compartment	383
61	Test Run No. 0422 Sunbury Baghouse Simulation - Linear Printout of Input Data for Baghouse Analysis	384
62	Test Run No. 0422 Sunbury Baghouse Simulation - Nonlinear Printout of Input Data for Baghouse Analysis	385

LIST OF TABLES (Continued)

No.		Page
63	Predicted and Measured Resistance Characteristics for Nucla Filter System	389
64	Comparison of Observed and Predicted Fly Ash Penetration Value, Sunbury Installation	405
65	Summary Table Showing Measured and Predicted Value for Filter System Penetration and Resistance, Coal Fly Ash Filtration With Woven Glass Fabrics	408
66	Data Used to Determine Constants in Dust Penetration Model	419
67	Input Specifications for Various Types of Cleaning Cycles	425
68	Baghouse Simulation Program Listing	426
69	Variables and Arrays Used in Baghouse Simulation Program	442
70	Data Input Format	446

ACKNOWLEDGMENTS

The authors express their appreciation to Dr. James H. Turner, EPA Project Officer, for his advise and technical support throughout the program. We also wish to acknowledge the assistance of the following GCA personnel: Dr. Michael T. Mills in the computer program area, Messrs. Mark I. Bornstein, Lyle Powers and Manuel T. Rei for technical support in the laboratory program, and Mr. Norman F. Surprenant for his technical reviews.

NOMENCLATURE

Roman

a	Proportionality factor, Leith and First efficiency model
a	Concentration decay function
a_c	Fraction of fabric area cleaned
a_d	Fraction of fabric area not cleaned
a_i	System constant in Walsh and Spaite model
a_u	Fraction of fabric area not cleaned
$\bar{a}$	Average acceleration
b	Proportionality factor, Leith and First efficiency model
c	Proportionality factor, Leith and First efficiency model
c	Concentration
cm	Centimeters
d	Pore diameter
d_c	Collector diameter
d_f	Fiber diameter
d_{min}	Pore diameter at greatest pore depth
d_{max}	Pore diameter at pore surface
d_o	Particle specific surface diameter
d_p	Particle diameter
d_s	Particle surface mean diameter

NOMENCLATURE (continued)

d_v	Particle volume mean diameter
f	Shaking frequency
g	grams, or gravitational force
k	Constant in Equation (25) = $(d_{max} - d_{min})/W_I$
k	Constant in Equation (50) for determination of average acceleration
k'	Parameter defined by Equation (77) for the calculation of efficiency
k''	Constant defined in Equation (77)
k_1	Cleaning period for a single compartment in Solbach model
m	Meter
min	Minute
n	Number of filters or compartments operated in parallel
n	Total number of areas in the system
Δt	Cleaning interval for a compartment
Σt	Combined operating time for a cycle
p	Pressure
t	Time
v	Gas velocity
x_i	System constant in Walsh and Spaite Model
A	Amplitude
ΔA_d	Rate of increase of collector surface area per unit area of filter cross section
A_i	Cloth face area of the i^{th} compartment
A_p	Particle surface area based on surface mean particle diameter, d_s
A_p	Ratio of total projected fiber surface to filter cross sectional area

NOMENCLATURE (continued)

A_p	Cross sectional area of a single pore
A_v	Particle volume, based on particle volume mean diameter, d_v
C	Concentration
C	Inlet dust concentration
C_c	Cunningham slip correction factor
C_i	Inlet concentration
C_o	Orifice coefficient
C_o	Outlet concentration
C_R	Residual concentration due to rear face slough-off
D_B	Diffusion coefficient
$\overline{E}$	Average collection efficiency in Fraser and Foley model
F_a	Adhesive force
F_{50}	Median adhesion force
I	Total number of compartments
J	Total number of areas on a bag
K	Reciprocal of K_2 in Stinessen drag model
K_2	Specific resistance coefficient
K_2^o	Specific resistance coefficient measured at 0.61 m/min and actual gas temperature
K_{FS}	Fabric surface correction factor for K_2
K_{perm}	Fabric permeability correction factor for K_2
K_{sh}	Particle shape correction factor for K_2
K_R	Initial slope of drag versus loading curve
K_v	Velocity correction factor for K_2
L	Filter thickness

NOMENCLATURE (continued)

L	Fiber bed depth
$\overline{M}$	Average hydraulic radius
N	Newton
N	Number of pores
N	Number of particles in a unit mass of filter bed
N_S	Limiting number of shakes beyond which no appreciable reduction of residual drag occurs
N_W	Limiting number of shakes beyond which no increase in filtration capacity is attained
P	Pressure drop
ΔP	Increase in pressure drop
P_c	Constant system pressure drop
P_E	Pressure drop based on system velocity and effective drag, S_E
P_{max}	Specified maximum pressure during a cleaning cycle
Pn	Penetration
Pn_o	Penetration at a residual loading
Pn_s	Steady state penetration
P_W	Pressure used to determine the fabric loading W_P
$P_{\overline{W}_P}$	Pressure drop at the average loading, $\overline{W}_P$
Q	Volumetric gas flow rate
Q	Volume flow per pore
Q_i	Volume flow rate through the i^{th} compartment
R_D	Ratio of particle diameter to fiber diameter
$\overline{R}$	Pore radius (based on minimum pore area)
S	Total filter drag

NOMENCLATURE (continued)

S	Total system drag
S_c	Cleaned area drag
S_d	Uncleaned area drag
S_E	Effective drag for cleaned filter area
S'_E	Average effective drag
S_i	Overall drag of the i^{th} compartment
S_o	Particle specific surface parameter
S_o	New fabric drag
S_R	Average resultant drag of a partially cleaned filter
S_R	Residual drag
$\overline{S}_R$	Average drag after cleaning
S_u	Uncleaned area drag
V	Average pore velocity
V	Face velocity
V_c	Constant average system face velocity
V_i	Velocity through the i^{th} compartment
V'_i	Average velocity through the i^{th} compartment when one compartment is off-line
V_R	Reverse flow velocity
W'	Absolute fabric loading minus the residual loading = $W - W_R$
W^*	Constant used in the nonlinear drag model, specified for each dust/fabric combination
W_f	Weight of clean fabric at the start of filtration, Noll, David and Shelton drag model
W_I	Fabric loading at inception of pure cake filtration (linear drag)

NOMENCLATURE (continued)

W_P	Fabric loading at the limiting pressure
W_P'	Corrected value for W_P
$\overline{W}_P$	Average fabric loading for a system operating under continuous sequential cleaning conditions
W_R	Residual fabric loading; i.e., the loading on a cleaned area
W_R'	Average fabric loading after cleaning
W_T	Average fabric loading before cleaning
X	Deposit thickness, Leith and First efficiency model

Dimensionless groups

Re_f	Fiber Reynolds number
Pe	Peclet number

Greek

α	Ratio of bed packing density to particle density
ε	Porosity
η	Single particle-single fiber efficiency
η_{DI}	Interception efficiency
η_I	Impaction efficiency
η_D'	Diffusion parameter
ρ_f	Discrete fiber density
ρ_P	Discrete particle density
$\overline{\rho}$	Bulk fiber density
σ_g	Particle size distribution geometric standard deviation
ϕ	Function specific to fabric and dust
μ	Gas viscosity

NOMENCLATURE (continued)

μm	Micron or micrometer
μ_f	Fluid viscosity

Subscripts

c	Cleaned area
i	Interval of size distribution
i	Number of the time increment
i	Refers to the i^{th} compartment
j	Refers to the j^{th} area on a bag
t	Refers to time = t
u	Uncleaned area

SPECIAL NOMENCLATURE

ENGLISH AND METRIC EQUIVALENCIES FOR KEY FILTRATION PARAMETERS

	Units		
	Metric	English	Equivalency
Filter resistance	N/m^2	in. H_2O	249 N/m^2 = 1 in. water
Filter drag	$N\ min/m^3$	in. H_2O min/ft	817 $N\ min/m^3$ = 1 in. water min/ft
Velocity	m/min	ft/min	0.305 m/min = 1 ft/min
Volume flow	m^3/min	ft^3/min	0.0283 m^3/min = 1 ft^3/min
Fabric area	m^2	ft^2	0.093 m^2 = 1 ft^2
Areal density	g/m^2	lb/ft^2	4882 g/m^2 = 1 lb/ft^2
Specific resistance coefficient	N min/g-m	in. H_2O min ft/lb	0.167 N min/ g-m = 1 in. H_2O min ft/lb
Dust concentration	g/m^3	$grains/ft^3$	2.29 g/m^3 = 1 $grain/ft^3$

SECTION I

SUMMARY

The overall objective of this program was to develop mathematical models to predict fabric filter behavior with emphasis on systems for the control of particulate emissions from coal-fired boilers. In conjunction with the development of drag and efficiency models, a laboratory experimental program was conducted to provide insight into critical filtration parameters (e.g., fabric structure, particulate deposition and removal) affecting field and laboratory filter performance. The laboratory program has been directed mainly to the collection of coal fly ash with woven glass fabrics of the type used at Nucla, Colorado, and Sunbury, Pennsylvania fabric filter installations. The results of both field and laboratory testing and research have been utilized in the development of the model. Further experimental work was carried out on full scale bags to verify the results of the bench scale program and to test and improve the models.

The literature with respect to filtration is vast, but the efforts to model fabric filtration have been limited in number and usefulness. In fact, the results of a detailed survey suggest that many parameters are best determined by carefully controlled experiments until an adequate theory is developed. Modeling approaches have usually depended upon a linear approximation to define the increase of fabric drag with fabric dust loading and many fabric collectors have been described as an array of cylinders. The latter (cylinder) approaches treat particle collection by concepts developed for bulk fiber filters for which randomly or preferentially oriented discrete fibers appear to capture particles in fair accord with "single particle-single fiber" collection theory.

A woven fabric filter, however, is more properly viewed as an array of pores whose number relate approximately to fabric thread count and whose boundaries are formed by the intertwined warp and fill yarns. Because of the low yarn porosity per se, ~10 percent, only those fibers constituting the napped, bulked or protruding staple fibers are available for effective "single fiber" collection. Conversely, negligible gas flow, and, hence, filtration, can take place within the yarns because of their very low permeability.

The fiber fraction that extends into and across the pore openings, which is fairly uniformly distributed in a good filter, actually constitutes the supporting substrate for initial dust cake formation. (If a filter fabric is composed entirely of multifilament yarns, the yarn proximity must be significantly increased before effective particle collection ensues.)

Considering particle capture to consist first of a bridging over of pore openings at the substrate level (a process that commences somewhat below the superficial fabric surface and continues until an appreciable dust cake has developed) has enabled the development of a new, nonlinear model. The new model (or assemblage of predictive equations) has the capability to describe more accurately the filter resistance and particle capture properties during the initial filtration phase than the simplified linear model when a large fraction of the filter surface is cleaned.

Bench and pilot scale tests showed that certain portions of the fabric were cleaned to a very low residual dust level whereas the remaining surface experienced no cleaning whatsoever. Exploratory tests with two element systems (dust removed from only 50 percent of the fabric surface) indicated that filter resistances were significantly lower while penetrations were correspondingly higher for nonuniformly loaded fabrics.

Higher penetrations result from the initial high velocity transients through the "just cleaned" fabric areas. Under the more rigorous analysis of velocity distributions afforded by the nonlinear drag model, even higher penetration levels would be predicted. When the model system is composed of six or more separate bag compartments in which the degree of cleaning is like that observed for many collapse or mechanical shaking systems (~10 to 20 percent) the difference between linear and nonlinear modeling diminishes.

The drag and efficiency models for a full scale system appear to give results which are both reasonable and informative. With respect to the Sunbury and Nucla type fabrics, experiment and theory indicate that by far the largest fraction of all dust penetrating these filters is that which passes through unblocked or unbridged pores immediately after filter cleaning or through oversize pores (pinholes) that fail to close at any time during the filtering cycle. Since very little dust is separated from that fraction of the inlet air that passes through a pore and, since pore velocities may exceed cake velocities by a factor of 10^3 or greater, the particle size properties of the filter effluent are dominated by the properties of the inlet dust that passes through the pore. Those changes in particle size efficiency attributable to either preliminary fiber filtration and subsequent cake filtration are usually completely obscured by direct dust penetration and/or clean face slough-off components. The above statement applies specifically to the common woven glass fabrics used for fly ash filtration.

Over the range of face velocities studied, 0.40 to 4.3 m/min (1.3 to 14 ft/min) velocity was observed to exert a strong influence on mass penetration while having little impact on size properties. Theory and confirming microscopic observations of filter surfaces suggested that complete pore bridging is more difficult to obtain at higher velocities due to increased reentrainment of deposited dust.

As the cake built up, the penetration decreased rapidly in exponential fashion followed by a leveling-off to an asymptotic value determined by penetration through the pinholes or by seepage and/or slough-off from the rear face of the dust layer.

The mathematical model developed within this study represents a new and very effective technique for predicting the average and instantaneous values for resistance and emission characteristics during the filtration of coal fly ash with woven glass fabrics.

Two basic concepts used in the model design: (1) the quantitative description of the filtration properties of partially cleaned fabric surfaces and (2) the correct description of effluent particle size properties for fabrics in which direct pore or pinhole penetration constitutes the major source of emission, have played important roles in structuring the predictive equation.

A third key factor in the model development was the formulation of explicit functions to describe quantitatively the cleaning process in terms of the method, intensity and frequency of cleaning. By cleaning we refer specifically to the amount of dust removed during the cleaning of any one compartment and the effect of its removal on filter resistance and penetration characteristics.

The drag and efficiency models have been combined to form an experimental computer program for a complete multichamber filtration system. The results of such modeling are presented for both flow resistance and particle penetration behavior. The linear drag model will probably satisfy most practical field filtration applications. However, the nonlinear model, which also visualizes fabric performance from the pore array concept, may provide a better fit in those cases where an unusually high dust removal is achieved during filter cleaning. The above (cleaning) process creates a filter surface that provides not only low resistance to air flow but also a highly permeable region for dust particles.

SECTION II

INTRODUCTION

The development and evaluation of a predictive model for fabric filtration with special emphasis on the control of coal fly ash emissions from boilers are described in this report. The primary goals of this project were to relate basic filtration parameters including dust properties, dust loadings and air-to-cloth ratios to key performance parameters, pressure loss and dust penetration characteristics. Laboratory experiments conducted as part of this program as well as the results of prior field and laboratory investigations by many researchers constituted the bases for the modeling concepts developed under the present program.

The following factors can be expected to influence the efficiency and the pressure/flow relationship:

1. Dust - chemical composition, particle size distribution, particle shape, particle phase, particle concentration.
2. Gas - chemical composition (especially moisture content), temperature, pressure.
3. Fabric - material, weave (including fill and warp counts), finish, history (especially accumulated dust).
4. Cleaning operations - cleaning type, intensity, frequency, duration.

Although it is desired that both resistance and efficiency characteristics be predictable for the conditions cited above, this goal is not easily attained. In forming a useful model, therefore, one treads a narrow path between untractable complexity and impractical simplicity, particularly so in the case of fabric filtration.

Several research programs are being conducted in the fabric filtration area because of the importance of fine particle removal by air and gas cleaning processes. By and large, the Environmental Protection Agency has provided the recent impetus for such activities, either through its in-house research programs or the sponsorship of outside research.

Completion of the "Handbook of Fabric Filter Technology" in 1970 by Billings and Wilder[1] along with supporting appendices, bibliography and recommendations for research under Contract CPA-22-69-38 represented the first major step to bring together and evaluate available data on filtration technology. The state-of-the-art in filtration technology was reviewed more recently in a joint EPA/GCA sponsored symposium whose papers appear in the December 1974 issue of the APCA journal.[2] Since that time, additional in-house and field studies performed by EPA have dealt with filter performance versus fabric structure, Draemel;[3] the performance of nonwoven (spun bonded) nylon fabrics, Turner;[4] and field filtration of metal oxide fumes, Harris and Drehmel.[5]

Various EPA contractor groups have investigated the use of fabric filtration with coal-fired industrial boiler effluents, McKenna;[6] the performance of field filter systems for bronze smelting operations, asphalt concrete production and coal-fired cyclone boilers, Hall and Dennis,[7] and more recently the performance of commercial glass fabric filter systems at two coal-fired power plants by Bradway, et al.[8] and Cass, et al.[9] The role of fabric filter cleaning mechanisms in controlling resistance characteristics and dust penetration has been studied extensively in the laboratory by Dennis and Wilder.[10] Based upon studies of the type described above, attempts have been made to develop mathematical models for describing fabric filter performance. Although one can argue that almost all models proposed to date have at best only limited application, their deficiencies are often due to a lack of reliable field and laboratory data. This situation has prevailed because of (1) the number of variables encountered in a filter system and (2) the often complex relationships among these variables.

DESCRIPTION OF A FILTRATION SYSTEM

Figure 1 shows a very simple schematic of a fabric filter installation. A dust-laden flow of gas enters the filter installation with a volumetric flow rate Q and a concentration c. The flow is divided among n compartments, the bags within each compartment having a fabric loading of average dust weight per unit fabric area W_i. The pressure drop across the i^{th} compartment's bags is given by the equation:

$$\Delta p_i = Q_i S_i / A_i,$$

in which Q_i is the volume flow rate, A_i is the cloth face area and S_i is the overall drag caused by the fabric and any accumulated dust. The ratio S_i/A_i is analogous to electrical resistance (with Q_i depicting the current and Δp_i the voltage). The total flow, Q, is the sum of the individual flows, Q_i (as long as temperature and pressure corrections are made). Usually the compartments are operated in parallel and so constructed that the pressure drop at any given time is expected to be essentially the same across all of them.

The relationship between the pressure drop and the volume flow for a particular installation will depend upon the locus of the intersections of the system fan curve and the system resistance curve,[11] each of which can be expressed as volume rate of flow versus pressure drop. Usually, one of the following conditions holds approximately for the installation:

1. The fan produces a constant volume of flow while the pressure drop changes with system resistance.
2. The fan produces a constant pressure drop, while the volume flow changes with system resistance.

OBJECTIVES

The cost of the installation will depend, in part, upon the type and quantity of fabric and a major operating cost will be that required to overcome filter resistance to gas flow.

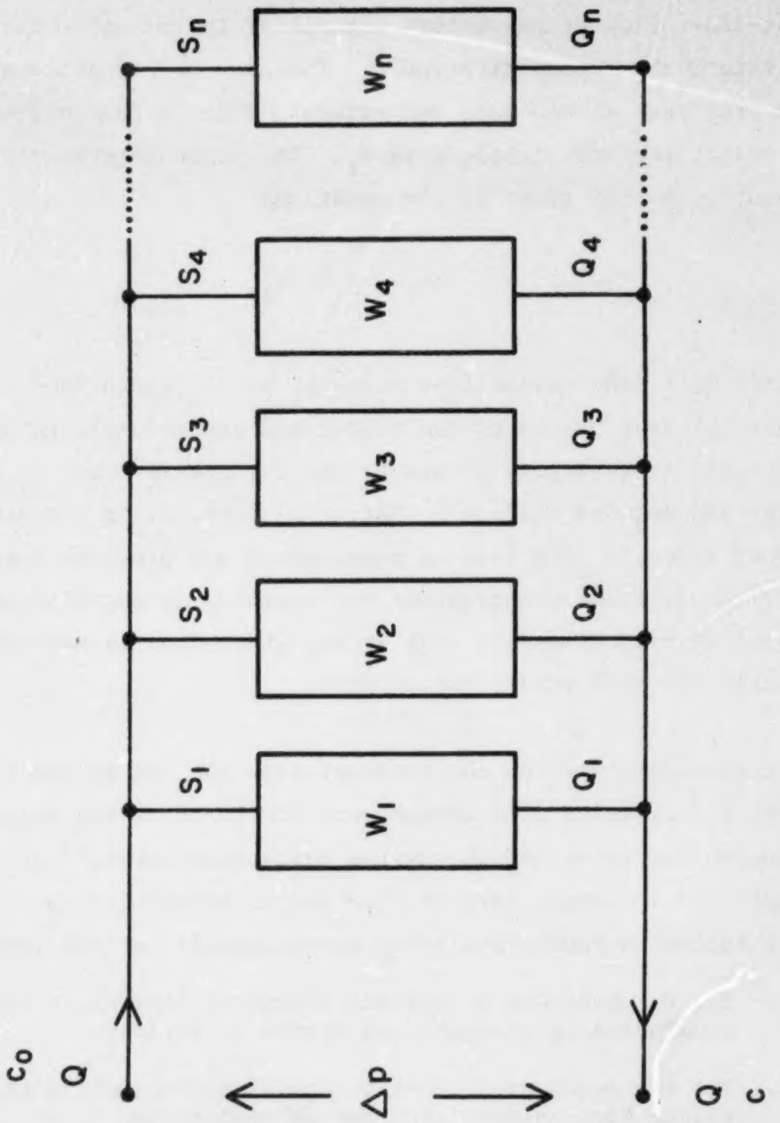
c_o
Q
Δp
Q
c
S_1
S_2
S_3
S_4
S_n
W_1
W_2
W_3
W_4
W_n
Q_1
Q_2
Q_3
Q_4
Q_n

Figure 1. Schematic of n-compartment baghouse

Often the available choice of fabrics will be limited, so that the major question becomes the area of cloth needed to handle a specified volume flow rate of gas.

The cloth area required has as its criterion "operation at an acceptable pressure drop across the cloth for a predetermined cycle."[12] One might add that this assumes that the collection efficiency is adequate under these conditions. Thus, an important goal is to be able to predict the pressure drop for a particular dust and fabric combination at a given air-to-cloth ratio. The drag will depend upon how much dust is on the filter surface, how it is distributed, the geometrical structure of the cake, the geometry of the fabric and the viscosity of the gas. A second and equally important goal is to predict the system emissions.

OUTLINE OF MODEL

A procedure for calculating the pressure/flow relationship and filter efficiency can be developed by first subdividing the fabric area into smaller homogeneous subunits (compartments, bags, or areas on bags) and then performing the following operations.

1. Calculate the drag (the pressure drop per unit face velocity) for the subunit.
2. Determine the flow from the drag and the instantaneous pressure drop.
3. Determine the penetration, or fraction of the particulate concentration reaching the subunit which penetrates to the clean air side.
4. Calculate the emissions rate from the subunit (penetration times inlet concentration times volume flow rate).
5. Calculate the new dust loading of the subunit.
6. Determine the new pressure drop or the new total flow rate by combining the resistance of the subunits according to the law for the addition of parallel resistances:

$$Q = \Delta p \frac{A}{S} = \Delta p \sum_{i=1}^{n} A_i/S_i$$

$$S = \left(\sum_{i=1}^{n} A_i/S_i \right)^{-1} A$$

To develop a time profile of the performance, this procedure must be done iteratively, with any cleaning taken into account as well.

The program goal was to develop those modeling concepts as diagrammed in Figure 2. With such a model one should be able to predict the collection efficiency and the relationship between flow and pressure drop for fabric installations for rational combinations of variables relating to dust, gas, fabric, and cleaning method.

SUMMARY OF METHODOLOGY

The model is built up from individual units:

1. Analysis of the system elements.
2. Analysis of operating modes.
3. Determination of flow through the elements during these processes.
4. Determination of particulate emissions during these processes.
5. Calculation of the pressure drop, flow, and emissions.

The steps involved in obtaining the necessary information to construct these units have been:

1. Review previous work.
2. Develop working model with regard to drag and particle removal.

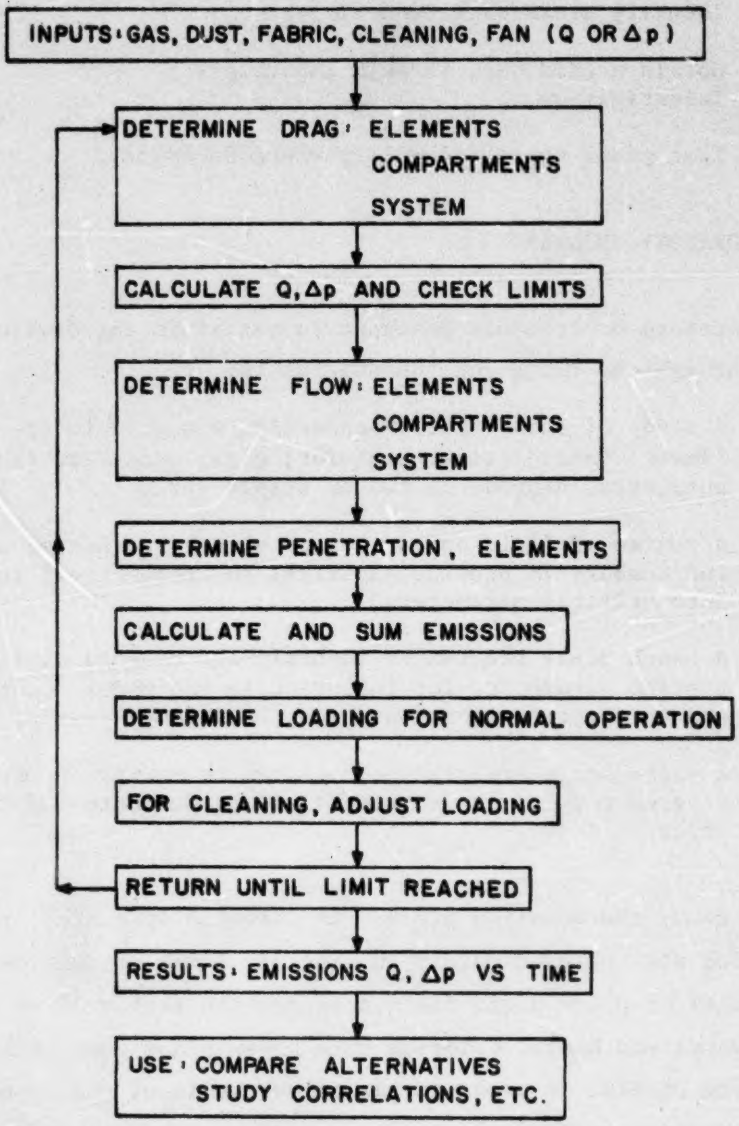
INPUTS: GAS, DUST, FABRIC, CLEANING, FAN (Q OR Δp)
DETERMINE DRAG: ELEMENTS
COMPARTMENTS
SYSTEM
CALCULATE Q, Δp AND CHECK LIMITS
DETERMINE FLOW: ELEMENTS
COMPARTMENTS
SYSTEM
DETERMINE PENETRATION, ELEMENTS
CALCULATE AND SUM EMISSIONS
DETERMINE LOADING FOR NORMAL OPERATION
FOR CLEANING, ADJUST LOADING
RETURN UNTIL LIMIT REACHED
RESULTS: EMISSIONS Q, Δp VS TIME
USE: COMPARE ALTERNATIVES
STUDY CORRELATIONS, ETC.

Figure 2. Flowchart for baghouse model

3. Compare model with existing data.

4. Alter hypotheses where necessary.

5. Identify areas of data deficiency.

6. Obtain needed data through laboratory investigation.

7. Test model again and modify where necessary.

THE LABORATORY PROGRAM

The laboratory program was designed to assist in the development of the model through the following investigations:

- A study of those fabric properties expected to influence fabric filter behavior; e.g., pore structure, pore area, napped, bulked or staple yarns.
- A review of field operations previously conducted at Nucla and Sunbury to provide empirical and theoretical insights into critical parameters.
- A bench scale program to identify and measure critical filtration parameters for inclusion in the model and to test and validate the model and its possible revisions.
- A pilot scale experimental program to verify the bench scale program results and to supply additional data for the modeling effort.

At this time, the modeling process is directed specifically to coal-fired combustion systems used mainly in electric power production. Therefore, the results of power plant field measurements performed at Sunbury, Pennsylvania and Nucla, Colorado with woven glass bags plus supporting laboratory studies on used and new filter media of the types employed at the aforementioned field locations are described in this report in the light of their contributions to mathematical model design.

The results of several field measurements at both Sunbury and Nucla have been presented in earlier reports. It was the aim of the previous tests to provide as much data on filter system performance as possible. To this end, mass concentration and particle size information were obtained over several days of typical power plant operations. Although it is believed that these measurements described accurately the inlet and outlet dust properties, the inability to make certain measurements in the field makes it difficult (1) to ascertain whether in fact certain system components were operating as intended and (2) to vary basic plant operating parameters without interfering with electric power production.

Because it was not possible to install instrumentation describing the performance of individual bag compartments (and bags), most field data depict average performance characteristics with respect to gas stream composition, temperature, pressure drop across the baghouse and emission characteristics. Therefore, although these data should enable reliable projections for the performance of replicate systems, caution must be exercised in applying the findings to coal-burning power plant operations where kW capacity, gas flows, number of compartments and cleaning cycles differ. To extrapolate these data for the filtration of noncombustion aerosols with glass fabric at different temperatures and with other modes of cleaning could lead to serious errors unless particle/fabric relationships are clearly understood. For the above reasons, several tests were performed in the laboratory not only to provide supplemental data but also to make maximum use of field measurements. Past and present field measurements plus those from carefully-designed laboratory experiments have provided the base for further testing and improvement of the model.

SECTION III

A REVIEW OF FABRIC FILTRATION MODELS

Although filtration processes have been treated extensively in the technical literature, most data are only tangentially related to fabric filtration. The remaining information more often examines the behavior of isolated cylindrical fibers or fibers which are part of a high-porosity matrix, as, for example, deep bed or bulk fiber filters. The literature describing models for determining pressure drop, flow rate and collection efficiency for fabric filters is much more limited.

PREDICTIVE MODELS

The efforts of several investigators to develop predictive models for fabric filtration processes are reviewed in the following paragraphs.

Robinson, Harrington and Spaite Model

One of the first modeling attempts was made by Robinson, Harrington and Spaite[13] who designed a mathematical model for predicting performance of a multicompartment, parallel flow baghouse. Their basic equation for calculating the drag, S, of an individual compartment was:

$$S = S_R + K_2 V c t \quad (1)$$

The relationship between the drag of the individual compartments within equal filter areas and the total drag of a parallel filter system is given by:

$$\frac{n}{S} = \frac{1}{S_1} + \frac{1}{S_2} + \cdots + \frac{1}{S_n} \qquad (2)$$

The symbols appearing in Equations (1) and (2) are defined here and in the following sections as shown below:

S = Total filter drag
S_R = Residual drag
K_2 = Specific resistance coefficient
c = Inlet dust concentration
t = Time
n = Number of filters or compartments operated in parallel.

Their model was derived from experimental data obtained on a pilot filtration unit consisting of 3 parallel flow compartments, each with eight cotton sateen bags cleaned by mechanical shaking.

The air flow distributions during these experiments as determined by Walsh and Spaite[14] are shown in Figure 3.

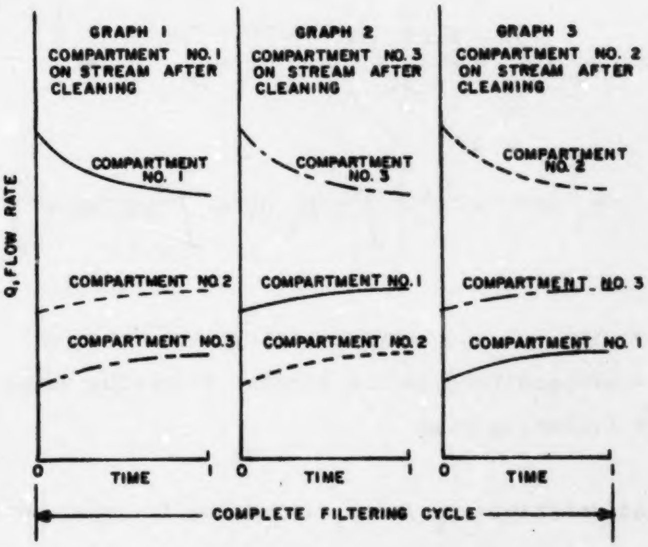

Figure 3. Three-compartment baghouse with sequential cleaning.

The three curves on each single graph represent the air flow through individual compartments over the same time interval, whereas the three graphs indicate the changes in compartment flow over a complete filtration cycle. Note that each compartment has assumed three distinct flow characteristics over the complete filtration cycle.

Analysis of the volume flow rate, Q, versus time curve for each compartment indicated the following approximate relationship:

$$Q_1 = a_i \, t^{x_i} \tag{3}$$

where the numbers i = 1, 2, 3, n refer to the order of cleaning with "1" indicating the most recently cleaned compartment and the terms a_i and x_i are system constants requiring experimental evaluation.

The drag values for the individual compartments were obtained as follows:

$$S_1 = S_R + \frac{K_2c}{A}\int_o^t Q_o \, dt$$

$$S_2 = S_R + \frac{K_2c}{A}\left[\int_o^{t_i} Q_1 \, dt + \int_o^t Q_2 \, dt\right]$$

$$S_3 = S_R + \frac{K_2c}{A}\left[\int_o^{t_i} Q_1 \, dt + \int_o^{t_i} Q_2 \, dt + \int_o^t Q_3 \, dt\right]$$

where t_i = time for one complete filtration interval

t = elapsed time in the current filtering interval

A = filtering area

Although the constants a_i and x_i appearing in Equation (3) can be defined in terms of operating variables and a combination of simple and multiple regression analyses, the overall mathematical manipulations are cumbersome, and, in the long run, provide data outputs that cannot be safely extrapolated beyond the operating conditions used to calculate the system constants.

The authors state that the values for the constants will also depend upon baghouse configuration and inlet concentration. Additionally, correct evaluation of K_2 is claimed to be very important. Although not mentioned by the authors, knowledge of the actual residual dust loadings and the degree of dust removal attained by various cleaning methods whether it be mechanical shaking or bag collapse with reverse flow is essential to any useful extrapolation of their proposed modeling equation.

If the residual drag denotes the drag obtained by the extrapolation of the linear zone, S_E, Equation (1) calculates the straight line shown in Figure 4 by the solid line. If their use of the term "residual drag" refers to S_R, then in Figure 4 their equation must be represented by the dashed line. In either case, Equation (1) considers the linear portion only, omitting the dust cake repair zone where the drag may exhibit initially a steep nonlinear rise. The model they present does not predict collection efficiency or effluent loadings.

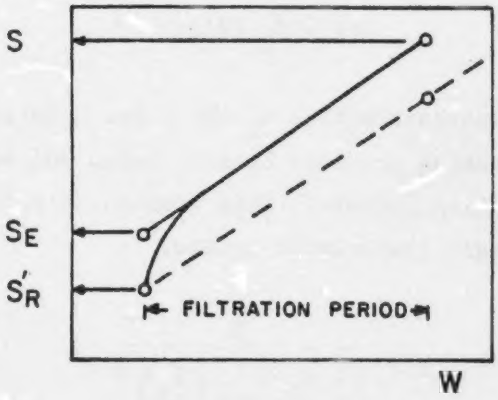

Figure 4. Fabric drag versus loading

Solbach Model

Based on bench-scale tests, Solbach[15] derived a simplified model for single and multicompartment filters. His approach was to extrapolate linearly the upper portion of the drag versus fabric loading curve so that an effective drag intercept, S_E, was obtained for the residual fabric loading condition W_R. This simplifying concept has been used by many previous investigators. Solbach also assumed that once the filter was conditioned or stabilized, repetitive values for either S_E or S_R would be obtained for successive filtering and cleaning cycles.

Solbach has also used the common expression for predicting total filter drag, i.e.:

$$S = S_E + K_2 W' \tag{4}$$

where W' indicates the amount of dust added to the filter since resumption of filtration.

He again uses the classical expression:

$$dS = K_2\, cV\, dt$$

with the added constraints that K_2 and c are constant for a given operation and that the operating pressure loss is known and maintained constant during the filtration process. This enables calculation of the gas velocity within a single compartment system.

$$V = \frac{1}{\sqrt{\frac{2\, K_2 c}{\Delta p}\, t + \left(\frac{S_E}{\Delta p}\right)^2}} \tag{5}$$

If the cleaning period for the filter compartment is k_1 and n is the number of the compartments, the total filtration period of each compartment is:

$$t = k_1 n$$

Thus the average gas velocity through the filter becomes:

$$V_{avg} = \frac{\sum_{i=1}^{n} V_i}{n}$$

or as a good approximation:

$$V_{avg} = \int V dt/t \qquad (6)$$

Solbach obtained an expression for the average gas velocity through the multicompartment system by combining Equations (5) and (6):

$$V_{avg} = \frac{\Delta p}{K_2\ c\ t} \left(\sqrt{\frac{2\ K_2 ct}{\Delta p} + \left(\frac{S_E}{\Delta p}\right)^2} - \sqrt{\left(\frac{S_E}{\Delta p}\right)^2} \right) \qquad (7)$$

The required total filter area for the multicompartment fabric filtration system is given by:

$$A = \frac{Q}{n\ V_{avg}} \qquad (8)$$

In order to estimate average face velocity and fabric area by Equations (7) and (8), it is necessary to select an operating pressure that will not change appreciably over a filtering cycle and to determine K_2 and S_E by methods described previously.

By rearranging Equation (7) a simplified form of this equation can be obtained in terms of the amount of dust deposited in time t:

$$S_{avg} \equiv \frac{\Delta p}{V_{avg}} = S_E + \frac{K_2W'}{2} \qquad (9)$$

showing that, according to Solbach, the "average" total drag S_{avg} is equal to the effective drag plus one-half the drag of the dust cake before cleaning. Dust penetration characteristics are not considered in the above models.

Dennis and Wilder Model

A somewhat similar expression for the average total drag of the multi-compartment system was obtained by Dennis and Wilder[10] by an independent analysis.

At any time, the pressure drop is equal to the instantaneous product of the filtration velocity and the drag so that the total drag can be described by the well-known approximate equation:

$$S = S_E + K_2W' \qquad (4)$$

and the instantaneous increase of the drag with the time is given by:

$$\frac{dS}{dt} = K_2 \frac{dW'}{dt} = K_2cV$$

By expressing W' as a function of dust concentration, filtration velocity and time, the instantaneous pressure drop is equal to:

$$\Delta p = \frac{S}{K_2c} \frac{dS}{dt} \qquad (10)$$

Because the pressure drop is essentially constant across each compartment and each bag, the instantaneous drag times the rate of increase of the drag is also the same over any area of the filter.

Thus, the average pressure drop over a time period $t_2 - t_1$, is:

$$\overline{\Delta p} \equiv \frac{1}{t_2 - t_1} \int_{t_1}^{t_2} \Delta p \, dt$$

By substituting Δp from Equation (10), the average pressure drop $\overline{\Delta p}$ is expressed as follows:

$$\overline{\Delta p} = \frac{1}{t_2 - t_1} \int_{S_1}^{S_2} \frac{S \cdot dS}{K_2 \ c} = \frac{S_2^{\ 2} - S_1^{\ 2}}{2 \ K_2 c \left(t_2 - t_1\right)} \tag{11}$$

In a baghouse with n identical compartments in a total filtration cycle τ, in minutes, one compartment is cleaned every τ/n minutes. By averaging the pressure drop over the total filtration cycle period, we obtain:

$$\overline{\Delta p} = \frac{n \ \Delta S^2}{2 \ K_2 \ c\tau} \tag{12}$$

Equation (12) was modified for use with any number of bags or compartments undergoing sequential filtering and cleaning as shown below:

$$\frac{\Delta p}{V_{avg}} = S_{avg} = S_E + \frac{K_2 W'}{2} \tag{13}$$

This form, which is almost identical to that developed by Solbach, Equation (9), does not require the assumption of constant operating pressure.

Because both models use the identical basic equations, it is understandable that they agree in predicting the average drag. The average of a linear function of W' is that function evaluated at the midpoint of the W' interval.

Noll, Davis and Shelton Model

In a model proposed by Noll, Davis and Shelton,[16] the same drag/fabric loading relationships cited previously are presented in equation form as:

$$S = S_E + S_c = S_E + K_2W'$$

Again, K_2 is the specific resistance coefficient as described by Williams, Hatch and Greenberg.[17] The term S_c is the increase in drag resulting from the increase in fabric loading, W', over the filtration interval. The authors have used what they refer to as a "triangulation method" to define the effective drag S_E in terms of K_2 and W_f, that is:

$$S_E = K_2W_f \qquad (14)$$

The term W_f is defined as the weight of the clean fabric at the start of a filtration. Although Equation (14) may apply over a narrow test range, it cannot have broad application because the nature of the fabric weave as well as its density and the presence of residual dust all exert a significant influence on the effective drag. The data presented in Table 1 show clearly that even clean cloth permeability shows no consistent relationship to fabric areal density, W_f.

Table 1. SOME PERMEABILITIES AND FABRIC WEIGHTS PER UNIT AREA[a]

Fabric description	Frasier permeability, fpm at 0.5 in. H_2O	Weight, oz/yd^2
Nomex filament 3 x 1 twill	15 - 20	4.5
Cotton sateen	15 - 20	9 - 10
Spun acrylic 2 x 2 twill	60	9.8
Nomex filament (combination cotton-fill) 3 x 1 twill	30 - 50	4.5
Nomex felt	20 - 40	14. - 16.0

[a] These data were obtained from Durham[18] and a DuPont research report.[19]

Noll, Davis, and LaRosa (1975) Model

In a more recent paper, Noll, Davis and LaRosa[20] evaluated the parameters K_2 and S_E by means of performance tests on clean and conditioned fabrics of polyester. According to this work, the K_2 values depend on the properties of the dust only. It also appears that the earlier concept of expressing S_E by the product K_2 W_f (Equation 14) has been abandoned.

These published data along with numerous tests performed on other types of fabric filters (glass fiber, Nomex, cotton, polypropylene) may represent "the potential for producing generalized methods of the performance prediction - and optimization for application to industrial fabric filter design." This statement was confirmed by P. J. LaRosa[21] from Pollution Control Division of Carborundum, Environmental Systems, Inc., who stated that a predictive model, based on these data, has been established for the strict use of the company.

Although the authors report successful curve fitting, it is emphasized that their so-called dust loading range in the nonlinear region (0.01 to 0.05 lb/ft^2) does not represent the true fabric dust loading. The reported values were obtained by extrapolating data from uniformly loaded fabrics to full scale bags that had experienced only partial cleaning.

Therefore, the models and constants derived from these measurement should apply only to filter systems that have identical residual dust holdings. This presumes, therefore, very similar cleaning processes. As stated earlier, the original modeling studies by Robinson et al.[13] involve the same oversights in treating the state and behavior of cleaned fabric filters in real, commercial applications.

Stinessen's Approach

Stinessen[22] has also studied the relationship between filter drag, S, and the permeability, K, and mass, W, of the dust cake:

$$\Delta S = \Delta W/K$$

The term K is the reciprocal of the well known term K_2 (specific resistance coefficient) that has been defined previously in Equation (1).

Stinessen's equation for estimating total filter drag:

$$S = S_E + \frac{1}{K}\int_o^t cV\,dt$$

uses the effective drag, S_E, thus avoiding the nonlinearity factor encountered in many real filtering applications. Although Stinessen introduces no new concepts, he does correctly surmise that K or K_2 should depend mainly upon dust cake and fluid properties. Furthermore, he does point out that misleading values for K will obtain until the cake undergoes "repair." In effect, a repaired cake is one that displays a nearly uniform dust deposit density over the entire filter surface. Stinessen did not include provisions in his model for predicting particle emissions properties.

Fraser and Foley Model

Fraser and Foley[23] have also presented a predictive model for single bag or single compartment performance. Their basic equation again assumed the classical form:

$$S = S_E + K_2 \int_0^t cV \, \overline{E} \, dt$$

except that average collection efficiency, $\overline{E}$, was introduced. The latter refinement appears unnecessary, however, because few practical fabric filters operate much below 98 percent efficiency.

At the time of their modeling effort, the authors found it necessary to depend upon the best available data in the literature (which did not provide strong support). The major failing in the Fraser and Foley model, however, is that it attempts to treat a fabric filtration process as a highly specialized bulk fiber system. Thus, a complex series of empirical corrections are applied to the filtration theory for high porosity filters to explain the performance of a woven fabric filter. Considerable effort is also devoted to determining how much dust must fill the filter void volume, when in fact most dust captured by a filter resides upon the surface with a relatively shallow interstitial penetration. The net result is that no successful application of these models can be expected unless they are applied to situations that replicate the conditions used to develop the modeling equations.

Leith and First Model

By using tagged fly ash aerosols, Leith and First[24] were able to distinguish between those fly ash particles which, under laboratory conditions, penetrated a needled felt fabric filter immediately and those particles which exhibited a delay in their penetration. These researchers postulated three types of penetration mechanisms: direct penetration, gradual seepage of the dust, and the breakage and penetration of plugs of material in the vicinity of pinholes. To summarize the results of their work, we quote:[24]

> "Penetration by 'straight through' dust loss was found to fall off rapidly after cleaning, to reach a minimum, and then to increase. 'Seepage' of dust through the fabric was found to be constant throughout the filtration cycle. Dust loss as 'pinhole plugs' was found to increase after cleaning, to pass through a maximum, then to decline. The pinholes appear to open the way for further emission by the 'straight through' mechanism."

The experiments were performed at face velocities from 5 cm/s to 15 cm/s and for dust cakes up to 60 μm thick. These velocities are higher than those in normal use for the filtration of fly ash (~ 1 cm/s) and these cake thicknesses are rather low. The efficiency as a function of particle size was such that the penetration was found to "remain relatively constant for particles from 0.3 to 4.0 micrometers in diameter." The penetration increased with face velocity.

The results quoted from the abstract are for the relative contributions, rather than the absolute mass flux for the different mechanisms. From their figures for mass flux versus time (at 10 cm/s), one would conclude:

1. Straight through mass flux seemed to decrease (roughly exponentially) with deposit thickness, but may have gone through a minimum near 20 μm thickness.
2. Seepage mass flux remained fairly constant with time and deposit thickness.
3. Pinhole plug mass flux decreased with increasing deposit thickness.

The fraction of the total penetration which was due to pinhole plugs and seepage was greater than the direct (straight through) contribution (at 60 μm thickness) for 15 cm/s but substantially less than the direct for 10 cm/s, which suggests seepage and pinhole plugs might be very much less than the direct at 1 cm/s.

Leith and First postulated the following functional forms for the three types of penetration:

1. Direct penetration proportional to e^{-aX^b}, where X is the deposit thickness.
2. Constant seepage mass flux versus thickness of deposit.
3. Pinhole plug mass flux proportional to Xe^{-cX}

where a,b,c are proportionality factors. The correlations they found in using these equations ranged from 0.86 to 0.91 correlation coefficients, for mechanism-by-mechanism comparison, adding support for their proposed mechanisms.

Leith and First found only a weak particle size dependence for efficiency, with the efficiency decreasing slightly as particle size increased. The particle size dependence, the velocity dependence, and their general appraisal of the filtration process led them to conclude:

> "Because media filtration theory does not describe the trends in penetration found in a fabric filter, and was not developed for the operational conditions found there, it should not be used to predict or interpret the penetration characteristics of fabric filters."

CONCLUSIONS

1. All but one of the models for fabric filtration reviewed here used a linear dependence for drag versus fabric dust loading (in weight per unit area). Such models ignore the possible effects of the zone of cake repair in the drag versus loading curves and they lack a means for predicting the effective drag, S_E.
2. Except for the models of Fraser, et al.,[23] and, to an extent, Leith and First,[24] the work thus far has not attempted to predict collection efficiency. The Fraser model to predict efficiency relied on a questionable combination of the concept of effective diameter with an equation for the effects of mutual fiber interference. The Leith and First model is supported by evidence from tests with unusually high face velocities.
3. With the exception of the work by Fraser, et al.[23] values of K_2 and S_E (S_R) were assumed or obtained experimentally rather than derived from a predictive analytical equation.

Improvements in the state-of-the-art should include the following:

1. Further development of models which apply to the nonlinear portion of the drag versus dust loading relationship.
2. Analysis and prediction of the parameters K_2, S_E, S_R, S_O, based upon at least semitheoretical equations rather than purely upon correlations.
3. Formulation of collection efficiency relationships starting from another basis other than isolated fibers in a flow and including such facets as collection by dust already captured, dislodgement and flow through pinholes.

SECTION IV

LABORATORY TEST EQUIPMENT AND MEASUREMENT PROCEDURES FOR DETERMINATION OF FILTER PERFORMANCE

BENCH SCALE FILTRATION EQUIPMENT

The laboratory program was designed so that filter performance tests involving fabric resistance and particulate retention characteristics could be carried out on either bench or pilot plant scales. Although the bench approach is always attractive, it was recognized that in those cases where dimensional or dynamic similarity could not be satisfactorily attained with small scale apparatus, it would be necessary to resort to the pilot approach in which the filter bags and system operating parameters would be essentially full scale at least on a single bag basis.

Because the bench approach affords the potential advantages of reduced testing time, higher measurement precision, less expensive equipment, and less space, a special test assembly was fabricated for this program in which the filtration area was reduced to a 15 cm x 23 cm (6 in. x 9 in.) flat test panel and the system air flow rate reduced to 0.0213 m^3/min (0.75 ft^3/min) at 0.61 m/min (2 ft/min) filtration velocity. Sufficient flexibility in fan capacity was provided to operate at air to cloth ratios up to 6.0.

There was no special reason for selecting a nominal 6 in. x 9 in. filter area except that stainless steel filter holders used routinely for suspended particulate sampling were available. By fabricating a rigid, steel picture frame assembly as the actual filter holder (Figure 5), a vehicle was provided by which clean or used filter panels could be easily removed and subsequently replaced after weight determination or microscopic observations.

In order to maintain some semblance of similarity with respect to full scale systems, the filter medium was installed in the normal vertical field position with no physical support or backing behind the fabric. Because the air approach to most filter bags consists of a parallel flow either inside or outside the bag whose initial velocity is characterized either by the ratio of bag volume flow to bag cross section (or external separation distance between bags), a flat distribution manifold section was installed upstream of the filtering surface as shown in Figure 5. The photographs of the test equipment shown in Figures 6 and 7 provide more details on the experimental system. The depth of the manifold, 2.5 cm, was reduced as much as possible so that the vertical velocity component of the entering aerosol would be sufficiently high to support all fly ash particles less than 30 μm diameter.

With respect to size distribution measurements of the GCA fly ash by (a) Andersen impactor before any appreciable particle fallout or (b) by light field microscope examination of an oil resuspension of the parent dust, Figure 8, it appeared that greater than 99 percent of the dust was represented by particles less than 30 μm in diameter. Therefore, a negligible fraction of the particle mass would fail to reach the filter when the average air velocity at the base of the filter panel is 6.8 cm/sec. The latter velocity corresponds to an air to cloth ratio of 2/1. At the filter midpoint, the average rise velocity of 3.4 cm/sec would fail to entrain only those particles greater than 23 μm in diameter (roughly 2 percent of the entering dust).

On the basis of the above analysis, it does not appear that the somewhat lower vertical rise velocities of the bench scale system requires special consideration in data treatment. The dimensions of the hopper beneath the level of the filter face were selected to provide gas retention times

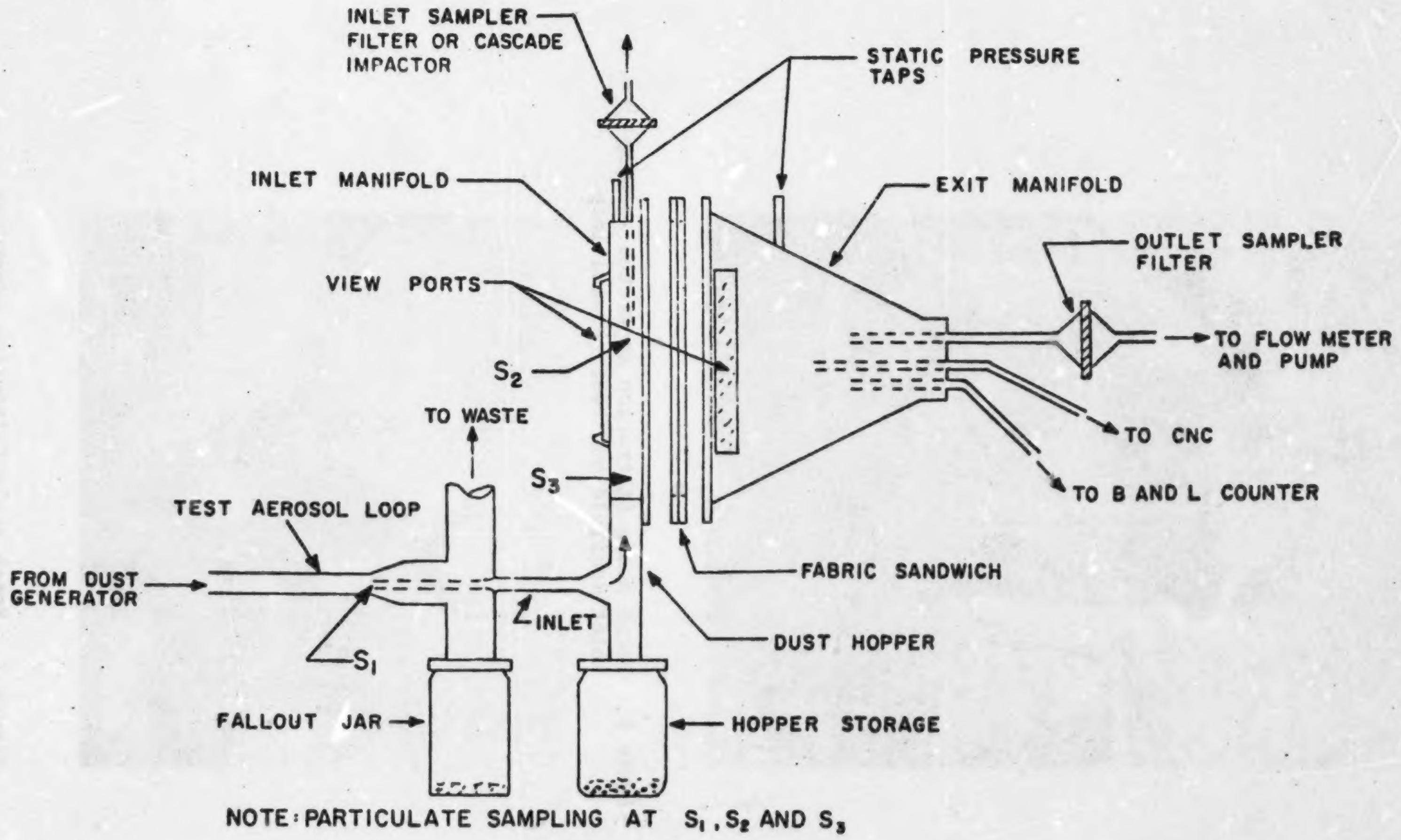
INLET SAMPLER FILTER OR CASCADE IMPACTOR
STATIC PRESSURE TAPS
INLET MANIFOLD
EXIT MANIFOLD
OUTLET SAMPLER FILTER
VIEW PORTS
TO FLOW METER AND PUMP
S_2
TO WASTE
TO CNC
S_3
TO B AND L COUNTER
TEST AEROSOL LOOP
FROM DUST GENERATOR
FABRIC SANDWICH
INLET
S_1
DUST HOPPER
FALLOUT JAR
HOPPER STORAGE
NOTE: PARTICULATE SAMPLING AT S_1, S_2 AND S_3

Figure 5. Schematic of filter test assembly with exploded view of fabric sandwich

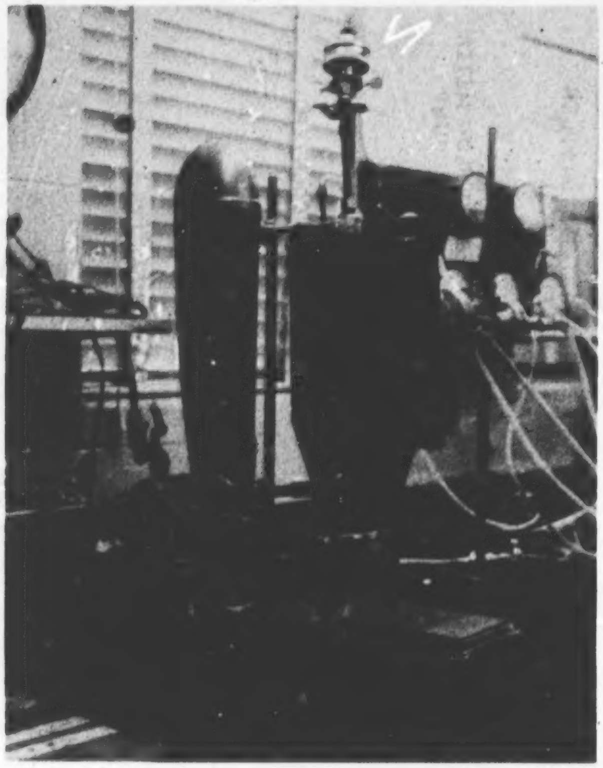

Figure 6. Bench scale filtration apparatus showing inlet manifold and test aerosol loop

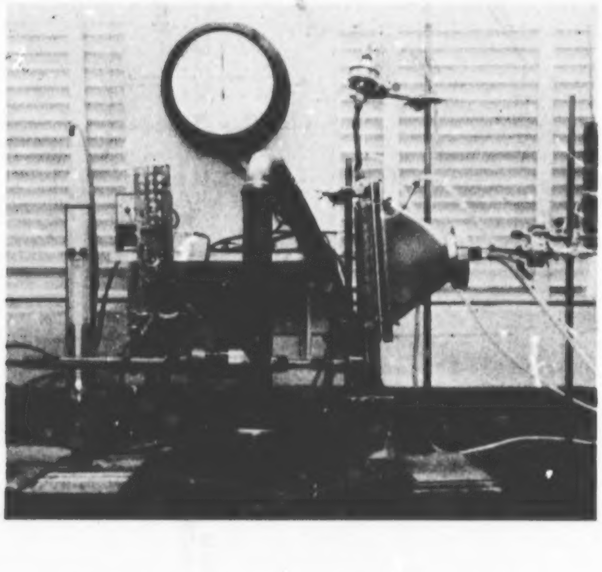

Figure 7. Bench scale filtration apparatus

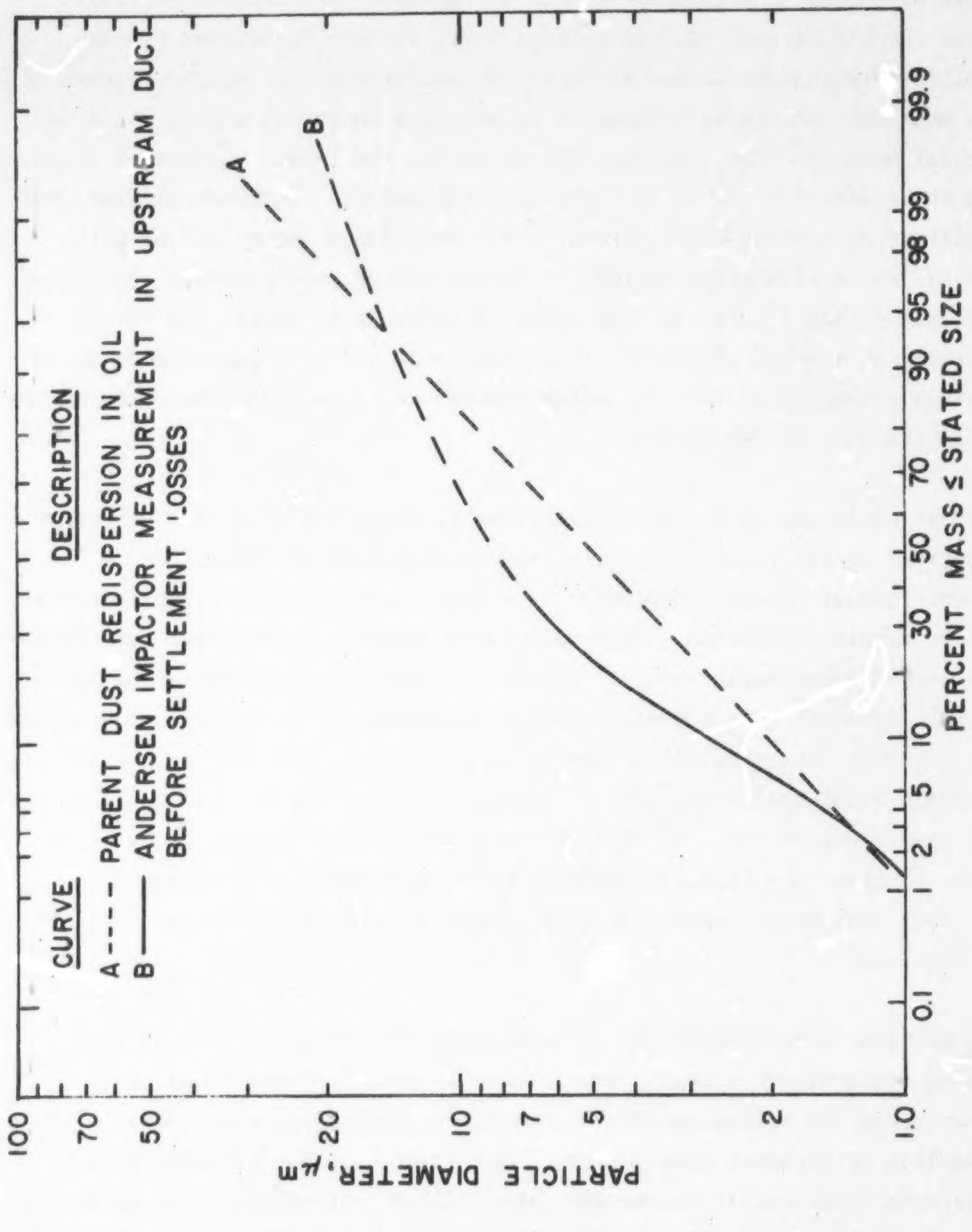

Figure 8. Size distribution measurements for GCA fly ash, for particle density of 2 grams/cm^3

in the 0.2 minute range to simulate field hopper settlement conditions. This allows for the typical selective removal of the coarser particles from the air stream. At the present time, roughly 50 percent of the solids entering the hopper falls to the collection jar located beneath it. By means of this inlet system, it is possible to obtain a good solid material balance. The dust deposits either on the fabric surface or falls to the collection jar at the bottom of the hopper. Fortunately, wall disposition has proven to be minimal. The manifold geometry allows for installation of a glass window for observing and photographing the filter surface during a test and also makes it possible to sample the inlet aerosol at several locations. The inlet pipe to the hopper was designed with a diverging section to reduce the chance of particle impaction on the opposite wall of the hopper.

Attention is called to two singular disadvantages of flat test panels as compared to the usual cylindrical bag configurations. First, it is nearly impossible to pre-tension the panels without going to an impractically complex apparatus. More important, however, is the fact that application of aerodynamic pressure causes the panel to dish inward so that a uniformly sized pore structure cannot be maintained because of the warping. In contrast, the pores in a tubular configuration such as a bag filter will undergo simultaneous and uniform changes under a tensile loading generated by pressure gradient. As pointed out later in this report, the size of pore openings may actually decrease with increased filter load and an extreme lack of uniformity in pore sizes may lead to very poor particle collection.

No problems were encountered in working on the clean air side of the bench scale filter system. Several probes could be introduced to the downstream converging section of the filter holder for particulate sampling or pressure measurements. To measure average effluent concentrations (mass basis) the entire fabric filter effluent was passed through an all-glass filter prior to flow measurement. Ordinarily, several hours were required to collect weighable effluent samples when high fabric efficiencies prevailed. Therefore, a condensation nuclei counter (CNC) and a Bausch and Lomb single particle light scattering counter (B&L) were used to indicate system performance against fine particles over brief, ∿ minutes, time periods.

DUST GENERATION APPARATUS

An NBS dust generator[25] was constructed to provide an accurately regulated dust feed to the system at a working range of 0.1 to 2 grams/minute. This device, Figure 9, consists of a small hopper, ∿ 200 grams capacity, that discharges to a slowly rotating spur gear located below it. By adjusting the rotation rate (∿ minutes) and the clearance between the hopper distributing plate and the gear teeth, dust is transported to an aspirating tube leading to a compressed air ejector. A clean, dried compressed air supply of about 3 ft^3/min at 50 psig, which entrains and shears the dry dust at sonic velocities within the nozzle, provides the test aerosol system from which the desired volume is extracted by the fabric filter pump. Excess aerosol is vented to a waste gas treatment system. By providing a separate test loop for the aerosol generator, the flow requirements for the filtration process are uncoupled from the stringent flow regulation requirements of the dust generator. Because the generator system operates under positive pressure, it augments the fabric filter fan system such that the negative pressure behind the fabric filter is seldom more than a few inches of water. This prevents sampling difficulties with the CNC equipment which is not designed for sample extraction from negative pressure regions. Figure 10 shows all the components of the bench scale system as assembled for testing.

PILOT SCALE FILTRATION EQUIPMENT

A pilot scale fabric filter system was used to make measurements which were impossible or impractical to make on a field scale system. Data to supplement and verify the bench scale tests were also obtained with the pilot

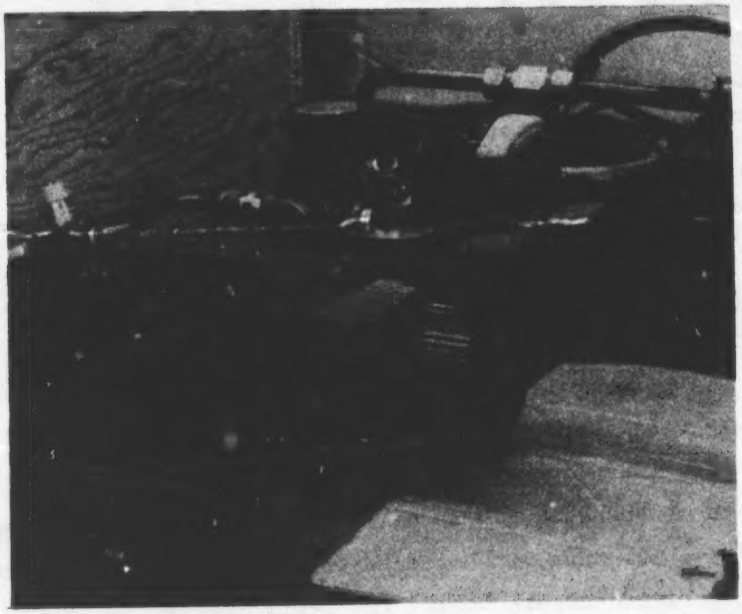

Figure 9. NBS type dust generator

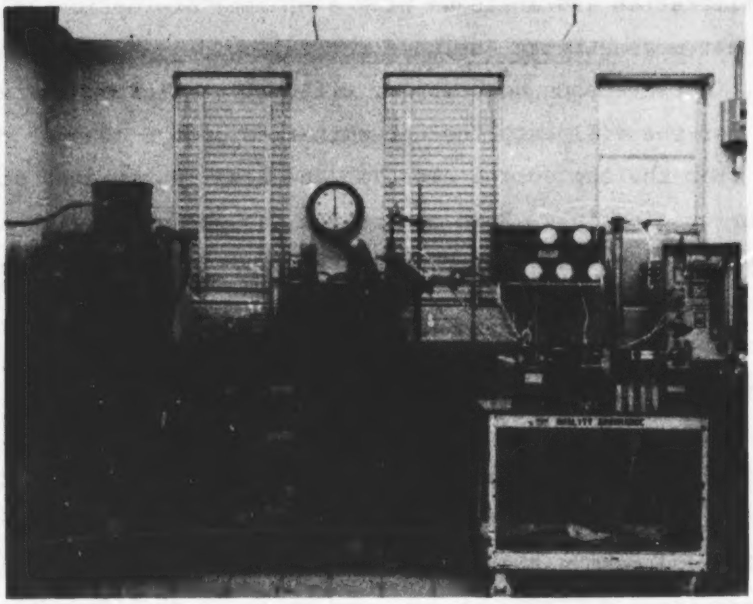

Figure 10. All components of bench scale filtration system

scale equipment. The pilot scale system simulates the full scale system geometry in that it has a normally tensioned cylindrical bag instead of a slack panel. In addition, full scale cleaning operations can be performed on the pilot scale system.

The apparatus was operated at flow rates, dust concentrations and with fabrics selected to represent typical field applications. To obtain accurate measurements, the pilot scale system was designed for startup, normal filtration and shutdown with a minimal disruption of the filter cake. Test measurements included the following: average mass effluent loading, instantaneous counting of effluent particles, average size properties for the effluent, the determination of the mass of particulate removed from the bag during cleaning and location of dust dislodgement sites during cleaning. Dust generation was performed with a commercial, auger type, feeder and a high pressure (90 psig) air ejection nozzle to attain maximum dispersion of the bulk fly ash.

The basic pilot scale fabric filter system was developed at GCA/Technology Division during a previous study.[10] A schematic of the pilot scale system as modified for this study is shown in Figure 11. Some of the important design features of the system are: the by-pass loop which permits the initiation and termination of flow to the bag with a minimum of system flow excursions; a Plexiglas cylinder to catch dust dislodged from the bag, thus permitting determination of the mass of dust removed and the time of removal; a removable filter housing which was made of from flexible hose to allow its removal without disturbing the bag and an 8-foot fluorescent lamp (not shown in Figure 11) that was installed within the bag to allow for observations of the bag surface. A turnbuckle located between the cap and spring assembly and the load cell was used to adjust the bag tension.

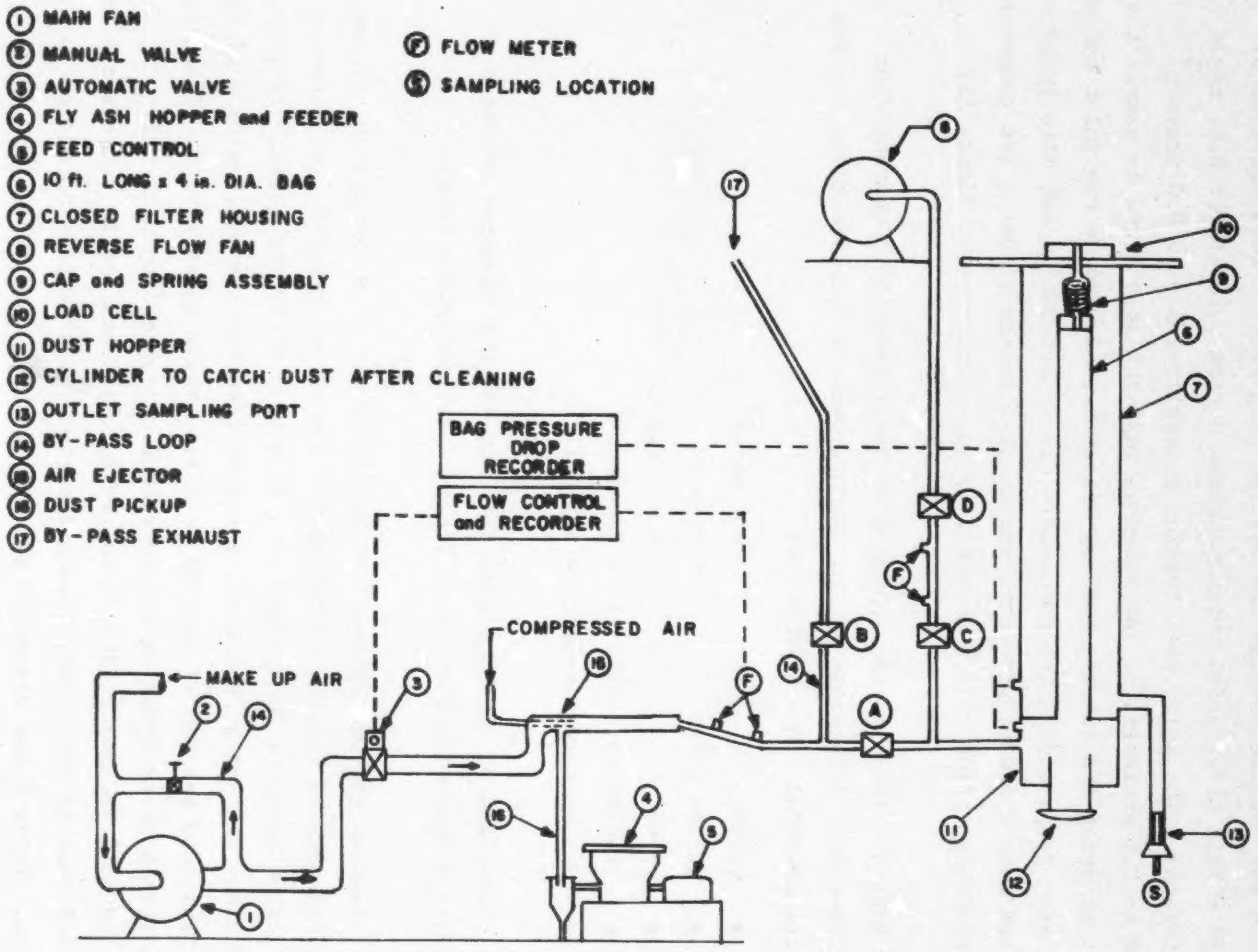
① MAIN FAN
② MANUAL VALVE
③ AUTOMATIC VALVE
④ FLY ASH HOPPER and FEEDER
⑤ FEED CONTROL
⑥ 10 ft. LONG x 4 in. DIA. BAG
⑦ CLOSED FILTER HOUSING
⑧ REVERSE FLOW FAN
⑨ CAP and SPRING ASSEMBLY
⑩ LOAD CELL
⑪ DUST HOPPER
⑫ CYLINDER TO CATCH DUST AFTER CLEANING
⑬ OUTLET SAMPLING PORT
⑭ BY-PASS LOOP
⑮ AIR EJECTOR
⑯ DUST PICKUP
⑰ BY-PASS EXHAUST
Ⓕ FLOW METER
Ⓢ SAMPLING LOCATION
BAG PRESSURE DROP RECORDER
FLOW CONTROL and RECORDER
COMPRESSED AIR
MAKE UP AIR
A
B
C
D
F
S

Figure 11. Schematic of pilot scale fabric filter system

Filtration parameters were selected to typify field operations. The pilot system was operated during the testing program at a constant flow of 0.498 m^3/min (17.6 acfm) which provided a face velocity of 0.61 m/min (2 ft/min). The inlet dust loading ranged from 6.9 to 8.0 grams/m^3 (3.0 to 3.5 grains/ft^3). An Andersen impactor positioned to sample the dust entering and leaving the bag was used to determine the inlet and outlet size properties. The cumulative size distribution for both inlet and outlet were the same with aerodynamic mass median diameter and geometric standard deviation of 5.8 μm and 2.42 μm, respectively, Figure 12.

The bags studied were manufactured by Menardi-Southern Company from Teflon-coated fiberglass cloth. Manufacturer's specifications for the fabric material are listed below:

- weight = 9.5 oz/yd^2
- thread count = 54 x 30
- weave = 3 x 1 twill
- Frasier permeability = 75 cfm/ft^2
- Mullen burst strength = 595 psi

The dimensions of the bags were 10.16 cm (4 in.) diameter by 304.8 cm (10 ft) length with five equally spaced antideflation rings.

Bag cleaning was accomplished by reversing the flow through the system, thereby causing the bag to collapse. The normal reverse flow produced a face velocity of 0.52 m/min (1.7 ft/min). After the normal filtering (loading) portion of the test, the dust feed was stopped; valve B of the by-pass loop was opened and the main flow valve A was closed. Cleaning was initiated by starting the reverse flow fan and opening valve C over a period of 2 seconds. Valve C was kept fully open for 56 seconds and then closed over an additional 2-second period, thus completing the cleaning cycle. Valve D was preset to give the desired flow rate. The above cleaning regimen was chosen to replicate the field operating system used at the Nucla, Colorado plant. Immediately after cleaning, the dust

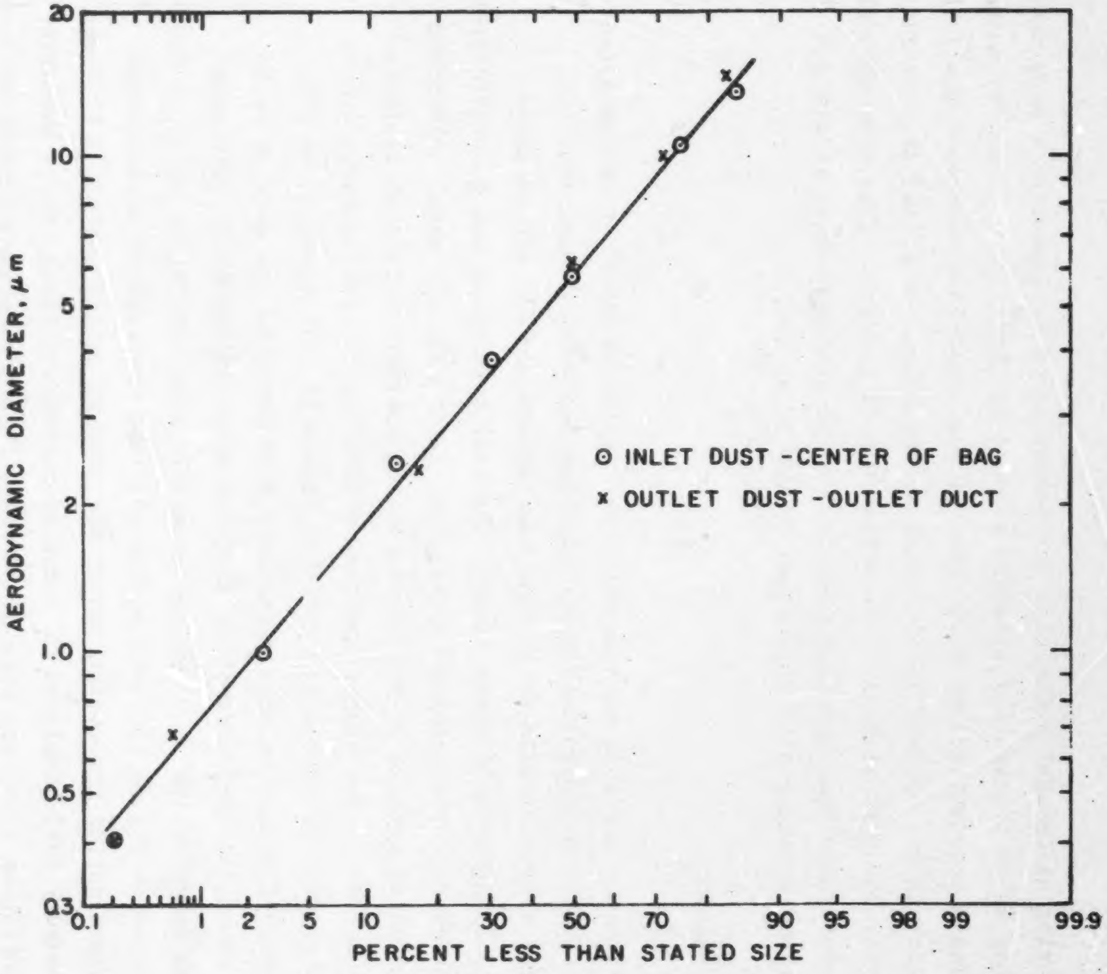

Figure 12. Inlet and outlet fly ash size distributions for a 10 ft x 4 in. woven glass bag, Sunbury fabric

collected in the catch cylinder was removed and weighed. The resumption of normal flow was accomplished by slowly opening valve A and slowly closing valve B. This step eliminated the problem of flow surges in the system which would have caused abnormal flexing of the bag.

Filtering at several velocities was accomplished by inserting a plug into the bag which blocked off selected regions of the fabric. Thus, by maintaining a constant volume flow rate, it was possible to increase the face velocity to any desired level. Without the plug, the normal face or filter velocity was approximately 0.61 meters/min (2 ft/min). This approach was more desirable than changing the flow in the system because it did not alter the particle size properties of the inlet dust.

TEST AEROSOLS

The simulant aerosols used during these tests consisted of resuspensions of a GCA fly ash obtained from a coal-burning power plant, rhyolite, a type of granite used in shingle manufacture and fly ash obtained from a lignite-fired power plant. The coal ash, which was recovered from electrostatic precipitator hoppers, was finer than the usual pulverized coal product because of the fractionating characteristics of cyclone-fired boilers. The size properties of the GCA fly ash as dispersed by NBS type dust generator are given in Figure 13. It appeared that no significant change in size parameters took place as the dust traveled from the S_1 to the S_3 sampling stations shown in Figure 5. The mass median diameter (MMD = 9 μm) and geometric standard deviation (σ_g = 3.0) indicated in Figure 13, fell within the band for similar measurements performed during the evaluation of the Sunbury filter system.[9] Although the Sunbury fuel consisted of a mix of anthracite fines, No. 5 buckwheat and petroleum coke, its size properties, Figure 14 actually appeared very similar to the GCA test fly ash. Therefore, it is believed that much of the test data deriving from the current laboratory studies with GCA fly ash can be used directly to support the field measurements. It was also

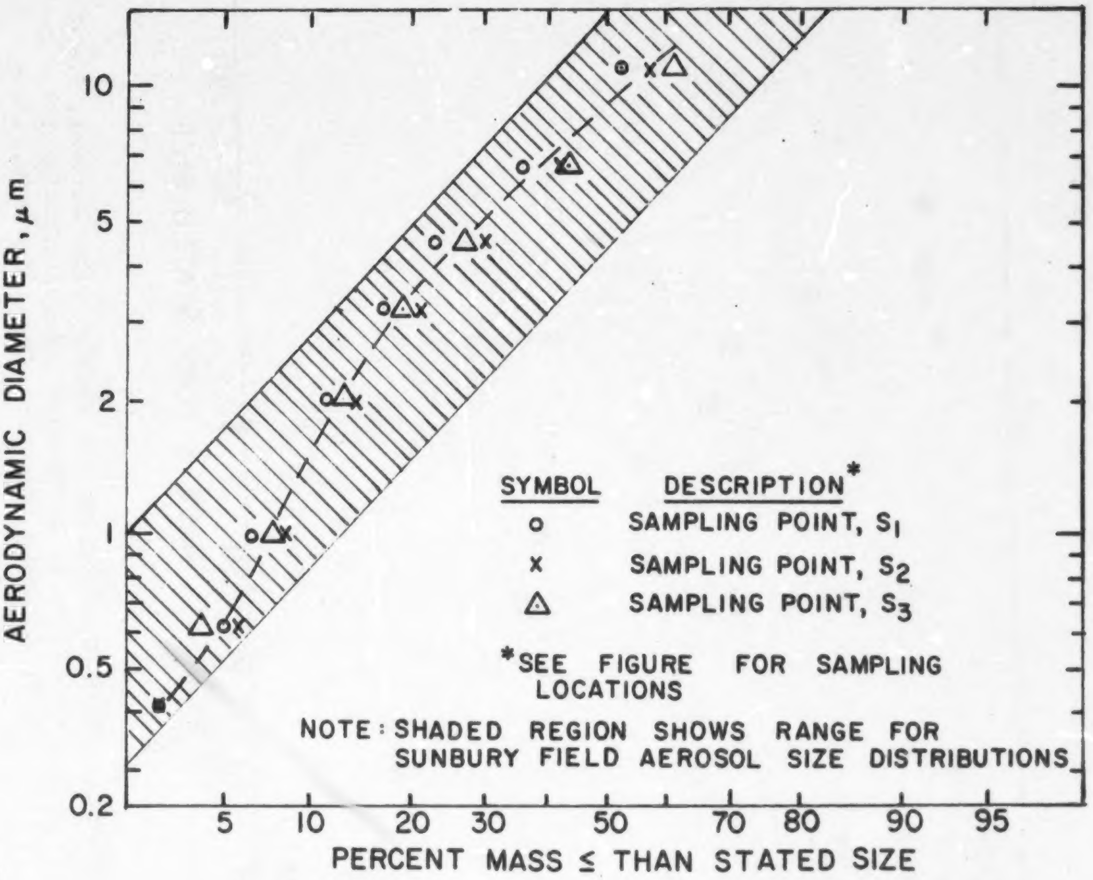

Figure 13. Size distribution for GCA fly ash entering bench scale filter system, Andersen in-stack impactor measurements

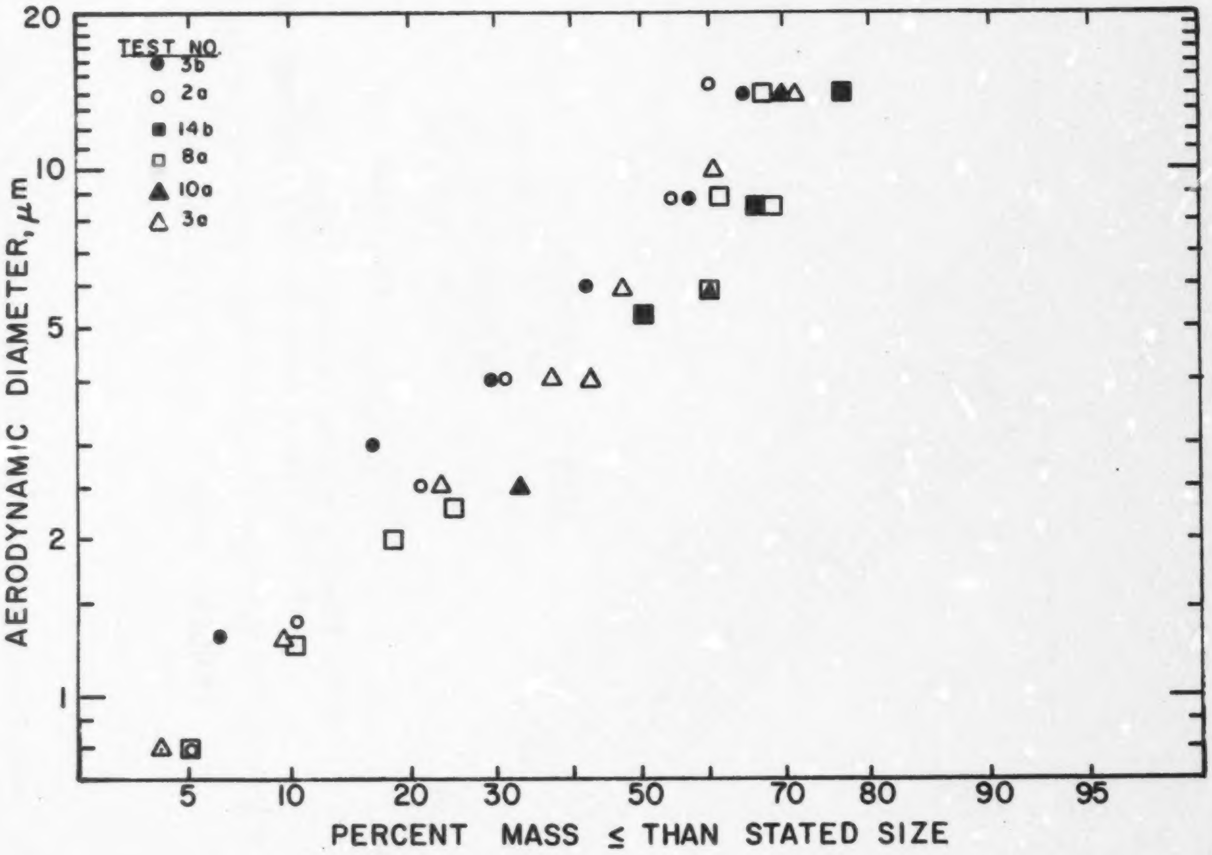

Figure 14. Mass distribution for Sunbury inlet aerosol, field measurements, based upon aerodynamic diameter. In-stack Andersen Impactor. Data from Reference 9

noted that the size parameters for the Sunbury effluent were nearly the same as those for the inlet.

The fly ash size properties for the pilot system were approximately the same as those for the bench tests. Dust dispersion was accomplished with an auger-type Acrison feeder in conjunction with a 90 psig air ejector. No significant differences between inlet and outlet size distributions were noted as shown in Figure 12. This observation has played an important role in explaining filter performance.

Similar size measurements by Andersen cascade impactor for the rhyolite (granite) and lignite test dusts are shown in Figures 15 and 16. Under normal testing procedures, the redispersed granite and lignite dusts were slightly coarser with mass median diameters of 15 μm and 12.5 μm, respectively.

A special, but very simple, extraction technique was used to provide much finer rhyolite particles. By reversing the manifold extraction probe (180^{o} from isokinetic) the mass median diameter for the rhyolite was reduced to 2 μm, Figure 15. The object of this procedure was to provide radically different size parameters for a specified dust for which prior analysis had indicated that chemical composition, density, shape factor (and other physical properties) were essentially invariant with respect to size. Under the above circumstances, the effect of dust size parameters alone upon specific resistance coefficient could be established.

PARTICULATE SAMPLING AND ASSESSMENT

Basic Sampling Equipment

The selection of instrumentation for determining mass concentrations, efficiencies and particle size properties was based mainly on the equipment used in prior EPA, GCA or other EPA sponsored programs.

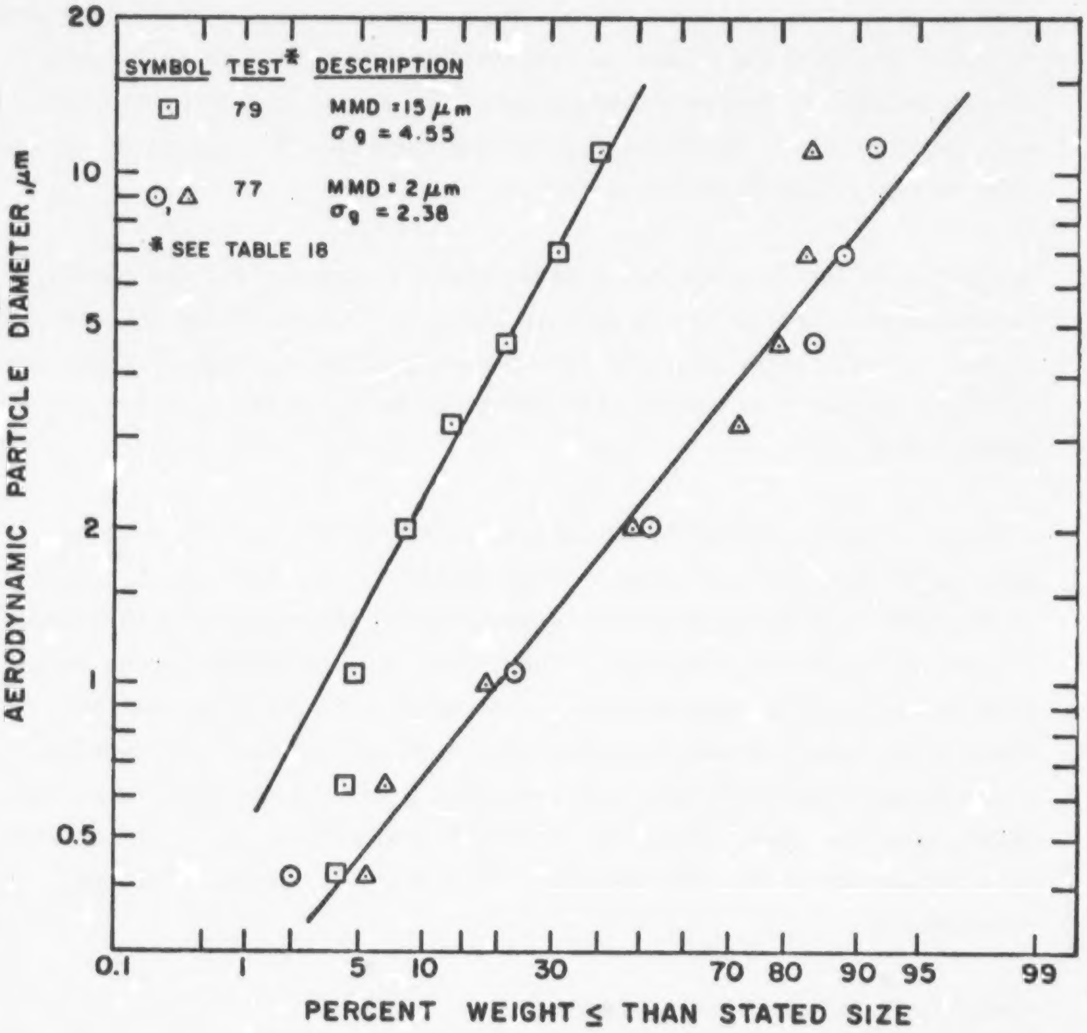

Figure 15. Size properties for coarse and fine rhyolite dust

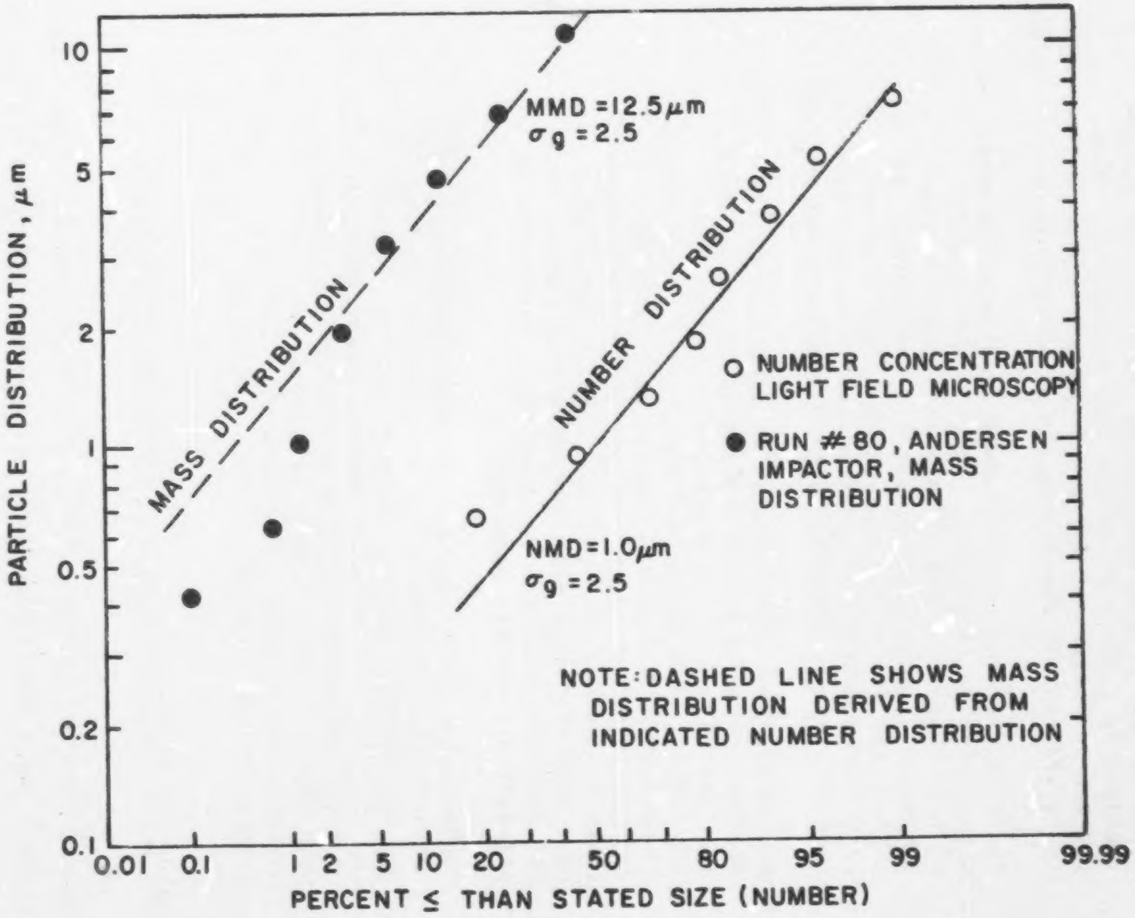

Figure 16. Particle size properties for lignite ash from precipitator hopper

Four basic sampling methods have been used:

- All-glass, Method 5 type filters for determination of both inlet and outlet mass concentrations. The only disadvantage to this approach is the long-time period required to collect weighable dust quantities. Thus, one can seldom detect important changes in concentrations that aid in describing the cleaning process.

- Andersen, in-stack type, cascade impactors for estimation of size properties. For a fixed aerosol system, this technique affords reasonable precise estimates of mass distribution for the central, 90 percent region, of the size range. Very high or very low concentrations present the respective problems of stage overloading or very long sampling periods.

- Bausch and Lomb Single Particle Light Scattering Counter (B&L) for number concentration and particle size distribution. Although its accuracy may be questioned, this instrument can provide time resolutions down to 0.1 minute insofar as reflecting changes in number concentrations for particle diameters in the 0.3 to 5 μm range. Prior GCA studies have indicated that mass concentrations derived from B&L data are usually lower than those determined by parallel gravimetric sampling.

- Condensation Nuclei Counter for detecting number concentration changes in the very fine, 0.0025 to 0.5 μm, diameter range. Although one may dispute the absolute concentration values, the capability of this instrument to follow concentration changes over brief, ∿ seconds, time periods makes it a useful adjunct to the B&L system that traces changes in the ∿ 0.5 μm particle size range.

Assessments and Interpretation of CNC and B&L Measurements

A condensation nuclei counter, CNC*, and a single particle light scattering counter, B&L+, were used extensively to delineate the rapid changes in effluent mass concentration and particle size distribution that take place over a filtration cycle (here defined as the period between resumption and termination of filtration). Periodic measurements were made on the background laboratory air throughout the testing programs to ascertain that the instrument performance characteristics remained unchanged. Additionally, these tests provided background data for nuclei concentrations (which, according to the CNC manufacturer, indicated particles less than the size range 0.3 μm to 0.5 μm and greater than 0.0025 μm.

---

*Model Rich 100 Condensation Nuclei Monitor manufactured by Environmental One Corporation, Schenectady, New York.

+Model 40-1 Dust Counter manufactured by Bausch & Lomb, Rochester, New York.

The above nuclei always constituted a small fraction of all test aerosols unless the ambient air underwent special filtration prior to entering the dust generating system.

Reference to Figure 17 indicates that the size properties for the ambient atmospheric dust did not change greatly over the testing period. The B&L measurements showed that the number median diameters, NMD, ranged from 0.3 to 0.4 μm and the geometric standard deviations, σ_g, from 2 to 2.5. These results were in fair agreement with light field microscope sizing data for atmospheric dust, 0.3 to 0.5 μm NMD and a σ_g value of 1.5 to 2.0, depending upon the dust generating activity in the area.

Those measurements depicted within the shaded region, Figure 17, represent the usual range of size parameters observed over the testing intervals. The calculated weight concentrations associated with each of these curves were developed by converting the fractional number concentrations to their equivalent weights by assuming that the particles were spherical with a density of 1.91 g/cm^3. The above density was selected so that in combination with the shape factor of $\pi/6$ for spheres, particle mass in grams would be expressed directly as D^3.

A separate graphing of the parallel CNC counts versus the matching weight concentrations derived from the B&L measurements is shown in Figure 18. Those points that fell outside the dashed envelope lines were, with one

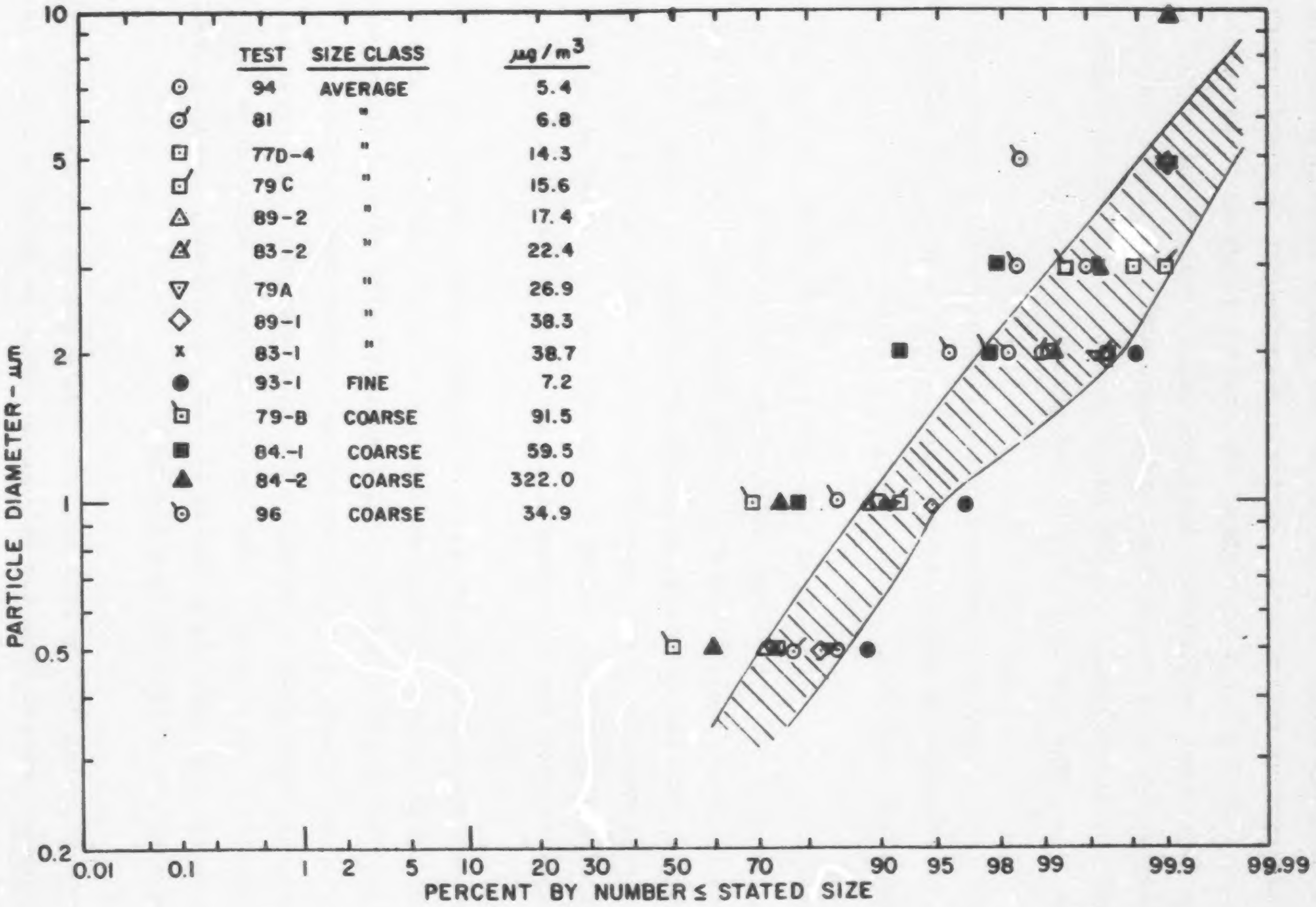

Figure 17. Number size distributions for background (laboratory) dust based on B&L counter measurements

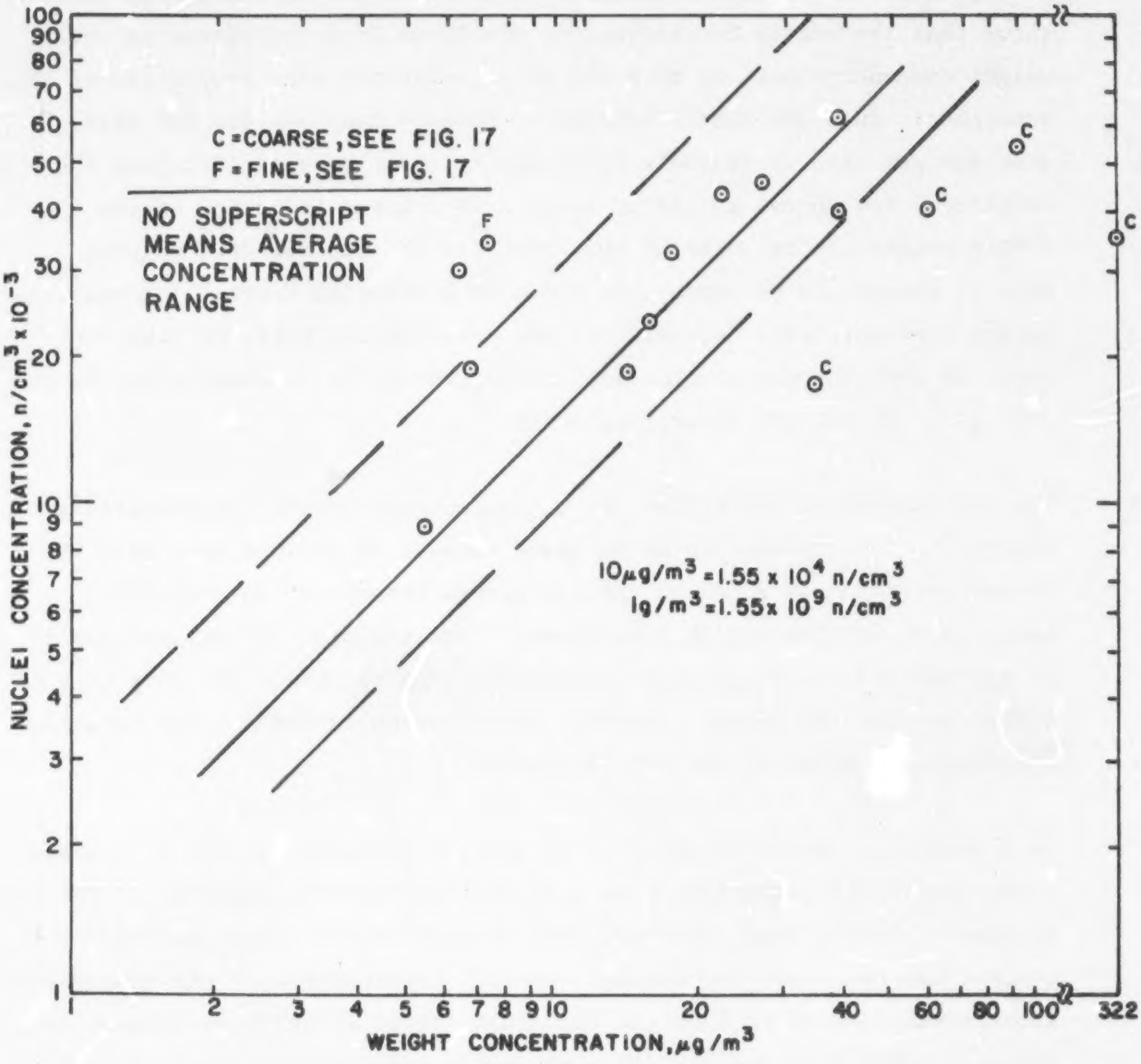

Figure 18. Relationship between nuclei concentrations by CNC measurements and weight concentrations derived from B&L data

exception, associated with tests where the dust was either coarser or finer than the average background aerosol (shaded region, Figure 17).

The approximate 45° slope displayed by the data points within the envelope shows that the nuclei concentrations are directly proportional to the weight concentrations, as they should be, when the size properties of the atmospheric dust are fairly constant. Because the complete B&L size spectrum was used to estimate mass concentration values, including the relatively few coarse particles that exert a large influence on the sample weight, it is believed that both the CNC and B&L data outputs were in reasonable agreement, at least on a relative basis. The calculated weight concentrations derived from B&L measurements were, for the most part, in good agreement with independent gravimetric measurements, 20 to 100 $\mu g/m^3$, in the GCA laboratory areas.

The few unsusually low values for the calculated weight concentrations, Figure 18, are believed to be in error because of failure to sample the coarse particles, > 5 μm, in the air stream because of anisokinetic sampling conditions and/or line losses. For example, the sloughing off of agglomerates in significant quantities from the clean air face of a filter may produce a highly bimodal distribution in which large particles are seldom detected by the B&L instrument.

As a result of extensive comparisons between effluent fly ash concentrations determined concurrently by gravimetric (filter) sampling and CNC measurements, it was concluded that the ratio of nuclei counts to mass concentrations was nearly a constant quantity irrespective of the concentration level. In the case of the previously cited comparisons between CNC, B&L and filter measurements for atmospheric dust, it was expected that a fixed proportionality would exist provided that the size distribution of the ambient aerosol did not change.

It was deduced, therefore, that the entering fly ash aerosol underwent no change in size properties after passing through the filter. The reason for this behavior, which appears to contradict all classical filtration theory, is discussed in a later section of this report. At this point, we only wish to point out that the existence of this very convenient proportionality between nuclei and mass concentrations allows CNC measurements to be used in conjunction with a calibration curve to determient changes in mass concentrations over brief, ∿ seconds, time intervals. The latter operation is essential if one is to make accurate forecasts of particulate emission levels from sequentially cleaned, multicompartmental filter systems.

Comparisons were also made between indicated nuclei concentrations and B&L measurements with respect to the number concentrations in specific size ranges, > 0.3 to 0.5 μm and > 0.5 μm. The regression lines shown in Figure 19 indicate a closer correlation between the finer size fraction than that shown for the coarser, > 0.5 μm particles. These data suggest properly that the nuclei counter, in accordance with its specifications, probably gives very little response for particles larger than 0.5 μm. The point scatter for both correlations results from the range in size distributions occurring within the data set.

The sampling procedures described above, in conjunction with pre- and post-drying and desiccation of samples in accordance with Method 5 protocol, represent standard EPA test methods. By weighing the fabric test panels before, during, and after filtration tests, accurate estimates of average inlet dust concentration and fabric loading were obtained. Temperature and humidity measurements by recording hygrothermograph with periodic checks by wet and dry bulb sling psychrometer were also included with the instrumental methods used in this study.

TENSILE PROPERTIES

Figure 20 shows the bench scale apparatus used to determine stress/strain relationships for the glass fabric under static loading conditions. Horizontal clamps were secured to the top and bottom of a fabric strip

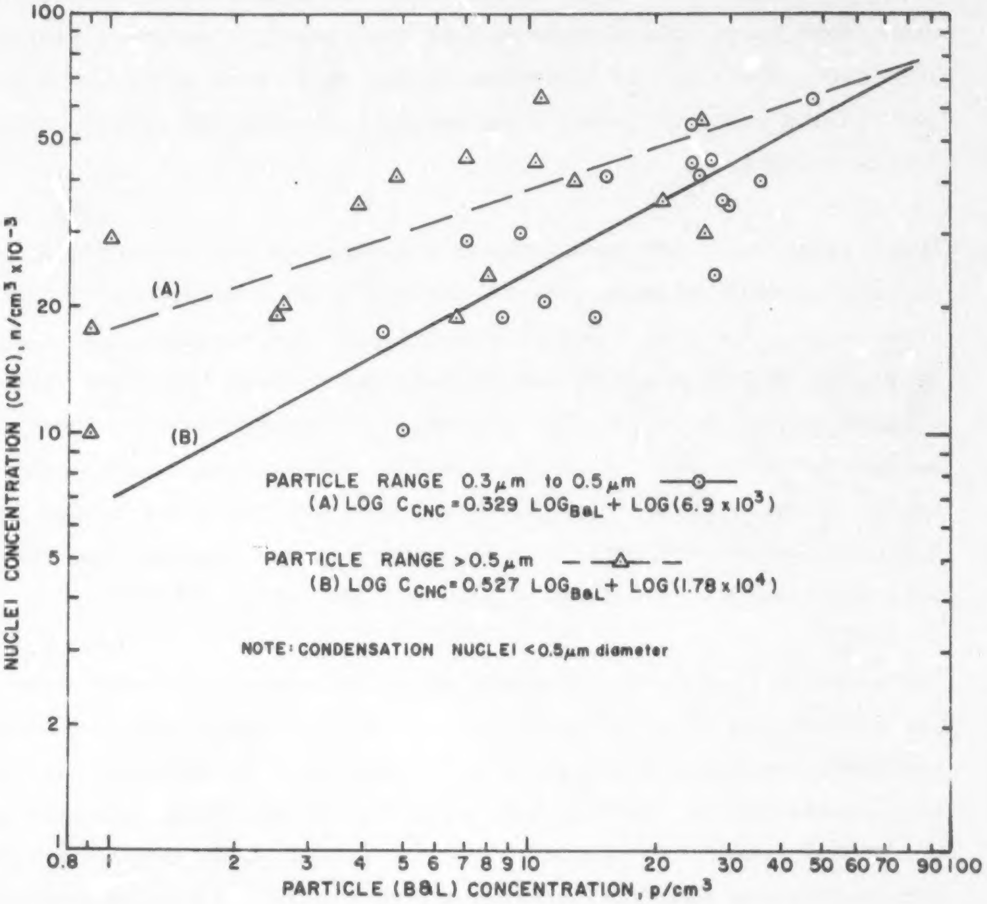

Figure 19. Concurrent measurements for nuclei concentrations (CNC) and particle concentrations by Bausch and Lomb counter in different size ranges

Figure 20. Test apparatus for measurement of fabric tensile properties

(6 in. x 18 in. or 3 in. x 18 in.) so that any applied load would be exerted uniformly over the width of the strip. A free floating ring was attached to the loading cable to assist in distributing the load evenly. Parallel scales on each side of the strip in conjunction with pointers attached to both sides of the lower clamp furnished replicate indications of fabric elongation under load. During the present test series, the maximum applied tension was 380 N or 85 lbs.

A similar system for static tension measurements was used for full scale, (10 ft long by 4 in. diameter), glass bags prepared from the Sunbury (Menardi) and Nucla (Criswell) fabrics. A strain gauge incorporated within the hanger arm in conjunction with a turnbuckle adjustment allowed for the determination of bag elongation as a function of applied tension. This arrangement also permitted precise control of tension levels during permeability and filtration tests.

SECTION V

FABRIC STRUCTURE STUDIES

INTRODUCTION

Classical approaches to modeling filter performance frequently begin with the clean (unused) fabric which is studied from the perspective of resistance to air flow, dust retention characteristics and interstitial particle deposits. Although tests with different, unused fabrics permit relative comparisons, these measurements can seldom be extrapolated directly to predict overall fabric performance under normal steady state filtration and cleaning conditions. In the latter case, continued filter usage followed by periodic cleaning leads to initial and terminal equilibria for which characteristic filter drag and dust holding levels may be assigned. The magnitudes of these terms are functions of both specific dust/fabric relationships and the method of fabric cleaning employed. It is emphasized that the path (e.g., filter resistance versus fabric dust holding) by which one progresses from the residual to the terminal states is seldom a simple linear function.

In addition, the manner in which the total filter dust loading is distributed over the fabric surface plays a controlling role in determining the filter resistance/fabric loading relationship. Consideration of this factor has enabled us to analyze the performance of both mechanical shaking and bag collapse-reverse flow cleaning systems in terms of the same basic variables.

A careful examination of fabric structure can provide several insights as to the probably performance of many dust/fabric combinations. The previously cited work of Draemel[3] and studies reported by Butterworth[26] and Pedersen[27] consider both the aerodynamic and dust retention characteristics of filters as functions of structure. Fabrics have been analyzed in terms of free area, thread count, weave, nap, size distribution for pore dimensions, and the yarn type such as number of strands, twist, multifilament or staple. Although the correlations deriving from these (structure) studies are frequently broad, particularly so with respect to the tighter and denser weaves, they still represent useful data inputs that can be readily obtained by simple laboratory microscopy.

Basic Manufacturer or User Specifications

Fabric properties as specified by the manufacture and/or user are given in Table 2 for the Sunbury, Pennsylvania and the Nucla, Colorado power plants. Despite the differences in fabric treatment, the two woven glass fabrics are very similar. It was observed, however, that certain of the descriptive parameters (Table 2) were not always internally consistent nor the same as those measured by GCA. For example, despite similar measurement techniques, clean cloth permeabilities appear to vary considerably, ~ ± 30 percent. It is suspected that these differences depend upon the fabric bolt from which the bag is made, the section of the bolt from which the test specimen is removed, and the handling of the fabric before and during the testing process. In view of these differences, it does not appear advisable to depend heavily on any filtration parameter derived from clean cloth permeability. Although these differences were not large, Tables 2 and 3, they may, in certain cases, be important in determining fabric performance.

The mixture of English and metric units in Table 3 is a result of commercial fabric descriptions being given in English or specialized textile units. Thus, replicate GCA measurements are also given in English units. Where no comparisons are made, however, metric dimensions have been assigned to such parameters as yarn dimensions and fabric thickness.

Table 2. FABRIC PROPERTIES FOR GLASS BAG FILTERS USED AT SUNBURY, PENNSYLVANIA AND NUCLA, COLORADO COAL-BURNING POWER PLANTS

	Sunbury[a]	Nucla
Dimension, length x diameter - ft x in.	30 x 12	22 x 8
Fabric weight - oz/yd^2	9.2	10.5
Weave	3 x 1 Twill	3 x 1 Twill
Warp (w) yarn	150's 1/2	Multifilament
Fill (f) yarn	Bulked 1/4	Bulked staple
Yarn (thread) count - w/in. x f/in.	54 x 30	66 x 30
Permeability at 0.5 in. - ft^3/min	54.3[b]	86.5[c]
Primary application	Reverse flow	Shaking and reverse flow
Fabric treatment	Teflon coating	Graphite-silicone coating
Manufacturer and fabric designation	Menardi Southern 601 T(Tuflex)	W.W. Criswell No. 640048

[a] Seven anticollapse rings.

[b] GCA test, Perm at 0.5 in. = 42.5 ft^3/min.

[c] GCA test, Perm at 0.5 in. = 112 ft^3/min.

Table 3. SPECIAL PROPERTIES, SUNBURY AND NUCLA FABRICS

	Sunbury fabric			Nucla fabric	
	Menardi Southern parameters	GCA measurements	Menardi Southern data, GCA calculations	W.W. Criswell parameters	GCA measurements
Fabric weight oz/yd^2	9.2	9.88	9.2	10.5	9.4
Fabric thickness µm	-	400	-	-	400
Yarn count per inch warp/fill	54 x 30	53.4 x 30.5	56.6 x 31.6[a]	66 x 30	66 x 30
Warp weight oz/yd^2	4.35	4.67	4.35	-	4.29
yds strand x 10^{-2}/lb yarn	-	-	150 - 1/2[b]	-	-
Fill weight oz/yd^2	4.85	5.21	4.85	-	5.11
yds strand x 10^{-2}/lb yarn	-	-	150 x 1/4[b]	-	-
Warp yarns Max/min diam, µm	-	450/200	-	-	375/200
Fill yarns Max/min diam, µm	-	650/200	-	-	600/200

[a] Thread count derived from (b) and weight of 9.2 oz/yd^2.

[b] 150 x 10^2 = yards of strand per pound of yarn.
1/2, 1/4 indicate 2 and 4 strands (plys) per yarn.

With respect to clean fabric weight, the differences may be attributable to variations in protective coating because GCA and manufacturers values for yarn count were in good agreement. The weight of yarn representing warp and fill densities was determined for this study by the microbalance weighing of 50 to 100 individual yarns of 5 cm length to determine the weight per unit length. These data, in combination with the measured yarn count, provided the GCA fabric weight values given in Table 3. It is not clear why the predicted thread counts for the Menardi Southern fabric (Sunbury) are significantly higher when estimated on the basis of a 9.2 oz yd^2 weight and the GCA yarn parameters (strand weight per unit length).

Fabric properties for the cotton and Dacron media tested in this study are given in Table 4. Although the above materials would not be used for hot fly ash filtration, they have been evaluated in earlier GCA tests in the form of 10 ft x 6 in. or 10 ft x 4 in. bags with conventional mechanical shaking. Thus, by conducting similar tests with 6 in. x 9 in. flat panels it was possible to ascertain whether the bench test geometry had any significant effect on performance parameters. At the same time, it was expected that any unique interaction between a given dust and various fabrics would be revealed.

Bag Resistance Versus Pore Velocity

A special sequence of measurements was made to determine fabric resistance levels at very high pore velocities, Figure 21. The object of these tests was to establish reasonable estimates of the maximum pore or pinhole velocities when the filter pressure loss is relatively high, ~500 to 750 N/m^2 (2 to 3 in. H_2O). In the case of the Sunbury fabric whose free area was estimated to be about 3 percent, the pore velocity is 33.3 times the face velocity. Use of Figure 21 in conjunction with the minimum cross sectional area of a pore or pinhole will indicate the volume of air passing through a pore at a specified pressure drop.

Table 4. DACRON AND COTTON PROPERTIES FOR FABRIC TEST PANELS STUDIED IN LABORATORY

	Sateen weave cotton-unnapped	Dacron crowfoot
Panel dimension - in. x in.	9 x 6	9 x 6
Fabric weight - oz/yd^2	10	10
Weave	Sateen	1/3 Crowfoot
Warp (w) yarn	Staple	Multifilament
Fill (f) yarn	Staple	Bulked staple
Yarn (thread) count w/in. x f/in.	95 x 38	71 x 51
Permeability at 0.5 in. H^2O - ft^3/min	13	33
Design application	Mechanical shaking	Mechanical shaking bag collapse
Manufacture and fabric designation	Albany International No. 960	Albany International No. 865B

Simplified Weave Representations

A schematic drawing of the Sunbury fabrics in accordance with textile conventions is given in Figure 22. The original bags installed in 1973 were characterized by a right-hand diagonal as depicted by the warp yarn surfaces seen on the filtering face. On the other hand, the replacement bags installed in 1975 were woven with a left-hand diagonal. Although this variation had no apparent bearing upon filter performance, it required that care by exercised in interpreting microscopic images with respect to pore shape and location. Note that warp (vertical) and fill yarn (horizontal) alignments and pore locations are indicated in Figure 22. The bags used at the Nucla, Colorado power station were also fabricated from a 3/1 twill weave with a left-hand diagonal, as shown in Figure 22.

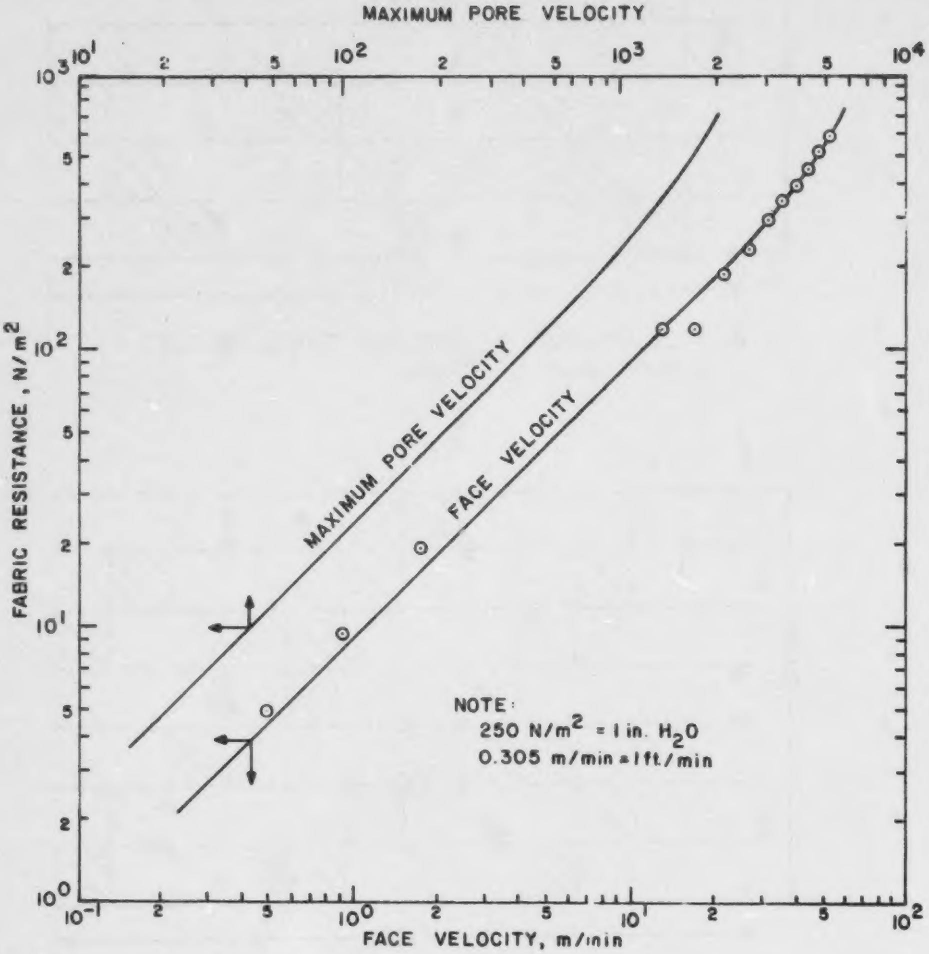

Figure 21. Resistance versus face and maximum pore velocity for clean (unused) Sunbury glass fabric

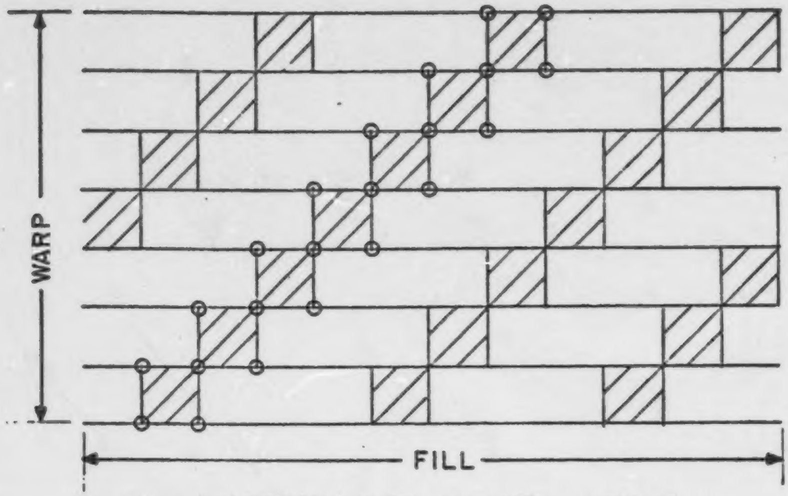

A. FILL (FILTERING) FACE 3/1 TWILL WEAVE,
RIGHT HAND DIAGONAL

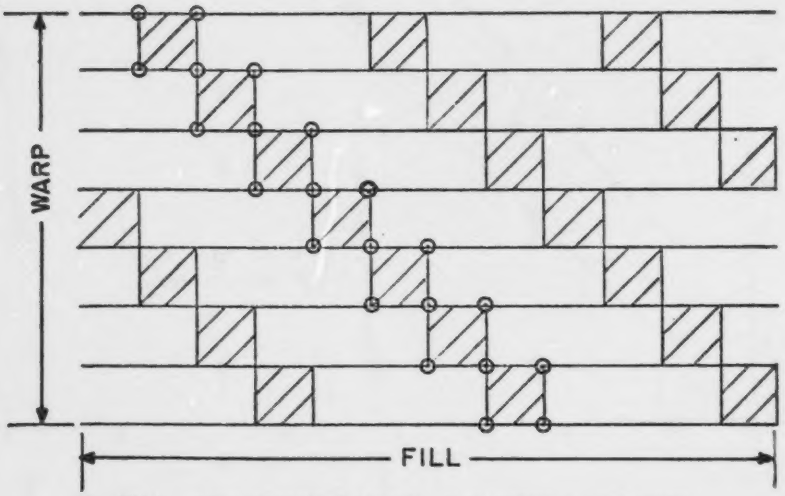

B. FILL (FILTERING) FACE, 3/1 TWILL WEAVE,
LEFT HAND DIAGONAL

Figure 22. Textile schematic drawing of Sunbury fabrics A. 1973 bags, B. 1975 bags. Circles on diagonal, warp yarn crossovers, indicate open pore locations

A simplified version of the appearance of the fill (filtering) face for the Sunbury media is given in Figure 23. Except for the differences in pore sizes, Figure 23 applies equally well to the Nucla fabric which is also a 3/1 twill weave. The average spacing between all fill yarns was 200 μm whereas all warps yarns were contiguous except for a 27 μm separation at yarn crossover points. The locations of the three characteristic pore types are shown by the encircled areas. Note that type III pores are blocked by virtue of the contacting warp yarns.

In Figures 24 and 25, photomicrographs of warp and fill faces for the Sunbury and Nucla fabrics, respectively, are shown at 20Xmag. The warp faces for both fabrics show clearly the smooth, compact appearance of the multifilament warp yarns which, with a 3/1 twill weave, occupy approximately 75 percent of the downstream (clean side) fabric surface. On the other hand, the bulk staple constituting the fill yarns presents a relatively loose structure in which a large fraction of the individual glass fibers (about 7.5 to 8.0 μm diameter) are separated from one another. The graphite in the Nucla surface coating is responsible for the black metallic luster of the yarns, Figure 25.

The density and porosity is relatively easy to establish for the multifilament yarns because the fibers are tightly twisted. Assuming that the spinning process layers the parallel fibers in a 60° offset array, the porosity is only about 10 percent. It is apparent that with void spaces or interyarn porosities of the order of 50 percent, air flow through high density warp yarns will be inconsequential. On the other hand, the bulked or fluffy character of the fill yarns as indicated in Figures 24 through 27 provides an extended surface for aerosol permeation and particle capture.

PORE PROPERTIES

Microscopic viewing of the fabrics, Figures 24 and 25, indicated that there were no spaces between the warp yarns except where they looped over the fill yarns. Due to distortion of yarns (Sunbury fabric) by stressing at

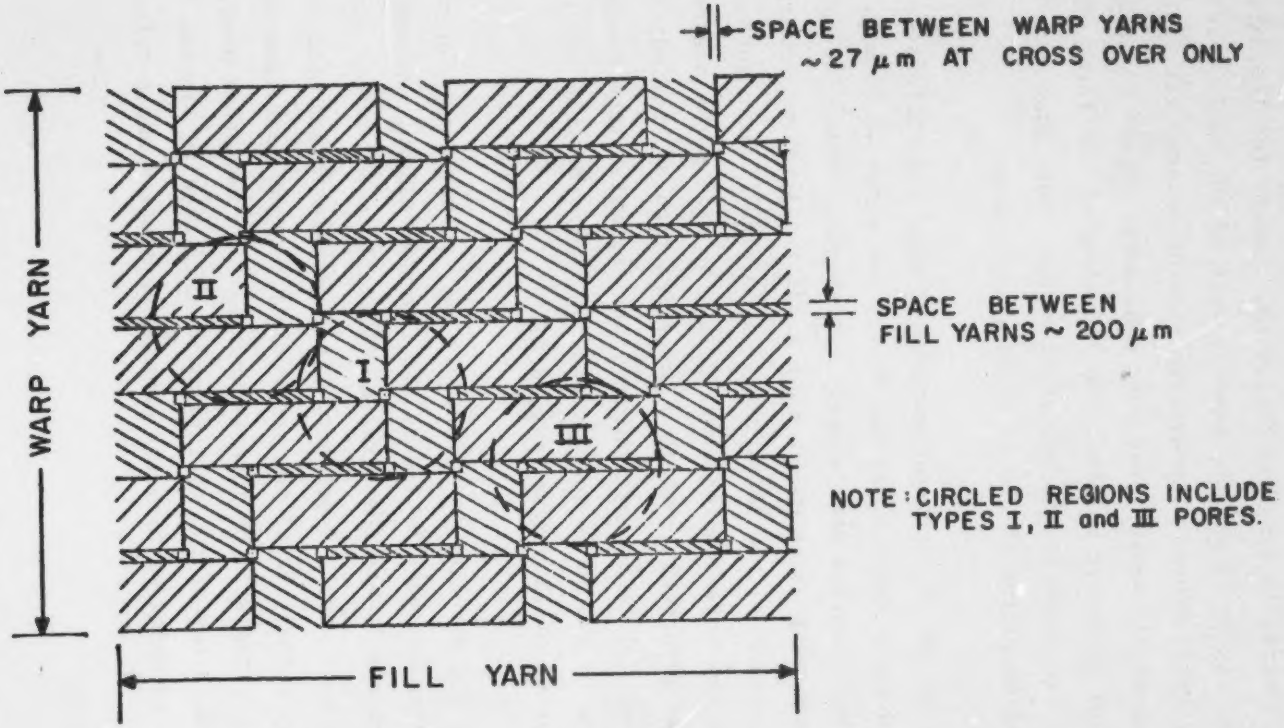
SPACE BETWEEN WARP YARNS
~27 μm AT CROSS OVER ONLY
SPACE BETWEEN
FILL YARNS ~ 200 μm
NOTE: CIRCLED REGIONS INCLUDE
TYPES I, II and III PORES.
I
II
III
WARP YARN
FILL YARN

Figure 23. Schematic of Sunbury fabric, filtering face, 3/1 twill, left-hand diagonal indicating pore locations and average dimensions. No space between warp yarns except at crossing points

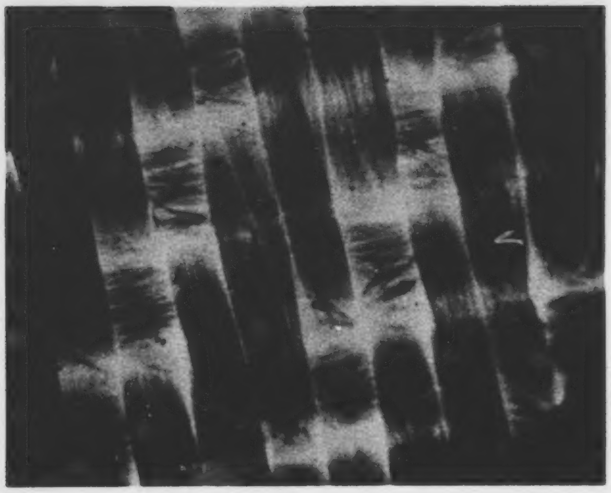

A. Warp surface

B. Fill surface

Figure 24. Warp and fill surfaces of clean (unused) Sunbury fabric with substage illumination (20X mag)

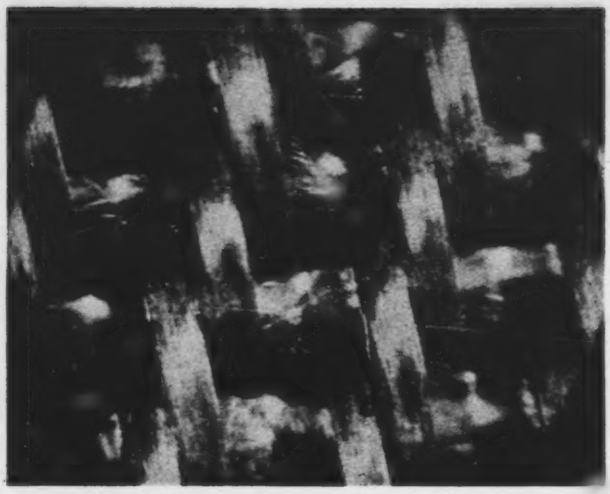

A. Warp surface

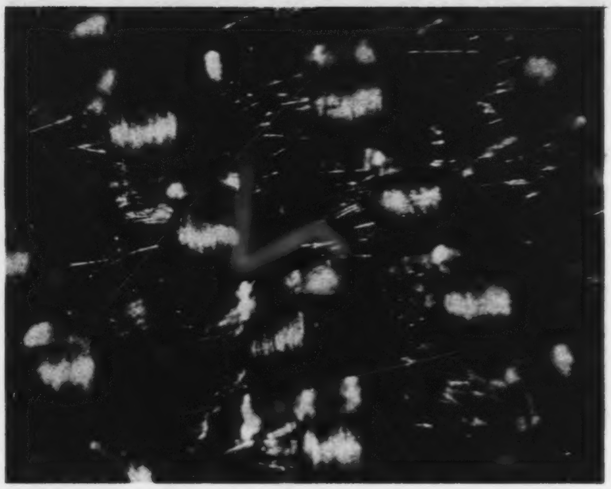

B. Fill surface

Figure 25. Warp and fill surfaces of clean (unused) Nucla fabric with substage illumination (20X mag)

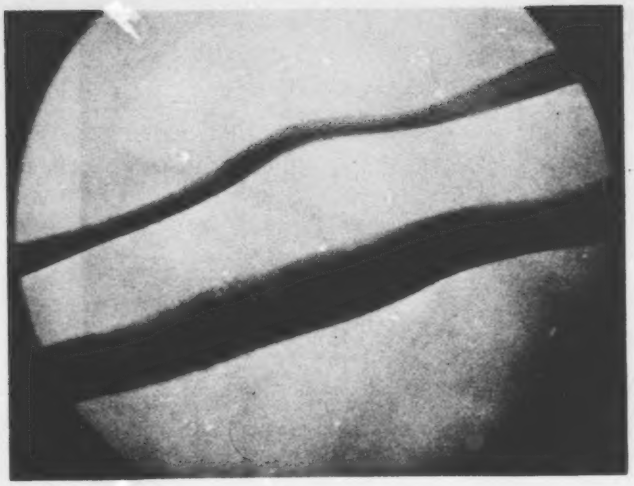

Warp yarns

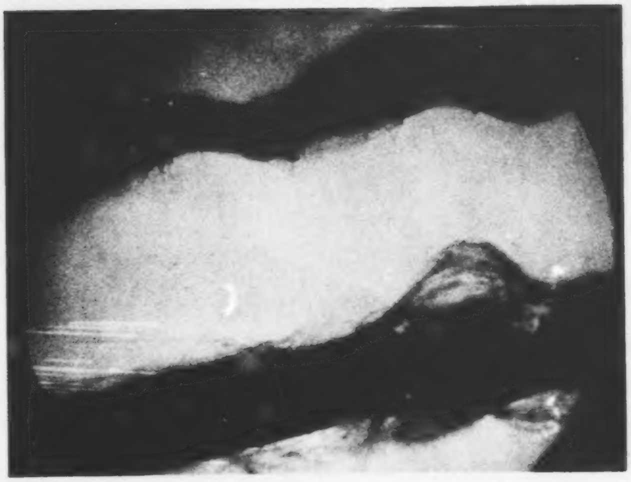

Fill yarns

Figure 26. Individual Sunbury warp and fill yarns as seen in plane of fabric showing maximum and minimum dimensions (20X mag)

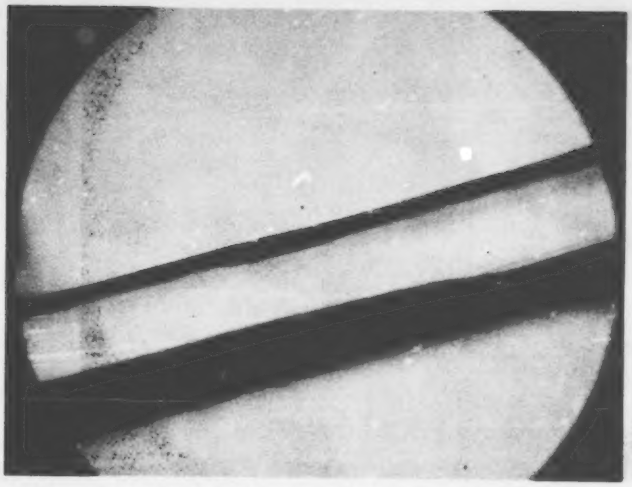

Warp yarns

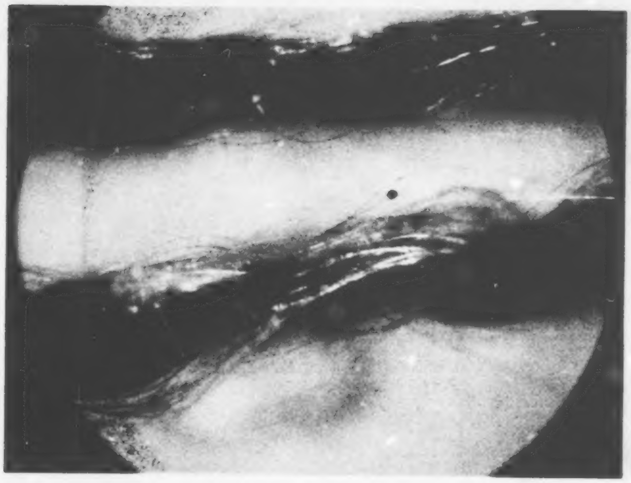

Fill yarns

Figure 27. Individual Nucla warp and fill yarns as seen in plane of fabric showing maximum and minimum dimensions (20X mag)

crossover points, perceptible openings having an average width in projection of about 27 μm appeared at these locations. Since there was a significant separation between adjacent Sunbury fill yarns of approximately 200 μm, Figure 24, slotted apertures or "see through" regions with projected cross sectional areas of about $5.4 \times 10^{-3} cm^2$ appeared at each pore location. Inspection of Figures 24 and 25 shows that open pores exist only at warp/fill crossings. Hence, the Sunbury and Nucla fabrics lose 25 percent of the potential pore count in both the warp and fill directions. The net result is that the number of pores per $in.^2$ appears as

$$(54-1)\ (30-1)\ (0.75)^2 = 865$$

for the Sunbury fabric, and

$$(66-1)\ (30-1)\ (0.75)^2 = 1060$$

for the Nucla media.

The thread counts are corrected by minus one because there always exists one less pore than the number of bounding surfaces generating the pores. Inspection of Figure 23 also shows that there are two Type II pores for every Type I pore.

Yarn Shape

As near as can be ascertained, the warp and fill yarns for the glass fabrics assume approximately elliptical cross sections typified by the maximum and minimum diameters given in Table 3. By assuming elliptical cross sections, however, misleading information are furnished with respect to the true fabric interstitial volumes and true internal surface area relative to skin friction. Hence, we have assumed a modified rectangular cross section in which the ends are depicted as having the minor diameter for the yarn cross section, Figure 28. Separate micrometer measurements on the Sunbury media indicated a thickness of about 400 μm. This value agrees with the thickness estimated by the sum of the minor diameters.

The geometry shown in Figure 28 appears to be an acceptable representation of the actual yarn contacts according to the edge section photomicrographs shown in Figure 29. Because the yarns are deformable, they are brought into intimate contact over large sections of their surfaces. In the case of the Sunbury fabrics, adjacent warp yarns were in direct contact except at crossing points as shown in Figure 28.

The average projected pore dimensions cited previously do not describe the true minimum pore cross section. Actually, the interstitial geometry is quite complex, even when the presence of protruding fibers and separated strands and yarns are ignored (which is often the case).

Pore Type and Area

First, according to the fabric weave, there are several possible pore types. In the case of the Sunbury, (Menardi Southern) fabric, three distinct pore types are found, Figure 23, two of which, Nos. I and II, constitute the passageways through which the air flows. The type III pores represent closed cells or blocked passages for the Sunbury and Nucla fabrics because there are no open spaces between adjacent warp yarns except at the previously designated crossing points.

The sectional views shown in Figure 30 provide a better indication of the effective cross sectional areas for the pores and their respective orientations. Displacement of the warp yarns as shown for a type I pore produces an opening between the bounding edges of the fill yarns resembling two apex-to-apex, truncated triangular openings. Furthermore, the curvature of the fill yarns creates the additional areas which are concealed beneath the surface of the fill yarns. The estimated cross-sectional areas per effective pore shown in Figure 30 were attained by rotation of the actual warped surface generated by the minimum separation distance between yarns into the same plane. In the present case, the error introduced by this approach for calculating the area of a warped surface was estimated to be less than 10 percent.

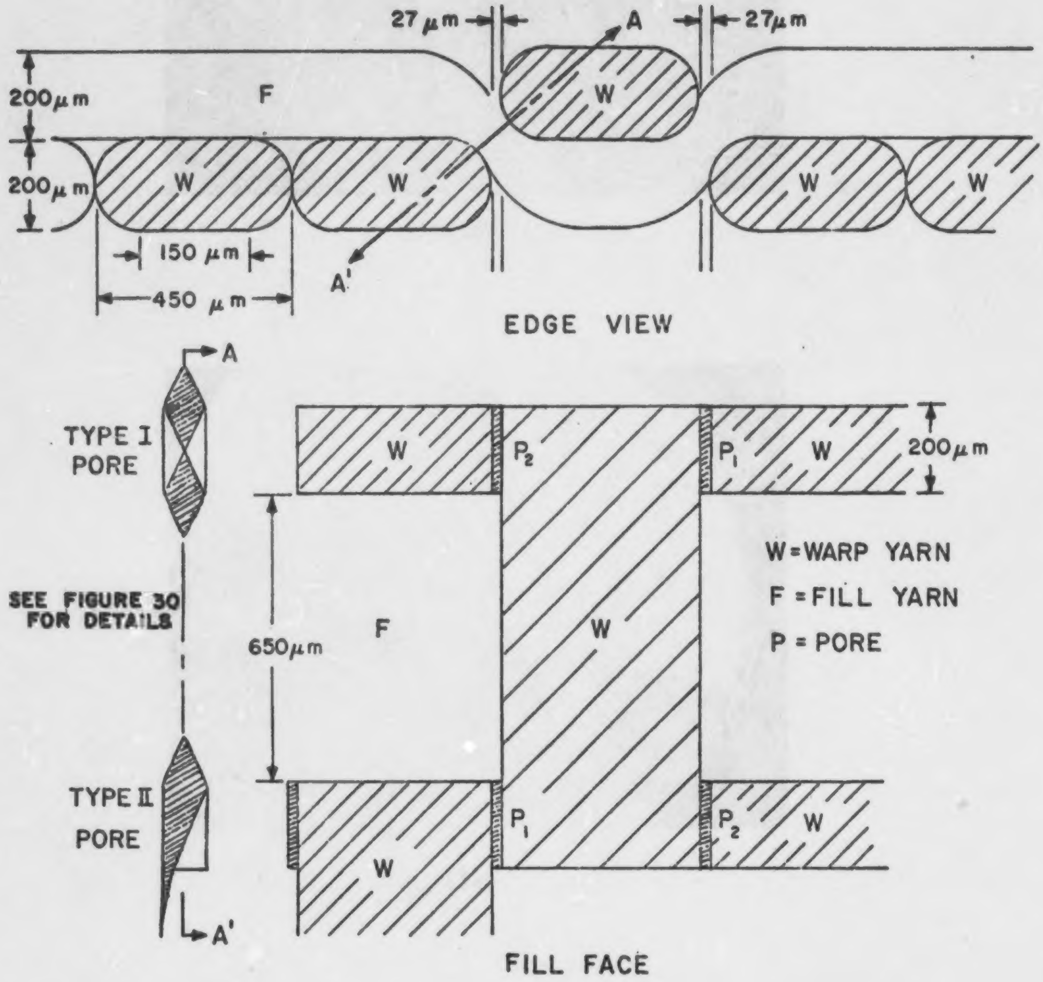
27 μm
A
27μm
200μm
F
W
200μm
W
W
W
W
150 μm
A'
450 μm
EDGE VIEW
A
TYPE I
PORE
SEE FIGURE 30
FOR DETAILS
TYPE II
PORE
A'
W
P2
P1
W
200μm
W=WARP YARN
F=FILL YARN
P=PORE
650μm
F
W
P1
P2
W
W
FILL FACE

Figure 28. Schematic drawing showing alignment, approximate form, and spacing of yarns and pores in Sunbury filter bags (Menardi Southern woven glass media)

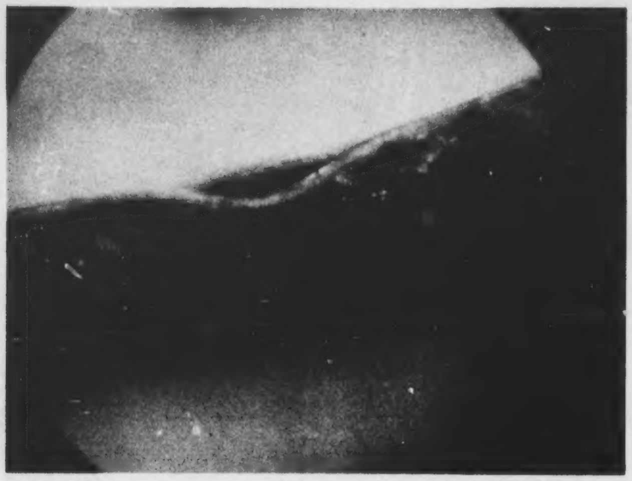

Warp

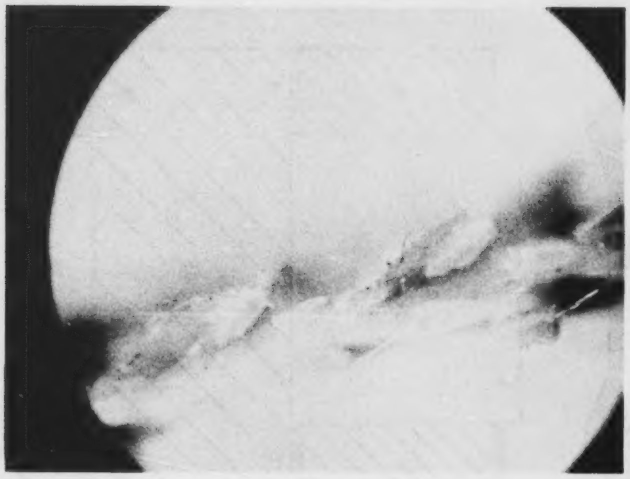

Fill

Figure 29. Edge views of clean Sunbury fabric (20X mag)

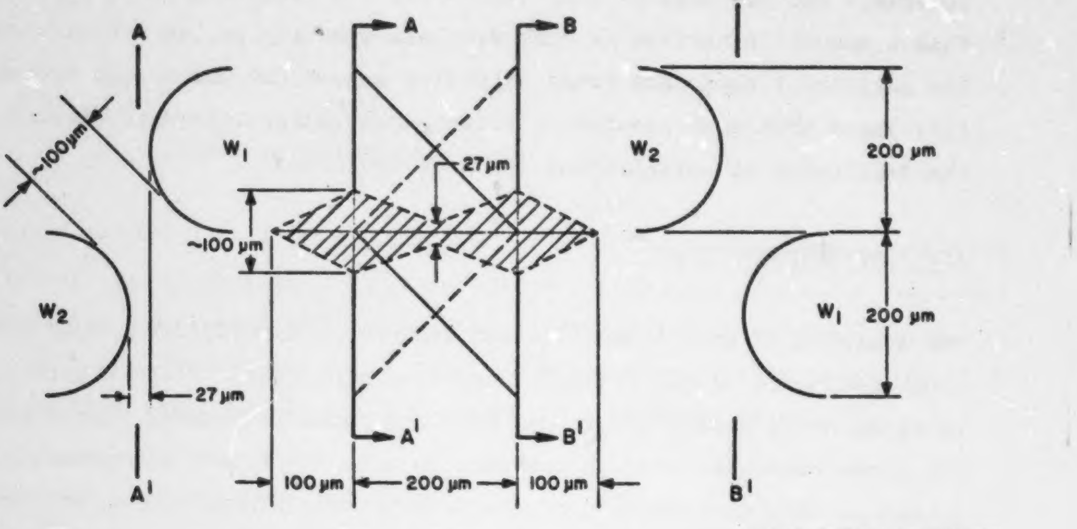
A
A
B
B
W1
W2
W2
W1
~100 µm
~100 µm
27 µm
27 µm
200 µm
200 µm
A'
A'
B'
B'
100 µm
200 µm
100 µm

TYPE I PORE

NOTE: SHADED REGION IS WARPED PORE SECTION ROTATED INTO A SINGLE PLANE

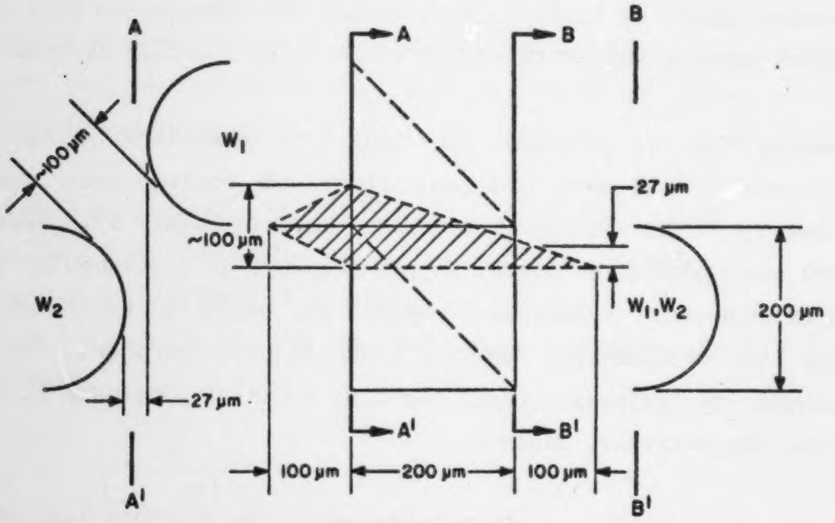
A
A
B
B
W1
W2
W1, W2
~100 µm
~100 µm
27 µm
27 µm
200 µm
A'
A'
B'
B'
100 µm
200 µm
100 µm

TYPE II PORE

Figure 30. Schematic drawing showing idealized alignment of parallel yarns and maximum pore cross section (shaded area)

The development of the contours for a type II pore followed the same process. For purposes of simplification, the yarns show an abrupt rather than a smooth transition as they displace from top to bottom locations. The additional expansion areas extending beyond the 200 μm gap between fill yarns have been treated as triangularly shaped elements because of the difficulty in establishing the true contours.

Air Flow Through Pores

The analysis of pore dimensions and general yarn structure should permit rough estimates of the probable performance of fabric filters with respect to clean media resistance to gas flow and particle removal characteristics. Two approaches were used in conjunction with the fabric measurements discussed in this section to estimate probable resistance characteristics. The first was based upon the average pore dimensions shown in Figure 28. These values were calculated by using the yarn counts and maximum/minimum yarn dimensions given in Table 3 coupled with the observation that there are no spaces between warp yarn except at the type I and II locations.

If one assumes that the principal pore length is established by the 200 μm space between each fill yarn, one can estimate the minimum pore cross section from the schematic representations given in Figure 30. Because the assumed pore boundaries appear (approximately) as a triangular and truncated triangular or trapezoidal shapes, the hydraulic radii have been computed in lieu of diameters for type I and II pore openings. For the Sunbury fabric, the hydraulic radii for type I and II pores are 17.8 μm and 17.9 μm, respectively, Table 5.

According to the Hagen-Poiseuille relationship, the pressure loss through a cylindrical pore of the Sunbury fabric under laminar flow conditions can be expressed by the following relation:

$$\Delta p = 8\mu QL/10\pi R^4 \tag{15}$$

Table 5. CHARACTERISTIC PORE DIMENSIONS[a] FOR SUNBURY (MENARDI SOUTHERN) AND NUCLA (CRISWELL) GLASS FABRICS

	Sunbury		Nucla	
	Type I pore	Type II pore	Type I pore	Type II pore
Cross-sectional area, μm^2	22,700	19,050	24,130	19,800
Perimeter, μm	1,276	1,065	1,368	1,157
Hydraulic radius,[b] (M) μm	17.8	17.9	18.4	17.2
Equivalent pore radius, μm				
Based on R = 2 M	35.6	35.8	36.8	34.4
Based on minimum pore area	85.0	77.8	87.5	79.5
Measured resistance[c] GCA tests, in. water	0.024	0.024	0.009	0.009
Calculated resistance[d] in. water	0.011	0.015	0.008	0.012
Calculated resistance[e] in. water	0.062	0.074	0.045	0.062
Calculated resistance[f] in. water	0.016	0.018	0.011	0.016

[a] Based on analysis of Figure 30.

[b] Average M values for type I and II pores - 17.8 μm for Sunbury and Nucla fabrics.

[c] Measured values, GCA tests.

[d] Calculated from Equation (1), $\overline{R}$ depicts circular equivalent of pore cross-sectional area.

[e] Calculated from Equation (2), using $\overline{M}$ values.

[f] Calculated from Equation (2), with $\overline{V} = \overline{V}_{max}/2$ and $\overline{M} = M_{min}\sqrt{2}$.

where Δp = pressure loss N/m^2

μ = gas viscosity 1.84×10^{-4} poise

Q = volume flow per pore 7.57×10^{-3} cm^3/sec

L = filter thickness 4.0×10^{-2} cm

$\overline{R}$ = pore (capillary) radius (based on minimum pore area) 8.5×10^{-3} cm

Use of Equation (15), in conjunction with a pore radius derived from the circular equivalent of the pore cross sectional area, provides estimates of filter resistance that agree roughly with measured values. The actual results for Sunbury and Nucla fabrics, respectively, show predicted values 50 percent lower and 33 percent higher than measures values.

Equation (15) may also be expressed in the form:

$$\Delta p = 2\mu VL/10\overline{M}^2 \tag{16}$$

where V is the average pore velocity based upon the pore cross sections given in Table 5 and the pore flow of 7.57×10^{-3} cited above and $\overline{M}$ the average hydraulic radius.

Estimates based upon Equation (16) showed resistances of 15.5 N/m^2 (0.062 in. water) and 18.4 N/m^2 (0.074 in. water), respectively, for types I and II pores in the Sunbury fabric. GCA measurements with flat test panels 15 cm x 23 cm (6 in. x 9 in.) indicated a pressure loss of 6.0 N/m^2 (0.024 in. water).

Similar calculations for the Nucla fabric at the same air flow rate (1.015 $cm^3/sec/cm^2$ fabric), a pore count of $164/cm^2$, and the pore dimensions given in Table 5, indicated filter resistances of 11.1 N/m^2 (0.045 in. water) and 15.5 N/m^2 (0.062 in. water), respectively, for types I and II pores. The GCA measured value for the clean fabrics was roughly 2.2 N/m^2 for identical flow conditions. Thus, both the Sunbury and Nucla estimates were unsatisfactory when the effective radii were computed as twice the hydraulic radii. Although both assume a capillary structure, which does not describe the filter interstices, one can argue that Equation (16) offers a better approximation because it takes into account the highly irregular pore boundaries tbrough the use of hydraulic radius.

In using Equation (16), the assigned values for the hydraulic radii were computed from the pore geometry shown in Figure 30. Thus, the use of a maximum value for average pore velocity and a minimum value for hydraulic radius automatically leads to a high predicted pressure loss.

Since the velocity at the surface of the fabric and the pore inlet is small compared to that at the throat of the pore, a better estimate of average pore velocity is one-half the throat value. For continuity of flow it is then required that the hydraulic radius at the throat be increased by the $\sqrt{2}$. When the adjusted values for V and M are substitute in Equation (16), the computed clean fabric resistance for the Sunbury fabric becomes 3.86 N/m^2 or 0.0155 in. water for a type I pore which is in good agreement with the GCA measured value, 0.024 in. water.

Similar calculations for type II Sunbury pores and types I and II Nucla pores are shown in Table 5. Despite the fact that a very simplistic model of the filter pore structure has been used (basically a symmetrical Venturi type opening with a minimum circular cross section at the center and a depth equal to the filter thickness), Equation (16) appears to provide reasonable values for fabric resistance characteristics when good estimates of effective pore count and minimum pore cross sectional area are available.

In applying Equation (16), it must be remembered that average pore velocity is based upon the gas flow per pore and the best estimate of pore cross sectional area. On the other hand, the hydraulic radius was computed on the basis of pore cross sectional area and pore circumference.

Except for square or circular cross sections where $M = L'/4$ and $D/4$, respectively, the $\overline{M}$ value satisfying resistance criteria in Equation (16) will not, at the same time, define the true pore cross sectional area and hence true average pore velocity. Therefore, if by successive measurements of filter resistance versus time one desires to estimate the average or effective open area per pore, it will be necessary to define the relationship between the M values characterizing resistance and pore areas, respectively. For example, with respect to a type I pore in the Sunbury fabric, the hydraulic radius is 17.8 μm for resistance computation and 42.5 μm for pore area estimation.

PHYSICAL PROPERTIES OF FABRICS

Several measurements of selected physical properties of previously used and new Sunbury and Nucla bags were performed by FRL* as part of the field sampling phase of this project. These data, which are summarized in Tables 6 and 7, are intended to help explain field performance, including resistance, dust retention characterisitcs, and evidence of undue wear and tear.

Most of the changes shown in Tables 6 and 7 are consistent with what one expects to see in fabrics with extended field use; i.e., decreased permeability due to interstitial dust fill and a corresponding increase in fabric weight; a detectible reduction in breaking strength and elongation prior to breaking; and a very pronounced increase in flexural rigidity.

One might infer that decreased permeability will result in improved dust retention at the expense of higher resistance. However, it is also possible for the permeability to increase due to partial blinding while at the same time the dust retention characteristics are reduced because

---

*Fabric Research Laboratories
1000 Providence Highway
Dedham, Mass., 02026

Table 6. RESULTS OF PHYSICAL CHARACTERIZATION TESTS ON SUNBURY FABRIC FILTER BAGS[a]

Test description	New bag	Used bag No. 1	Used bag No. 2	Used bag No. 1, vacuum cleaned	Used bag No. 2, vacuum cleaned
ASTM D 1910, Sample weight, oz/sq yd	11.0	16.9	13.5	11.5	11.3
ASTM D 1777, Sample thickness, mils					
Range	10.3 - 13.0	15.6 - 18.6	13.7 - 14.7	12.8 - 14.8	11.7 - 13.0
Average	11.2	16.9	14.2	13.6	12.5
ASTM D 737, Air permeability, cfm/sq ft at ½" H_2O ΔP					
Range	49.5 - 58.0	0.7 - 1.5	1.1 - 2.1	28.0 - 31.4	35.7 - 44.1
Average	54.3	1.1	1.6	30.5	40.0
ASTM D 1602, Breaking strength and elongation					
Breaking strength, lb					
Warp: Range	187 - 200	137 - 200	123 - 167		
Average	197	166	152	194	186
Fill: Range	82 - 93	111 - 132	86 - 142		
Average	87	121	116	117	134
Elongation at break, percent					
Warp: Range	3.1 - 3.9	3.6 - 3.9	2.1 - 3.6		
Average	3.5	3.8	3.2	3.4	3.2
Fill: Range	2.6 - 2.8	2.8 - 2.9	1.9 - 2.2		
Average	2.6	2.9	2.1	2.0	2.3
Average energy to break, inch-lb					
Warp:	3.4	3.2	2.4	3.4	2.9
Fill:	1.1	1.8	1.2	1.2	1.5
Average:	2.3	2.5	1.8	2.3	2.2
Flexural rigidity-beam method, (10^{-3})lb/sq in. per inch of width					
As received					
Warp:	0.41, 0.47	1.5 , 2.1	1.5, 1.1		
Fill:	0.73, 0.73	3.0 , 2.4	1.9, 2.0		
Average:	0.58	2.2	1.6		
Adjusted for difference in mass					
Warp:	0.41, 0.47	0.98, 1.4	1.2, 0.89		
Fill:	0.73, 0.73	1.9 , 1.6	1.6, 1.6		
Average:	0.58	1.5	1.3		

[a] Tests performed by Fabric Research Laboratories for GCA Corporation.

Table 7. RESULTS OF PHYSICAL CHARACTERIZATION TESTS ON A NUCLA FABRIC FILTER BAG[a]

	New bag	Used bag, middle	Used bag, bottom
ASTM D1910, Sample weight, oz/sq yd			
range	7.4 - 7.5	7.7 - 7.8	11.3 - 11.7
average	7.4	7.8	11.4
ASTM D1777, Sample thickness, inches			
range	0.0135 - 0.0156	0.0139 - 0.0158	0.0149 - 0.0169
average	0.0147	0.0147	0.0156
ASTM D737, Air permeability, cfm/sq ft			
range	83.5 - 91.8	30.8 - 48.2	30.8 - 48.2
average	86.5	38.6	38.6
ADTM D1682, Breaking strength and elongation			
Breaking strength, lbs			
Warp: range	168.6 - 210.0	117.0 - 225.0	102.0 - 135.0
average	186	166	116
Fill: range	82.2 - 116.0	35.1 - 100.5	54.7 - 96.1
average	104	66.5	73.1
Elongation to break, percent			
Warp: range	8.9 - 11.7	6.2 - 8.1	6.0 - 8.1
average	10.7	7.6	6.9
Fill: range	4.6 - 5.2	2.4 - 4.0	2.0 - 3.7
average	4.8	3.1	2.9
Flexural rigidity, lbs $(in.)^2$/in. width			
average	6.26×10^{-4}	1.99×10^{-3}	2.04×10^{-3}

[a] Tests performed by Fabric Research Laboratories for GCA Corporation.

of the loss of the nap or loose staple fibers after extended usage. With respect to the cleaning of bags by collapse and reverse air flow, those properties related to flexure may also be related to stiffness and rigidity. If cake dislodgement is more dependent on the rate of flexing than the actual degree of curvature present when the bag is collapsed, the rigidity factor may be very important. On the other hand, if curvature alone determines when the interfacial bonds between particles and yarns are severed, filter cleanability, and hence resistance properties, may be less sensitive to rigidity changes.

The apparent spread in the descriptive parameters given in Tables 6 and 7 suggests that caution should be used in developing predictive models based on limited tests. When one examines field performance tests on the Sunbury system over a 2-year period, (see Analyses of Sunbury Field Measurements), it seems reasonable to conclude that the order of the change and/or variations reported has not highlighted any serious performance defects. In some cases, the main value of the measurements given in Tables 6 and 7 is relative; i.e., once field experience with one fabric is well defined, a set of very similar measurements for another fabric will probably indicate similar field performance.

Tensile Modulus

Tensile properties were determined for several new and used samples of Sunbury and Nucla fabric in accordance with procedures described in earlier GCA studies.[10] The present measurements were made by determining the elongation (warp direction) of 7.6 cm x 45.7 cm (3 in. x 18 in.) and 15.2 cm x 45.7 cm (6 in. x 18 in.) strips of fabric under applied static loads ranging from 22 to 336 N (5 to 75 lbs). The equipment used for these measurements is described in the section on instrumentation. A representative loading curve is shown in Figure 31 for a 3 in. x 18 in. fabric sample, Sunbury plant, from a Compartment 6 bag. During the loading phase, the tension/elongation relationship followed the path

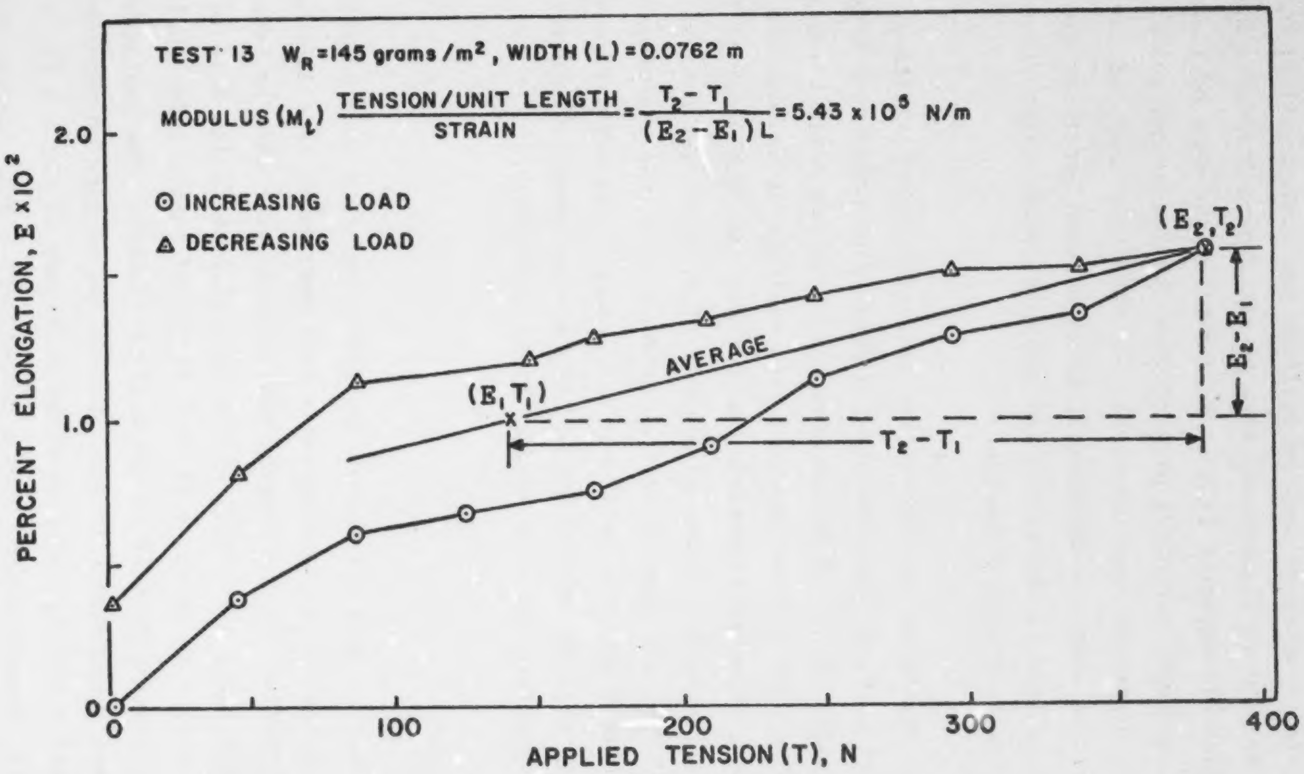

Figure 31. Stress/strain relationship for used Sunbury media, 7.6 cm x 45.7 cm (3 in. x 18 in.) strip with tension applied in warp direction

given by the circles. As the tension was relaxed, however, the return to original length displayed the same lag (or hysteresis) noted with many fabrics tested previously by GCA.[10] For general characterization of the elongation properties, the average slope of the curve at 222 N (a typical applied tension for field installed bags) can be used for the calculation of the stretch modulus, M. This approach applies to the utilization of tensile properties for estimating the average acceleration of mechanically shaken bags. However, when cleaning is dependent upon bag collapse, the tensile loading rather than the unloading curve appears to be a better indicator of bag installation and flex properties because tensile changes brought about by flow cessation and reversal are (a) very small compared to the installed tension levels 220 N (50 lbs) and (b) take place at low frequencies.

Because fabric thickness is often difficult to determine, the modulus for previous and present fabrics is expressed in terms of the periphery or width rather than the cross-sectional area of the material subjected to a tensile load. The tensile properties of the filter fabrics will be used to define the dynamic behavior of the fabric (acceleration or flex rate) during the cleaning process.

The results of several measurements are given in Table 8 for fabric samples from different compartments and with different residual dust loadings. These modulus estimates were based upon the curves generated while increasing loads were applied to the fabric rather than the average of load and unload conditions depicted in Figure 31. As stated above, it was believed that the former approach would provide a better indication of the dust holding/tension relationship.

If there is reasonable confidence in the estimation of fabric thickness, the tensile or elastic modulus values shown in Table 8 can be converted to the conventional form, N/m^2 or $lbs/in.^2$, by dividing each by the fabric thickness in the appropriate units. As discussed elsewhere, the thickness of the Sunbury and Nucla fabrics, 400 μm, was not difficult to ascertain.

Table 8. TENSILE MODULUS VALUES FOR GLASS BAGS USED FOR COAL FLY ASH FILTRATION

Test[a] number	Bag[b] compartment number	Residual dust load[c] grams/m^2	Tensile Modulus			
			15.2 cm x 45.7 cm		7.6 cm x 45.7 cm	
			N/m x 10^{-5}	lb/in x 10^{-3}	N/m x 10^{-5}	lb/in x 10^{-3}
12S	6	130	1.72	1.28	-	-
13S	6	145	-	-	3.85	3.0
14S	14	114	1.14	1.22	-	-
15S	14	149	-	-	4.16	3.14
16S	11	235	-	-	3.22	4.70
17S	11	203	1.58	1.51	-	-
18S	3	120	1.67	2.10	-	-
19S	3	162	-	-	3.80	3.50
20S	7	129	-	-	2.52	1.97
21S	10	141	-	-	2.34	2.47
22S	10	102	1.23	0.98	-	-
23S	7	102	1.10	0.94	-	-
28S	3	120	1.53	1.40	-	-
30S	14	115	1.28	1.36	-	-
31S	6	131	1.47	1.83	-	-
32S	-[e]	0.0 Unused	0.85	0.96	-	-
24N	2[f]	15.8	0.95	0.90	-	-
25N	1[f]	25.9	1.06	1.10	-	-
26N	1[f]	17.2	-	-	2.78	3.75
27N	2	12.9	-	-	2.97	2.10
33N	-[e]	0.0 Unused	0.85	1.04	-	-
34N	1[f]	2.9	0.86	0.94	-	-
35N	2[f]	0.0	1.26	2.12	-	-
32SB	g	0.0	0.67	1.65	-	-

[a] S, N refer to Sunbury, Pennsylvania and Nucla, Colorado power plants.

[b] Fourteen compartment baghouse, Sunbury, Pennsylvania.

[c] Resultant loading after laboratory cleaning.

[d] Tension applied in 18 in. (warp) direction.

[e] Clean, unused bag.

[f] Individual bag number.

[g] Clean Sunbury bag/ tension measured in fill direction.

Since the bag axis is usually aligned in the direction of the warp yarns to provide maximum bag strength, few tension determinations were made in the fill direction. The results of a single test, Table 8, Test 32SB, show the increased stretch properties of fill yarns (bulked staple) relative to the warp yarns. A comparison of modulus values for glass bags with those determined in previous GCA studies, Table 9, for cotton and Dacron fabrics shows that even with monofilament yarns, the elongation characteristics are far greater for synthetic fiber yarns than for glass.

Figure 32 indicates that the tensile modulus increases as the interstitial dust deposition increases. This behavior is attributed to the fact that dust particles within the pores and yarns prevent normal elongation and contraction which, in turn, reduces the elongation attainable per unit tensile force.

It should be noted that the indicated fabric modulus values for 7.6 cm wide strips were approximately twice those for the 15.2 cm x 45.7 cm strips, Table 8. Because woven glass fabrics fray badly (and the lubricated yarns slide over each other quite readily), it was expected that any contribution to tensile strength from the fill fibers would be less for narrow strips. If one assumes a constant yarn modulus, the doubling of the number of warp yarns (the principal support of the applied load) should show a decrease in elongation for a fixed load. Our measurements, however, refute this logic. It is expected that modulus determinations on full size bags, ~ 10 ft x 4 in., will explain this anomaly.

Bag Tension and Permeability

Test filters fabricated from new Sunbury and Nucla media were sewn with conventional stitching and internal support rings in the form of 10 ft. long by 4 in. diameter filter tubes. The resistance versus air flow relationship was determined over the approximate velocity range 0 to 1.83 m/min

Table 9. PROPERTIES OF COMMON WOVEN FABRICS INCLUDING TENSILE MODULUS

	Fabric	Weight[a]	Weave	Yarn[b] count	Perme-ability[c]	Tensile[d] Modulus lb/in.	Mfgr. No.	Mfgr.'s[e] comment
1.	Cotton	10	Sateen	95 x 58	13	105	960	S
2.	Cotton	10	Sateen	95 x 58 (Napped)	13	105	960C	S
3.	Dacron®	10	Plain	30 x 28 (Staple)	55	88.6	862B	S
4.	Dacron®	10	1/3 Crowfoot	71 x 51 (Filament)	33	466	865B	S,RF

[a] Weight: ounces per square yard.

[b] Yarn count: yarns per inch, warp x fill.

[c] Permeability: ft^3/min of air passing through 1 ft^2 of clean, new fabric at 1/2 in. H_2O pressure drop.

[d] GCA measurements.

[e] S indicates for shaking, RF indicates reverse flow cleaning.

[R] DuPont trademark.

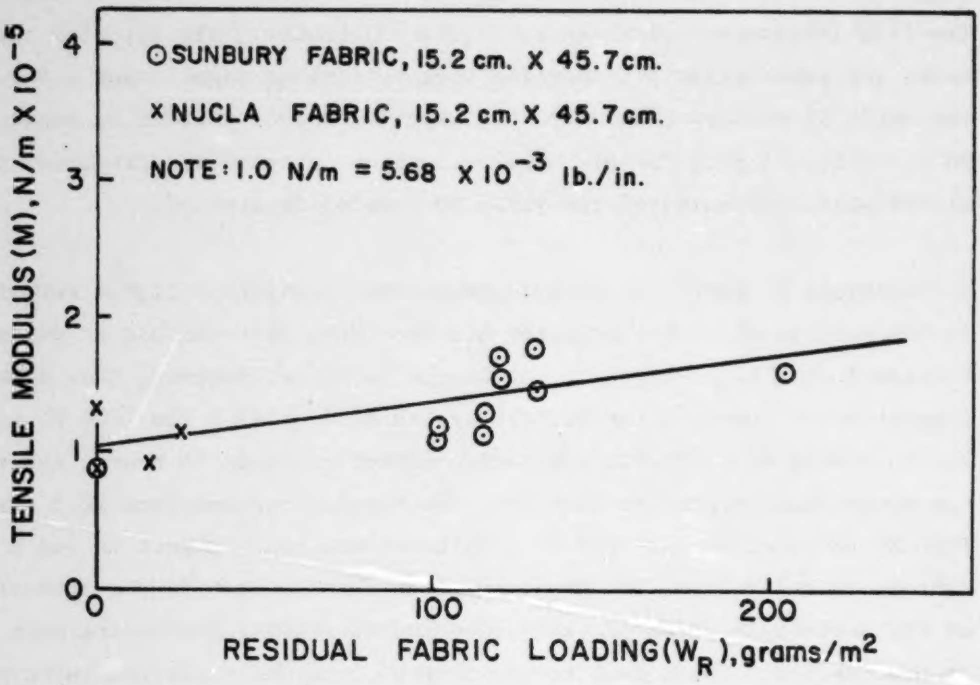

Figure 32. Effect of dust loading on tensile properties of woven glass bags

0 to 6 ft/min for each of several preselected tension values. The effect of bag tension upon resistance was then determined for a constant filtration velocity of 0.61 m/min as shown in Figure 33.

Examination of the resistance characteristics of clean glass bags indicates that the resistance to air flow actually undergoes an increase as bag tensioning increases from 0 (slack) to ~ 60 lbs (267 N). This behavior suggests that the effective pore or channel dimensions must decrease as the load increases. As shown in Figure 33, however, the apparent resistance (or permeability) properties does not change significantly for either the Nucla or Sunbury media over the expected normal tensioning range, 35 to 60 lbs (156 to 267 N). The resistance increase is attributed to an appreciable flattening of the yarns as tension is applied.

A comparison of Curves 2 and 3 suggests that a slightly higher resistance is encountered when flow measurements are begun with the bag at maximum tension level; e.g., Curve 2. It should be noted, however, that after completion of Curve 3, the filter bag was held at 48.5 lbs (216 N) tension. The following day, after a tensioning period of about 16 hours, the bag underwent some stretching such that the tension reduced from 48.5 lbs (216 N) to about 45 lbs (200 N). Although one might expect to see a reduction in resistance, it should be noted that the continuous stressing of the deformable yarns probably produced additional flattening over the 16-hour period. Thus, despite the lowered tensions reflected in Curve 2, there is a considerable lag or hystereris in the return of the yarn dimensions to its unstressed form.

Because the essentially slack installation condition noted for square test panels during bench scale tests leads to lower pressure loss, (and more open pore structure), it is quite possible that some filter media may show poorer performance as a flat test panel than in the form of a full scale filter bag. At the present time, there is no practical way to prepare a small, test panel such that a pre-set uniform tension can

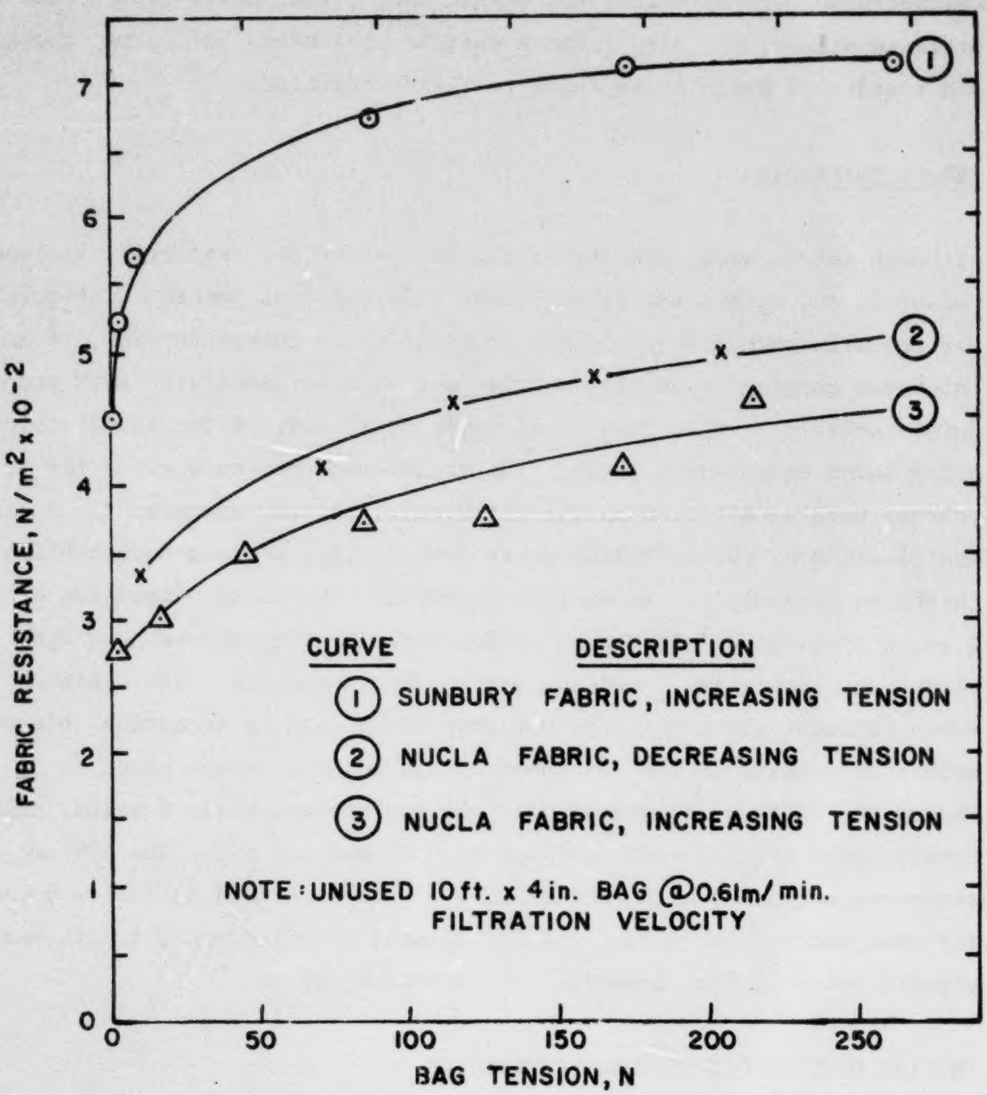

Figure 33. Effect of bag tension on resistance to airflow, with conventional bag suspension

be maintained during filtration. We have also observed that considerable assymetry in pore structure may ensure when a flat panel is deformed by pressure stressing. Both factors must be considered before extrapolating the results of bench scale tests to field conditions.

Fabric Thickness

Although fabric areal density; i.e., its weight per unit area, is readily measured, the determination of fabric thickness can present difficulties, particularly with highly napped, woven media or felted fabrics. Standard thickness gauging is usually carried out in accordance with ASTM procedures (D-1777-64) that involve accurate calipering of the fabric thickness under known compressive loads. The recommended pressure range for firm fabrics such as asbestos is 0.1 to 10 psi (7 to 700 grams/cm^2). A simple modification of the ASTM method was used in this program to establish thickness parameters. Glass fabric samples, cut to the dimension of 2 in. x 3 in. glass microscope slides were inserted between two such slides and compressed by adding various known weights. The distance between adjacent plate surfaces was then determined by an optical micrometer. According to the thickness versus loading curves shown in Figure 34, minimum thicknesses for the Sunbury and Nucla fabrics, respectively, were reached with loadings of 0.70 and 1.6 psi. The 400 μm thickness noted for both fabrics agreed well with data in Tables 6 and 7 for used media. Our values for the clean (unused) Sunbury fabric were significantly higher, however, 400 μm versus 280 μm.

INITIAL DUST DEPOSITION CHARACTERISTICS

A special experiment in which a succession of photomicrographs of the fabric surface were made during the filtration of fly ash with the Sunbury fabric suggests that pore closure takes place early in the filtration process and under conditions where parallel flow appears to predominate. The appearance of the fabric (shown schematically in Figure 35 for various

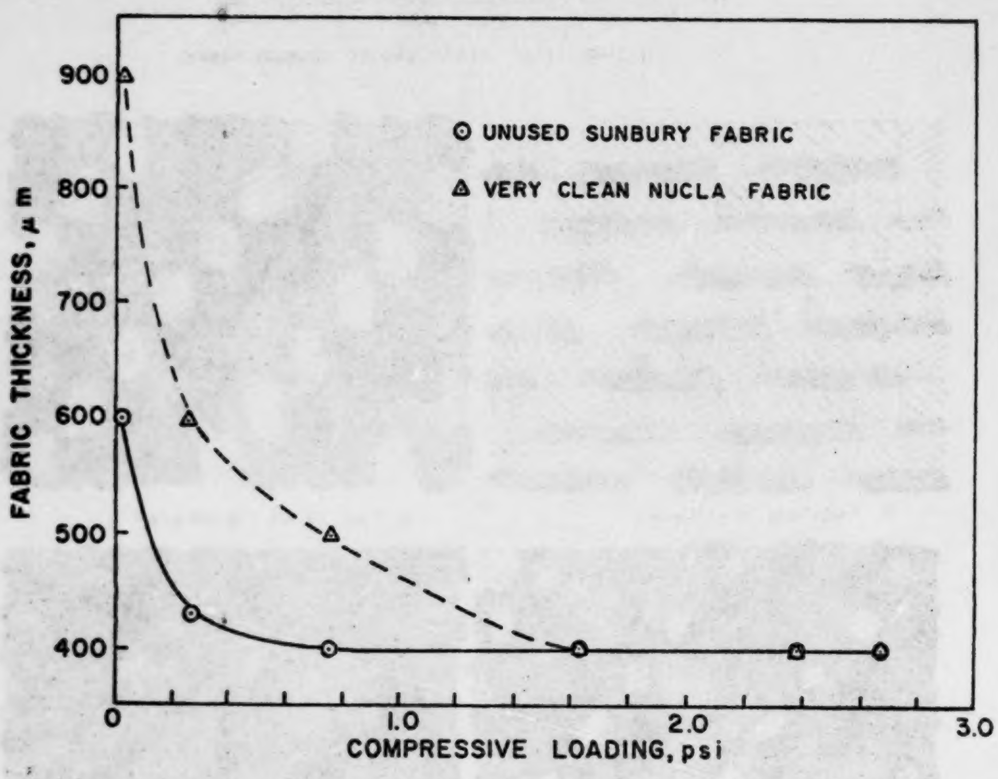

Figure 34. Fabric thickness versus compressive loading

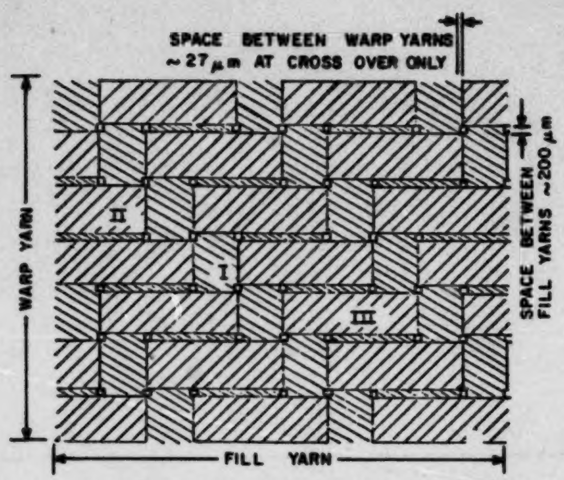
SPACE BETWEEN WARP YARNS
~27 μm AT CROSS OVER ONLY
SPACE BETWEEN FILL YARNS ~200 μm
WARP YARN
FILL YARN
II
I
III

1. TIME ZERO CLEAN, UNUSED SUNBURY FABRIC

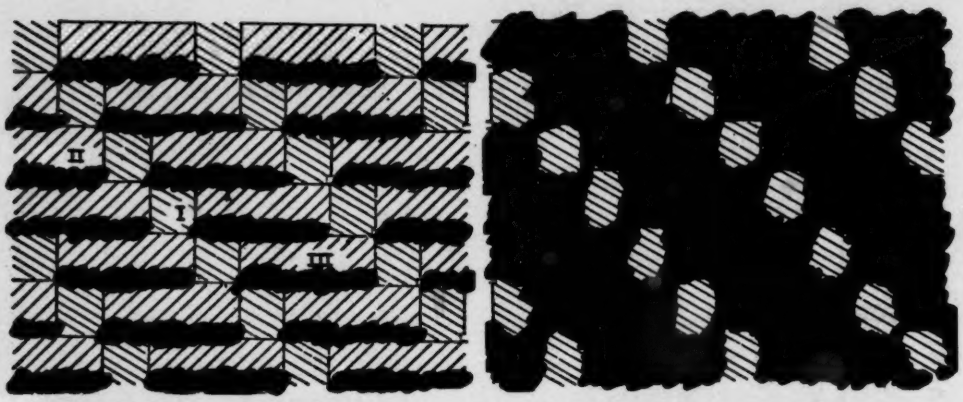

2. TIME 9min. W 47.7 g/m²

3. TIME 19 min. W 100 g/m²

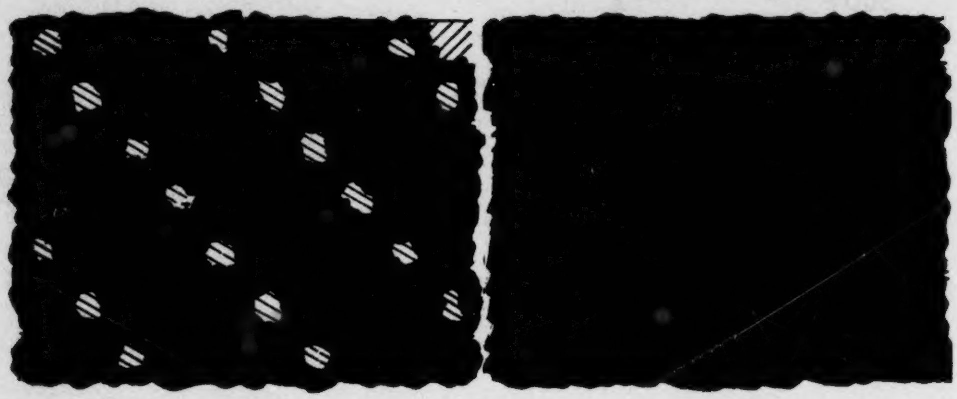

4. TIME 37min W 196 g/m²

5. TIME 50 min. W264 g/m²

Figure 35. Schematic of GCA fly ash filtration at 2 ft/min. Dark areas show dust deposits. Light areas indicate relatively clean warp yarns transmitting light with rear face illumination

surface loadings) indicates that dust first accumulates on and within the bulked fiber region about the Type 1 and Type 2 pores. Although we have referred to the sketches in Figure 1 as photos, they actually represent standardized and slightly simplified versions of the images seen by microscopy. As filtration progresses, the deposits spread such that the remaining surface of the fill yarns become covered, photos corresponding to filtration times of 37 and 50 minutes.

The open areas show the surface of deposit-free, multifilament warp yarns that transmit light when illuminated from the rear (clean) face. It should be noted that even when the fabric loading has reached 196 g/m^2, all "window sections" remained uncovered, thus suggesting a relatively even flow distribution through the regions of no dust deposit. It is emphasized that four pores, presumably completely bridged, constitute the boundaries or corners of the light transmitting region. High local velocities through these areas preclude dust deposition until the filling is complete above the underlying bridged pores. Unfortunately, when the filter surface is aligned normally to the viewing direction, the actual pores are concealed. However, light transmittancy as viewed by oblique camera angle indicated that clearly defined openings were present with clean (unused) fabrics. These open areas were observed to disappear shortly after filtration commenced. Finally, complete coverage is attained after 50 minutes. Variation in apparent "window" size suggests that all pores are not identical and that some sequential blockage must also take place. The presence of the uncoated warp yarns, photos after 19 and 37 minutes, do not indicate that the pores which act as sinks for these regions are unclosed or unbridged.

A second series of special fly ash filtration tests were made with a plain weave, pressed monofilament screen having a free area of 0.2 and 3120 square (0.025 cm x 0.025 cm) openings per inch.^{2} The maximum air velocity through the clean pore was about 43 m/min, approximately that estimated for the unused Sunbury fabric pores. Figures 36 through 38 (representing sequential tests on a single filter) show that only partial closure of the pores was

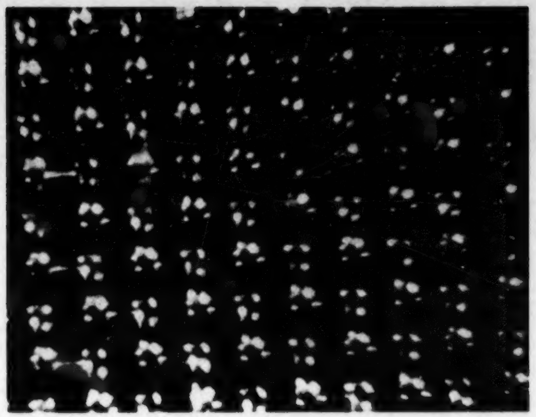

Zero minutes

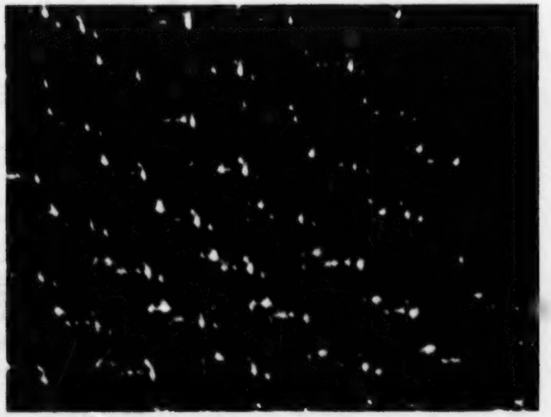

3 minutes

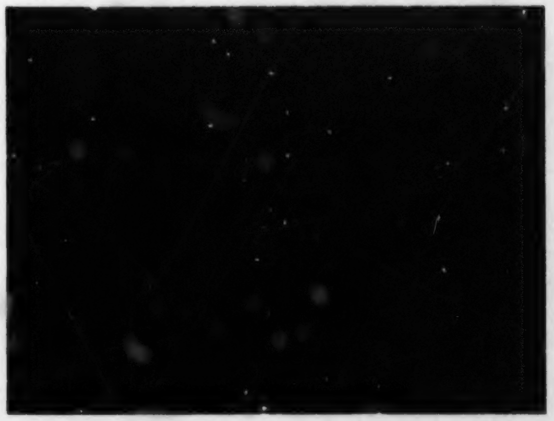

5 minutes

Figure 36. Fly ash deposition on monofilament screen versus filtration time, surface illumination

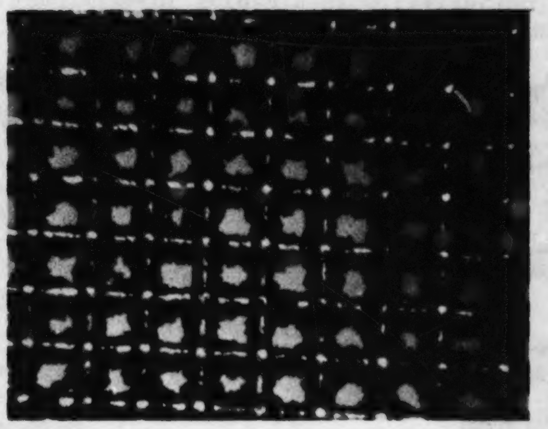

5 minutes

7 minutes

8 minutes

Figure 37. Fly ash deposition on monofilament screen versus filtration time, rear and surface illumination

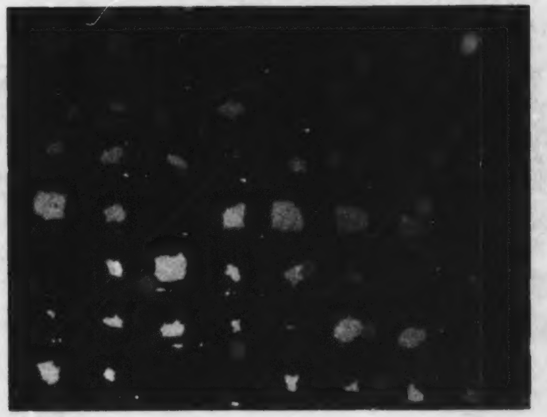

9 minutes

14 minutes

30 minutes

Figure 38. Fly ash deposition on monofilament screen versus filtration time, rear and surface illumination

attained after 5 minutes despite the fact that sufficient dust had approached or been "seen" by the filter to produce an areal density of 188 g/m^2 had dust retention been 100 percent. Observe, also, that no pore is completely bridged after 5 minutes filtration although for reasons of variable pore size, preferred deposition sites via dendrite formation and statistical randomness, the resulting apertures vary in size. The point to be emphasized, however, is that had the unobstructed openings between filaments been in the 10 μm to 25 μm range, the dendritic growth rate from the bounding filaments would have caused complete bridging well before a 5-minute filtration period. Thus, the degree of openness after 5 minutes seen in Figures 36 and 37 should probably scale to a time interval of the order of seconds. On the other hand, the distribution of opening sizes depicts the sequential aspects of pore bridging as demonstrated by real filters.

After 30 minutes filtration, several well defined pinholes appeared on the substrate which finally attained a loading density of 175 g/m^2, Figure 38. Although the average efficiency over the test period was 21 percent, the relatively high resistance of the blocked pore region causes most of the flow to pass through the pores or pinholes. No further closure of pores is expected; in fact, any slight vibration at this point in time would dislodge most of the dust. The openings shown in Figure 38 typify the appearance of many fabric surfaces that develop pinholes when face velocities are too large or the gradation of, and/or, absolute pore size is excessive.

If one assumes that pore bridging is accomplished in the very early period of filtration for a good filter, >99.5 percent efficiency, (thus excluding either a strict sequential or parallel pore closure process as the theoretical model), another description of the filtration process must be sought to explain the form of the resistance-loading curves for Sunbury and many similar woven fabrics.

SECTION VI

ANALYSIS OF SUNBURY AND NUCLA FIELD MEASUREMENTS

FABRIC DUST LOADINGS

Residual dust loadings for several Sunbury bags as received from the field are shown in Table 10.[9] These bags were removed after 2 years' service so that all replacements could be installed at the same time. Since the original guarantee had been only for 1 year there was also concern that future use might entail costly unscheduled plant shutdowns in the event of bag failure. Although there was no evidence of physical damage nor any significant change in collection efficiency (> 99.9 percent), average filtration resistance at 0.61 m/min (2 ft/min) filtration velocity had risen from 180 to 650 M/m^2 (0.6 to 2.6 in. water).

Filter bags were removed by first unfastening the bottom followed by placing a large box beneath the bag so that with the top disconnected the bag could be eased carefully into its container. Although some dust was undoubtedly lost to the hopper, it is believed that the dust holdings reported in Table 10 are reasonable estimates.

Examination of the residual dust holdings suggests that compartment 12 was probably cleaned most recently while the next in line for collapse was compartment 13. Because the individual compartments were cleaned in a 1 through 14 sequence, the graph of dust loading versus compartment number, Figure 39, should in theory display an increasing negative slope. Gross deviations from the curve, which we have attributed to accidental spills during handling, have been flagged. It is emphasized that despite

Table 10. RESIDUAL FABRIC DUST LOADING FOR SUNBURY BAGS AS RECEIVED FROM FIELD[a]

Compartment number	Fabric dust loading[b] grams/m^2	Weight ratio dust/bag
2	610	1.96
3	780	2.50
4	605	1.94
5	206	0.66
6	384	1.23
7	434	1.39
8	527	1.69
9	480	1.54
10	424	1.36
11	449	1.44
12	624	2.00
13	1430	4.60
14	920	-
Average	580	1.83

[a] Bags removed after 2 years service.

[b] Average of two bags sampled per compartment.

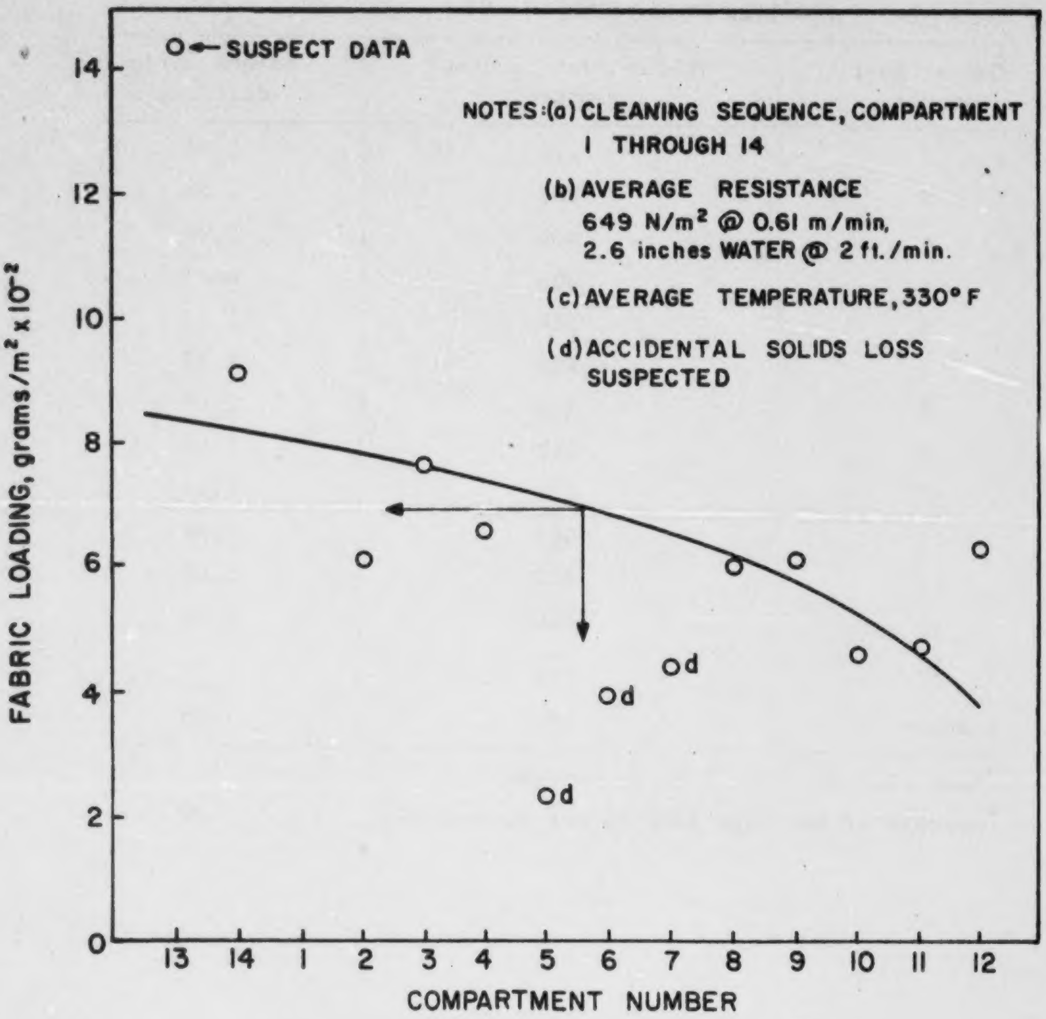

Figure 39. Residual dust loadings for bags in 14-compartment Sunbury collector. Cycle interrupted between cleaning of compartments 12 and 13 for removal and replacement of all bags[9]

the point scatter one can see from Figure 39 that the fabric loadings are considerable. Since it was not determined in the field whether uniform gas flow prevailed throughout the 14 compartments, the curve shape indicated in Figure 39 must be considered as speculative. On the average, however, it appears that the average system fabric loading is in the range of 650 to 700 grams/m^2. This loading level, in conjunctions with the field pressure measurements to be discussed in the next section will be compared with laboratory tests on the Sunbury media.

BAG RESISTANCE

Fabric resistance values as determined by GCA during field tests in March 1975 are shown in Figure 40 as a function of filtration velocity. No apparent increase was noted over a 35-day test period for which the average inlet dust loading was 6.4 grams/m^3 (2.78 grains/ft^3). The clustering of experimental points about the regression line suggests that variations in mass gas flow rate and not inlet loading were the main causes of resistance fluctuations shown in Table 11.

Analyses of old pressure charts provided by Sunbury personnel allowed us to trace the 2-year history of the glass bags that were evaluated by GCA during their last month of service, Figure 41. Based upon average monthly pressures, it appears that the main increase in fabric resistance occurs during the first few months of bag service. Once steady state conditions are attained, the increase in baseline resistance which is attributable to a gradual interstitial filling of the pores (which may be partially compensated by fabric stretching) is approximately 0.5 inches water. An improved time resolution of the pressure/time traces (daily basis) suggests that a near-steady state operating pattern may be reached in less than 3 weeks. Despite problems in instrument function and uncertainty as to system gas flow rates during the shakedown interval depicted in Figure 42, it appears safe to assume that a very radical increase in fabric resistance ($\sim$ 0.3 to 2 in. water) takes place in at least 3 weeks and possibly sooner.

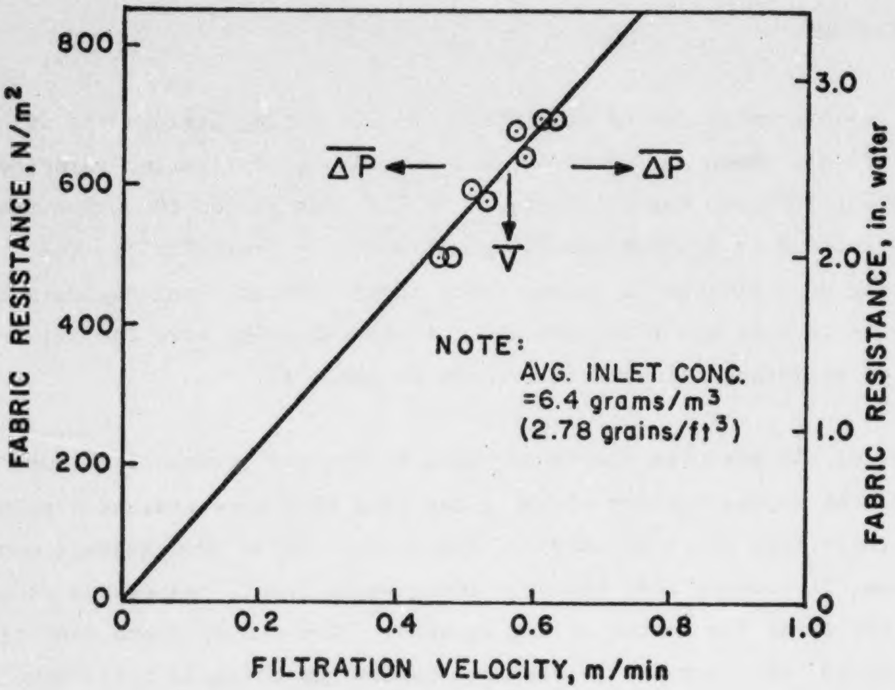

Figure 40. Average filter resistance for Sunbury glass bags, normal field use after 2 years service

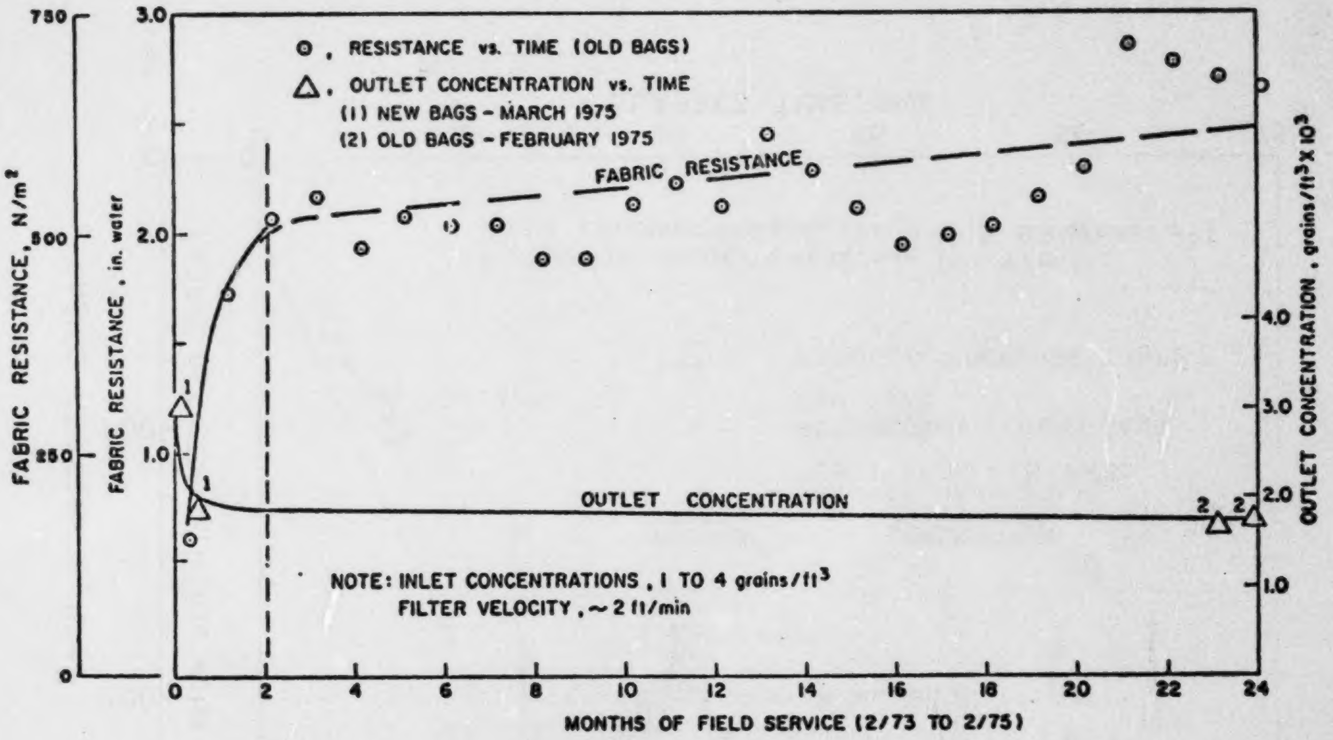

Figure 41. Filter resistance and outlet concentration versus time for glass bag filters at Sunbury, Pennsylvania power plant

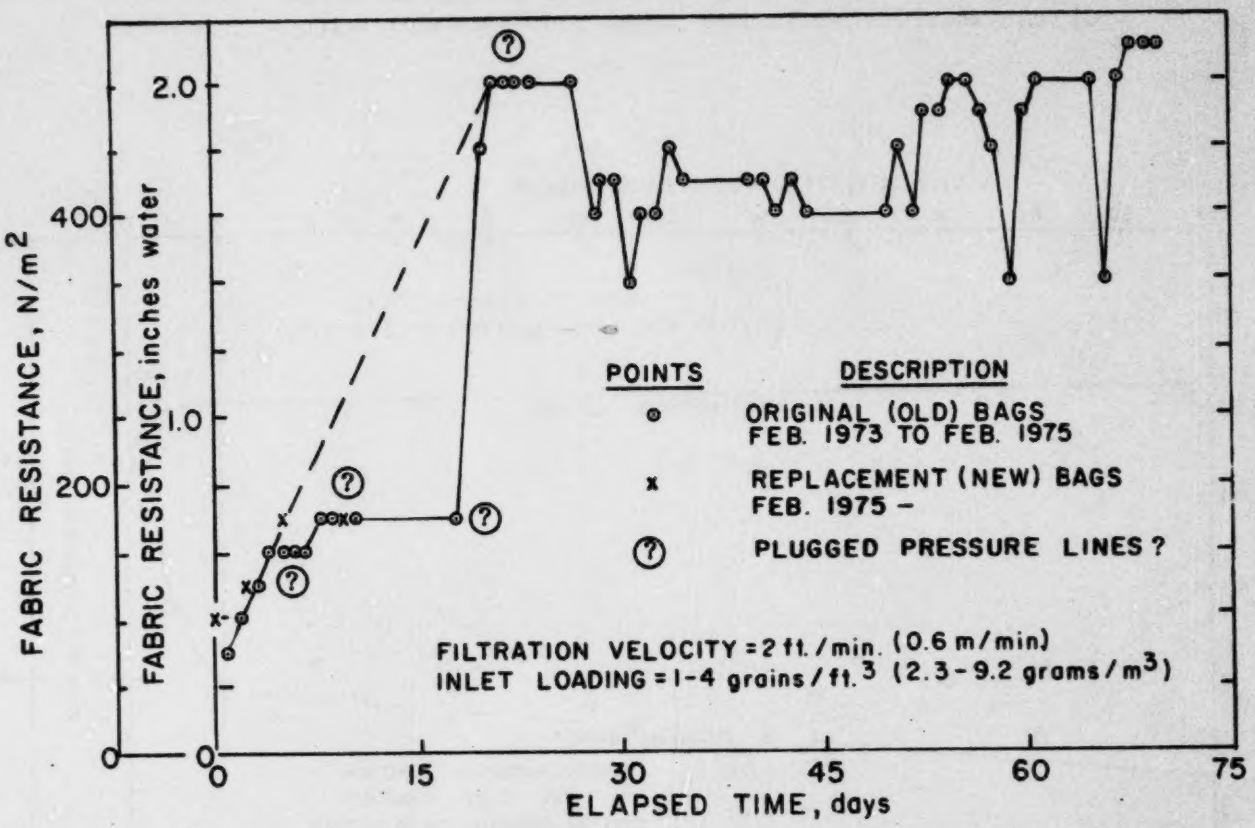

Figure 42. Resistance versus time for old and new Sunbury bags

Limited pressure data for new, replacement bags suggests that the operating characteristics for old and new bags are about the same. The rather abrupt rise to the 2 in. water operating level provides a practical guideline for modeling. In describing the greater fraction of the useful filter operating life (which Sunbury personnel believe may be as much as 3 years), it appears that the effective baseline for starting resistance might be considered as 2 in. water.

Although monthly and daily resistance - times curves suffice for practical estimates of power requirements, they do not provide the resolution necessary to assess the impact of successive cleanings on fabric resistance with multicompartment systems. A linearized 10-minute time trace from a Sunbury chart record of February 1975, Figure 43, gives a detailed picture of pressure loss patterns over successive filtering, cleaning, and manifold flushing cycles. Lowest fabric resistance values, 2.5 to 2.6 in. water, are indicated when all 14 Sunbury bag compartments are on-line. During the time interval between the sequential cleaning of compartments, no discernible increase in resistance was detectable for 13 and 14 chamber operation or during the admission of reverse flow air. This is readily explained by the fact that the amount of dust placed on the filtering surfaces during the period between cleanings represents but a very small fraction, $\sim$ 0.77 percent of the total estimated filter system dust holding. As soon as a compartment is isolated for cleaning, the handling of system flow by 13 compartments causes a resistance increase of about 0.25 in. water. With initiation of reverse flow (roughly 1.4 ft/min), the 13 on-line compartments must accommodate an additional flow volume (about 5 percent of primary flow). This leads to the observed maximum resistance levels of 2.9 to 3.1 in. water. The net result is that the average working fabric resistances is constrained to a relatively narrow range. Therefore, the modeling of system performance with respect to resistance, particulate emissions, and power needs is simplified.

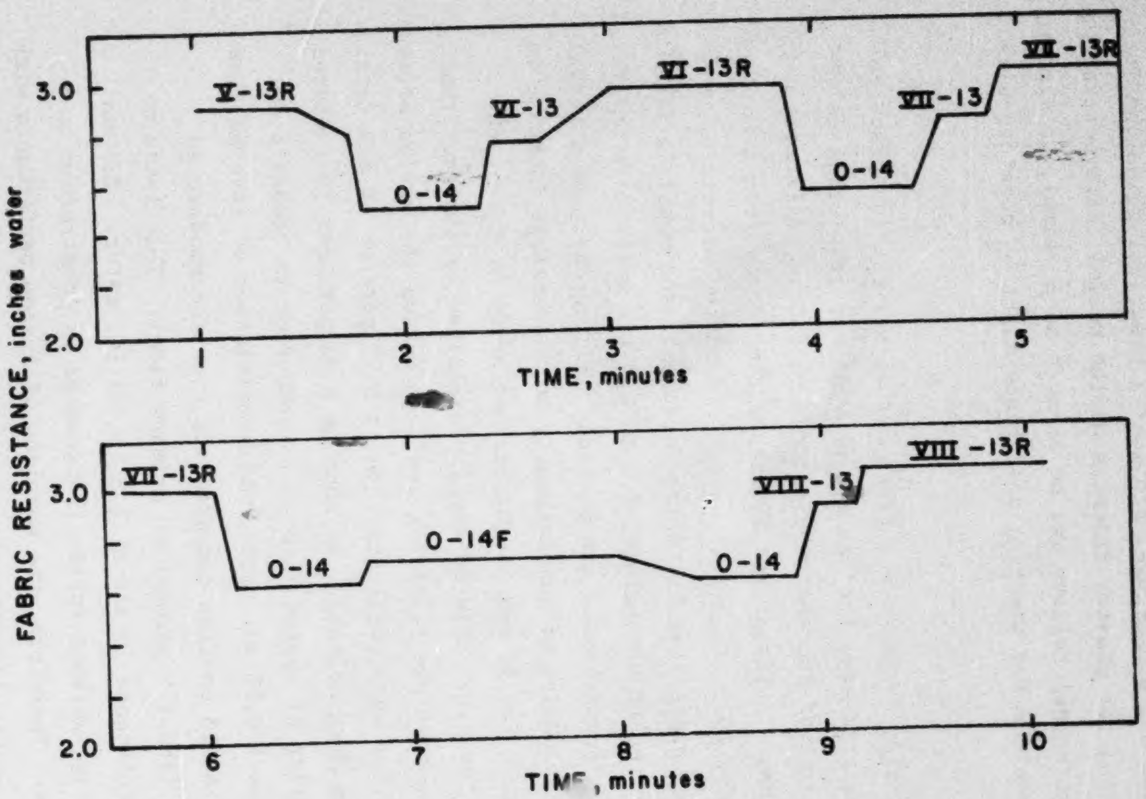

NOTES:

1. ROMAN NUMERAL REFERS TO COMPARTMENT BEING CLEANED.
2. 13 OR 14 INDICATES NUMBER OF COMPARTMENTS ON LINE.
3. R INDICATES REVERSE FLOW AIR IN USE.
4. F INDICATES MANIFOLD FLUSHING WITH REVERSE AIR.
5. O INDICATES ALL COMPARTMENTS FILTERING OR FLUSHING.

Figure 43. Filter resistance versus time for successive filtering, compartment cleaning and reverse flow manifold flushing, Sunbury field test of February 14, 1975

COLLECTION EFFICIENCY

The results of prior GCA field sampling of the Sunbury and Nucla effluents are summarized in Table 11. Inlet and outlet concentrations values, converted to their metric equivalents, are shown in Figures 44 and 45.

After 2 years service, Sunbury effluent concentrations averaged over several hours were about 1.7×10^{-3} grains/ft^3 (3.9 g/m^3) DSTP. Identical measurements upon new replacement bags some 10 days after installation showed slightly higher effluent concentrations, $\sim 2.1 \times 10^{-3}$ grains/ft^3 (4.89/m^3). Thus, it appears that no appreciable improvements in filtration capabilities are obtainable once steady state filtration conditions are realized. The fact that the emissions during the first day of use were significantly greater is consistent with the correspondingly lower filter resistance during the early shakedown period. There appears to be a rather good correlation between effluent concentration and fabric resistance properties according to the data shown in Figure 46. On the other hand, the outlet concentrations for both new and old bags show no significant dependency upon inlet concentration, Figure 44. This observation agrees with test results reported by GCA and others which indicate only weak correlations between influent and effluent concentrations for fabric filter systems.

The Nucla test data graphed in Figure 45 indicate essentially the same dust removal characteristics as shown by the Sunbury fabric. The significant difference between the two Nucla data sets resulted from the replacement of many faulty bags. It should be emphasized that the bag failures resulted from an air flow distribution problem that caused severe bag erosion. A modification in thimble design after the shake down test period corrected this problem.

Generally, a comparison of field and laboratory data for Sunbury and Nucla fabrics indicated comparable performance. Thus, it appears acceptable to extrapolate directly the results of many laboratory tests to estimate key modeling parameters.

Table 11. FIELD PERFORMANCE OF FILTER SYSTEMS WITH GLASS BAGS SUNBURY STATION[9]

Run No.[a]	Inlet concentration, gr/dscf	Outlet concentration, gr/dscf	Penetration, %	Inlet mmd, μm	Outlet mmd, μm	Fuel moisture, %	Fuel ash, %	Fuel sulfur, %	Steam flow, 1000 lbs/hr	Face velocity, ft/min	Baghouse pressure drop in. H_2O	Compartments cleaned per hour
1	3.6296	0.0022	0.06	5.8	7.1	2.9	18.5	2.1	400	2.02	2.8	28
4	4.1235	0.0013	0.03	7.0	7.7	3.1	25.1	1.7	395	2.07	2.6	28
5	2.6851	0.0017	0.06	4.6	3.7	3.0	23.6	1.6	400	2.18	2.8	28
6	2.5243	0.0014	0.06	4.7	4.5	2.6	21.1	2.2	410	2.21	2.8	28
7	3.1661	0.0014	0.04	5.5	4.4	3.4	31.6	1.8	410	2.03	2.7	28
8	2.2977	0.0014	0.06	5.1	5.6	2.9	29.5	1.5	400	2.05	2.7	28
9	2.4280	0.0015	0.06	4.4	10.4	3.2	22.6	2.2	400	2.07	2.6	28
10	3.2926	0.0016	0.05	4.8	6.6	3.0	23.0	1.4	370	2.08	2.6	28
11	2.6678	0.0033	0.12	11.9	6.1	2.5	19.7	2.2	360	1.88	2.3	28
12	2.0891	0.0017	0.08	7.2	3.6	2.1	16.0	3.2	325	1.82	2.4	28
13	2.6020	0.0020	0.08	11.0	3.4	2.6	18.8	1.6	325	1.69	2.0	28
14	2.8845	0.0015	0.05	6.5	6.6	1.7	18.7	1.7	310	1.64	2.0	28
15	2.6728	0.0016	0.06	9.1	5.0	3.0	22.2	1.3	390	2.05	2.7	28
16	2.4403	0.0013	0.05	5.6	6.1	2.7	20.6	1.2	390	2.05	2.7	14
17	2.5058	0.0016	0.06	6.1	10.0	3.2	23.5	1.6	375	1.98	2.7	14
18	1.8291	0.0013	0.07	8.0	6.4	2.4	19.0	1.5	400	2.07	2.7	28
19	2.8042	0.0016	0.06	3.2	7.5	2.8	21.6	1.5	400	2.45	3.6	28
20	2.2016	0.0018	0.08	5.9	6.6	2.6	22.2	1.2	380	2.36	3.5	28
21	1.6694	0.0019	0.11	3.4	7.4	1.8	21.7	1.4	375	2.01	2.8	28
22	1.3822	0.0031	0.22	8.2	6.4	2.3	20.7	2.1	370	2.10	0.4	28
23	3.2646	0.0028	0.09	5.4	3.1	3.5	22.3	1.8	380	2.02	0.5	28
24	2.0503	0.0029	0.14	7.0	5.0	3.6	22.6	1.8	410	1.96	0.6	28
25	3.0946	0.0025	0.08	5.6	5.8	4.1	20.6	2.4	380	2.01	0.6	28
26	2.3859	0.0022	0.09	9.6	11.5	3.5	23.2	1.6	400	2.05	0.6	28
27	1.3477	0.0022	0.16	8.0	12.0	2.7	18.3	2.1	400	2.22	0.7	28
28	3.0022	0.0022	0.07	6.8	5.9	3.2	21.1	2.1	410	2.15	0.7	28
29	2.0174	0.0023	0.11	9.2	2.6	3.6	23.8	1.6	370	1.95	0.7	28
30	2.0843	0.0020	0.10	6.7	2.4	2.7	23.1	1.5	390	1.99	0.7	28
31	2.2181	0.0022	0.10	7.5	4.4	3.3	22.0	2.0	400	2.05	0.7	28
Mean	2.5328	0.0020	0.08	6.4	6.1	2.9	22.0	1.8	384	2.04	2.0	27.0
Standard deviation	0.6346	0.0006	0.04	1.4	2.5	0.5	3.1	0.4	26	0.16	1.0	3.6

[a] Runs 1 through 22 - old bags with 2 years' service
Runs 22 through 31 - new bags, no prior service

Reproduced from best available copy.

Table 11 (continued). FIELD PERFORMANCE OF FILTER SYSTEMS WITH GLASS BAGS - NUCLA STATION[8]

Date	Run	Inlet mass loading grains/dscf			Outlet mass loading grains/dscf			Mass efficiency (percent)	Baghouse operation
		Method 5	Andersen A	Andersen B	Method 5	Andersen north	Andersen west		
9/21/74	1	2.0759	0.4984	-	0.0044	0.0101	0.0031	99.7880	Normal
9/22/74	2	2.1712	1.5078	1.4610	0.0049	0.0069	0.0034	99.7743	Normal
9/23/74	3	1.9753	1.4014	1.7176	0.0045	0.0034	0.0028	99.7722	Normal
9/24/74	4	1.7021	1.7092	1.1793	0.0063	0.0043	0.0021	99.6299	Normal
9/25/74	5	1.6768	1.4819	1.4382	0.0042	0.0031	0.0030	99.7495	Cont. cleaning
9/26/74	6	1.7995	1.3426	1.1600	0.0047	0.0048	0.0051	99.7388	Cont. cleaning
9/27/74	7	1.8516	1.3144	1.9251	0.0045	0.0033	0.0025	99.7570	Normal
9/28/74	8	11.4446	1.6248	2.0818	0.0016	0.0053	0.0015	99.9860	Long repressure
9/30/74	9	2.3878	1.6636	1.9608	0.0016	0.0021	0.0020	99.9330	Long repressure
10/1/74	10	1.6873	1.4206	1.3540	0.0010	0.0021	0.0034	99.9407	Normal
10/2/74	11	1.7422	1.0294	1.4893	0.0015	0.0035	0.0046	99.9139	No cleaning
10/3/74	12	2.1112	1.5900	1.3091	0.0092	0.0563	0.0796	99.5642	No cleaning
10/4/74	13	2.2693	1.8991	2.0574	0.0040	0.0034	0.0035	99.8237	Normal
10/5/74	14	1.7751	1.6593	1.4318	0.0029	0.0047	0.0154	99.8366	No repressure
10/6/74	15	1.3572	2.4579	1.6854	0.0007	0.0039	0.0036	99.9484	No repressure
10/7/74	16	2.1779	2.3232	1.5909	0.0019	0.0042	0.0037	99.9128	Normal
10/22/74	17	2.1098	1.8337	-	0.0022	0.0025	0.0025	99.8957	Normal
10/23/74	18	2.0669	1.5351	1.6651	0.0010	0.0024	0.0022	99.9516	Long repressure
10/24/74	19	1.9828	1.8120	1.7094	0.0015	0.0030	0.0021	99.9244	Normal
10/25/74	20	1.7791	2.9943	1.6683	0.0017	0.0025	0.0025	99.9045	No shaking
10/26/74	21	1.9502	1.5053	1.3352	0.0015	0.0028	0.0023	99.9231	No shaking
10/27/74	22	2.0572	1.9528	1.7008	-	0.0036	0.0035	-	Normal

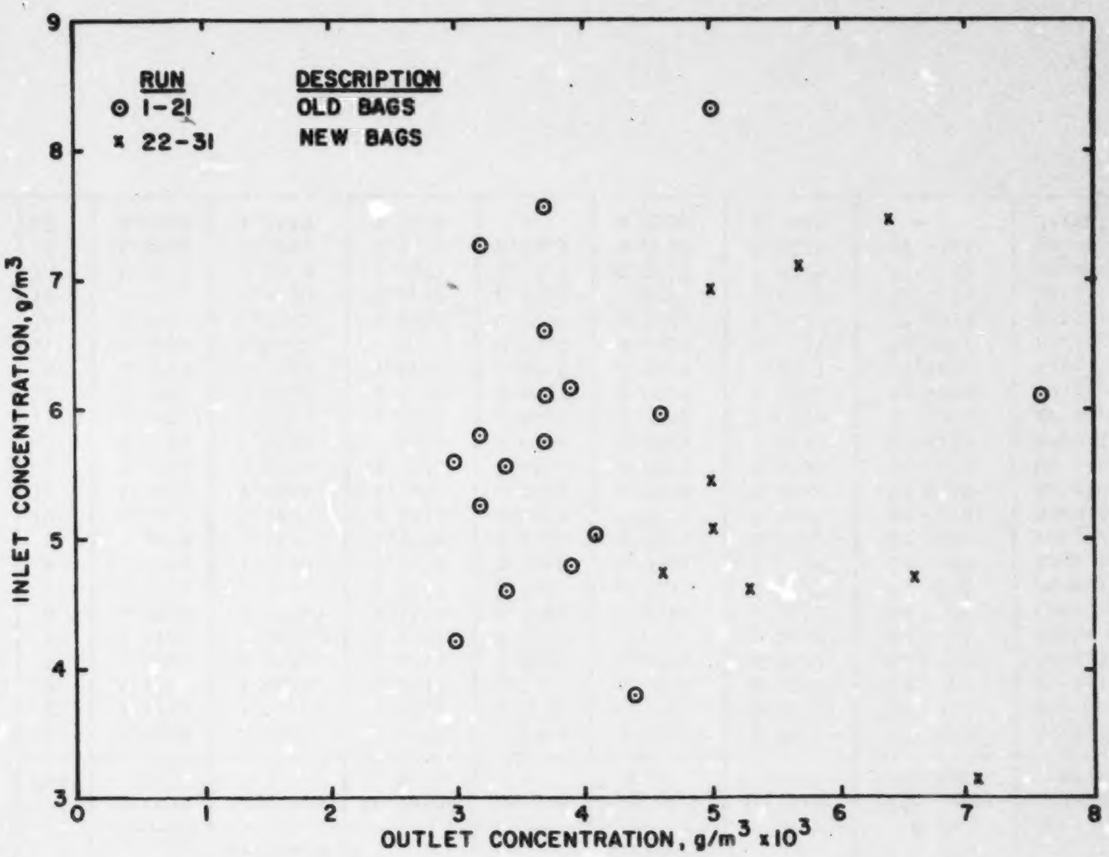

Figure 44. Inlet and outlet dust concentrations for Sunbury field tests

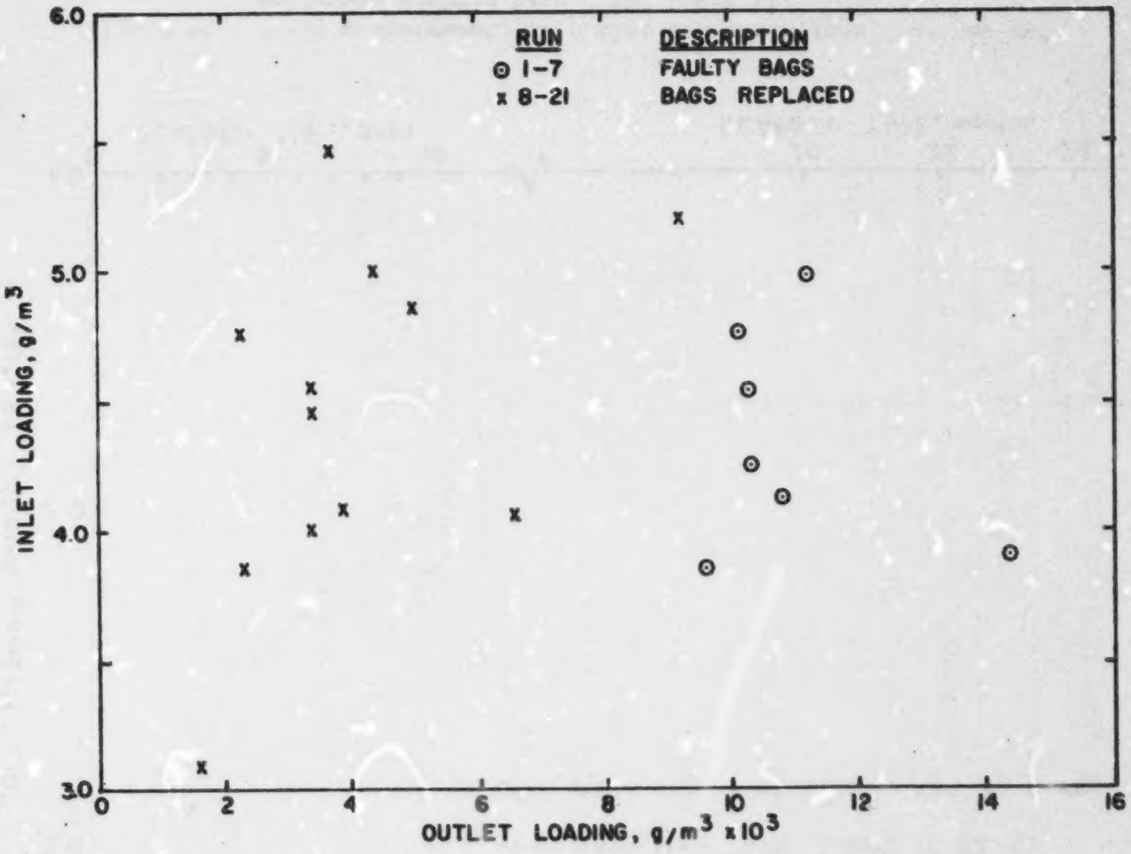

Figure 45. Inlet and outlet dust concentrations for Nucla field tests

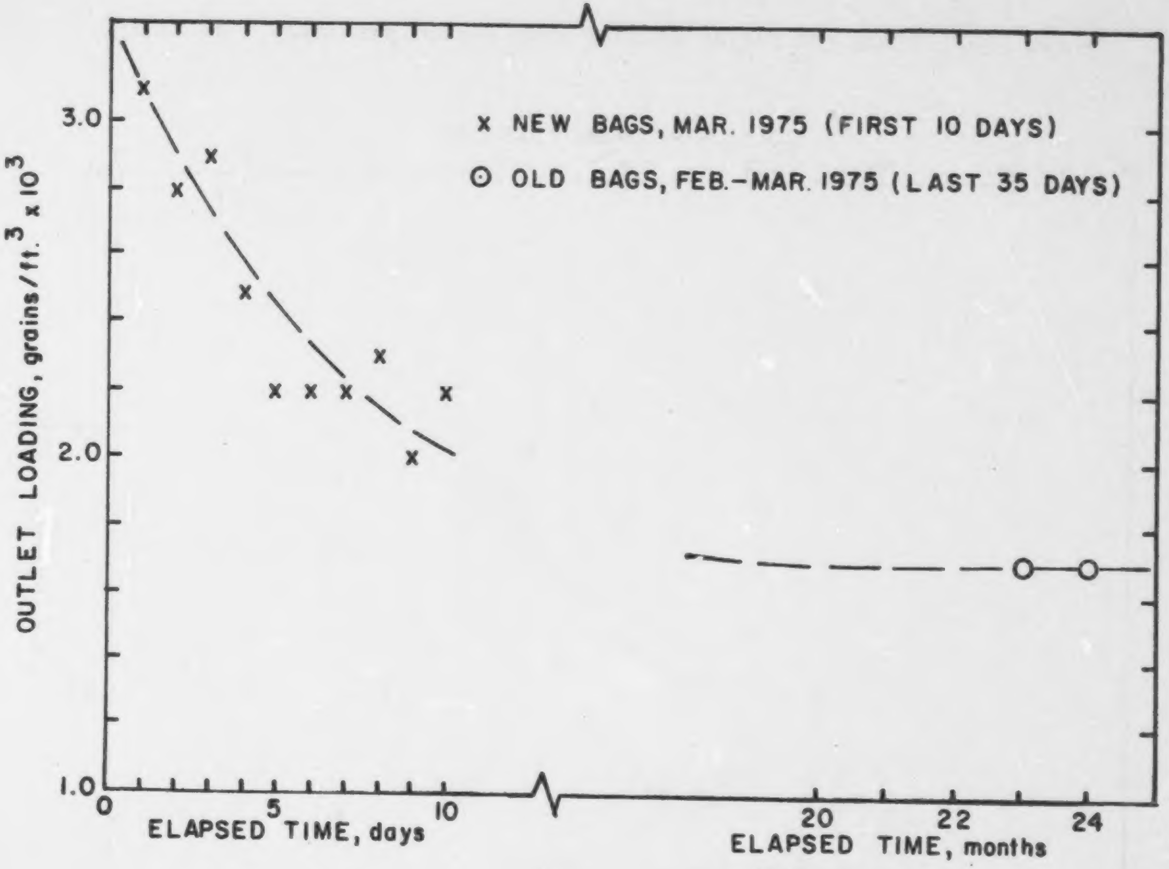

Figure 46. Field measurements of outlet concentrations from new and well-used Sunbury bags. See Table 11

SPECIFIC RESISTANCE COEFFICIENT

The operating mode for the fabric filter system used at the Sunbury Station did not allow the direct estimate of K_2 values because of a continuous cleaning schedule. Reference to Figure 43, for example, indicates that the interval between cleanings is too brief to detect any significant resistance versus loading trends. Additionally, any change in slope, $\Delta S/\Delta W$, reflects the integrated effect of a parallel flow through fabric surfaces of unequal dust loading. Therefore, without a complex differentiation process, the true K_2 values cannot be estimated.

On the other hand, many of the Nucla tests were carried out with very lengthy, 2 to 4 hour-filtering periods between cleanings. Hence it was possible to make determinations of K_2 for typical field aerosols. These results in both English and metric units are summarized in Table 12. A very detailed analysis of Nucla data relative to determining how reliably K_2 values can be predicted on the basis of dust and flow parameters is given in Section IX.

Table 12. MEASURED K_2 BASED ON FIELD TESTS AT NUCLA GENERATING SECTION

Run number	Measured K_2[a]	
	in H_2O min ft/lb	N min/g m
1-1-A	3.18	0.531
1-2-A	9.85	1.64
1-3-A	4.46	0.745
11-AB	6.03	1.00
14-AB	6.80	1.13
15-B	7.05	1.18
16-AB	6.76	1.13
16-B	6.76	1.13
19-1-AB	5.65	0.943
19-2-AB	5.95	1.16

[a] Based on actual face velocity of 2.76 ft/min (0.844 m/min), a flue gas temperature of 124°C, and an assumed dust cake porosity of 0.59.

Note: See Section IX and Table 36 for detailed analyses.

SECTION VII

BENCH SCALE LABORATORY TESTS

FABRIC RESISTANCE CHARACTERISTICS

Clean (Unused) Fabrics

Resistance measurements were performed on several samples of new and used glass bags from the Sunbury and Nucla power plants. These tests were made on 11 in. x 8 in. cloth panels which were clamped securely in the filter holder shown in Figure 5. An unsupported cloth area of 348 cm^2 (54 $in.^2$) (9 in. x 6 in.) was exposed. The results of tests on unused filters, Figure 47, were used to calculate Sunbury and Nucla permeabilities,[*] 42.5 and 112 ft^3/min, respectively. Independent measurements by FRL,[+] gave corresponding values of 54 and 86.5 ft^3/min. Since GCA and FRL used the same ASTM test methods, the differences are believed to result from the normal variability in fabric properties.

Cleaned (Used) Fabrics

Resistance measurements were also performed on several test panels removed from used Sunbury and Nucla filter bags shipped to the GCA laboratories. Because of handling, shaking, possible moisture absorption or chemical degradation, it is recognized that the laboratory measurements may not

---

[*] Volume flow (or air-to-cloth ratio) at 0.5 in. water filter resistance.

[+] FRL, Fabric Research Laboratories
1000 Providence Highway
Dedham, Mass. 02026

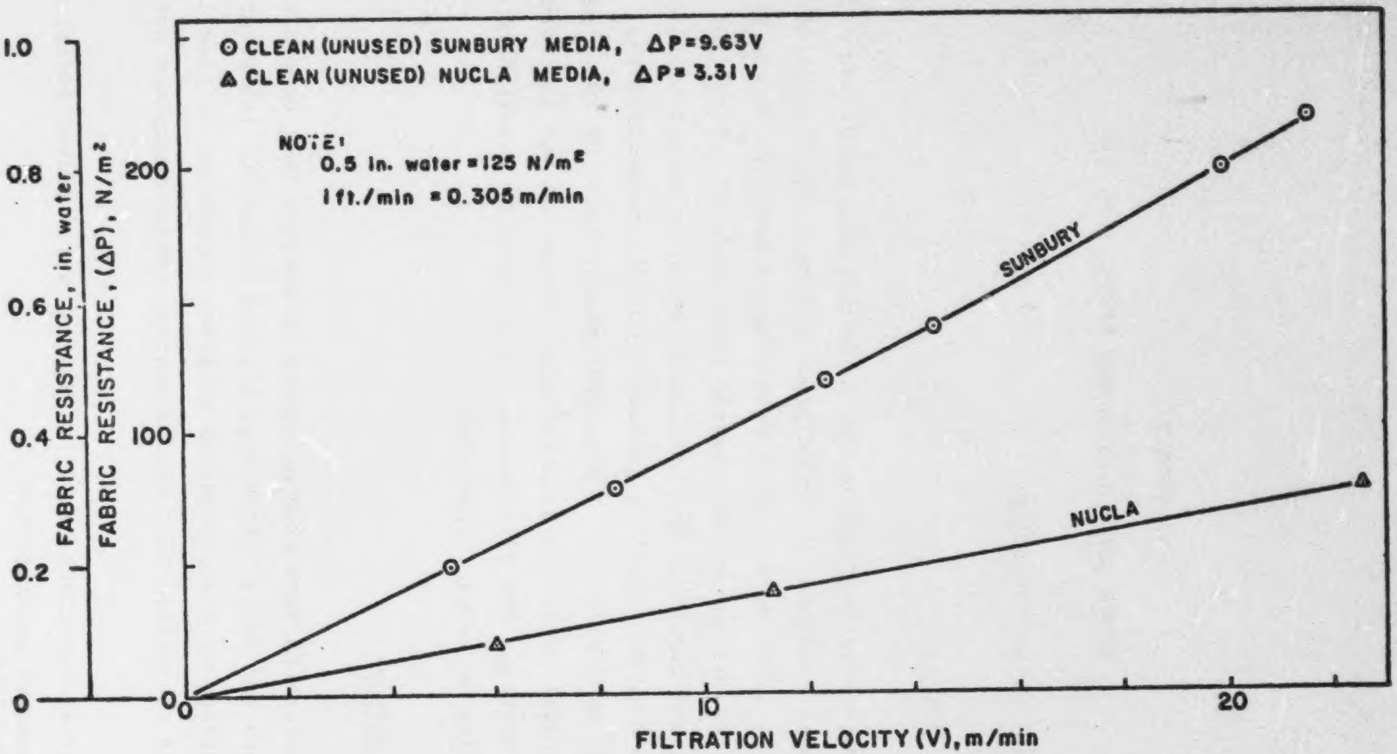

Figure 47. Filtration resistance for unused Sunbury and Nucla glass bags, laboratory measurements

represent true field conditions. However, it is believed that laboratory evaluation of the field media represent a useful supplement to the earlier field tests.

Prior to testing the used Sunbury and Nucla bags, a standard preparation and cleaning process was developed. The fabric test panels were first shaken by hand about 20 times at 1 cps to remove all dust that would fall off during normal handling of the filter. The clean air face was vacuumed to remove dust deposited during shipping, approximately 28 grams/m^2. During the latter process, there was negligible dust loss from the dirty air side. The three levels of cleaning applied to each test sample were arbitrarily defined as dirty, moderately cleaned, or well cleaned. The designations corresponded roughly to residual dust holdings of 135, 75 and 45 grams/m^2.

Figures 48 and 49 show resistance curves for fabric samples from the center sections of Sunbury bags removed from different bag compartments. Although test velocities were extended to the 10 m/min range with only minor deviations from a linear ΔP-V relationship, the plotted data were restricted to the probable filtration rates expected in the field. The code letters, T, C, and W appearing on Figures 48 and 49 refer, respectively, to the test number, bag compartment number, and the final fabric dust loading after cleaning the fabric panesl. Pressure velocity curves for the Nucla bags, Figure 50, indicate that the residual dust holdings for bags stated to have seen prior field service were exceptionally low. It was pointed out, however, that these bags had been stored in the open for some time such that considerable dust had washed off. In the case of bag No. 2, the resistance after cleaning returned to the same level observed for an unused (No. 3) bag.

Although these data are too limited to quantify, one might infer that the graphite-silicone treatment on the Nucla bags provides a greater dust unloading capacity than that for the Sunbury bags. This feature does not

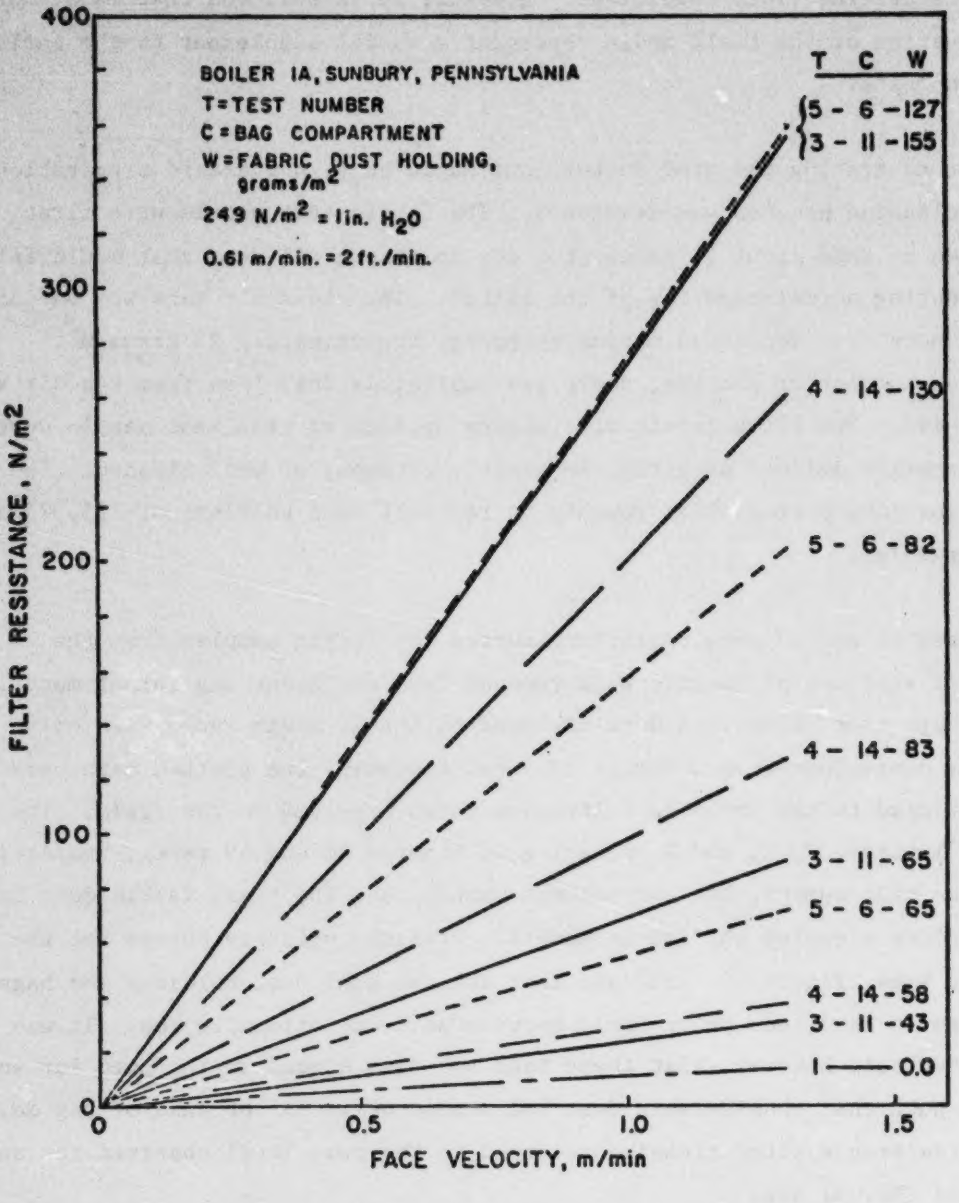

Figure 48. Resistance characteristics of used Sunbury fabrics cleaned in the laboratory to various residual dust holdings, Tests 1 to 5

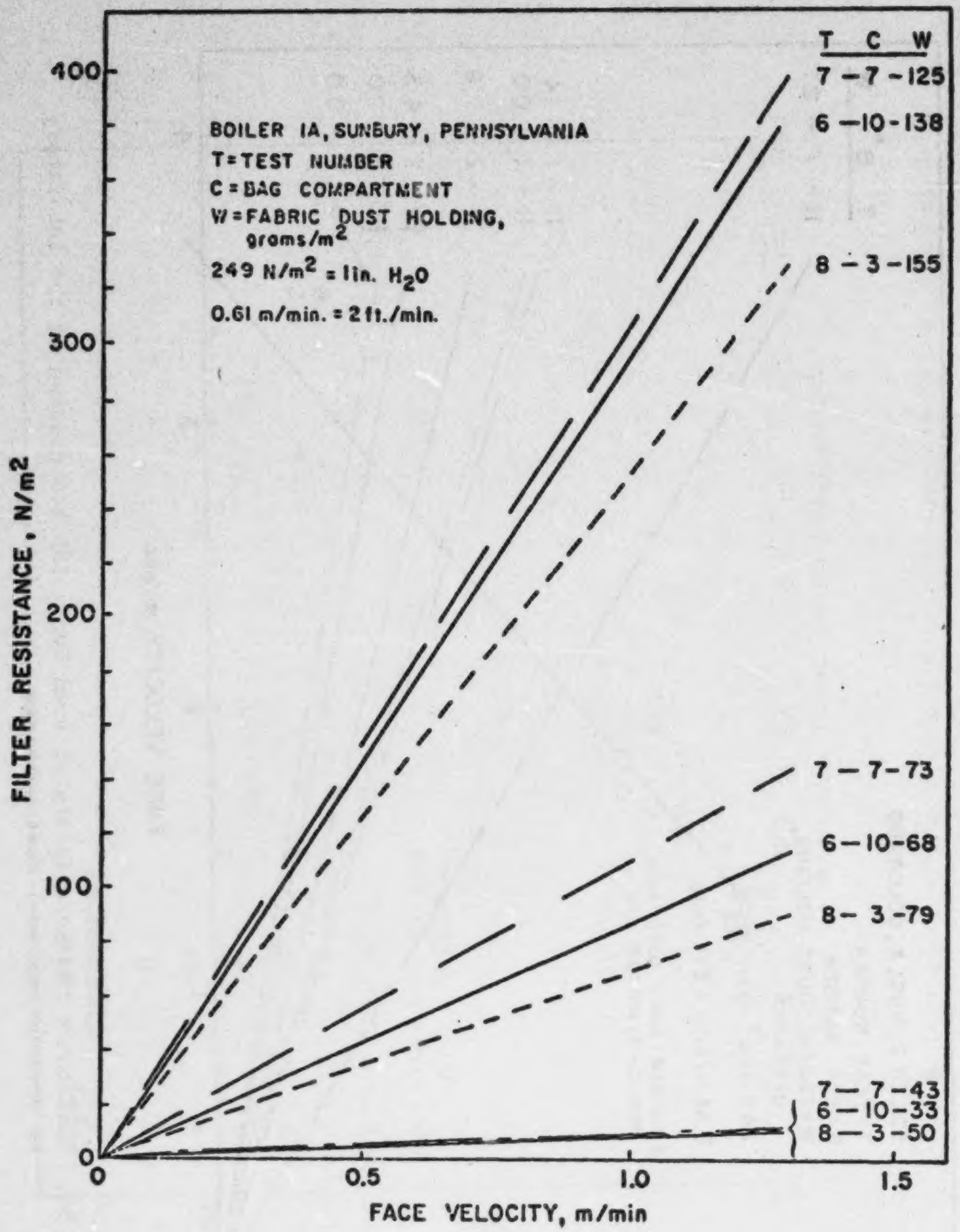

Figure 49. Resistance characteristics of used Sunbury fabrics cleaned in the laboratory to various residual dust holdings, Tests 6 to 8

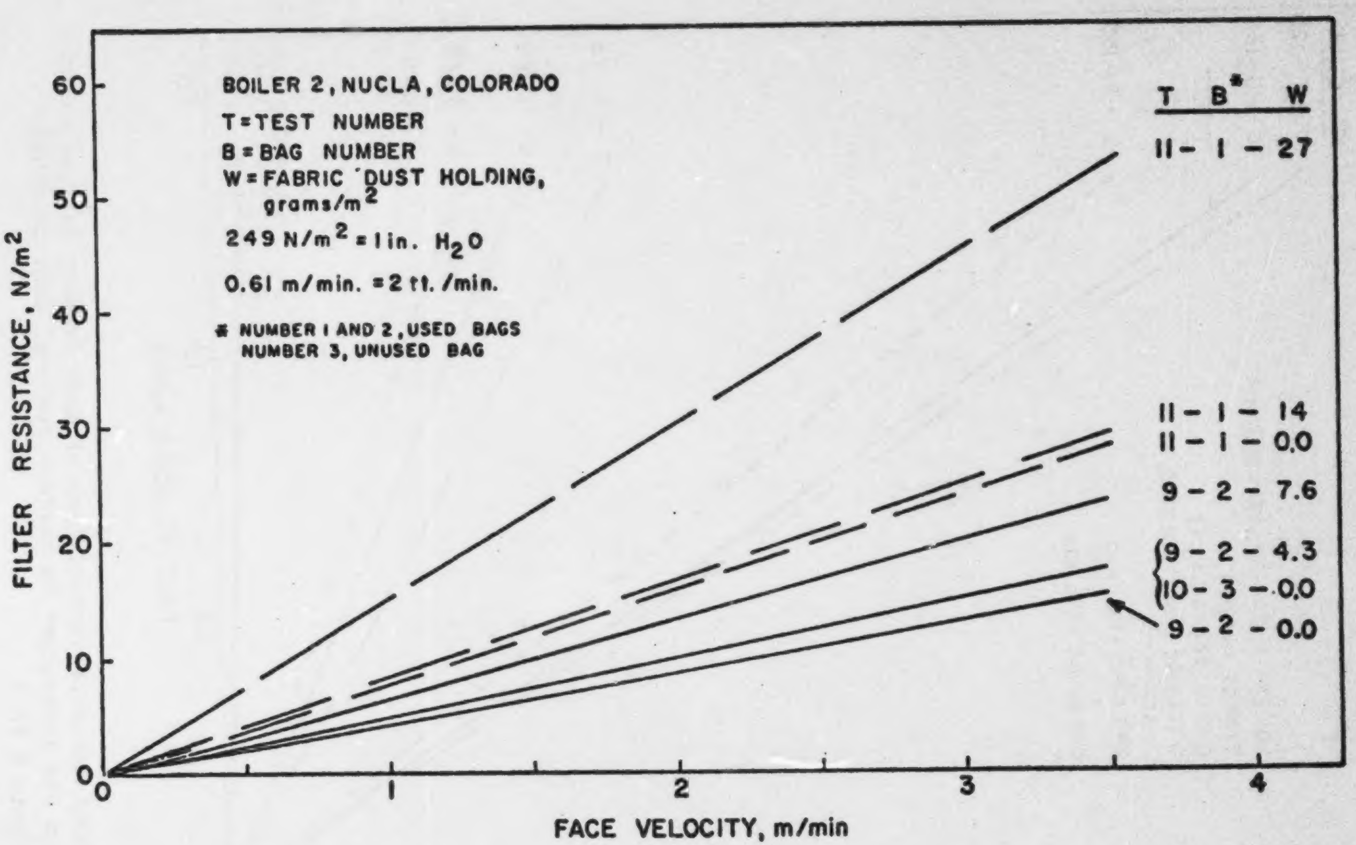

Figure 50. Resistance characteristics of used Nucla fabrics cleaned in the laboratory to various residual dust holdings

necessarily represent an advantage because it is the residual and deposited dust that provides the dust retention properties of the fabric. The effect of residual dust loading upon filter resistance is shown in Figure 51 for Sunbury media at 0.61 m/min (2 ft/min) filtration velocity. Despite the point scatterm the relation given by the empirical equation:

$$P = -72 + 1.68\ W_R \tag{17}$$

is in fair agreement with independent field measurements. For example, a resistance of 820 N/m^2 (3.3 in. water) is predicted by Equation (1) in contrast to an observed value of 670 N/m^2 (2.7 in. water) as shown in the field data of Figure 41. In Equation (17), P is expressed in Newtons per $meter^2$ and W_R in grams per $meter^2$.

Because of several unknown factors in field handling and the problems of simulating superficial and interstitial dust deposits by the laboratory shaking and vacuuming procedure, the point scatter noted in Figure 51 is not surprising. The minimal point scatter with low residual deposits suggests that the "most difficult to detach" particles must have rather specific alignment patterns and deposition sites.

It was not determined whether or not partial or complete blinding of some of the fabric pores had taken place during field use. On the other hand, if the hand cleaning and vacuuming of the field fabrics had not lead to uniform dust removal, a large point scatter would have been expected from fabric to fabric. This problem, which is treated in detail in later sections of this report, is described briefly in the following discussion. Reference to Figure 52 shows the form of resistance/fabric loading curves for GCA single bag filtration with cleaning by mechanical shaking. In both cases, dust removal was highly nonuniform with the actual surface consisting of two distinct regions, the first from which slabs of dust were separated from the fabric-dust interface, leaving a relatively clean area below and the second from which no dust was removed.

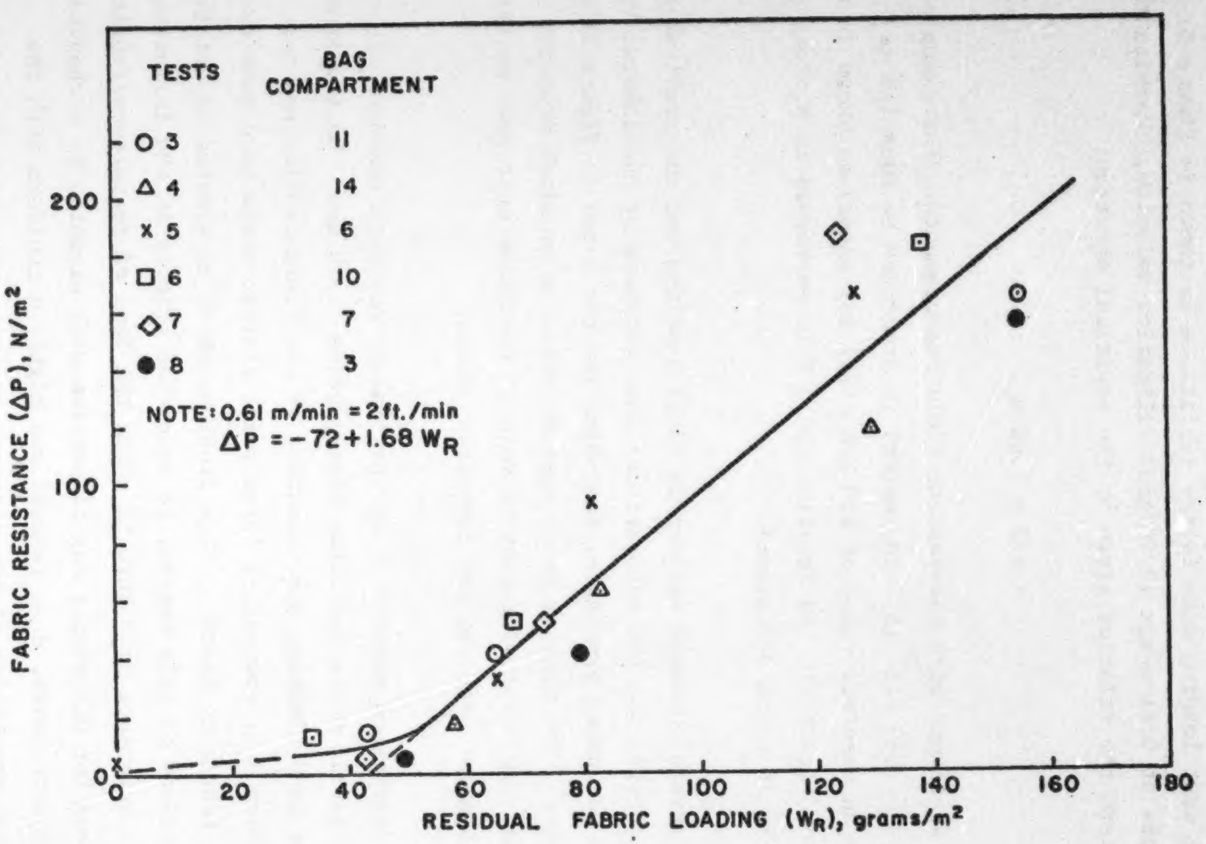

Figure 51. Fabric resistance versus residual fabric loading for Sunbury bags at 0.61 m/min (2 ft/min) filtration velocity

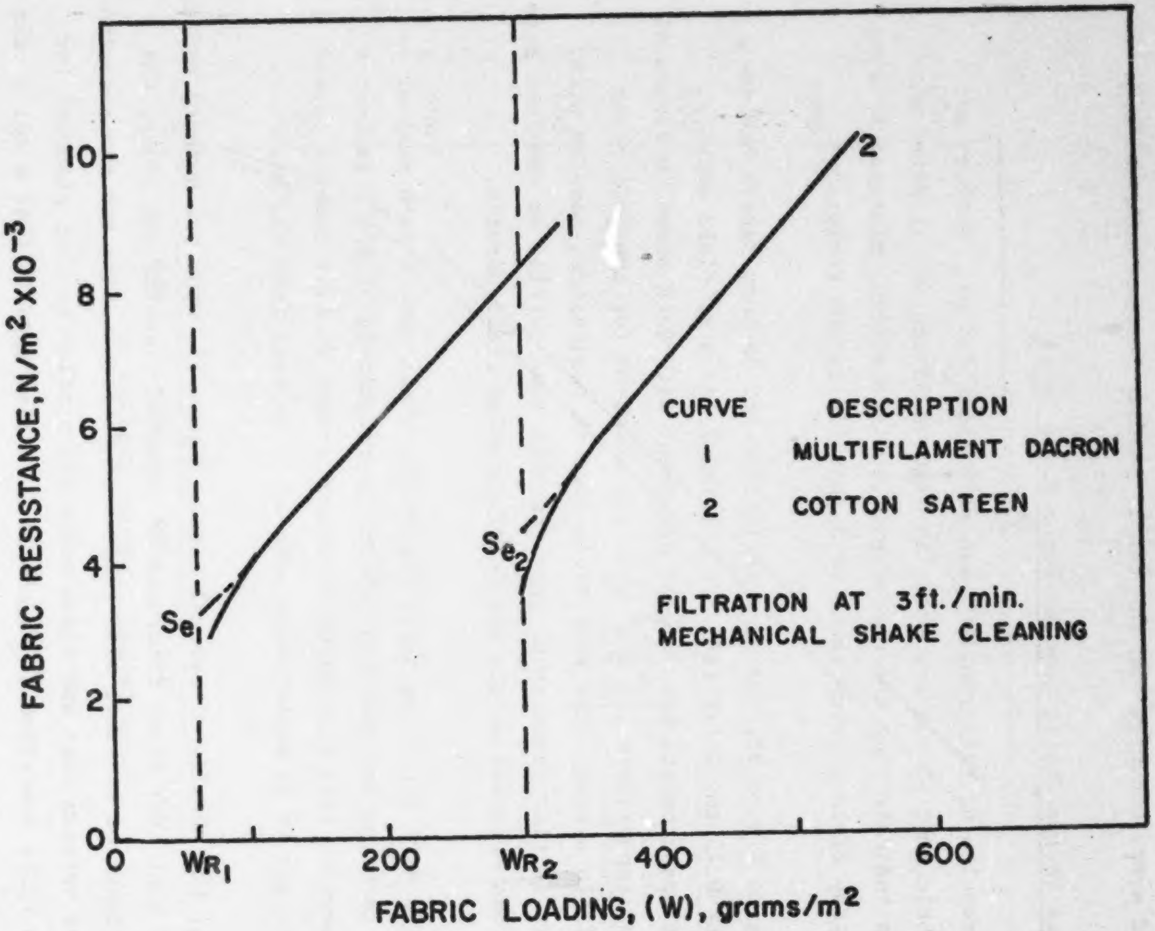

Figure 52. Typical resistance versus dust loading curves for fly ash filtration with staple and multifilament yarns

The net result is a parallel flow system in which each element has initially a different air flow (and dust loading) rate. As the filtration process continues, the flow and deposition rates through the cleaned and uncleaned areas converge and the fabric loading becomes more uniform.

Resistance Versus Fabric Loading-Bench Scale Tests

Typical results of filtering GCA ash with clean and used Sunbury and Nucla fabric test panels are shown in Figures 53 and 54. Limited measurements indicate that the characteristic interstitial plugging arising from lengthy field service leads to higher filtration resistance.

According to Figure 53, the base resistance for Sunbury fabric had increased by 0.75 in. water (185 N/m^2) after 2 years of field service. The above measurements are in good agreement with data shown in Figure 41 wherein an approximate 125 N/m^2 gain was observed for the full scale Sunbury field system. The more rapid rise in resistance, coupled with the higher initial resistance, suggests that some partial or complete pore blinding has occurred as the result of extended field service.

Comparative data for Nucla bags, Figure 54, which show a much smaller resistance increase for the used fabric (approximately 50 N/m^2) reflect a shorter service life plus an undetermined amount of dust removal caused by bag storage in an unsheltered area after removal from the baghouse.

Generally, the results of several tests, Figure 53, upon new Sunbury media, indicated that over short intervals of repeated cleaning and reuse, the initial change of pressure with respect to fabric loading and the resistance difference between used and clean media was similar to that observed for the Nucla tests described in Figure 54. It also appears that a solid cake formation has developed for both Nucla and Sunbury fabric after the fabric dust loading reaches about 175 g/m^2 (0.036 lb/ft^2) because slopes of the resistance-loading curves undergo no further change. The estimated K_2

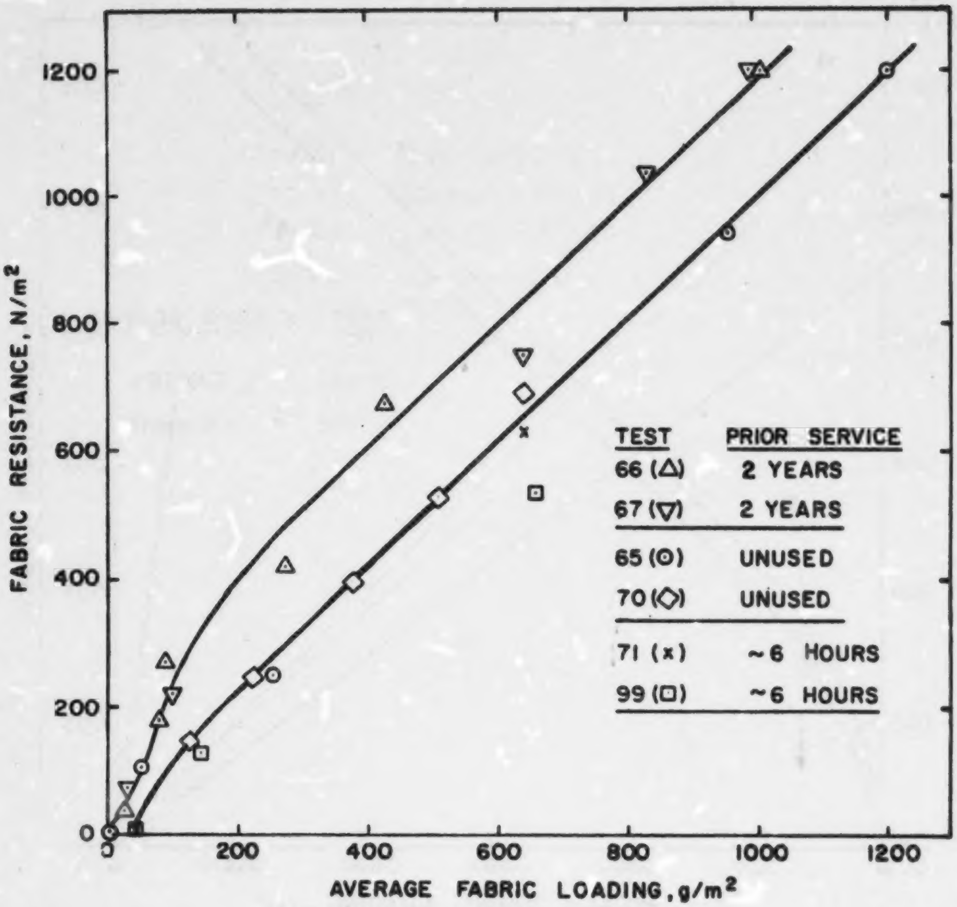

Figure 53. Resistance versus average fabric loading for Sunbury fabric with GCA fly ash at 0.61 m/min face velocity

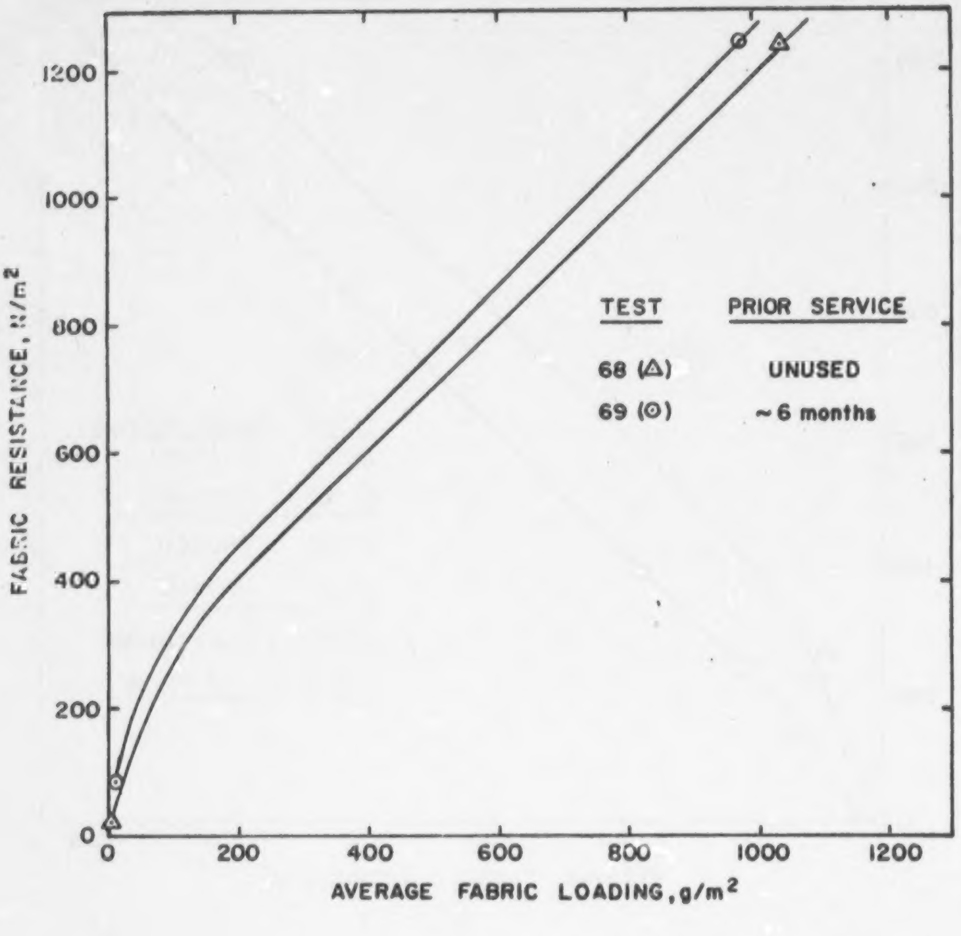

Figure 54. Resistance versus average fabric loading for Nucla fabric with GCA fly ash at 0.61 m/min face velocity

value in metric units, about 1.6 N min/gm (9.6 in. H_2O min ft/lb) was slightly lower than that reported previously for the filtration of GCA fly ash with cotton, 1.85 N min/gm. However, as will be discussed later, present tests indicated that corrections for differences in filtration velocity (0.92 m/min in prior GCA tests)[10] converted the K_2 value of 1.6 to 1.95 N min/ g m.

Filtration tests were also performed with other dust/fabric combinations, Table 13. Resistance/fabric loading curves and tabulations of key parameters deriving from these measurements are given in Figures 55 and 56 and Table 18, respectively. It is emphasized that the tests described in Figures 53 through 56 typify the behavior of uniformly loaded filters. Once the filter undergoes a partial cleaning, a decidely nonuniform loading condition prevails as mentioned previously.

Table 13. FABRIC/DUST COMBINATIONS STUDIED IN THE LABORATORY PROGRAM

Fabric	Dust
Sunbury (Menardi) glass bags, 3/1 twill	GCA fly ash Lignite Rhyolite
Nucla (Criswell) glass bags, 3/1 twill	GCA fly ash Lignite
Cotton sateen	GCA fly ash
Dacron crowfoot weave	GCA fly ash

DUST DEPOSITION AND REMOVAL CHARACTERISTICS

Deposition on Used Fabrics

The appearance of dust-laden and cleaned Sunbury fabrics was observed directly and microscopically to provide improved assessments of the overall filtration process. The photomicrographs prepared during this phase of the study answer several important questions as to (1) the disposition

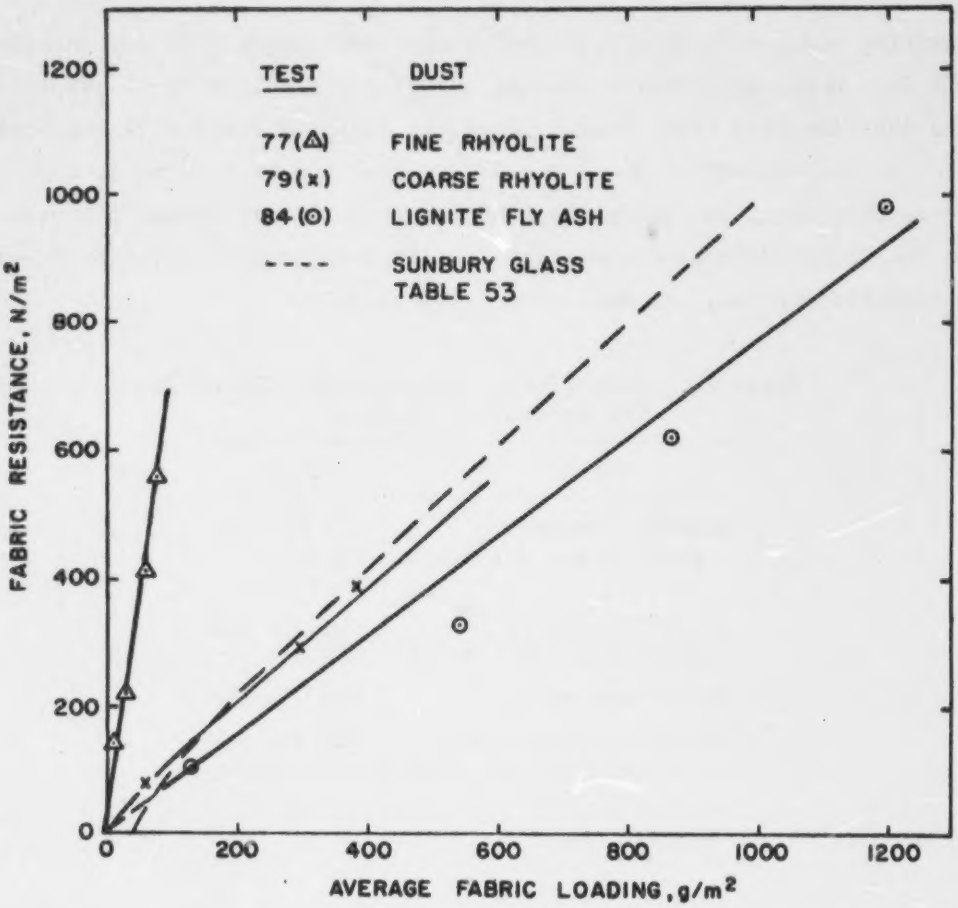

Figure 55. Filtration of granite dust (rhyolite) and lignite fly ash with Sunbury fabric at 0.61 m/min face velocity

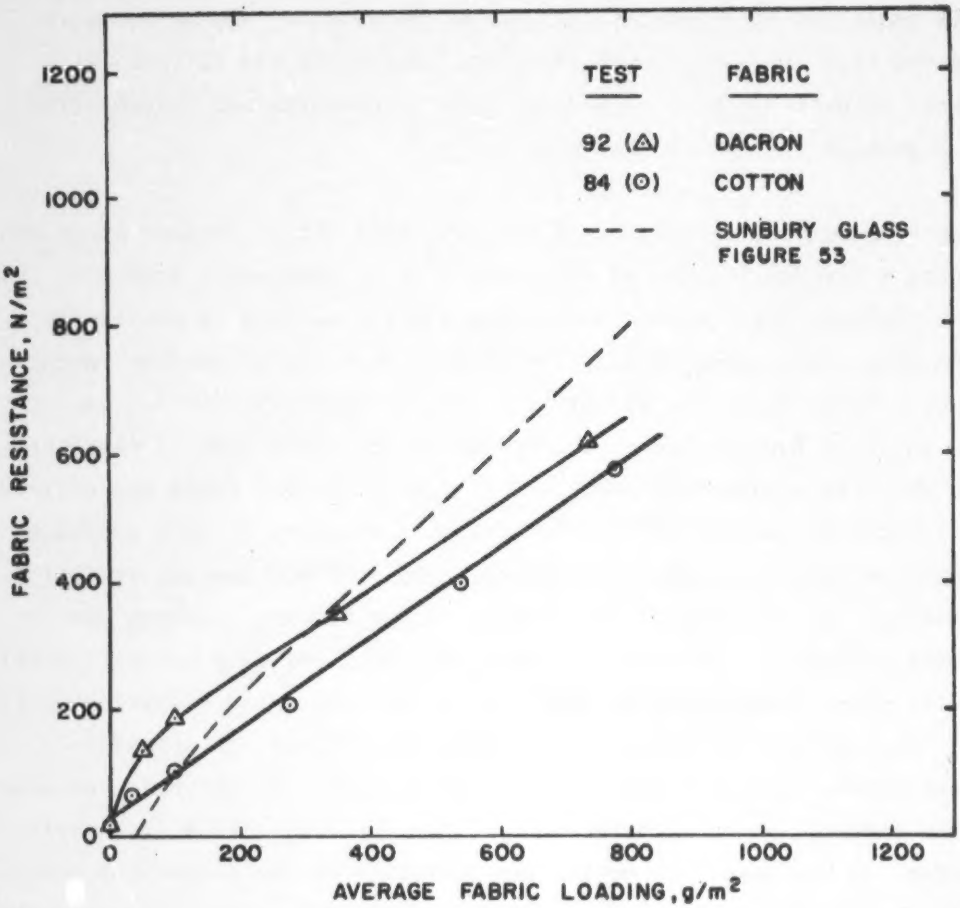

Figure 56. GCA fly ash filtration with unused sateen weave cotton (unnapped) and Dacron (crow foot weave) at 0.61 m/min face velocity

of the dust on the filter following cleaning, (2) the manner in which dust is detached, (3) the description of the dust cake per se, (4) the physical appearance and probable location of leak points on the filter, and (5) the appearance of the clean air side (warp surface) of the new filter fabric after 8 hours of fly ash filtration. The samples of filter fabric discussed in this section were removed from 6 in. x 9 in. test panels installed in a bench-scale system, Section IV, Figure 5. A resuspended coal fly ash aerosol described previously was filtered at a velocity of 0.61 m/min (2 ft/min) at inlet concentrations ranging from 2 to 3 grams/m^3 (1 to 1.5 grains/ft^3).

Figure 57 shows the appearance of the filtering (fill) surface after depositing a fly ash loading of 945 grams/m^2 on a previously used and cleaned Sunbury bag. At 20X magnification, the surface is relatively smooth with only a minor indication of the clean fabric surface perturbations. Grain detail is discernible down to approximately 2.5 μm. After inducing fabric flexure by depressing the clean side, a characteristic checking or cracking results which, under normal field bag collapse, is a prelude to dust release. The general appearance of this cracking resembles a highly polished and etched metal specimen showing crystal boundaries. In the case of the fabric, Figure 57, the cracking pattern conforms roughly to the maximum continuous length of warp yarns (500 μm) and fill yarns (approximately 2000 μm) as exposed on the filtering (fill) face. The far greater curvatures at warp yarn crossovers appear to represent cake failure zones where fabric curvature is altered. Because of this checking process, detachment of the dust layer from its fabric interface is hastened. By noting the curvature of the supporting fabric matrix during flexure, it is suggested that tensile, shear, and compressive properties of the dust layer might be estimated.

Figure 58 shows another fabric sample with a terminal fly ash holding of only 430 grams/m^2. Although the basic appearance is unchanged (see Figure 57, the shadowing technique indicates clearly the ridges or raised

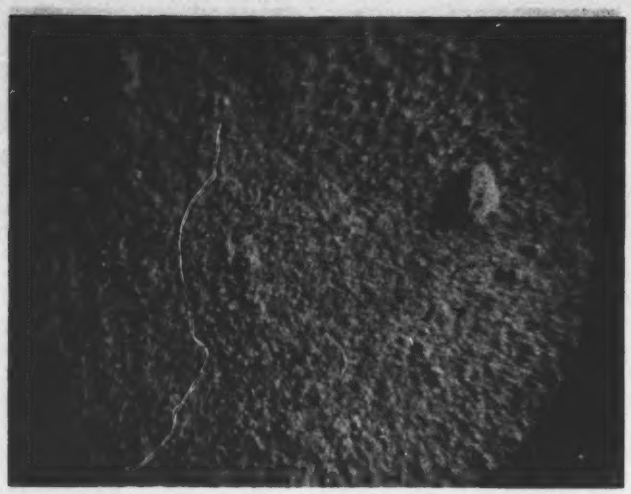

A. Dust surface prior to cleaning

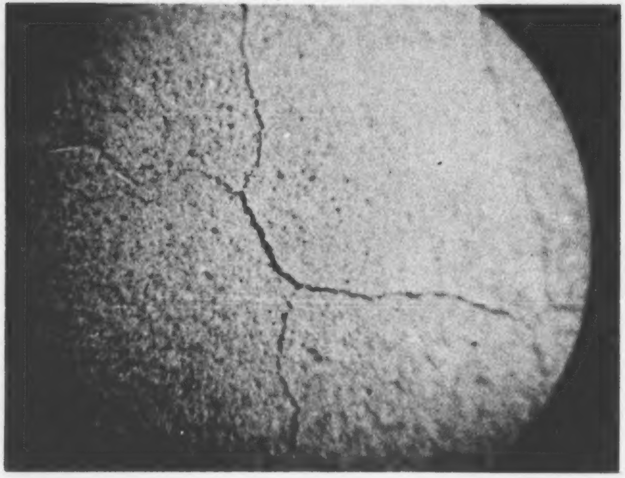

B. Checking or cracking induced by flexure

Figure 57. Fly ash dust layer on Sunbury fabric, laboratory tests prior to removal of 945 grams/m^2 cloth loading (20 X magnification)

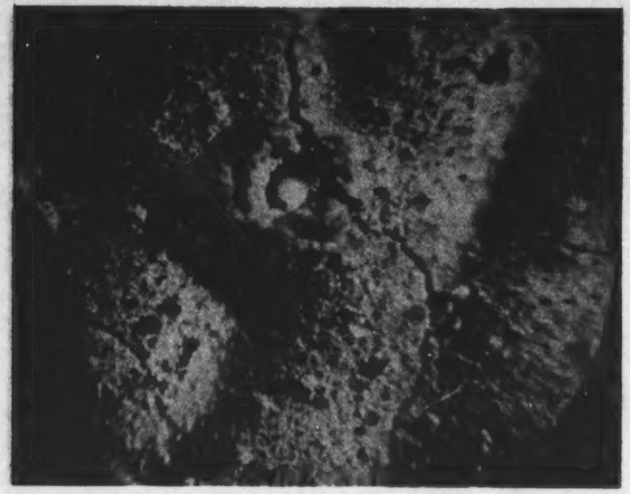

Figure 58. Photomicrograph of Sunbury media showing GCA fly ash loading with pinhole leak and cracks induced by flexure

diagonal portions caused by the underlying fill fibers. It is concluded that the presence of the supporting matrix is probably detectible except for very high surface loadings, approximately 1200 grams/m^2. A full-size and a three times enlargement of the same filter shown in Figure 58 with 430 grams/m^2 surface loading, indicate clearly in Figure 59 the ridge patterns mentioned previously. Both figures also indicate pinholes or punctures that can contribute significantly to dust penetration.

Pinholes and Air Leakage

Figure 59 reveals several surface perturbations whose true details are better evidenced in Figure 58. Aside from small depressions caused by the impact of occasional massive particles (probably agglomerates) of the order of 200 μm diameter, several "ant-hill" type mounds appear on the fabric surface. Substage microscope illuminations reveal these structures to be associated with open pores with diameters ranging from 100 to 200 μm. The circular ridges of dust surrounding these openings (pinholes), estimated to be about 1 mm high, result from the inertial separation of particulates as the aerosol changes direction and accelerates to flow through the apertures. The presence of these surface deposits points out that at least some of the dust is collected from that fraction of the air that leaks through these pores. A pore (pinhole) count indicated a concentration of 2500 per m^2 of the pore type shown in Figure 60A, Test 65-F.

Inspection of Figure 60B shows that a pinhole may act as a focus for the cake cracking process. This bears out an earlier observation that cracking or checking is initiated at the points of maximum yarn curvature; i.e., the yarn crossing points. Although it did not appear at first that an observed pinhole concentration of 2500 per m^2 would affect significantly the filter behavior, a subsequent analysis indicated that the pinhole flow was significant. It was noted that all pinholes were located above Type I and Type II pore openings in the fabric. Thus, the projected areas of the pinholes were essentially as described in Section V, Figure 28,

Full scale

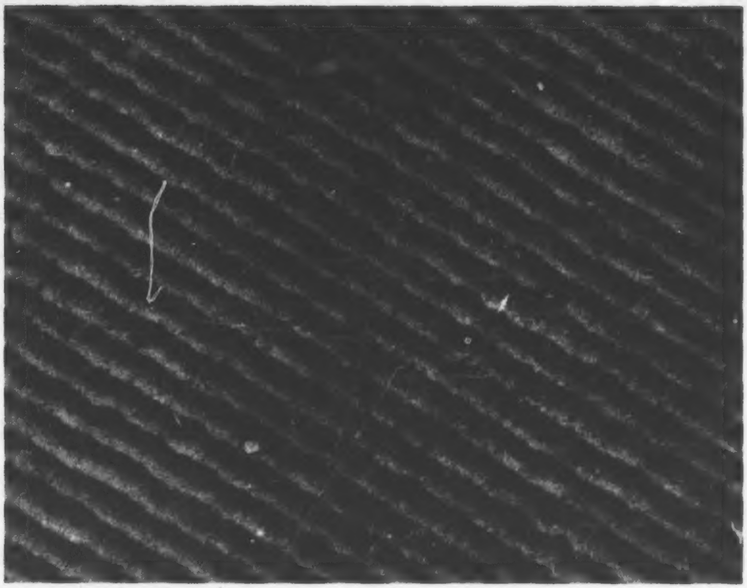

Enlarged 4/1

Figure 59. GCA fly ash deposit on previously used Sunbury fabric showing crater and pinholes, 430 grams/m^2 cloth loading

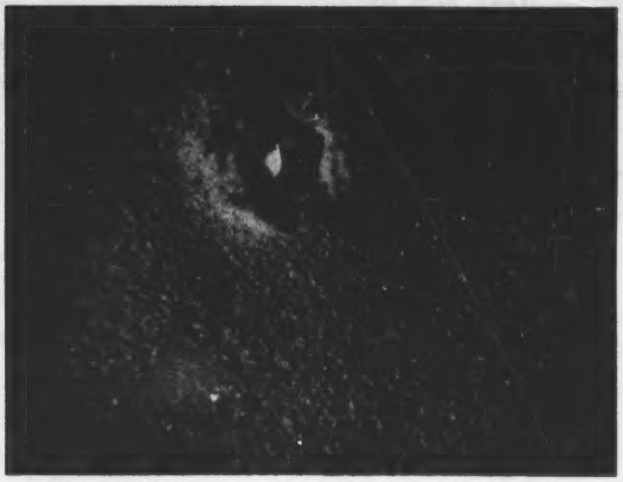

Pinhole leak, filtration surface, showing characteristic mound, substage lighting (20X magnification)

Pinhole leak as focus for radiating checking. Pore accentuated by substage lighting (60X magnification)

Figure 60. Pinhole leak structures, GCA fly ash filtration on Sunbury fabric

while the effective cross section defining the air flow should appear as shown in Figure 30. If one assumes that the interstitial air flow remains well within the laminar range, $N_{Re} \simeq 100$ to 200, Equation (18) may be used to calculate average (pinhole) velocity when the pore dimensions and filter resistance are known:

$$V = 10\ \Delta PM^3/2\mu L \tag{18}$$

The resulting calculation for a pressure differential of 1000 N/m^2 (4 in. water), pore depth (filter thickness) of 0.04 cm, and an average pore area of 2.27×10^{-4} cm^2 gives a pore (pinhole) velocity of 3230 cm/sec (6350 ft/min). The average pore cross-sectional area is that based upon best estimates of minimum pore dimensions, Figure 30 and Table 5. A second estimating procedure is to treat a pinhole opening as a sharp edge orifice so that the velocity is defined by the relation:

$$V_{(cm/sec)} = C_o\ 128.3\sqrt{\Delta p\ (N/m^2)} \tag{19}$$

Because the pinhole diameter is infinitely small relative to the flow cross section on either side of the filter, the orifice coefficient C_o, is approximately 0.62, irrespective of the flow type. By means of a trial calculation, the N_{Re} value was redefined, thus providing an improved estimate of 0.66 for C_o. The final outcome was a slightly lower value, 2650 cm/sec (5206 ft/min) for pore velocity. Even when the more conservative (lower) velocity was used to determine the fraction of the total filter flow that passed through the observed pore area (roughly 1.89×10^{-2} cm^2 for the 83 pinholes in the panel), the calculation indicated that nearly 14.1 percent of the air passed through these pinholes. Therefore, if dust removal were 99.5 percent or better for the undisturbed cake and zero percent for the pinholes, one would expect a weight collection efficiency of 86.5 percent. Actually, the sharp convergence of the streamlines for that fraction of the flow passing through a pinhole results in considerable dust collection as can be seen in Figure 60. Based on the angle of the incident surface illumination, approximately 45 degrees, and the shadow dimensions, the average height of the larger pinhole mounds is about 1 mm. By simple geometric approximations and as an estimated deposit density of 0.82 grams/cm^3, the amount of dust surrounding each pore is estimated as about 6.2 x 10^{-4} grams. Details for determining the density of the superficial dust layer are discussed in the next section. In the case of the test results illustrated in Figure 60 very few pinholes were visible when the test panel was removed for weighing after 33 grams of dust had been deposited. As the result of accidental jarring and flexure, however, it is postulated that the dust layer was cracked causing the pinhole leaks observed at the completion of the dust loading tests. The final dust deposit of 42 grams was equivalent to a cloth loading of approximately 1200 grams/m^2. Until the apparent damaging of the filter layer, the mass efficiency measurements over the filter loading process had ranged from 99.26 to 99.88 percent with an average value of 99.67 percent. However, during the pinhole leak period the average efficiency reduced to 96.67 percent based upon gravimetric analyses of filter samples.

A summary of the filtration parameters shown above is given in Table 14. There appears to be no positive time trend in either outlet concentration or collection efficiency until the last phase of the filter loading. Here, as indicated previously, the dust layer must have experienced severe internal damage, including the rupture of particle-to-fiber bonds at the dust/fabric interfaces.

At reduced pressure differentials during the early phase of filter loading, the predicted pore velocities are much lower if the concept of capillary flow is assumed, Figure 61. It is difficult, however, to state which geometric concept applies to the actual pinholes. If our interpretation of Figure 60A is correct, it would appear that the pore consists of a bell mouth entry converging over a depth of 2000 μm from a diameter of

Table 14. FILTRATION CHARACTERISTICS OF NEW (UNUSED) SUNBURY FABRIC WITH GCA FLY ASH[a]

Fabric dust loading[b] grams/m^2	Pressure drop		Outlet concentration[c]		Weight collection efficiency percent
	N/m^2	In. H_2O	grams/m^3 x 10^3	grains/ft^3 x 10^3	
130	170	0.68	9.2	4.00	99.26
210	210	0.84	1.8	0.783	99.88
250	240	0.96	5.3	2.31	99.52
345	320	1.28	2.1	0.913	99.93
960	950	3.80	3.5	1.52	99.88
1,200	1,200	4.80	99.0	43.0	96.67

[a] Test No. 65 A-F performed on flat test panel, 0.0348 m^2 (9 in. x 6 in.) at 0.61 m/min (2 ft/min). Average inlet concentration 2.6 grams/m^3 (1.1 grains/ft^3).

[b] Indicated fabric loading based on weighing test panel and its holder.

[c] Outlet samples collected on all-glass, Method 5 type filters.

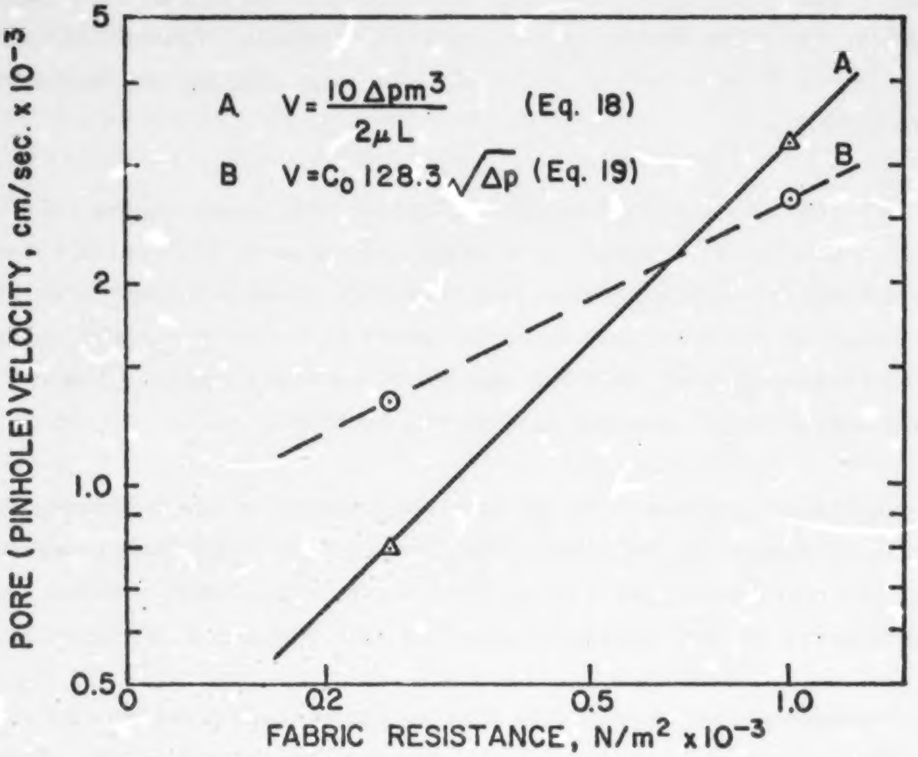

Figure 61. Estimation of pinhole velocities by capillary (A) and orifice (B) theory for fly ash loaded Sunbury fabric

roughly 750 μm to channel diameter of 350 μm. The channel depth is the sum of the mound height (1000 μm) and dust cake thickness (1000 μm).

Within the fabric structure itself, the channel seems to decrease abruptly in cross section to that of the Type I or Type II pore openings (approximately 200 μm) shown in Figure 30. The fact that the channel diameter decreases from about 350 to 200 μm over a distance of 100 μm, Figure 30, suggests that the orifice approach might be more appropriate for velocity estimates, at least at the higher resistance levels. Conversely, at lower resistances, viscous losses rather than inertial factors may dominate the flow picture.

The fact that the measured weight collection efficiency during test 65-F was 96.7 percent as compared to a predicted value of 86.5 percent based upon estimated average pore velocity and pore cross-sectional area is attributed to the following factors: overestimation of pinhole velocity and/or cross-sectional area and neglect of particle removal from the actual volume of air passing through the pinhole.

The results of previous permeability measurements on clean Sunbury fabric, Section V, Figure 21, indicated that laminar flow conditions persisted until the pore velocities reached 1000 m/min. The former results are in rough (factor of two) agreement with the data presented in Figure 61.

It is suspected that appreciable dust collects about a pinhole or oversize pore when gas velocities through the opening are not excessive. However, in the case of a sudden dislodgement of the dust mass bridging a pore, high, ~ 900 to 1500 m/min velocities rapidly lead to a steady state collection/reentrainment condition such that net particle removal from the gas penetrating the pore is negligible.

A distinction should be made between those openings or pinholes that are present when filtration is initiated through new or cleaned fabric areas and those openings that can be seen during the later stages of filtration when lowered efficiencies have been observed.

When filtration begins, the actual number of open pores is determined by the weave or thread count and yarn proximity. Because there are a large number of openings, the air velocity through any one pore is not sufficiently large to prevent a gradual accumulation of dust in the form of bridging over the pore entrance. Provided that the range in effective pore diameter is not excessive (a necessary fabric characteristic for high efficiency filtration), complete pore bridging can usually be accomplished before particle reentrainment rate equals or exceeds particle deposition rate.

If the range in pore (interyarn spacings) is too large, complete bridging of most of the pores may take place while a few still remain open. Due to the much lowered resistance to air flow compared to the caked-over region of the filter, the air velocities through the remaining openings as described for test 65-F become too high to allow particle deposition. Hence, a permanent opening(s) remains and increased particle penetration takes place. It is emphasized that rough handling, shock, or vibration may also dislodge dust blocking a pore(s) so that the same problem arises; i.e., no further chance of sealing the opening until the filter is cleaned for the next cycle.

In any case, it appears reasonable to assume that a few pinholes may contribute significantly to effluent loadings when fabric loadings (and fabric resistance) are high. Therefore, it becomes very important to determine which factors cause pinhole formation in industrial practice. One can postulate that poor quality control in fabric manufacture or careless handling during bag sewing, shipping, and system installation can lead to breaks, discontinuities or oversize pore openings. In addition, gross mechanical vibrations, fan pulsation, sticky dampers or other accidental disturbances may lead to unintended cake flexure that initiates penetration at critical pore openings.

Fabric Appearance After Cleaning

Previous microscope observations, Figures 57 through 60, have revealed the filter surface characteristics before any dust removal took place such as the texture of the dust layer, the presence of pinhole leaks, and particularly the cracking or checking of the dust cake induced by flexure. It appears that this cracking process, shown again at 60X magnification in Figure 62, is a necessary precursor to cake detachment. The photomicrographs of Figure 63 provide informative sectional views of the checking process as the loaded fabric is viewed from the edge. In Figure 63A a crack can be seen developing above the warp yarn (end view) that overlaps the fill yarn upon which much of the visible cake lies.

The density of the surface dust layer was estimated by carefully excising measured slabs of dust (length, width, and depth) followed by weighing on an analytical balance. This process indicated an apparent bulk density of 0.82 grams/cm^2. If one measures the actual depth of the dust layers shown in Figure 63 based upon 20X magnification, they are seen to be roughly consistent with the average fabric loadings determined for the filter prior to preparation of samples for photomicrographing.

When the loaded fabric is gently flexed, the dust falls as flakes or slabs as shown in Figure 64. It has been stated previously that the main point of separation takes place at the dust/fabric interface. Although the focal depth at 60X manification does not allow for clarity at the fabric surfaces when the outer surface of the dust is in sharp focus, the use of substage illumination shows very clearly the light transmitted through the cleaned portions of the filter. By focusing upon the resultant fabric surface after detachment of the dust layer, Figure 64, it can be seen that the warp yarns (the light regions) retain relatively little dust while the fill yarns hold much larger quantities within the bulked staple material.

Figure 62. Checking or cracking of deposited fly ash layer on glass fabric by intentional flexing (60X magnification). Test with clean (unused) Sunbury fabric with cloth loading of 945 grams/m^2

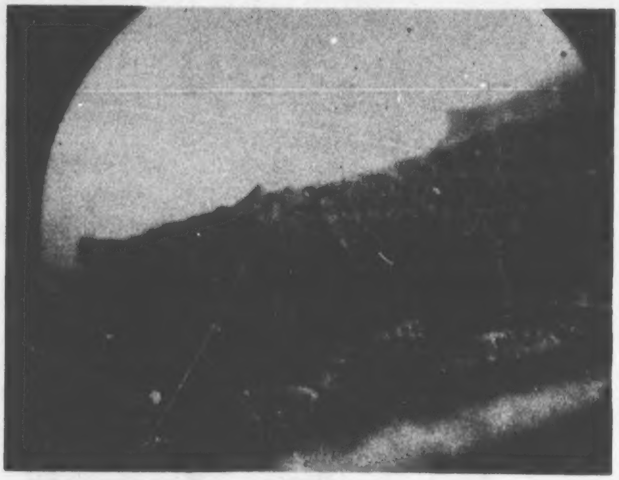

Edge view warp yarns seen on end, cloth loading order approximately 1200 grams/m^2

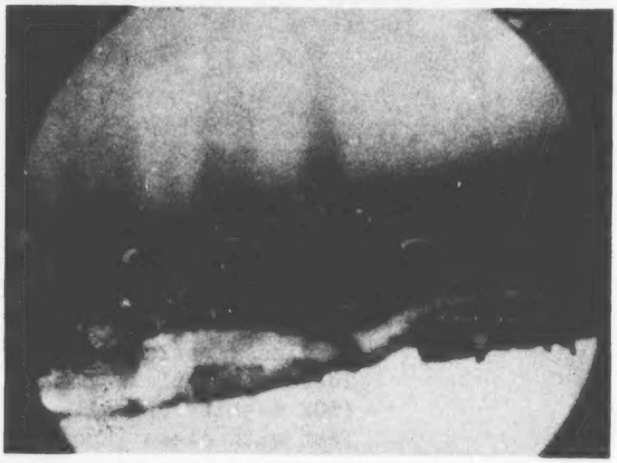

Edge view showing checking and fill yarn cloth loading approximately 440 grams/m^2

Figure 63. Dust cake as seen in sectional views with GCA fly ash on Sunbury fabrics (20X magnification)

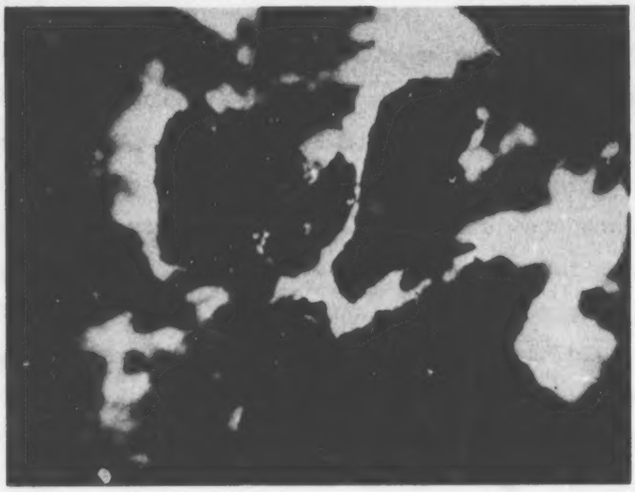

Filtering face immediately preceding cake dislodgement. Bright, out-of-focus regions, are clean, warp yarns (60X magnification)

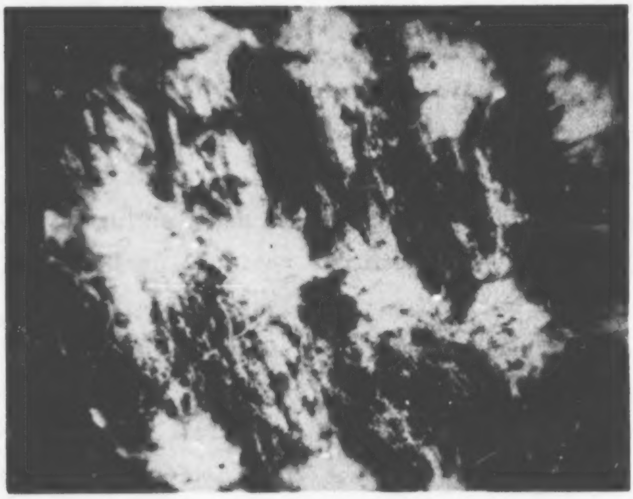

Filter surface after cake dislodgement showing relatively clean (bright) warp surfaces and residual dust on fill surfaces (20X magnification)

Figure 64. Before and after appearance of dirty and cleaned Sunbury fabric with GCA fly ash filtration

To put things in proper perspective, the terminal fabric dust loadings during current tests ranged from 500 to 1200 grams/m^2 whereas the cleaned surfaces retained only about 50 to 80 grams/m^2. Thus, when a section of the fabric is cleaned by bag collapse and reverse flow, the surface immediately beneath the detached slab contains very little dust per unit area in contrast to many fabrics cleaned by mechanical shaking. Prior tests with Dacron, cotton and glass fabrics, for example, showed average residual dust holdings in the 54 to 300 grams/m^2 range, the latter also representing the approximate areal density of many common filtration fabrics including the Sunbury and Nucla glass media. The reasons for these variations in fabric loadings and their impact upon filter performance are discussed in the section on weight collection. The photomicrographs of Figure 65 show the appearance of the cleaned surface and the downstream face at 60X magnification. By means of substage illumination, the bounding yarns for a Type I pore, approximately 120 μm diameter, are shown as well as the nearly particle-free (bright) warp yarns. Figure 65 shows the presence of dust in a Type II pore opening as viewed from the clean face of the filter. Generally, the clean air faces of the filters loaded in the laboratory for the first time gave very little indication of the encroaching penetration shown in Figure 65.

Despite the fact that the graphite-silicone coating on the Nucla fabric tended to mask the true character of residual dust deposits, the residual dust loading for the Nucla bags closely approximated that of the Sunbury media. The undisturbed loaded fabric, Figure 66 (approximately 1200 grams/m^2 of GCA fly ash) looked the same as its Sunbury counterpart. It can also be seen, Figure 66, that the residual dust is concentrated on or within the fill yarns. Although there was actually very little difference in residual dust holdings for samples shown in Figures 66 and 67 (top), it is believed that the fuzzier appearance of Figure 67 is due to the extra dust retentivity of many protruding fill fibers on the new fabric which are eroded or broken off after a filter has seen 2 years of field

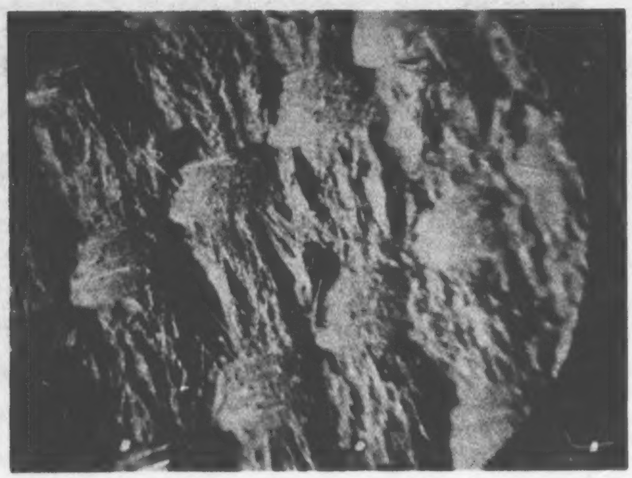

Cleaned filtering surface, bright spot is substage lighting, Type I pore

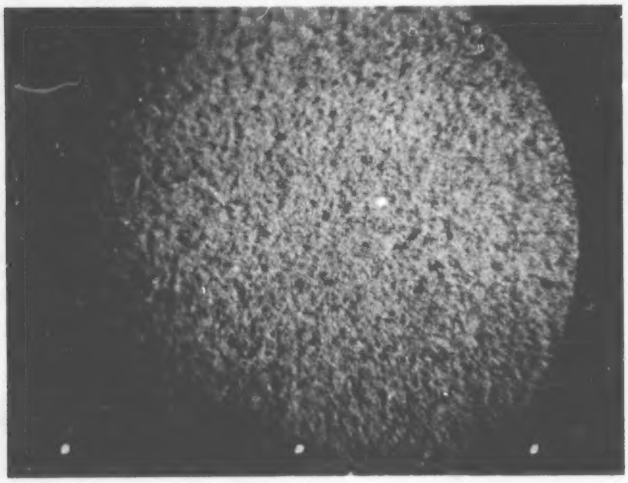

Clean, warp face showing dust seepage at Type II pore

Figure 65. Pore appearances for clean and dirty faces of cleaned Sunbury fabric with GCA fly ash filtration (60X magnification)

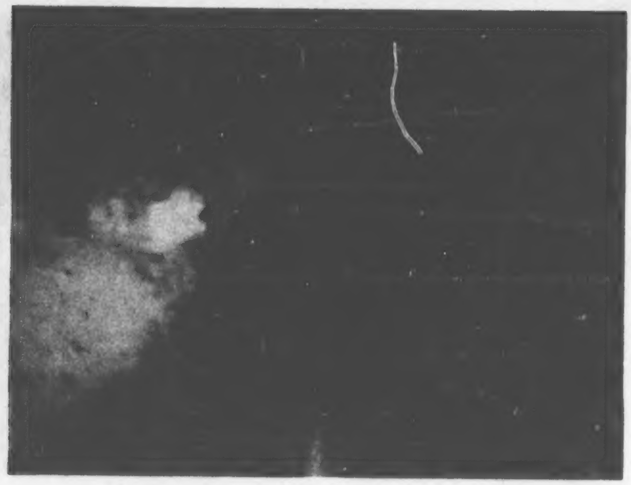

Filter surface after cake dislodgement light-dust deposit on warp yarns

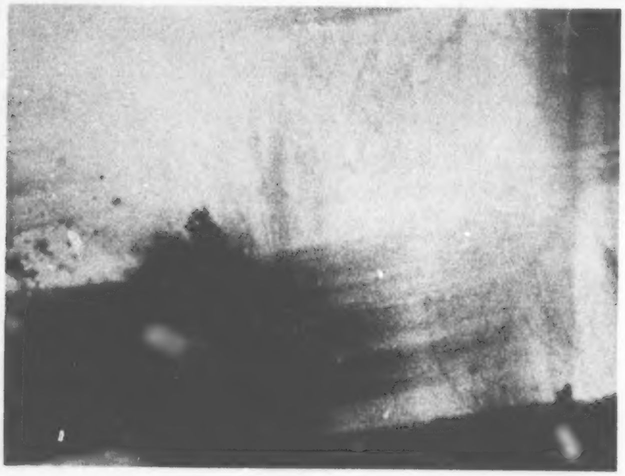

Filter face before cleaning

Figure 66. Appearance of previously used Nucla fabric befire and after cleaning. GCA fly ash loading of 1200 grams/m^2 (20X magnification)

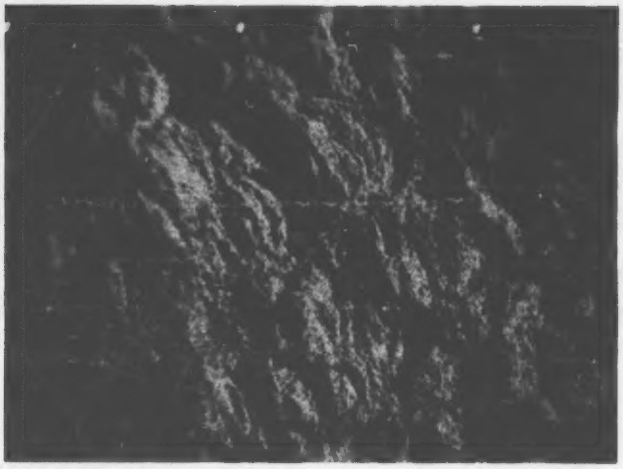

Filter surface after cake dislodgement. In-focus granular areas are warp yarns with light dust coating

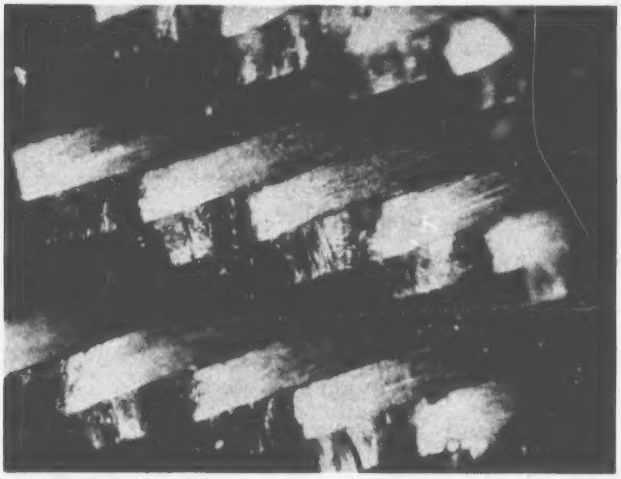

Clean (downstream) surface after dust removal. Minimal indication of particle penetration at pore locations

Figure 67. Appearance of fill and warp faces of Nucla fabric after removal of GCA fly ash loading of approximately 1000 grams/m^2, previously clean (unused) fabric (20X magnification)

service. Although the reflection from the graphite flakes obscure some structural details, one can detect little evidence of dust penetration on the clean air side of the filter shown in Figure 67.

The unmagnified photograph, Figure 68, shows a 150 cm x 100 cm section of a Nucla test panel in which the dust has been removed from the center section. Although it is not apparent in this photograph, transmitted light can be readily seen if the "cleaned" portion is viewed obliquely at about 45 degrees.

Although dust layers in excess of 1 mm in depth are extremely thick relative to what one encounters with many mechanical shaking systems (approximately 0.2 to 0.3 mm at most), it should be remembered that the fabric acceleration level and that of the adhering dust must reach approximately 4 to 5 g's (4.4×10^3 cm/sec^2) before the dust layer can be dislodged by tensile or shearing forces.[1] The forces necessary to overcome dust layer-to-fabric layer adhesion, estimated by Zimon[28,29] to range from 100 to 300 dynes/cm^2, require therefore that the products (mass) x (fabric acceleration) or (mass) x (gravity acceleration) attain the 100 to 300 dynes/cm^2 level during the cleaning action. Since the bag collapse process usually involves low acceleration, gravity alone at the 1-g level must be augmented by a correspondingly larger dust mass to exceed the adhesive forces cited above.

The result of this analysis suggests that where 4.5 g's is sufficient to bring about dust removal by mechanical shaking when the dust layer is roughly 0.25 mm thick, the dust layer when subjected to gravity forces alone must attain a thickness of 1 mm or larger before separation occurs with a simple, reverse-air-supplemented, bag collapse process. Prior GCA measurements[10] and the present tests indicate that terminal dust holdings for the glass bags used in the field are in the 500 to greater than 1000 grams/m^2 range (approximately 0.5 to greater than 1.0 mm thickness).

Figure 68. Photograph showing a section of Nucla test panel from which dust has been dislodged. Roughly 3/4 actual size

Dust Release From Glass Fabrics

Because of the excellent dust release properties of the glass fabrics, it is possible to remove a large fraction of the dust deposit by repeated flexing. The dust detaches in the form of flakes or slabs from the dust/fabric interface such that the residual dust beneath the detached slab constitutes about 10 to 20 percent of the total bag fabric weight. It is emphasized that in normal filtration practice no more than a small fraction of the fabric surface is ever stripped during collapse and reverse flow cleaning. Therefore, the relationships indicated in Figures 53 through 56 can be applied directly only to the cleaned areas of field systems and only when the filtration velocity is constant.

As far as fly ash filtration with glass fabrics is concerned, the loading curve appears to be the important one from an operating viewpoint. According to our microscopic and weighing observations of dust removal by mechanical (flexural) dislodgement of dust, it appears that once sufficient force is applied at the dust/fabric interface to detach the dust layer, the separation process appears to leave approximately the same amount of residual dust, Table 15.

The above effect is not unexpected because the dust layer, irrespective of its physical properties, detaches from the interface region between the fabric yarns and the dust cake. Even though the sateen weave cotton has a more pronounced nap structure because of its all-staple yarn construction, its residual fly ash holding was roughly the same as that for the glass fabrics. In the absence of more detailed information, it appears that the assumption that the residual dust holdings and residual resistances for many dust fabric combinations will not vary greatly in magnitude may be a good first approximation. It is again emphasized that the residual levels cited above are those for the fabric surface beneath the detached "slab" of dust.

Table 15. RESIDUAL LOADING AND RESISTANCE AFTER FABRIC CLEANING

Test No.	Test Aerosol	Filter fabric[a]	Terminal dust loading grams/m^2	Residual dust loading grams/m^2	Residual[b] resistance N/m^2
66	Fly ash	Sunbury fabric[c] 2 years' service	432	31.0	31.0
67	Fly ash	Sunbury fabric[c] 2 years' service	1011	29.0	67.0
65	Fly ash	Sunbury fabric, new, cleaned	1220	66.0	17.4 (2.5)
71	Fly ash	Sunbury fabric, new, cleaned	660	32.0	7.5 (2.5)
98A	Fly ash	Sunbury fabric, new, cleaned	390	47.0	10.0 (2.5)
99B	Fly ash	Sunbury fabric, new, cleaned	660	56.0	15.0 (2.5)
69	Fly ash	Nucla fabric[c] <6 months' service	1000	11.0	82.0 (1.2)
68	Fly ash	Nucla fabric new, cleaned	1000	40.2	18.7 (2.5)
83A	Lignite	Sunbury fabric new, cleaned	1200	63.0	7.5 (2.5)

Table 15 (continued). RESIDUAL LOADING AND RESISTANCE AFTER FABRIC CLEANING

Test No.	Test Aerosol	Filter fabric[a]	Terminal dust loading grams/m^2	Residual dust loading grams/m^2	Residual[b] resistance N/m^2
81	Lignite	Nucla fabric new, cleaned	1200	92.0	25.0 (2.5)
82	Lignite	Nucla fabric new, cleaned	1200	63.0	7.5 (1.2)
85	Fly ash	Cotton sateen new, cleaned	920	42.0	56.2 (20)
95	Fly ash	Dacron crowsfoot previously used	210	16.0	6.2 (2.5)

[a] All fabrics used at least once prior to cleaning and retesting.

[b] Term in parentheses indicates clean (unused) resistance at 0.61 m/min (2 ft/min).

[c] Fabric previously used in field application.

The information presented in Table 15 does not indicate the actual energy required to dislodge the dust. It should not be assumed that because of similar residual resistances and fabric dust loadings that all dusts are detached with equal ease.

Filtration With Partially Cleaned Filters

Several tests were performed in which roughly half of the fabric dust holding was removed from test panels before resuming filtration. Tests 84 and 85 in Figure 69 illustrate, respectively, the difference in resistance properties for uniformly and nonuniformly loaded fabrics. The resistance versus fabric loading relationship is also indicated for the same fly ash/cotton fabric combination when evaluated on a pilot mechanical shaking system.[10]

The appearance of the partially cleaned media has been shown in Figure 68. It was also pointed out that dust separation took place at the dust/fabric interface. Thus, if the filter initially bore a uniform dust layer, the partially cleaned unit would display two characteristic regions, the first from which no dust was detached and the second, a cleaned region having a *uniformly* distributed residual loading of the order of 50 to 75 g/m^2, Table 15.

The results of three tests in this category, which are reviewed in detail in Section IX, were instrumental in the validation of modeling concepts developed under this program.

In Table 16, weight collection efficiencies are reported for various uniform dust loadings on the cotton fabric for different time intervals, Curve 1. In Curve 2, the loading process was repeated except that the test began after about 50 percent of the original fabric dust holding 800 $grams/m^2$ was removed. The net result was that the cleaned fabric area held 42 $grams/m^2$ and the uncleaned section about 800 $grams/m^2$ at the start of filtration.

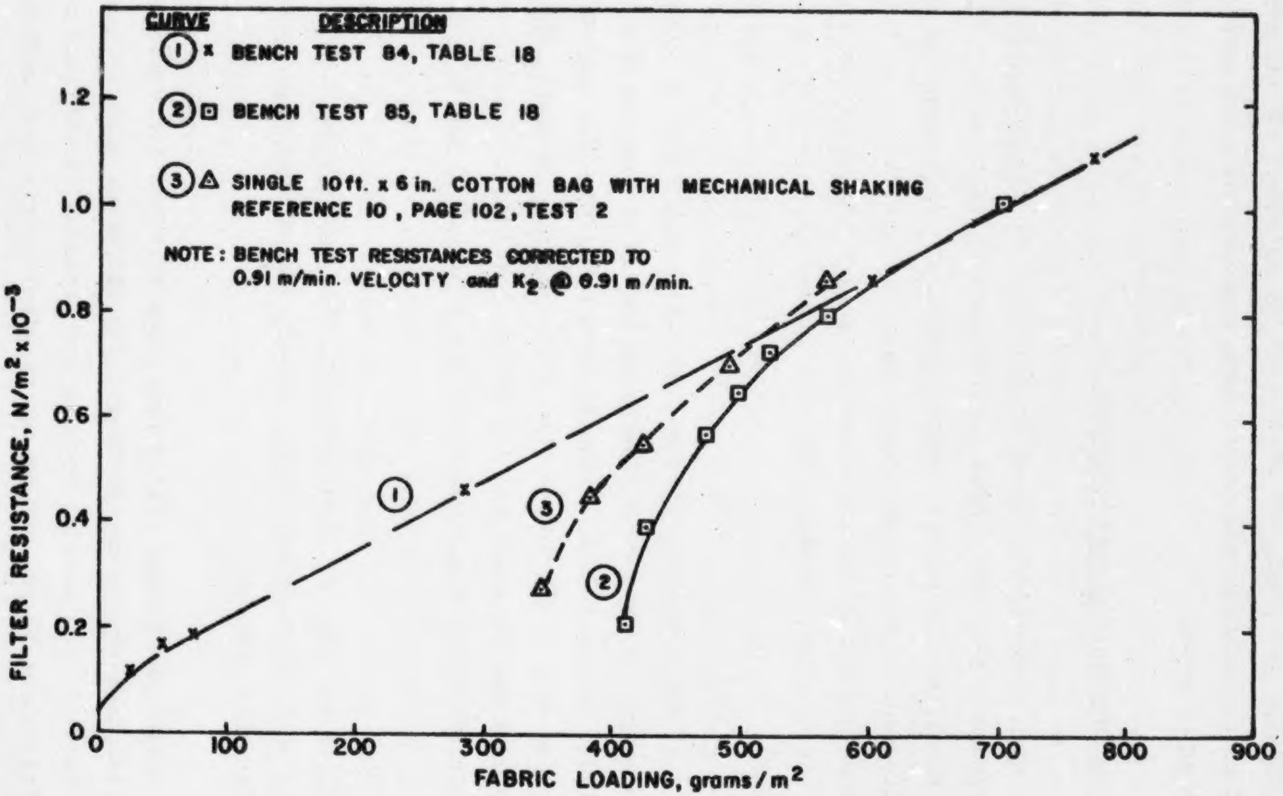

Figure 69. Fly ash filtration with clean and partially cleaned sateen weave cotton, flat panel and bag tests

Table 16. WEIGHT COLLECTION EFFICIENCY FOR SATEEN WEAVE COTTON WITH GCA FLY ASH (SEE FIGURE 69)

Time interval, min	Average fabric loading, g/m^2	Weight collection efficiency percent
Curve 1[a,b] - Uniform fabric dust loading		
0 - 15	0 - 67	99.8711
15 - 180	67 - 800	99.9990
0 - 180	0 - 800	99.9871
Curve 2[a,b] - Nonuniform dust loading		
0 - 10	400 - 417	99.9732
10 - 90	417 - 775	99.9970
0 - 90	400 - 775	99.9940

[a] Curve 1 C_{inlet} = 7.1 g/m^3, Curve 2 C_{inlet} = 7.7 g/m^3

[b] Average filtration velocity, 0.61 m/min (2 ft/min)

In both cases, the overall efficiency levels are seen to increase as more dust deposits on the fabric surface. In the case of Curve 2, the residual dust holding of the cleaned portion of the fabric, ~ 50 to 100 grams/m^2, presented a more efficient collection surface than the unused fabric because of partial plugging. Overall performance for the fly ash/cotton system was approximately the same as reported in earlier GCA mechanical shaking studies.[10]

Figure 69 also allows a comparison between flat panel (Curve 2) and full scale bag filtration tests with the fly ash/unnapped sateen weave cotton combination, Curve 3. It is indicated that by plotting bag resistance versus absolute fabric dust holding (rather than against the amount of dust added during a steady state filtration cycle) the curve assumes a form very similar to that for the partially cleaned test panel.

Examination of Curve 3 shows that its slope differs considerably over most of its length from that depicting the true K_2 value (Curve 1). Unless the filtration process is carried out far enough so that dust accumulations on the previously cleaned and uncleaned surfaces are almost the same, it is not possible to estimate K_2 directly from either field or laboratory measurements unless (1) the fraction of cleaned and uncleaned areas can be determined and/or (2) the drag properties of these respective areas have been determined.

SPECIFIC RESISTANCE COEFFICIENT

Effect of Velocity

Limited bench tests, Figure 70, were performed with Sunbury glass fabrics and the GCA fly ash aerosol to determine the effect of average filtration velocity on the specific resistance coeffcient. Filtration velocity was varied from about 0.38 to 1.52 m/min (1.3 to 5.0 ft/min), the approximate range over which glass fabrics appear to operate most effectively when filtering hot flue gases.

Because of the spherical nature of the fly ash particles (which should assist in establishing a reasonably stable bed structure), it had been assumed that the K_2 values (specific resistance coefficient) would not change appreciably over a moderate range, < 1.52 m/min (5 ft/min). Test results, however, showed a consistent increase in K_2 with velocity, Figure 71, which can be described quite accurately for the fly ash/glass fabric system by the relationships:

$$K_2 \text{ (N min/g m)} = 1.8\ V^{\frac{1}{2}},\ V \text{ in m/min} \qquad (20a)$$

$$K_2 \text{ (in. } H_2O \text{ min ft/lb)} = 5.95\ V^{\frac{1}{2}},\ V \text{ in ft/min} \qquad (20b)$$

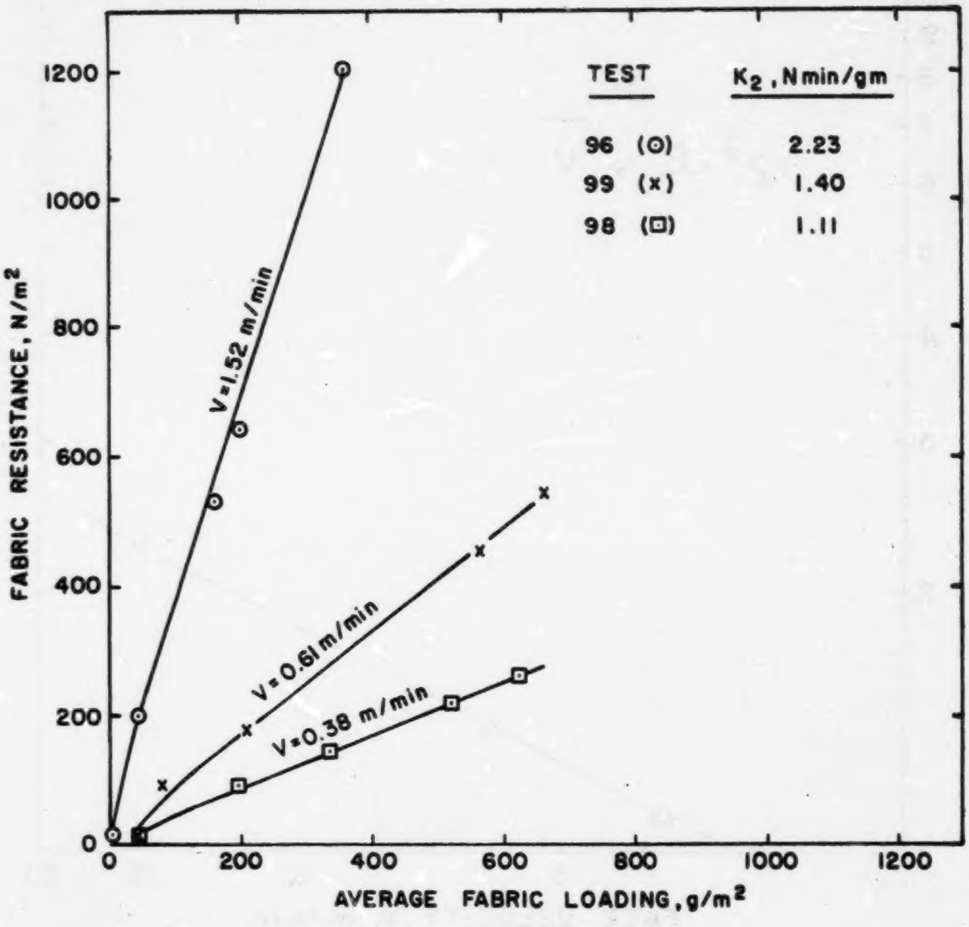

Figure 70. Effect of filtration velocity (V) on specific resistance coefficient (K_2). Sunbury fabric with GCA fly ash

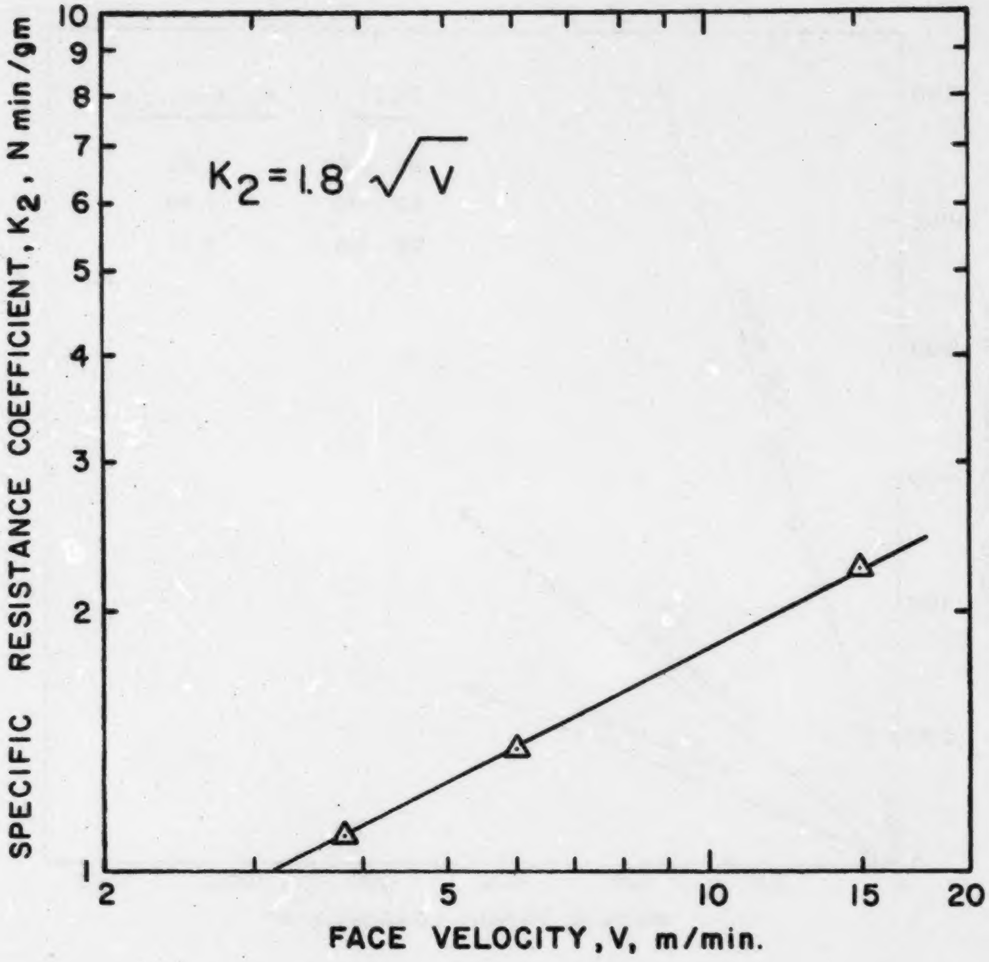

Figure 71. Effect of face velocity on K_2, Sunbury fabric with GCA fly ash

No electrical charge effects were studied during the above test series. However, air temperature and relative humidity were maintained nearly constant at 70°F and 55 percent R.H.

Effect of Particle Size

The effect of particle size on filter resistance coefficients was also examined via tests on selected size ranges of a rhyolite (granite type) dust with the Sunbury fabric. These measurements were performed with rhyolite because density and shape factor appeared to be nearly independent of size.

The simple procedure of reversing the extraction probe from the aerosol loop provided the finer of the two size distributions shown previously in Figure 13. The resistance/fabric loading curves for the coarse and fine ryholite are shown in Figure 55.

The results indicated that the K_2 values for the two rhyolite size distributions, 1.4 and 9.9 N min/ g m, varied inversely as their respective mass mean diameters (MMD). The Carman-Kozeny[10] theory indicates, however, an inverse square relationship, i.e.:

$$K_2 = \phi \, (d_p)^{-2}$$

for granular beds comprised of uniformly sized particles.

Therefore, the inverse relationship, $K_2 = \theta \, (\text{MMD})^{-1}$, determined for the rhyolite is a purely empirical function resulting from the choice of mass median diameter as the characterizing parameter.

It should be noted that the Carman-Kozeny[10] relationship can also be expressed in the form:

$$K_2 = \psi \, (S_o)^2 = \phi \, (d_o)^{-2} \qquad (21)$$

where S_o is the specific surface parameter. In the case of a monodisperse particle system, S_o is a simple linear function of $1/d_p$. When the system is polydisperse, it appears reasonable to express S_o as the ratio of particle surface area to the volume occupied by the particle, A_p/A_v. The terms A_p and A_v, respectively, are calculated from the characteristic surface mean and volume mean diameters, d_s and d_v, for the size distribution of interest.

If the size parameters can be computed from a logaritmic normal distribution, the following relationships obtain:

$$\log_{d_s} = \log \text{MMD} - 4.605 \log^2 \sigma_g \tag{22}$$

$$\log_{d_v} = \log \text{MMD} - 3.454 \log^2 \sigma_g \tag{23}$$

Use of the above equations in conjunction with the size parameters shown in Figure 13, gave an S_o ratio of 2.52 for the coarse and fine ryholite dusts. Thus, one would expect the respective K_2 values to differ by a factor S_o^2 or 6.35. Actually, the ratio of measured K_2 values for the fine and coarse dust was 7.07 suggesting that the calculation of the specific surface term provides a better estimate of K_2 values for polydisperse systems than use of the MMD value alone. In Section IX, the results of a detailed analysis of the relationship between K_2 and S_o are presented for the field and laboratory measurements conducted during or related to the present study.

Dacron Filtration Tests

Additional tests were performed to determine why the collection efficiency for crowfoot (1/3) Dacron media was so low, ~ 80 percent, with GCA fly ash compared to prior measurements, ~ 99.5 percent, with full scale filter bags (10 ft x 6 in.). Summaries of all Dacron bench tests are given in Table 17 and Figure 56.

Table 17. GCA FLY ASH FILTRATION WITH CROWFOOT DACRON, BENCH SCALE TESTS

Test no.[a]	Fabric resistance N/M^2	Fabric loading grams/m^2 (range)	Filtration surface[b]	Dry bulb temperature °C	Relative humidity	Weight collection efficiency percent[d]
92 N	200	0-100	Warp	23.3	40[c]	69.9
92 N	350	100-352	Warp	24.5	42[c]	78.7
92 N	726	352-726	Warp	25.0	38[c]	79.8
93 N	196	0-100	Warp	22.0	16[c]	76.4
93 N	298	100-325	Warp	22.0	16	78.5
94 N	188	0-184	Fill	23.2	40	79.3
95 U	284	45-195	Warp	23.5	23	80.5

[a] N = new (unused) fabric; U = used fabric.

[b] Warp yarns constitute 75 percent of upstream (filtering) surface.
Fill yarns constitute 75 percent of upstream (filtering) surface.

[c] Indicates poor electrical ground. All other tests well grounded.

[d] Reported efficiencies apply to indicated fabric loading range.

Note: DACRON - Globe Albany No. 856B, 10 oz/yd^2, 1/3 Crowfoot, 71F x 51F (bulked) thread count, 33 perm.

All tests indicated a slight increase in efficiency as fabric loading increased but hardly at the levels needed for effective performance. Although one expects to see some differences due to relative humidity, the degree of electrical grounding, or the direction of air flow through the fabric (warp or fill face as the filtering surface), the data in Table 17 showed consistently poor and uniform performance irrespective of test conditions. Because of anomalies in attempted charge measurements (possibly due to a defective instrument) electrical charge per se either on the dust particles and/or on the Dacron fabric could not be related to the efficiency results although is suspected to be involved.

Earlier resistance tests, Figure 33, suggest, however, that the difference in fabric pore structure between full scale bags and small, flat test panels may explain the gross differences in dust collection. Clean fabric resistance measurements showed a significant increase in resistance (and hence reduced permeability) with full scale bags in contrast to equivalent measurements with flat panels. The results indicate, therefore, that reduced pore dimensions occur with a tubular (bag) configuration as well as a distortion feature which should represent a "one way" rather than a "two way" stretch with a nearly square flat panel. Although the present rationale is qualitative, it appears possible that the larger pore openings coupled with less uniformity in pore dimensions, may explain the poor performance encountered with bench scale tests. Several other dust/fabric combinations including lignite, GCA fly ash and granite dust with glass fabric (Sunbury and Nucla) and GCA fly ash with sateen weave cotton encompassed the same range of humidity and inlet loading levels while showing efficiencies ranging from 99.9 to 99.999 percent.

It was noted that a large pinhole population, ~ 5300/m^2 was present at the end of test 92. Because the resistance, 625 N/M^2, was comparatively high, there was probably little chance that these pinholes would ever have become blocked. On the other hand, the pinhole density of 9000/m^2 observed for test 93, might have undergone some reduction if the test had been continued because of the lower air velocity through the pores at test termination.

If one assumes that those pores that remained unbridged for Dacron media are about 1.5 times larger than the corresponding pores for the Sunbury fabric (as indicated by preliminary microscope observations), the estimated pore areas/cm^2 for tests 92 and 93 are 10^{-4} cm^2 and 1.7×10^{-4} cm^2, respectively. In conjunction with estimated pore velocities of 4000 and 2000 ft/min, respectively, for tests 92 and 93 and assumed 0 percent dust removal for air passing through the pores, overall weight collection efficiencies of 83 and 85 percent are predicted. The observed values, Table 18, were in the 80 percent range.

Aside from demonstrating the extent to which a comparatively small pinhole area can contribute to dust penetration, the analyses of the above data also suggest that one might use penetration data in conjunction with the observed pinhole count and filter resistance to estimate the effective cross-sectional areas of the larger pores.

COLLECTION EFFICIENCY AND PENETRATION

Weight Collection Efficiency Measurements

Weight collection efficiencies, inlet and outlet dust concentrations, fabric loadings and other relevant test parameters are summarized in Table 18 for bench scale filtration tests with various aerosol and fabric combinations. All tests were performed in the filter assembly shown in Figure 5. During some tests, the filter panels were removed at intermediate loading levels for visual inspection and determination of fabric dust holdings. For all practical purposes, the increase in filter dust holding divided by the air volume passed through the filter provided an accurate measure of true inlet dust concentration when efficiencies exceeded 99 percent. Otherwise, Method 5 type filter samples were collected upstream to establish inlet load levels. All outlet concentrations were determined by the Method 5 type sampling of the test airstream as well as by supplemental condensation nuclei counting (CNC), Bausch and Lomb (B&L) single particle light scattering measurements and Andersen cascade impactor samples.

According to Table 18, effluent loadings and collection efficiencies were about the same for clean (unused) samples of the Sunbury and Nucla filter fabrics. Except for Tests 65A and 65F, there appeared to be no dependency upon fabric dust holding. However, inspection of CNC and B&L measurements in the next section shows a rapid decrease in particle number concentration up to the point when a fabric dust loading of about 150 grams/m^2 has

Table 18. SUMMARY OF BENCH SCALE FILTRATION TESTS

Test No.	Test dust[a]	Fabric tested	Fabric loading, g/m²		Resistance, N/m²		Dust concentration		Weight efficiency, percent	Comments
			Initial	Final	Initial	Final	Influent, g/m³	Effluent, g/m³ x 10³		
65 A	FA[c]	New Sunbury	0.0	130	2.5	170	1.24	9.2	99.26	
65 B	FA	New Sunbury	130	210	160	210	1.53	1.8	99.88	
65 C	FA	New Sunbury	210	250	180	240	1.10	5.3	99.52	
65 D	FA	New Sunbury	250	-	220	320	2.96	2.1	99.93	
65 E	FA	New Sunbury	-	960	320	950	2.96	3.5	99.88	
65 F	FA	New Sunbury	960	1200	750	1200	2.99	99	96.69	Pinholes detected, 2500/m² of fabric.
65 A-F	FA	New Sunbury	0.0	1200	2.5	1200	2.33	20.6	99.12	
66 A	FA	Used Sunbury	31	77	31	190	0.63	58	90.79	Fabric from Sunbury Steam Electric Station No. 1 A Baghouse, cleaned.
66 B	FA	Used Sunbury	77	100	170	290	0.31	41	86.77	
66 C	FA	Used Sunbury	100	280	290	500	2.02	35	98.27	
66 D	FA	Used Sunbury	280	430	410	670	1.41	39	97.23	Pinholes detected 680/m² of fabric.
66 A-D	FA	Used Sunbury	31	430	31	670	1.09	40.3	96.31	
67	FA	Used Sunbury	29	1000	67	1200	8.05	68	99.16	Fabric from Sunbury Steam Electric Station No. 1 A Baghouse, cleaned, pinholes detected.
68	FA	New Nucla	0.0	1000	2.5	1200	6.36	6.9	99.89	
69	FA	Used Nucla	11	1000	82	1200	6.25	6.9	99.89	Fabric from Nucla Generating Station No. 2 Baghouse, cleaned.
70 A	FA	New Sunbury	0.0	95	2.5	150	5.18	41	99.21	
70 B	FA	New Sunbury	95	230	150	240	7.38	9.2	99.88	
70 C	FA	New Sunbury	230	380	250	370	-	-	-	
70 D	FA	New Sunbury	380	510	400	540	-	-	-	
70 E	FA	New Sunbury	510	640	560	700	-	-	-	
70 C-E	FA	New Sunbury	230	640	250	700	8.00	2.3	99.97	
70 A-E	FA	New Sunbury	0.0	640	2.5	700	7.03	11.2	99.84	
71	FA	Used Sunbury	32	660	7.5	630	6.84	4.58	99.93	Fabric from test 70, cleaned.
72 A	FA	Used Sunbury	340	450	25	370	-	-	-	Fabric from test 71, partially cleaned to residual dust holding of 340 grams/m² of fabric. Pinholes detected, 402/m² of fabric.

Table 18 (continued). SUMMARY OF BENCH SCALE FILTRATION TESTS

Test No.	Test dust[a]	Fabric tested	Fabric loading, g/m^2		Resistance, N/m^2		Dust concentration		Weight efficiency, percent	Comments
			Initial	Final	Initial	Final	Influent, g/m^3	Effluent, g/m^3 x 10^3		
72 B	FA	Used Sunbury	450	540	370	520	-	-	-	
72 C	FA	Used Sunbury	540	750	520	710	-	-	-	
72 A-C	FA	Used Sunbury	340	750	25	710	6.73	90.83	98.65	
77 A	RF	New Sunbury	0.0	13	2.5	150	0.34	18.53	94.55	
77 B	RF	New Sunbury	13	30	140	220	0.34	2.29	99.33	
77 C	RF	New Sunbury	30	53	220	320	0.34	0.23	99.93	
77 D	RF	New Sunbury	53	64	320	410	0.34	0.69	99.80	
77 E	RF	New Sunbury	64	79	410	560	0.34	0.92	99.73	
77 A-E	RF	New Sunbury	0.0	79	2.5	560	0.34	3.66	98.92	
79 A	RC	New Sunbury	0.0	57	2.5	75	1.65	5.72	99.65	
79 B	RC	New Sunbury	57	180	75	160	1.65	0.69	99.96	
79 C	RC	New Sunbury	180	300	160	290	-	-	-	
79 D	RC	New Sunbury	300	390	290	390	-	-	-	
79 C-D	RC	New Sunbury	180	390	160	390	1.65	0.09	99.99	
79 A-D	RC	New Sunbury	0.0	390	2.5	390	1.65	1.14	99.93	
81 A	L	New Nucla	0.0	550	1.2	330	9.08	10.07	99.88	
81 B	L	New Nucla	550	870	300	620	8.63	7.78	99.91	
81 C	L	New Nucla	870	1200	550	980	8.35	24.02	99.71	Pinholes detected, 287/m^2 of fabric.
81 A-C	L	New Nucla	0.0	1200	1.2	980	8.76	13.3	99.85	
82 A	L	New Sunbury	0.0	540	2.5	310	9.83	4.80	99.95	Pinholes detected, 29/m^2 of fabric.
82 B	L	New Sunbury	540	790	290	520	-	-	-	
82 C	L	New Sunbury	790	1200	500	910	-	-	-	
82 B-C	L	New Sunbury	540	1200	290	910	10.11	16.47	99.84	
82 A-C	L	New Sunbury	0.0	1200	2.5	910	9.98	11.0	99.89	
83 A	L	Used Sunbury	63	130[b]	7.5	87	7.43	1.37	99.98	Fabric from test 82, cleaned.
83 B	L	Used Sunbury	130[b]	480	87	280	7.43	1.14	99.98	
83 C	L	Used Sunbury	480	760	280	570	7.85	0.92	99.99	
83 A-C	L	Used Sunbury	63	760	7.5	570	7.66	1.14	99.981	

Table 18 (continued). SUMMARY OF BENCH SCALE FILTRATION TESTS

Test No.	Test dust[a]	Fabric tested	Fabric loading, g/m^2		Resistance, N/m^2		Dust concentration		Weight efficiency, percent	Comments
			Initial	Final	Initial	Final	Influent, g/m^3	Effluent, g/m^3 x 10^3		
84 A	FA	New Cotton	0	70[b]	20	100	7.10	9.15	99.87	
84 B	FA	New Cotton	70	280	100	220	-	-	-	
84 C	FA	New Cotton	280	540	210	420	-	-	-	
84 D	FA	New Cotton	540	780	400	580	-	-	-	
84 B-D	FA	New Cotton	70[b]	780	100	580	7.10	0.07	99.999	
84 A-D	FA	New Cotton	0	780	20	580	7.10	0.92	99.99	
85 A	FA	Used Cotton	400	450[b]	110	260	7.69	2.06	99.97	Fabric from test 84, partially cleaned to residual dust holding of 400 grams/m^2 of fabric.
85 B	FA	Used Cotton	450[b]	820	260	700	7.69	0.23	99.997	
85 A-B	FA	Used Cotton	400	820	110	700	7.69	0.46	99.991	
89 A	L	Used Sunbury	340	410[b]	17	190	7.60	21.05	99.72	Tests 89 A-B, fabric from test 83, partially cleaned to residual dust holding of 340 grams/m^2 of fabric.
89 B	L	Used Sunbury	410[b]	870	190	600	7.60	12.58	99.83	Pinholes detected, 86 m/^{2} of fabric.
89 A-B	L	Used Sunbury	340	870	17	600	7.60	13.7	99.82	
92 A	FA	New Dacron	0.0	100	5.0	200	7.33	2208	69.88	Tests 92 A-C, outlet side of fabric very dirty after filtration.
92 B	FA	New Dacron	100	350	200	350	8.53	1818	78.69	Pinholes detected, 5223/m^2 of fabric.
92 C	FA	New Dacron	350	740	340	620	8.72	1767	79.74	Pinholes detected, 5310/m^2 of fabric.
92 A-C	FA	New Dacron	0.0	740	5.0	620	8.43	1850	78.05	
93 A	FA	New Dacron	0.0	100	3.7	190	7.48	2081	72.18	
93 B	FA	New Dacron	100	320	150	290	7.48	1605	78.54	System well grounded, pinholes detected, 8897/m^2 of fabric.
93 A-B	FA	New Dacron	0.0	320	3.7	290	7.48	1762	76.44	
94	FA	New Dacron	0.0	180	2.5	190	6.18	1275	79.37	Air flow through fabric opposite normal filtering direction. Pinholes detected but not countable.
95	FA	Used Dacron	16	210	6.2	280	6.50	1269	80.48	Fabric from previous lab studies, pinholes detected but not countable.
96	FA	New Sunbury	0	400	11.2	1370	5.37	58.34	98.91	Filtered at 1.51 meters/minute, pinholes detected, 603/m^2 of fabric.

Table 18 (continued). SUMMARY OF BENCH SCALE FILTRATION TESTS

Test No.	Test dust[a]	Fabric tested	Fabric loading, g/m^2		Resistance, N/m^2		Dust concentration		Weight efficiency, percent	Comments
			Initial	Final	Initial	Final	Influent, g/m^3	Effluent, g/m^3 x 10^3		
97	FA	Used Sunbury	270	390	162	1100	4.60	562.8	87.77	Fabric from test 96, partially cleaned to residual dust holding of 270 grams/m^2 of fabric, filtered at 1.52 meters/minute, pinholes detected, 3588/m^2 of fabric.
98 A	FA	Used Sunbury	47	90[b]	5	62	8.09	16.7	99.79	Fabric from test 97, cleaned, tests 98 A-B filtered at 0.39 meters/minute.
98 B	FA		90[b]	620	62	260	8.09	1.83	99.98	
98 A-B	FA		47	620	5	260	8.09	3.20	99.96	
99 A	FA	Used Sunbury	56	140[b]	15	130	8.40	43.01	99.49	Fabric from test 98, cleaned, tests 99 A-B filtered at 0.60 meters/minute.
99 B	FA		140[b]	660	130	540	8.40	1.60	99.98	
99 A-B	FA		56	660	15	540	8.40	6.86	99.92	

[a] FA = fly ash; RF = Rhyolite fine; RC = Rhyolite coarse; L = Lignite.

[b] Fabric loading estimated from inlet concentration, flow rate and time; i.e., W = CQt.

[c] GCA fly ash was filtered at 0.61 meters/minute for all tests except those indicated. GCA fly ash MMD = 9 μm; σg = 3.0.

accumulated. Test 65A indicates a high effluent concentration during the early filtration phase. A very significant decrease in efficiency was observed for Test 66F as the result of severe pinhole formation or puncture damage.

It was concluded that accidental overstressing or vibration of the filter cake before or during reinstallation for the final filtration sequence was at last partly responsible for the pinhole formation. Details on the appearance, number, approximate dimensions and the total volume of air flow diverted through the pinholes have been discussed previously. Tests on one previously used Sunbury fabric, Test 66, indicated the presence of pinholes throughout the entire measurement interval. Semiquantitatively, the estimated total pinhole area in the latter case appeared consistent with the reported effluent concentrations and efficiencies, ~ 88 to 99 percent.

By not disturbing a second sample of the used Sunbury fabric, Test 67, an overall test efficiency of 99.15 percent was obtained. Based upon these data, it appears possible that the less effective performance of the used Sunbury fabric may have resulted in part from its 2 years of field service. On the other hand, since previously reported field data indicated fairly high efficiency levels, ~ 99.5 percent or greater,[8,9] it is suspected that bag removal and shipment to our laboratories plus subsequent cleaning and handling were the main contributors to poorer performance.

Little can be said for the Nucla tests, Nos. 68 and 69, except that high efficiency levels were observed for both used and unused fabrics. However, the Nucla media had seen less than 6 month's field service.

New Sunbury fabric did not indicate relatively high efficiencies, ~ 99.9+ percent for all test conditions. When the fabric surface was partially cleaned, Test 72A-C, the overall efficiency during the dust reloading process was 98.65 percent. It is again pointed out that resumption of filtration with a partially cleaned filter surface leads to transient high velocities, about 1.5 m/min (5 ft/min) in the present case, that lower the collection efficiency. In most cases, the effluent concentrations from the glass fabrics were in the range of 2 to 5 x 10^{-3} grains/ft^3 (~ 4.6 to 10 mg/m^3).

The fact that very thick dust cakes deposited on the glass fabrics (~ 0.5 to 1 mm) compared to those for mechanically shaken cotton fabrics (~ 0.2 mm) does not necessarily imply equivalent performance.

If the pore structures for the cotton and glass fabrics are examined, it is seen that the volume of fiber obstructing the pores is greater and the distance between individual fibers is less for the sateen weave cotton. Therefore, the particulate emissions are expected to be lower for the cotton fabric for two reasons: (a) the "tighter" weave provides a firmer support upon which to develop a uniform, unbroken dust layer, and (b) the greater number of interlacing fibers obstructing the pores will reduce agglomerate slough-off from the rear face of the filter. The above release is not to be confused with the "pinhole plug" emissions described by Leith et al.[24]. In the latter case, an open channel or pore is created, perhaps 50 to 200 μm in diameter, through which the upstream aerosol passes with very little dust removal. As a result, the "pinhole" plug effluents are also expected to reflect the upstream concentration level. On the other hand, rear face slough-off without breakthrough is expected to consist of a low order emission that may depend upon face velocity but not necessarily relate to the inlet loading. Limited cascade impactor measurements suggest that the mass median diameter for the slough-off material is roughly half that of the inlet dust, 3 versus 6 μm. As far as the fly ash/woven glass fabric combinations are concerned, it is suspected that the effluent loadings reflect both rear face slough-off and direct penetration through pinholes.

Because the size parameters for the rear face slough-off are not radically different from those of the inlet duct and because the former effluent ordinarily represents only a small fraction of the total effluent, the dust fraction that penetrates the filter directly is the one that controls the overall effluent particle size properties.

In some cases, the confirmed presence of pinhole leaks provided a ready explanation for the observed penetration values. However, it is very important to note that a careful inspection of the dirty surface of a filter often revealed no pinholes despite the observed downstream emissions. Thus, it was assumed that periodic sloughing-off of dust from the dust layer/fabric interface region was the major source of such emissions, once all pores were completely bridged.

It should be noted, however, that many mass samples were collected over long averaging periods. Thus, the greater part of the dust collected downstream probably penetrated the fabric before the pore bridging process was completed. Unfortunately, although CNC measurements provided excellent time resolution for effluent loadings, the instrument sensitivity usually precluded detection of concentrations less than 0.5 mg/m^3. The net result was that instrument limitations often prevented any sharp differentiation among the factors contributing to the filter effluents.

When the effluent concentrations for a sateen weave cotton are compared with those for the glass fabrics, it is seen that the former are as much as 50 times less, Test 85b, Table 18. As stated previously, it is believed that the much higher fraction of staple fibers in the cotton fabric provides a stronger bridging mechanism over the pore regions so that less material is sheared off by aerodynamic drag. The more substantial pore bridging with the cotton fabric also reduces the chance for cracking and pinhole formation in the overlying dust cake.

Condensation Nuclei Measurements

CNC concentrations were observed to undergo extreme fluctuations during Test 65, Figure 72, whenever the filter panel was removed and reinstalled. Subsequently, the removal difficulties were eliminated by maintaining air

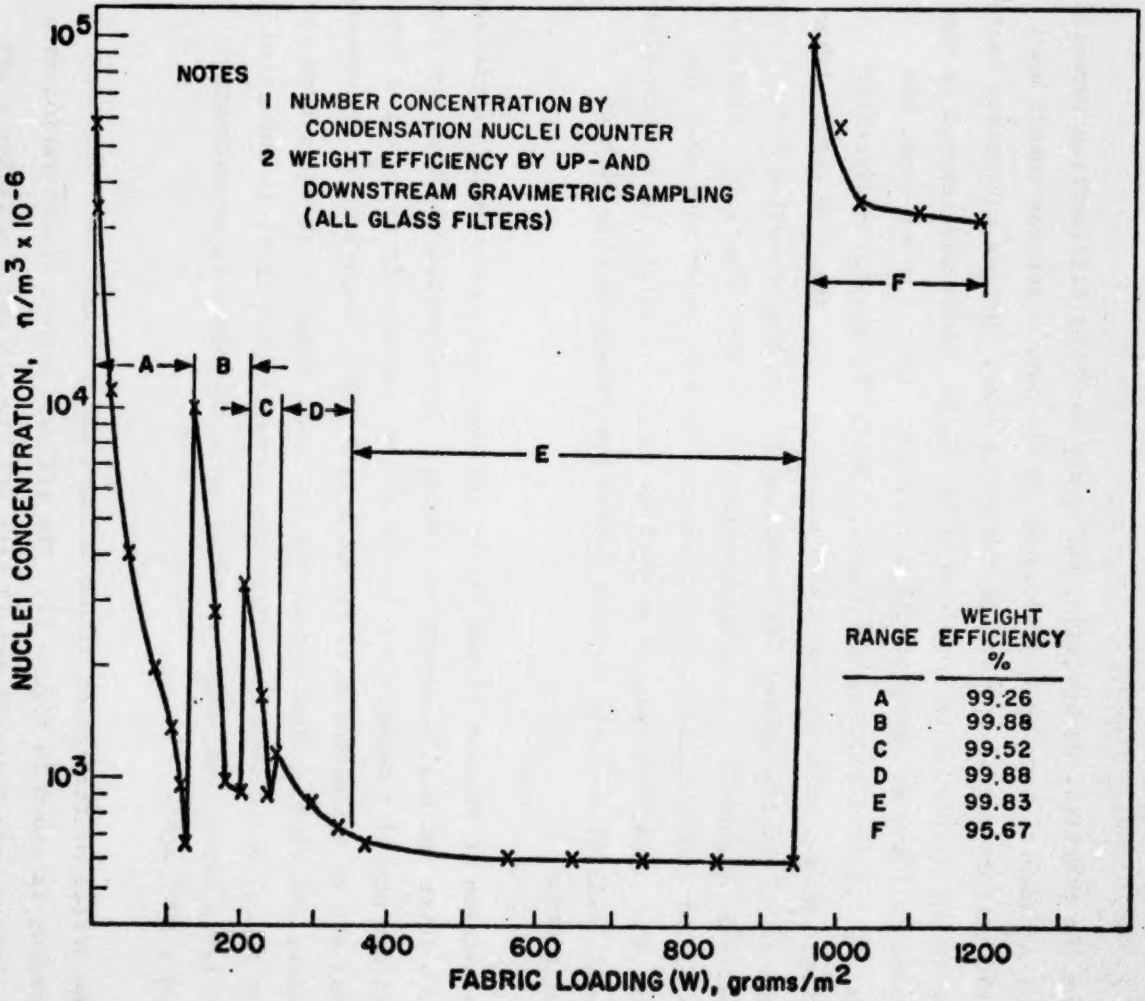

Figure 72. Effluent concentration versus fabric loading for unused Sunbury media with GCA fly ash, Test 65

flow through the filter until it was rotated into a "dust face up" position. Since the fabric surface was already bowed downward as it would be under the normal static dust load, stopping the air flow produced only minimal filter flexure (and minimal cake compression).

From the practical perspective, the early handling difficulties revealed that accidental jarring and vibration could have a serious impact upon field performance if applied at the wrong time. During subsequent testing it was difficult to detect when the filter panel was removed as the result of improved experimental techniques. On the other hand, the Test 66 filter (used Sunbury media), Figure 73, showed consistently erratic nuclei emissions at a concentration level about 30 times higher than noted for the unused fabric during its stable operation phase, Test 65E, Figure 72. A replicate test, No. 67, on Figure 74, indicates an outlet concentration level which was not much lower than that for Test 66. Thus, CNC results as well as those for weight collection efficiency suggest that the Sunbury fabric has undergone some form of degradation.

Inspection of Figures 75 and 76 for the used and unused Nucla fabric show much lower and nearly identical results. It is emphasized that the final uniform nuclei concentration levels do not necessarily represent a levelling off at a concentration of 800×10^{-6} n/m^3. According to the manufacturer, the true minimum nuclei concentration might be anywhere from zero to the actual value when a constant low concentration level is indicated. In later tests, the lowest recorded value decreased to approximately 200×10^{-6} n/m^3.

The effect of filtration with a uniform and a nonuniform fabric dust loading is shown in Figure 77. The effluent nuclei concentration data are based upon Tests 71 and 72 with GCA fly ash and a relatively new Sunbury fabric test panel. In the case of Test 72, approximately half of the dust was removed prior to resuming filtration. As stated previously, that area from which the dust cake had been removed performed initially as a completely cleaned fabric with a W_R value of the order of 50 grams/m^2

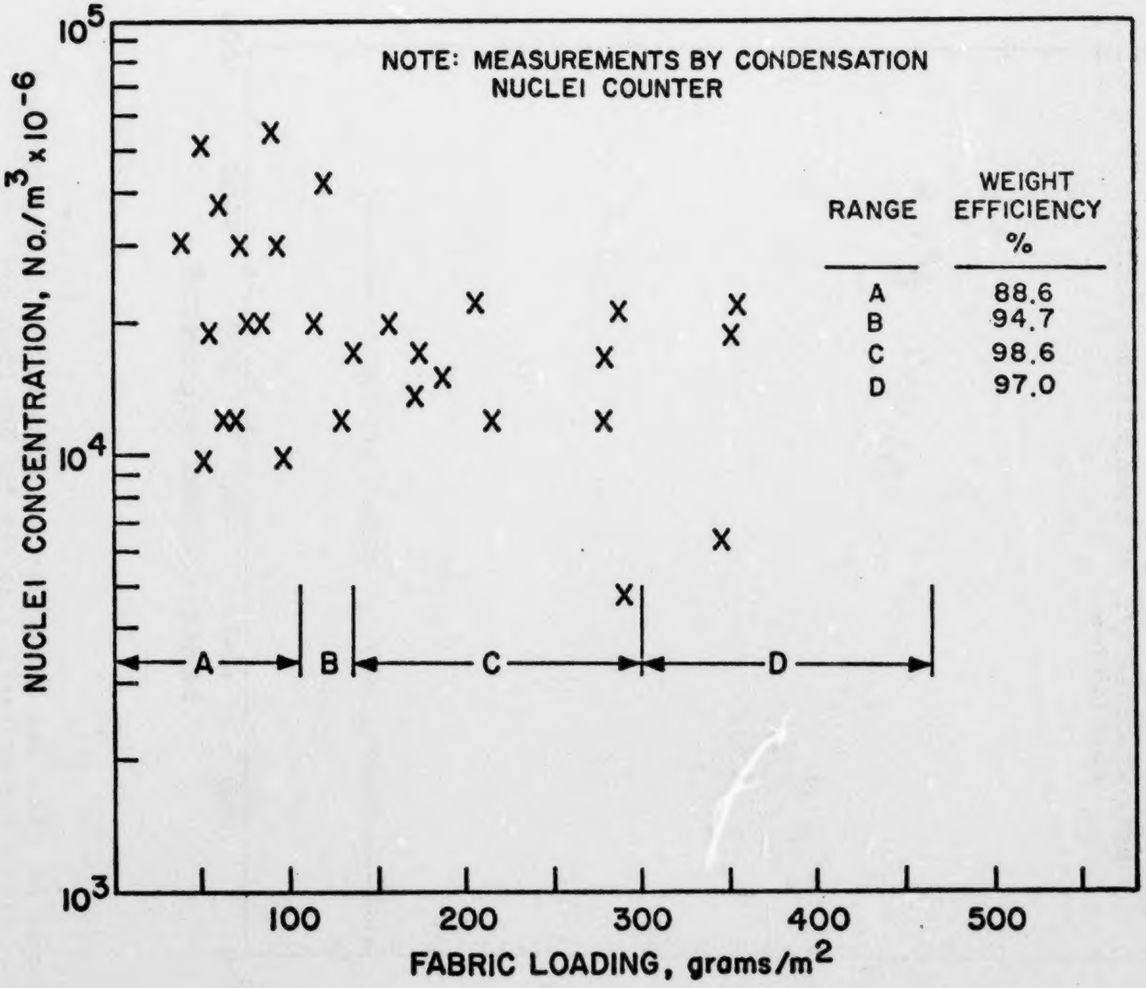

Figure 73. Effluent concentration versus fabric loading for used Sunbury fabric (Test 66) with GCA fly ash

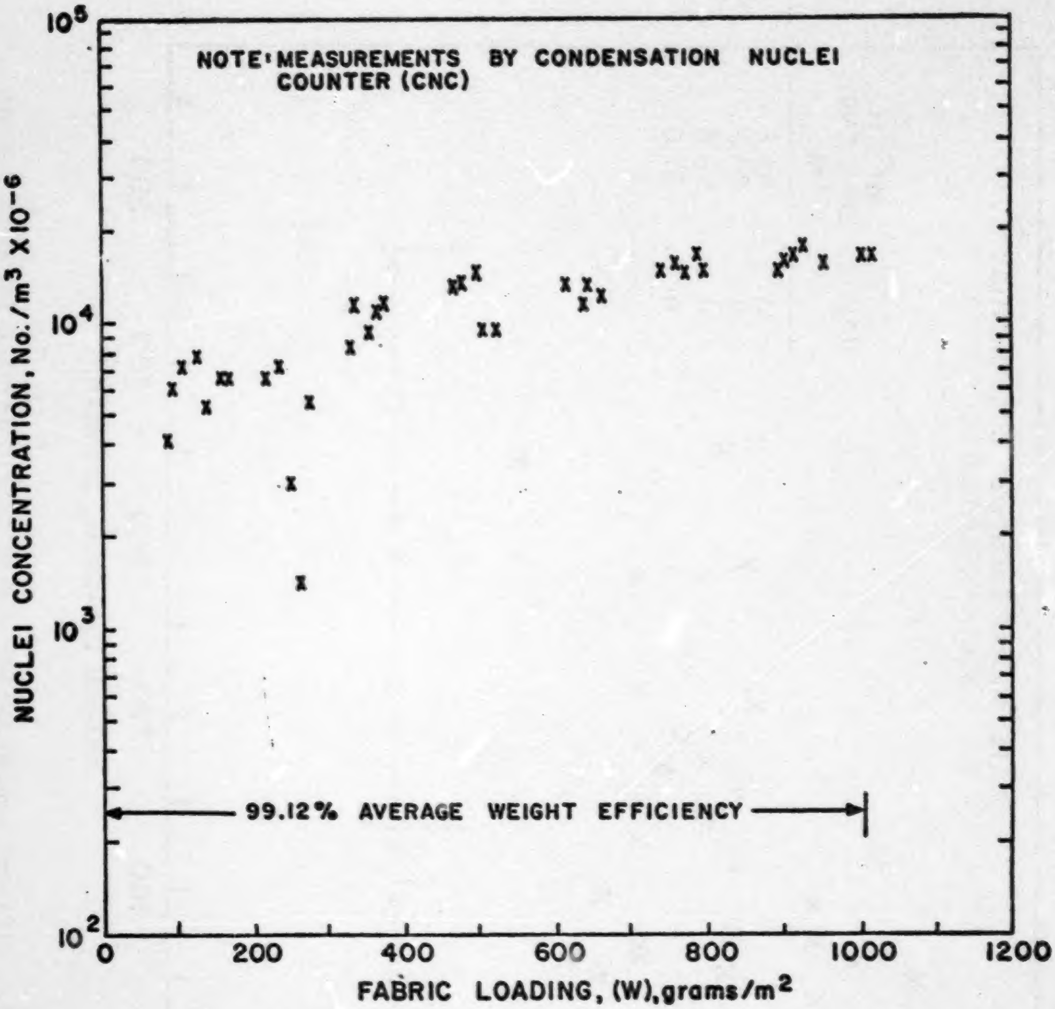

Figure 74. Effluent concentration versus fabric loading for used Sunbury media with GCA fly ash (Test 67)

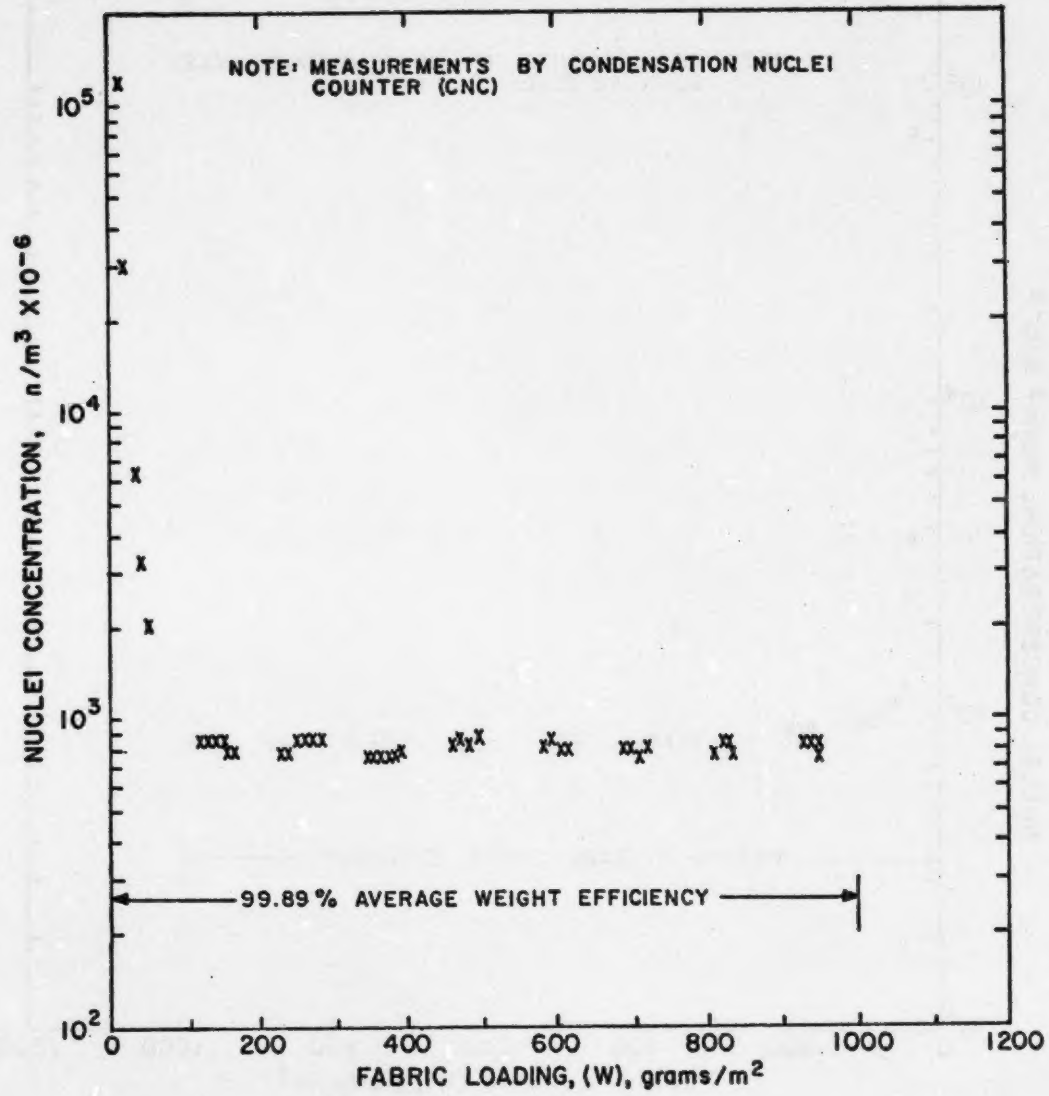

Figure 75. Effluent concentration versus fabric loading for unused Nucla (Test 68) media with GCA fly ash

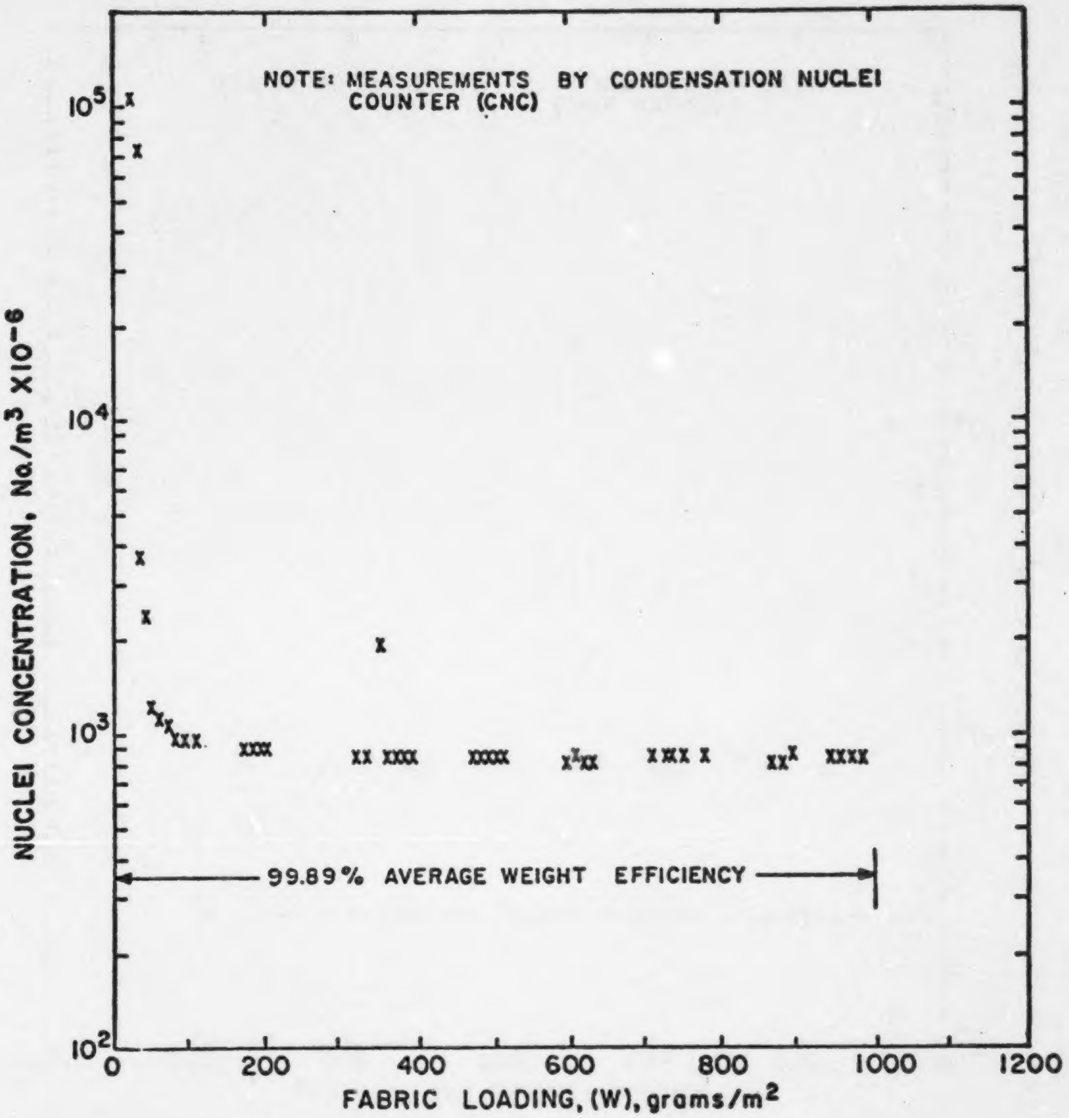

Figure 76. Effluent concentration versus fabric loading for used Nucla fabric (Test 69) with GCA fly ash

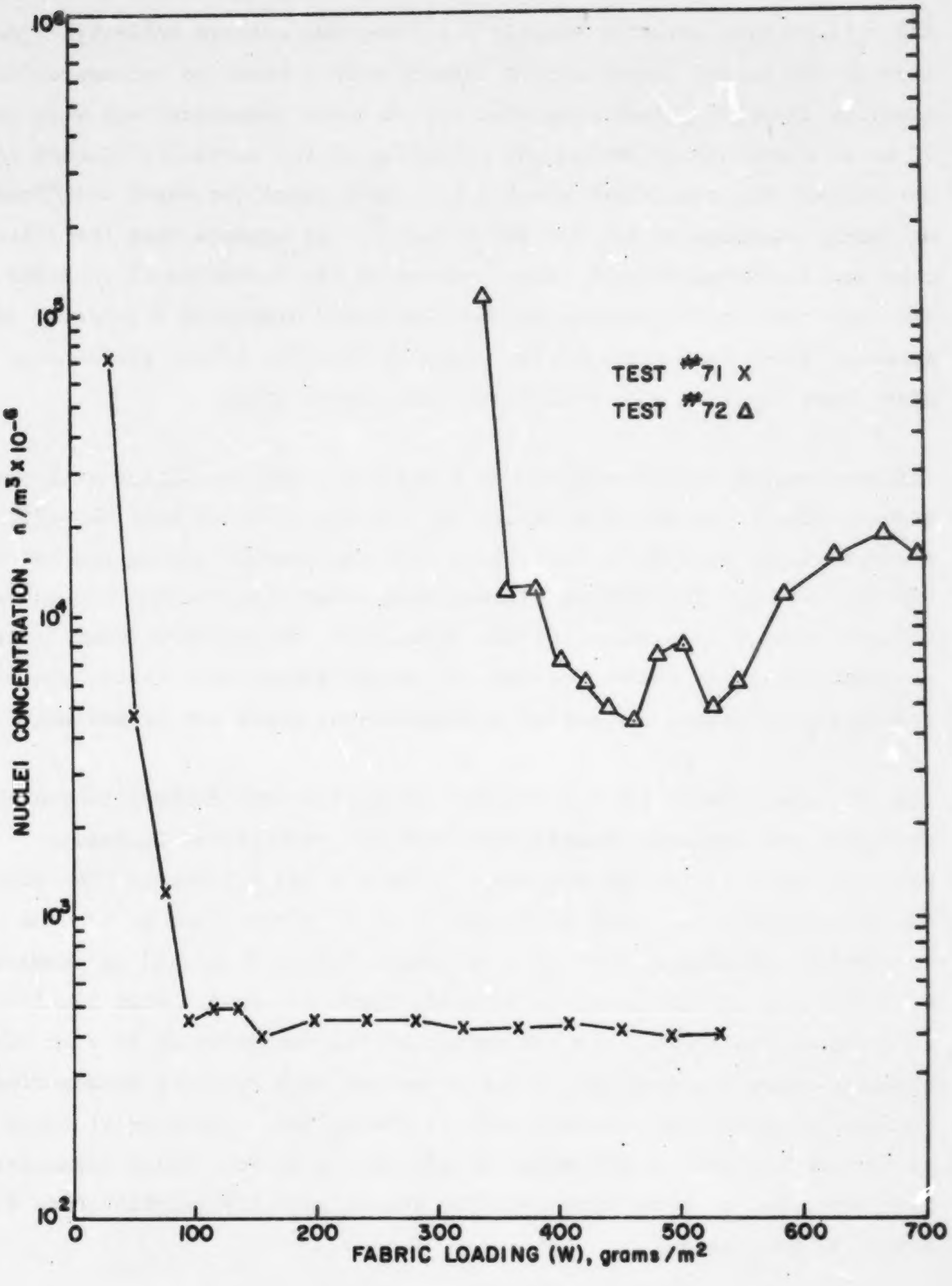

Figure 77. Effluent concentration versus fabric loading for used Sunbury fabric and GCA fly ash with uniform (Test 71) and nonuniform (Test 72) dust loading

and a filtration velocity roughly 2.5 times the average velocity. Inspection of the nuclei concentration changes with respect to increased fabric loading, Figure 77, indicates that the effluent concentrations were from 10 to 60 times higher during the reloading of the partially cleaned fabric. During Test 65, the filter panel was removed twice for check weighings at fabric loadings of 450 and 540 grams/m^2. It appears that the filter cake was disturbed in both cases leading to the formation of pinholes. The fact that nuclei concentrations eventually displayed a tendency to decrease after each perturbation suggests that the filter performance might have improved with additional dust accumulation.

Effluent nuclei concentrations for lignite fly ash filtration with the Sunbury fabric are shown in Figure 78. It was observed that the effluent concentrations dropped to low values once the fabric loading reached the 150 g/m^2 level. The same conditions were noted when the GCA fly ash was filtered with sateen weave cotton, Figure 79. Because the lower limit of sensitivity was reached by the CNC device during some tests, the true instantaneous values for outlet concentrations could not be estimated.

The CNC measurements for GCA fly ash filtration with Sunbury fabric shown in Figure 80, indicate clearly that particle penetration increases with increased filtration velocity. Curves 3 and 4 indicate that effluent nuclei concentrations were generally 30 to 40 times lower at reduced filtration velocities, 0.37 to 0.61 m/min (1.3 to 2 ft/min) as compared to filtration at 1.51 m/min (5 ft/min), Curve 1. Again after partial cleaning of the fabric, the resumption of filtration leads to even higher effluent concentrations during the transient high velocity flow period through the previously cleaned area of the filter. Analyses of these data, in conjunction with measurements of effluent mass and nuclei concentrations have been used to model concentration versus velocity relationships discussed in Section X.

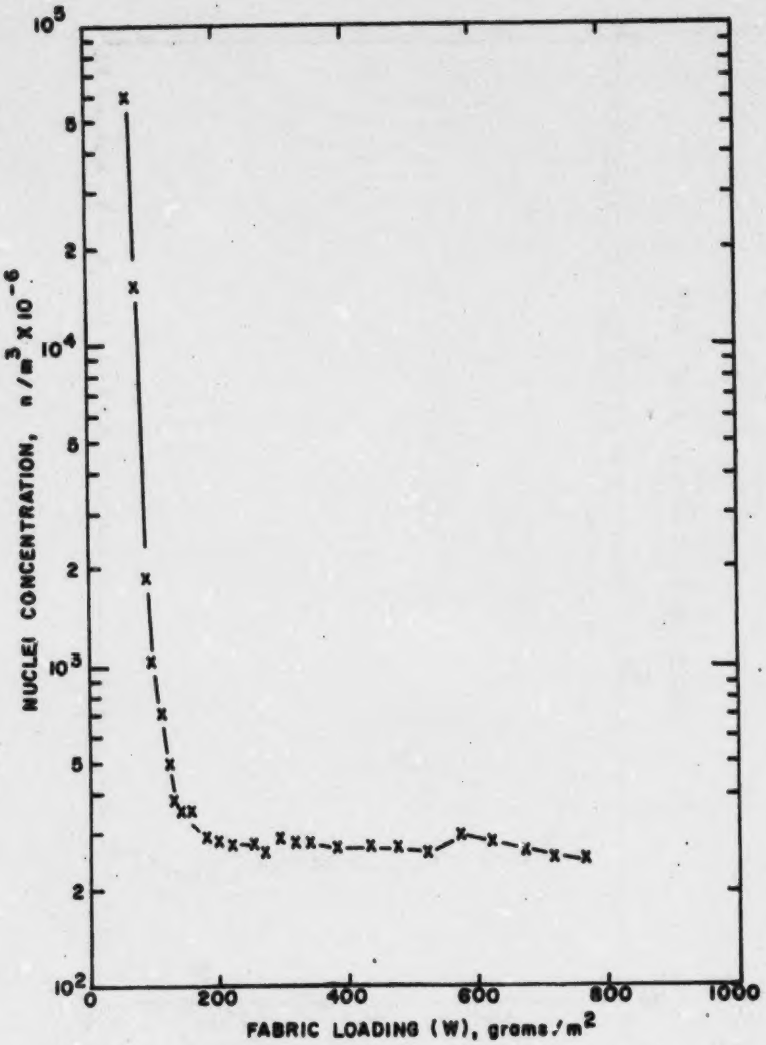

Figure 78. Effluent nuclei concentration versus fabric loading for used Sunbury fabric with lignite fly ash, Test 83

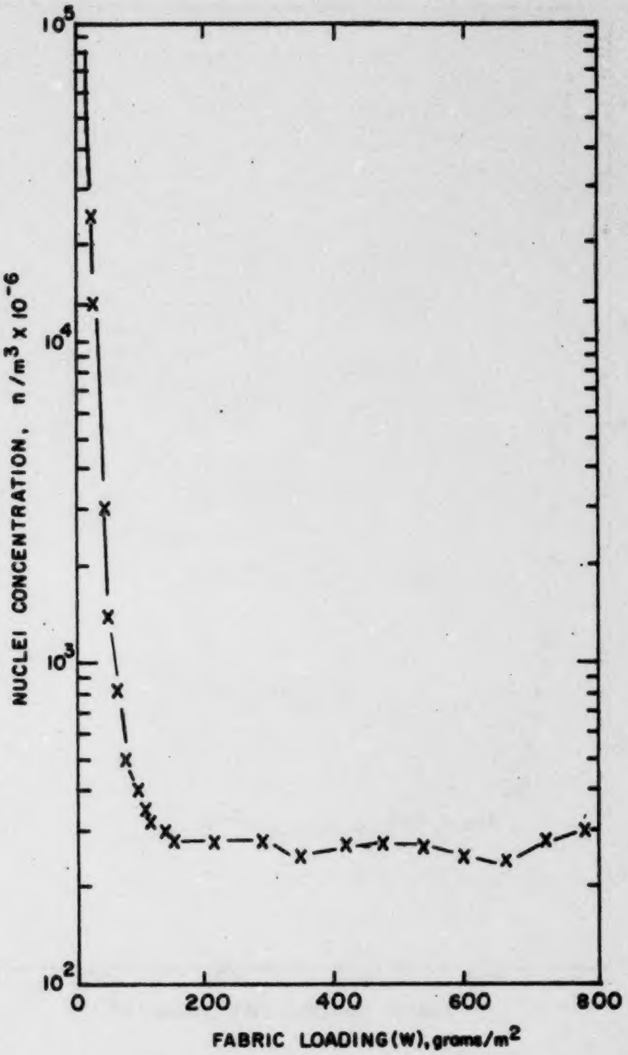

Figure 79. Effluent nuclei concentration versus fabric loading with used cotton sateen and GCA fly ash, Test 84

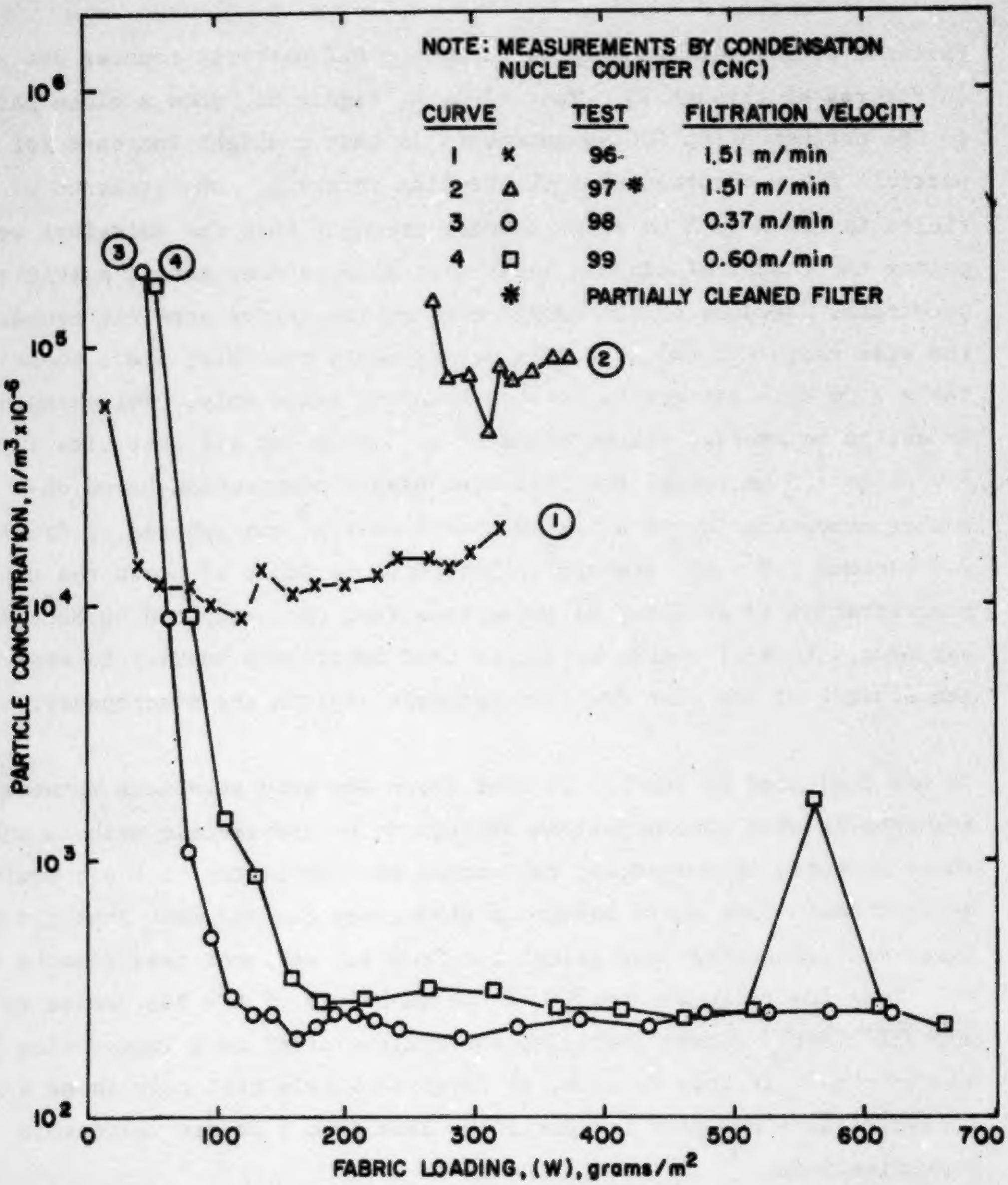

Figure 80. Effect of filtration velocity on effluent nuclei concentration, GCA fly ash with new Sunbury fabric

Particle Size and Concentration by Optical Counter

Particle sizing measurements performed by B&L particle counter are given in Figures 81 through 83. Test 67 data, Figure 81, show a close parallel to the corresponding CNC measurements in that a slight increase for all particle sizes occurred over the testing interval. The presence of particles in the 2 to 5 μm range suggest strongly that the emissions were mainly the result of pinhole leaks that allowed many coarse particles to penetrate. Because of electronic choking (excessive particle numbers in the size range < 2 μm), the only measurements possible; i.e., those for the > 2 μm size categories have qualitative value only. For example, if we assign an average volume diameter of 3.5 μm for all particles in the > 2 μm to > 5 μm range, the predicted mass concentration based on a number concentration of 6.5×10^7 particles/cm^3 and spheres of density 2.0 becomes 2.9×10^3 grams/m^3. Reference to Table 18 shows the above concentration to be about 24 times less than that computed by Method 5 sampling. Loss of coarse particles that contribute heavily to mass and the neglect of the fine fraction probable explain the discrepancy.

It was indicated in Section IV that there was good agreement between atmospheric dust concentrations determined by gravimetric methods and those computed by converting B&L number concentrations to their equivalent mass values. This would appear to strengthen the argument that the much lower mass concentrations calculated from B&L effluent measurements (20 to 100 times lower) is the result of the inability of the B&L device to collect and efficiently detect particles (or agglomerates) much larger than 5 μm in diameter. If this is true, it is quite likely that only those number concentrations reported for particles less than 5 μm are reasonable approximations.

Bausch and Lomb measurements for the Nucla fabric tests, Figures 82 and 83, indicate both lower effluent concentrations and finer size distributions relative to the Sunbury tests. Despite the fact that the absolute values of CNC and B&L tests may be subject to question under some test conditions, they are not only consistent with each other but also follow the same

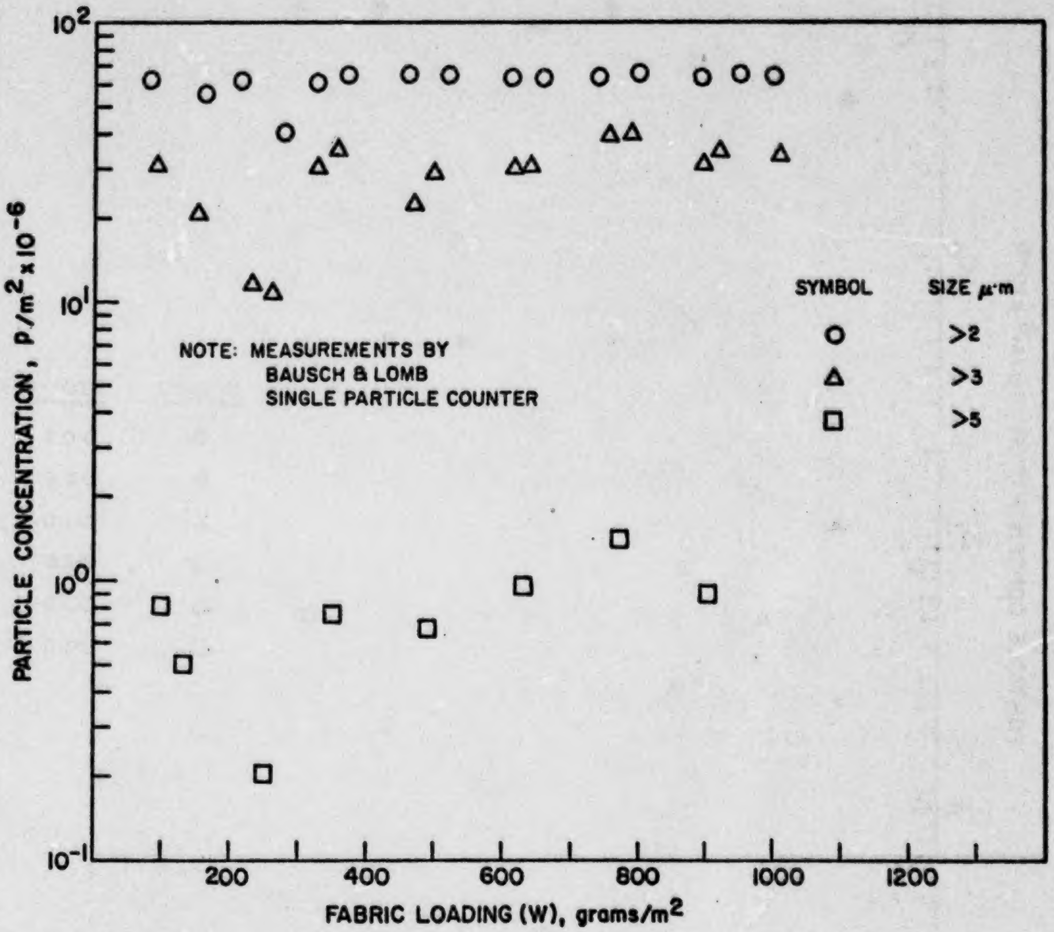

Figure 81. Effluent concentration versus fabric loading and particle size for used Sunbury media with GCA fly ash, Test 67

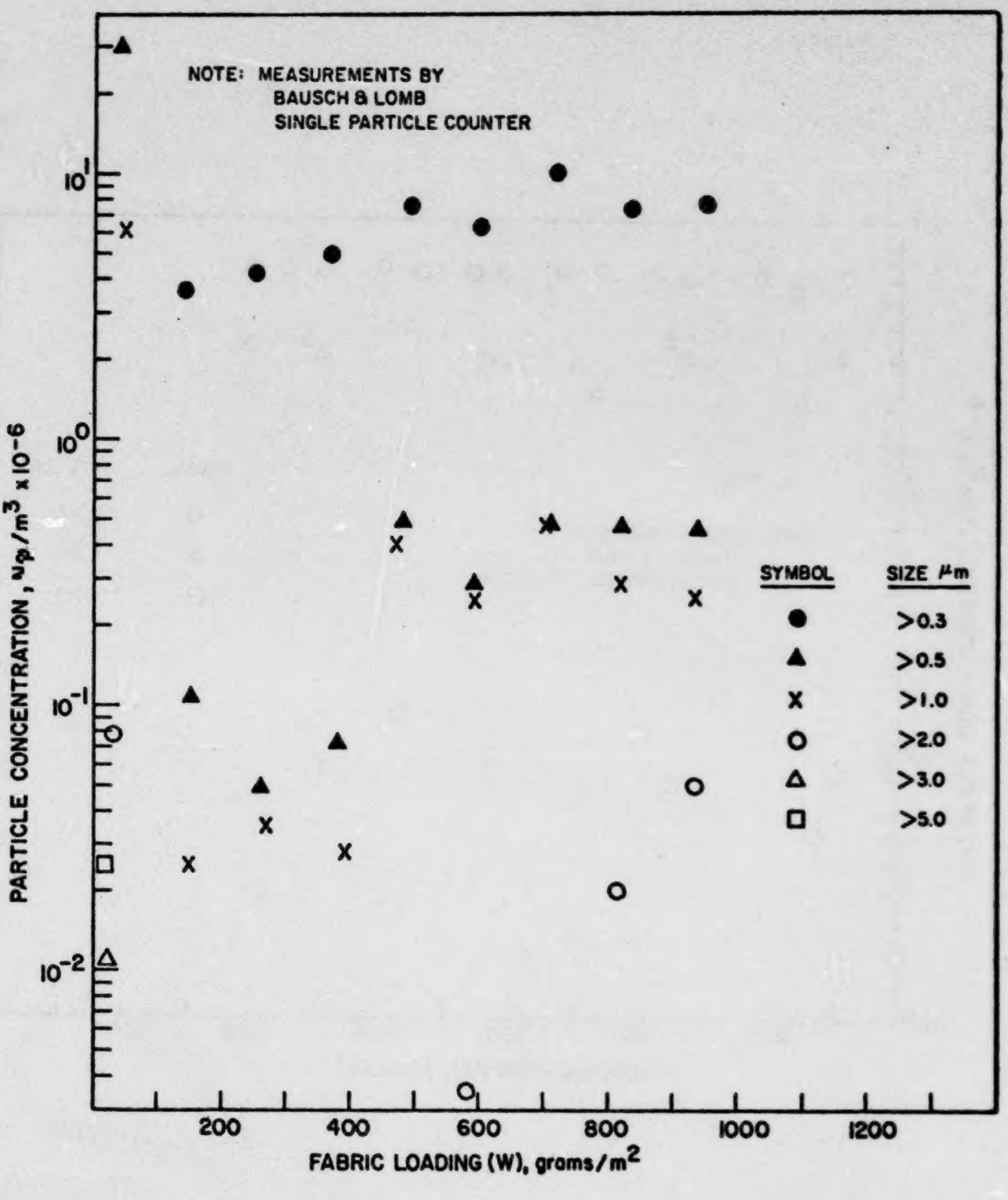

Figure 82. Effluent concentration versus fabric loading and particle size for unused Nucla fabric with GCA fly ash, Test 68

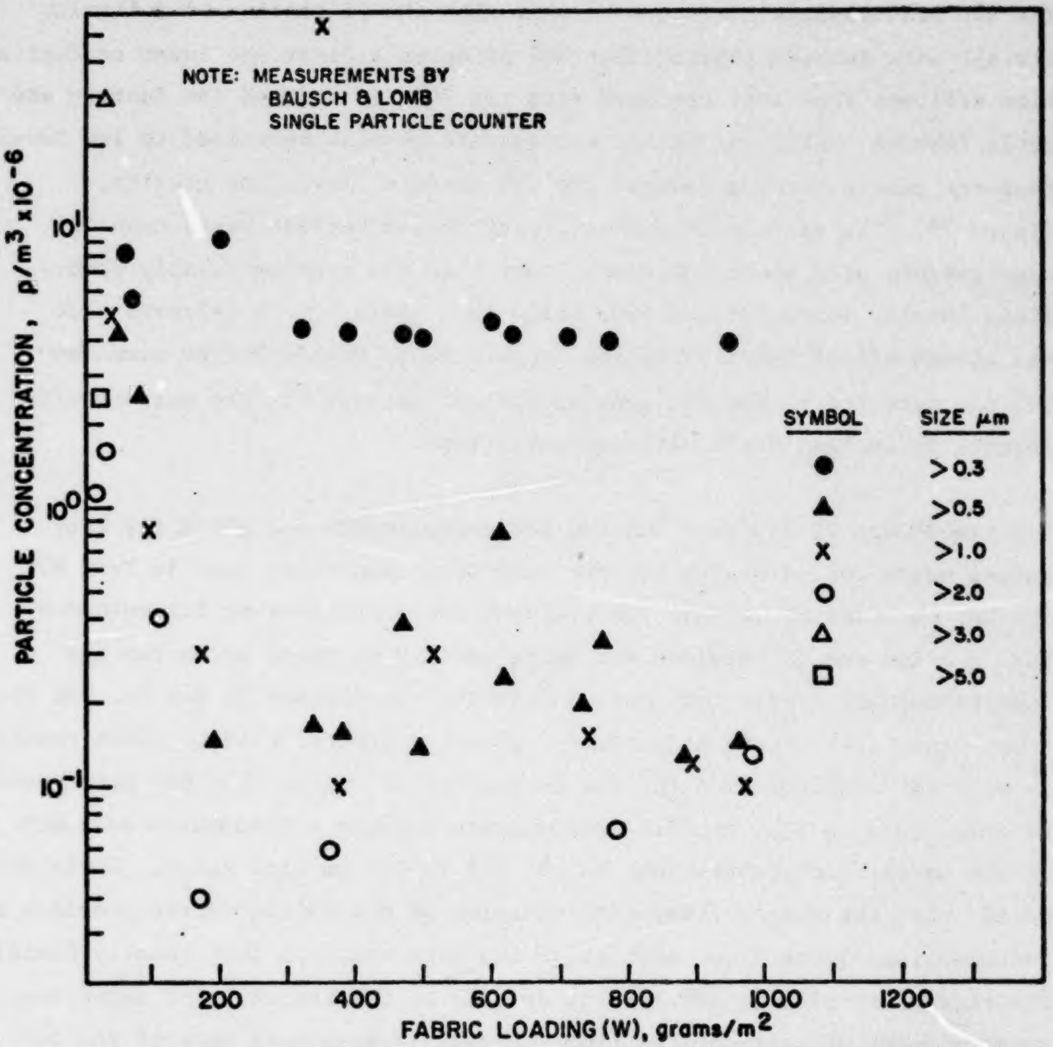

Figure 83. Effluent concentration versus fabric loading and particle size for used Nucla media with GCA fly ash, Test 69

trends set by the gravimetric measurements. Therefore, we believe that the present program again demonstrates the value of both techniques as means for detecting and/or explaining rapid changes in filter system function.

The B&L measurements of Figure 84 show that the filtration of a lignite fly ash with Sunbury fabric (Test 83) produces a finer and lower concentration effluent than that obtained with the GCA fly ash and the Sunbury and Nucla fabrics. Effluent nuclei concentrations also decreased to low levels once the fabric loading reached the 150 grams/m^2 level and greater, Figure 78. The calculated mass effluent concentrations based upon B&L measurements were about 200 times lower than the gravimetrically determined levels, Tests 83B and 83C, Table 18. Again, it is believed that the slough-off of large particles capturable by Method 5 type sampling but not detected by the B&L sensing system, account for the extreme difference in estimated effluent concentrations.

Figures 85 and 79 indicate B&L and CNC measurements for a GCA fly ash/ sateen weave cotton system for the same test conditions used in Test 83. The key observation is that the effluent concentrations as determined by both the B&L and CNC devices are quite similar to those noted for the lignite/Sunbury fabric combination described in Figures 84 and 78. On the other hand, gravimetric measurements showed a greater than 10 times reduction in effluent concentration for the cotton system, Table 18. Our interpretation of these data is that the B&L measurements provide a reasonable estimate of the particle concentrations in the 0.3 to 1.0 μm size range. It is suspected that the staple fiber configuration of the cotton fabric provides an intercepting, loose fiber mesh above the pore openings that greatly diminishes the chances of pinhole development as well as the tendency for aerodynamic reentrainment of agglomerates from the rear (downstream) face of the dust layer.

Nuclei Versus Mass Concentrations

An extensive review and assessment of condensation nuclei measurements performed during GCA laboratory and pilot tests have revealed that these

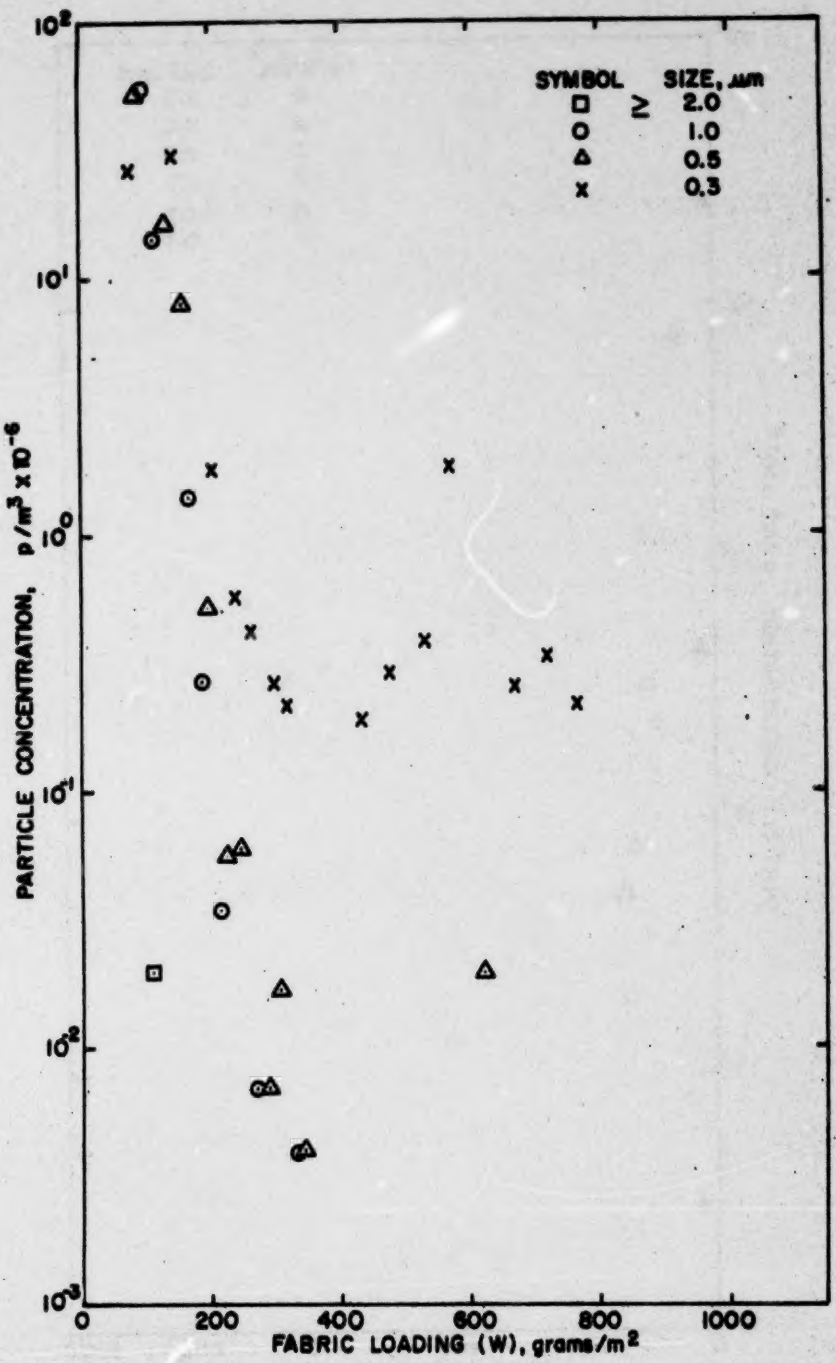

Figure 84. Effluent particle concentration versus fabric loading and particle size for used Sunbury fabric and lignite, Test 83, B&L measurements

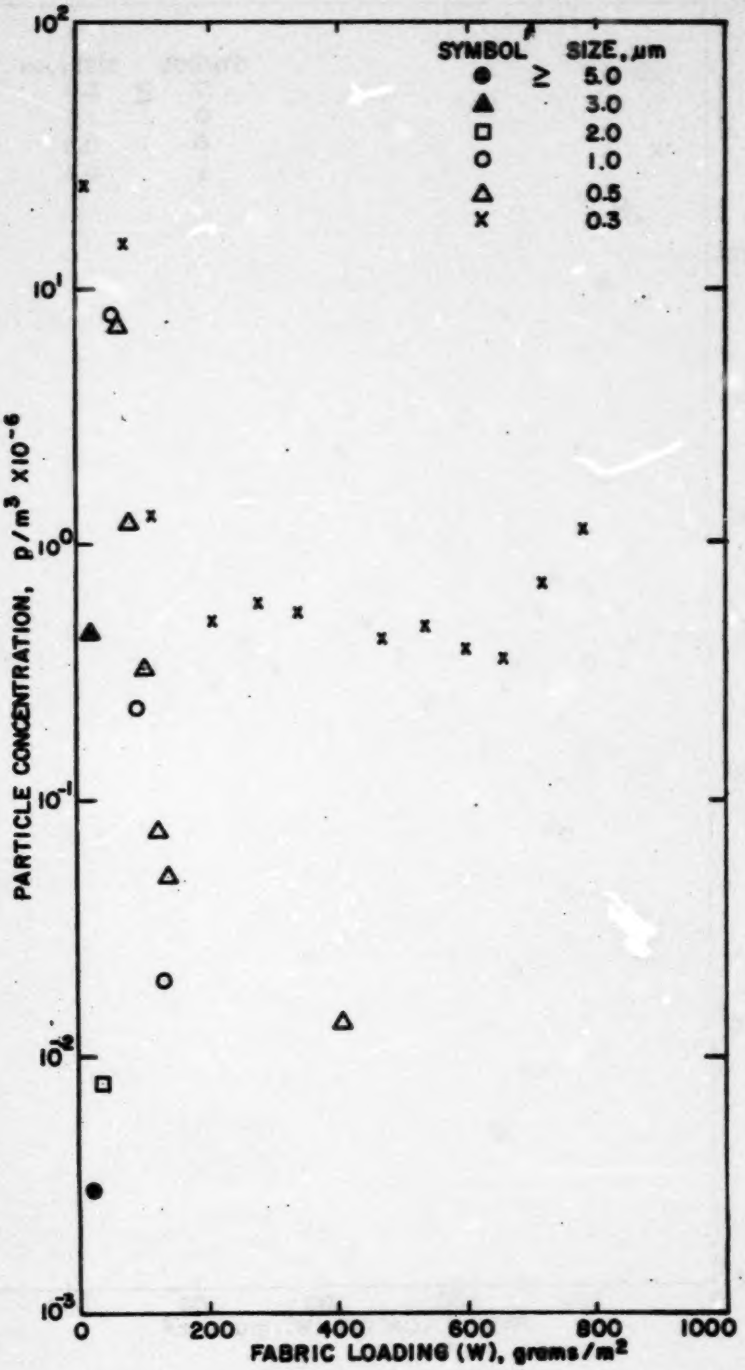

Figure 85. Effluent concentration versus fabric loading for unused cotton sateen with GCA fly ash (Test 84) B&L measurements

data, when used properly, provide an excellent record of the rapid changes in mass effluent concentrations that take place during a typical filtration cycle. Average nuclei concentrations, which were determined by conventional graphical integration methods, embraced the same fabric loading intervals used to establish the corresponding average mass concentration by filter sampling.

A graph of the average nuclei concentrations observed or calculated for the filter effluents versus concurrent mass measurements by all-glass filters indicates a linear relationship over the concentration range $\sim 10^{-3}$ g/m^3 to 10 g/m^3 (see Figure 86). Although one can question the absolute nuclei counts as displayed by a CNC device, one expects a properly functioning unit to provide reproducible measurements. Thus, with respect to any aerosol the nuclei population should bear a constant relationship to the corresponding total mass concentration.

The fact that a linear relationship previals for the effluent measurements has some interesting implications. First, any significant downstream nuclei concentration must arise from penetration through the filter, either through open pores (or pinholes) or through a "thin" freshly formed dust layer. No nuclei-sized particles should be generated by particle slough-off from the filter because adhesive forces preclude the release of anything but agglomerates or discrete particles in the 5 to 10 μm range or larger. Secondly, the existence of the same proportionality between nuclei and mass concentration in the filter effluent indicates that the observed mass penetration is principally that which escapes through unblocked pores during the early filtration period or through large pores (pinholes) that fail to bridge over at any time during the filtering cycle. One can also infer that the persistence of this proportionality means that very little dust is removed from that fraction of the gas volume which passes through these unblocked pores.

The end result is that the dust that passes through the open pores prior to their bridging dominates the size properties of the filter effluent. Accordingly, when we examine the comparative size properties of inlet

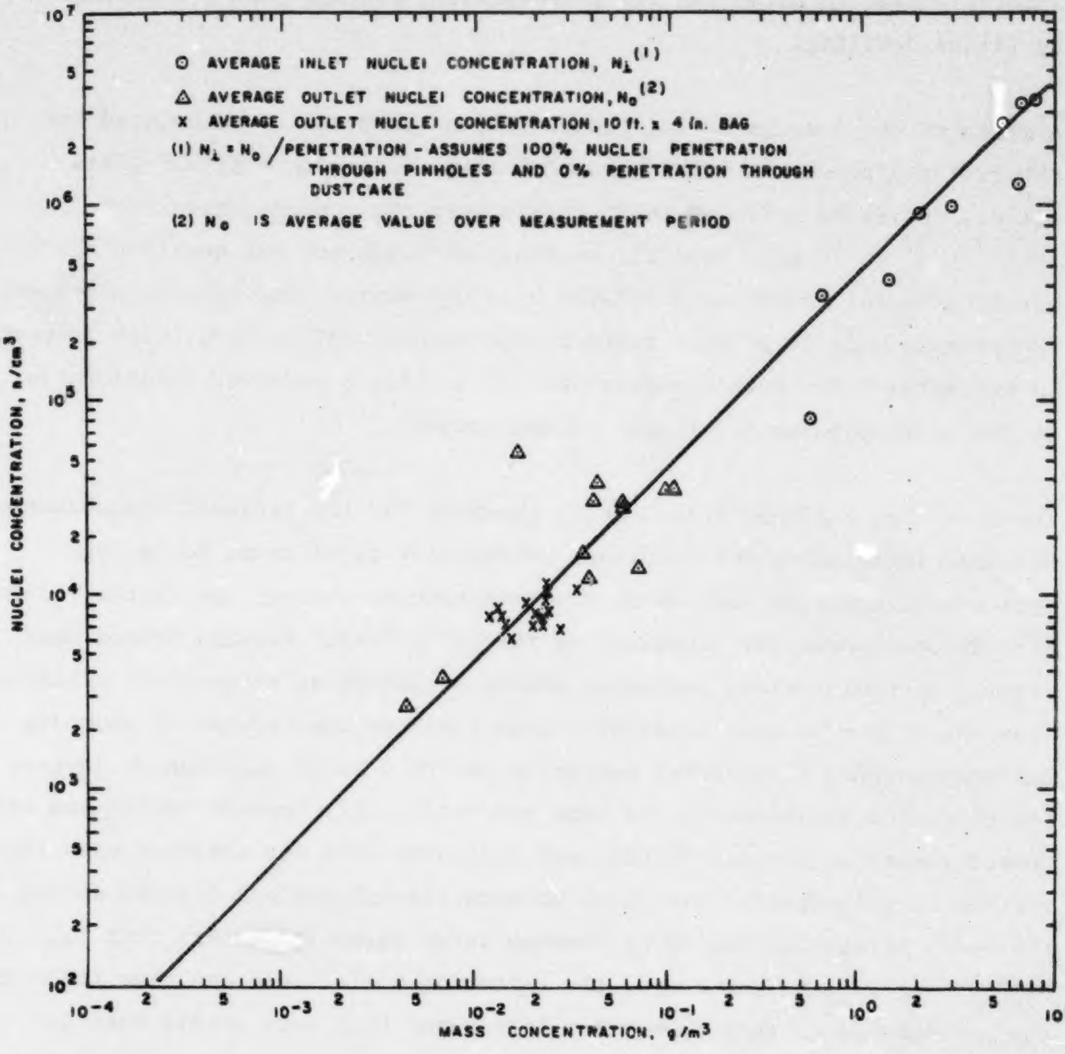

Figure 86. Calibration curve - nuclei and related mass concentrations for GCA fly ash

and effluent dusts we see very little difference in size distribution measurements by cascade impactor provided that all phases of the filtration cycle are properly represented. For this reason, practically all field and laboratory tests performed with identical and properly functioning sizing apparatus show essentially the same collection efficiency for all but the largest particles, 30 μm or larger. The basic problem is that so much more of the inlet dust passes through the pores with little or no dust removal as compared to that which passes through the dust cake, that the real fractionating potential of the dust cake is completely obscured.

The inlet nuclei concentrations were estimated by the following indirect method. It was assumed that the observed outlet nuclei concentrations were attributable to the direct penetration of nuclei through pores or pinholes. It was also assumed that the total dust concentration penetrating a pinhole is directly proportional to the nuclei concentration because dust removal from the fraction of air passing through the pinhole is negligible for glass fabrics of the Sunbury or Nucla types. Therefore, if mass measurements are available to define inlet and outlet concentrations, the penetration value can be applied to the outlet nuclei concentration to estimate the corresponding inlet value; i.e., $C_i = C_o/P_n$. As stated previously, this step appeared reasonable because size distribution measurements for upstream and downstream aerosols are nearly the same.

The relationship between nuclei and mass concentrations shown in Figure 86 actually constitutes a calibration curve. These data have been used to transpose point values for outlet nuclei concentrations determined under several test conditions to their equivalent mass values.

A summary of concentration, efficiency and penetration data for fly ash filtration with glass fabrics is given in Table 19. Information on the state of the filters during these tests with respect to pinholes (if any), prior service of the filter and its dust holding range during each test are also presented. A similar data tabulation, Table 20, compares inlet

Table 19. SUMMARY OF CONCENTRATION, EFFICIENCY AND PENETRATION MEASUREMENTS FOR GCA FLY ASH FILTRATION WITH WOVEN GLASS FABRICS AT 0.61 m/min FACE VELOCITY

Test no.	Inlet concentration g/m^3 gravimetric[a]	Outlet concentration $g/m^3 \times 10^3$		Fractional penetration		Fractional efficiency		Comments		
		Gravimetric	CNC[b]	Gravimetric and CNC	Gravimetric	Gravimetric and CNC	Gravimetric	Initial filter state[c]	Pinhold leaks m/m^2[d]	Fabric loading range - g/m^2
65 A	1.24	9.2	28.0	0.023	0.0074	0.977	0.9926	new	-	0 - 130
65 B	1.53	1.8	1.6	0.0010	0.0012	0.9990	0.9988	loaded	-	130 - 210
65 F	3.00	99	96.0	0.032	0.033	0.968	0.967	loaded	2,500	750 - 1200
66 A	0.63	58	80.0	0.126	0.102	0.874	0.908	just cleaned	yes	31 - 77
66 C	2.02	35	32.0	0.016	0.017	0.984	0.983	loaded	680	106 - 280
66 D	1.41	39	28	0.028	0.022	0.978	0.972	loaded	680	280 - 430
67	8.05	68	33	0.0041	0.0084	0.9959	0.9916	just cleaned	yes	29 - 1000
68[e]	6.36	6.9	8.0	0.0013	0.0011	0.9987	0.9989	new	yes	0 - 1000
69[e]	6.25	6.9	8.0	0.0013	0.0011	0.9987	0.9989	just cleaned	yes	11 - 1000
70 A	5.18	41	95.0	0.018	0.008	0.982	0.992	new	yes	0 - 128
70 B	7.38	9.2	1.5	0.0002	0.0012	0.9998	0.9988	loaded	?	95 - 230
96[f]	5.37	58.3	65.0	0.012	0.011	0.988	0.989	new	603	0 - 400
97[f]	4.60	563	220	0.048	0.122	0.952	0.878	just cleaned	3,588	270 - 390
98 A[g]	8.09	16.7	120	0.014	0.0021	0.986	0.9979	just cleaned	yes	47 - 90
98 B	8.09	1.8	0.4	0.00005	0.0002	0.9999	0.9998	loaded	no	90 - 620
99 A	8.40	43	89	0.010	0.0051	0.990	0.9949	just cleaned	yes	56 - 140
99 B	8.40	1.6	0.9	0.0001	0.0002	0.9999	0.9998	loaded	no	140 - 660
71	6.84	4.6	5.5	0.0008	0.0007	0.9992	0.9993	just cleaned	yes	32 - 660
72 A-C	6.73	90.8	60.0	0.0089	0.0135	0.9911	0.9865	just cleaned	402	340 - 750

[a] Gravimetric refers to Method 5 filter sampling or direct weighing of test panels.

[b] CNC measurements converted to equivalent mass concentration based on calibration curve.

[c] New indicates first use of filter; loaded designates intermediate test; just cleaned refers to partial or complete cleaning.

[d] Observed number of pinholes per m^2; yes means pinholes detected but not counted; all new or cleaned filters.

[e] Nuclo fabric for Tests 68 and 69; Sunbury fabric for other tests.

[f] Face velocity = 1.52 m/min (5.0 ft/min).

[g] Face velocity = 0.38 m/min (1.3 ft/min).

Table 20. INITIAL AND AVERAGE OUTLET CONCENTRATIONS AND RELATED PENETRATION DATA FOR FLY ASH/WOVEN GLASS FABRIC FILTERS

Test No.[a]	Inlet concentration nuclei/cm^3		Initial outlet[d] concentration		Fractional penetration		Average outlet concentration	Initial fabric loading[g]
	CNC[b]	Calibration[c]	Nuclei/cm^3	g/m^3[e]	Initial[d]	Average[f]	Nuclei/cm^3	g/m^2
65 A		5.6×10^5	1.5×10^5	0.335	0.27	0.0074	1.27×10^4	0.76
65 B							7×10^2	
65 F	1.0×10^6	1.36×10^6					4.67×10^4	
66 A	3.4×10^5	3.0×10^5	1.5×10^5	0.315	0.500	0.102	3.6×10^4	0.38
66 C	9.2×10^5	9.0×10^5					1.6×10^4	
66 D	4.3×10^5	6.5×10^5					1.25×10^4	
67		3.8×10^6					15×10^4	
68		3.0×10^6	3×10^5	0.636	0.100	0.0011	3.7×10^3	3.9
69		2.9×10^6	2.5×10^5	0.537	0.086	0.0011	3.6×10^3	3.8
70 A		2.4×10^6	2.7×10^5	0.580	0.112	0.008	4.3×10^4	3.2
70 B							0.7×10^3	
96	2.8×10^6	2.5×10^6	1.5×10^5	0.322	0.060	0.011	2.9×10^4	3.3
97		2.1×10^6	1.5×10^5				1.0×10^5	
98 A		3.8×10^6	2×10^5	0.428	0.053	0.0021	5.2×10^4	4.9
98 B							2.5×10^2	
99 A		3.9×10^6	1.8×10^5				3.8×10^4	
99 B							3.9×10^2	
71	3.5×10^6	3.2×10^6	7.2×10^4	0.150	0.022	0.0007	2.5×10^3	4.2
72 A-C	1.3×10^6	3.1×10^6	2.6×10^5	0.565	0.084	0.0135	2.7×10^4	4.1

[a] See Table for additional concentration and penetration data.

[b] Estimated from outlet nuclei concentration and filter penetration computer from gravimetric measurement. Nuclei penetration assumed to reflect air volume passing through open pores or pinholes that collect no dust.

[c] Estimated from gravimetric equivalent and calibration curve.

[d] First measurable CNC data; assumed to relate to added dust increment of 4 g/m^2 (roughly one minute after initiation of filtration).

[e] Equivalent mass concentration from calibration curve.

[f] Average penetration over test interval, see Table 19.

[g] Corresponds to initial fractional penetration.

and outlet concentrations on the basis of nuclei counts. Initial penetration values are based upon the initial measurements of condensation nuclei concentrations.

The "initial" value depicts the nuclei concentration about one minute following resumption of filtration after which time the flow has stabilized. If the average inlet concentration is assumed to be about 6.5 g/m^3, the average fabric holding after 1 minute is about 4 g/m^2. However, in the subsequent development of the relationship between effluent concentration and filtration velocity, the actual fabric loadings at 1 minute (last column, Table 20) were computed based upon the observed inlet loadings.

Effluent Concentrations Versus Face Velocity

Data for Sunbury and Nucla fabrics are shown in Figure 87 for fly ash filtration at 0.61 m/min face velocity and for Sunbury fabrics at three filtration velocities in Figure 88. The coordinates for the origin of each curve are the inlet dust concentration and the increment of fabric loading added following initiation of filtration. It is expected that the true "instantaneous" effluent concentration is about one half that of the inlet value as will be discussed in Section X. Additionally, it was also expected that the initial effluent concentration would increase, although not necessarily linearly, with the inlet concentration. Data points for these curves are summarized in Table 21 for both nuclei and mass concentrations, as a function of time. Mass concentrations were estimated from point values of nuclei counts and the calibration curve, Figure 86.

Rating Fabrics With Atmospheric Dust

Most woven fabric filters perform poorly when filtering atmospheric dust only because there is no solid dust layer for particle removal. Only after several months does sufficient dust accumulate to provide effective filtration. For this reason, precoating or flocking techniques have been

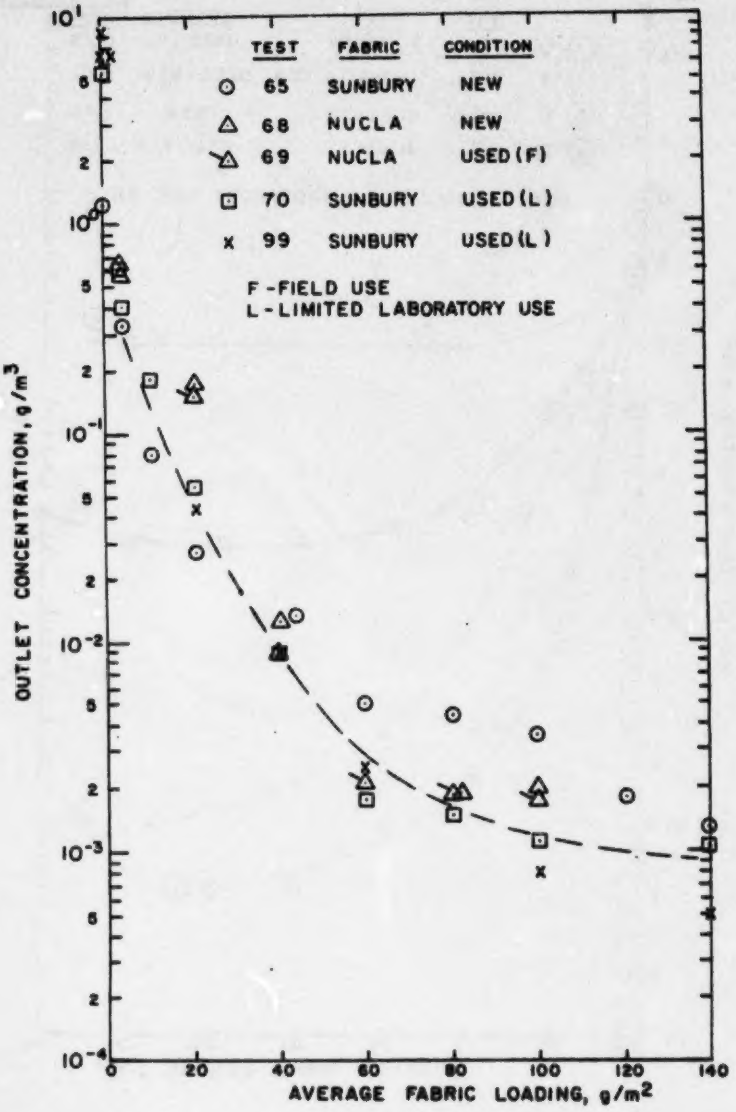

Figure 87. Outlet concentration versus fabric loading at 0.61 m/min (2 ft/min) face velocity. GCA fly ash with Sunbury and Nucla fabrics. Loading increase referred to start of filtering cycle

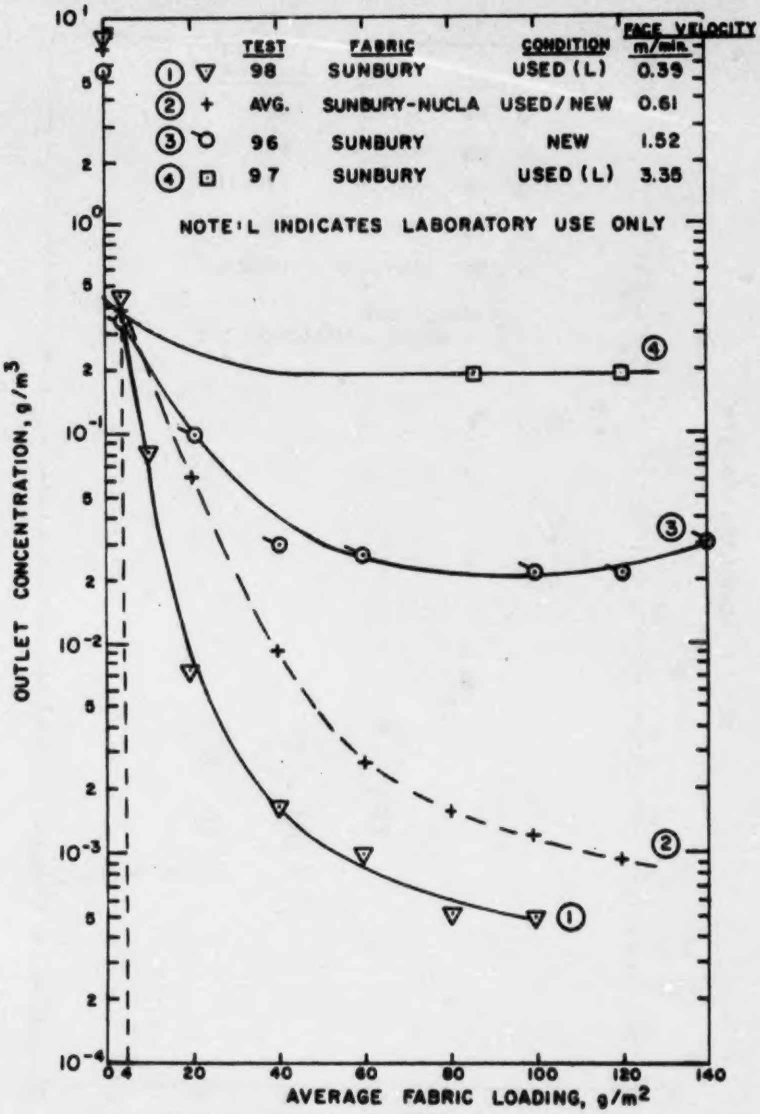

Figure 88. Outlet concentration versus fabric loading for three face velocities. GCA fly ash and Sunbury fabric. Loading increase referred to start of filtering cycle

Table 21. CHANGE IN EFFLUENT CONCENTRATION WITH INCREASING FABRIC LOADING FOR FLY ASH FILTRATION WITH WOVEN GLASS FABRICS

W	C_o (Outlet concentration) g/m^3															
	Test 65		Test 68		Test 69		Test 70		Test 96		Test 66		Test 72		Test 97	
g/m^2	N/cm^3	g/m^3	N/cm^3	g/m^3	N/m^3	g/m^3	N/m^3	g/m^3	N/m^3	g/m^3	N/m^3	g/m^3	N/m^3	g/m^2	N/m^3	g/m^3
0[a]	1.24		6.36		6.25		5.18		5.37		0.63		6.73		4.60	
4	$1.5\text{x}10^5$	0.34	$3\text{x}10^5$	0.64	$2.5\text{x}10^5$	0.55	$2.7\text{x}10^5$	0.60	$1.5\text{x}10^5$	0.34	$1.5\text{x}10^5$	0.34	$2.6\text{x}10^5$	0.56	$1.5\text{x}10^5$	0.34
10	$3.5\text{x}10^4$	0.08					$8\text{x}10^4$	0.18	$8\text{x}10^4$	0.18	$3.2\text{x}10^4$	0.07	$2\text{x}10^4$	0.045		
20	$1.2\text{x}10^4$	0.027	$8\text{x}10^4$	0.18	$7\text{x}10^4$	0.15	$2.5\text{x}10^4$	0.055	$4.5\text{x}10^4$	0.10	$2\text{x}10^4$	0.044				
40	$4.2\text{x}10^3$	0.0092	$6\text{x}10^3$	0.013	$4\text{x}10^3$	0.009	$4\text{x}10^3$	0.009	$1.4\text{x}10^4$	0.031	$1.1\text{x}10^4$	0.025	$9\text{x}10^4$	0.020	$7.5\text{x}10^4$	0.17
60	$2.3\text{x}10^3$	0.005	$1\text{x}10^3$	0.0022	$1\text{x}10^3$	0.0022	$8\text{x}10^2$	0.0018	$1.2\text{x}10^4$	0.027	$3\text{x}10^4$	0.065	$7\text{x}10^3$	0.015	$7\text{x}10^4$	0.15
80	$2\text{x}10^3$	0.0045	$9\text{x}10^2$	0.0020	$9\text{x}10^2$	0.0020	$6.5\text{x}10^2$	0.0015			$3\text{x}10^4$				$8.2\text{x}10^4$	0.18
100	$1.6\text{x}10^3$	0.0036	$8\text{x}10^2$	0.0018	$9\text{x}10^2$	0.0020	$5\text{x}10^2$	0.0011	$1\text{x}10^4$	0.022			$4.7\text{x}10^3$	0.010		
120	$8\text{x}10^2$	0.0018							$9\text{x}10^3$	0.020					$1\text{x}10^5$	0.22
130													$5\text{x}10^3$	0.011	$9.5\text{x}10^4$	0.21
140	$6\text{x}10^2$ [b]	0.0013			$8\text{x}10^2$ [b]		$4\text{x}10^2$	0.0009	$1.4\text{x}10^4$	0.031	$3\text{x}10^4$					
							$3.5\text{x}10^2$ [b]		$2.5\text{x}10^2$ [b]		$6\text{x}10^2$ [b]			0.018		

[a] Indicated concentrations are inlet values. True outlet concentration at time zero should be less than inlet value.

[b] Apparent lower detection limit for CNC during measurement period.

employed when fabric filters have been selected to remove low concentrations of highly toxic particles from the atmosphere. It was believed, however, that considerable insight might be gained as to the ultimate performance of many woven fabric filters if their atmospheric dust collection characteristics could be observed over the short term.

The rational behind this testing procedure is that many fabrics which possess essentially the same pore structure will display the same clean permeability characteristics even when there are differing amounts of loose fiber extending into the pore zone. Although the loose fiber substrate obstructing a pore may make a negligible contribution to (clean) resistance to air flow, the subsequent accumulation of particles upon it will change this picture radically. Interlaced fibers with dust accumulation now effectively subdivided a single pore into several smaller areas as well as causing an appreciable reduction in pore cross section. The net result is that a significant increase in filter resistance is expected within a short time when filtering industrial aerosols whose concentrations are typically 10^5 to 10^6 times greater than ambient dust concentrations. In contrast, the absence of a fiber substrate within a pore limits early particle removal to the inlet and wall surfaces such that extended time periods are required before appreciable blocking and resistance increases can take place.

Although there are several choices of test aerosol generators and materials,[30] ambient dust affords the major advantage of availability at no cost. Therefore, various fabric test panels were mounted in the bench scale apparatus, Figure 5, so that alternate measurements of particle concentrations as determined by condensation nuclei and B&L optical counters could be performed immediately upstream and downstream of the filter. Minimal length sampling lines ran to a glass switching valve so that upstream or downstream samples could be directed to the sensing areas of the CNC and B&L units. Approximately 2.5 minute intervals were allowed between upstream and downstream to allow for flush out and equilibration.

Figure 89 shows inlet and outlet concentrations for the two woven glass fabrics (Sunbury and Nucla types) and a sateen weave cotton. Whereas the fill fibers alone produce the discrete fiber phase of the glass filters, the cotton yarns are spun from staple fibers such that there are many more free fibers as evidenced by the napped appearance. Over the brief testing periods, < 50 minutes, it is unlikely that sufficient dust is deposited upon fibers to alter their base collection efficiency. Therefore, the temporal changes merely reflect normal variations in ambient dust levels. Data summaries in Table 22 indicate that the cotton fabric is the more efficient fine particle collector. Hence, one ultimately expects that better overall performance will be afforded by the cotton fabric insofar as efficiency and effluent characteristics are concerned. Many prior measurements confirm the above observation.[7,8,9,10,31]

The failure of B&L and CNC measurements to display a constant proportionality is due to significant variations within the coarse cost particle fraction of the ambient dust. Thus, the nuclei concentrations are relatively stable because only the coarse particle concentrations have increased.

The data presented here are too limited to allow prediction of the probable residual drag levels for a fabric impregnated with a specific dust when its clean (unused) permeability is known. However, the measuring technique is so simple that it is believed that examination of several fabrics whose structure and fiber array were known could develop this approach into a useful quantitative tool.

Table 22. ATMOSPHERIC DUST PENETRATION WITH WOVEN GLASS AND COTTON FABRICS

Instrument	Average penetration		
	Sunbury fabric	Nucla fabric	Sateen weave cotton
CNC	0.64	0.73	0.40
B&L	0.45	0.76	0.38

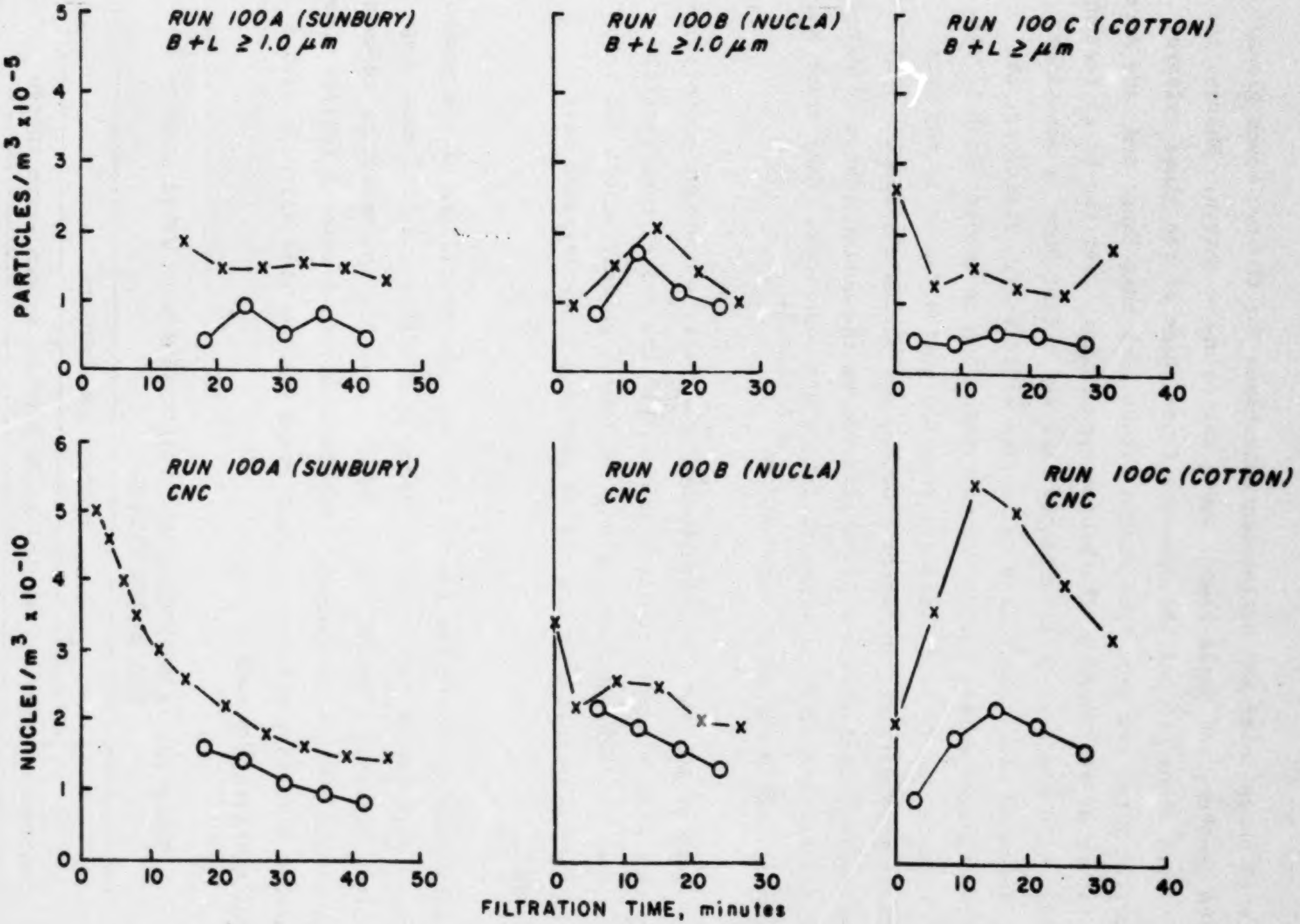

Figure 89. Room air filtration with clean (unused) woven fabrics at 0.61 m/min face velocity, inlet (x) and outlet (o) concentrations

SECTION VIII

PILOT PLANT TESTS

INTRODUCTION

Although the several bench scale tests described previously in this report have played a major role in providing a data base for model development, there were some areas where extrapolations from bench to full scale systems entailed considerable risk. It was pointed out, for example, that flat, unsupported test panels would experience more distortion in pore dimensions than a cylindrical bag because of the warping introduced in the former case. Additionally, bench scale tests afforded no acceptable means to simulate the collapse and reverse flow (or mechanical shaking) operations normally used to clean a woven fabric filter. However, the final state of a cleaned fabric panel was very accurately simulated by bench scale flexing and/or tapping such that the modeling concepts deriving from those measurements could be directly extrapolated to full scale units.

Field or pilot scale measurements, therefore, furnish the only practical means to properly relate the cleaning process and its associated energy input to the resultant cleaning. Here by resultant cleaning is meant how much dust is removed and what fraction of the fabric surface is exposed after application of the cleaning action.

SUMMARY OF TESTING PROCEDURES

Several tests were carried out with the pilot filter system described in Section IV, Figure 11. The filter bag was sewn from Sunbury type fabric into a 10 ft x 4 in. tube with five, equally-spaced internal rings to prevent complete bag collapse. Bag tension was adjusted by a turnbuckle built into the hangar arm attached to the cap section closing off the top of the bag. Filtration velocity 0.61 n/m (2 ft/min) and inlet dust concentration 7.16 g/m^3 (3.13 $grains/ft^3$) were maintained constant throughout the test series unless otherwise specified. Bag cleaning was accomplished by diverting the air flow from the bag through a by-pass loop followed by the use of reverse flow air at 0.48 m/min for a period of 1 minute. Dust dislodged during cleaning was collected in a special, readily-removed hopper for transfer and weighing. Rigorous bag cleaning was accomplished by hand shaking for those tests where it was desired that filtration begin with nothing but the "limiting," uniformly-distributed residual loading, W_R. The latter value was determined by separate weighings of the new and cleaned bags on a triple beam balance. Particle sizing measurements were performed with the same instrumentation used for bench tests; i.e., Andersen impactor, condensation nuclei counter (CNC) and optical counter (B&L). Inlet and outlet mass concentrations were determined by a combination of Method 5 type filtration, dust dislodgement and material balance. Special interior lighting for the bag (8 ft fluorescent tube) was installed so that dust removal patterns could be documented photographically.

GENERAL COMMENTS

The pilot test results are presented in several tables in which the pilot (P) plant measurements have been grouped, whenever possible, according to the specific purpose of each test series. Test P-1-1, Table 23, was a shake down operation after which it was ascertained that the bag was not properly sealed. However, an important observation during this test was that vibration of the baghouse structure by persons working on the elevated platform while making measurements led to erratic and excessive dust dislodgement from the bag. This problem was eliminated by relocation of instrumentation and sampling locations. This test demonstrated clearly that vibrations or shocks induced by heavy equipment operation, damper

Table 23. EFFLUENT CONCENTRATION FROM NEW (UNUSED) AND PARTIALLY LOADED SUNBURY TYPE FABRIC WITH GCA FLY ASH AND ATMOSPHERIC DUST

Run No.	Fabric loading at beginning of run, g/m^2	Fabric loading before cleaning, g/m^2	Fabric loading after cleaning, g/m^2	Dust removed by cleaning, g/m^2	Percent dust removed by cleaning	Outlet concentration[a] g/m^3	Average penetration percent
P-1-1[a]	0.0	1253	113	929	91.0[b]	0.0559	0.87
P-6-2	743	743	491	205	33.9	0.00063[c]	-
P-7-1[a]	491	843	147	567	82.6	0.0319	0.45
P-9-1[a]	0.0	461	461	0.0	0.0	0.0903	1.26

[a] Inlet concentration = 7.16 g/m^3, fly ash.

[b] Dust removed by hand-shaking.

[c] Inlet concentration ~ 0.00005 g/m^3, (atmosphere dust).

closings or fan pulsations can contribute to dust removal in the field. However, from the point of view of field validation or laboratory measurements, it would be difficult to quantitate their role in the cleaning process.

A second factor that could lead to a significant difference between field and laboratory performance was the presence of pinholes and the evidence of fabric distortion or stretching apparently arising from bag sewing operations. Tests performed with new (unused) fabrics, Table 23, and used bags, Tables 24 and 25, showed generally higher emission levels (2 to 3 times) than noted for the bench scale test panels. However, normal variability in fabric properties aside from sewing factors may also account for differences in performance.

DUST REMOVAL VERSUS FABRIC LOADING

The tests summarized in Tables 23, 24, 25 and 26 and Figure 90, indicate the amount of dust dislodged from a filter as the result of a single cleaning by collapse and reverse flow. Bags were tensioned at either 50 or 15 lbs and the reverse flow velocity and duration were identical at 0.49 ft/min and 1 minute, respectively. The amount of dust removed was observed to depend upon the prior dust holding of the fabric. This behavior appears to confirm the hypothesis that the dust separating force must increase as the deposit areal density increases while the opposing interfacial adhesive force depends upon the specific dust/fabric combination but not the areal density of the dust layer. The above factors are treated in detail in Section IX.

In appraising the dust removal relationship shown in Figure 90, it should be noted that several factors may influence dust removal. Generally speaking, one set of variables determines the adhesive forces which are controlled mainly by the specific dust and fabric properties and the related environmental effects of temperature, humidity and electrical charge.

Table 24. RELATIONSHIP BETWEEN DUST REMOVAL AND PREVIOUS FABRIC LOADING, GCA FLY ASH FILTRATION WITH 10 ft x 4 in. WOVEN GLASS BAG (SUNBURY TYPE) AT 0.61 m/min FACE VELOCITY

Run No.	Fabric loading at beginning of run, g/m^2	Fabric loading before cleaning, g/m^2	Fabric loading after cleaning, g/m^2	Dust removed by cleaning,[a] g/m^2	Percent dust removed by cleaning	Outlet concentration g/m^3	Average penetration percent
P-2-1	113	937	345	592	63.3	0.0501	0.70
P-2-2	327	422	387	35	8.4	0.0311	0.43
P-2-3	387	545	498	48	8.7	0.0230	0.32
P-2-4	498	723	598	126	17.4	0.0296	0.41
P-4-1[b]	85.9	696	274	422	60.6	0.0272	0.38
P-4-2	274	429	382	47.3	11.0	0.0281	0.39
P-4-3	382	536	476	49.1	11.2	0.0235	0.33
P-4-4	476	631	549	67.0	13.0	0.0286	0.40
P-4-5	549	704	550	125	21.8	0.0300	0.42

[a] Cleaning by bag collapse and reverse flow.

[b] P-4 series also used to demonstrate appearance of cleaned bag surface by means of light source inside the bag.

Table 25. REPETITIVE CLEANING AND FILTRATION CYCLES WITH GCA FLY ASH AND WOVEN GLASS (SUNBURY TYPE) FABRIC AT 0.61 ft/min FACE VELOCITY AND 50 lbs TENSION

Run No.	Fabric loading at beginning of run, g/m^2	Fabric loading before cleaning, g/m^2	Fabric loading after cleaning, g/m^2	Dust removed by cleaning, g/m^2	Percent dust removed cleaning	Outlet concen-tration, g/m^3	Penetration during run, percent
P-3-1	576	725	513	211	29.2	0.0353	0.49
P-3-2	513	662	552	111	16.7	0.0259	0.36
P-3-3	552	701	563	138	19.6	0.0144	0.20
P-3-4	563	713	602	111	15.6	0.0137	0.19
P-3-5	602	751	630	121	16.0	0.0279	0.39
P-3-6	630	780	633	147	18.9	0.0236	0.33
P-3-7	633	782	623	159	20.4	0.0227	0.31
P-3-8	623	772	615	157	20.3	0.0227	0.32
P-3-9	615	764	623	142	18.5	0.0252	0.35
P-3-10	623	772	657	115	14.9	0.0243	0.34
P-3-11	657	806	668	138	17.2	0.0213	0.29
P-3-12	668	817	663	154	18.9	0.0215	0.30
P-3-13	663	812	668	145	17.8	0.0206	0.28
P-3-14	667	817	616	201	24.6	0.0215	0.30
P-3-15	588	737	609	128	17.4	0.0190	0.27
P-3-16	609	758	625	133	17.6	0.0162	0.23
P-3-17	625	775	613	161	20.8	0.0144	0.20
P-3-18	613	763	629	134	17.6	0.0137	0.19
P-3-19	629	778	657	121	15.6	0.0121	0.17

Table 26. EFFECT OF REDUCED BAG TENSION, 15 lbs, ON DUST REMOVAL AND PENETRATION GCA FLY ASH WITH 10 ft x 4 in. BAG, SUNBURY FABRIC, AT 0.61 m/min FACE VELOCITY

Run No.	Fabric loading at beginning of run, g/m^2	Fabric loading before cleaning, g/m^2	Fabric loading after cleaning, g/m^2	Dust removed by cleaning, g/m^2	Percent dust removed by cleaning	Outlet concentration, g/m^3	Average penetraion, percent
P-5-1	550	705	501	167	29.0	0.0305	0.43
P-5-2	501	656	537	97.0	18.2	0.0234	0.33
P-5-3	537	692	554	112	19.9	0.0158	0.22
P-5-4	554	709	553	127	21.9	0.0224	0.31
P-5-5	553	708	559	122	21.1	0.0225	0.31
P-5-6	559	714	579	110	18.9	0.0190	0.26

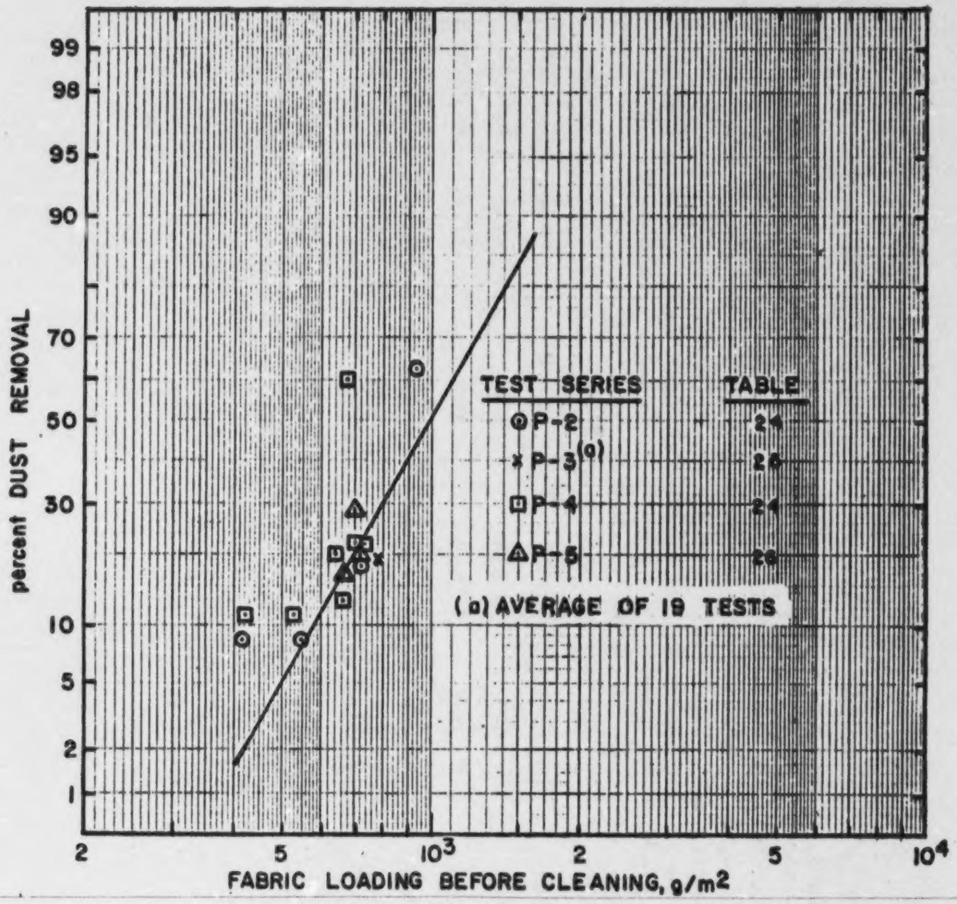

Figure 90. Dust removal versus fabric loading and estimated distribution of interfacial adhesive forces for GCA fly ash and Sunbury type fabric

The latter factors were considered to be constant during the laboratory studies. Except for the effect of gas temperature on viscosity and local gas velocities, the above items were not observed to cause any distinguishable performance differences between laboratory measurements and field filtration tests with coal-fired boilers.

The second set of variables relates to the description and quantitation of dust dislodgement effects. Prior mechanical shaking studies[10] and the sequence of tests described in Table 27 and Figure 91 show that repeated cleaning action removes additional dust although in rapidly diminishing quantities. One infers, therefore, that use of a single collapse and reverse flow cleaning cycle not only dislodges a specified quantity of dust but also alters the distribution of interface adhesive forces for the dust remaining on the fabric. Hence a second application of the same cleaning process will dislodge an additional increment of dust and so forth until further removal becomes negligible.

It was assumed that all dust removed from the fabric was attached with an adhesive force less than the applied dislodging force, the latter defined as the product of the fabric loading and the local gravitational acceleration. Therefore, if the curve shown in Figure 90 represents the results of a single bag cleaning at each of the indicated load levels, it is expected that a smaller slope would be displayed if multiple cleanings were performed at each fabric loading. The rationale for this statement is that at very high fabric loadings (1200 to 1500 g/m^2)[1,10] as much as 90 percent of the dust cake can dislodge. Thus, even with repeated cleanings, the maximum increase in percent dust removal could not exceed 10 percent. On the other hand, at lower fabric loadings a very significant increase in dust removal is possible by repetitive cleanings.

Percent dust removal was graphed on logarithmic probability paper because the data presented in Figure 90 also describe the distribution of adhesive forces over the interfacial region of the fabric. The estimated curve

Table 27. EFFECT OF SEVERAL SUCCESSIVE CLEANINGS BY BAG COLLAPSE AND REVERSE FLOW, GCA FLY ASH WITH WOVEN GLASS FABRIC (SUNBURY TYPE)

Number of cleanings[a]	Fabric loading before cleaning W_T g/m^2	Cumulative dust removed by cleaning $W_T' - W_R$ g/m^2	Fabric loading after cleaning W_R' g/m^2	Cumulative dust removed by cleaning percent	Cleaned area fraction[b] a_c	Uncleaned area fraction[c] a_u
1	778	121	657	15.6	0.167	0.833
2	657	169	609	21.7	0.232	0.768
3	609	194	584	24.9	0.266	0.734
4	584	214	564	27.5	0.299	0.701
5	564	222	556	28.5	0.309	0.691
6	554	232	546	29.8	0.319	0.681
7	546	238	540	30.6	0.328	0.672
8	540	245	533	31.5	0.337	0.663
9	533	251	527	32.2	0.345	0.655
10	527	256	522	32.9	0.352	0.648
11	522	259	519	33.2	0.356	0.644

[a] These tests represent a continuation of the cleaning process with the first cleaning corresponding to Run P-3-19, Table 25.

[b] $a_c = 1 - a_u$

[c] $a_u = W_R' - W_R/W_{T_1} - W_R$, where W_R is the residual uniformly distributed loading on the cleaned fabric surface and WT_1 is the cloth loading before the first cleaning.

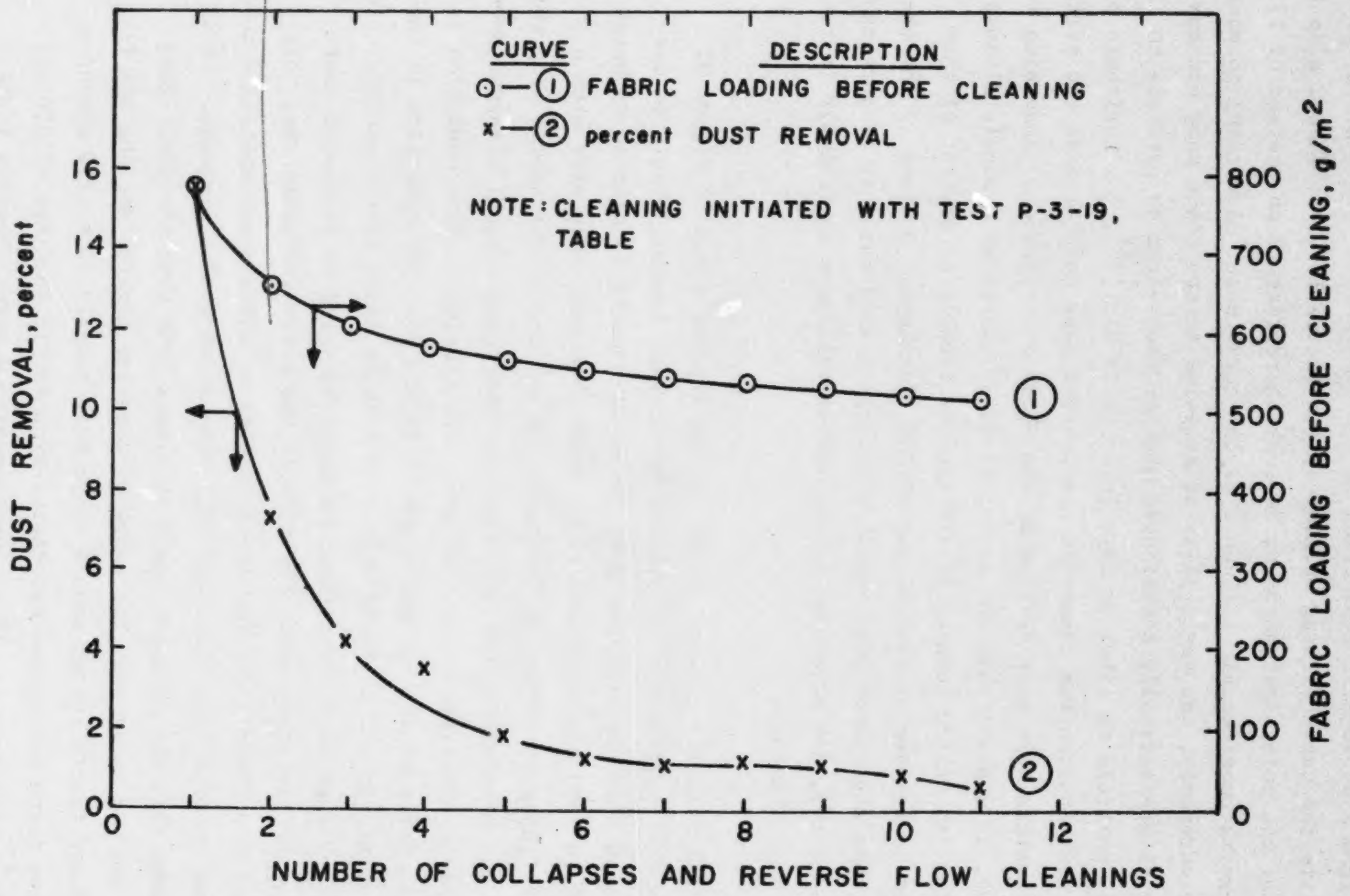

Figure 91. Dust removal characteristics for repetitive cleaning cycles, Sunbury type fabric with GCA fly ash

derives from a subsequent replotting of the data points on a log-log scale to simplify the curve fitting mechanics, see Figure 119. It should also be noted that the point designated as P-3, which represents an average of 19 tests, exerts considerable influence on the curve path. According to many prior measurements, the variability of adhesive forces about some central tendency is statistically distributed whether the system be particle to particle, particle to fiber or dust layer to fabric.[1,28] A logarithmic probability distribution was chosen in the present case only because the particle size parameters were best defined by the above distribution. According to Figure 91, it appears that the amount of dust removed by a single cleaning for an initial fabric loading of 778 g/m^2 is roughly 67 percent of that which can be removed by several repetitive cleanings. Because of the extended times associated with repeated collapses (and the loss of working fabric surface), any advantage of successive collapses is probably lost after a few cleanings.

Extrapolation of the removal versus fabric loading curve of Figure 90 suggests that practically all of the fabric dust loading should be dislodged with a single collapse when the areal density is allowed to reach the 1200 to 1500 g/m^2. It should be noted, however, that even with a single collapse per cleaning interval, the surface of the fabric from which no dust has previously been dislodged has undergone several flexures once steady-state operating conditions have been attained. This condition is reflected for most data points shown in Figure 90. The exception is the single point for one collapse only of a heavily laden fabric surface. It is expected that repetitive flexings would have led to increased dust removal. On the other hand, the form of the curve indicates that there is probably a lower level for areal density at which even repetitive collapse and reverse flow cleanings will accomplish little cleaning. If it is assumed that the adhesive force is always less than the dislodging force, one can infer that the range of adhesive bonding for the GCA fly ash/Sunbury fabric system should range from roughly 50 to 150 dynes/cm. The above force values are associated with fabric loadings of 510 and 1530 g/m^2, respectively, in conjunction with a normal gravity field.

Although the preceding data analyses are considered to be correct from the qualitative viewpoint, it is recognized that more testing is needed to strengthen their quantitative value. With respect to a coal fly ash-woven glass fabric system, however, these data have provided very useful guidelines for the modeling discussed in Section IX.

DUST REMOVAL WITH SUCCESSIVE FILTRATION AND CLEANING CYCLES

Successive filtration and cleaning tests, Table 25, were carried out at representative field operating conditions to determine how many cycles would be required before achieving steady state conditions with a single bag. Reference to Curves 1 and 2, Figure 92, indicates that after 5 to 6 operational cycles, the dust deposition and removal rates become equal. Dust penetration values for essentially constant inlet concentration show a consistent downward trend, however, suggesting that progressively more dust is accumulating within the filter pore structure. Field measurements at the Sunbury Plant, Section VI, Figure 42, indicated that 10 to 12 days of operation were required before a relatively constant emission rate was reached with a multicompartment system.

DUST REMOVAL AND BAG TENSION

A limited test sequence, Table 26, indicated that reducing bag tension from 50 to 15 lbs had little effect on dust removal and penetration characteristics. The above tension range encompasses the values commonly used in the field with glass bags used for fly ash filtration. Prior measurements showing the effect of bag tensioning on clean cloth permeability, Section V, Figure 33, also indicated that there was little change in fabric permeability over the 15 to 50 lb tension range. The Table 27 tests also showed that dust removal appeared to level off after five to six successive cleaning cycles. This finding seems to corroborate the test results of Figure 92 which show that five to six repetitive cleanings of the fabric between loading intervals is sufficient to reach a practical limiting level.

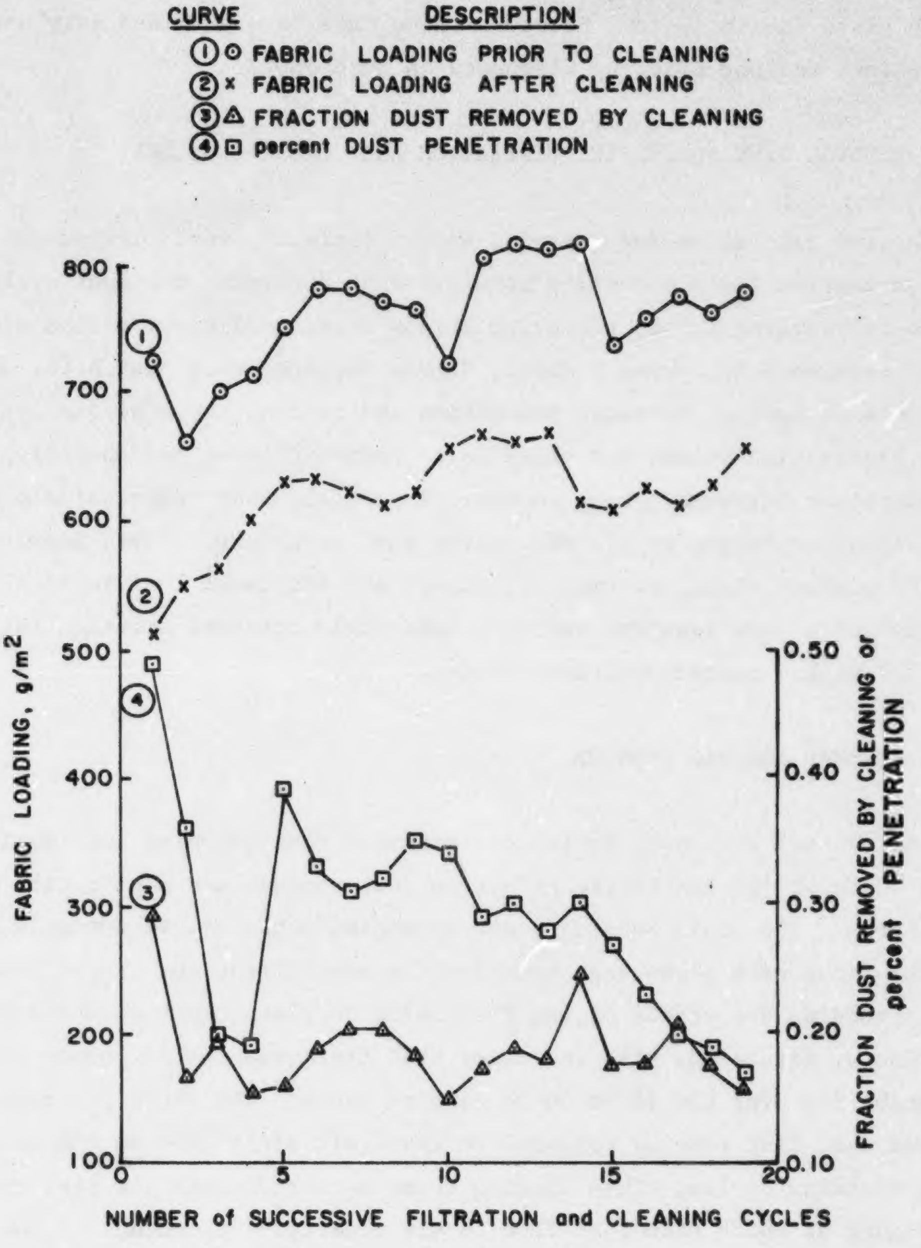

Figure 92. Performance of Sunbury fabric with GCA fly ash with repetitive filtration and cleaning cycles

RESISTANCE VERSUS FABRIC LOADING

The resistance versus fabric loading curves for the tests summarized in Table 25 are shown in Figure 93. Approximate steady-state conditions appear to have been reached after 8 to 9 successive cleaning and filtration intervals. The discontinuities indicated in Curves 1 through 9 resulted from a flow regulation problem that was subsequently corrected. It is emphasized that the slopes of these curves do not enable computation of K_2 values because the filtering intervals were too brief to allow for regeneration of a uniform thickness dust cake.

On the other hand, the extended filtering times used for the tests described in Table 23 and Figure 94 show that the resistance versus fabric loading curves eventually approach the slope obtained when the dust deposit is uniformly distributed. The estimated K_2 value for the linear section of the curve is 1.35 N min/g min, which is fair agreement with K_2 values determined previously for GCA fly ash.

DUST PENETRATION MEASUREMENTS

Constant Velocity Tests

Figure 95 indicates that short-term changes in filter emissions are defined by condensation nuclei concentrations are quite similar to corresponding bench tests performed with test panels. When the average nuclei concentrations were computed for each of the 19 tests listed in Table 25, their equivalent mass concentrations derived from the calibration curve of Figure 86, Section VII, were in close agreement with values determined by concurrent gravimetric sampling. One can infer, therefore, that the test aerosol properties for the pilot system were very similar to those of the bench tests.

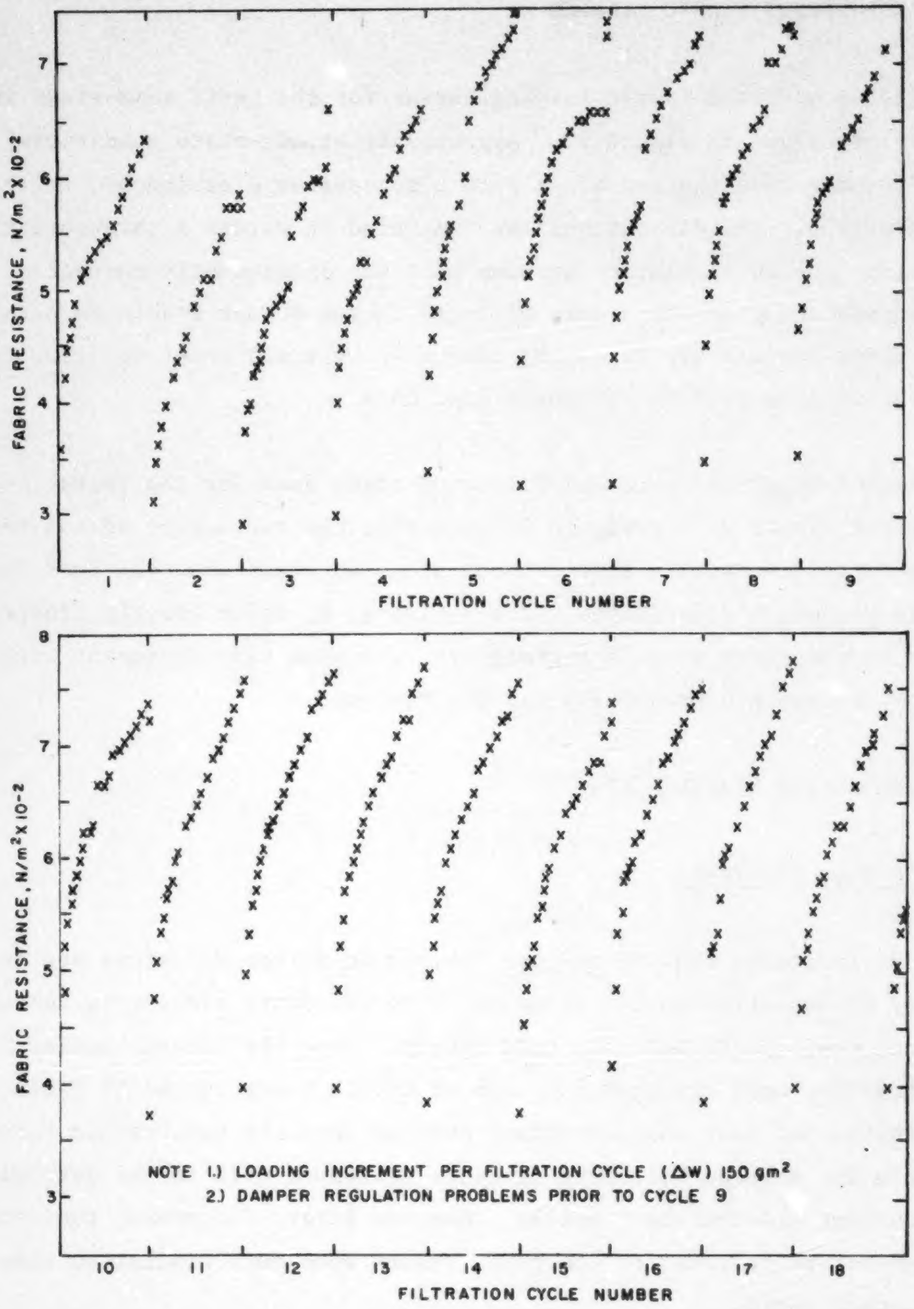

NOTE 1.) LOADING INCREMENT PER FILTRATION CYCLE (ΔW) 150 gm^2
2.) DAMPER REGULATION PROBLEMS PRIOR TO CYCLE 9

Figure 93. Successive filtration and cleaning cycles for Sunbury fabric with GCA fly ash based on data of Table 25

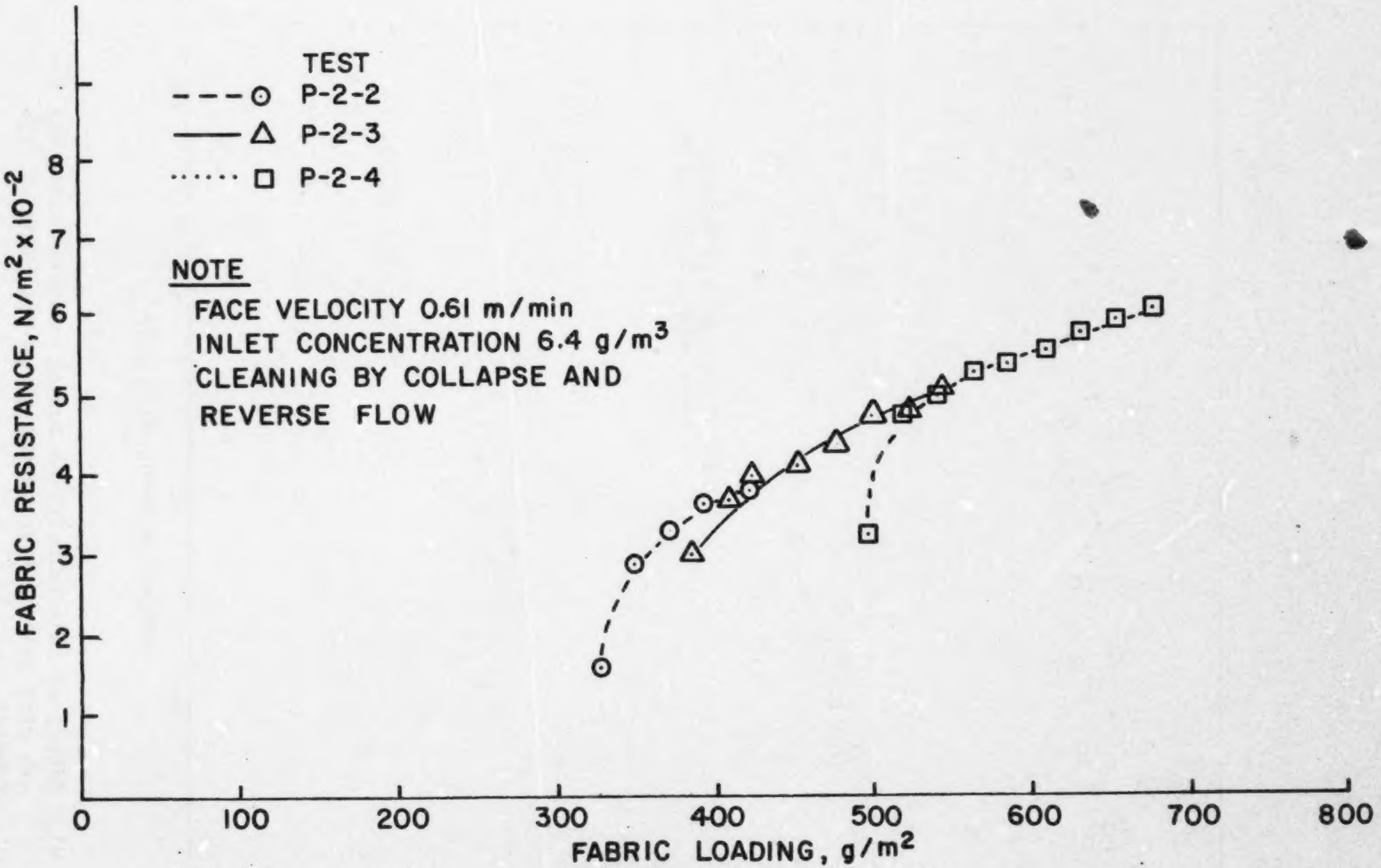

Figure 94. Single bag (10 ft x 4 in.) filtration of GCA fly ash with Sunbury fabric - three cleaning cycles with variations in residual loading

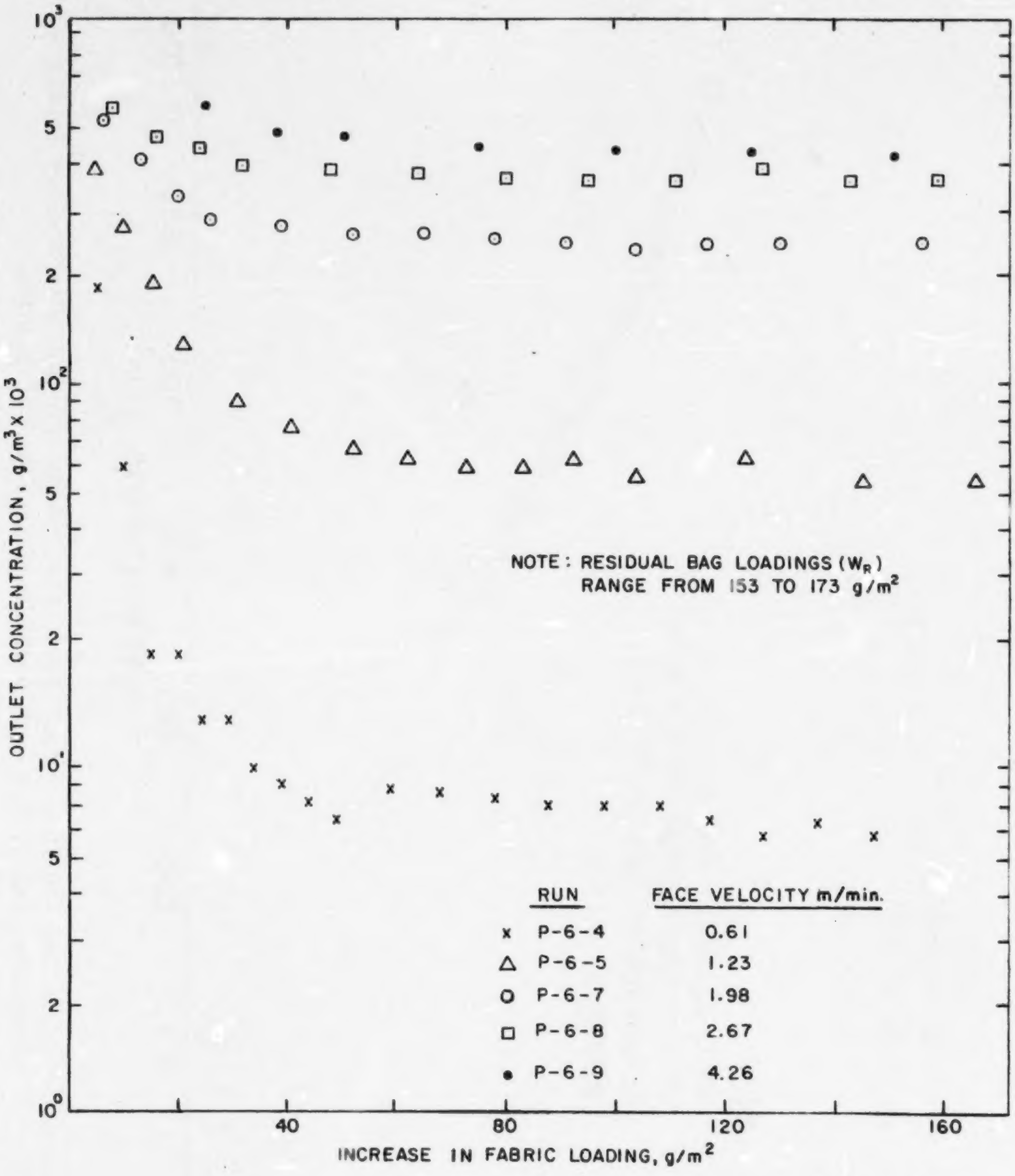

Figure 95. Effect of face velocity on outlet concentration, GCA fly ash with 10 ft x 4 in. woven glass bag (Sunbury type fabric)

PENETRATION VERSUS FACE VELOCITY

Previous measurements with bench scale equipment, Section VII, Figure 88, indicated that filtration velocity had a very significant effect upon effluent concentrations. In order to reduce the chance of serious scaling errors, a second series of tests was performed over the velocity range 0.61 to 4.25 m/min, each test starting with essentially the same fabric loading (150 to 175 g/m^2), Table 28. Manual shaking was used to remove the dust. These tests confirmed the adverse effect of increased face velocity on effluent concentration. Figure 95 shows plots of effluent concentration versus fabric loading for several face velocities.

Figure 96 shows the relationships between average and final outlet concentration and face velocity for the bag tests described in Figure 95 and the panel tests discussed previously in Section VII and Figure 88. Final concentration refers to the essentially constant outlet concentration that follows the rapid decay phase. According to the curves of Figure 96, bag and test panel average concentrations appear to increase as the 2.22 power of the face velocity whereas the final or limiting concentrations increase as the cube of the velocity. The indicated exponential relationship applies fairly well for face velocities less than 2.5 m/min. At higher velocities a marked decrease in slope is observed. Again, the main impression gained from these data is that high air-to-cloth ratios even if acceptable from the point of view of operating resistance, may lead to excessively high dust emissions.

REAR FACE SLOUGH-OFF

Only one pilot test was run to establish the approximate magnitude of particulate emissions when room air alone was passed through a previously loaded bag, Run P-6-2, Table 23. The indicated outlet concentration was 0.63 mg/m^3, about six times greater than the estimated inlet atmospheric dust concentration. The source of the emission was the slough-off or

Table 28. EFFECT OF FACE VELOCITY ON OUTLET CONCENTRATION, GCA FLY ASH 10 ft x 4 in. WOVEN GLASS BAG, SUNBURY FABRIC

Run No.	Face velocity, m/min	Fabric loading at beginning of run,[a] g/m^2	Fabric loading before cleaning, g/m^2	Fabric loading after cleaning, g/m^2	Outlet concentration,[b] g/m^2	Average penetration, percent
P-8-1	0.62	155.9	302.5	153.5	0.0355	0.50
P-8-2	1.23	153.5	360.5	158.6	0.1615	2.25
P-8-4	1.98	173.3	368.5	165.1	0.7128	9.95
P-8-5	2.67	165.1	403.2	131.4	1.0868	15.15
P-8-6	4.26	131.4	507.6	-	1.2750	17.80

[a] Bag hand shaken to attain indicated residual loading.

[b] Inlet loading constant at 7.16 g/m^3.

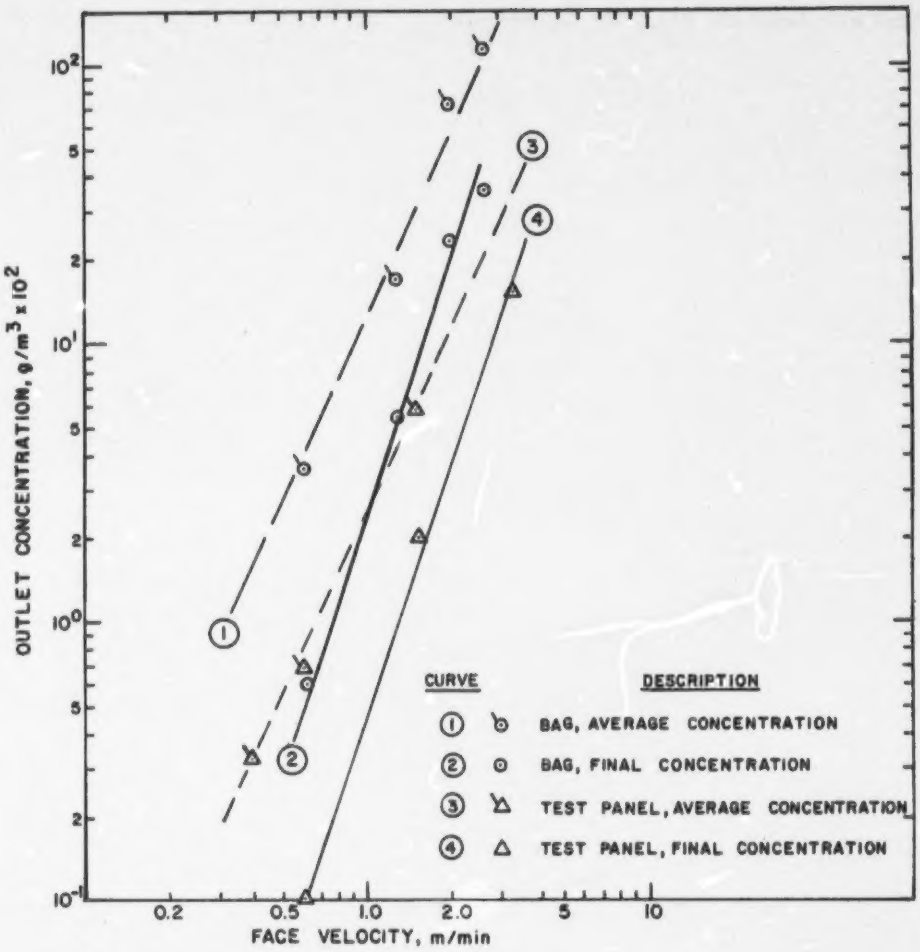

Figure 96. Relationship between final and average outlet concentration and face velocity for 10 ft x 4 in. bag and test panel with GCA fly ash and Sunbury type fabric

detachment of particle agglomerates from the rear of the pore regions caused by air reentrainment and perhaps aided by random mechanical vibrations in the system. The particle size distribution for the above emission source is shown in Figure 97. It is emphasized that such dust releases do not mean that pinholes have developed in the fabric, although they might ultimately lead to pinhole formation.

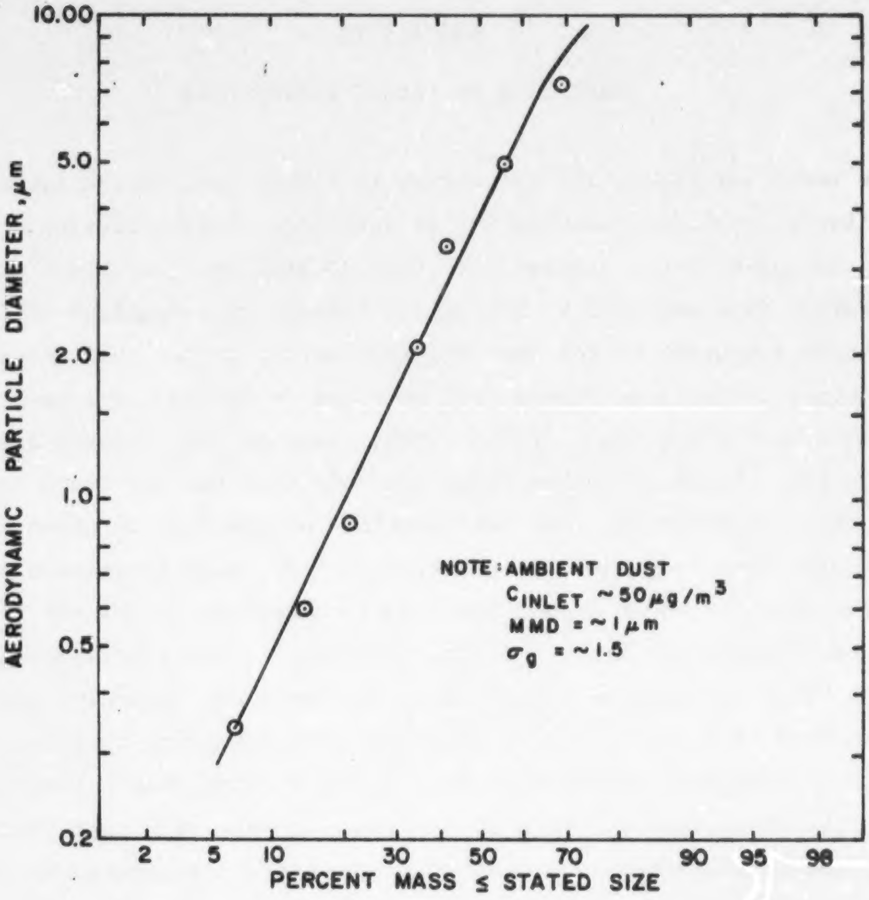

Figure 97. Effluent particle size parameters from GCA fly ash loaded Sunbury fabric when filtering atmospheric dust

SECTION IX

PREDICTION OF FABRIC FILTER DRAG

A new model for predicting the change in fabric drag (S) in terms of the fabric areal dust loading (W) is described in this section. The model is based upon a concept discussed by Billings and Wilder[1] in which filtration is considered to take place through an assemblage of pores or channels bounded by the warp and fill yarns, rather than through an assemblage of isolated fibers such as found in felted media or high porosity bulk fiber beds. It is further assumed that several discrete fibers from staple or bulked yarns protrude into the interyarn region to form a substrate for dust cake growth. Observation of clean and used woven glass fabrics under low power, 4x to 10x, magnification appears to substantiate the above assumption. Dust collection is assumed to result from two processes; first, the rapid blocking of the interspersed bulk fibers by an essentially superficial dust layer and secondly, the development of a dust layer or cake upon this substrate that results in particle removal by direct sieving. In the ensuing dust collection process, the characteristic rate of resistance change with dust loading for the glass fabric appears to conform to the pattern suggested by fabric geometry and classical fluid dynamics.

Empirical equations have been developed that simplify calculating procedures although rational physical processes that explain observed filter behavior can be postulated in most cases. The above statement applies to the mathematical model developed to describe the typical drag versus fabric loading relationship noted for the fly ash/woven glass fabric systems.

CRITIQUE OF LINEAR DRAG MODEL

The linear model of fabric drag ($S = S_E + K_2 W$) discussed in the preceding review section has the advantage of simplicity. The drag is modeled as increasing from the artificial value S_E with a constant slope K_2. The extension of this line is superimposed upon the linear section of the curve at the latter's juncture with the curvilinear section. The disadvantage of the linear model is that it becomes increasingly incorrect as W' decreases from 175 to 0 g/m^2 (0.03 to 0 lb/ft^2. The consequence of this error is that the linear model is most incorrect when the flow and the emissions through the bag are greatest. The extent of the error, however, depends upon the difference between the S_E and the S_R values, the number of compartments operated in parallel and the amount of dust removal during cleaning.

The development of a nonlinear model that provides a good approximation of the actual performance curve and a means by which S_E can be evaluated when a linear approximation suffices are presented in the next section.

DERIVATION OF NONLINEAR (PORE) MODEL

The curve shown in Figure 98 shows the typical form assumed by a drag versus fabric loading curve for a fly ash/woven glass fabric filter after several repetitive cleaning cycles. It is very important to note that complete cleaning has taken place such that the residual dust holding, W_R, is only that retained within the loose fiber structure obstructing the pores. Careful observation of the region from which a dust layer or element of the dust cake has been dislodged shows that separation occurs principally at the interfacing between the dust cake and the fabric. Analysis of adhesive and cohesive forces suggests that dust loss through surface spallation should be minimal because the cohesive forces within the dust cake exceed the adhesive bonds between the dust and fabric surface.

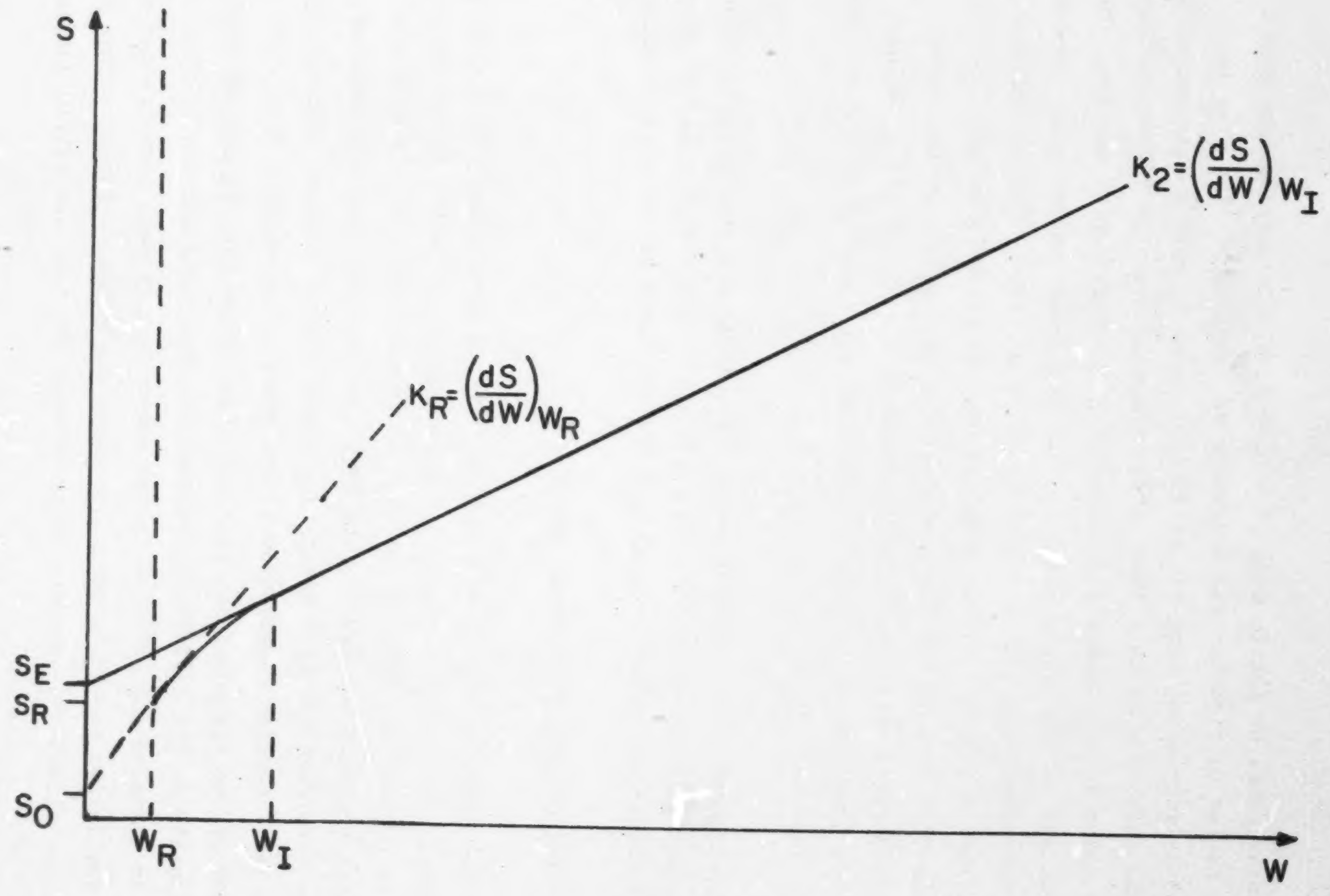

Figure 98. Typical drag versus fabric loading curve for a uniformly distributed dust holding

Therefore, if a filter with a uniformly distributed dust deposit, W, is cleaned at some pre-selected intensity, the cleaned filter will display two distinct surfaces; the first, the unchanged or uncleaned region with its original surface loading, W, and the second, the region from which the surface layer has been detached that now is characterized by the residual loading, W_R. Several measurements and observations during this study have shown that with more intense cleaning, the total cleaned area is increased but the surface loading upon the cleaned regions is uniformly distributed at a near constant areal density irrespective of cleaning intensity. Residual fly ash loadings for Sunbury and Nucla type glass fabrics generally fell within the loading range 50 to 100 gram/m^2. Additionally, limited tests with other dust/fabric combinations indicated that W_R values generally fell within the same 50 to 100 gram/m^2 range although the amount of dust dislodged by a fixed energy input was strongly dependent upon the individual dust and fabric properties.

The cleaning process as it bears upon filter drag and dust penetration characteristics will be discussed in more detail in succeeding sections of this report. The key factor to be noted at this time is that a cleaned element of the filter surface is one from which the surface dust cake is completely detached. The resulting surface with its residual loading, W_R, presents the same pore array present in the clean (unused) filter except that dust particles (essentially irreversibly retained within the loose fiber substrate blocking the pores) lead to an increase in the residual filter drag.

The residual drag, S_R, for a uniformly cleaned filter is associated with the characteristic residual fabric loading, W_R. Over the surface loading interval W_I-W_R, the rate of change of drag with fabric loading, dS/dW, gradually decreases from its initial value of K_R at W_R until it assumes a final constant rate, K_2, for all surface loadings in excess of W_I. The term W_I indicates the fabric loading at the point where the curve assumes a linear path. The effective drag, S_E, is shown as the lower linear extrapolation of the drag curve. Because the clean drag of the filter, S_o, is seen only once in any practical filter application, it is of interest only to the extent that it may aid in predicting the behavior of the fabric with new applications.

Several physical mechanisms were considered in an attempt to provide a rational physical explanation for the path of the drag/fabric loading curves studied in the course of this program. Although it appeared reasonable to consider the curve path between W_R and W_I as the result of a gradual reduction in unobstructed pores, several measurements and tests described earlier in this report indicate that nearly all pores ~ 99.99 percent or greater must be completely blocked within a very brief period of filter use. Otherwise, the extremely high permeability of open pores would cause most of the air to vent through them. Furthermore, a completely sequential pore blocking process over the W_R to W_I interval would dictate a concave upward curve form rather than the path shown in Figure 98 as discussed in Appendix A. In the case of filtration with heavily napped cotton fabrics, one may encounter a concave upward resistance versus fabric loading relationship due to a gradual compression of the more porous dust layer as the resistance increases.

One comparatively simple explanation for the observed curve shape lies with the fact that once initial bridging is accomplished (which is greatly enhanced by the presence of bulked yarns or staple) the dust layer develops gradually, first below and finally above the fabric surface. Although the depth of the dust penetration within the fabric structure is restricted by the location of the fiber substrate, there still remains the possibility of an appreciable reduction in pore cross section for the subsurface regions.

Under these conditions, two factors contribute to a rapid increase in filter resistance when filtration commences. First, if the porosity of the deposit is assumed to be constant irrespective of deposition site, the first increments of dust collected below the filter surface will exhibit a greater depth per unit of mass because their cross sections are reduced. Thus, under laminar flow conditions the resistance per unit mass will be larger because of the increased depth. Secondly, the flow cross section is reduced for the initial deposits requiring that the velocity increase proportionally to maintain continuity of flow. Both the depth per unit increment of deposit and the velocity through the deposit decrease as the surface of the fabric is approached. Conversely, once dust fill reaches the filter surface level the cake depth is directly proportional to unit mass of deposit and cake velocity is constant (assuming no porosity changes due to cake compression).

Figure 99 depicts a fabric pore with a low density bridging of discrete fibers within the gap separating the yarns. The latter structure constitutes the principal supporting substrate for the dust layer. Particle penetration into the bulked fiber mass is relatively small compared to the surface deposition. The pore cross section is seen to increase as the surface of the filter is approached. In the simplified model of the pore structure in Figure 99, the convergence is treated as a truncated conical section. This allows the pore diameter between the surface of the fabric and the bottom (or start) of the dust layer to be defined by a simple linear equation.

$$d = d_{min} + \left(\frac{d_{max} - d_{min}}{W_I}\right) W \qquad (24)$$

where d_{min} is the cake diameter at its greatest pore depth, d_{max} the cake diameter at the surface of the pore, W_I the average surface loading at the inception of cake filtration, and d the cake diameter at any average fabric loading W. The development of the above approach results in the following expression for the change in drag ΔS over the loading range W_R to W_I;

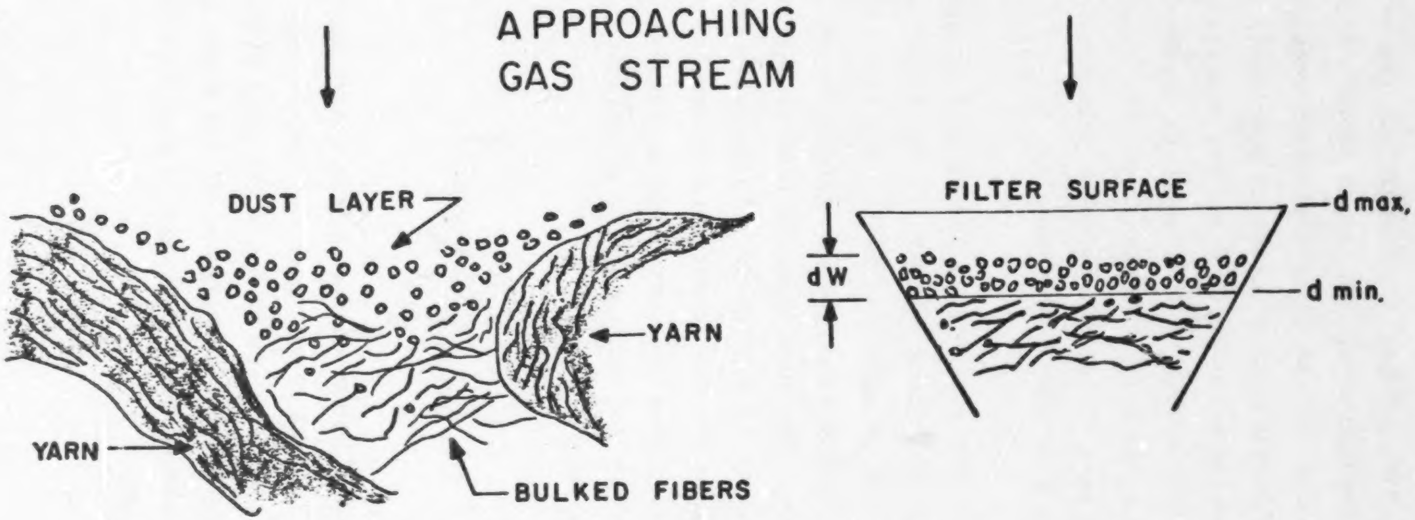
APPROACHING
GAS STREAM
DUST LAYER
YARN
YARN
BULKED FIBERS
FILTER SURFACE
d max,
d min.
d W

SKETCH OF FILTER SECTION, DUST LAYER BUILDUP ON SUPPORTING BULKED FIBER SUBSTRATE

SIMPLIFIED PORE FORM, TRUNCATED CONE

Figure 99. Schematic, dust accumulation below surface of fabric with bulked fiber or staple support

$$\Delta S \Bigg|_{W_R}^{W_I} = \frac{K_2}{3k}\left(d_{max}\right)^4 \left[-\frac{1}{\left(d_{min} + kW\right)}^{3}\right]\Bigg|_{W_R}^{W_I} \qquad (25)$$

where $k = \dfrac{d_{max} - d_{min}}{W_I}$

According to microscopic inspection of the fabric, and examination of Figure 28, it appears that the ratio of d_{max} to d_{min} should be in the range of 1.5 to 1.7. The above values allow the development of a drag versus fabric loading curve using Equation (25) that describe our laboratory measurements.

The calculation of S over the range W_I to W follows the standard relation

$$\Delta S \Bigg|_{W_I}^{W} = K_2 W \Bigg|_{W_I}^{W} \qquad (26)$$

Unfortunately, Equation 25 is cumbersome and the constants d_{max} and d_{min} are difficult to determine. Additionally, the complete filtration range must be defined by two separate equations, each with its specific limits.

Therefore, a simpler approach was sought to define the curvilinear relationship shown in Figure 98. To satisfy the mathematical, if not the physical picture, the model should reflect the following:

$$S = S_R \text{ at } W = W_R$$

$$dS/dW = K_R \text{ at } W = W_R$$

$$dS/dW = K_2 \text{ for } W \geq W_I$$

and

$$S = S(W_I) \text{ at } = W_I.$$

Such a model would display the correct initial and final slopes, K_R and K_2, respectively, while satisfying the experimental values at W_R and for $W \geq W_I$.

The above terms were examined in the derivative form; i.e.,

$$\frac{dS}{dW} = f(W)\ K_R + g(W)\ K_2 \text{ for } W \geq W_R$$

which shows that the following conditions must prevail in the successful model.

$$f(W) = 1 \text{ and } g(W) = 0 \text{ at } W = W_R$$

$$f(W) = 0 \text{ and } g(W) = 1 \text{ at } W \geq W_I$$

In order to approximate the physical situation discussed previously, that is, the effective reduction in specific resistance coefficient from K_R to K_2 over the fabric loading range W_R to W_I an exponential decay process was selected. The reason for this approach is that the necessary increases and decreases in the functions $f(W')$ and $g(W')$ can be accommodated by a single equation. Here W' refers to $W-W_R$ so that the curve path is traced from its true origin (W_R, S_R).

If $f(W')$ and $g(W')$ are arbitrarily defined by the following equations

$$f(W') = \exp\ (-W'/W^*)$$

$$g(W') = 1 - f(W') = 1-\exp\ (-W'/W^*)$$

the differential equation defining the drag versus loading relationship appears as

$$\frac{dS}{dW} = K_R \exp\ (-W'/W^*) + K_2\ [(1-\exp\ (-W'/W^*)] \qquad (27)$$

Upon integration, Equation (27) reduces to the form:

$$\boxed{S = S_R + K_2 W' + (K_R - K_2)\ W^*\ \ 1-\exp\ (-W'/W^*)} \qquad (28)$$

In later sections of this report, approximate methods for estimating such parameters as K_2, S_R and S_o are given. Until the state-of-the-art advances well beyond our present understanding of the several factors defining the above variables, however, the direct experimental determination of these parameters is strongly recommended.

The terms S_R, S_E, K_R and K_2 are readily determined by the graphical analysis of fabric loading curves of the type shown in Figure 98. Such curves can be generated from comparatively simple laboratory or field testing procedures with the specific dust/fabric combination and air-to-cloth-ratio of interest.

The term W^* is a system constant whose value is best derived from the direct graphical measurements of S_R, S_E, K_R and K_2.

$$W^* = (S_E - S_R + K_2\ W_R)/(K_R - K_2) \qquad (29)$$

Alternatively, W^* also appears to be closely related to W_I based upon examination of data described later in this section; i.e.,

$$W^* = 0.35\ W_I \qquad (30)$$

At the present time, it appears preferable to treat the residual drag - residual loading coordinates as the starting point for the modeling process. Aside from the fact that the clean (unused) fabric drag is encountered but once, there is no existing relationship to determine how the clean and effective drags are related for specific dust/fabric systems.

The concave form for the drag/loading curve, Figure 98, has been attributed to the higher velocities and greater cake depth per unit mass of dust for dust deposits below the fabric surface. If the fabric is very highly napped, however, there will be less chance for interstitial dust penetration. Hence, as noted for napped cotton sateen filters, the initial (K_R) and final (K_2) slopes are nearly the same. In fact, if the napped medium is at all compressible, the resistance increase with fabric loading may display a concave upward shape as the porosity of the dust/fabric mass decreases. The same phenomena are observed when the compaction is apparently increased by filtration at higher velocities as discussed in a later section.

It has been emphasized that the filtration model presented here involves oversimplification of some very complex interactions. The assumption has been made that the pores or interyarn spaces are identical in shape and dimensions. The weave characteristics alone, however, indicate that at least two distinct pore geometries are encountered with a 3/1 twill, Figures 23 and 28, Section V.

Additionally, a certain lack of uniformity in pore dimensions arises directly from the weaving process while rough handling and improper installation can also contribute to an undesirable spread in pore sizes. It was also assumed that loose loops or free fiber ends extending into or across a pore cross section presented a fairly uniform substrate. In practice, however, oversize pores can be found that may or may not be bridged over during the filtering cycle. Thus, there exists a limiting pore size beyond which a fabric ceases to be a highly effective filter. GCA measurements suggest that open pore area must be reduced to the order of 10^{-6} times that of the total filter surface before good filtration can ensue; i.e., effluent concentrations in the 10^{-3} g/m^3 range.

Although 100 percent multifilament weaves were not investigated with respect to coal fly ash filtration, it should be noted that the absence of bulk fiber fill in the interyarn region will reduce particle collection significantly unless the interyarn spacing is greatly reduced. Tests performed with a plain weave plastic screen in which the velocity through 200 μm diameter pores simulated that for the ~100 to 150 μm pores in woven glass fabric showed that complete bridging was impossible to attain without a supporting fiber structure. Performance of the plastic screen described in Figure 36 suggests that pore diameters should be of the order of 10 to 20 μm to achieve collection comparable to that attained with the 50 to 150 μm diameter pores for common woven glass fabrics. Note that the adverse effect of oversize pores can be counterbalanced by the bulk fibers that constitute the substrate for cake formation.

In the preceding analysis it is assumed that all pores are identical with respect to cross section, depth and quantity of fiber dispersed within the pores. Thus, aside from any randomness resulting from the spatial variability of the inlet dust concentrations, pore bridging and the development of a dust layer should proceed as "n" parallel filtering operations where "n" is the effective pore count per unit filter cross section. Should the degree of dust accumulation increase at any point on the filter, the concurrent increase in resistance would tend to redistribute the dust laden gas to areas of less resistance. Thus, minor deviations from pore dimension uniformity, which typifies a useful woven fabric, would not seriously hamper the bridging process. However, should there be too large a range in pore diameters, there exists the probability that complete pore bridging or blockage might never be attained. Hence, unsatisfactory performance may be encountered in the field for the above reason due to damage or improper fabric selection.

VERIFICATION OF NONLINEAR DRAG MODEL

The experimental performance curves for five different fabric filters were selected to evaluate the curve fitting capability of the nonlinear model. Fabric descriptions and test data sources are listed in Table 29.

It was assumed that the fabric dust loadings were uniformly distributed upon the filters and that the filters had been especially cleaned down to their minimum W_R values, ~50 g/m^2. Although subsequent investigations

Table 29. PHYSICAL PROPERTIES OF FABRICS INVOLVED IN MODEL TESTING

Test number	Type of fabric	Weight,[a] oz/yd^2	Weave and yarn count, yarns per inch	Frasier permeability, ft^3/min @ 0.5 in water[b]	Reference
1	Glass fiber	9.06	3/1 crowfoot, filament 55 x 58	7.9	Spaite and Walsh[13]
2	Polypropylene	4.30	3 x 1 twill, filament 74 x 33	15.0	Durham[15]
3	Dacron	10.0	Plain, staple 30 x 28	55.0	Dennis and Wilder[16]
4	Cotton	10.0	Unnapped sateen 95 x 58	13.0	Dennis and Wilder[16]
5	Polyacrylester	9.8	2 x 2 twill, spun 39 x 35	60.0	Durham[15]

[a] 1 oz/yd^2 = 33.9 g/m^2.

[b] 1 in. water = 250 N/m^2.

suggested that the W_R values were larger and that the dust was not distributed uniformly upon the filters after cleaning, the validation of the nonlinear model was in no way affected because the curve fitting process relates only to the operating conditions assumed for each curve. Thus, in testing the model, K_R is the initial curve slope for the coordinates S_R, W_R; $W' = W-W_R$ is the amount of dust added to the filter following the filter cycle; and W_I-W_R is the dust deposit required before the drag versus loading curve assumes its linear form with its characteristic slope of K_2.

The values for K_2, K_R, S_R, W_I and W* and relevant operating information for the test fabrics are shown in Table 30. The values for these constants were determined by the graphical analysis of pressure versus loading curves of the type shown in Figure 98. These data, in conjunction with Equations (27) and (28), were used to compute the curve trajectories for the different fabrics, Figure 100. Comparisons of the predicted and experimental results show excellent agreement over the range of input parameters tested.

It is therefore concluded that model Equations (27) and (28) are appropriate for describing nonlinear drag versus fabric loading relationships.

EMPIRICAL CORRELATIONS

If the terms appearing in Equation (28) were easy to define, the modeling of any filter system would be a comparatively simple process. Unfortunately, except by the avenues of direct measurement or system replication it is not yet possible to determine such parameters as K_R, K_2, S_E, S_R and W* with the desired degree of accuracy.

In the following sections, data from several sources have been analyzed to determine their potential usefulness. The close inspection of filter performance statistics appearing in the literature often shows that critical data are not available. The most serious omission is the absence of true residual dust holding data for a single element (or bag)

Table 30. SUMMARY OF MEASURED FILTRATION PARAMETERS FOR MODEL TESTING

Test number	Fabric type[a]	S_R[b] N min/m^3	S_E[b] N min/m^3	K_R[c] N min/gm	K_2[c] N min/gm	W_I[d] g/m^2	W*[d] g/m^2	Dust type	Filtration[e] velocity v m/min	Type of cleaning	Reference
1	Glass fiber	689	943	67.2	2.69	17.57	3.9	Wet ground mica	0.61	Shaking	Spaite and Walsh[13]
2	Polypropylene	287	779	22.7	1.02	65.9	22.0	Fly ash	1.22	Shaking	Durham[15]
3	Dacron	66	246	15.7	2.08	32.2	13.2	Fly ash	0.92	Shaking, reverse air	Dennis and Wilder[16]
4	Cotton	410	558	12.1	2.52	36.6	15.1	Fly ash	0.92	Shaking, reverse air	Dennis and Wilder[16]
5	Polyacrylester	41	205	4.42	0.77	146	44.9	Fly ash	1.22	Shaking	Durham[15]

[a] Refer to Table 2 for fabric properties.

[b] S_R, S_E 1 in. water min/ft = 820 N min/m^3.

[c] K_R, K_2 1 in. water min ft/lb = 0.168 N min/gm.

[d] W_I, W* 1 lb/ft^2 = 4882 g/m^2.

[e] V 1 ft/min = 0.305 m/min.

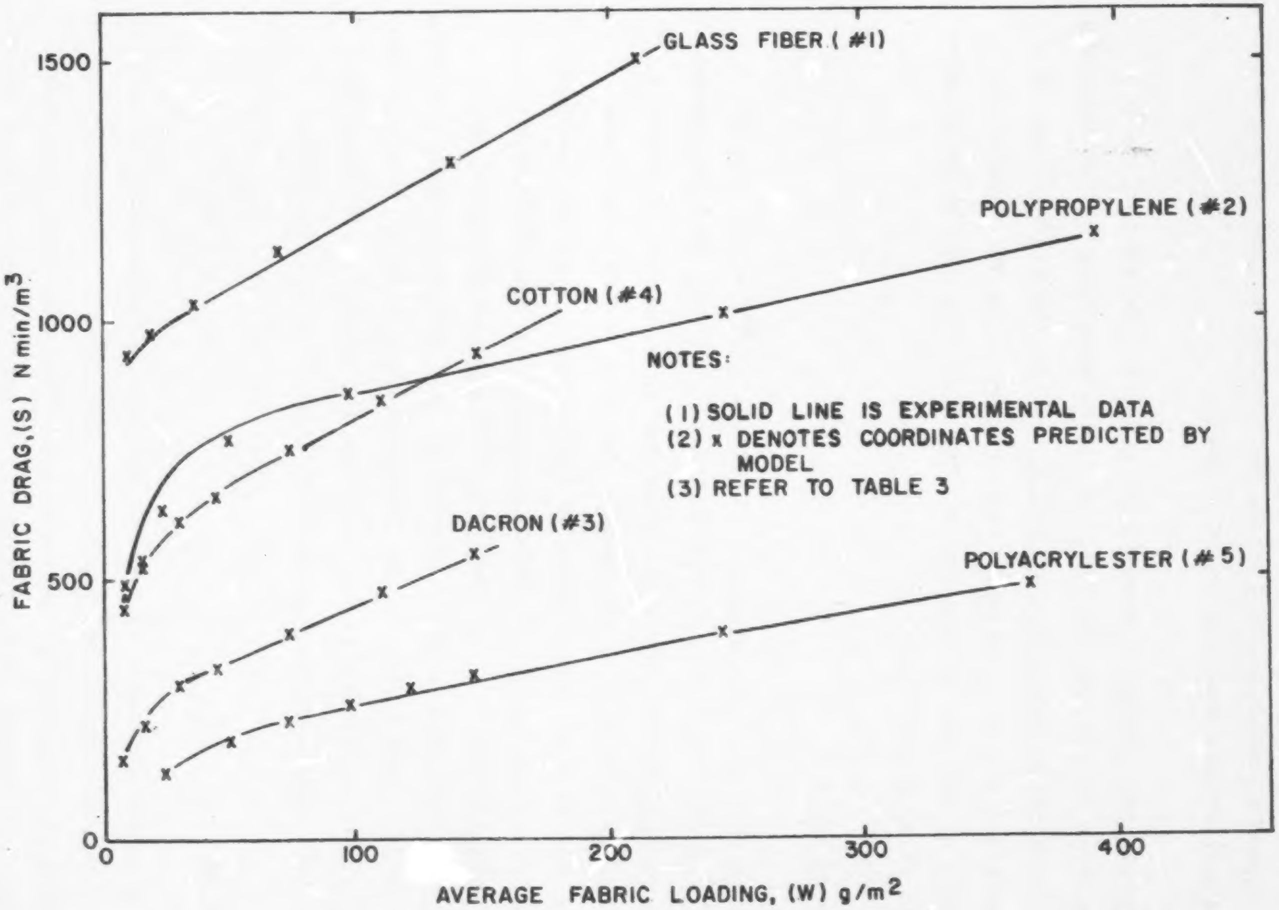

Figure 100. Comparison between experimental and predicted drag properties

within a filter system. This problem is encountered with many laboratory and field measurements. Additionally, the cleaning operations are usually defined as vigorous, moderate or typical but without regard to the precise energy input and/or the amount of dust removal.

Data reviewed in the following paragraphs provide some insight as to probable range of values for the critical terms appearing in the modeling equations. With reference to S_o, S_E and K_R values the correlations are strictly empirical for want of basic measurements. On the other hand, the estimation of specific resistance coefficient, K_2, can be undertaken on the basis of existing theory.

Clean Fabric Drag, S_o

The clean fabric drag, which depicts the permeability of the unused fabric, is related to the Frasier permeability. In the English system, it is given as the volume flow rate per unit fabric area that produces a resistance to air flow of 0.5 in. water. In this report, the clean fabric drag, S_o, is simply expressed as fabric resistance, P, divided by the filter face velocity, V. Because S_o can be determined quite easily and inexpensively, it is hardly justifiable to resort to any involved theoretical approaches to determine its numerical value. However, because there is a rational although rather complex process by which the use of a modified filtration theory enables reasonable predictions for S_o, methods for evaluating S_o are discussed later in this section.

Effective Drag, S_E

As part of a comprehensive study of the effects of fabric weave on filter performance, Draemel[3] performed tests with several experimental and commercial fabrics in the form of conventional filter bags and flat test panels, Table 31. Steady state filtration parameters are depicted for mechanically-shaken bags whereas single tests are described for unused

Table 31. CLEAN (UNUSED) AND EFFECTIVE DRAG VALUES FOR COMMERCIAL AND EXPERIMENTAL FABRICS BY DRAEMEL[3] WITH RESUSPENDED COAL FLY ASH[a]

Fabric type	Weave and yarn count	Clean fabric drag, S_o		Effective drag, S_E	
		in H_2O/fpm	N min/m^3	in H_2O/fpm	N min/m^3
Single bag - Mechanical shaking[b]					
Dacron 1-39703	3 x 1 twill 78 x 65	0.027	22.1	1.29	1058
Dacron 39707	3 x 1 twill 68 x 54	0.0085	7.0	0.36	295
Dralon 3039577 (acrylester)	3 x 1 twill 78 x 70	0.043	35.3	0.79	648
Spun-acrylic 4-4589	3 x 1 twill 76 x 51	0.015	12.3	0.50	410
Polypropylene 5-33106	3 x 1 twill 67 x 53	0.0038	3.2	0.22	180
Dacron 6-39704	3 x 1 twill 67 x 58	0.0106	8.7	0.49	402
Spun rayon 7-884 (cellulose)	sateen 96 x 86	0.0034	2.8	0.21	172
Polyester 8-4388	3 x 1 twill, comb. fill-spun 77 x 77	0.026	21.3	0.76	623
Nomex 9-4400	plain - spun 46 x 38	0.013	10.6	0.54	443
Test panels - 1 ft^2, one-filtration cycle[c]					
Dacron 011	3 x 1 twill, filament 77 x 63	0.014	11.5	0.83	681
Dacron 020	sateen, filament 76 x 63	0.046	37.7	0.83	681
Dacron 015	3 x 1 twill 76 x 82	0.033	27.1	0.80	656
Dacron 038	3 x 1 twill, staple 76 x 73	0.009	7.4	0.51	418
Dacron 088	3 x 1 twill, staple 76 x 82	0.0056	4.6	0.18	148

[a] Fly ash, MMD = 3.7 μm, $_g$ = 2.42.

[b] Repetitive filtration at steady state operation with commercial fabric.

[c] Single tests on new test panels, experimental fabrics.

filter test panels. In both cases, a redispersed coal fly ash aerosol was used. Most test fabrics were 3/1 twill weaves of Dacron or related synthetics. Their areal densities were about 206 g/m^2 as compared to about 312 g/m^2 for the woven glass fabrics evaluated in the present study. The estimated fiber surfaces of the Dacron and glass media, however, were roughly similar because of the much lower Dacron density (1.4 g/cm^3 versus 2.2 g/cm^3 for glass). Based upon prior GCA experience with Dacron fabrics cleaned by mechanical shaking, Draemel's single bag measurements are assumed to reflect relatively low residual dust holdings. Therefore, his reported values of effective drag, S_E, are assumed to be approximately correct. In Figure 101, Draemel's data from Table 31 and the results of the present study, Table 32, have been graphed to determine whether effective drag, S_E, might be predicted on the basis of clean fabric drag.

Because test dusts, basic fabric properties and length of fabric service were quite similar it appeared reasonable that clean fabric permeability, (which reflects among other things the degree of openness or pore area), should exert a significant effect on the ultimate filter effective, S_E, drag or the residual drag, S_R. It is emphasized, however, that as pointed out in Draemel's studies, several factors other than clean fabric permeability influence the working drag parameters for a filter.

These variables include the size, amount, and location of bulk fiber collecting area within the pore structure; the number of effective pores per unit area, the actual pore geometry and the size distribution of the particles to be collected.

Therefore, in using S_o alone as the key parameter, a fairly wide spread in data points should be expected, Figure 101. Effective drag values for new fabric can be estimated by the relationship

$$S_E \text{ (N min/m}^3\text{)} = 189 + 18\, S_o \tag{31}$$

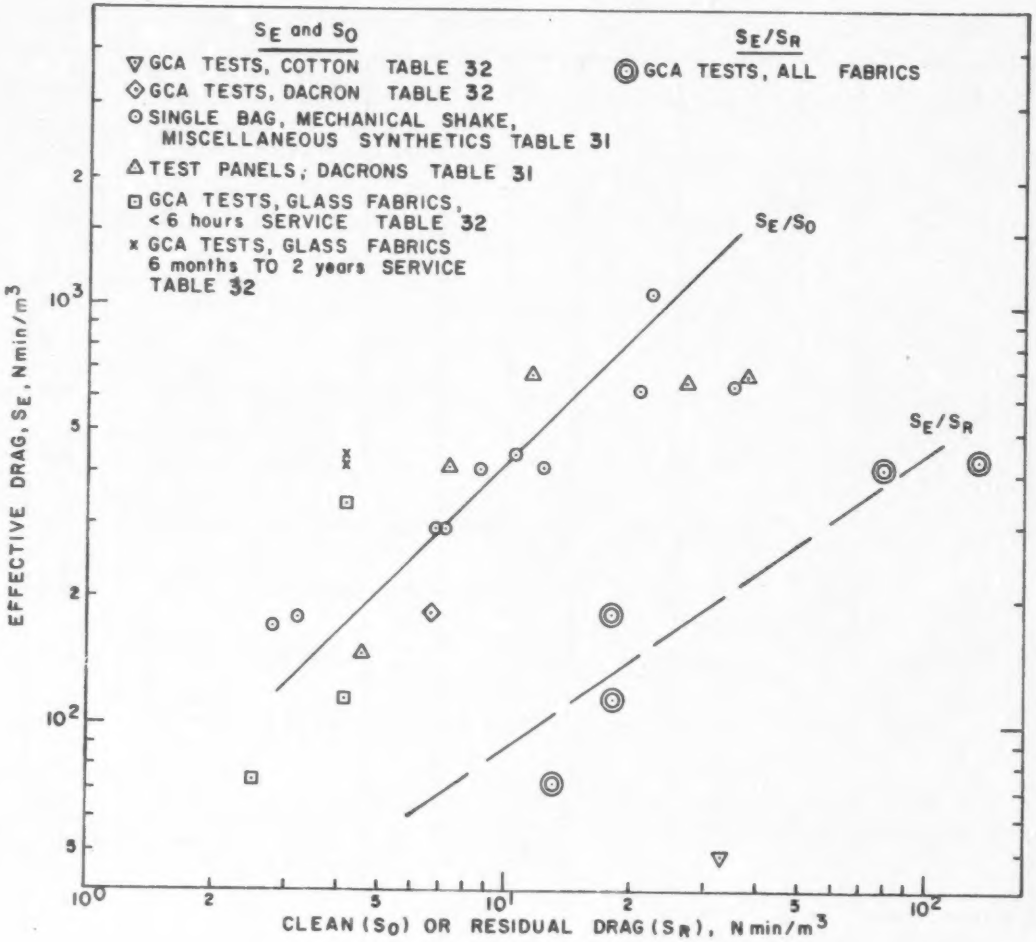

Figure 101. Relationship between effective (S_E) and clean (S_O) or residual (S_R) drag

Table 32. SUMMARY OF EXPERIMENTALLY DERIVED MODEL INPUT PARAMETERS USED TO PREDICT DRAG VERSUS FABRIC LOADING RELATIONSHIP

				Drag N min/m^3			Specific resistance coefficient N min/gm		W*	Residual fabric leading	W_I [d]	
Test no. [a]	Test dust	Fabric	Service life	S_o	S_R	S_E	K_R	K_2	g/m^2	g/m^2	g/m^2	W^*/W_I
65, 70 71, 99	GCA fly ash	Sunbury glass	<6 hours	4.1	18	115	2.65	1.60	72.9	44	175	0.42
66, 67	GCA fly ash	Sunbury glass	2 years	4.1	80.3	352	7.54	1.60	45.7	30	150	0.38
68	GCA fly ash	Nucla glass	Unused	4.1	-	205	6.56	1.60	-	0.0	-	-
69	GCA fly ash	Nucla glass	~6 months	4.1	134	434	5.85	1.60	60.5	11	175	0.35
98 [b]	GCA fly ash	Sunbury glass	<6 hours	2.5	13.2	74	2.84	1.08	34.5	47	110	0.32
96 [c]	GCA fly ash	Sunbury glass	Unused	15	-	60	-	2.06	-	0.0	-	-
84	GCA fly ash	Sateen weave cotton	Unused	32.8	-	49.2	2.32	1.14	13.9	0.0	50	0.28
92	GCA fly ash	Dacron crowfoot weave	<6 hours	6.6	18.8	188	6.23	1.11	-	16.0	-	-
77	Rhyclite, line	Sunbury glass	Unused	4.1	-	-	-	12.3	-	-	-	-
79	Rhyclite coarse	Sunbury glass	Unused	4.1	-	-	-	1.39	-	-	-	-
84	Lignite fly ash	Sunbury glass	Unused	4.1	-	-	-	1.26	-	-	-	-

[a] Face velocity is 0.61 m/min unless otherwise indicated

[b] Face velocity = 0.38 m/min

[c] Face velocity = 1.52 m/min

[d] Fabric loading at inception of linearity

Residual Drag, S_R

It was expected that the relationship between effective drag, S_E, and residual drag, S_R, would parallel that for the previously discussed effective drag versus clean drag. This follows from the fact that an increase in S_R, which is the result of increased particle entrapment within the fiber blocked pores, should lead to a higher starting resistance for the cleaned filter. Figure 101 appears to support this hypothesis despite the limited data.

Examination of Figure 102 also indicates that the residual drag does not show any clearcut dependency on the dust/fabric combination. It does appear, as expected, that extended filter usage increases the residual drag. In comparing the behavior of filters that have seen very limited use, there seems to be a slight correlation between the amount of dust on the filter before cleaning and the residual loading. Since the resistance across the filter is loading dependent, it is fair to assume that increased loading may cause increased compression of the residual dust/fabric substrate. This could account for the higher residual loadings shown in Figure 102. Aside from calling attention to these factors, however, it should be noted that there are not yet sufficient data available to develop the resistance properties of any dust/fabric combination to the point where they constitute a reliable data input for predictive models.

Initial Slope, K_R

The initial slope, K_R of a nonlinear drag versus dust loading curve is best estimated by careful experimental measurements. Although the early changes in slope, dS/dW, are logically expressible as functions of weave characteristics (which determine interstitial deposit geometry) and intrinsic dust properties (which determine cake permeability), current

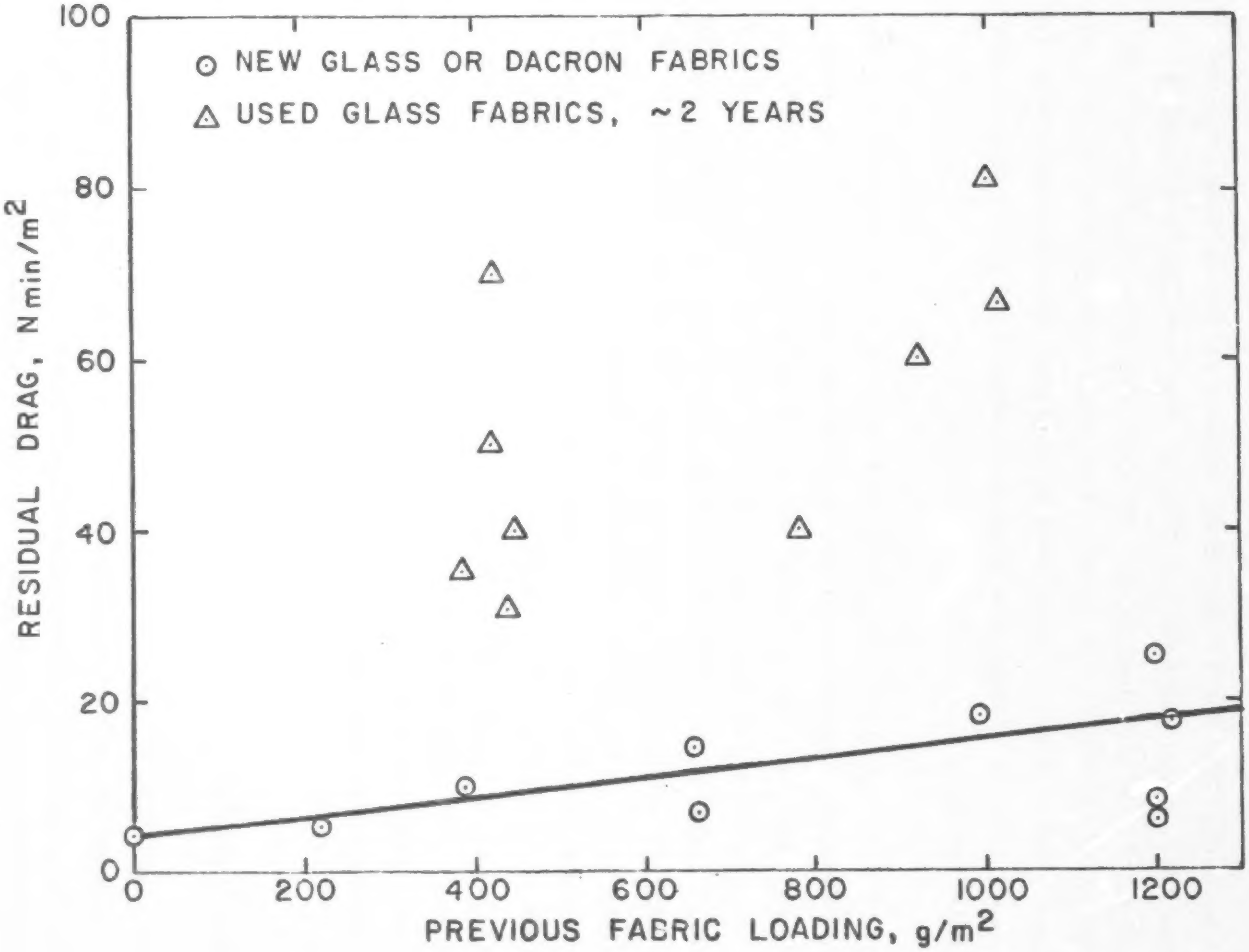

Figure 102. Effect of previous fabric loading on residual drag for new and well used fabric

analyses indicate that it would be difficult to make accurate determinations of the necessary input parameters in this relationship:

$$- dS/dW = \emptyset(W)(K_2)$$

Estimation of W^*

Given the situation where experimental measurements of S_E, S_R, K_R and K_2 are available (or can be readily obtained) it was indicated previously that the term W^* could be determined empirically as:

$$W^* = (S_E - S_R + K_2 W_R)/(K_R - K_2) \qquad (29)$$

An alternative approach is to define W^*, the constant appearing in Equations (13) and (14) in terms of the fabric areal density, W_I, characterizing the start of the linear portion of the drag versus fabric loading curve. According to test parameters summarized in Tables 30 and 32, W^* may be estimated by the following expression:

$$W^* = 0.35\ W_I \qquad (30)$$

It is emphasized that Equation (30) should be used only as a guideline and never as a substitute for actual test measurements.

THEORETICAL CORRELATIONS

Clean Fabric Permeability

A detailed examination of fabric properties in which microscopic observations played a large role provided several insights as to the probable performance of many dust/fabric combinations. In Section V of this report, it was shown that the number, type and approximate shape of pore openings in woven fabrics could be established by simple geometric considerations.

If the filter pores are treated as capillaries, the Hagen-Poiseuille relationship provides an approximate means to calculate resistance characteristics.

$$\Delta p = 8\mu QL/10\pi\bar{R}^4 \qquad (15)$$

where Δp = pressure loss N/m^2
μ = gas viscosity poise
Q = volume flow per pore cm^3/sec
L = filter thickness cm
$\bar{R}$ = pore (capillary) radius (based on minimum pore area) cm

Reasonably good agreement was found between measured and observed resistance values (50 percent lower and 33 percent higher, respectively, for Sunbury and Nucla fabrics). However, the determination of the minimum pore cross section Figure 30, Section V by a combination of geometric and microscopic analyses represents considerable effort.

The value of $\bar{R}$ appearing in Equation (15) is based upon the circular equivalent of the minimum pore cross section. Since the pores vary in cross section and present tortuous rather than straight channels, several fabric weaves should be studied with special attention directed to pore geometry before any version of the Hagen-Poiseuille equation can be applied with confidence. In almost every case, direct measurement of clean cloth permeability (a very simple procedure) is the preferred approach.

Specific Resistance Coefficient, K_2

The specific resistance coefficient, K_2, has been discussed extensively in the filtration literature.[1] It is directly calculable from the true linear portion of the drag versus fabric loading curve where $K_2 = dS/dW$

which is constant for a specified dust/fabric combination. In accordance with the Carman-Kozeny theory,[1] K_2 can also be predicted by the relationships

$$K_2 = k \mu S_o^2 (1 - \varepsilon)/\rho_p \varepsilon^3 \tag{31a}$$

or

$$K_2 = k \mu \frac{36}{d_p^2} (1 - \varepsilon)/\rho_p \varepsilon^3 \tag{31b}$$

in which the terms are defined as follows:

k = Carman-Kozeny constant, frequently assumed to be 5.0.
μ = gas viscosity
S_o = ratio of particle surface to particle volume
d_p = particle diameter with a monodisperse system
ε = dust cake porosity
ρ_p = particle density

Equation (31a) was developed for use with granular beds composed of uniformly sized spheres in which porosity, ε, would ordinarily range from roughly 0.3 to 0.7. If the porosity is very high, ~ 0.9, and/or the particle shape deviates significantly from the spherical, Equation (32a) has little predictive value. The same can be said for those circumstances in which the particle sizing data are incomplete or incorrect for the dust of interest.

A detailed review of the filtration literature by Billings and Wilder[1] revealed no reliable means for predicting K_2 values except for direct experimental measurements. Their attempts to correlate data from several sources were not successful because of the absence of many critical data inputs. Additionally, the common failing of reporting filter drag as a function of the dust increment added during the filtering cycle rather than on the basis of total fabric dust loading, makes it impossible to interpret correctly most field and laboratory data.

Only if one assumes that there are lengthy filtration periods without interruption for cleaning can the K_2 values be considered as approximately correct. In those instances where a drag versus fabric loading curve involves a nonuniform dust distribution upon the fabric, the true K_2 value cannot be determined.

K_2 Versus Face Velocity - Attempts to correct or modify K_2 values in accordance with changes observed when particle shape factor, fabric surface properties and clean cloth permeability differed for a new set of dust and operating parameters have been cited by Billings and Wilder[1] in the form of tabulated correction factors, see Table 33.

The term K_v is defined roughly by the expression

$$K_v \doteq V(\text{ft/min})/3 \tag{32}$$

Borgwardt et al[32] have indicated that K_2 can be defined as

$$K_2 = a\ V^{1.5} \tag{33}$$

where a is a characteristic constant for the dust in question. One can infer from the above that K_2 varies as V to the 1 to 1.5 power.

The correctness of these relationships, however, is seriously questioned because of measurement techniques and lack of critical data. As stated previously, the nature of the cleaned fabric surface is seldom defined and the dust is often characterized by a single parameter only such as the mass mediam diameter.

Experimental data from various laboratory sources,[1,14,18,20] Table 34, are graphed in Figure 103, in order to estimate the impact of particle size and face velocity upon K_2. If the probable variations in the physical properties of the dusts (i.e., size, distribution, shape and density) and the face velocities are assumed to balance one another the point array in Figure 103 suggests that K_2 varies nearly inversely with mass median diameter.

Table 33. CORRECTIONS FACTORS FOR K_2

Particle shape, K_{sh}

Dust material	K_{sh}
Crushed	10.0
Ash	4.
Irregular	3.
Collapsible	0.2
Fumes	0.05

Fabric permeability, K_{perm}

S_o^a	K_{perm}
10	1.3
20	1.2
30	1.1
40	1.0
50	0.9
60	0.8
70	0.7
80	0.6
90	0.5

[a] Clean (unused) permeability CFM/ft^2 at 0.5 in. H_2O

Fabric surface, K_{Fs}

Fabric	K_{Fs}
Smooth	1.0
Napped	1/2
Felts	1/4

These correction factors are intended for use in the empirical equation:

$$K_2 = 1000\ K_{sh}\ K_{Fs}\ K_{perm}\ K_v/d_p^{\,2}$$

Table 34. DATA SUMMARIES FOR ESTIMATING K_2 AS A FUNCTION OF FACE VELOCITY AND PARTICLE SIZE

K_2 in. H_2O min ft/lb	Type of filter	Weave yarn count	Dust type size, MMD, μm	Gas velocity, ft/min	Ref. no.
57.0	Dacron	No data	As. salts 3.3	1.0	1
42.6	Glass fiber	3x1 Crowfoot 55x58	Mica 6.0	6	14
40.0	Dacron RP	Plain staple 30x28	Fly ash 5.0	3	10
37.0	Dacron AN	3x1 Twill 78x69	Talc 5.1	3	20
37.0	Glass fiber	3x1 Twill 53x51	Fly ash 3.5	3	14
28.0	Dacron DN	3x1 Twill 79x81	Talc 5.1	3	20
27.0	Dacron EN	3x1 Twill 42x28	Talc 5.1	3	20
24.4	Glass fiber 1	3x1 Crowfoot 55x50	Mica 6.	6	14
23.0	Glass fiber 1	3x1 Crowfoot 55x50	Mica 6.0	4	14
22.5	Glass fiber 1	3x1 Crowfoot 55x50	Mica 6.0	2	14
21.4	Glass fiber 3	3x1 Crowfoot 55x58	Mica 6.0	4	14
21.3	Glass fiber 1	3x1 Crowfoot 55x55	Mica 6.0	2	14
21.2	Dacron A	3x1 Twill, fil. 82x62	Mica 6.0	2	14
16.5	Glass fiber 3	3x1 Crowfoot 55x58	Mica 6.0	2	14
16	Glass fiber 3	3x1 Crowfoot 55x58	Mica 6.0	2	14
16.3	Dacron RC	3x1 Crowfoot 71x51	Fly ash 8.0	3	10
15.0	Dacron B	3x1 Twill 82x76	Mica	2	14
15.0	Nomex A	3x1 Twill 96x78	Fly ash 15.0	4	18
14.7	Nomex A	3x1 Twill 96x78	Fly ash 15.0	4	18
14.4	Dacron B	3x1 Twill 82x76	Mica 6.0	2	14
12.4	Dacron RP	Plain staple 30x28	Fly ash 8.0	3	16
11.6	Nomex filament	3x1 Twill 96x78	Fly ash 15.0	4	18
11.2	Dacron RP	Plain staple 30x28	Fly ash 8.0	3	10
9.6	Glass fiber N	3x1 Twill 66x30	Fly ash 9.0	2	Fig. 54
9.6	Glass fiber S	3x1 Twill 54x30	Fly ash 9.0	2	Fig. 53
9.6	Glass fiber S	3x1 Twill 54x30	Fly ash 9.0	2	Fig. 53
8.	Nomex B	3x1 Twill, spun comb. 95x58	Fly ash 15.0	4	18
7.8	Glass fiber	3x1 Twill, fil. bulk 54x30	Fly ash 18.0	2	32
7.7	Dacron C	3x1 Twill 77x81	Fly ash 15.0	4	18
7.2	Dacron C	3x1 Twill 77x81	Fly ash 15.0	4	18
7.1	Dacron C	3x1 Twill 77x81	Fly ash 15	4	18

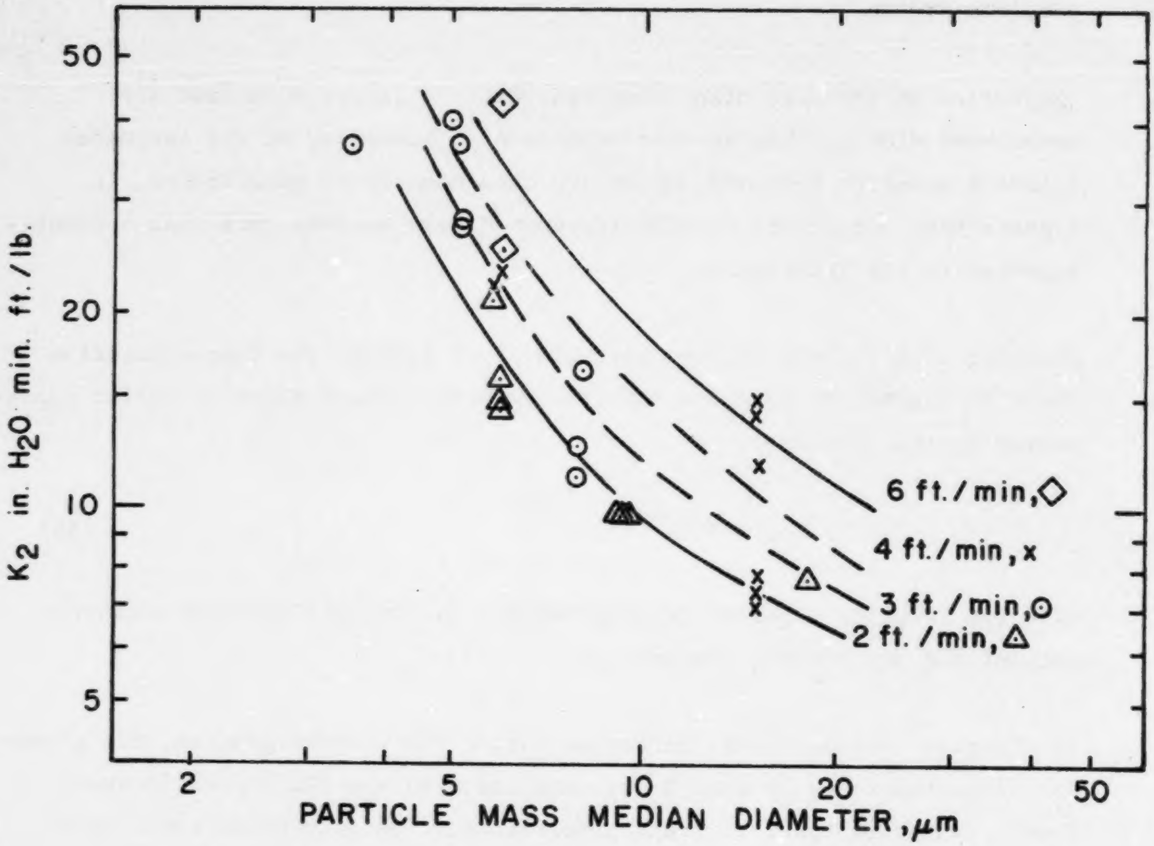

Figure 103. Specific resistance coefficient (K_2) versus mass median diameter and face velocity. Data from Table 34

$$K_2 \doteq (d^{-1}) \qquad (34)$$

Although, this observation appears to contradict theory, which indicates that the diameter exponent should be -2 (see Equation (31b)), it should be noted that Equation (31b) assumes a monodisperse and not a polydisperse particle system.

Inspection of the data also indicates that the larger K_2 values are associated with the higher face velocities. According to the estimated constant velocity contours, which are conceeded to be speculative, it appears that the effect of velocity upon K_2 may be less than that currently reported in the literature.

Plotting of K_2 values for two particle sizes against the face velocities shown in Figure 104 suggests that the velocity effect might be better represented by the following

$$K_2 = \phi\ (V^{0.5}) \qquad (35)$$

with the velocity exponent ranging between 0.5 and 1.0 for many commonly encountered dust/fabric combinations.

In a series of experiments performed during the current program, the effect of filtration velocity upon K_2 was studied with the GCA fly ash/Sunbury fabric system at three filtration velocities. Because these tests were carried out under carefully controlled conditions, there seems little reason to question the approximate square root relationship shown by the dotted line on Figure 104, at least with respect to fly ash and closely related dusts. For this reason, we have elected to define the effect of face velocity on K_2 by an expression such as Equation (35) to correct for K_2 variations during real filtration processes involving coal fly ash and woven glass fabrics. With reference to a specific dust/fabric system K_2 should probably be defined as

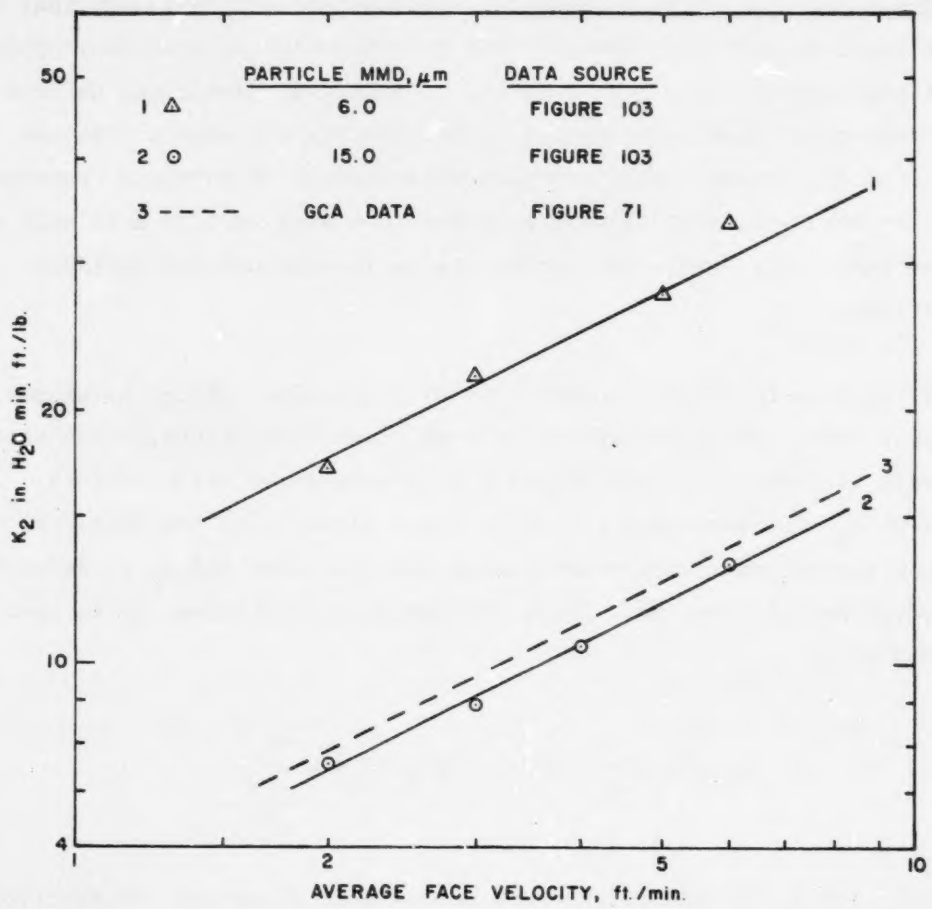

Figure 104. Estimated effect of face velocity on K_2 based upon literature review, Table 6

$$K_2 = a\ V^{0.5}$$

where the constant, a, is determined from the actual measurement of K_2 at any velocity within the expected working velocity range for the system.

K_2 Versus Specific Surface Parameter - It was stated previously that a major limitation of the Carman-Kozeny relationships is that they apply to ideal structures; i.e., beds composed of spherical particles, uniform with respect to size and physical properties and bed depth. However, the fact that the present study provided more details on particle characteristics and other relevant filtration parameters than usually available suggested that their predictive capability be re-examined for nonideal situations.

The first step involved determination of a specific surface parameter, S_o, that more clearly describes the pore properties-channel cross sections and wall surface area - associated with polydisperse distributions Thus the term A_p was considered to define total superficial (or envelope) surface for all particles constituting the dust cake and V_p to describe the total particle volume. Thus, for spherical particles, S_o is then defined as

$$S_o = A_p/V_p = N\ \pi\ d_s^{\ 2}/N\ \frac{\pi}{6}\ d_v^{\ 3} = \frac{6d_s^{\ 2}}{d_v^{\ 3}} \qquad (36)$$

where d_s and d_v are the surface and volume mean diameters, respectively, and N the number of particles in a unit mass of filter bed.

The characteristic diameters cited above are easily determined from the linear approximations to logarithmic-normal mass distributions for inlet fly ash aerosols; i.e.

$$\log d_s = \log \mathrm{MMD} - 4.605 \log^2 \sigma_g$$

$$\log d_v = \log \mathrm{MMD} - 3.454 \log^2 \sigma g$$

Such measurements were performed both in the field and in the laboratory with the Andersen impactor, a commonly used device to determine mass size distributions.

K_2 Versus Dust Cake Porosity - A second critical parameter appearing in the Carman-Kozeny equation is bed porosity, ε. In the case of coarse granular materials, Dalla Valle reports that particles > 10 μm form moderate porosity beds, ~0.3 to 0.7, whereas powders in the 1 to 10 μm range may have larger void volumes, 0.5 to 0.9.[33] Two approaches for estimating porosity were used in this study. Actual filter cakes deposited under normal filtration conditions upon woven all glass fabrics, Section VII, were excised by micro manipulation so that their volume and weight could be determined. These tests showed a bulk density of 0.82 g/cm^3, which when related to an assumed discrete particle density of 2.0 g/cm^3, indicates a bed or filter cake porosity of 0.59.

A second approach for estimating porosity was to determine the bulk density of test dusts prior to re-aerosolizing. Generally the "as received," moderately shaken or vibrated, and shaken and heated samples showed that the bulk densities were roughly one-half the assumed fly ash density of 2.0 g/cm^3.

It is emphasized that highly accurate estimates of ε are necessary before K_2 can be predicted with any high degree of confidence. Reference to Table 35 shows that small, ~10 percent, variations in porosity lead to large differences, ~50 percent, in the porosity function, $(1 - \varepsilon)/\varepsilon^3$.

Calculated and Observed K_2 Values, Field and Laboratory Tests - Measurements at the Nucla power station were analyzed to determine the probable value of K_2 for the field aerosols. Several tests were reviewed, Table 36, in which lengthy filtration periods (1 to 4 hours) were maintained between the cleaning cycles. The Nucla operating procedure usually involved continuous cleaning of all six compartments over a 25-minute period once the cleaning cycle was pressure actuated. Because of the long filtering periods, the characteristic lack of uniformity in fabric dust loadings from one compartment to another immediately after cleaning decreased greatly as filtration progressed. Therefore, it is justifiable to estimate the specific resistance coefficient, K_2, directly from the resistance change, ΔP, noted at constant velocity, V, for the change in fabric loading, ΔW, over the measurement period. It was assumed that the inlet loadings, filtration velocities and temperatures were constant over the indicated averaging periods, although some variations were apparent as evidenced by the change in slope of the resistance versus time chart traces.

Table 35. POROSITY FUNCTION FOR GRANULAR POROUS MEDIA

Porosity ε	$\frac{1-\varepsilon}{\varepsilon^3}$	Particle diameter, μm
0.90	0.14	1.0
0.85	0.24	1.5
0.80	0.39	1.5
0.75	0.60	2.0
0.70	0.88	2.5-3.0
0.65	1.27	3.5
0.60	1.85	5.0
0.55	2.70	8.0
0.50	4.0	10-12
0.45	6.0	20
0.40	9.4	25-30
0.35	15.1	30
0.30	25.9	30
0.25	48.0	30

Table 36. MEASURED AND CALCULATED K_2 VALUES FOR NUCLA FIELD TESTS[8]

Run no.[a]	Measurement period, minutes	Inlet dust concentrations,[b] g/m^3 dstp	Particle size parameters[c]				Measured K_2,[e] N min/g m	Calculated K_2,[f] N min/g m
			MMD μm	σ_g	ρ_p g/cm^3	S_o^2[d] cm^{-2}		
1-1-A	110	4.76	14.8	5.2	2.0	2.37×10^8	0.531	3.39
1-2-A	90						1.64	3.39
1-3-A	80						0.745	3.39
11-AB	140	3.98	10.2	2.68	2.0	6.98×10^7	1.00	0.962
14-AB	100	4.05	14.1	3.33	2.0	7.79×10^7	1.13	1.72
15-B	22	3.07	10.6	3.58	2.0	2.13×10^{11}	1.18	3.39
16-AB	60	4.99	11.3	3.55	2.0	2.28×10^8	1.13	2.02
16-B	60	4.99	12.7	3.27	2.0	9.03×10^7	1.13	1.33
19-1-AB	141	4.53	11.3	2.5	2.0	6.51×10^7	0.943	0.843
19-2-AB	72	4.53	11.3	2.5	2.0	6.51×10^7	1.16	0.843

[a] First number refers to test; second number to different, non-overlapping measurement periods during test; A or B refers to separate Andersen impactor analyses; and AB to the average of analyses A and B.

[b] Average dust concentration by Method 5 type sampling.

[c] Andersen impactor estimates of mass distribution parameters by log-normal distribution with assumed particle (discrete) density of 2 g/cm^3.

[d] S_o^2 computed from $S_o^2 = (6\, d_s^2/d_v^3)^2$ for assumed spherical particles with indicated surface (d_s) and volume (d_v) diameters computed from mass distribution parameters.

[e] Measured K_2 for actual filtration velocity, ~0.84 m/min and a gas temperature of ~124°C.

[f] K_2 computed by Carman-Kozeny relation $K_2 = \underline{k\mu\, S_o^2}\left(\frac{1-\epsilon}{\epsilon^3}\right)$, where $\epsilon = 0.59$ and $\left(\frac{1-\epsilon}{\epsilon^3}\right) = 1.9$.

Note 1: Run no. 1 - Sizing data suspect, poor agreement between Method 5 (4.76 g/m^3) and Andersen impactor (1.14 g/m^3) loadings

Run no. 1 - Average measured K_2 at operating conditions = 0.974 N min/g m.

Note 2: Tor convert K_2 (metric) to K_2 (English) multiply N min/g m by 6.0 to obtain in H_2O min ft/lb.

In performing these analyses, the cake porosity, ε, was estimated to be 0.59 on the basis of laboratory bulk density measurements on a filter dust layer, 0.82 g/cm^3, and a discrete particle density for fly ash of 2 g/cm^3.

The results of these calculations, Table 36, showed an average predicted K_2 value about two times greater than the measured value. The apparent agreement with theory is surprisingly good in view of the acknowledged limitations of input parameter measurements.

For example, linear extrapolations beyond the observed size classes for cascade impactor size distributions may not afford an accurate description of all size properties. Additionally, one is usually compelled to assume that the particles depositing on the various impactor stages are discrete particles having the density of the parent material. Actually, there may be agglomerates present to the extent of 10 to 15 percent of the total number count when compressed air is used to redisperse dry powders. Most real gas streams also contain agglomerated particles. Thus, conversion of aerodynamic size to actual size may give erroneous results for estimates of surface and volume mean diameters even if all particles are spheres.

Another potential problem is to decide whether a population of agglomerated particles will produce a deposit whose porosity is at least partially controlled by the external dimensions of the agglomerated particles. Were this to be true, a system composed of agglomerates, each of stable structure and having a porosity of 0.5, might conceivably form a dust layer with an interagglomerate porosity of 0.5 and an overall porosity of 0.75. At this time, it does not appear that a precise definition of the above conditions is possible. In lieu of rather difficult and time consuming laboratory measurements where sections of dust cake are excised for analysis, it appears that a practical measure of cake porosity may be obtained by noting bulk density values for the loose dust under a variety of tamping (vibration) and heating conditions. Average values for all Nucla tests are summarized in Table 37. Note that the K_2 values for ambient conditions include corrections for gas viscosity and filtration velocity.

Table 37. SUMMARY OF AVERAGE K_2 VALUE FROM NUCLA FIELD STUDIES

	Test conditions 124°C, 0.844 m/min	Ambient conditions 21°C, 0.61 m/min
	N min/g m	N min/g m
Measured K_2	1.05	0.75
Calculated K_2	2.09	1.49
Calculated S_o	1.28×10^8 cm^{-2} (Average of all tests, Table 36)	

Further indication of the degree of conformity found between measured and predicted K_2 values (the latter calculated from the Carman-Kozeny relationship) is shown in Table 38 for several past and current GCA tests with fly ash and other test dusts. In these tests, the porosity values for coal fly ash deposits were taken as 0.59 based on GCA laboratory tests. Porosity values for lignite fly ash, talc and granite dust were based upon bulk density measurements on the dry dust using graduated containers and a laboratory balance. The first set of size parameters listed for any dust-fabric combination, Table 38, is the original analysis of size distribution curve. These (original size parameters) were used to calculate the indicated S_o^2 values.

In the case of tests with coarse granite dust, supplemental trial estimates were made to ascertain what impact variations in estimated size parameters (MMD and σ_g) might have upon S_o^2. The variations in size parameters represent different visual estimates of the best linear fit to the size distributions shown in Figure 15, Section IV. The same exercise was carried out

Table 38. CALCULATED AND MEASURED VALUES FOR SPECIFIC RESISTANCE COEFFICIENTS FOR VARIOUS DUSTS

	Dust parameters					Filtration Parameters				Measured K_2,			
Test dust	MMD,[a] um	σ_g	Particle density g/cm^3	S_o^2 cm^{-2}	Cake porosity, ε	Velocity, m/min	Temp., °C	Filter fabric	Test scale	Test conditions	Ambient conditions 21°C 0.605 m/min	Calculated K_2, 21°C	Ratio, calc. K_2 / meas. K_2
Coal fly ash Public Service Co., NH (GCA)	4.17(I)	2.44	2.0	4.73×10^8	0.59	0.915	21	—	Pilot	2.29	1.85	5.72	3.09
	5.0 (M)	2.13	2.0	2.58×10^8	0.59	0.915	21	Napped cotton, sateen weave	Pilot	2.29	1.85	3.74	2.02
	6.38(I)	3.28	2.0	3.55×10^8	0.59	0.605	21	Glass, 3/1 twill	Bench	1.40	1.40	5.14	3.67
Coal fly ash Public Service Co., NH	3.8 (I)	3.28	2.0	9.94×10^8	0.59	0.823	138	Glass, 3/1 twill	Field	6.35	4.45	14.4	3.23
Coal fly ash Detroit Edison (EPA)	3.2 (M)	1.8	2.0	4.78×10^8	0.59	0.915	21	Napped cotton, sateen weave	Pilot	1.22	1.00	6.19	6.18
Coal fly ash Public Service Co., NH (GCA)	2.42(M)	1.77	2.0	8.49×10^8	0.59	0.915	21	Napped cotton, sateen weave	Pilot	2.17	1.77	11.0	6.20
Coal fly ash Nucla, CO	11.3(I)	3.55	2.0	1.28×10^8	0.59	0.851	124	Glass, 3/1 twill	Field	1.05	0.75	1.84	1.98
Lignite fly ash Texas Power and Light	8.85(I)	2.5	2.4	1.06×10^8	0.46	0.605	21	Glass, 3/1 twill	Bench	1.34	1.34	3.67	2.78
	8.85(I)	2.5	2.4	1.06×10^8	0.42	0.605	21	Glass, 3/1 twill	Bench	1.34	1.34	5.16	3.86
	8.85(I)	2.78	2.4	1.30×10^8	0.46	0.605	21	Glass, 3/1 twill	Bench	1.34	1.34	4.49	3.36

Table 38 (continued). CALCULATED AND MEASURED VALUES FOR SPECIFIC RESISTANCE COEFFICIENTS FOR VARIOUS DUSTS

	Dust parameters					Filtration Parameters				Measured K_2,			
Test dust	MMD,[a] μm	σ_g	Particle density, g/cm^3	S_o^2 cm^{-2}	Cake porosity, ε	Velocity, m/min	Temp., °C	Filter fabric	Test scale	Test conditions	Ambient conditions 21°C 0.605 m/min	Calculated K_2, 21°C	Ratio, $\frac{\text{calc. } K_2}{\text{meas. } K_2}$
Granite dust	9.21(I)	4.83	2.2	5.05×10^8	0.68	0.605	21	Glass, 3/1 twill	Bench	1.38	1.38	2.64	1.92
	9.21(I)	4.55	2.2	4.13×10^8	0.68	0.605	21	Glass, 3/1 twill	Bench	1.38	1.38	2.15	1.56
	9.21(I)	4.05	2.2	2.88×10^8	0.68	0.605	21	Glass, 3/1 twill	Bench	1.38	1.38	1.50	1.09
	8.1 (I)	3.88	2.2	3.24×10^8	0.68	0.605	21	Glass, 3/1 twill	Bench	1.38	1.38	1.70	1.23
	9.84(I)	4.32	2.2	3.44×10^8	0.68	0.605	21	Glass, 3/1 twill	Bench	1.38	1.38	1.69	1.22
	9.21(I)	4.83	2.2	1.01×10^8	0.60	0.605	21	Glass, 3/1 twill	Bench	1.38	1.38	5.28	3.84
	1.23(I)	2.38	2.2	5.10×10^9	0.68	0.605	21	Glass 3/1 twill	Bench	12.3	12.3	26.7	1.94
Talc	2.77(I)	2.9	2.2	1.51×10^9	0.84	0.915	21	Cotton, 3/1 twill	Pilot	5.76	4.71	2.35	0.50
	2.77(I)	2.9	2.2	1.51×10^9	0.82	0.915	21	Cotton, 3/1 twill	Pilot	5.76	4.71	2.72	0.58
	2.77(I)	2.9	2.2	1.51×10^9	0.73	0.915	21	Cotton, 3/1 twill	Pilot	5.76	4.71	5.78	1.23

[a] (I) refers to cascade impactor sizing.
(M) refers to microscope sizing (light field, oil immersion).

with respect to both size parameters and porosity for the lignite tests and with respect to porosity alone for the talc measurements.

The relationship between K_2 values and the specific surface parameters, S_o^2, Figure 105, indicates that grouping of data points by type of dust (and/or type of measurement) shows a strong linear correlation between K_2 and S_o^2 as postulated the Carman-Kozeny theory. It is emphasized that the difference between the MMD value for a highly polydisperse distribution and the diameter that characterizes the term S_o may be considereable. In the case of the coarse granite dust, the MMD was 9.21 μm whereas the single diameter used to compute S_o was 2.65 μm. Since the S_o term is squared in calculating K_2, a twelvefold difference in the estimate of K_2 would result.

Of particular interest to the present program is the fact that bench, pilot and laboratory tests with the same fly ash type (Public Service Co. of New Hampshire) as well as field tests with a similar (sizewise) Nucla stoker fly ash show surprisingly good agreement with the K_2-S_o^2 correlation. At the same time, the predicted K_2 values are consistently high based upon the data summaries given in Table 39.

Table 39. MEASURED AND PREDICTED K2 VALUES

Fly ash	Test scale	Predicted K_2	Measured K_2	K_2 pred./meas.
Public Service Co., N.H., coal-cyclone boiler	Pilot	5.72	1.85	3.09
	Bench	5.14	1.40	3.67
	Field	14.4	4.45	3.23
Nucla, Colorado coal-stoker-fired	Field	1.84	0.75	1.98
Texas Power and Light lignite	Bench	4.44	1.34	3.31

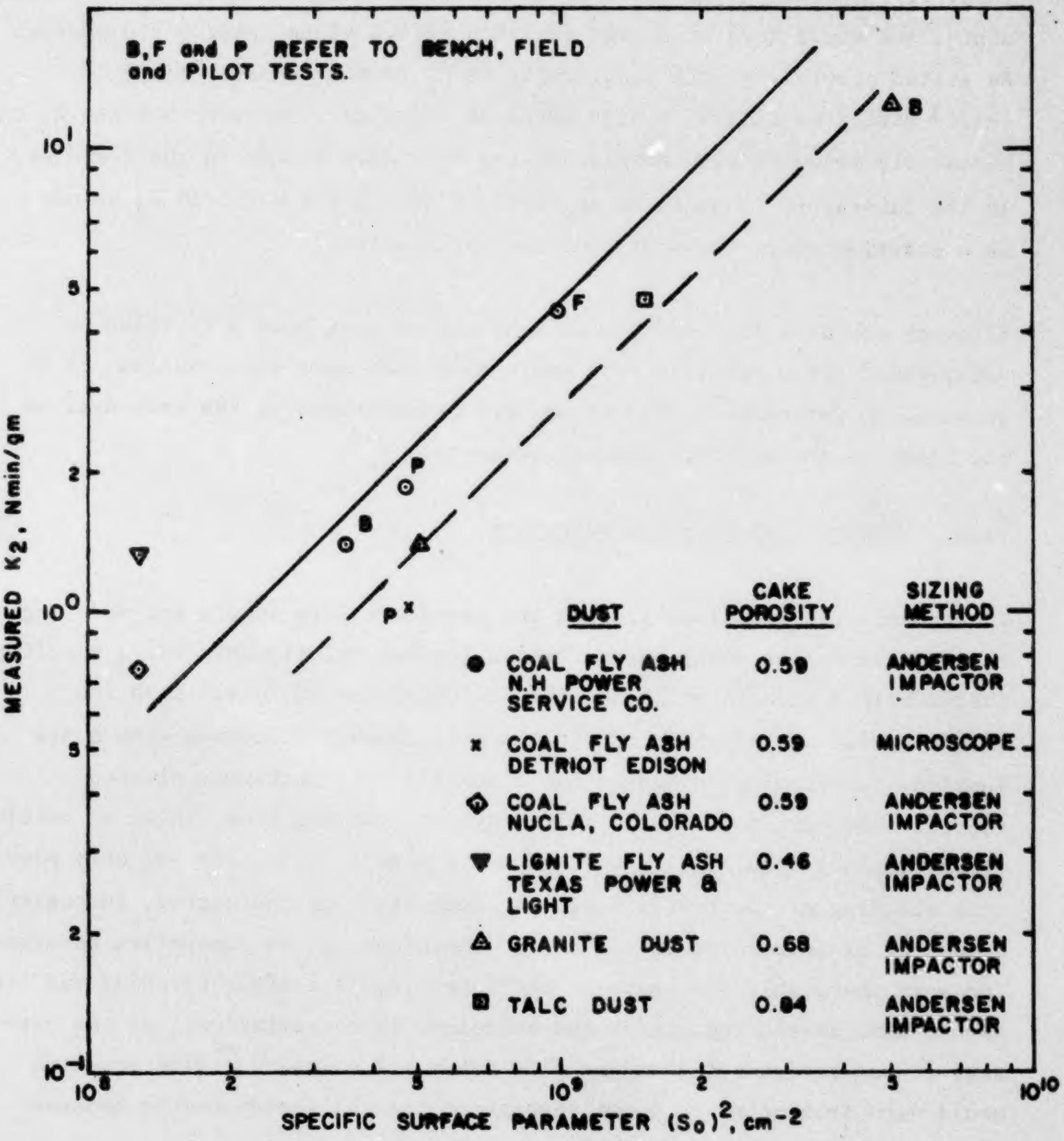

Figure 105. Specific resistance coefficient versus specific surface parameter (S_o^2) for various dusts

As far as the tests with three different fly ashes are concerned, the ratios for predicted and measured values appear to range between 2 and 4. Thus, if compelled to estimate K_2 without resorting to experimental measurements, one would have to accept possible errors of at least ± 100 percent. As stated previously, the sensitivity of K_2 to the porosity function, $1-\varepsilon/\varepsilon^3$ mitigates against a high level of accuracy. However, because K_2 can be readily measured with simple testing apparatus either in the field or in the laboratory it would be impractical not to use measured K_2 values as a starting point for most modeling applications.

Although the data are limited, it does appear that once a K_2 value is established for a specific dust and a specified size distribution, it is possible to determine K_2 for other size permutations of the same dust on the basis of the specific surface parameter, S_o^2.

FABRIC CLEANING AND FILTER PERFORMANCE

The preceding discussions provide the necessary data inputs for modeling the resistance (or drag) versus fabric loading relationship for a specified dust/fabric system in which the dust is deposited uniformly upon the fabric surface. The above conditions prevail when filtering with a new (unused) fabric or with a used but completely and uniformly cleaned fabric. However, real fabric filter systems ranging from single to multi-compartmented, sequentially cleaned units almost invariable see only partial cleaning of the fabric surfaces, regardless of the method, intensity, frequency or sequencing of cleaning. Therefore, it is imperative to examine very thoroughly the state of the fabric surface after cleaning and its impact upon system resistance and emissions characteristics. At the outset, it was recognized that gas flow rates and emission characteristics would vary from point to point throughout the collection system because of local variations in filter drag.

Resistance (Drag) Versus Dust Distribution on Fabric

The results of the GCA fabric filter cleaning study[10] indicated that the actual removal of dust from a fabric by mechanical action usually took place as a spallation process in which the dust separation occurred at the interface between the dust layer and the fabric. Except for unique circumstances, the resistance to tensile or shear forces at this boundary is much less than within the cake itself.

Examination of the forces needed to dislodge a dust cake by collapse or mechanical shaking has indicated that shearing or tensile forces in the 100 to 300 dynes/cm^2 range are required to cause cake detachment.[28] In the case of bag collapse systems, a 0.1 cm layer of fly ash having a bulk density of 1 g/cm^3 exerts a shearing force of roughly 100 dynes/cm^2 in a gravity field of 1g. On the other hand, the acceleration levels imparted to the dust layer in a mechanical shaking system are in the 5 to 6g range for a shaking frequency of 7 cps and a 1-inch shaking amplitude. Therefore, a tensile force of the order of 100 to 300 dynes/cm^2 is generated at the dust fabric interface with a 0.02 cm layer of dust. One infers that mechanical shaking will remove considerably more dust than simple bag collapse. The above line of reasoning also suggests strongly that the physical behavior and ultimate performance of both bag collapse and mechanical shaking cleaning systems can be treated in similar fashion.

Although the same approach should be applicable to pulse jet systems, two important factors should be kept in mind. First, estimated accelerations imparted to the fabric by reverse pulse air are much higher, ~200 g, such that the areal dust deposit density needed to achieve separating forces in the 100 to 300 dynes/cm^2 range is very low, approximate micrometers. Because of the napped character of most felts used in pulse jet systems, it appears unlikely that a distinct, fiber-free layer can develop in most filtration applications. Second, the felted media presents many more pores with much smaller diameters and greater depths than encountered with most woven fabrics. Hence, the basic substrate is a much more effective dust arrester than the typical woven fabric.

Analytical complications had been anticipated in applying the dust separation concept used for collapse and shake cleaning systems because of the difficulty in determining which fractions of the dust were interstitially or superficially deposited for a given set of operating variables. Subsequent laboratory tests, Section VII, indicated that these and other critical measurements could be made with ease.

By means of laboratory measurements, it was possible to estimate filter performance by two different approaches.

- The drag values for loaded and cleaned filters in conjunction with the fraction of dust removed (or the fraction of cleaned filter surface exposed) allowed computation of all intermediate system resistance values as well as the variations in areal dust deposit density with time.
- The measurement of total system drag in conjunction with the fraction of surface cleaned by flexure at two specific levels of cleaning, provided a direct mechanism for calculating residual and terminal drag values for the system.

Examination of Figure 106 shows how extreme the changes in systems resistance or drag are when filter cleaning is achieved by the dislodgment of dust layers from the dust/fabric interface rather than as a uniform surface spallation. The numbers used in developing Figure 106 and Table 40 relate closely to the drag values measured in actual laboratory tests. The average drag values after cleaning, $\overline{S}_R$, have been calculated from the following relationship:

$$\frac{1}{\overline{S}_R} = \frac{a_c}{S_c} + \frac{a_d}{S_d} \qquad (37)$$

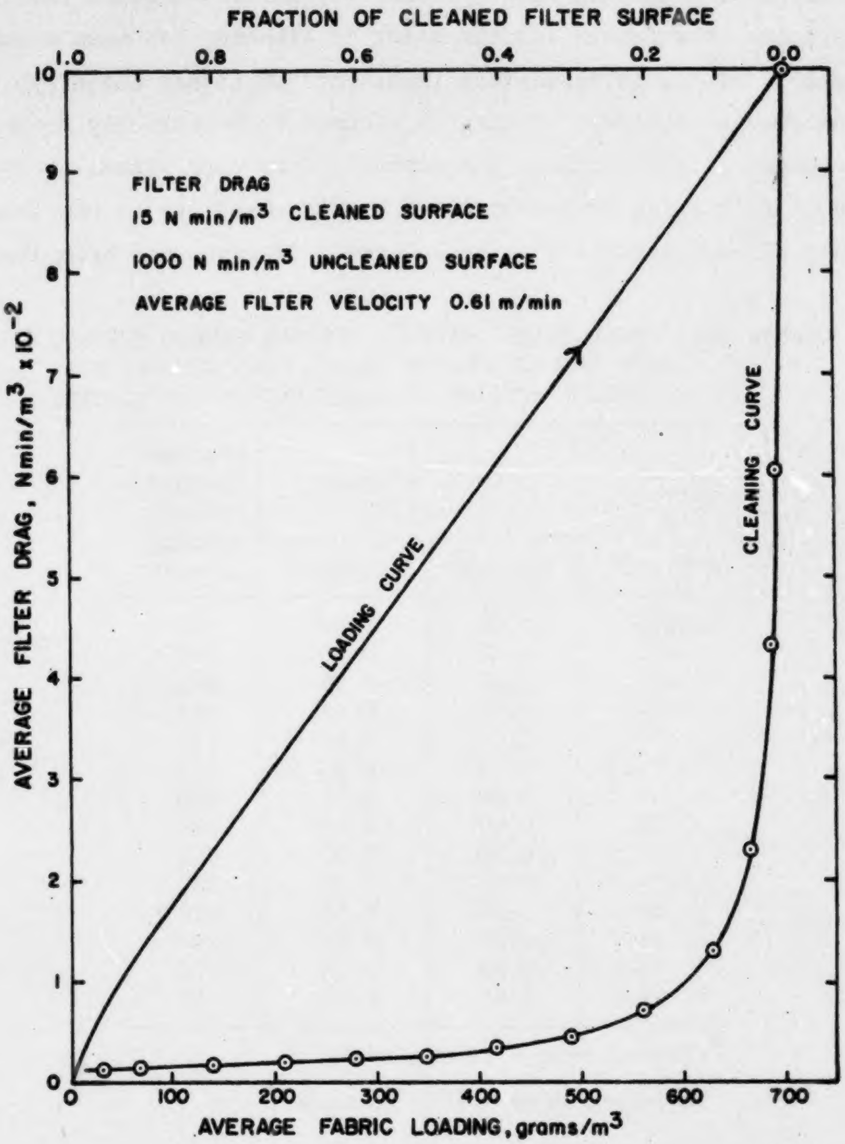

Figure 106. Average filter drag with various degrees of dust removal - fly ash filtration with woven glass fabric

where a_c and a_d are the fractions of cleaned and uncleaned fabric, respectively. S_c and S_d represent filter drag values for cleaned and uncleaned regions with estimated values of 15 and 1000 N-min/m^3, respectively. To keep within the working range of coal fly ash/woven glass fabric filter systems, the fabric loading prior to cleaning has been assumed to be 700 g/m^2. By assigning various levels of fractional cleaning, for which the average residual loading is assumed to be directly proportional to the cleaned filter surface, the actual system drag values at the resumption of filtration are shown to be highly sensitive to the fraction of freshly cleaned surface when only a small fraction has been cleaned.

Table 40. RELATIONSHIP BETWEEN CLEANED FABRIC SURFACE AND AVERAGE FILTER DRAG - COAL FLY ASH FILTRATION WITH WOVEN GLASS FABRIC (PREDICTED)

Average $\bar{S}_R$ N-min/m^3	Surface area fraction		Average residual dust holding grams/m^2
	Cleaned[a]	Uncleaned[b]	
1,000	0.00	1.00	700
603	0.01	0.99	693
432	0.02	0.98	686
234	0.05	0.95	665
132	0.10	0.90	630
70.8	0.20	0.80	560
48.3	0.30	0.70	490
36.7	0.40	0.60	420
29.6	0.50	0.50	350
24.7	0.60	0.40	280
21.6	0.70	0.30	210
18.7	0.80	0.20	140
16.6	0.90	0.10	70
15.8	0.95	0.05	35

[a] Cleaned drag = 15 N/min/m^3.

[b] Uncleaned drag = 1000 N-min/m^3.

Since the fabric drag resulting from successive flexing as depicted in Figure 106 rapidly approaches the cleaned fabric drag as a limiting value, one should consider the situation where the flexing process has been stopped after 50 percent of the dust has been removed. Within the expected accuracy limits for such measurements, there would appear to be no advantage, in terms of resistance, to continued flexing beyond the 350 g/m^2 load level. However, were flexing continued, much more cleaned fabric area would become available with an attendant increase in filtration capacity (the loading present at the maximum allowed pressure drop) during the next filtration cycle. We do not imply it is best that woven glass bags cleaned by collapse and reverse flow be flexed until nearly all of the dust is removed. There would be little reduction in resistance and there would be a probable penalty in terms of increased dust emissions.

The main objective for the calculations illustrated in Figure 106 is to show how closely the process relates to the data presented several years ago by Walsh and Spaite in Figures 107 and 108. For a specified mechanical shaking system (defined in terms of amplitude and frequency), there was a limiting number of shakes, N_s, beyond which no appreciable reduction in residual drag was attainable. There was also a limiting number of shakes, N_w, beyond which no increase in filtration capacity could be attained. The latter number of shakes, N_w, always exceeded the number required to reach a practical minimum resistance. More recent shaking studies performed by GCA indicated that no appreciable increase in dust removal was obtainable after about 200 shakes.

According to Walsh and Spaite, the additional number of shakes, $N_w - N_s$, required to reach a maximum holding capacity for a specified shaking mode was assumed to re-orient or restructure the cake such that discontinuities were minimized. Based upon the behavior of fabrics cleaned by collapse and the other analyses presented in this discussion, it appears more likely that significant dust removal and additional cleaned surface is gained during the $N_w - N_s$ shaking interval with a negligible decrease in drag as shown in Figure 106.

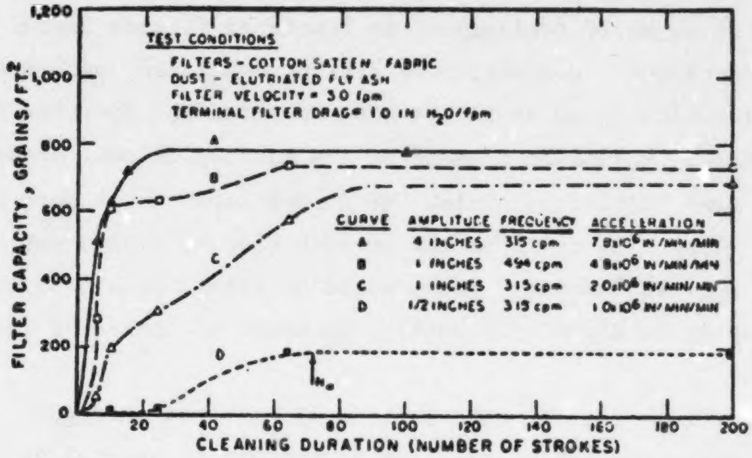

Figure 107. Effect of cleaning duration on filter capacity for several shaking conditions[14]

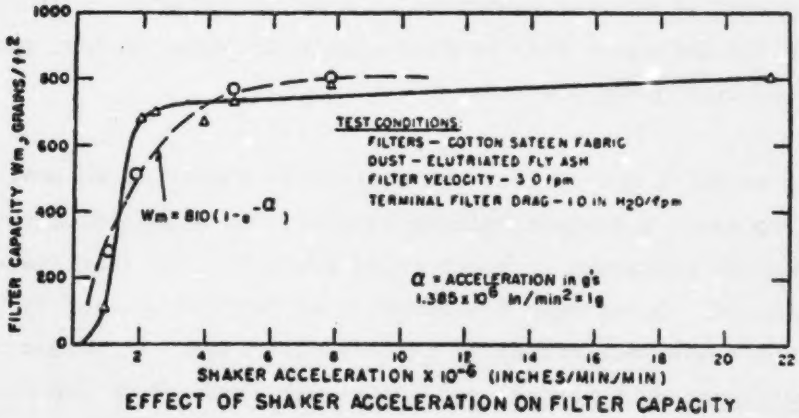

EFFECT OF SHAKER ACCELERATION ON FILTER CAPACITY

Figure 108. Effect of shaker acceleration on filter capacity[14]

In the case of many mechanical shaking systems, the energy transmitted via the shaking process is sufficient to dislodge only the more loosely bonded or thicker (and heavier) sections of the dust layer. Hence, a limiting residual holding is reached by a path resembling an exponential decay process. Most measurements reported by GCA in their study of fabric filter cleaning mechanisms[10] showed that after 200 individual shakes, only about 5 percent more of the potentially dislodgeable dust (assumed to be equivalent to an additional 5 percent of cleaned filter surface) could be removed with the specified cleaning mode.

The curves of Figure 109 illustrate why many past modeling efforts have not been successful. Curve 1 depicts the cleaned condition described previously where complete dislodgment of the overlying dust layer has been accomplished by hand cleaning. Curves 2, 3 and 4 describe the characteristic drag versus loading curves that result when the fabric surface has undergone partial cleaning. Note that whereas the abscissa denotes the average areal dust loading, the actual filter surface displays two characteristic regions at the resumption of filtration, the first from which the areal density has been reduced to the W_R level and the second which retains the former uncleaned fabric loading, W_T. Thus, for the fraction of cleaned and uncleaned surfaces relating to Curve 3, the average starting areal density is 0.5 W_T. In the case of large terminal loadings (W_T) and small residual loadings (W_R), the ratio, W_R/W_T, is an approximate measure of the fraction of uncleaned area.

Reference to the literature indicates that filter performance is often characterized by curves such as shown in Figure 109 except that the zero point on the abscissa refers to the residual dust holding which may be 0.25, 0.5, 0.75 or any other fraction of the terminal loading, W_T, depending upon the intensity of cleaning. Since the cleaning intensity and the actual residual dust holding (which is very difficult to measure) are seldom indicated, it is possible to draw several distinct conclusions from such drag versus fabric loading relationships, most of which will be erroneous. For example, if Curves 2, 3, and 4 are graphed so that the abscissa

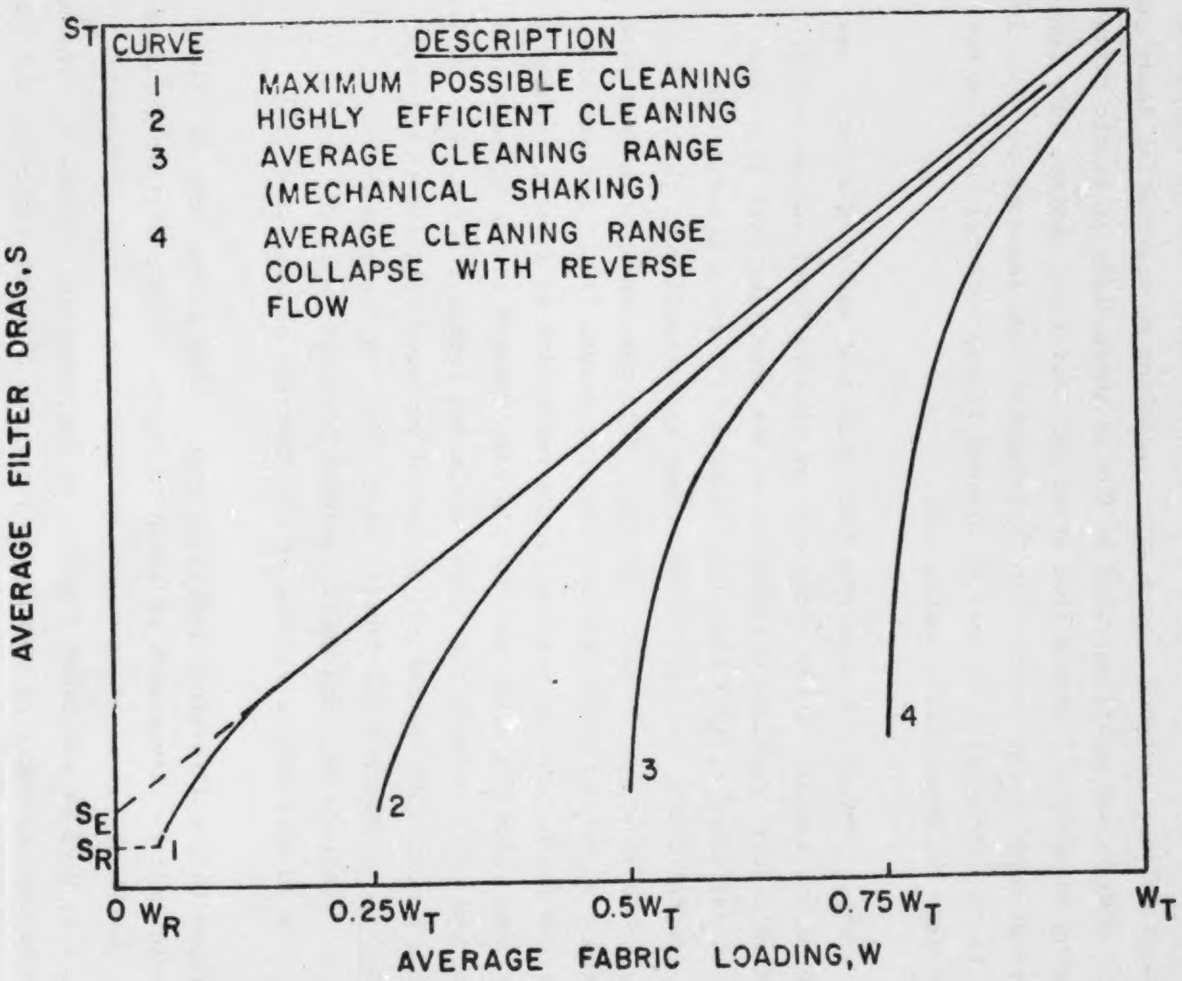

Figure 109. Typical drag versus loading curves for filters with different degrees of cleaning and a maximum allowable level for terminal drag, S_T, and terminal fabric loading, W_T

refers to the dust increment deposited during a typical filtration cycle and the system drag is constrained to values $\leq S_T$, it is apparent that the upper, nearly linear portion of Curve 2 will display the same slope, K_2, shown by Curve 1. The latter value, dS/dW, gives the correct K_2 value for the dust at the specified filtration velocity. However, as the residual dust holding increases, the near linear sections of Curves 3 and 4 no longer display the same slope and a reduction in the permissible S_T value further accentuates this difference.

The high degree of initial curvature in Curves 2, 3, and 4 results from a constantly changing air flow (and dust deposition rate) for the initial high (cleaned) and low (uncleaned) permeability regions of the fabric surface. Since the dust accumulation is most rapid on the "just cleaned" regions, the areal densities for both elements of the fabric surface will converge, thus leading to the dS/dW or K_2 relationship shown for a uniformly loaded fabric. The net result is that one cannot use curves of the type shown in Figure 109, to determine K_2 and S_E for any generalized modeling procedures. Only if the parameters deriving from any of the Figure 109 curves are applied to replicate filtration conditions will the empirically based equations provide useful data.

The problems discussed above can be avoided if the curves of Figure 109 are correctly recognized as reflecting the results of rapidly changing, parallel flows through fabric regions of changing permeability. The latter concept is frequently described in the literature with respect to sequentially cleaned, multicompartment filters.[1,13,16] The compartment approach, however, fails to take the behavior of individual bags into consideration.

Several experiments were performed to test the hypothesis that fabric filter performance could be defined by analyzing the behavior of partially cleaned fabrics after filtration was resumed. The starting assumptions are reiterated below to make clear the ground rules for the modeling process. When a uniformly loaded filter has undergone partial cleaning, the resultant surface is composed of two distinct areas; the first from which no dust has been removed and the second which is cleaned down to its characteristic W_R value.

Figure 110 indicates the actual appearances of (1) a woven glass fabric in the form of a 10 ft × 4 in. bag that was cleaned by collapse and reverse flow under normal field conditions, and (2) a partially cleaned filter panel cleaned by hand-flexing. Both photographs show that the dust has dislodged as slabs or flakes from the interface region with little indication of spallation from the surface layer. The special fluorescent tube mounted within the bag reveals the high degree of light transmittancy (and the minimal residual dust holdings) in those areas from which the dust has dislodged. Although the use of surface rather than transmitted light does not permit the same sharp light contrast, the presence of two distinct surfaces is indicated and the weave structure is clearly displayed on the cleaned, central section of the panel.

As shown earlier, the residual dust holdings are small, uniformly distributed and not strongly dependent upon the type of dust or woven fabric. The uncleaned portion represented by the area fraction a_u has a drag value of S_u based upon the filter resistance just before cleaning. The cleaned fraction, a_c, displays the characteristic residual drag, S_c which, for purposes of simplification, may be defined by S_E rather than S_R. Therefore, given the initial and final filter dust holdings or the fraction of cleaned filter area, the average effective drag, S'_E, for the two element system immediately after cleaning can be expressed by the equation:

$$\frac{1}{S'_E} = \frac{a_c}{S_c} + \frac{a_u}{S_u} = \left(\frac{V}{P}\right)_E \qquad (38)$$

Since K_2, in theory, depends only upon particle and fluid properties it should not vary with a fixed dust/fabric system. However, tests performed during this study and many past studies have demonstrated that K_2 may often increase with filtration velocity. The increase in K_2 is attributed mainly

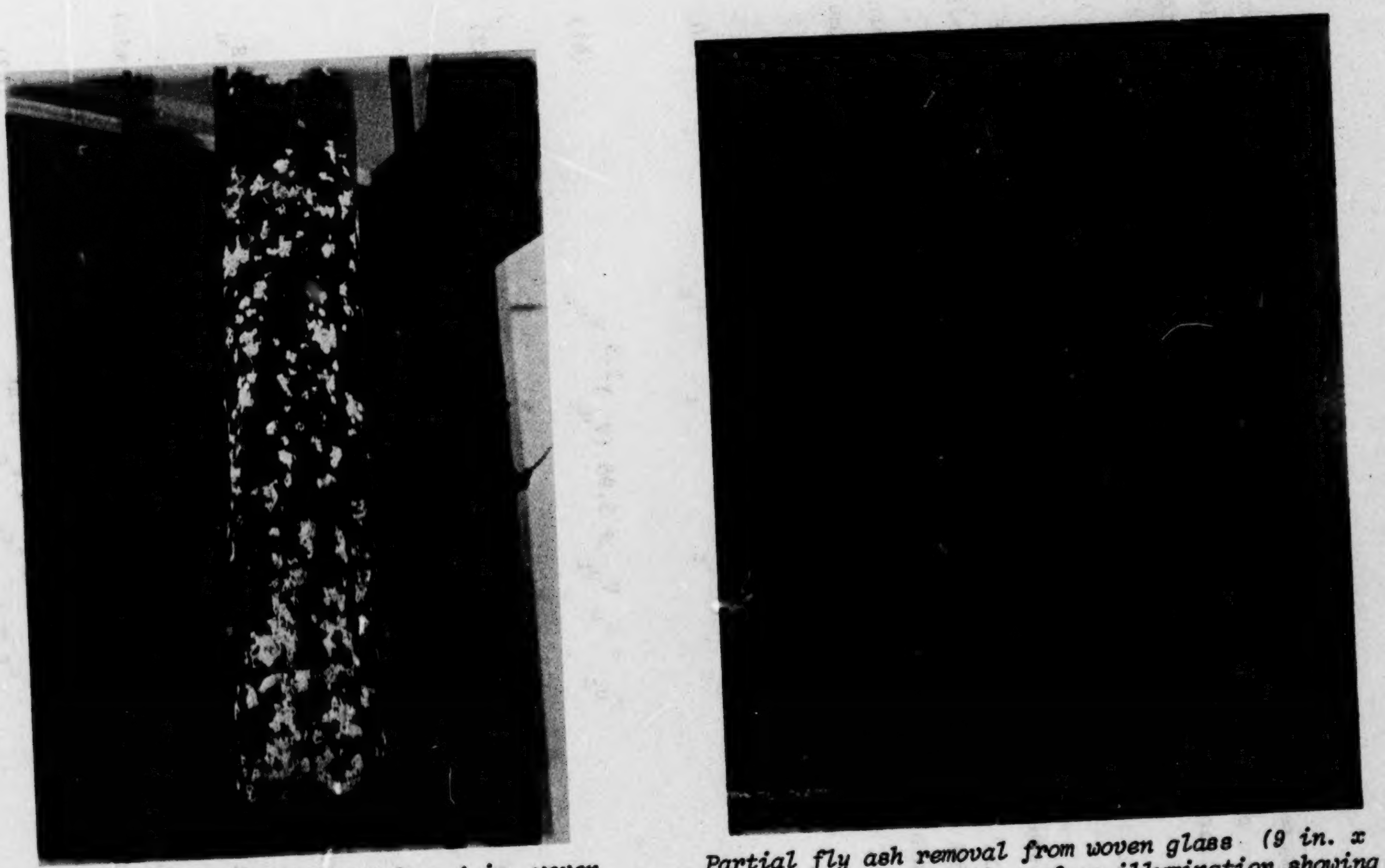

Fly ash dislodgment from 10 ft x 4 in. woven glass bag with inside illumination showing cleaned (bright) areas

Partial fly ash removal from woven glass (9 in. x 6 in.) test panel with surface illumination showing cleaned central region

Figure 110. Appearance of partially cleaned fabrics

to a decrease in cake porosity that results from higher particle momentum when the particle strikes the filter. For the fly ash/glass fabric system investigated in this study, K_2 can be expressed by the empirical equation:

$$K_2 = 5.95\ V^{1/2}\ \text{(English units)} \qquad (39)$$

If the specific resistance coefficient, K_2, is defined as a function of velocity, Equation 40, a simple iterative solution based upon the following equations can be used to predict the fabric resistance/fabric loading relationship. Using the subscripts c and u to denote cleaned and uncleaned surfaces, respectively, and t to depict the system parameters at the time equals t:

$$P_{c_t} = S_c V_{c_t} + 5.95\ (V_{c_t})^{1.5}\ W_{c_t} \qquad (40)$$

$$P_{u_t} = S_u V_{u_t} + 5.95\ (V_{u_t})^{1.5}\ W_{u_t} \qquad (41)$$

$$\overline{V} = a_c V_{c_t} + a_u V_{u_t} \qquad (42)$$

P_{c_t} is always equal to P_{u_t} and average filtration velocity, $\overline{V}$, inlet dust concentration, C, and the characteristic drag terms, S_c and S_u are system constants.

The average fabric dust loading after a small time change Δt (~ 1 to 5 min) can be approximated by the following equations:

$$W_{c_{t+1}} \doteq W_{c_t} + V_{c_t}\ C\ \Delta t \qquad (43)$$

$$W_{u_{t+\Delta t}} \doteq W_{u_t} + V_{u_{\Delta t}} C \Delta t \quad (44)$$

Then the equations listed below will indicate the new fabric resistance at the end of the time interval Δt:

$$P_{c_{t+\Delta t}} = S_c V_{c_{t+\Delta t}} + 5.95 \left(V_{c_{t+\Delta t}}\right)^{1.5} W_{c_{t+\Delta t}} \quad (45)$$

$$P_{u_{t+\Delta t}} = S_u V_{u_{t+\Delta t}} + 5.95 \left(V_{u_{t+\Delta t}}\right)^{1.5} W_{u_{t+\Delta t}} \quad (46)$$

By substituting $V_{u_{t+\Delta t}} = \left(\overline{V} - V_{c_{t+\Delta t}} a_c\right)/a_u$, and equating Equations (45) and (46) the relationships between effective pressure drop and velocity and dust holding for the two fabric surfaces are readily computed for successive time increments by a simple programming operation.

The system of equations described above is suitable for describing the drag versus fabric loading relationship for a partially cleaned, single bag or a two bag system in which one bag is completely cleaned.

The performance of a large, multicompartment filter system can be determined in similar fashion by introducing as many equations for the pressure and fabric loading terms as there are compartments and/or different filtering surfaces in the system. In a generalized form

$$S = \left(\sum_{j=1}^{n} A_j/S_j \right)^{-1} A \quad (47)$$

where S refers to system drag, A_j to the area of the j^{th} element and A, to the total filtration area.

The modeling concepts described above were applied to the experimental data shown in Figures 111 through 113. In each instance, fabric test panels

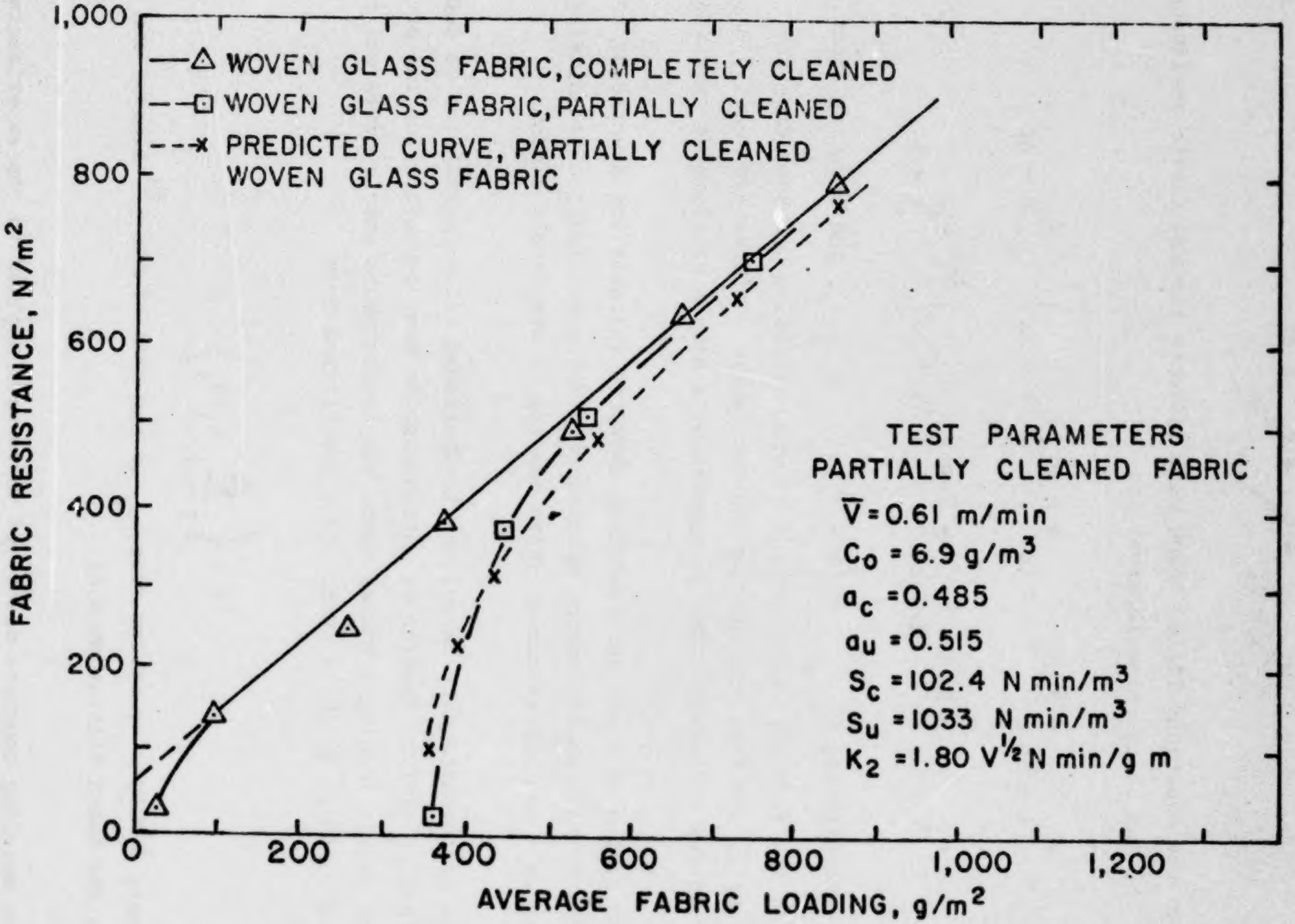

Figure 111. Fly ash filtration with completely and partially cleaned woven glass fabric (Menardi Southern), Tests 71 and 72

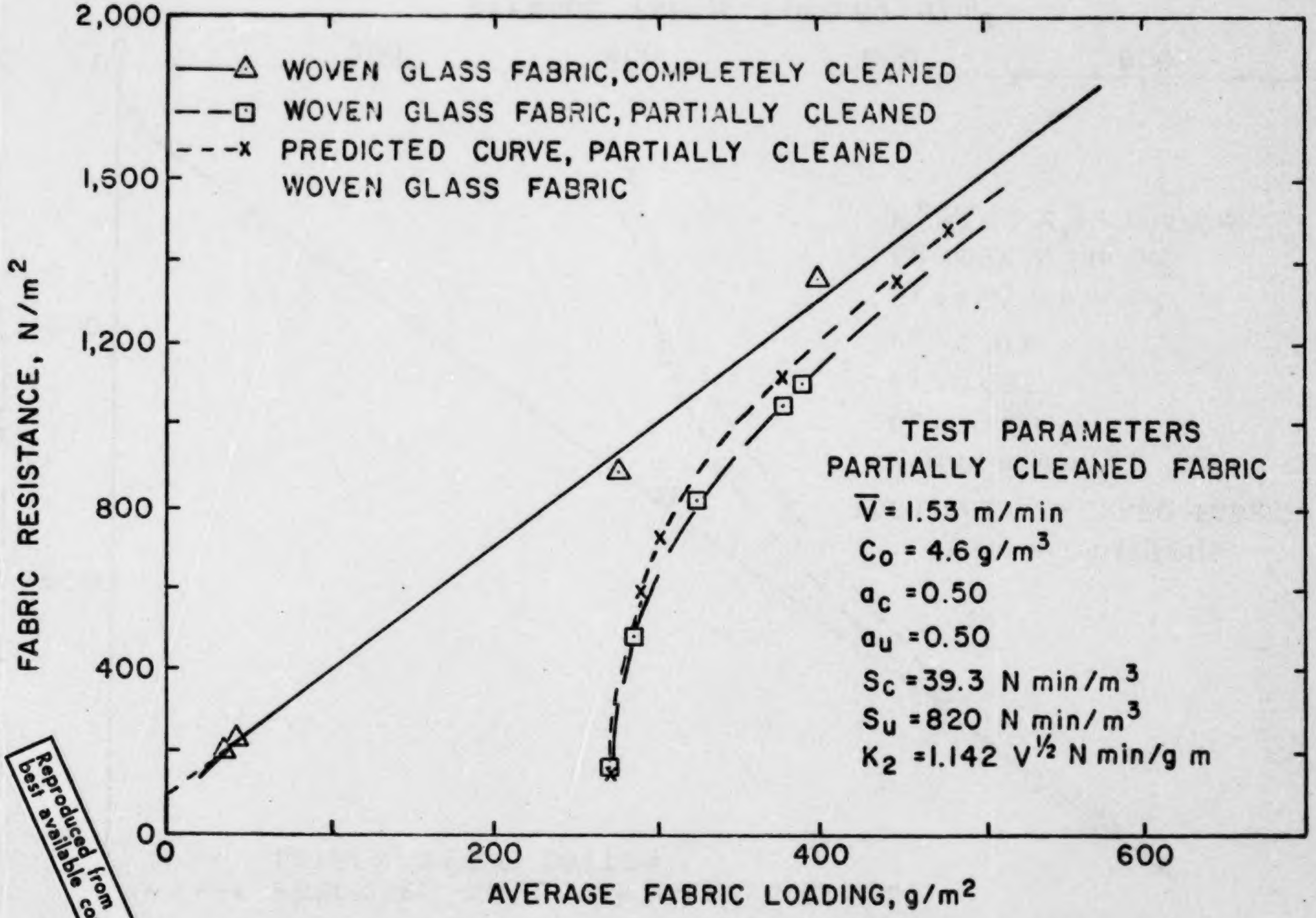

Figure 112. Fly ash filtration with completely and partially cleaned woven glass fabric (Menardi Southern), Tests 96 and 97

Reproduced from best available copy.

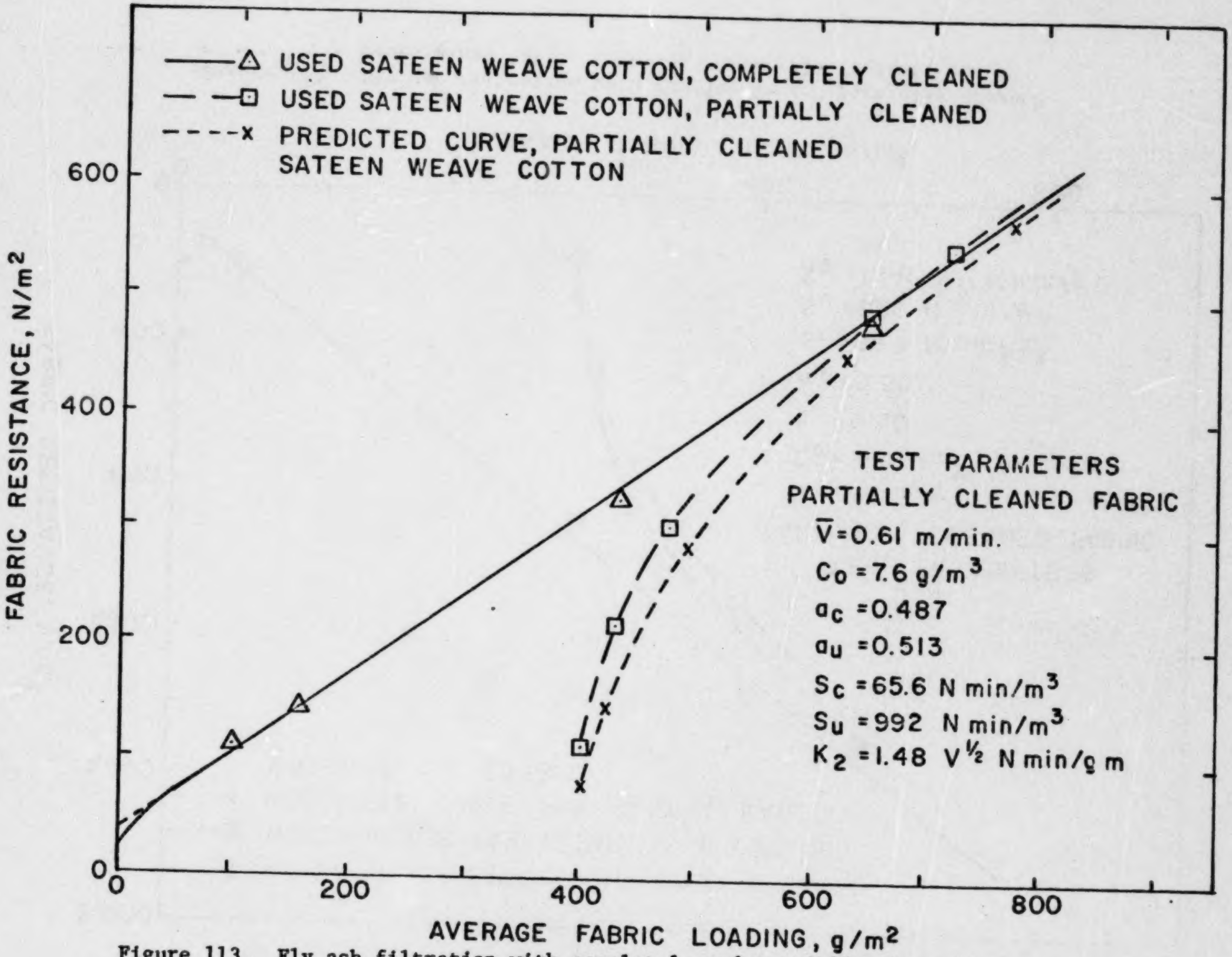

Figure 113. Fly ash filtration with completely and partially cleaned sateen weave cotton, unnapped (Albany International), Tests 84 and 85

that had been uniformly loaded with fly ash were partially cleaned so that approximately half the filter surface was stripped of its dust layer. The subsequent experimental loading curves followed much steeper paths and only at the higher average cloth loadings did the slope of each curve, K_2, approach that of the uniformly loaded fabric.

The drag value for the uncleaned area, S_u, is that based upon the filter resistance, face velocity, and fabric loading immediately before cleaning. Conversely, S_c is the drag value for the cleaned area only which is determined by removing completely the overlying dust layer from the fabric. It (S_c) is associated with the residual dust holding, W_R, for the cleaned portion of the fabric. The fraction of cleaned area, a_c, and uncleaned area can be determined by actual measurement of the cleaned and uncleaned areas. However, it is simpler to use the following mathematical relationship when the magnitude of the fabric loading before cleaning (W_P) the average dust loading (ΔW) added to the filter over the filtration cycle and the true fabric residual dust holding W_R are determinable; i. e.,

$$a_c = 1 - \frac{W_P - \Delta W - W_R}{W_P - W_R} = 1 - a_u \qquad (48)$$

From Equation (48) the uncleaned area fraction is computed as indicated. When W_P is very large, approximately 1000 g/m^2, the relationship $(W_P - \Delta W)/W_P$ provides a good approximation of a_u.

The curves designated by "X" on Figures 111 through 113 were generated by the modeling equations cited previously using the input parameters shown on each figure. The fact that the theoretical and experimental curves agree as well as they do suggests that the hypothesized filtration process is essentially correct.

Although it suffices for modeling purposes to treat the preliminary substrate plugging and subsequent cake growth on the basis of parallel flow through the pore array, it should be realized that normal statistical variations in pore dimensions and discrete fiber distribution will cause some pores to bridge over more rapidly than others. In the event of gross differences in pore size (or excessive filtration velocities) there is a real possibility that complete pore bridging will never occur. The later factor is responsible for high dust penetration and, in extreme cases, erroneously low estimates of K_2.

The modeling presented in Figures 111 through 113 is based upon the simplifying assumption that the nonlinear section of the drag curve can be ignored. A trial test was made, however, in which the drag versus loading relationship was broken down into two straight lines. The initial, curvilinear section was approximated by a straight line having a steeper slope than the normally linear portion of the curve. Reference to Figure 114 shows a slight shift of the predicted drag curve during the early loading phase. Despite the fact that the model is improved, it does not appear that much has been gained insofar as predicting average resistance is concerned.

Dust Removal Versus Cleaning Conditions

It has been determined previously that resistance characteristics for partially cleaned fabrics can be readily computed once the state of the filtration surface is established in terms of cleaned and uncleaned areas. From an operating viewpoint, however, it is also necessary that the method, intensity and duration of the fabric cleaning process be directly relatable to the state of the fabric surface. This means that the dust separating forces generated by the cleaning process and the adhesive forces that oppose dust dislodgment must be defined quantitatively.

Dust separating forces have been discussed for both bag collapse and reverse flow cleaning, and mechanical shaking. In the former case, it has been assumed that the shearing force exerted at the interface between the vertically aligned fabric and the dust cake is equal to the product of cake areal density, W, and the local gravitational constant, g. The force

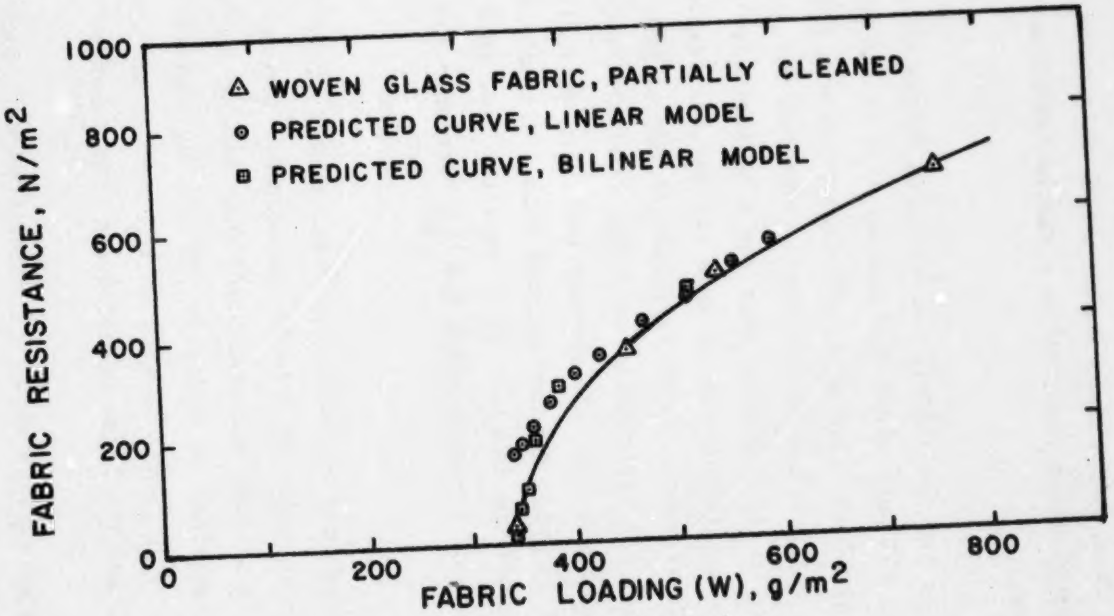

Figure 114. Resistance versus fabric loading for partially-loaded fabric, measured and predicted (using linear and bi-linear models) Test 72

causing dislodgment is also equal to the tensile force (W x g) exerted at the interface when the dust deposit is attached to the underside of a horizontally aligned filter. It is assumed that the interfacial adhesive force is approximately equal to the separating force at the instant of cake detachment. Thus, measurement of the areal density of a dust deposit at its dislodgement location constitutes a simple method to estimate interfacial adhesion levels.

If the areal density and the interfacial adhesive forces were uniform over the fabric surface, all dust would dislodge as soon as the areal density reached the critical level. Actually, all laboratory and field measurements indicate that only partial dust separation is attained for a fixed separating force. Therefore, one concludes that for a multiplicity of reasons the adhesive forces are distributed in some statistical fashion over the fabric surface . Furthermore, there is reason to expect that the applied separating forces are not distributed uniformly over the fabric surface. Qualitative observations during the current test program indicated that a vertical gradient in areal density existed with a slightly denser deposit on the lower surface of the fabric. It is expected that this gradient will increase as the range of particle sizes (or σ_g) increases for the entering aerosol.

What is actually determined by laboratory measurements is an "effective" gradient for the distribution of interfacial adhesion forces. Computations are given in Table 41 showing the equivalent dust separating force for each of the tests summarized in Tables 24, 25 and 26, Section VIII. The separating force for each fabric loading is the product of fabric loading before cleaning (W_T) and the local acceleration (980 dynes/cm^2).

The fraction of cleaned surface area, a_c, associated with each dust removal value has also been calculated for each test in accordance with the expression:

Table 41. FRACTION OF FILTER SURFACE CLEANED VERSUS DUST SEPARATION FORCE, GCA FLY ASH WITH WOVEN GLASS FABRIC (SUNBURY TYPE)

Run No.	Dust separation force,[a] dynes/cm^2	Fraction of fabric surface cleaned,[b] a_c	Run No.	Dust separation force,[a] dynes/cm^2	Fraction of fabric surface cleaned,[b] a_c
P-2-1	92	0.67	P-3-1	71	0.31
P-2-2	41	0.09	P-3-2	65	0.18
P-2-3	53	0.10	P-3-3	69	0.21
P-2-4	71	0.19	P-3-4	70	0.15
P-4-1	68	0.6	P-3-5	74	0.17
P-4-2	42	0.12	P-3-6	76	0.20
P-4-3	53	0.12	P-3-7	77	0.22
P-4-4	62	0.21	P-3-8	76	0.22
P-4-5	69	0.23	P-3-9	75	0.20
P-5-1	69	0.32	P-3-10	76	0.16
P-5-2	64	0.20	P-3-11	79	0.18
P-5-3	68	0.21	P-3-12	80	0.20
P-5-4	69	0.24	P-3-13	80	0.19
P-5-5	69	0.23	P-3-14	85	0.26
P-5-6	70	0.20	P-3-15	72	0.19
			P-3-16	74	0.19
			P-3-17	76	0.23
			P-3-18	75	0.19
			P-3-19	76	0.17
			P-3-1 to P-3-19	avg. 75	0.20

[a] Dust separation force = (W)(g) prior to cleaning. Equal to interfacial adhesive force when dust layer detaches.

[b] Dust detached from cleaned area held by adhesive force less than applied separating force.

$$a_c = 1 - \frac{W_R' - W_R}{W_T - W_R}$$

where W_T and W_R' refer to the average fabric loading before and after cleaning and W_R is the characteristic residual loading (50 g/m^2) for the fly ash/glass fabric systems.

The statistical nature of adhesive force distributions has been demonstrated by many present and past tests[10,14] in which successive repetitions or continuations of collapse-reverse or mechanical shaking has led to increased dust removal. Test results for various dust and fabric combinations show that a limiting removal level is attained after about six repetitive collapse and reverse flow treatments or 360 individual mechanical shakes, Figure 115 and Table 42. In the latter case, the bag was shaken at a frequency, f, of 8 cps with a 1 in. amplitude, A, (horizontal displacement) for the shaker arm such that the approximate maximum acceleration imparted to the dust layer was 5 gs ($\sim$4900 cm/sec^2).

It should be noted that the separation forces generated by mechanical shaking are also dependent upon fabric loading, W. However, the "g" factor, which is now governed by the shaking parameters, is much greater than that afforded by gravity separation. Average acceleration $\bar{a}$ was estimated by the relationship:[10]

$$\bar{a} = k4\pi^2 f^2 A \tag{49}$$

where k ranges from 0.7 to 0.8 for the previously cited amplitude and frequency conditions.

The most important observation with respect to multiple cleanings is that beyond a fixed number of collapses (or flexes) or a fixed number of shakes no further dust removal is attained for a specified energy input.

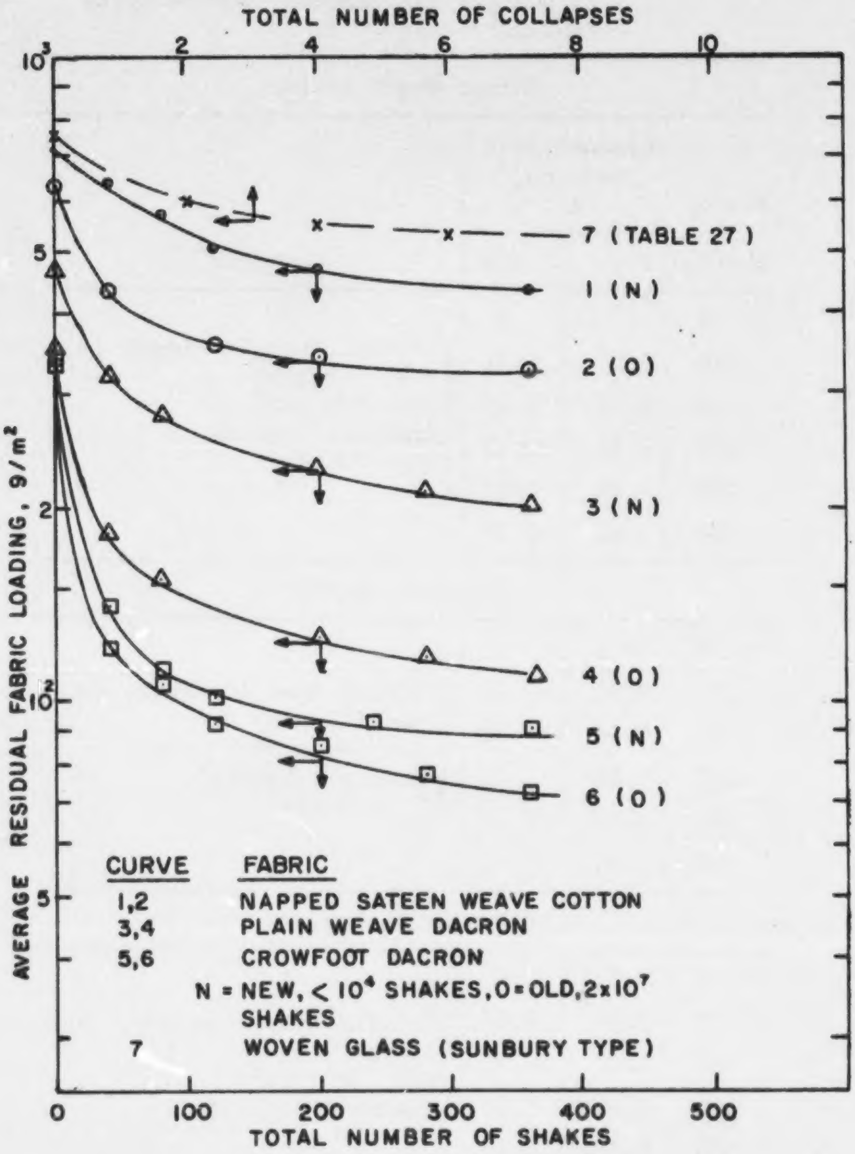

Figure 115. Average residual fly ash loadings versus fabric type and number of mechanical shakes (8 cps at 1 in. amplitude), Reference 10

Table 42. EFFECT OF NUMBER OF MECHANICAL SHAKES ON GCA FLY ASH REMOVAL FROM SELECTED FABRICS[10]

Number of shakes	Cleaned area fraction,[a] a_c		Comments[b]
	New	Old	
Sateen weave cotton			
0	-	-	
40	0.11	0.31	Initial dust loadings, (W_T), New, 729 g/m^2 Old, 635 g/m^2 Residual loading W_R = 70 g/m^2
80	0.22	0.45	
120	0.32	0.48	
200	0.37	0.51	
360	0.43	0.54	
Crowfoot Dacron			
0	-	-	
40	0.70	0.75	Initial dust loadings, (W_T), New, 361 g/m^2 Old, 341 g/m^2 Residual loading W_R = 70 g/m^2
80	0.80	0.80	
120	0.83	0.85	
200	0.84	0.90	
360	0.86	0.93	
Plain weave Dacron			
0	-	-	
40	0.32	0.60	Initial dust loadings, (W_T), New, 475 g/m^2 Old, 360 g/m^2 Residual loading W_R = 70 g/m^2
80	0.47	0.70	
200	0.60	0.80	
280	0.65	0.83	
360	0.67	0.86	

[a] a_c = Fraction of surface cleaned to W_R level.

[b] Cleaning accomplished by mechanical shaking of 8 cps with 1 in. amplitude. Bag acceleration = 5 g s (4900 cm/sec^2).

Only by increasing the thickness of the dust layer or by increasing the dust layer with a concurrent increase in acceleration by inducing an oscillating motion can a further increase in dust removal be attained.

With respect to dust dislodgement by the collapse and reverse flow process, the precise nature of the dust separation process is difficult to describe except for the simplified system in which the dust cake "hangs" from the underside of a horizontally mounted filter (not a conventional field procedure).

Figure 115 shows that the type and service life of a fabric affect significantly the degree of cleaning for a fixed energy input. For immediate reference, the relevant properties of all fabrics discussed in this section have been summarized in Table 43. The presence of bulk or staple fiber enhances the interfacial adhesion, thus making dust release more difficult. Additionally, the gradual "shedding" of staple with extended filter usage appears to decrease the adhesive bonding as suggested by the "new" and "old" values for average residual loadings. It is emphasized, however, that reduced average residual loadings may not indicate lowered filter resistance and decreased penetration. Examination of cleaned fabric shows that a large fraction of the bulk staple is attached to portions of the fill yarn that do not enter into the filtration process because of yarn proximity. Thus, shedding of the superficial staple reduces surface loadings in this area without any change in the interstitial region which may, in the long term, experience reduced flow cross section due to gradual plugging. It is necessary to assume first that the fabric loading is already at the level where it produces a separation force equal to that of the local adhesive force. When air flow is diverted from the bag, a bending ensues that produces cracking or checking of the surface because the bending moment of the dust layer has been exceeded. As reported earlier, many repeated flexings produce a crack pattern whose boundaries relate closely to the weave structure, Figure 28, Section V. Observations

Table 43. PHYSICAL PROPERTIES AND PENETRATION DATA FOR WOVEN FABRIC EXAMINED FOR DUST CAKE ADHESION

Fabric	Weight, oz/yd^2	Weave	Yarn count,[a] w/in. x f/in.	Frasier permeability, ft^3/min at 0.5 in. H_2O	Mfgr. and code number[c]	Application	Average penetration, percent
Woven glass	9.2	3x1 Twill	54x30[b]	42.5	MS, 601 Tuflex	Field[9] Sunbury, Pa.	0.08
Woven glass	10.5	3x1 Twill	66x30[b]	86.5	WWC, No. 640048	Field[8] Nucla, Colo.	0.16
Woven glass	8.4	3x1 Twill	53x51[b]	45-60	AI Q53-875	Field[7] Bow, N.H.	0.38
Woven Dacron	10	1/3 Crowfoot	71x51[b]	33	AI No. 865B	Laboratory,[10] GCA	0.07-0.29
Woven Dacron	10	Plain	30x28 staple	55	AI No. 862B	Laboratory,[10] GCA	0.05-0.23
Cotton	10	Sateen weave napped	95x58 staple	13	AI No. 960	Laboratory,[10] GCA	<0.001

[a] Yarn count warp (w) yarn/in. x fill (f) yarns/in.

[b] Multifilament warp yarns, bulked fill yarns.

[c] MS - Menardi Southern
WWC - W.W. Criswell
AI - Albany International

of the dust dislogement process indicated that collapse alone led to relatively low release rates compared to the amount detached after reverse flow was initiated (5 to 10 percent). The role of the reverse air flow appears to be that of applying a mechanical thrust to a slab or flake of dust whose bonds to the fabric have already been severed by shearing action. Since the dust layer is vertically aligned in commercial filter systems, it is necessary to assume that local curvature of the fabric surface between anticollapse rings (if used) coupled with a statistical distribution of adhesive forces is sufficient to initiate the dust separation process. Once a preliminary release takes place, a cascading or avalanche effect appears to take place until the maximum removal is obtained for a fixed set of cleaning parameters.

Based upon the dust removal data presented in Tables 24 through 26 and Figure 115, the fraction of the fabric surface cleaned (a_c) and the estimated separating forces, F_s, have been computed for these tests, Tables 41 and 42. As stated previously, it has been assumed that all dust dislodged from the fabric was held by a force less than or equal to the applied separating force. The dust removals noted for the collapse and reverse flow tests actually reflect the results of several collapses for each element of the fabric surface. For example, both the P-3 and P-5 test series indicated that after five or six filtration cycles the dust deposition and dust removal rates came into equilibrium. This finding is consistent with the results of the special tests shown in Figure 91, Section VIII, that indicate no appreciable gain in dust removal after six successive collapses between filtration intervals. It is assumed that a layer of dust that has not separated until the sixth filtration cycle, Table 27, has essentially the same adhesive properties as those for a similar dust layer that has experience six successive collapses.

Figure 116 shows a graph in which the fraction of cleaned area, a_c, is plotted against the dust separating force, F_s, immediately before cleaning. The fraction of cleaned area also represents the fraction of the fabric surface for which the interfacial adhesion, F_a, is equal to or less than

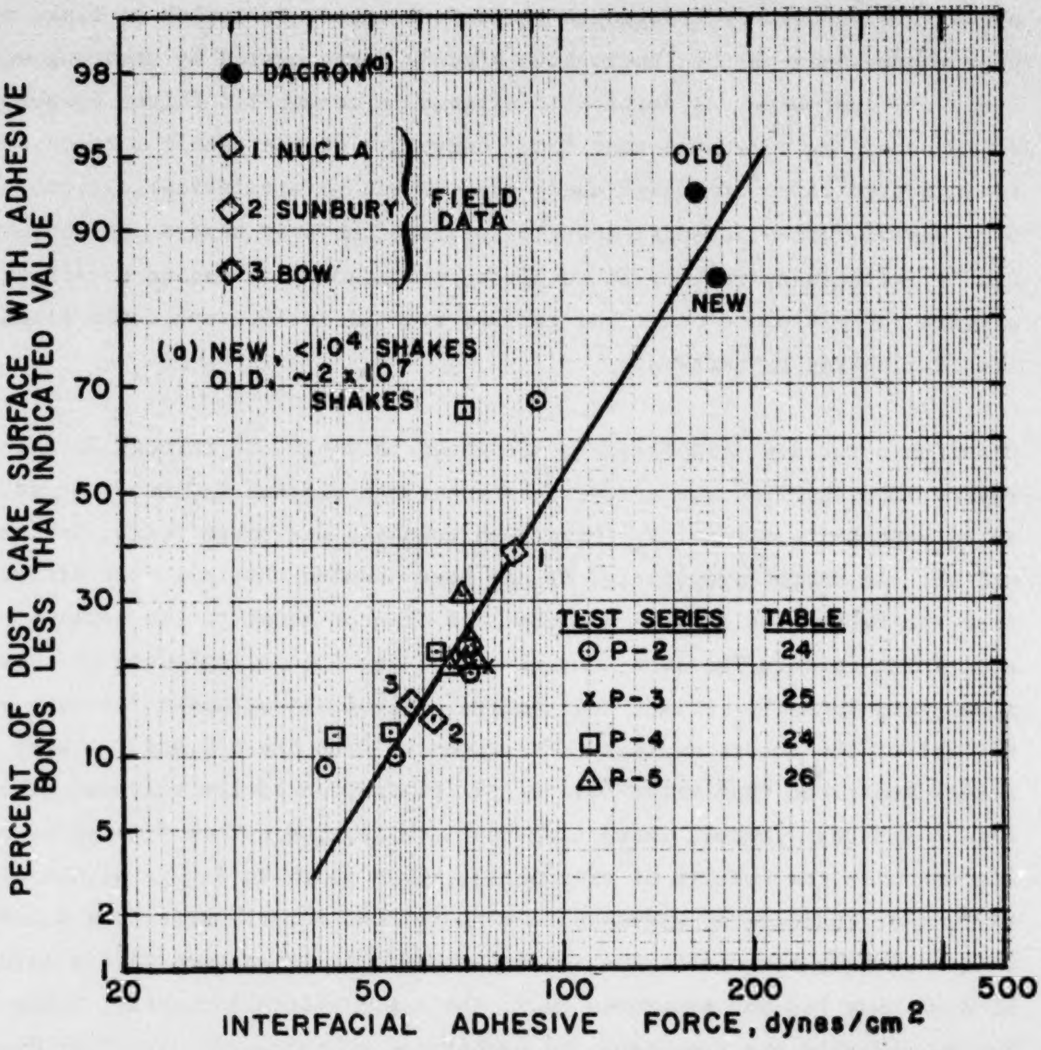

Figure 116. Estimated distribution of adhesive forces for woven glass fabrics and one Dacron fabric with coal fly ash

the applied separating force. Therefore, the abscissa can also be interpreted as the interfacial adhesive force. The results of all current pilot tests, Tables 24 through 26, as well as those for GCA field measurements at coal burning utility boilers located in Sunbury, Pa., Nucla, Colo., and Bow, N.H. are presented.

Two additional data points are given that are based upon laboratory measurements with a fly ash/woven Dacron fabric system.[10] Similarities in weave, fabric density, bulk fiber content and penetration characteristics, Table 43, suggest that the Dacron behavior at the indicated adhesive force level might simulate glass fabric performance. Unfortunately, there was not sufficient time within this program to carry out a rigorous study of dust dislodgment phenomena. Hence, we have used as much peripheral information as possible to support the existing measurements.

Noting that the field tests represent independent observations, it appears that laboratory pilot tests with single bags provide a very reasonable estimate of field performance insofar as dust removal is concerned. It is also concluded that mechanical shaking and collapse systems can be treated in similar fashion just as long as the acceleration imparted to the dust cake can be defined. For example, if one elects to initiate cleaning at the Nucla station after the average fabric loading has risen to 850 g/m^2, the curve shows that 38 percent of the cleaned compartment surface will have been cleaned to its true residual level of 50 g/m^2. The predicted area fraction cleaned for the Sunbury and Bow operations based upon the measured average residual dust loadings, also fall within a few percent of the actual values.

It must be remembered, however, that these correlations apply only to fly ash/glass fabric systems. The magnitude and distribution of estimated interfacial adhesive forces for other fabrics are indicated in Figure 115. Although one can make qualitative predictions as to what adhesive properties might be anticipated for various dust/fabric systems, there do not exist sufficient data or working theory to make any generalized predictions. The problem of predicting adhesive properties, even for single element systems; i.e., particle to particle, particle to fiber or particle to plane is a highly complex one because several factors acting in concert such as particle, fiber and gas properties in the presence of external field forces contribute to adhesion and cohesion.

A fairly extensive review of particle adhesion phenomena as applied to fabric filtration was prepared by Billings and Wilder.[1] In all but a few cases, the major research in this area was restricted to analyses of the adhesive or cohesive forces betweeh a single particle and other objects; i.e., particles, fiber or plane surfaces. The rather discouraging aspect of the many reported measurements is that the use of radically different instrumental approaches coupled with a lack of clarity in defining what fraction of adhering material is removed by a given force and the doubtful nature of the "monodispersity" of some particle distributions makes difficult any quantitative comparisons among the various studies. Many investigators indicate that the range of measured adhesion for uniformly sized particles can be described by a logarithmic-normal distribution[28,34-36] with perhaps a 20 to 100 fold difference in force between the 1 and 99 percentiles. Data excerpted from a study by Boehme[36] are presented in Figure 117. Atmospheric humidity has been shown to exert a significant effect on adhesion with respect to large ~ 100 μm particles.[10,34,35,37] It appears, however, that the observed increase in adhesion over the 50 to 100 percent R.H. range is relatively small for particle diameters less than 15 μm, Figure 118. Examination of Figure 118 also suggests that the physical nature of the particles and/or fiber also have a strong influence on adhesion. As far as natural charging is concerned, the magnitude of the image forces arising from 100 electrons per 10 μm particle appear to be many orders of magnitude less than the noncharge-related adhesive forms.[1] Charged to their maximum potential, the electrical attraction is only roughly the same as that for natural adhesion forces, approximately 0.5 dynes.

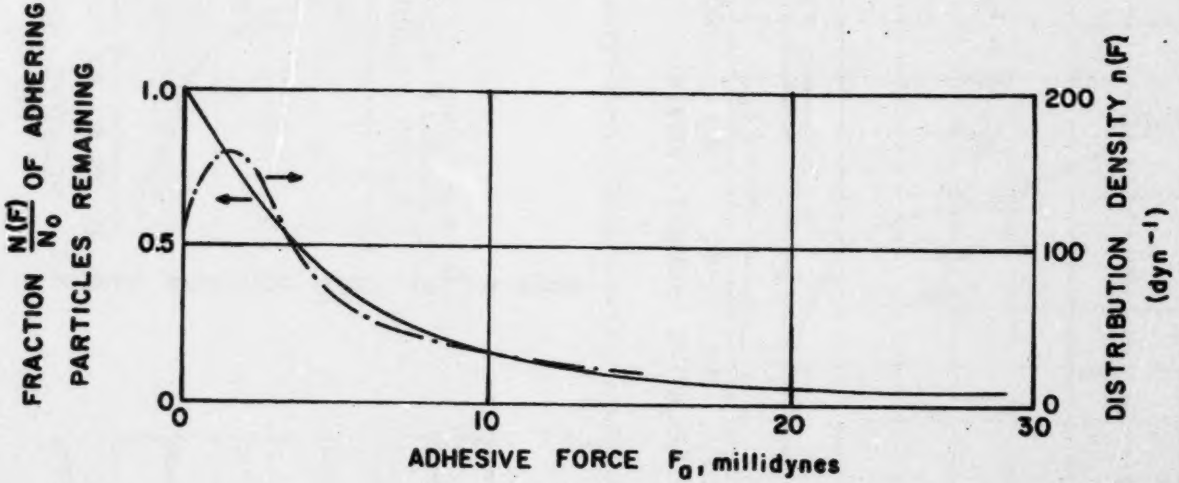

Figure 117. Adhesion of spherical Fe particles of 4 μm diameter to Fe substrate at room temperature in air as a function of applied force (from Bohme, et al., Reference 36) and Reference 1

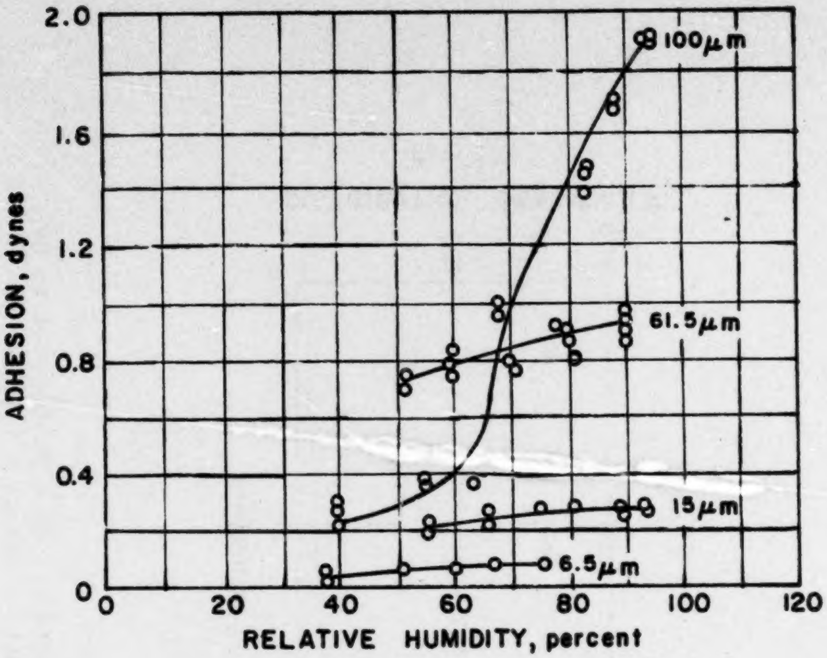

A. From Corn, Reference 37, Pyrex-Pyrex

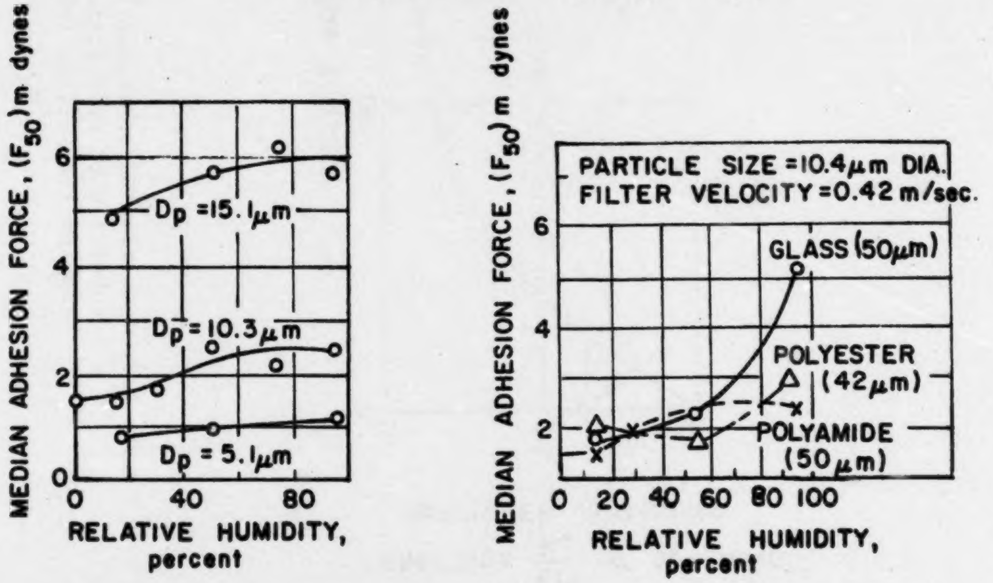

B. From Löffler, Reference 35, granular quartz on 50 μm nylon fiber

C. From Löffler, Reference 36, granular quartz on indicated fibers

Figure 118. Effect of particle size and relative humidity on adhesion for various materials (Reference 1)

Corn[37] and others[28,35] have developed their adhesion theories on the premise that liquid condensation at the interface between particles or particles and other surface geometries produces strong capillary forces that resist separation. Minimum and maximum forces for a particle-to-particle system and a particle-to-plane system, which differ by a factor of two, can be estimated by the following relationship:[1]

$$F_a = 10^2\ dp_1\ dp_2/\left(dp_1 + dp_2\right) \quad \text{(particle to particle)}$$

$$F_a \cong 10^2\ dp \quad \text{(particle to plane)}$$

Given a 10 μm particle without specification as to physical nature of the particle or deposition surface, the estimated adhesive force (with dp expressed in centimeters) is about 0.1 dyne. If a dust cake composed of 10 μm particles were in contact with a flat surface, the number of individual particles in contact with a 1 cm^2 surface would be of the order of 10^6 and the resultant interfacial force would be 10^5 $dynes/cm^2$. Even in the event of much greater porosities, the magnitude of the internal cohesive forces would probably exceed 10^3 $dynes/cm^2$.

On the other hand, the best estimates of cake adhesion to a fabric based upon the present study indicate that 50 to 150 $dynes/cm^2$ is the approximate range of interfacial adhesive forces. The disparity in adhesion between intracake and interfacial structures is attributed to the greatly reduced contact area between dust particles and fibers due to the inherent openness of the fabric. The above analysis appears to support the observations that the cake detaches at the dust/fabric interface.

The preceding review provides at best only a qualitative treatment of the factors that affect adhesion. It does, however, point out that unless particle charging is induced by outside means and unless electrical fields are impressed across the filter media, that electrical phenomena should not play a major role in determining the performance of woven glass fabrics against cool fly ash. Based upon laboratory tests with Dacron fabrics, relative humidites ranging from 16 to 42 percent had no discernible effect on efficiency or resistance to air flow. The good agreement between present field and laboratory studies also suggests that humidity is not an important factor with fly ash/woven glass systems provided that filter operation is maintained well above the dew point. It is also concluded that the only way to estimate cleanability at the present is by direct laboratory (or field) measurement. At this time the cleaning parameters derived from Figure 116 afford the best predicting capability.

Although the relationship between dust removal (and/or the fraction of cleaned fabric area exposed after cleaning) and the initial fabric loading appears to be logically defined by a probability type function, it can also be described conveniently by the log-log plot shown in Figure 119 if the degree of cleaning is constrained to the approximate range, 5 to 60 percent of the fabric surface. Based upon present field and laboratory tests, the above range encompasses most observations of dust removal. Until further data become available to refine the mathematical description of the postulated cleaning process, it appears acceptable to use the simpler relationship indicated below:

$$a_c = 1.51 \times 10^{-8} W^{2.52} \tag{50}$$

in which a_c is the fraction of filter surface from which the dust cake is dislodged and W is the fabric loading just before dust dislodgement.

Application of Equation (50) is restricted to collapse and reverse flow cleaning systems. If fabric cleaning is by mechanical shaking, the following relationship should be used:

$$a_c = 5.24 \times 10^{-6} (F_A)^{2.52}$$

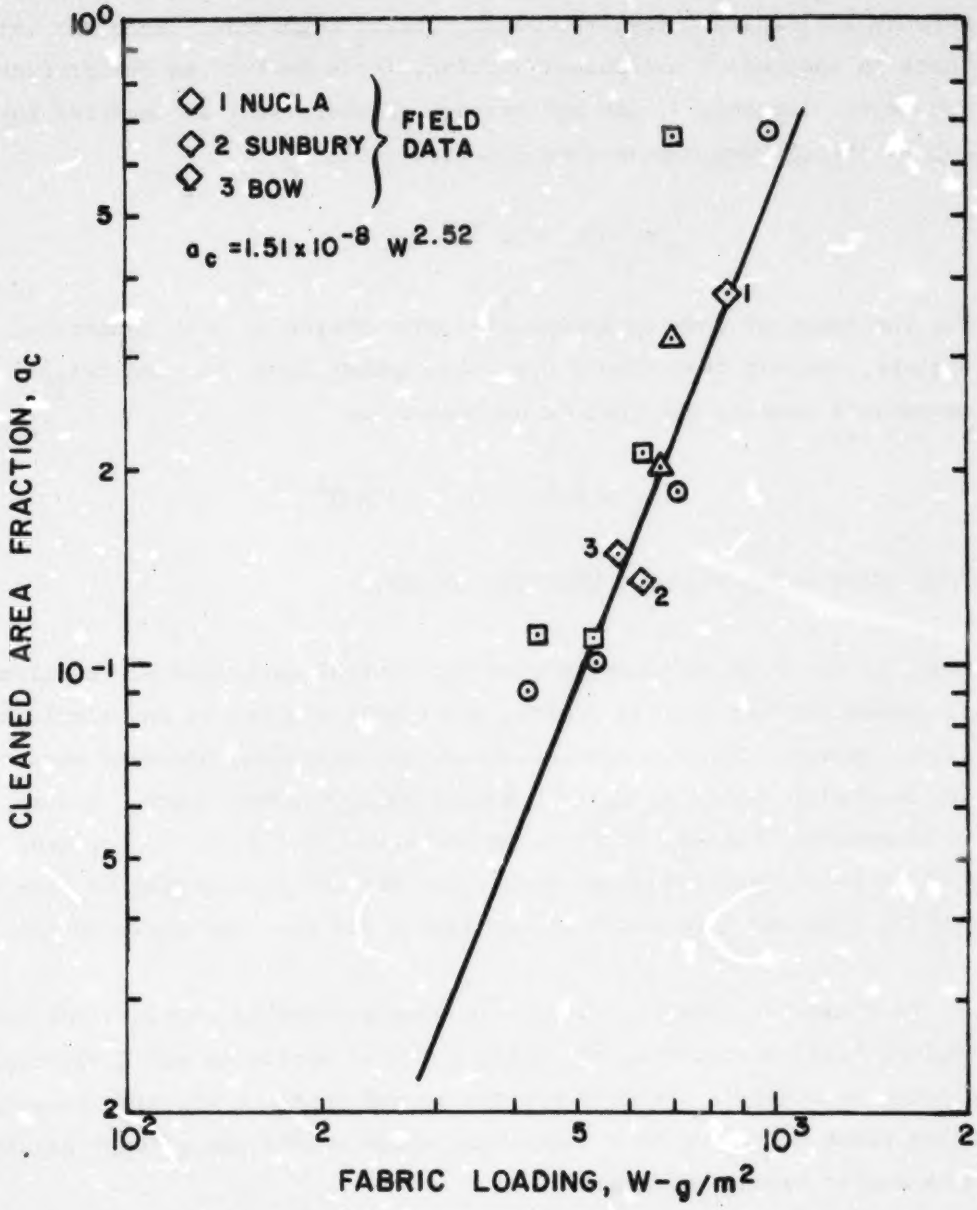

Figure 119. Relationship between cleaned area fraction and initial fabric loading. GCA fly ash and woven glass fabric, see Figure 116.

in which F_A represents the adhesive force (dynes/cm^2) that must be overcome by a cleaning force, F_c, of equivalent magnitude. When the latter force is induced by mechanical shaking, it is defined as the product of the fabric loading, W, and the average acceleration, $\bar{a}$, imparted to the bag by the shaking motion (see Equation (49)):

$$F_A = F_c = W\bar{a} = Wk4\pi^2 f^2 A$$

For the range of shaking frequencies encountered in most commercial applications, usually less than 6 cps, the cleaned area fraction resulting from mechanical shaking can then be expressed as:

$$a_c = 2.23 \times 10^{-2} (f^2AW)^{2.52} \qquad (51)$$

FULL SCALE APPLICATIONS - MODELING CONCEPTS

Equation (50), in conjunction with the several mathematical relationships discussed earlier in this report, are easily applied to any single bag filter system. Special considerations are involved, however, when they are used with multicompartment, sequentially cleaned units. Ordinarily, it is assumed that all filter bags installed in a given compartment function in identical fashion although this may not necessarily be true depending upon bag deployment and proximity and gas flow distribution.

In the following paragraphs, the cleaning process is examined for two typical field situations, the first a filter system in which the cleaning process is pressure actuated and the second approach wherein cleaning takes place according to a fixed-time cycle regardless of dust deposition rate and/or fabric loading.

PRESSURE CONTROLLED CLEANING

The ultimate selection of operating parameters for pressure-controlled cleaning is based upon the following data inputs:

- A maximum allowable resistance across the fabric filter prior to cleaning.
- A fixed inlet dust concentration, C_i, and volume flow rate, Q_i, as determined by fuel burning rate, fuel composition and excess air rate.
- A fixed average filtration velocity, $\overline{V}_i$, that has been selected upon the basis of dust penetration properties for the selected fabric.
- Steady-state operation as defined by equilibrium between dust collection rate and dust removal rate.
- Sequential cleaning of all compartments followed by extended filtration with all compartments on-line until the pressure limit is again reached.

The first step is to determine what fabric dust loading, W_{Pmax}, corresponds to the maximum allowable operating resistance, P_W. Since the filter system will operate for lengthy time intervals, ~2 to 3 hours, between cleaning cycles (roughly 30-minute duration) the dust distribution over the fabric surface will be nearly uniform just before initiation of cleaning. Therefore, the term W_P may be estimated from the characteristic pressure or drag curve for the specific dust/fabric combination for which the terms S_E and K_2 have already been defined; e.g., Figures 43 and 54, Section VII, and Table 32. Assuming that the fabric undergoes a conventional collapse and reverse flow cleaning, the amount of dust dislodged and the fraction of cleaned fabric area exposed, a_c, is readily estimated from Figures 90 and 119 and Equation (50).

The actual dust removal associated with a given a_c level is determined from the relationships:

$$\Delta W = W_P - W_R' \tag{52}$$

and

$$W_R' = (1 - a_c)(W_P - W_R) + W_R \tag{53}$$

Where W_R' is the average residual dust holding after cleaning, W_P, the fabric loading at the limiting pressure, and W_R the characteristic residual loading of the cleaned fabric surface only. The total dust removed, ΣW, following the sequentially cleaning of n compartments expressed in terms of fabric filtration area then becomes:

$$\Sigma W = n\ (W_P - W_R') \qquad (54)$$

Since the amount of dust dislodged during the cleaning process must equal the quantity of dust deposited between successive cleaning and filtration cycles, the combined operating time, Σt, for the overall cycle is estimated from the following relationship:

$$\Sigma t = n\ (W_P - W_R')/C_i V_i \qquad (55)$$

and the time interval over which all filters are on-line is computed as:

$$t_{\text{on-line}} = \Sigma t - n\Delta t \qquad (56)$$

where n is the number of compartments and Δt the cleaning interval for each compartment.

Equations (52) through (56) provide a practical estimate of the necessary cleaning frequency if one is not to exceed the specified operating pressure. An improved estimate may be obtained, however, by noting that at the inception of the cleaning process only the first compartment has a fabric loading of W_P. The remaining compartments will acquire succesive increments of loading as cleaning continues throughout the cycle such that the last or n^{th} compartment to be cleaned will have an increased fabric loading, ΣW; i.e.:

$$\Sigma W = W_P + (n-1)\ C_i V_i'\ \Delta t \qquad (57)$$

During the actual cleaning period, $n\Delta t$, all filtration must take place through the (n-1) on-line compartments. Hence, assuming that overall system volume flow is relatively insensitive to small pressure changes, the average velocity throughout the on-line compartments must increase by the ratio n/n-1; i.e.:

$$V_i' = V_i \ (n/n-1)$$

Equation (57), therefore, is reduced to the form:

$$\Sigma W = W_p + n \ C_i \ V_i \ \Delta t \tag{58}$$

One can infer from the above relationship and Figure 119 that more dust should be removed and, hence, more filtration surface exposed as the cleaning cycle progresses.

To avoid undue complications in the estimating process and yet take into account the gradual increase in fabric loading, the original W_p value based on pressure limitations has been modified as follows:

$$W_p' = W_p + n \ C_i \ V_i \ \Delta t/2 \tag{59}$$

where V_i is again the average face velocity when all filter compartments are operating. It is emphasized that use of the procedure described above assumes that the transient pressure increases associated with the start of the cleaning process will not reduce the gas handling capacity of the boiler fans. When the first compartment is taken off line for cleaning, the system flow must be accommodated by the remaining n-1 compartments leading to an automatic rise in system resistance.

If the upper pressure criterion is based upon the peak transient values, the following approach must be used.

The increment of dust added to the remaining on-line (n-1) compartments while cleaning the first compartment can be expressed as:

$$\Delta W = C_i \; V_i \; (n/n-1) \; \Delta t$$

and the corresponding increase in pressure, ΔP, over that observed just before cleaning appears as:

$$\Delta P = K_2' \; V_i \; (n/n-1) \; \Delta W \qquad (60)$$

Because K_2 has also been shown to be velocity dependent; i.e.: $K_2 = 1.8 \; (V)^{\frac{1}{2}}$ (metric units), Equation (60) must be further modified:

$$\Delta P = 1.8 \; C_i \left[(V_i) \; (n/n-1) \right]^{2.5} \Delta t \qquad (61)$$

When the indicated pressure is now specified as a not-to-be-exceeded value, the pressure used to determine the required fabric loading W_P just before cleaning is defined as:

$$P_W = P_{max} - \Delta P \qquad (62)$$

Once the term P_W is determined, the estimate of cleaning frequency is carried out according to the previously described procedure, Equations (52) through (56).

It should be noted that in the limiting case, a pressure controlled cleaning system with intermittent cleaning cycles will reduce to a continuously cleaned system with back-to-back cleaning cycles when dust removal during the cleaning cycle equals that deposited during the same period. If the deposition rate exceeds the capability of the removal cycle, a new, higher pressure equilibrium automatically evolves. In the case of cleaning by bag collapse and reverse flow, the increase in surface loading provides the added dislodgement force. Where mechanical shaking is employed, it might be possible to avoid a pressure increase altogether by increasing either the amplitude and/or frequency of shaking.

TIME CYCLE CLEANING

Under conditions of constant flow and constant loading, the behavior and analysis of filtration systems cleaned on either a pressure or time control cycle would be the same. During a variable loading process, initiation of cleaning during periods of low inlet loading may lead to undesirably high outlet concentrations due to loss of dust cake. To a certain extent, however, dust removal at lower cloth loadings (and lower operating resistances) is significantly lower with both collapse and mechanically shaking because the dust layer itself contributes to the separating forces. Hence, the impact of overcleaning may not be as severe as anticipated.

In the following section, the cleaning versus resistance parameters are examined with respect to a Sunbury type filtration system in which the cleaning cycles are repeated sequentially. The analysis of the above system is carried out on the premise that C_i, V_i and the collapse and reverse flow process per se are constant terms. Hence, it can again be stated that once steady state conditions are established, the total quantity of dust dislodged over a complete cleaning cycle (each bag cleaned once) must equal the amount of dust deposited over the same time interval. The latter amount, ΔW, is again determined as:

$$\Delta W = n\ C_i\ V_i\ \Delta t = C_i\ V_i\ \Sigma t$$

where n is the number of compartments and Δt the nominal time between successive cleanings. At the start of any filtration cycle, the fabric loading for the compartment about to be cleaned can be expressed by W_P, which, in the present case, is an unknown quantity. The fraction of cleaned fabric area exposed, a_c, can be described as indicated earlier by the relationship:

$$a_c = 1 - \frac{W_P - \Delta W - W_R}{W_P - W_R} \qquad (63)$$

The term a_c is also definable by the relationship:

$$a_c = 1.51 \times 10^{-8} W_P^{2.52} \qquad (51)$$

By combining Equations (63) and (51), a relationship is obtained that allows solving for W_P:

$$W_P^{2.52} (W_P - W_R) = 6.62 \times 10^7 \Delta W \qquad (64)$$

If W_P is significantly greater than W_R, 10 times or greater, Equation (64) can be reduced to the simple form:

$$W_P^{3.52} = 6.62 \times 10^7 \Delta W \qquad (65)$$

Having determined W_P, the magnitude of the cleaning parameter, a_c, can be estimated from Equation (51). Similarly, the equilibrium pressure and drag associated with all "n" compartments in operation are determined from the previously established performance data for the dust/fabric combinatios of interest.

The maximum pressure level displayed during the cleaning cycle will again take place when one compartment is taken off-line for cleaning. Although Equation (61) serves to indicate the increase in resistance, ΔP, it should be noted that the fabric dust loading computed by Equations (64) or (65) applies only to the compartment just taken off-line. The remaining compartments through which all flow is diverted have instantaneous fabric loadings that range from:

$$W_P - C_i\ V_i\ \Sigma t/(n-1)$$

to

$$W_P - C_i\ V_i\ \Sigma t$$

for the next and last compartments to be cleaned in sequence and the time interval, Σt, cited above represents the total elapsed time for the cleaning cycle.

Thus, as a reasonable approximation, the average fabric loading just before cleaning, $\overline{W}_P$, can be expressed as:

$$\overline{W}_P = W_P - C_i\ V_i \frac{\Sigma t}{2}\ (n/n-1) \tag{66a}$$

The resistance corresponding to the $\overline{W}_P$ level then becomes:

$$P_{\overline{W}_P} = P_E + K_2 \left[W_P - C_i\ V_i \frac{\Delta t}{2}\ n/n-1 \right] V_i\ (n/n-1) \tag{66b}$$

The term P_E in Equation (66b), which is defined as the effective resistance, is related to the effective drag, S_E.

If there are many compartments in the system, the maximum or peak resistance, P_{max}, occurring when one compartment is undergoing cleaning may not be much greater than that predicted by Equation (66b).

If there are only a few, approximately five, compartments in the system, it might be safe to design on the basis of the maximum expected pressure, P_{max}, in the system; i.e.:

$$P_{max} = P_E + K_2\ \overline{W}_P\ V_i\ (n/n-1) + \Delta P \tag{66c}$$

Where $\overline{W}_P$ and ΔP are determined by Equations (66a) and (61), respectively.

When several compartments are involved as with the Sunbury system, the difference between maximum and minimum pressures becomes relatively small, approximately 2.5 to 2.75 in. water (550 to 687 N/m^2) without the introduction of reverse air. Reverse air flow with its added volume increment further increases the pressure range; i.e., 550 to 750 N/m^2.

SECTION X

PREDICTION OF FABRIC FILTER PENETRATION

In this section, the development of a new model to predict the particle collection characteristics of woven fabric filters is discussed. The model is intended to describe the behavior of fabrics in which at least the fill yarns are spun from staple fibers or are made up of bulked multifilament yarns. In both cases, many loosened, discrete fibers protrude into the interyarn spaces (or pores) thus forming a convenient substrate for initial dust cake formation. For present purposes, the application of the model is directed mainly to woven glass fabric filters used for the collection of coal fly ash. Thus, the approximate pore structure shown in Figure 99, Section IX, is the one for which particle collection characteristics have been modeled.

As indicated in the literature review, most techniques for estimating filter collection efficiency apply to low porosity, bulk fiber filters or felted media. They are not intended for use with fabric filter systems in which particle capture occurs as the dusty gas passes through a parallel array of pores or channels whose boundaries are defined by the specific weave or interlacing of the warp and fill yarns. Therefore, syntheses of the type attempted for fabric filters by Fraser et al.,[23] the latter based upon a highly modified single fiber/single particle theory, are not successful except for describing closely replicated filter systems.

On the other hand, treatment of collection on the basis of particle capture by obstructed or unobstructed pores (the obstructions consisting of low porosity, bulk fiber plugs or screens) and by a dust cake composed of the collected particles appear to provide a satisfactory means for completely describing the particle collection characteristics of a woven fabric filter.

PARTICLE CAPTURE BY UNOBSTRUCTED PORES

Although it would be highly desirable both from the performance and analytical viewpoints that (1) all filter pore dimensions be identical and (2) that any fiber substrate bridging the pores be uniformly distributed, a real fabric filter may show considerable deviation from the ideal pattern. In the former (ideal) case, the substrate deposition and bridging processes will proceed in parallel. Conversely, the imperfections encountered with real filters will lead to some sequential bridging of pores although the latter process must occur over a brief time span if the filter is to provide satisfactory performance. The more serious deviation or defect is where the loose, interpore fiber substrate fails to bridge all or part of the pore opening. Depending upon the dimensions of the unobstructed opening and the pressure gradient across it, the initial gap must either be bridged during the early stage of filtration before pore velocities become excessive or fail to be bridged and thus constitute a permanent opening or pinhole leak in the filter. Within the context of this report the only distinction made between a pinhole and a pore is that the pinhole or "see-through" opening is either an oversized pore or a pore that contains no fiber substrate or plug.

In some cases, it is suspected that a tenuous bridging of the pore opening by the fiber substrate at the onset of filtration may actually rupture because of the aerodynamic stresses induced by the dust deposit on and within it. The microscopic examination of several pinholes on heavily loaded fabrics, Figure 60, Section VII, shows only the bounding yarn surfaces and no loose fiber structure whatsoever. Microscopic measurements of dust accumulation about these pinholes in conjunction with the estimated air volumes passing through these openings also suggest that a pinhole is a very poor fly ash collector, with actual efficiencies in the 10 percent range or lower.

The above observation led to the conclusion that a rigorous analysis of the dust collection capability of a pore was unjustified insofar as woven glass fabrics and coal fly ash collection are concerned.

The special tests described in Figure 37 indicated that the rate of dust accumulation within the pores of a plain weave, monofilament screen, was very slow. Furthermore, a declining rate of resistance rise coupled with the fact that previously obstructed pores "blew out," confirming the pinhole plug releases described by Leith et al.,[24] suggested that collection efficiency would soon fall to negligible levels, Figure 38.

Despite the fact that the openings were slightly larger than the 170 μm, nominal pore size for the Sunbury fabric, it was very evident from the 5-minute photograph, Figure 37, that very little of the approaching dust load, ~200 g/m^2, had remained on the fabric. At test completion, the screen filter retained only 15 percent of the average input loading. The 5-minute photo relates to a free area of roughly 10 percent whereas the final 30-minute picture shows less than 5 percent free area. Hence the pore velocity, which was roughly twice as large in the latter case, also exerted a greater entraining force on the previously deposited dust.

A different approach for predicting pore capture was based upon the relative efficiencies reported by Fuchs[29] for extraction sampling from stagnant air masses. Figure 120 shows fractional particle size recoveries with a constant sampling velocity of 6 m/sec at several air-stream velocities. Those values that relate to pore penetration appear at zero flow field velocity. They indicate that the sampling probe will capture 95 percent or more of all particles equal to or less than 15 μm. In the present situation, the acceleration of the air velocity from 0.61 m/min at the filter face to roughly 20 m/min at the minimum pore cross section is analogous to withdrawing a sample from stagnant air. According to Fuchs,[29] when the air velocities are low relative to the sampling velocities, the approaching streamlines are either straight or slightly convex with respect to the axis of flow. Therefore, minimal sampling losses should be expected under stagnant flow conditions. The maximum losses should occur in the region where the sampling velocity is roughly twice that of the flow field velocity. Particle losses are minimized when isokinetic sampling conditions are attained.

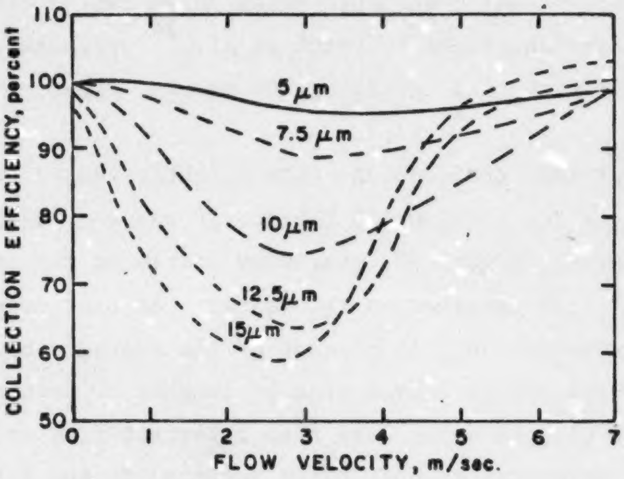

Figure 120. Efficiency of sampling an aerosol from a variable velocity flow field at a constant sampling velocity of 6 m/sec.

Although it is not proposed here that a highly anisokinetic sampling process is an exact replication of a dust laden gas stream converging to pass through a fabric pore, the similarity was considered sufficient to justify treating open pores or pinholes as non- or very-low efficiency collectors.

An extensive series of measurements involving simultaneous gravimetric sampling of inlet and outlet concentrations and condensation nuclei (CNC) measurements for filter effluents are given in Tables 19 and 20, Section VII.

The CNC data have played two roles in the present study. First, despite the fact that CNC data do not represent absolute values, they do provide a relative measure of rapid changes in effluent concentration as filtration progresses.

More importantly, it was observed that the outlet nuclei concentrations related directly to the measured outlet mass concentrations as shown in Figure 86, signifying that all dust particle sizes were collected equally well by the filter. Since this observation contradicts accepted filtration theory, which dictates preferential collection of the larger particle sizes, an explanation was sought for this inconsistency.

First, it was noted that insofar as concurrent upstream and downstream cascade impactor measurements were concerned, field and laboratory tests showed no significant differences between the respective mass distributions. In the case of Nucla measurements, the coarseness of the inlet dust coupled with the fact that significant gravitational and inertial losses were possible between the upstream sampling point and the filter face appears to explain the size reduction in the effluent dust. Although the slough-off of agglomerated particles from the rear filter face can lead to a coarser downstream size distribution than expected, test measurements, Section VII, suggested that agglomerate slough-off can only partially explain the observed downstream size parameters.

However, when the total number of pinhole leaks were actually measured in conjunction with an estimate of the air volume passing through them with an assumed 100 percent penetration, the predicted filter efficiency values were very close to the actual measured values, see Section VII. Volume flow through the pinholes was based upon the observed dimensions as determined microscopically, the measured filter pressure loss and the flow versus resistance parameters developed from special permeability tests, Figure 21, Section V.

The conclusion drawn from the tests cited here was that the downstream effluent for the fly ash/glass fabric systems, was essentially that which had passed untreated through pores or pinholes in the filter.

Because of the very low resistance levels for unbridged pores, a very small fraction of the total filter surface in the form of unbridged pores will cause a relatively large quantity of gas to pass through them. An extreme case noted for a Dacron fabric, Section VII, showed that a fractional pore area of approximately 10^{-4} resulted in 20 percent fly ash penetration.

The fraction of the inlet aerosol that actually passes through the bulked fiber region and the superimposed dust layer is expected to follow the classical filtration rules as discussed in the following paragraphs. From a very practical perspective, however, the contributions from the above sources are usually very small compared to the dust fraction conveyed by the air penetrating the pores. As discussed in a later section, direct pore penetration accounts for nearly all the effluent with fly ash/woven glass filter systems.

PARTICLE CAPTURE BY BULK FIBER SUBSTRATES

The appearance of the pore structure for clean (unused), woven glass fabric has been presented schematically in Figure 28. Microscopic examination of the filter surface during the filtration process shows that the initial dust accumulation is confined almost entirely to the bulked fiber regions with no buildup upon the multifilament yarns until the interfiber depressions are filled. The filter loading process as viewed by microscope is shown in a simplified sketch of the fabric surface, Figure 35, Section V.

Based upon the observed pore structure, it is believed that the initial dust collection process is essentially that of bulk fiber or deep bed filtration. Because the inlet aerosol is highly polydisperse, the preliminary dust deposition will be confined mainly to the upstream region of the substrate such that a distinct and separate dust cake rapidly evolves. The early dust capture process can be described quite well by classical bulk fiber filtration theory provided that reasonable estimates can be made for certain physical and operating parameters.

Dust penetration may be approximated by the relation:

$$Pn = \exp\left[-\frac{4\,\bar{\rho}\,\eta L}{\pi\, d_f\, \rho_f}\right] \qquad (67)$$

where bed porosity is high, ≥ 0.90. The terms $\bar{\rho}$ and ρ_f refer to bulk and discrete fiber densities, respectively; L is the bed thickness, d_f the fiber diameter and η the single particle-single fiber collection efficiency for the particle size and particle capture mechanisms(s) of interest. In the above case the term $(1 - \bar{\rho}/\rho_f)$, or $(1 - \alpha)$, which appears in the denominator of the exponent form discussed by Dennis,[30] has been deleted. Equation (67) may also be expressed in the form:

$$Pn = \exp\left[-A_p\, L\eta\right] \qquad (68)$$

where the product, A_p L, can be considered as the ratio of total projected fiber surface to the filter cross-sectional area.

The key fabric properties, operating parameters and the assumptions made in apply Equation (67) are summarized in Table 44.

The bases for the input parameters listed in Table 44 are as follows: microscopic observations indicated that roughly 10 percent of the total yarns, item 4, were dispersed as discrete fibers. Due to the tightness of the 3 x 1 twill weave, 25 percent of the pores were effectively blocked in both the warp and fill directions. Thus, the fabric porosity, item 5, was reduced from 0.64 to 0.363. It was assumed that the average pore diameter at the midpoint of the substrate region was roughly 2.5 times smaller than the inlet diameter at the surface of the fabric. This leads to a 6.3 times velocity increase, item 6, within the bulked fiber region. If the bulk fiber occupies about 50 percent of the total void volume (0.646), dispersion of 10 percent of the fabric weight results in a bulk density value of 0.241 g/cm^3, item 7, for the substrate. The above development is discussed further in Appendix B.

Table 44. INPUT PARAMETERS FOR ESTIMATING BULK FIBER EFFICIENCY

1.	Average fiber diameter	8.5 μm
2.	Fabric weight	312 g/m^2
3.	Average face velocity	0.61 m/min
4.	Only 10 percent of the total fabric fiber content is dispersed as discrete fibers within the effective pore volume.	
5.	Because of many contiguous yarns, the effective filter void volume (i.e., that through which flow takes place) is reduced from 0.646 to 0.363.	
6.	Average air velocity through the loose fiber occupying the void volume is increased 6.3 times due to channel shape.	
7.	The bulk density of the fiber within the effective pores is 0.241 g/cm^3.	

By substitution of numerical values given in Table 44, Equation (67) is reduced to the functional form:

$$Pn = \exp\left[- 5.84\ \eta \right] \qquad (69)$$

The term η was then examined with respect to particle collection by interception and impaction mechanisms which were considered to predominate as far as mass accumulation was concerned.

The interception efficiency, η_{DI}, was computed in accordance with procedures described by Dennis:[30]

$$\eta_{DI} = k' R_D^2,\ R_D = d_p/d_f \text{ and } k' = (2 - \ln Re_f) \qquad (70)$$

where d_p and d_f refer to particle and fiber diameters, respectively, and Re_f is the fiber Reynolds number.

The impaction efficiencies, η_I, were computed in accordance with conventional procedures;[30] i.e.:

$$\phi\ (\eta_I) = \frac{C_c\ \rho_p\ d_p^{\ 2}\ v}{18\ \mu_f\ d_f}, \tag{71}$$

and the classical target efficiency curves given in the literature.[7,29] In Equation (71), C_c is the Cunningham slip factor, ρ_p the particle density, v the air velocity and μ_f the fluid viscosity.

The calculated efficiency parameter, η, for capture by either interception or impaction and the predicted initial filter efficiencies resulting from impaction alone are listed for several particle sizes in Table 45.

Table 45. COLLECTION PARAMETERS AND INITIAL EFFICIENCY FOR WOVEN FABRIC FILTERS FOR FIBER PHASE COLLECTION

d_p µm	η_I	η_{DI}	Fractional[a] penetration	Fractional[a] efficiency
1	~0.02	0.003	0.86	0.14
2	0.10	0.01	0.56	0.44
3	0.30	0.023	0.17	0.83
4	0.45	0.041	0.072	0.93
5	0.60	0.064	0.030	0.97
10	0.80	0.26	0.004	0.996

[a] Conservative estimates based on η_I alone, the larger of the collection parameters. Note that effective η should be greater than η_I.

An estimate of the diffusion parameter, η_D', for a 0.5 µm particle by the approximate relation, $\eta_D' = (Pe)^{-1} = D_B/Vd_f$,[30] indicated a value of 0.005. Since η_D continues to decrease with decreasing diffusion coefficient (and increasing particle size), it appears that diffusion collection plays a very minor role in the capture of those particles accounting for most of the projected surface area, > 80 percent.

According to the predicted penetration levels in Table 45, the initial filter efficiency is low for particles less than 2 μm and greater than 93 percent for all particles greater than 4 μm. In a relatively short time period, however, sufficient dust will accumulate within the loose fiber structure to significantly increase its collection capability.

In the following paragraphs, an approximate method is developed for predicting the increase in efficiency during the first few minutes of filtration based upon the filtration parameters summarized in Table 46.

Table 46. FILTRATION PARAMETERS FOR COMBINED FIBER-PARTICLE COLLECTION

1. Size properties for inlet fly ash aerosol, MMD @ $\rho_p = 2\ g/cm^3$ = 6.36 μm, $\sigma g = 3.28$.
2. Projected particle surface per gram of dust = $2.366 \times 10^3\ cm^2/g$.
3. Inlet dust concentration = $3.5\ g/m^3$.
4. Dust arrival rate at reduced pore cross section = $13.42\ g/m^2/min = 1.342 \times 10^{-3}\ g/cm^2/min$.
5. Increase in collector surface area per cm^2 of filter cross section for 1 minute is $\frac{3.175\ cm^2\ \text{dust area}}{cm^2\ \text{filter cross section}} = \Delta A_d$

If one assumes that the increment of collector surface contributed by the dust, ΔA_d, is as effective as an equal quantity of fiber surface, A_p, Equation (68) can be expressed in the form:

$$Pn = \exp\left[-\left(A_p + \Delta A_d\right)\eta\right] \tag{72}$$

This allows us to calculate the theoretical penetration levels as the dust loading builds within and upon the fiber substrate as shown in Table 47. Since these data refer only to the collection of 2 μm particles, it is necessary to integrate across the particle size distribution with respect to impaction efficiency to determine the overall weight efficiency for the fly ash aerosol. The simple incremental solution to this problem is summarized in Table 48 for the previously cited GCA fly ash.

Table 47. PENETRATION ESTIMATES FOR A 2 μm PARTICLE AS A FUNCTION OF FABRIC LOADING AND INLET CONCENTRATION AT 0.61 m/min FACE VELOCITY, FIBER FILTRATION PHASE

Time	Average[a] fabric loading, g/m^2	$(A_p + \Delta A_d)\eta$ dimensionless	Fractional	
			Penetration	Efficiency
Inlet loading = 3.5 g/m^3				
0	0.0	(5.84 + 0) 0.1	0.56	0.44
1	2.14	(5.84 + 3.17) 0.1	0.41	0.59
2	4.28	(5.84 + 6.34) 0.1	0.29	0.71
3	6.42	(5.84 + 9.51) 0.1	0.22	0.78
Inlet loading = 7.0 g/m^3				
0	0.0	(5.84 + 0) 0.1	0.56	0.44
1	4.28	(5.84 + 6.34) 0.1	0.29	0.71
2	8.56	(5.84 + 12.68) 0.1	0.16	0.84
3	12.84	(5.84 + 19.02) 0.1	0.083	0.917

[a] Refers to dust loading distributed over complete filter face with 100 percent retention.

The primary reason for exploring the preceding collection concept is to demonstrate that the proper use of classical theory in conjunction with some simplifying assumptions provides estimates of early filtration behavior which are in good agreement with the actual experimental measurements. For example, the initial fractional penetration values given in Table 20, Section VII, are generally in the 0.1 range (0.9 fractional efficiency).

It should be realized that once the fabric undergoes its first cleaning, there will be a permanent residual loading of roughly 50 g/m^2 of which some 25 percent will reside within the active pore regions. The other 75 percent will be retained in the continuous fill yarns that form blind pores. If the added particle surface is factored into Equation (72), the

Table 48. PARAMETERS FOR, AND ESTIMATION OF, OVERALL WEIGHT COLLECTION FOR FLY ASH DURING FIBER PHASE FILTRATION

Size range µm	$\bar{d}$ µm	Percent[a] mass in range	Time[b]					
			Zero		1 minute		3 minutes	
			Fractional[c] efficiency	Fraction[d] collected	Fractional efficiency	Fraction collected	Fractional efficiency	Fraction collected
0.5 - 1.5	1.0	9.7	0.14	0.0136	0.20	0.0194	0.32	0.031
1.5 - 2.5	2.0	10.7	0.44	0.0471	0.59	0.0631	0.785	0.084
2.5 - 3.5	3.0	9.0	0.83	0.0747	0.933	0.0840	0.990	0.089
3.5 - 4.5	4.0	6.0	0.93	0.0557	0.983	0.0590	0.999	0.67
4.5 - 5.5	5.0	6.0	0.97	0.0582	0.995	0.0597	↓	
5.5 → ∞		55.0	0.98	0.5417	0.999	0.55		
Total fly ash collection				0.791		0.835		0.874

[a] Indicates mass distribution for inlet fly ash aerosol.

[b] Time from initiation of filtration with unused fabric.

[c] Efficiency for specified size based on total projected collector surface.

[d] Fraction of inlet aerosol collected.

pentration values for time zero and 1, 2, and 3 minutes, respectively, would decrease from the initially clean values, Table 47, as follows: 0.56 to 0.088, 0.41 to 0.063, 0.29 to 0.046 and 0.22 to 0.034. Again these predicted values appear to be in line with the measured results shown in Table 20. Additionally, it should be expected that the entrapment of residual dust within the fiber matrix should improve particle collection.

PARTICLE CAPTURE BY DUST CAKE (GRANULAR BED)

Fabric filters, which depend upon the deposited dust layer to provide the collection capability, would always operate at 100 percent efficiency with monodisperse aerosols if there were no defects in the supporting substrate and particle contacts with adjacent particles were at a maximum for the solid geometric array.[6]

Furthermore, the nominal pore openings in a bed of uniformly sized particles would automatically sieve out any particles greater than about 0.15 times the diameter of the base particle size. Pursuing this analysis to its logical end indicates that even a polydisperse aerosol will eventually generate a dust layer that for all practical purposes is impenetrable. The only problem is to establish at what point particulate emissions are no longer detectable.

Unfortunately, most real filter systems fail to demonstrate the postulated "zero" penetration conditions because the supporting fabric either does not permit the development of a uniformly structured bed or the gaps in the supporting fabric may allow low level entrainment of agglomerates from the clean air face of the filter. These problem areas will be discussed in detail in a later section. At this point, it is appropriate to examine the theoretical particle collection efficiency during the early stages of cake formation to determine how rapidly particle penetration levels will decrease.

In the simple modeling process discussed here, it is assumed that the supporting substrate enables the development of a dust layer of uniform density and thickness. The selected penetration expression:

$$Pn = \exp \left[\frac{3 \alpha L \eta}{2d_c (1 - \alpha)} \right] \qquad (73)$$

is one that has been discussed extensively in the literature.[10,29,30] The term α is the ratio of bed packing density to particle density,[30] d_c is the granule (collector) diameter and η again is the single particle-single granule collection efficiency for the system of interest. It follows from the definition of α, that the term $1 - \alpha$ is the bed porosity, ε.

Unfortunately, Equation (73) applies directly only to a highly specialized system involving a single collector (granule) size and monodisperse aerosol. In order to justify its use, for example, with a dust cake produced by filtering a polydisperse aerosol, certain modifications were necessary. As a starting point, the situation has been examined wherein the "polydisperse" bed is analyzed with respect to its capability to capture specific particle sizes. Therefore, Equation (73) has been converted to the form:

$$Pn = \exp \left[- \frac{3 L}{2 (1-\alpha)} \left(\sum \frac{\alpha_i \eta_i}{d_{c_i}} \right) \right] \qquad (74)$$

where $1 - \alpha$ refers to the overall cake porosity (which is assumed to be 0.5 based upon present experiments) and α_i, η_i and d_{c_i} are the characteristic porosity, collection efficiency and collector diameter, respectively, for the i^{th} intervals of the size distribution describing the inlet GCA fly ash aerosol.

The mechanisms of particle collection by diffusion, interception and impaction were then examined in accordance with procedures described for granular beds.[30]

$$\text{Diffusion parameter} = \eta_D' = 5\,(k'')^{-1/3}\,Pe^{-2/3} \qquad (75)$$

where Pe is the Peclet number ($d_c\ V/D_B$) and D_B the diffusion coefficient.

$$\text{Interception parameter} = \eta_{DI} = 3\,R_D^2\,(k'')^{-1} \qquad (76)$$

The term k" is defined by the equation:

$$k'' = (2 - 3\,\alpha^{1/3} + 3\,\alpha^{5/3} - 2\,\alpha^2)/(1 - \alpha^{5/3}) \qquad (77)$$

and $R_D = d_p/d_c$

$$\text{Impaction parameter} = \eta_I = \frac{C_c\ \rho_p\ d_p^2\ v}{9\ \mu_f\ d_c} \qquad (78)$$

where all terms are described as indicated for Equation (71). In Table 49, a summary of collection parameters is given for the particle diameters constituting the polydisperse dust layer (granular bed) and two inlet particle diameters, 0.25 μm and 1.0 μm.

Inspection of Table 49 shows that the interception parameter predominates for the indicated particle sizes. Although the combined effect of these mechanisms when functioning in concert will exceed the largest indicated value; i.e., η_{DI}, it will also always be less than the algebraic sum of the components. For present purposes, a conservative approach was selected wherein the η_{DI} values alone were used to describe the collection parameter.

The values for the term, $\alpha_i\ \eta_i/d_{c_i}$, were computed for the individual volume fractions of the fly ash distribution and for two inlet particle sizes as shown in Table 50. The sum of the terms, $\Sigma\ \alpha_i\ \eta_i/d_{c_i}$, provides a partial data input for use in Equation (74). By assuming various bed thicknesses, L, and a porosity, ε, of 0.5, the overall penetration values for 0.25 and 1.0 μm particles were computed, Table 51.

Table 49. ESTIMATED VALUES FOR DIFFUSION, INTERCEPTION AND IMPACTION PARAMTERS, GRANULAR BED COLLECTION[a]

Collector diameter, d_c μm	Particle diameter					
	d_p = 0.25 μm			d_p = 1.0 μm		
	Diffusion η_D'	Interception η_{DI}	Impaction η_I	Diffusion η_D'	Interception η_{DI}	Impaction η_I
0.25	0.35	2.27	0.08	0.32	36.4	0.5
1.0	0.17	0.25	0.02	0.12	4.0	0.2
2.0	0.10	0.058	0.01	0.069	0.94	0.1
5.0	0.069	0.018	0.005	0.037	0.29	0.05
10.0	0.035	0.002	0.003	0.022	0.038	0.02

[a] Refer to Equations (75), (76) and (78).

Table 50. PARAMETERS USED TO COMPUTE DUST CAKE PARTICLE COLLECTION EFFICIENCY

Particle size range µm	Mean diameter for range d_{c_i} µm	Volume of i^{th} fraction	α_i	k"	Particle diameter = 0.25 µm			Particle diameter = 1.0 µm		
					R_D	η_{DI}	$\alpha_i\ \eta_i/d_{c_i}$ x 10^{-4}	R_D	η_{DI}	$\alpha_i\ \eta_i/d_{c_i}$ x 10^{-4}
5 - 0.5	0.25	0.023	0.0115	1.32	1.0	2.27	0.1044	4.0	36.4	1.67
0.5 - 1.5	1.0	0.157	0.0785	0.75	0.25	0.25	0.0196	1.0	4.0	0.315
1.5 - 2.5	2.0	0.140	0.0700	0.80	0.125	0.058	0.0020	0.5	0.938	0.033
2.5 - 7.5	5.0	0.380	0.1900	0.42	0.05	0.0178	0.0006	0.2	0.286	0.011
7.5 - 12.5	10.0	0.140	0.0700	0.80	0.025	0.002	0.00001	0.1	0.0375	0.0003
> 12.5		0.160	0.0800					0.05		
Totals		1.000	0.5000				0.1266			2.028

Table 51. ESTIMATED OVERALL WEIGHT COLLECTION EFFICIENCIES AS A FUNCTION OF CAKE THICKNESS AND INLET PARTICLE SIZE FOR FLY ASH

Bed thickness μm	Areal[a] density g/m^2	Estimated fraction penetration	
		Particle diameter, μm	
		0.25	1.0
10	10	2.2×10^{-2}	10^{-27}
20	20	5.0×10^{-4}	$<10^{-27}$
30	30	1.1×10^{-5}	$<10^{-27}$
100	100	10^{-17}	$<10^{-27}$

[a] Estimated values for added dust increment with an assumed bulk density of 1 g/cm^3

The preceding analysis of dust cake efficiency suggests that one should anticipate minimal dust penetration through the cake provided that there are no pinholes or other surface discontinuities.

No attempt was made to estimate the retention properties for particles greater than 1.0 μm for the obvious reason that capture by interception must automatically increase. Measured values for penetration based upon determinations with a condensation nuclei counter indicated that penetrations for nuclei in the 0.0025 to approximately 0.5 μm range were generally less than 10^{-2} after fabric loading reached 10 to 20 g/m^2. In the above case, however, the nuclei penetration resulted mainly from direct air leakage through unbridged pores.

In the evaluation of both size and concentration properties in the following section, one is forced to conclude that as far as fly ash/woven glass systems are concerned, there is no point to include bed capture in the overall penetration model. As stated earlier, direct pore penetration, which does not alter particle size properties appreciably, may readily exceed penetration from all other sources by a factor of at least 100.

FLY ASH PENETRATION FOR WOVEN GLASS FABRICS

Based upon the preceding analyses, it appears that most dust emissions from woven glass fabrics of the type commonly used for hot fly ash filtration are the result of direct penetration through pores or pinholes. It has been pointed out previously that a freshly cleaned filter surface contains several open pores which, for the most part, become bridged over during the first part of the filtering cycle. Those pores or pinholes that fail to close at any time during the filter cycle are usually larger, ~150 μm in diameter, than the average pore size or contain no fiber obstructions. As far as fly ash/woven glass systems are concerned, the pinholes are the major dust penetration source.

The above statements have been substantiated by the many field and laboratory measurements discussed in Section VII. Additionally, the fact that measurements of particle size distributions immediately upstream and downstream of the filters showed no statistically significant differences suggests that the filter collects all particles at essentially the same efficiency.

Penetration Versus Pore Properties

If one considers a fabric filter that operates at a constant face velocity and inlet dust loading, the fractional mass penetration will be directly proportional to the fraction of the airstream that passes through the pinholes. Therefore, the changes in effluent concentration as the average fabric loading increases shown in Section VII, Figures 75 and 76, indicate that pore area must decrease rapidly once filtration is initiated. Based upon effluent measurements for face velocities of 0.61 m/min or lower, the outlet concentrations appears to level out at about 0.3 to 0.5 mg/m^3.

Unfortunately, with regard to those filters showing the lowest effluent concentrations, the detection capability of the CNC system did not permit estimation of true minimum values. Depending upon the calibration characteristics of the condensation nuclei counter, the minimum detectable effluent concentrations ranged from an apparent 0.3 to 0.5 mg/m^3, whereas the actual levels may have been considerably lower. Thus, the assumption made in designing the penetration model that effluent concentrations never go below 0.5 mg/m^3 represents a safe or conservative approach in so far as predicting system emissions.

Since particulate emissions are attributed almost entirely to pore or pinhole penetration, the actual quantity of dust passing the filter must depend directly on the volume of gas passing through the openings. In turn, the volume of gas passing through the open pores is determined by the pore cross sectional area and the pore velocity. Because the velocity through any pore or pinhole must increase as the pressure gradient increases across the filter, the fraction of the approaching air passing through the pores will also increase unless the pore dimensions are reduced greatly by effective bridging as filtration progresses. Therefore, the very rapid decrease in dust penetration observed during the early stages of filtration must denote a rapid closure of pore openings.

The major problem at this time is to determine precisely what fabric parameters control its capability to provide an essentially unbroken substrate for support of the dust cake. It is evident, based upon both theoretical analyses and experimental observations, that high efficiency filtration of typical inlet concentrations, ~1 to 5 g/m^3, could always be attained where there was no problem of pore closure. As this study progressed, it became apparent that a rigorous study of the basic fabric variables determining the ultimate performance of the dust/fabric structure could not be undertaken without detracting from the specific objective of developing a predictive model for coal fly ash filtration. Hence, the working parameters proposed for the model described in this report are based mainly upon practical field and laboratory measurements relating to coal-fired boiler operations.

It has been indicated that certain semiquantitative measurements may provide key guidelines as to filter performance, clean cloth permeability being a prime example. However, the caution has been extended that the presence or absence of bulk fibers within a pore while having little influence on clean (unused) cloth permeability may affect dramatically its dust retention capability.

If one compares the woven glass fabrics commonly used for hot gas filtration with sateen weave cotton, for example, the Frasier permeabilities are roughly 60 and 15, respectively (i.e., initial cotton resistance is four times that for woven glass). Here the permeability does provides a reliable index of dust collection potential since, as shown in Table 18, fly ash effluents from sateen weave cotton were appreciably lower, ~10 times. Comparative emission measurements with atmospheric dust as the test aerosol, using an optical counter and a condensation nuclei counter, Section VII, have also indicated that sateen weave cotton is a more efficient fine particle and nuclei collector. The point that must be stressed is that only the presence of fine, well dispersed fibers, with separation distances of the order of the fiber diameters can provide firm supporting substrates for cake development.

It is also emphasized that in conjunction with the reduction of pore size to enhance pore bridging, it is also important that the number of pores per unit area be maximized so that the free area is kept as high as practicable and, conversely, the resistance as low as possible. In the case of the Sunbury and Nucla twill weave fabrics, the continuous yarns were responsible for a reduction in the number of active pores, Section V. However, it is also possible that a looser weave structure (which at first appears as a possible way to reduce resistance by providing additional flow would simultaneously lead to a lack of uniformity in pore dimensions. The latter situation has been demonstrated in this and prior studies[3] to be a primary cause of pinhole leakage.

In the modeling relationships proposed in this section for particle penetration, the constants appearing in the working equation apply specifically to coal fly ash/glass fabric systems. If different fabrics are substituted or the properties of the dusts differ significantly from the types used in this study; i.e., coal and lignite fly ashes, and granite dust, a change in constants should be expected. However, it is again emphasized that the ease with which bench scale measurements can be performed suggests that direct measurement, rather than uncertain extrapolation of unproven theoretical concepts, is the best approach for estimating many basic modeling parameters. Methods of performing these measurements have been described in Section IV.

Penetration and Inlet Concentration

It has been reported previously[10,31] that effluent concentrations from fabric filters are not strongly dependent upon the influent concentration, particularly so in the case of fabrics such as sateen weave cotton that provide a good support for the overlying dust cake. The above situation prevails because once the dust cake develops (and in the absence of pinhole leaks) the amount of dust penetrating the undisturbed cake is negligible for cake thicknesses greater than 10 to 20 μm. Therefore, only in the case of very frequent cleaning wherein a larger fraction of the gas stream passes through the yet unblocked pores would one expect to see the effect of inlet concentration changes.

Woven glass fabrics, however, and other similar weaves, often posses sufficient pinhole leaks to cause a constant low order dust emission. In those cases where the problem is serious; e.g., penetrations at the 1 percent level or greater, the magnitude of the pinhole leakage will vary directly with the inlet concentration because the volume of unfiltered air passing through the pinholes far exceeds that passing through the dust cake.

Low order emissions may arise from two sources, direct pinhole penetration or the previously discussed rear-face slough-off. Limited gravimetric tests during the present program with a full scale (10 ft. x 4 in.) woven glass (Sunbury type) bag indicated that slough-off contributed about 0.5 mg/m^3 to the total effluent concentration. This (0.5 mg/m^3) value also corresponds to the lowest mass concentration that can be estimated from CNC measurements. For this reason, use of 0.5 mg/m^3 as a constant background emission rate to be added to that resulting from pinhole penetration appears to be an acceptable procedure.

Penetration Versus Face Velocity

The measurement of dust penetration and effluent concentration at various face velocities, Section VII, Figures 87 and 88, indicated that velocity plays a very important role in filtration. The discouraging aspects of these tests as far as the fly ash/glass fabric combinations are concerned is that a serious penalty in the form of increased emission levels (roughly eight times greater) must be accepted if one elects to increase the air-to-cloth ratio by a factor of 2.5 (0.61 to 1.52 m/min or 2 to 5 ft/min).

The fact that emission rates increase at the higher velocities is consistent with the characteristic pore and pinhole structures noted for the glass fabrics. Despite the fact that the deposition velocity for the dust is greater, which should accelerate the pore bridging process, the higher velocity also causes a greater entraining force to act upon particles deposited in any partially bridged region. The end result is that more pores remain unbridged at the higher face velocities.

The most important aspect of the above findings, however, is that any sequentially cleaned, multicompartment filter is automatically subjected to a rather broad spectrum of velocities at various points in the system at any instant depending upon the surface loading distribution. Hence, in computing local dust penetration levels, one must take into account both the local fabric loadings and velocities. For example, previously discussed tests showing the resistance versus loading characteristics for filters from which approximately 50 percent of the dust had been removed, Table 18, Section VII, showed significant increases in penetration. The corresponding changes in penetration are summarized in Table 52. Reference to tests 71 and 96 shows that penetration is about 16 times greater for a 150 percent velocity increase with uniformly loaded glass fabrics. Partially loaded fabrics, tests 72A-C and 97, indicate a nine times increase in penetration for a similar, 150 percent, velocity increase. Most important, when a filter operating at an average velocity of 1.52 m/min was partially cleaned, its emission levels were 11 times greater than those for the uniformly loaded fabric when filtration was resumed.

The data in Table 52 indicate that overcleaning of fabrics as well as high velocities can lead to undesirably high emission rates. Therefore, it is very important to determine precisely what contribution is made by each element of a filter system under parallel flow conditions in which the filtration velocities over the complete system can easily vary by a factor of 10 at the initiation of filtration.

Figure 121 shows the velocity versus fabric loading relationship for the partially cleaned woven glass fiber described in test 72, Table 52. The maximum velocity is seen to be nearly twice the average velocity and the initial velocities through the cleaned and uncleaned fractions of the surface differ by a factor of 10. If the terminal loadings remain the same and 10 percent, rather than 50 percent of the filter surface is cleaned, a fivefold increase over the average velocity would be expected at the resumption of filtration.

Table 52. COMPARATIVE PENETRATION CHARACTERISTICS FOR UNIFORMLY LOADED AND PARTIALLY LOADED FABRICS, GCA FLY ASH

Test[a]	Fabric	Average face velocity, m/min	Dust loading range, g/m^2	Dust distribution	Cleaning	Fractional penetration mass basis
71	Used Sunbury	0.61	32-660	Uniform	Complete	0.0007
72-A-C	Used Sunbury	0.61	340-750	Nonuniform	Partial	0.0135
96	New Sunbury	1.52	0-400	Uniform	Complete	0.0109
97	Used Sunbury	1.52	270-390	Nonuniform	Partial	0.1223

[a] Data excerpted from Table 18, Section VII.

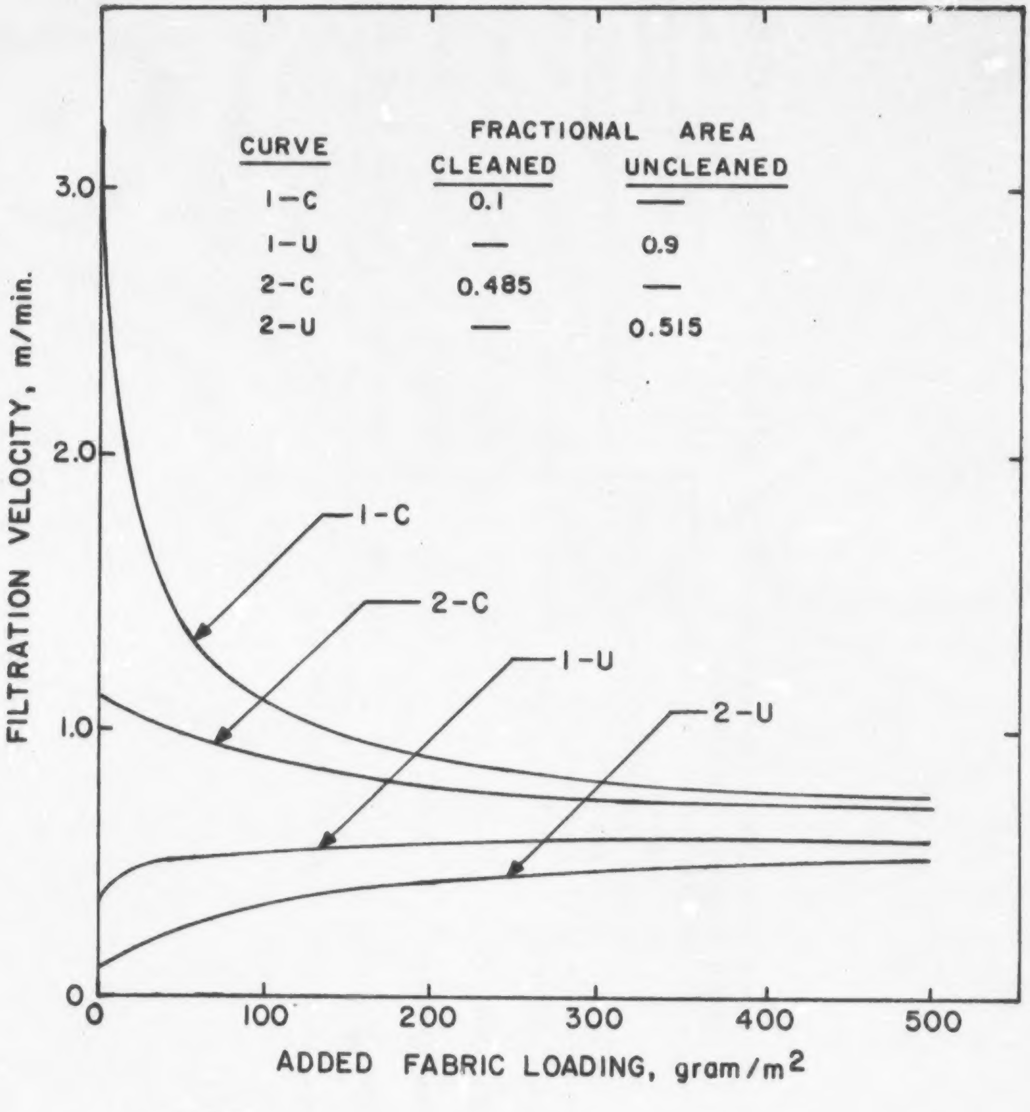

Figure 121. Filtration velocity through cleaned and uncleaned areas of filter. GCA fly ash and Sunbury fabric

DUST PENETRATION MODEL

Based upon the available field data and the results of the laboratory testing program, it was decided that the model for predicting coal fly ash penetration through woven glass fabrics should take into account the following variables:

• The unique functional relationship between a specific dust and a specific fabric	ϕ
• Inlet dust concentration	C_i
• Fabric loading	W
• Filtration velocity	V
• Residual outlet concentration	C_R
• Outlet dust concentration	C_o

Thus, in notational form the fractional penetration can be expressed as:

$$Pn = \psi \left[\phi, C_i, V, C_R, C_o \right]$$

The term, ϕ, should appear as a constant that characterizes the unique interrelationship between coal fly ash and the Sunbury or Nucla type glass fabrics. The inlet concentration, C_i, will appear as an independent variable and remain unchanged for a specific set of operating parameters. As indicated previously, C_R, depicts a low-order, relatively constant emission that is assumed (a) to derive mainly from rear face slough-off, (b) to be independent of inlet loading, and (c) to be unique to the fly ash/glass fabric system.

The velocity term, V, refers not to average velocity but to the actual local face velocity at a specific fabric loading as determined by the model describing the fabric drag versus fabric loading relationship. The term, C_o, is the computed filter effluent concentration associated with the parameters cited above; i.e.:

$$C_o = \theta \left[\phi, C_i, W, V, C_R \right]$$

Working equations for the estimation of outlet concentration and filter penetration in terms of the previously cited variables are developed in the following paragraphs. The mathematical relationships indicated in Figures 87 and 88 and Table 21 provide the data base. The curves show the effects of both inlet concentration and filtration velocity on outlet concentration as dust accumulates upon the fabric surface. Because the overall efficiencies attain the 98 percent or greater level within a very brief time, the increases in fabric loading per unit time are equivalent to the quantity of dust approaching the fabric.

Since outlet concentrations showed a dependency on inlet concentration and since the inlet concentrations varied from test to test, the curves were normalized prior to the data analysis. This was done by graphing actual penetrations versus fabric loadings for each of the tests. Plotting an effective penetration (outlet concentration divided by inlet concentration) would have dampened the effect of the residual outlet concentration on total outlet concentration. Thus, the penetration values used in the analysis were the effective penetration minus the residual penetration (residual outlet concentration divided by inlet concentration).

The procedure used in developing an expression for actual penetration as a function of fabric loading and velocity was based upon conventional curve fitting methods. An empirical relationship was sought which would accomplish the following:

- Predict penetration as a function of fabric loading at constant face velocity
- Predict a penetration level $\leq$ 100 percent for zero fabric loading
- Attain a limiting, steady state penetration once filtration is dominated by cake filtration.

The general form selected for the mathematical function was:

$$Pn = Pn_s + (Pn_o - Pn_s) \exp(-aW) \qquad (79)$$

where Pn = penetration

Pn_s = penetration at steady state

Pn_o = initial penetration at $W = W_R$

W = increase in fabric loading above the residual value, W_R

a = concentration decay function

Equation (79) reflects both the rapid exponential decay observed for outlet loadings as well as their ultimate leveling off at a fixed emission rate as filtration progresses.

The constants Pn_s, Pn_o and a were evaluated for the 0.39, 0.61 and 1.52 m/min velocity tests along with the steady state value for the 3.35 m/min test. The initial fractional penetration values, which were obtained by extrapolation, ranged from approximately 0.09 to 0.11. A Pn_o value of 0.1 was used irrespective of velocity. After the steady state values and the initial slopes were plotted versus face velocity, the constants were computed and the working equations developed:

$$Pn_s = 1.5 \times 10^{-7} \exp \left\{ 12.7 \left[1 - \exp(-1.03V) \right] \right\} \qquad (80)$$

$$a = \frac{3.6 \times 10^{-3}}{V^4} + 0.094 \qquad (81)$$

where V is the local face velocity, m/min. The development of these equations is presented in Appendix C.

Equations (79) through (81) provide the means for predicting penetration as a function of face velocity and fabric loading. The outlet concentration, C_o is found by multiplying the inlet concentration, C_i, by the actual penetration followed by the addition of the residual outlet concentration, C_R:

$$C_o = Pn\ C_i + C_R \qquad (82)$$

The solid curves shown in Figure 122 represent the computed values for effluent concentrations whereas the symbols depict the actual data points. Despite the obvious curve fitting problem for the low velocity (0.39 m/min) test in the 20 to 80 g/m^2 fabric loading range, it is emphasized that the fit is excellent in the very critical range where the outlet concentration decreases by at least two orders of magnitude.

The effect of inlet concentration upon effluent concentrations is shown in Figure 123. Note that the filter effluents tend to follow linearly the changes in inlet concentration during the early phases of filtration, approximately up to a fabric loading of 40 g/m^2. During this period the dominant emissions are those from direct penetration through unbridged pores. However, once significant bridging has taken place, direct pore penetration may play a minor role with respect to periodic slough-off of agglomerated particles from the rear (clean) filter face. Therefore, despite tenfold differences in inlet loadings, the ultimate emissions after cake stabilization may show relatively small, factor of 2, differences.

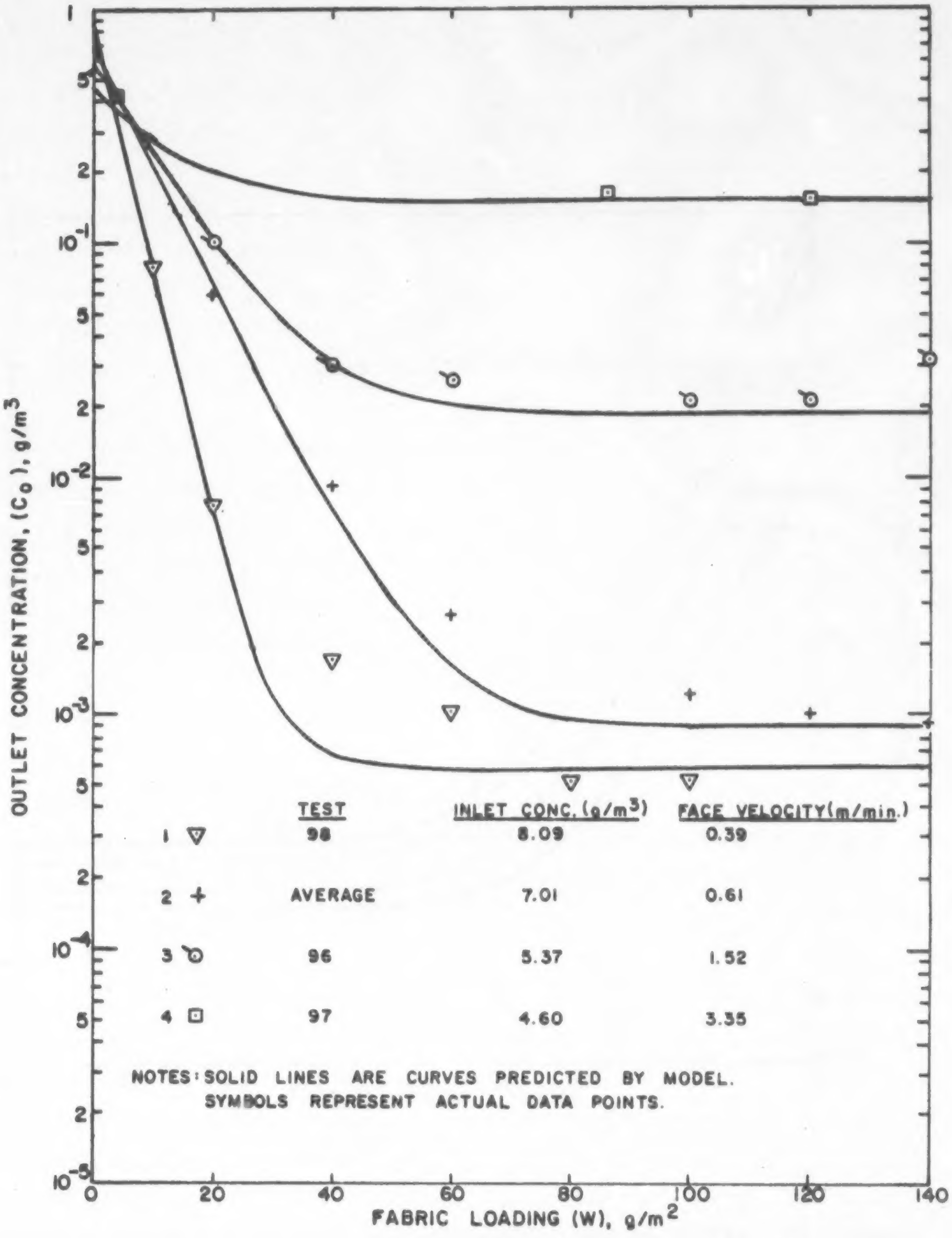

Figure 122. Predicted and observed outlet concentrations for bench scale tests. GCA fly ash and Sunbury fabric

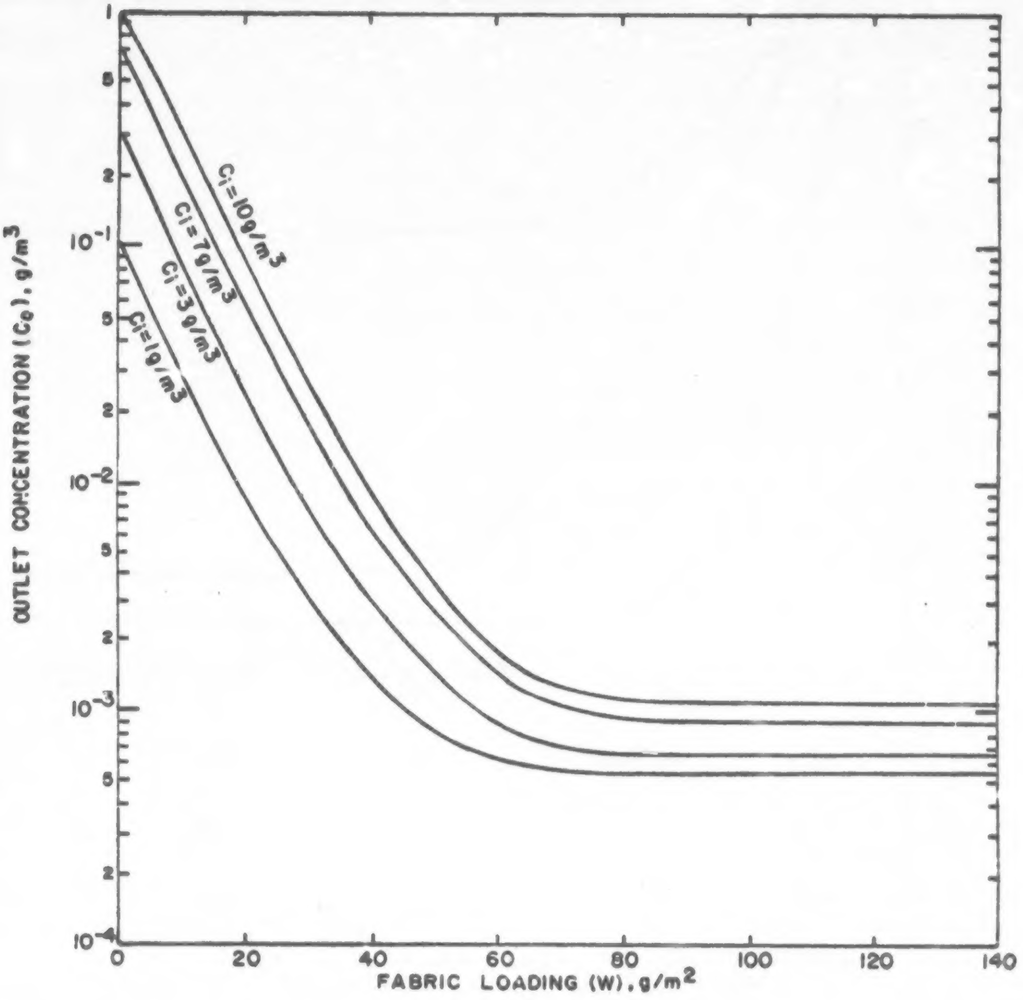

Figure 123. Effect of inlet concentration on predicted outlet concentrations at a face velocity of 0.61 m/min. GCA fly ash and Sunbury fabric

SECTION XI

MATHEMATICAL MODEL FOR A FABRIC FILTER SYSTEM

INTRODUCTION

The preceding sections of this report provide the technical background for the design of the mathematical model describing the filtration of coal fly ash. In general, it can be said that the literature furnished only qualitative guidelines and certainly no practical techniques for analyzing or predicting the behavior of large, multicompartmented baghouses. The sparsity of technical information from both field and laboratory sources required that a broad based series of laboratory studies be carried out to provide a rational basis for model development. As the present study progressed, complexities in experimental measurements coupled with unexpected performance data, made it clear that the research should be constrained mainly to the problem of filtering coal fly ash from utility boiler effluents, if a realistic predictive model were to be developed within the time frame for this study. By adhering to this resolve it was possible to identify and define the proper roles of the major variables entering in to the fly ash filtration process.

It is again pointed out that the predictive model is intended for use with a coal fly ash/woven glass fabric system in which the collecting media consists of twill weaves similar to those now commonly employed by large utilities installations. The performance characteristics of these glass fabrics (and related weaves of nonmineral composition) reveal that the particulate effluents consist mainly of dust that passes through unblocked pores or pinholes with minimal size fractionation and collection taking place during the ensuing process. Although such penetration occurs mainly during the early filtration phase, it may continue throughout the filtration cycle if the fabric pore structure is not uniform or the fabric has been damaged or worn by extended field service. The net result is that the modeling process for dust penetration is greatly simplified because the overwhelming dust penetration by direct leakage precludes any reduction in size parameters for the filter effluent. Thus, despite contrary reports in the literature, the fractional particle size efficiencies for all dimensions of interest are approximately the same and equal to that for the overall mass collection efficiency.

If radical changes in pore structure or staple fiber content are introduced, it is expected that the relationships proposed for fly ash/woven glass fabric systems would require modification. For example, limited tests with cotton sateen fabric (which have not been elaborated upon in this report) suggest that both effluent size properties and effluent concentrations were appreciably lower than those observed with glass fabrics.

PRINCIPAL MODELING RELATIONSHIPS

A brief summary of those mathematical relationships forming the basis for the predictive model is given in the following paragraphs. The key equations used to calculate filter drag and dust penetration behavior, each identified by its original number, are listed below along with the reasons for their selection.

Two mathematical functions were developed for describing the nonlinear drag versus fabric loading curves frequently encountered in industrial filtration processes. Despite a relatively close adherence to postulated filter behavior, the first approach, Equation (25), required the evaluation of several constants and the mathematical structure was overly cumbersome. On the other hand, the second approach, Equation (28), proved to be a good curve fitting tool despite its purely empirical structure. Therefore, Equation (28) as shown below is selected to describe all nonlinear drag/fabric loading curves when it is believed that the nonlinear segments play an important role in determining resistance and/or dust penetration characteristics:

$$S = S_R + K_2 W' + (K_R - K_2) W^*\left(1-\exp(-W'/W^*)\right) \qquad (28)$$

In those instances where the drag/loading relationship is essentially linear, or the nonlinear segment of the curve can be safely ignored, the simpler expression, Equation (4), is chosen:

$$S = S_E + K_2 W \qquad (4)$$

Because there exist no dependable means to predict the numerical value for the constants appearing in Equations (28) and (4), it is strongly recommended that the terms S_R, S_E, K_R, K_2, and W* be determined by experiment. Simple and inexpensive laboratory methods to achieve this end are described in this report (see Section IV). The term W* is readily computed from the relation:

$$W^* = (S_E - S_R + K_2 W_R)/(K_R - K_2) \qquad (29)$$

Although the most accurate estimates of K_2 values should derive from test measurements with the dust in question, allowance must also be made for the impact of increasing face velocity on K_2. An empirical function, Equation (20a), applying specifically to coal fly ash/woven glass fabric systems, satisfies this requirement:

$$K_2 = 1.8\, V^{1/2} \text{ metric units} \qquad (20a)$$

If a rough estimate of K_2 is required before confirming tests can be performed, the Carman-Kozeny equations (Equations (31) and (36)) can be modified as follows: (1) reduction of the constant k from 5.0 to 2.5 and (2) computing the specific surface parameter, S_o, for the distribution of particle sizes constituting the dust cake:

$$K_2 = 2.5\mu\ S_o^2(1-\varepsilon)/\rho_p\varepsilon^3 \qquad (31)$$

The above modification in conjunction with Equation (20a) provides key data inputs whose values constantly change during the iteration procedure used to determine local and average values for velocity, V, drag, S, and fabric loading, W, throughout the fabric filter system being modeled.

The degree of cleaning attained by collapse and reverse flow is determined by the empirical relationship developed for coal fly ash/woven glass fabric systems:

$$a_c = 1.51 \times 10^{-8}\ W^{2.52} \qquad (50)$$

In the case of mechanical shaking, a modified form of Equation (51) applies which takes into account shaking frequency f (cps), shaking amplitude A (cm) as well as fabric loading W (g/m^2):

$$a_c = 2.23 \times 10^{-2}\ (f^2\ AW)^{2.52} \qquad (51)$$

Penetration values and particle effluent concentrations that reflect the impact of dust inlet loading, face velocity, fabric areal density and the unique characteristics of the coal fly ash/woven glass fabric system are determined by the following equations:

$$Pn = Pn_s + \left(Pn_o - Pn_s\right) \exp(-\ aw) \qquad (79)$$

where $Pn_s = 1.5 \times 10^{-7} \exp\left\{12.7\left[1-\exp(-1.03V)\right]\right\}$ (80)

and $a = \dfrac{3.6 \times 10^{-3}}{V^4} + 0.094$ (81)

$$C_o = Pn\ C_i + C_R \qquad (82)$$

It is again emphasized that coal fly ash undergoes no significant reduction in size properties following filtration with woven glass media of the types used at the Sunbury and Nucla power stations. Hence, the fractional particle size efficiency values are constant, independent of size and, for all practical purposes, equal to the overall weight collection efficiency. This anomalous behavior is the result of gross, unfiltered air passage through unblocked pores or pinholes that far exceeds dust penetration through the dust cake, per se.

The key to the modeling process for predicting the performance of multicompartment systems is the concept that treats a cleaned fabric filter as two separate elements, one from which no dust has been removed and the other from which the dust layer has spalled off at the dust/fabric interface. The latter surface has a uniformly distributed drag characteristic which, for practical purposes, is essentially independent of previous surface loading, intensity of cleaning and the dust/fabric combination.

System drag values are computed by iterative methods using the several data inputs noted previously:

$$S = \left(\sum_{i=1}^{n} A_i / S_i \right)^{-1} A \qquad (47)$$

or

$$S = \left(\sum_{i=1}^{n} \frac{a_c}{S_c} + \frac{a_{u_1}}{S_{u_1}} \cdots \frac{a_{u_i}}{S_{u_i}} \right)^{-1}$$

where a_c refers to the fraction of cleaned surface, $a_{u_{1,2,i}}$ to the various uncleaned fractions, and $S_{u_{1,2,i}}$ indicates the associated drag values.

DESIGNED MODEL CAPABILITY

In the previous paragraphs the basic filtration equations and the iterative approach for treating multicompartment filtration systems have been reviewed for immediate reference. The following discussion is intended to outline the ground rules with respect to how closely the predictive model(s) describes the overall fly ash filtration processes for utility applications. The only major constraint for the model(s) is that (1) the inlet aerosol should consist of or possess the general physical properties of a coal fly ash and (2) the fabric characteristics be similar to the woven glass media of the types used at the Sunbury and Nucla installations. Aside from the above, the model is sufficiently flexible to meet the following criteria:

- The model is adaptable to either constant flow or constant pressure conditions. With respect to most large, multicompartmented systems, however, the available gas handling capacity must necessarily be controlled so that excursions from mean flow rates are minimal.
- The model can accommodate to a continuous cleaning regimen; i.e., the immediate repetition of the cleaning cycle following the sequential cleaning of successive individual compartments, or
- The model can also describe the situation where lengthy filtration intervals are encountered between the cleaning cycles. In both cases the term cleaning cycle refers to the uninterrupted cleaning of all compartments in the system. No provision is made for the random cleaning of less than all compartments followed by continuous on-line filtration of all compartments.

The system cleaning characteristics are determined by the fraction of fabric area cleaned, a_c, when individual compartments are taken off-line. With respect to bag collapse systems and/or low energy shaking, the dust removal parameter, a_c, is calculated from the fabric loading, W_T, before cleaning.

- The model can be used with collapse and reverse flow systems, mechanical shaking systems or combinations of the above. It is not intended for use with pulse jet or high velocity reverse jet cleaning systems.
- The model can be used equally well with pressure or time controlled cleaning cycles.
- The model provides estimates of average and point values of filter drag or resistance for the selected set of operating parameters and dust/fabric specifications.
- The model provides estimates of average and point values for penetration and mass effluent concentration for the selected set of operating parameters and dust/fabric specifications.

In the above instances, it is assumed that the following operating parameters are known: inlet concentration (C_i), average face velocity (V_i), cleaning parameters (frequency and intensity, energy level, of cleaning cycles) and the fabric loading before cleaning (W_T). In addition, the related parameters, S_R, S_E, K_R, K_2, and W* must also be specified for the given dust/fabric combination.

The model alternatively provides an estimate of the necessary frequency of cleaning when the maximum operating resistance P_{max} is cited as an operating specification along with the expected values of C_i and the selected value for V_i.

BASIC MODELING PROCESS

The basic model treats each of the "I" compartments of the filter system as a separate element. It is also assumed that the inlet dust concentrations and the filtration velocities are the same for each bag within a given compartment. However, the possibilities of both concentration and velocity gradients are recognized due to the particle size spectrum, bag proximity and air inlet location.

Figure 124 indicates the distribution of volume flow rates for a filter system consisting of "I" separate compartments. Because of the parallel arrangement, the resistance P across each compartment is the same just as the voltage drop would be for the analogous electrical circuit. The volume flow rate, q, and gas velocity, v, through each compartment vary inversely with the individual compartment drag.

The distinguishing feature between the new modeling concept introduced in this study and previously reported efforts is that the surface of each bag within a given compartment is subdivided into a number of secondary areas each of which displays its own characteristic fabric loading (W), drag (S), face velocity (V) and dust penetration (Pn). The fact that the contributive role of each of these areas with respect to overall system drag and penetration can be assessed at any time during the cleaning and/or filtering cycles is a unique feature of the new model. Note again that since all bags within a given compartment possess identical performance characteristics, an "I" compartment system could be described equally well as an "I" bag system.

The experimental models presented in Equations (40) through (46), Section IX, for a two-"element" or two-"surface" system have been expanded to define the performance of typical field, multisurface systems. In the former instance, the partial cleaning of a single bag led to an average residual fabric loading, $\overline{W}_R$, represented by two distinct surface loadings; the first or cleaned area, a_c, with its characteristics cleaned residual loading, W_R, and the second or uncleaned area, a_u, whose areal density, W_T, was the same as that before initiation of cleaning. By successive iterations, the temporal and spatial relationships for face velocity, fabric loading and drag for each surface were developed over varying periods. With extended filtering times, the areal densities for the distinct surfaces converged due to the self-equalizing feature of the filtering process.

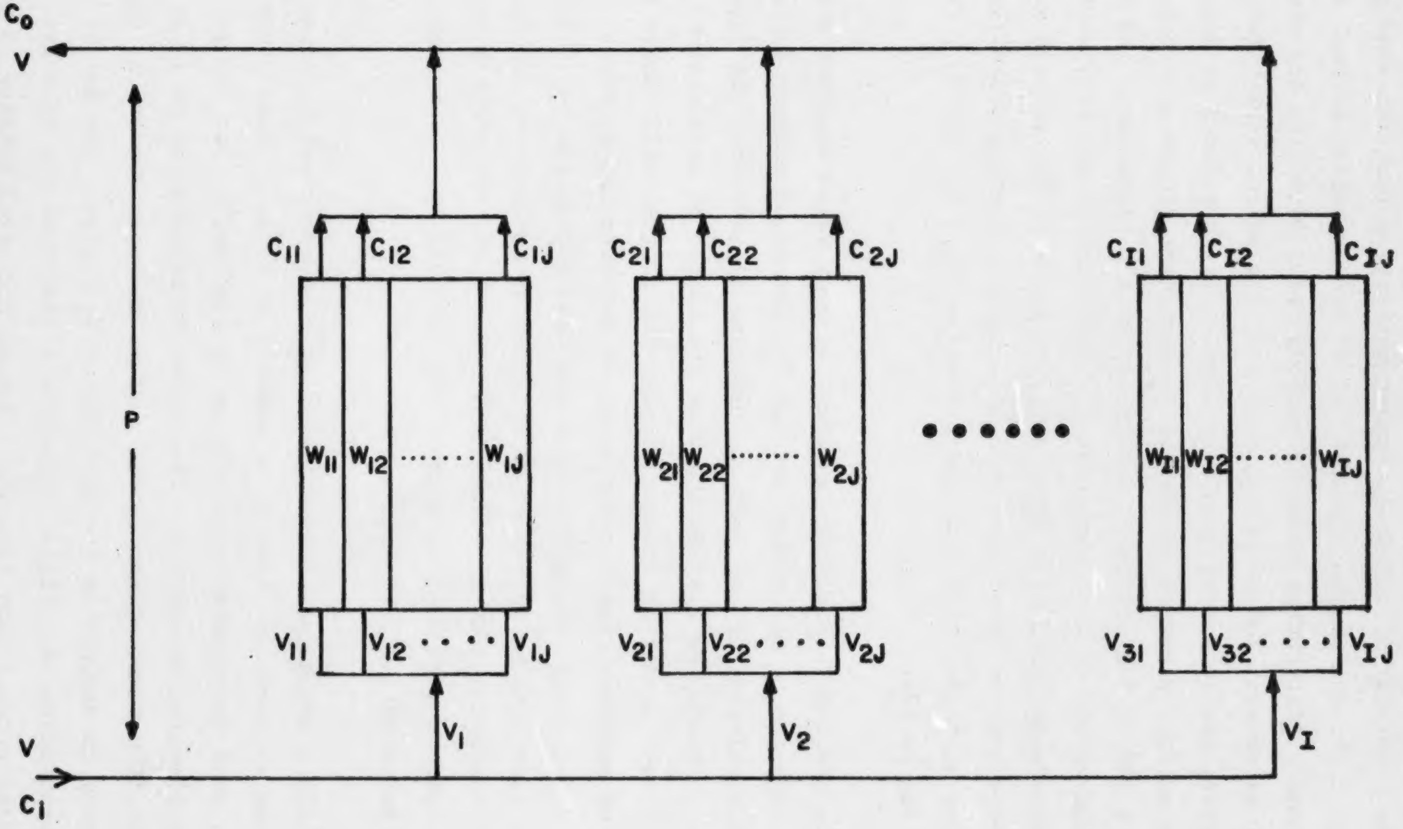
C_o
V
P
C_{11}
C_{12}
C_{1J}
C_{21}
C_{22}
C_{2J}
C_{I1}
C_{I2}
C_{IJ}
W_{11} W_{12} …… W_{1J}
W_{21} W_{22} …… W_{2J}
W_{I1} W_{I2} …… W_{IJ}
V_{11}
V_{12} · · · ·
V_{1J}
V_{21}
V_{22} · · · ·
V_{2J}
V_{31}
V_{32} · · · ·
V_{IJ}
V_1
V_2
V_I
V
C_I

Figure 124. System breakdown for I bags and J areas per bag

Although the treatment of multicompartment systems follows the same procedure as that for the single bag unit, it is now necessary to deal with several randomly distributed areas of varying areal densities for each bag as well as several compartments, each with its unique variability pattern. Thus, the following notational system is introduced to describe the various surface elements in the multicompartment system in which the subscripts i and j, respectively, designate the i^{th} compartment and the j^{th} area subdivision in each compartment. This enables one to identify the specific element of fabric area; e.g., compartment 2, 1st area subdivision for which the local face velocity, surface loading and effluent concentration at a specified time are defined as V_{21}, W_{21} and C_{21}, respectively, Figure 124.

Although the program is designed to accept as many as 10 separate areas (J=10) per bag, the actual number used in the iteration process (which is automatically selected by the computer program) depends upon the input value for a_c. Given the restriction that the number of subdivisions or areas must always appear as integer values, the program will always select the number of subareas that comes closest to matching the a_c input. Thus, a value of 3 for J will satisfy exactly the requirement that $a_c = 0.333$ whereas the same J value will also be selected as the nearest approximation to the condition that $a_c = 0.35$. If a_c is 0.38, the program will select and operate with 8 areas wherein the cleaning of 3 areas provides a cleaning parameter, a_c, of 0.375.

In Figure 125, a schematic representation of a hypothetical 3 compartment filter system is shown in which a_c is assumed to be 0.5. Under these conditions, each compartment need only to be subdivided into two areas to satisfy the cleaning parameters. The proper interpretation of a_c in this case is that 50 percent of the fabric surface in each compartment undergoing cleaning is reduced to its residual or W_R status. The height of the bar representing each filter compartment indicates the relative fabric loading prior to any cleaning. Hence, the areal density is uniform

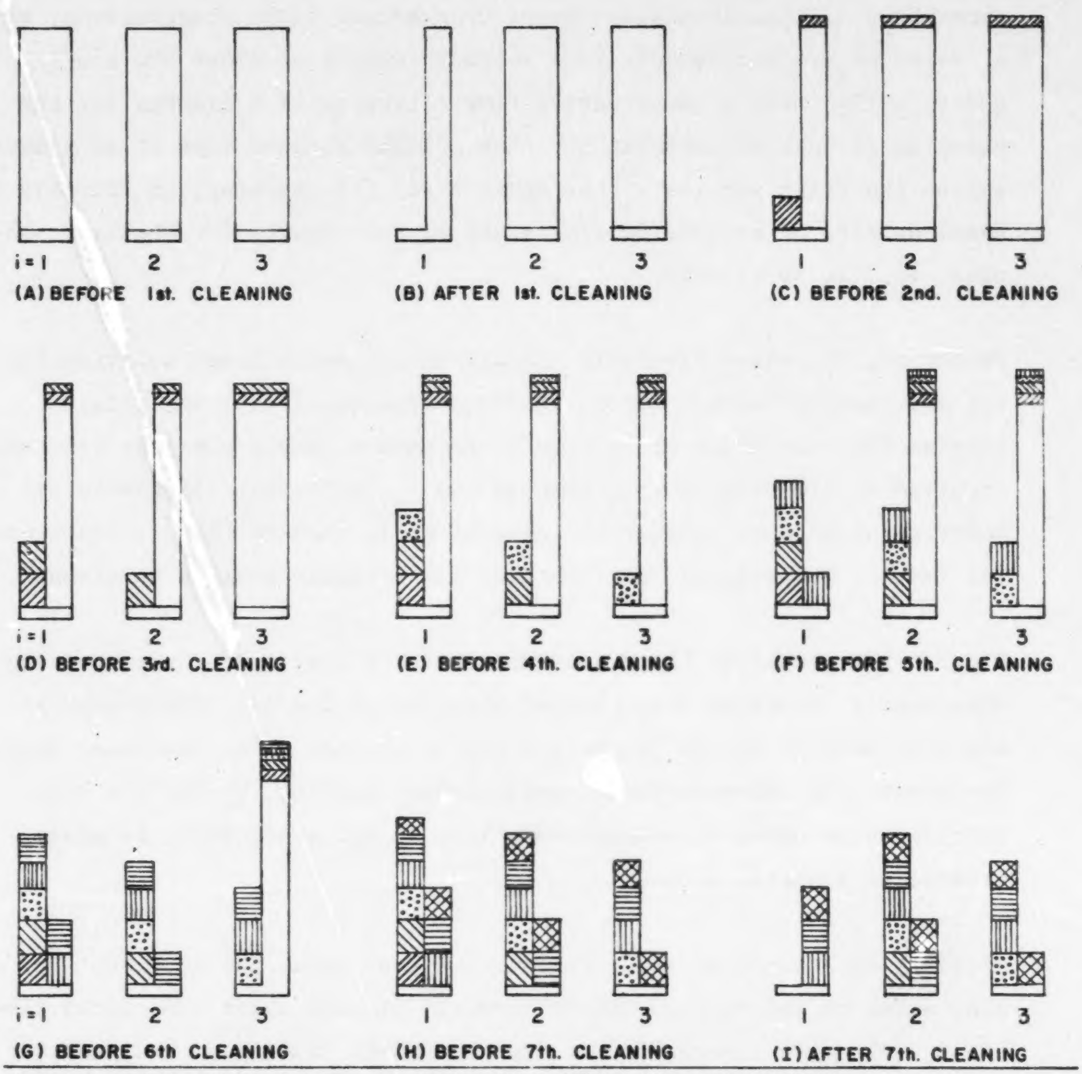
i=1
2
3
(A) BEFORE 1st. CLEANING
1
2
3
(B) AFTER 1st. CLEANING
1
2
3
(C) BEFORE 2nd. CLEANING
i=1
2
3
(D) BEFORE 3rd. CLEANING
1
2
3
(E) BEFORE 4th. CLEANING
1
2
3
(F) BEFORE 5th. CLEANING
i=1
2
3
(G) BEFORE 6th CLEANING
1
2
3
(H) BEFORE 7th. CLEANING
1
2
3
(I) AFTER 7th. CLEANING

NOTES 1. BAR HEIGHT A ROUGH MEASURE OF FABRIC LOADING AND/OR DUST CAKE THICKNESS
2. BEFORE AND AFTER 7th. CLEANING REPRESENTS STEADY STATE OPERATING RANGE
3. THREE COMPARTMENT SYSTEM (I=3) WITH a_c=0.50 (J=2)
4. MINIMAL RESIDUAL LOADING FOR ALL FILTERS REPRESENTED BY NARROW BAND AT BASE OF HISTOGRAM

DUST ADDED	AFTER	DUST ADDED	AFTER
▨	1st. CLEANING	▥	4th. CLEANING
▧	2nd. CLEANING	▤	5th. CLEANING
▒	3rd. CLEANING	▦	6th. CLEANING

Figure 125. Schematic representation of approach to steady state cleaning and fabric loading conditions for a three-compartment system with 50 percent of each compartment surface cleaned

throughout all compartments. Based upon actual field observations, an input a_c value of 0.5 corresponds to a surface loading of about 900 g/m^2. Additionally, with a conservative time allowance of 5 minutes for the cleaning of each compartment and thus a total elapsed time of 30 minutes before the first subarea a_{11} is again ready for cleaning, an increase in areal density of roughly 50 g/m^2 might be anticipated for the last subarea, a_{32}, to be cleaned.

Therefore, to follow precisely the previously established relationship for dust removal versus fabric loading, (Equations (51) and (51a), Section IX), the value of a_c should increase slightly over the time span involved in cleaning the a_{11} through the a_{32} subareas. In the actual modeling procedure, an average value of a_c is assumed that is based upon the initial loadings of the first and final compartment to be cleaned.

Figure 125B simulates the distribution of a filter system dust holding immediately following the collapse cleaning of the 1st compartment in which 50 percent of the fabric surface is cleaned. The resultant height represents the characteristic residual dust holding, W_R for the dust/fabric system under investigation which, in the short term, is always treated as a system constant.

Although no attempt at exact scaling has been made, the increments of dust added to the on-line filter compartments and their associated subareas, relate in inverse fashion to the fabric loading at the start of filtration; i.e., the "just cleaned" or lightly loaded subareas see the higher face velocities and hence the greater dust deposition rates. As the successive cleaning steps are traced from Figure 125B through H, it can be seen that the average filter dust holding has undergone a gradual decrease as the originally uniformly loaded subareas are reduced to the partially loaded regions shown in Figure 125H. However, with a continuation of the cleaning process in which subarea a_{11} experiences its second cleaning, the system will operate at a steady state condition.

The filter performance with respect to resistance and particulate emissions will now oscillate within a constant range whose upper and lower limits are dominated by the fabric loading profiles (without regard to sequence) shown in Figure 125H and 125I.

In addition to assuming that the dependence of a_c on point-by-point changes in fabric loading can be ignored, the impact of successive fabric collapses (which may weaken adhesive bonds but not necessarily lead to immediate dust dislodgment) has not been included in the modeling operations. It is assumed that for a specific cleaning method an equilibrium adhesion level is reached after 5 to 6 repetitions of the cleaning process. The above equilibrium process should not be confused with the relatively long, approximately 2 to 3 weeks, process required for the fiber dust holdings to reach a steady state. Beyond this point no significant increase in dust dislodgement can be attained without increasing the intensity of the dislodging force. As far as the modeling procedures for the fly ash/woven glass fabric systems are concerned, the two simplifying assumptions discussed above reduce significantly the data processing while introducing no obvious penalties in predicting filter system performance.

Once the decision is made (by the computer) as to how many subareas will be used for each compartment (and bag), the calculations proceed by successive iterations with the results from the first iteration constituting the input for the second, and so forth.

The general procedure for calculating all the system parameters at any time in a cycle is outlined in Figure 126. Individual subareas and compartment (bag) drags are first calculated so that the total (average) system values for drag, pressure drop, and flow rate can be determined. Based on the system pressure drop and individual bag drags, the volume flow is first partitioned among all the compartments followed by a further subdivision among the subareas of each bag. Penetration and outlet concentration are then computed for each subarea, each compartment (bag) and

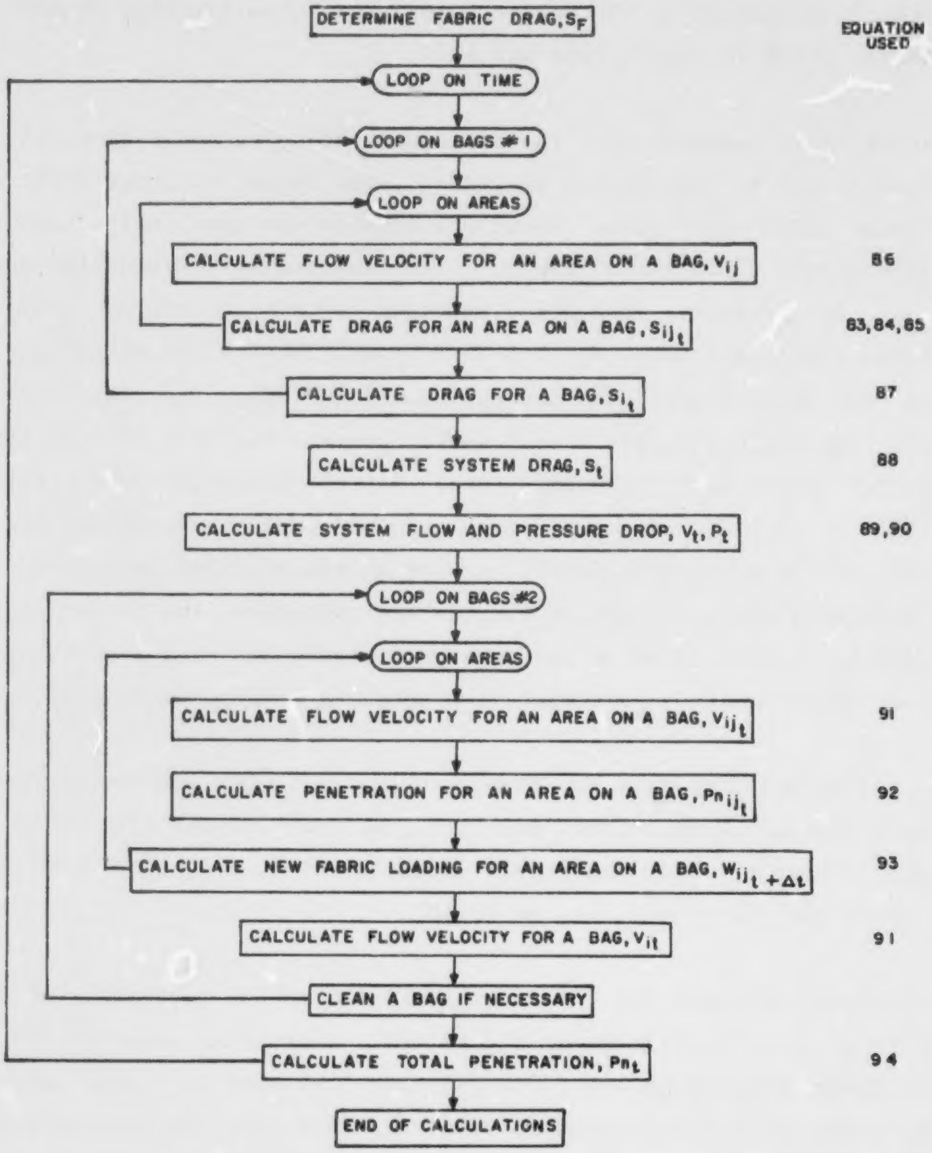
DETERMINE FABRIC DRAG, S_F
EQUATION USED
LOOP ON TIME
LOOP ON BAGS # 1
LOOP ON AREAS
CALCULATE FLOW VELOCITY FOR AN AREA ON A BAG, V_{ij}
86
CALCULATE DRAG FOR AN AREA ON A BAG, S_{ij_t}
83,84,85
CALCULATE DRAG FOR A BAG, S_{i_t}
87
CALCULATE SYSTEM DRAG, S_t
88
CALCULATE SYSTEM FLOW AND PRESSURE DROP, V_t, P_t
89,90
LOOP ON BAGS #2
LOOP ON AREAS
CALCULATE FLOW VELOCITY FOR AN AREA ON A BAG, V_{ij_t}
91
CALCULATE PENETRATION FOR AN AREA ON A BAG, Pn_{ij_t}
92
CALCULATE NEW FABRIC LOADING FOR AN AREA ON A BAG, $W_{ij_{t+\Delta t}}$
93
CALCULATE FLOW VELOCITY FOR A BAG, V_{it}
91
CLEAN A BAG IF NECESSARY
CALCULATE TOTAL PENETRATION, Pn_t
94
END OF CALCULATIONS

Figure 126. Baghouse model computational procedure

for the total system in the order named. Since the dust deposition rate is determined by a specified flow velocity and inlet concentration, the weight of dust added to any area on any bag can be calculated. Thus, the fabric loadings for all areas can be calculated for succeeding time increment.

The actual time increments chosen for the iteration represent a compromise between excessive computing and printout operations and the need to resolve excursions in resistance and/or emissions about their mean values that may bear upon the adequacy of the control process. The policy exercised here has been to select time increments that define key system operating and performance parameters; i.e., flow rates, resistance and outlet concentration, at the start, middle and end of the filtration interval during which a compartment has been taken off-line for cleaning. In the case of the Nucla operation, the overall cleaning period per filter compartment was 4 minutes. Hence, the selection of a 2-minute iteration time provides a measure of maximum, minimum and average system parameters while compartment cleaning is taking place.

PROGRAM DESCRIPTION

A flow diagram for the computer simulation program, which is comprised of two basic steps, is presented in Figure 127. The main program first calls the MODEL subroutine in which all calculations are performed and then transfers control to the SCRIBE subroutine in which the results are plotted. All data input and output and calculations are performed by the MODEL subroutine. Data are input to the program via the two subroutines READIM and READIT.

READIT inputs all operating parameters and constants used in the linear drag model. Cleaning parameters and constants used in the nonlinear model are input by READIM. READIM also performs the temperature correction on viscosity.

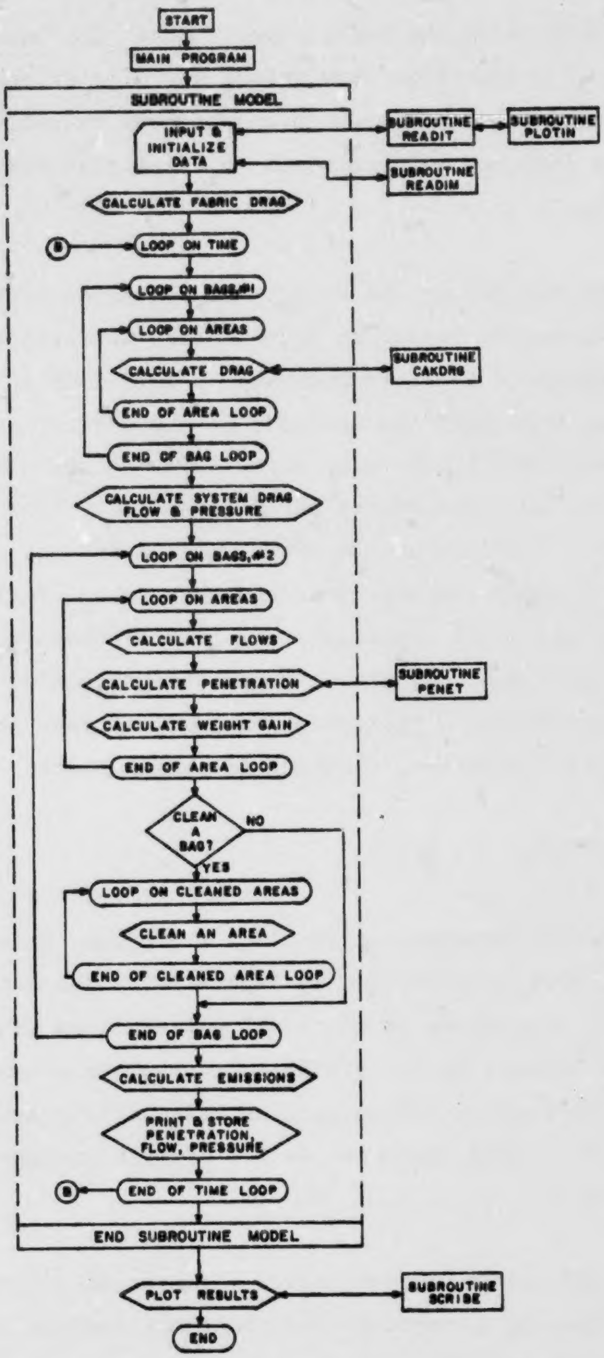
START
MAIN PROGRAM
SUBROUTINE MODEL
INPUT & INITIALIZE DATA
SUBROUTINE READIT
SUBROUTINE PLOTIN
SUBROUTINE READIM
CALCULATE FABRIC DRAG
B
LOOP ON TIME
LOOP ON BAGS,#1
LOOP ON AREAS
CALCULATE DRAG
SUBROUTINE CAKDRG
END OF AREA LOOP
END OF BAG LOOP
CALCULATE SYSTEM DRAG FLOW & PRESSURE
LOOP ON BAGS,#2
LOOP ON AREAS
CALCULATE FLOWS
CALCULATE PENETRATION
SUBROUTINE PENET
CALCULATE WEIGHT GAIN
END OF AREA LOOP
CLEAN A BAG?
NO
YES
LOOP ON CLEANED AREAS
CLEAN AN AREA
END OF CLEANED AREA LOOP
END OF BAG LOOP
CALCULATE EMISSIONS
PRINT & STORE PENETRATION, FLOW, PRESSURE
B
END OF TIME LOOP
END SUBROUTINE MODEL
PLOT RESULTS
SUBROUTINE SCRIBE
END

Figure 127. Baghouse simulation program flow diagram

Headings for graphical output are established by the PLOTIN subroutine. In performing the calculations for drag and penetration, the program utilizes the additional subroutines, CAKDRG and PENET, respectively.

COMPUTATIONAL PROCEDURES

The following paragraphs provide a description of the procedures and equations used to calculate system performance. A flow diagram for the entire program is presented in Figure 127 and a diagram of the basic computations performed is shown in Figure 126. A tabulation of relevant equations with reference to where they are treated in the report is also included in Figure 126.

Drag Computation

Cleaned fabric drag is a predetermined input that is not computed by the program. It is set equal to the effective drag, S_E, if the linear drag model is selected and to the residual drag, S_R, if the nonlinear drag model is used.

Area drag values are computed by the linear or nonlinear drag models with the subroutine CAKDRG. The choice of subroutines is automatically performed by the program which selects the nonlinear model when W^* has any nonzero value. A zero value for W^* will automatically lead to computer calculations by the linear drag model.

The area drag equations for the linear model are:

$$S_{ij_t} = S_E + K_{2_{ij}} \times W_{ij_t} \tag{83}$$

and for the nonlinear:

$$S_{ij_t} = S_R + K_{2_{ij}} \times W'_{ij_t} + (K_2 - K_{2_{ij}})W^* \left(1-e^{-W'_{ij_t}/W^*}\right) \tag{84}$$

Where S_{ij_t} = the drag for the j^{th} area on the i^{th} bag at time = t

S_E = effective drag for cleaned fabric

S_R = residual drag for cleaned fabric

$K_{2_{ij_t}}$ = specific cake resistance for the area

W'_{ij_t} = absolute fabric loading less the residual fabric loading

K_R = initial slope of the drag versus loading curve

W^* = constant dependent on fabric and dust properties

t = time

The specific cake resistance (K_2) is a function of velocity:

$$K_{2_{ij_t}} = K_2^\circ \sqrt{V_{ij}/0.61} \tag{85}$$

where K_2° is the specific resistance at 0.61 m/min and the actual gas temperature. A correction for gas viscosity changes is carried out within the program's initiation step.

Since the flow velocity for a specified area is not determined until the system pressure drop and area drag are known, it must be estimated from the previous system pressure drop and the previous drag on the area:

$$V_{ij} = P_{t-\Delta t}/S_{ij_{t-\Delta t}} = V_{ij_{t-\Delta t}} \tag{86}$$

The total or average drag for a compartment (bag) is calculated for a parallel resistance network of J equal areas as:

$$S_{i_t} = J/\sum_{j=1}^{J} 1/S_{ij_t} \tag{87}$$

Similarly, total system drag is calculated for I bags as:

$$S_t = I/\sum_{i=1}^{I} 1/S_{i_t} \tag{88}$$

For convenience in data processing, the drag value for any compartment undergoing cleaning is set equal to 10^{20} in lieu of plus infinity because the compartment velicity is zero. However, since the parameters describing overall system performance are based on total fabric area, the value of I in Equation (88), which designates the total number of system compartments, is not changed. Total baghouse flow or pressure drop can, therefore, be held constant while the average flow velocities for the individual compartments are permitted to vary.

The total or average system flow and/or pressure drop are calculated from the total system drag and the specified constant pressure drop and/or flow. Additionally, when a compartment is being cleaned via reverse flow, the reverse flow air is factored into the computed pressure drop and flow rate.

When the system pressure drop is specified as constant, the average gas velocity system is calculated by:

$$V_t = P_c/S_t + V_R/I \tag{89}$$

and when the system flow is specified as constant, the pressure drop is calculated by:

$$P_t = V_c\ S_t + V_R\ S_t/I \tag{90}$$

where P_C = specified constant system pressure drop

V_c = specified constant system velocity

V_R = reverse flow velocity for a single bag

It is again pointed out that a constant pressure drop system in most large field installations would not ordinarily be anticipated. Such a constraint could lead to unacceptable flow variation in most process or contaminant control operations.

If no reverse flow is used, V_R is zero in the above Equations (80) and (90). Once the system pressure drop is known, the calculated flow velocity through an area can be calculated:

$$V_{ij_t} = P_t/S_{ij_t} \tag{91}$$

Fabric Penetration

Penetration through a specified subarea is calculated by the subroutine PENET from the empirical relationships developed in Section X:

$$Pn_{ij_t} = \frac{C_o}{C_i} = Pn_s + (0.1 - Pn_s)e^{-aW_{ij_t}} + C_R/C_i \tag{92}$$

where Pn_{ij_t} = penetration through the j^{th} area on the i^{th} bag

W_{ij_t} = cloth loading minus residual loading at time t

C_R = residual concentration, 0.5 mg/m^3, a system constant

C_i = inlet concentration

$$Pn_s = 1.5 \times 10^{-7} e^{12.7(1-e^{-1.03 V_{ij_t}})} \tag{92a}$$

$$a = 3.6 \times 10^{-3}/(V_{ij_t})^4 + 0.094 \tag{92b}$$

and V_{ij_t} = face velocity of the j^{th} area on the i^{th} compartment (bag) at time t.

Once the face velocity and penetration have been established for an area, the dust deposition rate can be calculated. The fabric loading on the area used in the calculations for the succeeding time loop is:

$$W_{ij_{t+\Delta t}} = V_{ij_t} \times (1-Pn_{ij_t}) \times \Delta t \times C_i + W_{ij_t} \tag{93}$$

Note that when a compartment (bag) is being cleaned, its area velocities are zero and thus no dust is added to the bag. The average flow velocity through a compartment (bag) is calculated in the same manner as that for an area (Equation (91) except that the total compartment drag is used.

After the compartment filtering (or on-line) time has progressed to the point where it is equal to the cleaning cycle time minus the time required to clean one compartment, the cleaning cycle is initiated. This entails taking the compartment off line followed by setting its drag at 10^{20} to adjust for the zero flow condition.

Total or average system penetration is simply the total mass emitted divided by the total mass input:

$$P_t = \frac{1}{V_t IJ} \sum_{i=1}^{I} \sum_{j=1}^{J} Pn_{ij_t} V_{ij_t} \tag{94}$$

After all calculations for time = t have been completed and the fabric loading for the next time loop has been calculated, one proceeds to the next time iteration.

Program Input and Output

A summary of the program input data and their related units are presented in Table 53.

Table 53. SIMULATION PROGRAM INPUT DATA

Item	Units	Symbol[a]
Number of compartments	-	I
Cycle time	Minutes	t
Cleaning time	Minutes	t
Total area run time	Minutes	t
Number of cycles modeled	-	-
Number of increments per bag	-	-
Average system face velocity (constant)	m/min	V_c
Inlet concentration	g/m^3	C_i
Effective drag	$N\text{-}min/m^3$	S_E
Residual drag	$N\text{-}min/m^3$	S_R
Cake resistance at 0.61 m/min and 25°C	N-min/g-m	K_2
Reverse flow velocity	m/min	V_R
Residual loading	g/m^2	W_R
Initial cake loading	g/m^2	
Average system pressure (constant)	N/m^2	P_c
Maximum pressure	N/m^2	P_{max}
W*, System constant	g/m^2	W*
Initial S versus W slope	N-min/g-m	K_R
Temperature	°K	T
Caked area	-	a_u
Print diagnostics	True or false	
X and Y axis lengths	inches	

[a] Symbols used in main body of report. Symbols used in program appear in Appendix A.

The number of compartments (bags) specified is limited to 100. Cycle time is the time required to clean all compartments whereas claening time is the time required to clean only one compartment. Once the number of compartments and the total and individual cleaning times have been specified, the time between individual compartment cleanings is fixed. For example, if the cleaning cycle time is 30 minutes, the individual cleaning time is 5 minutes and the system has three compartments, then the time between the completion of cleaning in one compartment and the start of cleaning in the next compartment is 5 minutes. This intermediate 5-minute, on-line period plus the actual 5-minute cleaning time is considered to be the cleaning cycle time for a single compartment.

The total area run time is defined as the time between cleaning cycles when all compartments are filtering. This allows all compartments to filter for a specified amount of time after the cleaning cycle has been completed. To determine the time increment used in the calculations, the number of time increments per compartment between successive cleanings; i.e., the individual compartment cleaning cycle time, must be input. Referring to the previous example in which the time between cleanings is 10 minutes, if five increments were chosen, the incremental time would be 10 minutes/5 or 2 minutes. The number of time increments per cleaning cycle is simply the product of the number of increments per compartment and the number of bags (compartments) in the system. The time specifications are discussed further in Appendix D.

The air-to-cloth ratio should be specified only if operation at constant total flow rate is desired. If it is not specified, a constant pressure drop must be specified. Operation at constant pressure is assumed if both are nonzero. The actual gas temperature and pressure must be used in calculating the air-to-cloth ratio, the inlet concentration and the reverse flow velocity. Reverse flow velocity is the velocity of the reverse flow air through a single compartment.

If the system is operated at a constant volume flow rate, cleaning can be controlled by pressure. If a maximum pressure is specified, cleaning will be initiated when the total system pressure exceeds that value. This will override any total area run time specification. When pressure control is used, total time modeled is simply the number of cycles modeled times the sum of the cycle time and total area run time.

The residual fabric loading, W_R, is the loading which exists on the cleaned portion of a bag just after cleaning. The absolute cake loading, W_T, includes all dust on the fabric, the cleanable function as well as the fixed residual fraction, W_R. In the operation of the linear drag model, the absolute fabric loading is used, whereas the nonlinear drag and the penetration models are based on the cleanable or removal dust loading W' or $W_T - W_R$. Both the linear and nonlinear models (see Section IX) can be used to predict drag. The effective drag, S_E, must be specified in either case since it is used to determine flow velocity for the calculation of K_2 on a cleaned bag. The specific cake resistance, K_2, must also be specified at 0.61 m/min and 25°C for both models because the laboratory measurements of K_2 were made under the above conditions. The coefficient K_2 is allowed to vary linearly with viscosity and with the square root of velocity. Therefore, if a K_2 value is available for conditions other than indicated above, it may be corrected for input to the program. The gas temperature must be specified for the calculation of viscosity, which is subsequently used to correct the value of K_2 input.

The linear model is used to calculate drag if a zero value is entered for W^*, a constant quantity for the fabric and dust under investigation. A nonzero value for W^* indicates that the nonlinear model should be used. Values for the initial slope of the drag versus loading curve, K_R, and the residual drag, S_R, must be specified if the nonlinear model is selected.

The fractional area of a bag from which dust is not removed during cleaning is input as caked area, a_u. The number of areas into which a bag is subdivided and the number of those areas which will be cleaned is determined within the program. The fractional area which will be cleaned is then output. A maximum deviation of 3 percent may arise between the caked area input and the cleaned area selected by the program since the total number of areas on a bag is limited to 10. Cleaned area is limited to the 10 to 100 percent range which appears to embrace the observed field conditions. The model can be easily adjusted to handle 20 subareas per bag if, for example, the cleaned area were as low as 5 percent.

The type of output desired is controlled by the x and y axis specification and the print diagnostics. The x axis is limited to a length of 24 inches and the y axis to a length of 12 inches. If no values are specified, 6 and 5 inches, respectively, are used for the x and y axis lengths. If step-by-step values of individual area and bag flows and drags are desired, print diagnostics should be specified as TRUE.

A description of the card input formats to be used is presented in Appendix A.

A sample of the program output is shown in Table 54. If the print diagnostics have been specified as TRUE, the type of information shown in the table will be output for every time increment. The total number of areas per bag (compartment) here is eight, three of which will be cleaned to achieve a fractional cleaned area of 0.375. Drag, S, for each area on each bag (compartment) and the entire bag (compartment) is output in metric units, N-min/m^3. Note that compartment (bag) 5 is off line, as indicated by a drag of 10^{20} and a velocity of 0.0. Flow velocities are reported in m/min. The next line gives the time, T, min., system pressure drop, DELP, N/m^2, system flow velocity, DELQ, m/min and outlet concentration, g/m^3. These terms are summarized along with the individual bag (compartment) flow rates after all calculations have been

Table 54. SAMPLE PROGRAM OUTPUT WITH SUPPLEMENTARY DEFINITION OF TERMS

```
 BAG-DRAG=    AREA  1    AREA  2    AREA  3    AREA  4    AREA  5    AREA  6    AREA  7    AREA  8     SBAG
     1       1.77E+03   1.77E+03   1.77E+03   1.77E+03   1.77E+03   1.22E+03   1.22E+03   1.22E+03   1.51E+03
     2       1.77E+03   1.77E+03   1.77E+03   1.77E+03   1.77E+03   1.23E+03   1.23E+03   1.23E+03   1.52E+03
     3       1.77E+03   1.77E+03   1.77E+03   1.77E+03   1.77E+03   1.24E+03   1.24E+03   1.24E+03   1.52E+03
     4       1.76E+03   1.76E+03   1.76E+03   1.76E+03   1.76E+03   1.25E+03   1.25E+03   1.25E+03   1.53E+03
     5       1.00E+20   1.00E+20   1.00E+20   1.00E+20   1.00E+20   1.00E+20   1.00E+20   1.00E+20   1.00E+20
     6       1.77E+03   1.77E+03   1.77E+03   1.77E+03   1.77E+03   1.21E+03   1.21E+03   1.21E+03   1.51E+03
 BAG-FLOW=    AREA  1    AREA  2    AREA  3    AREA  4    AREA  5    AREA  6    AREA  7    AREA  8     QBAG
     1       8.57E-01   8.57E-01   3.57E-01   8.57E-01   8.57E-01   1.24E+00   1.24E+00   1.24E+00   1.00E+00
     2       8.58E-01   8.58E-01   8.58E-01   8.58E-01   8.58E-01   1.23E+00   1.23E+00   1.23E+00   9.97E-01
     3       8.58E-01   8.58E-01   8.58E-01   8.58E-01   8.58E-01   1.22E+00   1.22E+00   1.22E+00   9.94E-01
     4       8.58E-01   8.58E-01   6.58E-01   8.58E-01   8.58E-01   1.21E+00   1.21E+00   1.21E+00   9.90E-01
     5       0.0        0.0        0.0        0.0        0.0        0.0        0.0        0.0        1.51E-17
     6       8.57E-01   8.57E-01   8.57E-01   8.57E-01   8.57E-01   1.25E+00   1.25E+00   1.25E+00   1.00E+00
 T= 190.0                 DELP= 1514.                     DELQ= .8309              CONCENTRATION= .2455E-02
          BAG  1       BAG  2       BAG  3       BAG  4       BAG  5       BAG  6       BAG
 T=        6.00        10.00        14.00        18.00        22.00         2.00        WEIGHT DUMPED= .0
 CAKE  9.1977E+02   9.2291E+02   9.2621E+02   9.2969E+02   9.2874E+02   9.1676E+02
 SBAG  0.1513E+04   0.1518E+04   0.1524E+04   0.1530E+04   0.1000E+21   0.1508E+04
 QBAG  0.1001E+01   0.9972E+00   0.9936E+00   0.9897E+00   0.1514E-16   0.1004E+01
```

Notes:

BAG DRAG - Areas 1 through 8, N-min/m^3, drag for individual areas
SBAG - Drag for entire bag, N-min/m^3

BAG-FLOW - Areas 1 through 8, m/min, velocities for individual areas
QBAG - Average velocity for entire bag, m/min

T - Test time or operating time after cleaning, min
DELP - System pressure drop, N/m^2
DELQ - System (average) velocity, m/min
CONCENTRATION - System outlet concentration, g/m^3
CAKE - Indicated bag loading, g/m^2

completed. Print diagnostics do not affect the summary table. The amount of material cleaned from a bag is also output to the right of concentration. This wieght dumped (dislodged) is reported as grams of material per unit of bag area (m^2). The last four lines are again a summary of operating times, individual bag loadings, drags and flow velocities. The loading is the average fabric loading for the bag. The indicated time below the bag number is a measure of how long a bag has been operating after a cleaning. Bag 6 will be the last to be cleaned.

After each cycle is completed, the average system flow, pressure drop and penetration are printed regardless of the print diagnostics specifications. These are averaged over the time simulated up to that point rather than over an individual cycle. In addition, after each cleaning cycle is completed, the average penetration for that cycle is output. The print diagnostics affect this output.

In addition to the tabular output, the program generates four graphs: system pressure drop versus time, system flow rate versus time, individual compartment (bag) flow versus time, and total penetration versus time. To avoid a cluttered graph, the individual compartment (bag) flow graph is limited to five compartments (bags).

PREDICTIVE VALIDATION

Introduction

The filtration model described in the preceding section was tested by introducing measured and calculated input parameters for operating coal-fired utilities boilers at Sunbury, Pennsylvania and Nucla, Colorado. It is recognized that the validation procedures cannot be considered as completely independent checks because certain of the field measurements of the above plants were used to develop and/or to refine the laboratory tests that constituted the principal basis for the modeling process. On the other hand, the extent to which the measured and predicted performance characteristics agree with one another, suggests strongly that the original concepts introduced in this study relating to cleaning and dust penetration phenomena represent the correct modeling approach for fly ash/glass fabric systems.

System Parameters

Dust and fabric properties as well as field data analyses for both Sunbury and Nucla operations have been presented in Sections IV through VI of this report. Detailed field measurements at both installations have also been described in separate reports.[8,9]

The basic input parameters for modeling the Nucla and Sunbury operations are summarized in Table 55 under the subheadings Operating Parameters and Fabric and Flow Parameters. The system parameters were selected from specific field tests (Sunbury and Nucla) rather than using average operating conditions. The fabric and dust properties for the Nucla system were based mainly upon the field data described in Section VI of this report. On the other hand, the continuous cleaning procedures used at the Sunbury installation did not allow for direct field determination of some dust/fabric parameters. However, because the GCA test fly ash was quite similar to the Sunbury dust, the laboratory measurements with the Sunbury fabric were considered to provide a good index of field conditions.

Nucla Data Inputs - The cleaning process at Nucla was controlled by fabric pressure loss with a resistance of 1200 N/m^2 (4.8 in. water) actuating the cleaning cycle. Because the cyclical cleaning of six compartments reduced system resistance to well below 1200 N/m^2, the system operated with all compartments on-line for extended, ~2 hour periods, prior to again reaching the pressure level actuating cleaning. The actual cleaning sequence for each Nucla compartment is summarized in Table 56. It should be noted that during the 240 seconds (4 min) that each compartment is isolated from the

Table 55. DATA USED FOR MODEL TRIALS WITH THE NUCLA AND SUNBURY FABRIC FILTER SYSTEMS

	Nucla	Sunbury
Operating parameters		
Number of compartments	6	14
Cleaning cycle time, min	24	32.67
Compartment cleaning time, min	4	1.4
Face (filtration) velocity, m/min	0.824	0.545
Inlet concentration, g/m^3	2.6	5.19
Maximum pressure, N/m^2	1160	-
Gas temperature, ^oK	412	442
Reverse flow velocity, m/min	0.0415	0.300
Fabric and dust parameters		
Effective drag, S_E, $N\text{-}min/m^3$	434	352
Specific cake resistance, K_2, N-min/g-m	0.76[a]	1.6[a]
Residual drag, S_R, $N\text{-}min/m^3$	-	80
Initial slope, K_R, N-min/g-m	-	7.54
Residual loading, W_R, g/m^2	50	30
W*, g/m^2	-	46

[a] Measured at 25°C, 0.61 m/min

Table 56. NORMAL CLEANING SEQUENCE FOR EACH NUCLA COMPARTMENT[a]

Event	Duration, seconds	Damper positions
Settle	54	Main damper closed, repressure damper closed
Repressure	15	Main damper closed, repressure damper open
Settle	56	Main damper closed, repressure damper closed
Shake	10	Main damper closed, repressure damper closed
Settle	56	Main damper closed, repressure damper closed
Repressure	15	Main damper closed, repressure damper open
Settle	34	Main damper closed, repressure damper closed
		Main damper open, repressure damper closed
Interval	17	
		Initiate next compartment cleaning

[a] Table 13 from Reference 8.

main system, the bag (or compartment) undergoes two separate cleanings (collapse and reverse flow) and two separate, low intensity shakings. Field observations indicated no appreciable difference in performance as the result of the added shaking.

Since the estimated shaking frequency was 4 cps and the amplitude appeared to be no greater than 0.5 in., the acceleration introduced by shaking is less than 1 g. Hence, once equilibrium adhesive levels have been reached due to multiple perturbations of the fabric surface, the added shaking and a second collapse are not expected to have a significant effect on dust removal.

Therefore, the total time involved with the cleaning of a single compartment has, for filtration purposes, been subdivided into the two intervals shown in Table 57. The first 30-second period describes the total time that an additional reverse flow must be accommodated by the I-1 compartments remaining on-line. The second 210-second interval represents the period when the on-line I-1 compartments see only the increased flow due to reduced fabric area.

Table 57. SIMPLIFIED CLEANING SEQUENCE PER NUCLA COMPARTMENT USED IN PREDICTIVE MODELING

Event	Duration, seconds	Operation
Repressure	30	Main damper closed, repressure damper open
Settle, shake	210	Main damper closed, repressure damper closed
Filtration	240	Total off-line, cleaning, period per compartment

Rather than treating the reverse flow period as an intermittent function while cleaning is taking place, the total reverse air volume has been prorated over the complete 240-second cleaning cycle. The net result is that the average reverse flow velocity is reduced to 0.042 m/nin. The above simplification facilitates the data handling process while still taking into account the average effect on system resistance and particle penetration. The 17-second "left-over" time interval after 240 seconds was neglected because its inclusion would have required the use of smaller time increments in the model.

The input data used for the Nucla modeling is presented in Tables 55 and 58, the latter showing the formal computer printout. Since the actual filtration time between cleaning cylces is lengthy, about 2 hours, compared to the overall cleaning time, 24 minutes, the bags operate with comparatively high fabric loadings for a major portion of their on-line time. Additionally, the distribution of fabric loading is essentially uniform over the latter part of the filtration cycle so that a satisfactory field estimate of the specific resistance coefficient, K_2, for the dust could be made. On the other hand, it was not possible to extract sufficient information from the field data on the other descriptive parameters, K_R, S_R, S_E and W^*, used to define the system drag/fabric loading relationships nor was it possible to determine directly the total fabric dust holdings for the loaded Nucla bags at the time of the field survey. Hence, it was necessary to estimate S_E in conjunction with the measured K_2 value to determine the approximately drag versus fabric loading characteristics for the field system. Therefore, laboratory measurements with Nucla fabric test panels and the GCA fly ash (which was slightly finer than the field aerosol) were used to provide the best estimate of S_E.

The above step led to the choice of the linear drag model since it involved only one estimated parameter, S_E, rather than the three additional values, S_R, K_R and W^* required for the nonlinear model. Because of the extended filtration periods with all filters on-line, the early filtering phase with recently cleaned fabric surfaces constituted a relatively small fraction of the total filtering period. Thus, it appeared that any nonlinearity in the drag/fabric loading relationship might be ignored in the Nucla case. It is emphasized here that a few special, but comparatively

Table 58

```
TEST RUN # 0422 NUCLA BAGHOUSE SIMULATION-LINEAR
                                    PRINTOUT OF INPUT DATA FOR BAGHOUSE ANALYSIS
```

```
                                                  6
NUMBER OF COMPARTMENTS=                   24.00000 MINUTES
CYCLE TIME=                                4.00000 MINUTES
CLEAN TIME=                                0.0     MINUTES
TOTAL AREA RUN TIME=                        20 CYCLES
NUMBER OF CYCLES MODELED=                    2 INCREMENTS
NUMBER OF INCREMENTS PER BAG=              0.82400 M/MIN
Q/A=VELOCITY=                             2.600E+00 G/M3
CONCENTRATION=                            4.340E+02 N-MIN/M3
SE=EFFECTIVE BAG DRAG=                    7.600E-01 N-MIN/G-M
K2=CAKE RESISTANCE AT .61 M/MIN=            0.0415 M/MIN
REVERSE FLOW VELOCITY=

                                          50.0      G/M2
WR=RESIDUAL LOADING=                      806.      G/M2
INITIAL CAKE LOADING=

                                              T
PRINT DIAGNOSTICS=                        0.0       N/M2
CONSTANT PRESSURE=                        1.160E+03 N/M2
MAXIMUM PRESSURE=

                                          .0        G/M2
W*=

                                          0.0       N-MIN/G-M
KO=                                       0.2339E-01 CP
MU=GAS VISCOSITY=                         0.0       N-MIN/M3
SR=RESIDUAL DRAG=                         4.1200E+02 DEGREES KELVIN
TEMPERATURE=                              6.2000E-01
CAKED AREA=

                                          0.3750E+00
CLEANED AREA=
```

---

[a] All measurements referred to gas temperature of $412^{o}K$ except for K_2.

simple field tests might have been used to establish the drag versus fabric loading relationship had the need for these measurements been anticipated in the preceding field studies.[8,9]

In validating the predictive model with Nucla field measurements, it is emphasized that the starting point is a given set of field output parameters which one attempts to relate to the measured input parameters via the modeling route.

One of the first terms to define is the fraction of fabric surface that is cleaned in any given bag compartment when the cleaning process (collapse or mechanical shaking) is carried out. The above determination is readily made because once steady-state filtration conditions have been established, the amount of dust deposited over the period between the initiation of successive cleaning cycles (which in the case of Nucla operations involves both the cleaning cycle and an extensive filtering period without cleaning) must equal the amount of dust dislodged during the cleaning cycle.

Based upon the face velocity and inlet concentration values shown in the Table 58 and a total cycle time of 150 minutes, the dust deposited over this period, ΔW, was 321 g/m^2. The terminal fabric loading, W_p, just before cleaning was estimated to be 850 g/m^2 using the maximum pressure level, P_{max}, just before cleaning, 1160 N/m^2, Table 58, and the linear drag model in which K_2 was assumed to be 0.76 N min/g m and S_E to be 434 N-min/m^3.

$$W_P = (P_{max}/V - S_e)/K_2 \qquad (95)$$

and

$$a_c = 1 - \frac{W_P - \Delta W - W_R}{W_P - W_R} \qquad (63)$$

At the present time, the calculation of a_c by Equation (64) is executed outside the formal computer program, because of the great number of operating modes that may be encountered in the field. Since these calculations are also easily performed, their exclusion from the program appears advisable until more experience is attained with the model. With reference to the numerical values entered in Table 58, S_E and K_2 must be corrected for gas viscosity and K_2 must be further corrected for velocity as pointed out previously in Section VII, Equation (20a). Therefore, S_E at field operating temperature (and viscosity) must be expressed as

$$S_{E_{field}} = S_{E_{ambient}} \left(\frac{\mu_{field}}{\mu_{ambient}} \right) \quad (96)$$

The K_2 value at field conditions is calculated as

$$K_{2_{field}} = K_{2_{ambient}} \left(\frac{\mu_{field}}{\mu_{ambient}} \right) \left(\frac{V_{field}}{V_{ambient}} \right)^{0.5} \quad (97)$$

Sunbury Data Inputs - The Sunbury cleaning process consists of back-to-back cycles with all compartments on-line for brief, ~ 1 min, periods between each compartment cleaning. The actual cleaning cycle, presented on a compartment basis, is shown in Table 59. Reduced to its simplest terms, each compartment is off-line for 83 out of the 140 seconds associated with the cleaning of each compartment. For 51 seconds out of the 83 second period when I-1 (13) compartments remain on line, an additional reverse flow of 0.49 m/min must be accommodated by the on-line compartments. Again, because this flow persists only for the time fraction 51/83, its average value over the compartment cleaning cycle reduces to 0.30 m/min as indicated in Table 55.

A special feature of the Sunbury system is the air (sweep) flushing of the reverse flow manifold to minimize dust deposition. Practically speaking, this process, which requires about 125 seconds for every seven compartment cleanings, increases the on-line time of all compartments by 250 seconds per cleaning cycle. Thus, in redefining the cleaning cycle for

Table 59. NORMAL CLEANING SEQUENCE FOR SUNBURY[a] COMPARTMENTS

Step	Event	Duration, seconds	Operation	No. of compartments cleaned
1	Settle	17	Main damper closed, repressure damper closed	1[b]
2	Reverse flow	51	Main damper closed, repressure damper open	
3	Settle	15	Main damper closed, repressure damper closed	
4	Filtering	39	All compartments on line	
5	Collapse duct sweeping	80	Sweep valve open, all compartments on line	0
6	Filtering	45	All compartments on line	
Repeat Steps 1 through 6 for second group of seven compartments				
1-4		854	Cleaning interval for 7 compartments	7
5,6		125	Sweeping interval for 7 compartments	0
		1,958	Total elapsed time per cycle	14

[a] Excerpted from Table 7, Reference 9

[b] Steps 1 through 4 repeated seven times and Steps 5 and 6 one time for one-half the cleaning cycle

easier computer treatment, the cycle has been restructured as shown in Table 60. In the modeling process, the actual time that each compartment is off-line remains at 83 seconds, but the on-line time associated with the sweep cleaning is spread uniformly over each compartment cleaning interval. With respect to selecting time increments for the Sunbury operations, a basic time division of 140 seconds was chosen so that the beginning and end of each compartment cleaning interval could be properly described. The above interval was further subdivided into four increments so that intermediate resistance and penetration variations could be resolved by the program.

Table 60. SIMPLIFIED CLEANING SEQUENCE PER SUNBURY COMPARTMENT

Steps	Event	Duration	Operation	No. of compartments cleaned
1	Settle	32	Main damper closed, repressure damper closed	1[a]
2	Reverse flow	51	Main damper closed, repressure damper open	
3	Filtering	57	All compartments on line	b
		140	Cleaning interval per compartment	

[a] One compartment off line during Steps 1 and 2

[b] Total cleaning cycle = (140 sec/comp)(14 comp) = 1960 seconds

The fabric and dust properties and system operating parameters for the Sunbury installation have been presented in Table 55. Summary of all data inputs used in the modeling process are given in Tables 61 and 62, respectively, for the linear and nonlinear drag models. Since continuous cleaning is used at Sunbury, the fraction of cleaned area, a_c, could not be determined in the same manner as that for the Nucla plant. Instead, the average fabric loading was first determined by weighing several loaded Sunbury bags (see Section VI) after removal from the system.

Table 61

```
TEST RUN # 0422  SUNBURY BAGHOUSE SIMULATION-LINEAR
                                        PRINTOUT OF INPUT DATA FOR BAGHOUSE ANALYSIS

NUMBER OF COMPARTMENTS=
CYCLE TIME=                                14
CLEAN TIME=                             32.67000 MINUTES
TOTAL AREA RUN TIME=                     1.40000 MINUTES
NUMBER OF CYCLES MODELED=                0.0     MINUTES
NUMBER OF INCREMENTS PER BAG=             14 CYCLES
Q/A=VELOCITY=                              4 INCREMENTS
CONCENTRATION=                           0.54500 M/MIN
SE=EFFECTIVE BAG DRAG=                 5.190E+00 G/M3
K2=CAKE RESISTANCE AT .61 M/MIN=       3.520E+02 N-MIN/M3
REVERSE FLOW VELOCITY=                 1.600E+00 N-MIN/G-M
                                          0.3000 M/MIN
WR=RESIDUAL LOADING=
INITIAL CAKE LOADING=                   30.0      G/M2
                                        30.0      G/M2
PRINT DIAGNOSTICS=
CONSTANT PRESSURE=                         F
MAXIMUM PRESSURE=                      0.0        N/M2
                                       0.0        N/M2
W*=
                                        .0        G/M2
KO=
MU=GAS VISCOSITY=                     0.7540E+01 N-MIN/G-M
SR=RESIDUAL DRAG=                     0.2458E-01 CP
TEMPERATURE=                          8.0000E+01 N-MIN/M3
CAKED AREA=                           4.4200E+02 DEGREES KELVIN
                                      8.5500E-01
CLEANED AREA=
                                      0.1429E+00
```

Table 62

```
TEST RUN # 0422 SUNBURY BAGHOUSE SIMULATION-NON LINEAR
                                       PRINTOUT OF INPUT DATA FOR BAGHOUSE ANALYSIS
-----------------------------------------------------------------------------------

NUMBER OF COMPARTMENTS=                      14
CYCLE TIME=                               32.67000 MINUTES
CLEAN TIME=                                1.40000 MINUTES
TOTAL AREA RUN TIME=                       0.0     MINUTES
NUMBER OF CYCLES MODELED=                    14 CYCLES
NUMBER OF INCREMENTS PER BAG=                 4 INCREMENTS
Q/A=VELOCITY=                              0.54500 M/MIN
CONCENTRATION=                           5.190E+00 G/M3
SE=EFFECTIVE BAG DRAG=                   3.520E+02 N-MIN/M3
K2=CAKE RESISTANCE AT .61 M/MIN=         1.600E+00 N-MIN/G-M
REVERSE FLOW VELOCITY=                     0.3000 M/MIN

WR=RESIDUAL LOADING=                      30.0      G/M2
INITIAL CAKE LOADING=                     30.0      G/M2

PRINT DIAGNOSTICS=                           F
CONSTANT PRESSURE=                        0.0       N/M2
MAXIMUM PRESSURE=                         0.0       N/M2

W*=                                       46.00     G/M2

KO=                                      0.7540E+01 N-MIN/G-M
MU=GAS VISCOSITY=                        0.2458E-01 CP
SR=RESIDUAL DRAG=                        8.0000E+01 N-MIN/M3
TEMPERATURE=                             4.4200E+02 DEGREES KELVIN
CAKED AREA=                              8.5500E-01

CLEANED AREA=                            0.1429E+00
```

Reproduced from best available copy.

The fractional area cleaned, $a_c = 0.145$, calculated on the basis of the average fabric loading of the bags (compartments) and the quantity of dust added to the filter system over the cleaning cycle, the latter defined by the C_i, V_i and t values given in Table 55. The values shown in Tables 61 and 62 for K_2, K_R, S_R, S_E and W^* were based on laboratory measurements with both used and new Sunbury fabric and GCA fly ash. Since the size properties for the GCA and the Sunbury fly ash were very similar, it was considered acceptable to use the laboratory findings to describe the dust-related parameters involved in the modeling process.

Nucla Plant - Model Validation

Predicted Versus Actual Resistance Characteristics - The actual pressure-time curve for a typical Nucla field test (Run No. 1) is shown in Figure 128. These data, which were traced from a field strip chart, also apply to the operating and dust-fabric parameters summarized in Tables 55 and 58.

The predicted pressure-time curve, Figure 129, developed from the linear model and the data inputs appearing in Table 58 shows good agreement with the actual measurements. Peak pressure traces were generally lower during the cleaning cycle because the reverse flow air was averaged over the cycle rather than using the transient spike values. The multiple peaks shown in Figure 128 synchronize quite well with the two brief "repressuring" operations indicated in Table 56. Note that the extra pair of pressure spikes per compartment cleaning are not displayed on the predicted curve because of the averaging process.

Selected reference points for comparing the actual and precicted resistance measurements are outlined in Table 63.

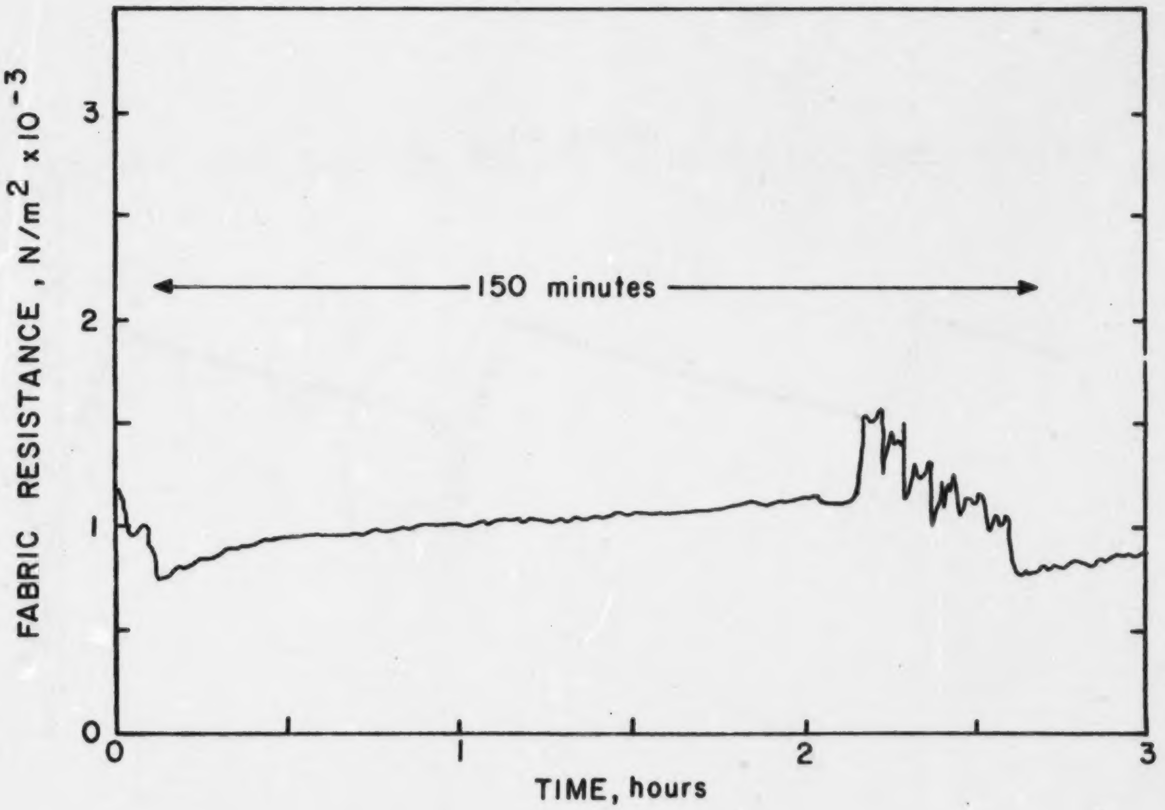

Figure 128. Pressure-time trace for run number 1, Nucla generating station (Reference 8)

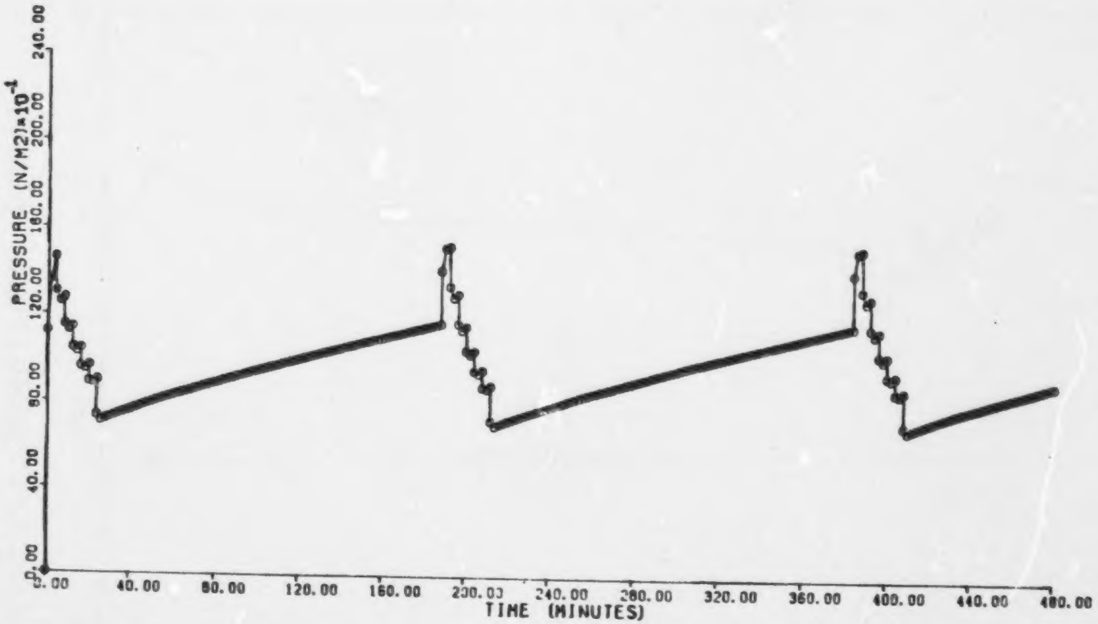

Figure 129. Test run No. 0422 Nucla baghouse simulation - linear pressure versus time graph

Table 63. PREDICTED AND MEASURED RESISTANCE CHARACTERISTICS FOR NUCLA FILTER SYSTEM

	Actual		Predicted	
	N/m^2	in. H_2O	N/m^2	in. H_2O
Maximum resistance during cleaning	1700	6.8	1520	6.1
Initial resistance following cleaning	850	3.4	720	2.9
Maximum resistance just before cleaning[a]	1160	4.7	1160	4.7
Time between successive cleaning cycles	150 min		188 min	

[a] Fixed value for predicted conditions.

The main differences between the actual and predicted resistance versus time curves are (1) the average resistance is slightly lower for the predicted curve and (2) the range between final and initial resistance values exclusive of the cleaning intervals is slightly higher for the predicted curve.

The above results would be expected if the estimated value for the fraction of cleaned area were too large.

If a lower a_c value were assumed, a smaller reduction in resistance would take place and the interval between cleaning cycles would also reduce. In the special case where the dust removed during the cleaning cycle equals exactly the amount deposited over the same period, the fabric operating resistance can be maintained at the same level. However, failure to keep up with the deposition rate will automatically drive the system to a new, higher equilibrium operating pressure. In the extreme case, lack of fan capacity, bag rupture or other irreversible changes would necessitate a complete reevaluation of the filter system design.

Predicted Velocity Relationships - Total or average system velocity is shown as a function of time in Figure 130. The average velocity is based on a constant volume flow rate, Q, and the total number of compartments (and fabric) in the system. Therefore, during the 24-minute cleaning cycle, the average velocity also remains constant except when reverse flow air is used. The short-term increases in flow velocity shown in Figure 130 are due to the addition of reverse flow air. Because the reverse flow was averaged over the entire cleaning cycle rather than over the actual transient (~15 second) period, the velocity spikes do not appear in the computer printout.

Figure 131 is a graph of the individual compartment velocities for compartments 1 through 5 as a function of time. A pressure spike appears when each compartment is taken on- and off-line. This explains the zero velocity points which are indicated as each of the six Nucla compartments is successively isolated over the 24-minute cleaning intervals. After 166 minutes of filtration with all compartments on-line, it can be seen that the velocity range for the "just" and the "first" cleaned compartments falls roughly within ± 2.5 percent of the average value. Hence, it is reasonable to assume that the fabric surface loadings have returned to nearly uniform levels.

Predicted Penetration - Total (overall) system fractional penetration for the Nucla filter installation is presented as a function of time in Figure 132. The emission characteristics of the system are best analyzed by starting at a point of minimum system penetration, roughly 5×10^{-4} at 188 minutes. The initial penetration increase from 5 to 9×10^{-4} during the cleaning of the first compartment is due to the increase in on-line compartment velocities when one compartment is taken out of service. According to Equation (96), Section VIII, particle concentration is expected to vary approximately as 2.2 power of the face velocity. Therefore, the observed penetration increase appears reasonably consistent with the fact that average face velocity has been increased by 20 percent.

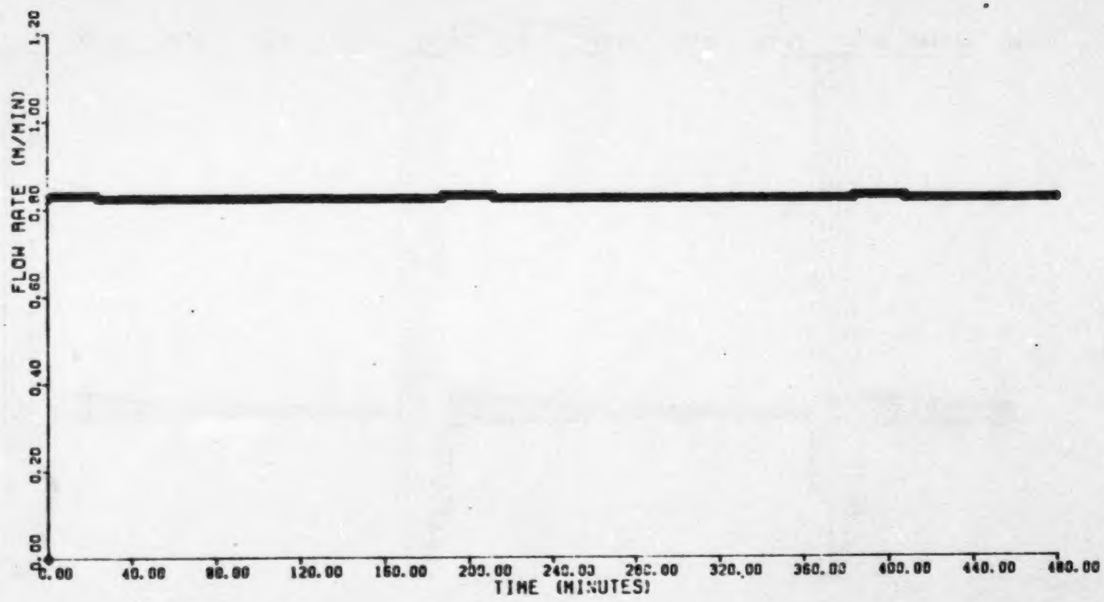

Figure 130. Test run No. 0422 Nucla baghouse simulation - linear flow rate versus time graph

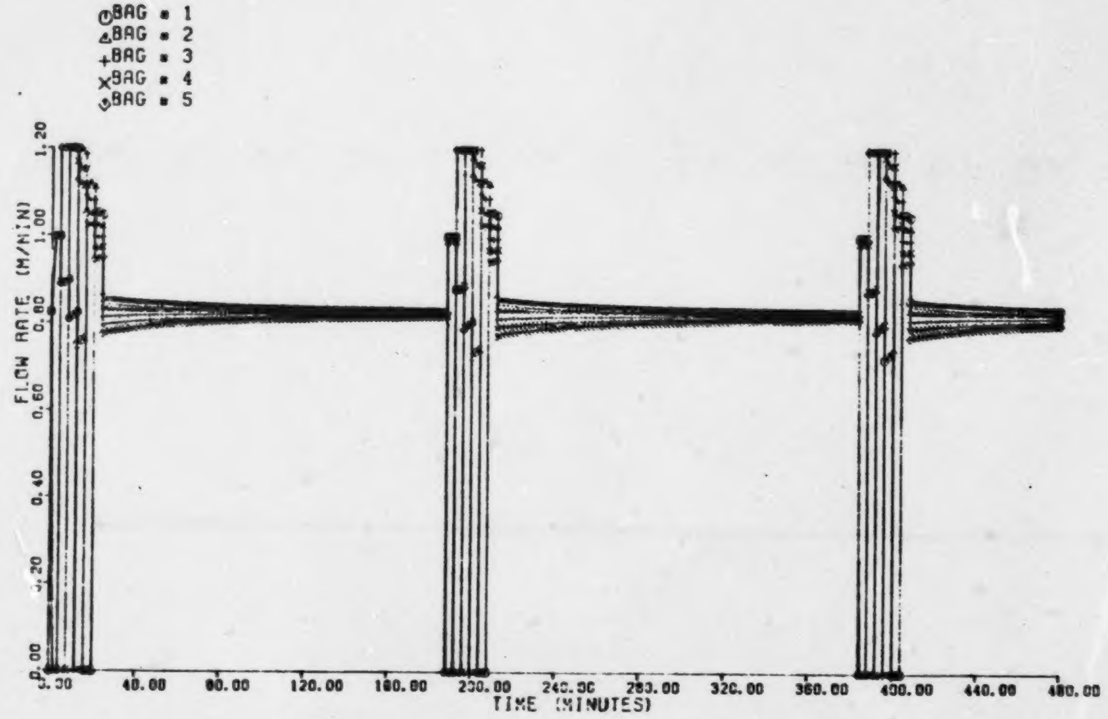

Figure 131. Test run No. 0422 Nucla baghouse simulation - linear individual flow rate graph

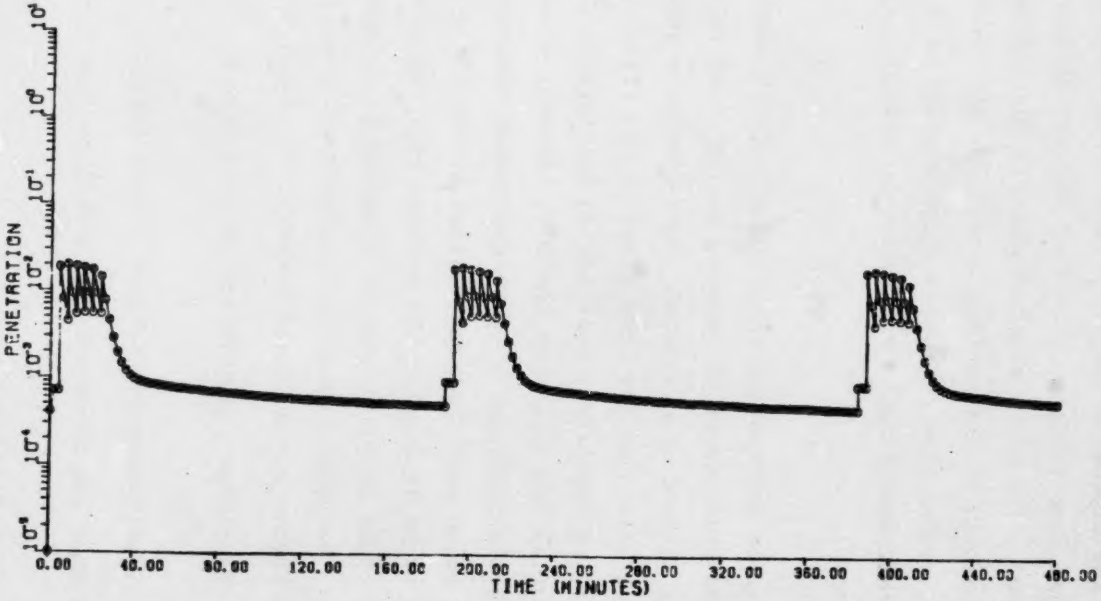

Figure 132. Test run No. 0422 Nucla baghouse simulation - linear penetration versus time graph

When the next compartment is returned to service, its dust loading is nonuniform with part of the fabric cleaned to its residual loading, a_c, and the remainder having a loading equivalent to that just prior to cleaning. Since the cleaned areas has a much lower resistance to flow and, thus, a higher face velocity than that for the uncleaned area, its efficiency is lower. The above process accounts for the second major increase in penetration to its maximum level. As more dust is added to the compartments, penetration decreases significantly to a new minimum value until the next compartment is returned to service, at which point emissions again rise.

As the cleaning cycle progresses, the availability of partially loaded, previously cleaned areas tends to reduce the high face velocity through the most recently cleaned area. Hence, one observes a gradual reduction in peak emission levels over the time frame of the cleaning cycle. When the cleaning cycle is completed, penetration initially decreases rapidly due to a preferential deposition on the most recently cleaned areas. The velocities and fabric loadings in all compartments then decrease slowly to an asymptotic value such that penetration is nearbly constant until another cleaning cycle is begun. The average efficiency for the 190-minute predicted cycle is 99.81 percent compared to an actual test result of 99.79 percent. Although the above results suggest excellent agreement between modeling theory and observed performance; i.e.:

Predicted penentration = 0.19 percent

versus

Observation penetration = 0.21 percent

it is recognized that the above statistic derives from a limited data base.

Sunbury Plant - Model Validation

Predicted Versus Actual Resistance Characteristics - The actual resistance history for Run No. 1, Sunbury plant, is presented in Figure 133 (see Table 21, Reference 9). Because of the time scale compression, the

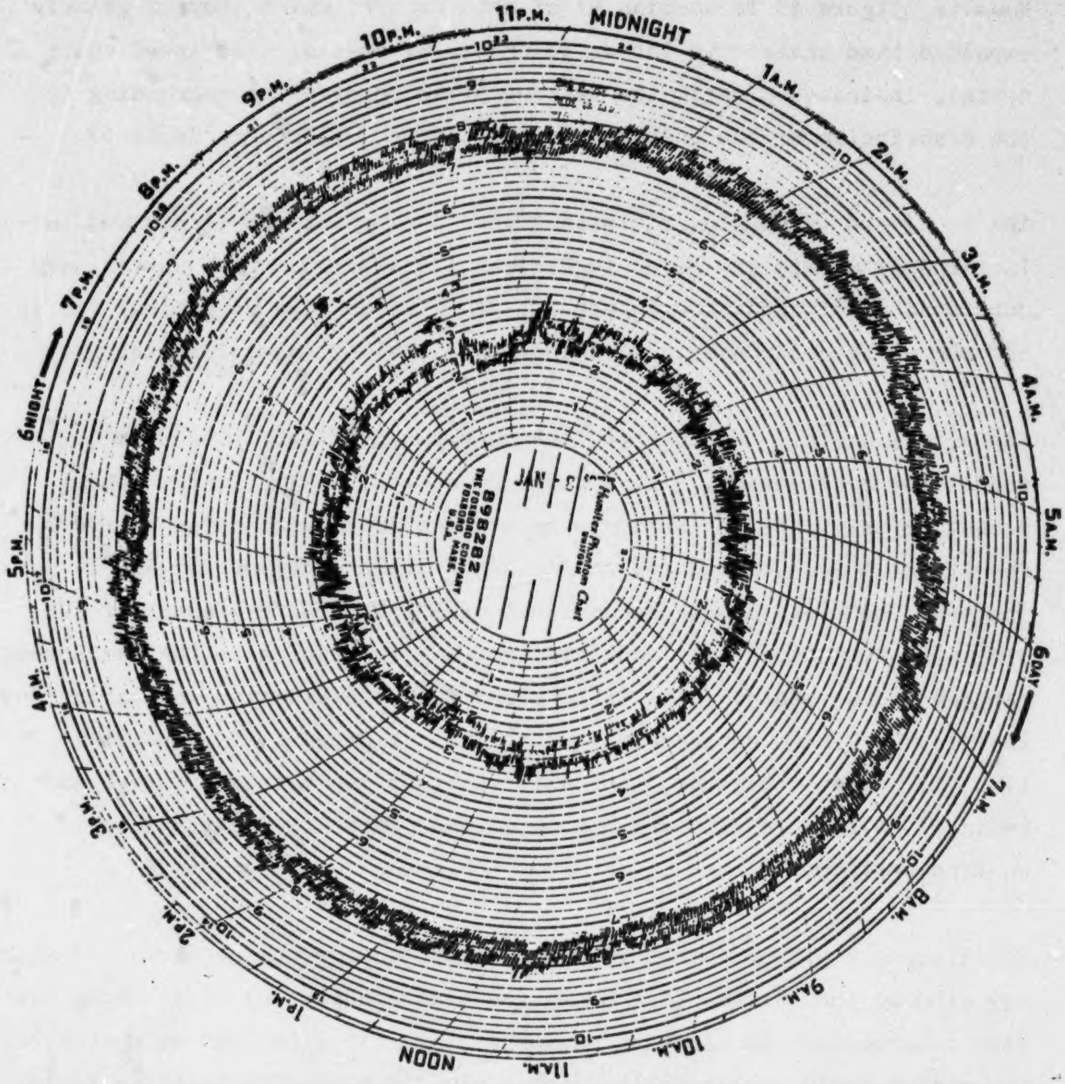

Figure 133. Pressure drop history of Sunbury baghouse - run No. 1 (Reference 9)

cyclical pattern for the resistance changes is obscured such that one can perceive only the nominal maximum and minimum pressure excursions. However, Figure 43 in Section VI of this report, which shows a greatly expanded time scale (the latter generated by special high speed chart tests), indicates clearly the various pressure steps corresponding to the description of the Sunbury cleaning cycle outlined in Table 59.

The predicted curves for resistance versus time for the linear and nonlinear drag models are given in Figures 134 and 135. Both curves were developed under conditions where the filtration began with clean fabric and where the continuously cleaning cycle was initiated immediately.

The actual average baghouse resistance was approximately 635 N/m^2 during the test period, with a range of about 150 N/m^2. After about 5 hours of simulated operation, the average resistance as predicted by the linear model leveled off at 550 N/m^2 with a range of 100 N/m^2. On the other hand, an average resistance of 525 N/m^2 with a range of 125 N/m^2 was predicted by the nonlinear model. In both cases the resistance reached a near steady state value after 4 to 5 hours time indicating how rapidly the system approaches equilibrium. Limited field data, Section VI, suggest, however, that a leveling off in both resistance and emission characteristics may not be reached until 10 days to 2 weeks on-line performance.

The discrepancy between observed and predicted resistance characteristics may also be the outcome (see Nucla resistance analysis) of assuming too high a value for the cleaning parameter, a_c. If less dust were removed, the system would automatically seek a new and higher equilibrium resistance. It is believed that the ratio of the resistance range to the average value will diminish at the higher operating resistances although the absolute difference between maximum and minimum pressure excursions may increase.

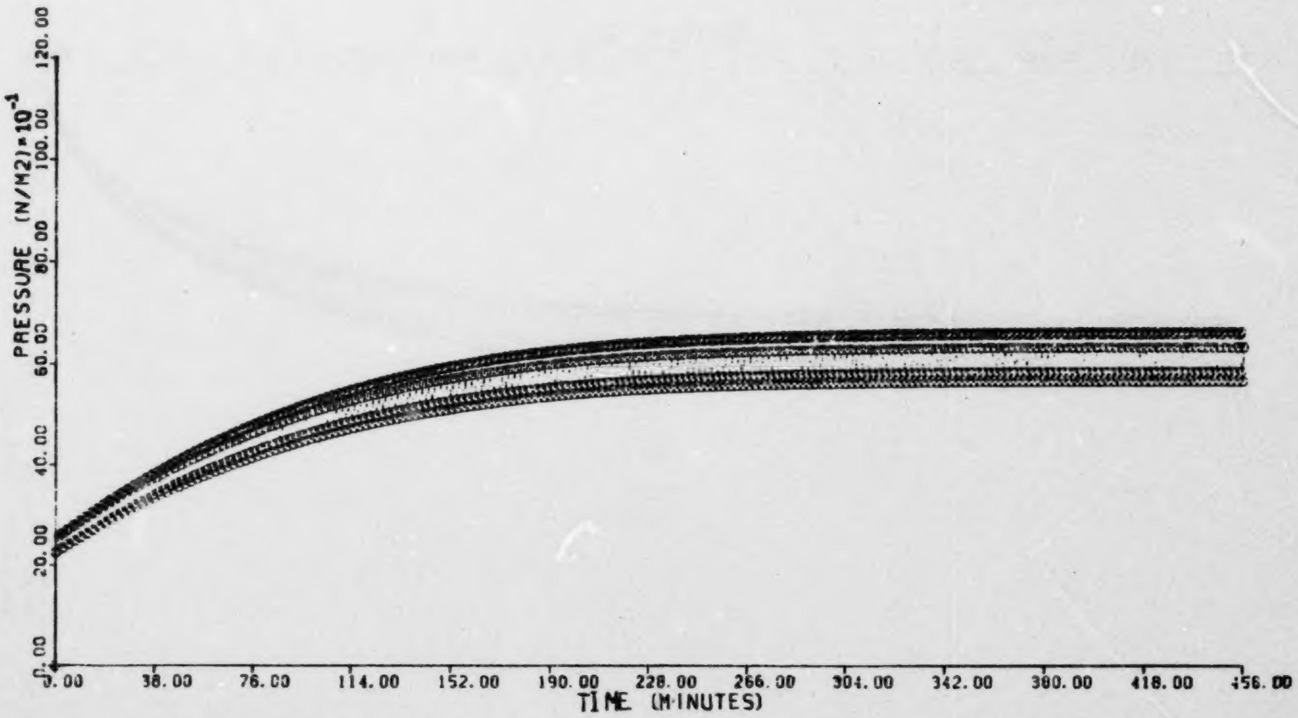

Figure 134. Test run No. 0422 Sunbury baghouse simulation - linear pressure versus time graph

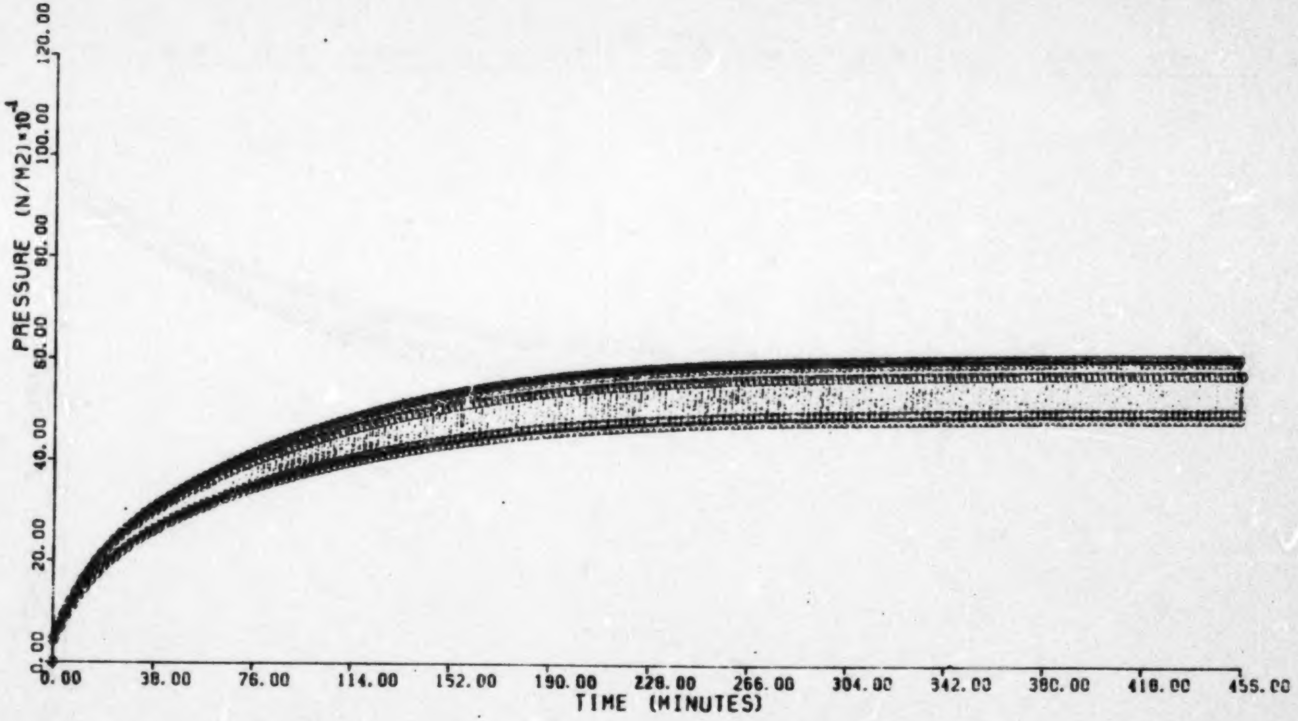

Figure 135. Test run No. 0422 Sunbury baghouse simulation - nonlinear pressure versus time graph

The lower average resistance and greater resistance range predicted by the nonlinear model is due to the lower value assumed for the starting drag of the cleaned fabric. The nonlinear model uses an S_R value of about 80 N-min/m^3 in contrast to an S_E value of 352 N-min/m^3 for the linear model. Therefore, when a cleaned compartment is first brought on line, its drag and that of the system are lower for the nonlinear model. In both cases the resistance just before a compartment is returned to service is about 600 N/m^2.

Both models are useful for design purposes. The linear model, which predicts a safely conservative average resistance, is a good estimator of power consumption. On the other hand, the nonlinear model provides a better index of transient pressure changes which might be important with respect to fan selection. Again, the accuracy of all predictions depends upon the reliability of the data inputs used in the modeling process.

Predicted Velocity Relationships - The average compartment velocity for compartments one through five as a function of time is shown in Figures 136 and 137 for the linear and nonlinear models, respectively. It was arbitrarily assumed that the velocities (and hence areal densities) were the same for all compartments at the initiation of the cleaning cycle. Once the cleaning cycle begins, however, the sequential compartment cleaning in conjunction with the data inputs given in Tables 61 and 62 will automatically drive the system to its steady state regimen characterized by the velocity gradients shown in Figure 136.

The minimum or zero velocity excursion occurs when a compartment goes off-line and the peak value indicated for each compartment represents the high transient velocity occurring when a cleaned filter is first returned to service. Reference to the point arrays on both curves shows that the second highest velocity for each compartment (0.6 minutes later) is very much lower. The data point dispersion for the nonlinear model

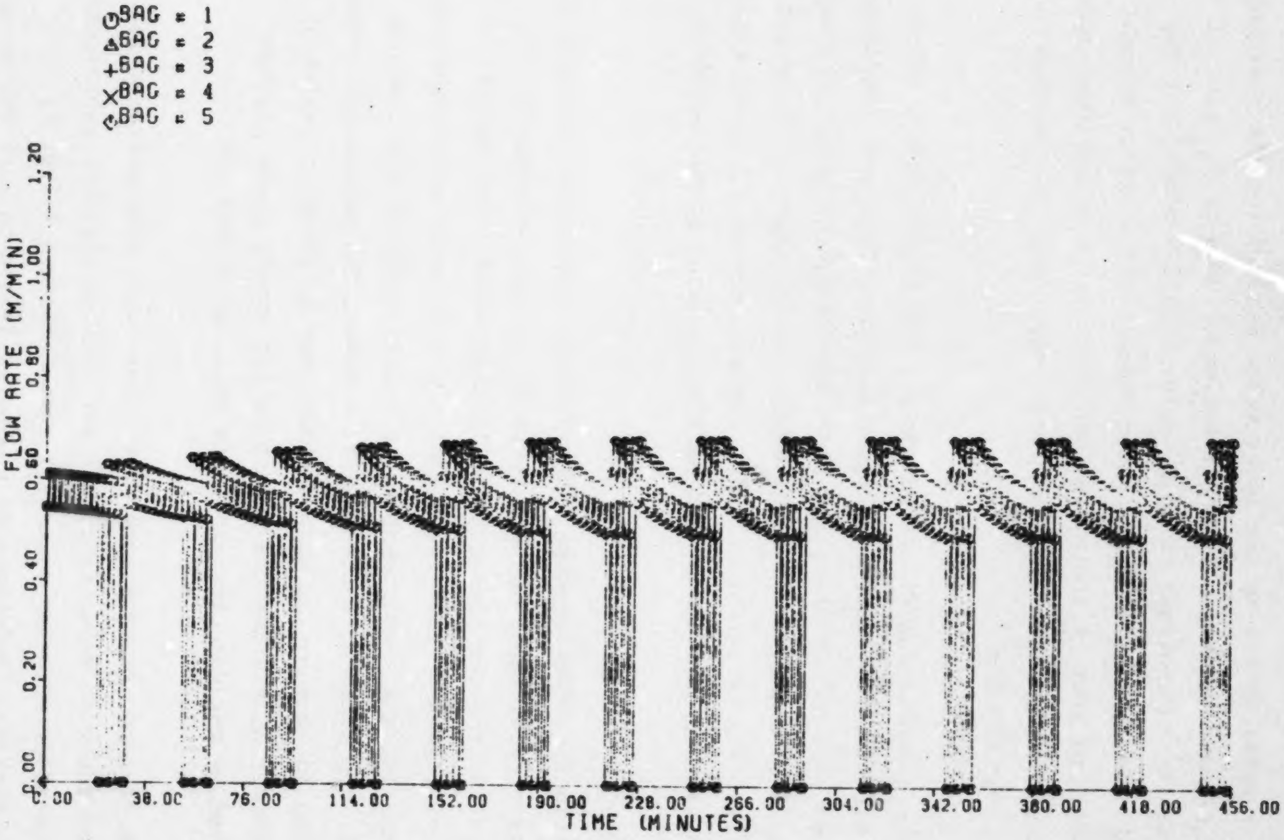

Figure 136. Test run No. 0422 Sunbury baghouse simulation - linear individual flow rate graph

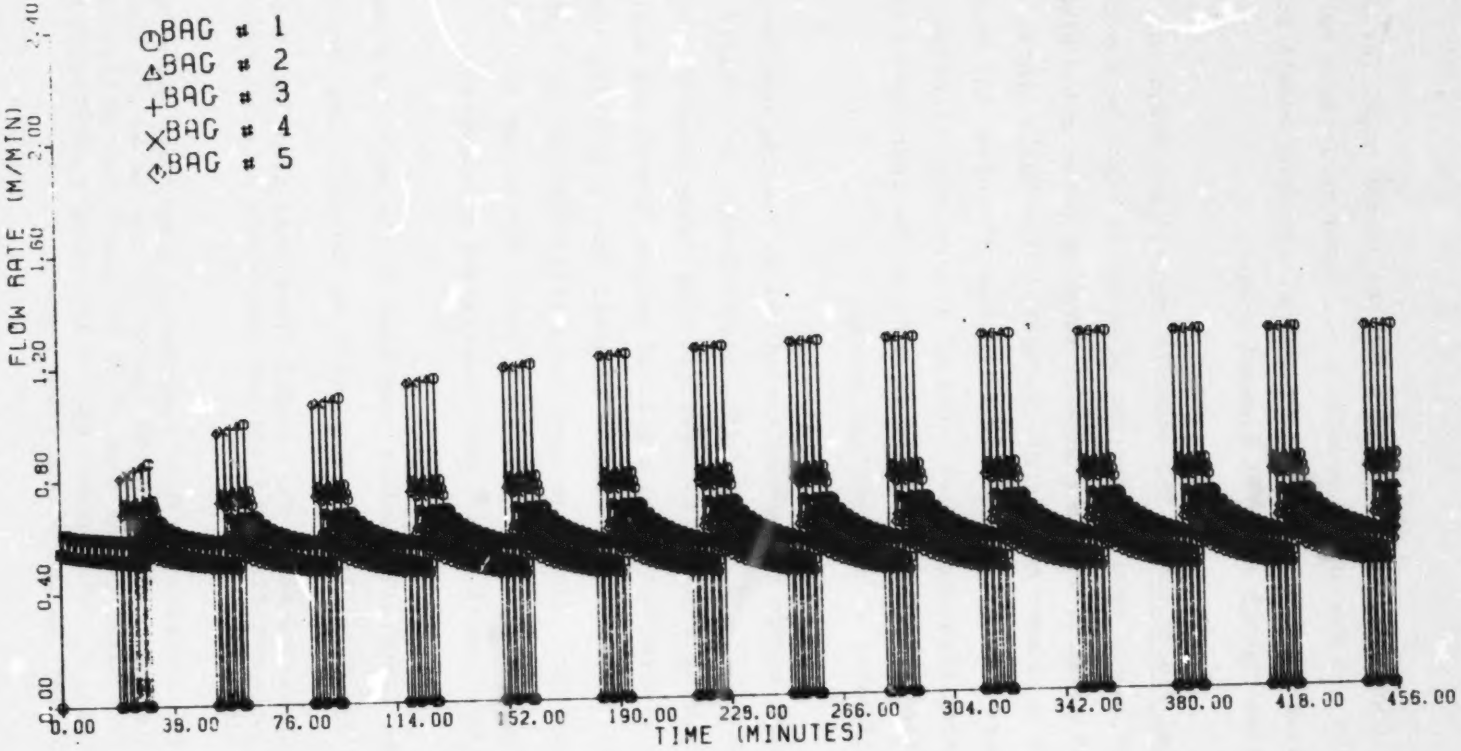

Figure 137. Test run No. 0422 Sunbury baghouse simulation - nonlinear individual flow rate graph

covers a greater range than that for the linear model for the same reason given for the resistance models; i.e., lower resistance during the early filtration phase (or nonlinear region of the drag model) leads to higher velocities through the just cleaned areas.

Predicted Penetration - The velocity variations described previously have a direct impact upon penetration behavior as might be expected, Figures 138 and 139, with the greater range in penetration also associated with the nonlinear model. In contrast to the Nucla operations in which there were lengthy time intervals between cleaning, the back-to-back compartment cleaning cycles leads to a constantly changing effluent concentration whose average value at any time is represented approximately by the midpoint of the envelope curves.

The average steady state penetration values for the nonlinear and linear models are 0.27 and 0.20 percent, respectively, as compared to an actual field value of 0.06 for the specific test being modeled. Again, the difference between the two predicted values (linear and nonlinear models) is attributed to the difference in local face velocities immediately after cleaning. Since the local velocities through the just cleaned areas as predicted by the nonlinear model are higher than those predicted by the linear model, the higher penetration is expected.

The higher penetration values predicted by the model as compared to the observed field results are attributed to the following factors:

1. The estimate of the cleaned fractional area, a_c, based upon interpretation of field and laboratory data may be on the high side.
2. The estimates of dust penetration properties based upon fabric surfaces cleaned in the laboratory may be on the high side. Such might be the case if field levels for residual dust holdings, W_R, were higher due to increased interstitial deposition of dust in the bulked fiber region.

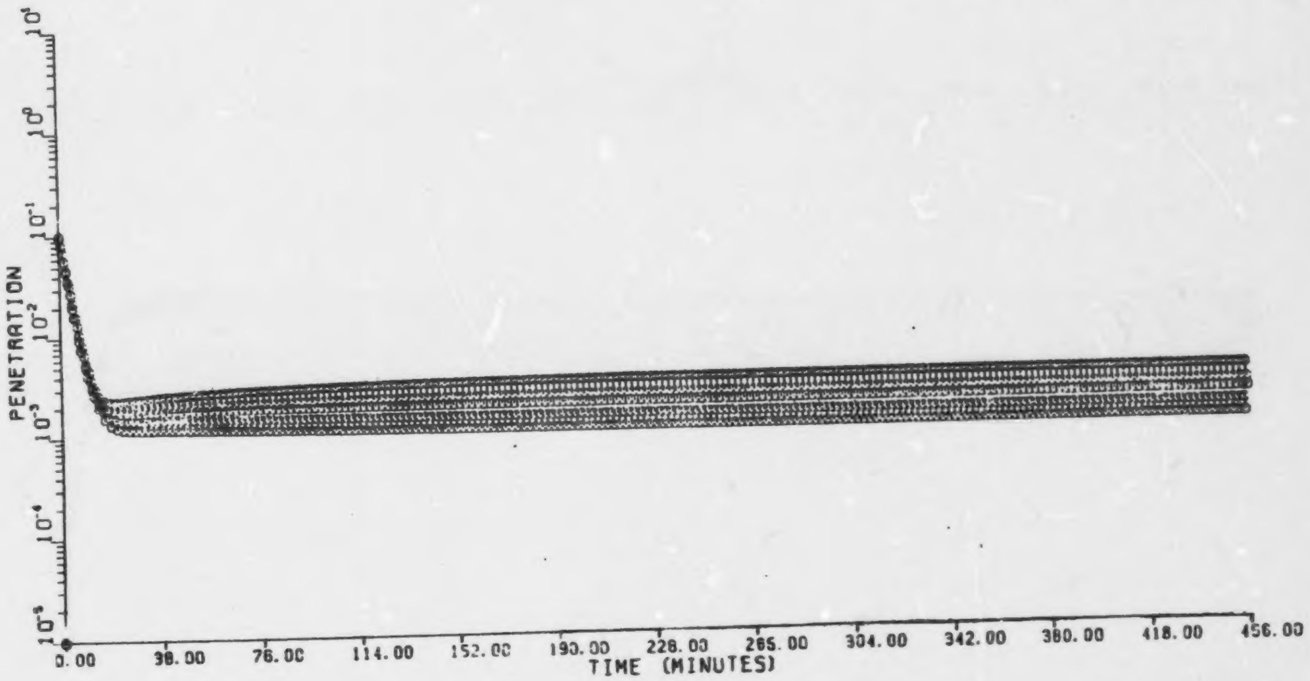

Figure 138. Test run No. 0422 Sunbury baghouse simulation - linear penetration versus time graph

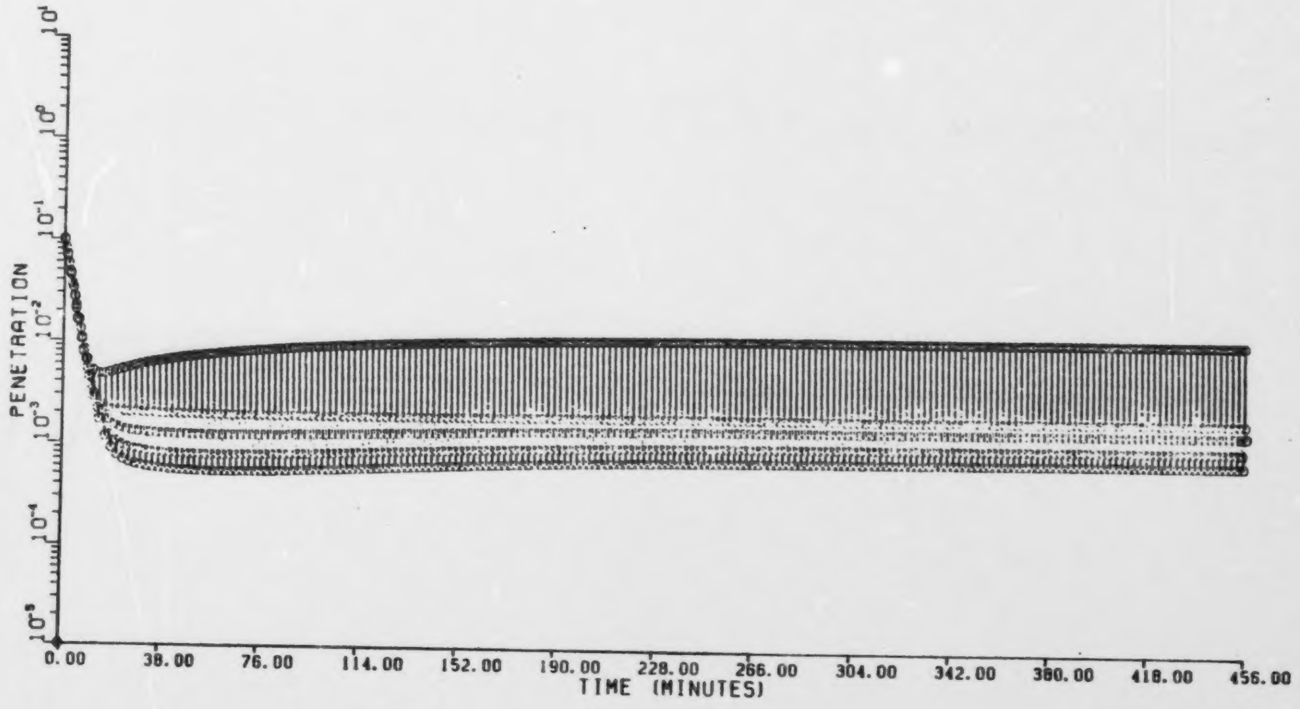

Figure 139. Test run No. 0422 Sunbury baghouse simulation - nonlinear penetration versus time graph

3. The field data relate to a test with fabric bags that have seen over 2 years' service.

Despite the fact that data are limited, inspection of Table 11A, Section VI, indicates that the dust penetration levels for recently installed Sunbury bags showed significantly higher penetrations than those that had seen over 2 years' field service. The same trend was also exhibited for particle concentrations over the same time span, Figure 41, Section VI.

Excerpted data from Table 11A provide an improved picture of the predictive potential of the new model. If one considers that the mathematical relationships developed within this study for calculating dust penetration were based upon tests with new fabric panels (generally less than 24 hours total use) the agreement between the linear model predictions and actual field observations is reasonable and safely conservative with respect to the nonlinear model, Table 64.

Table 64. COMPARISON OF OBSERVED AND PREDICTED FLY ASH PENETRATION VALUE, SUNBURY INSTALLATION

			Percent penetration		
				Predicted	
Runs[a]	Time period	Bag service life[b]	Measured[b]	Linear model	Nonlinear model
22,23,24	3/20/75 to 3/22/75	1.5 days	0.15	0.20	0.27
25,26,27	3/23/75 to 3/25/75	4.5 days	0.11	-	-
28,29,30,31	3/26/75 to 3/29/75	7.5 days	0.09	-	-
1 through 21	1/08/75 to 2/14/75	>2 years	0.07	-	-

[a] See Table 16, Section VI, and Table 1, Reference 9.

[b] Average values for indicated time frame.

SUMMARY OF MODEL HIGHLIGHTS AND DIRECTION FOR FUTURE WORK

The mathematical model developed within this study represents a new and very effective technique for predicting the average and instantaneous values for resistance and emission characteristics during the filtration of coal fly ash with woven glass fabrics.

Two basic concepts used in the model design: (1) the quantitative description of the filtration properties of partially cleaned fabric surfaces and (2) the correct description of effluent particle size properties for fabrics in which direct pore or pinhole penetration constitutes the major source of emission, have played important roles in structuring the predictive equations.

A third key factor in the model development was the formulation of explicit functions to describe quantitatively the cleaning process in terms of the method, intensity and frequency of cleaning. By cleaning we refer specifically to the amount of dust removed during the cleaning of any one compartment and the effect of its removal on filter resistance and penetration characteristics.

The derivation of two supporting mathematical functions based upon laboratory and field experiments provided improved definition of the specific resistance coefficient, K_2, for use in the modeling equation. The first function describes K_2 in terms of a specific surface parameter, S_o, that relates to the typical polydisperse particle size distributions encountered in the field. The second relationship takes into account, as others have also indicated, that K_2 should be expressed as an increasing function of face velocity.

Limited information on long-term filter service, ~2 years, suggests that woven glass fabrics now used for coal fly ash filtration will exhibit a gradual increase in drag in the range of 125 N-min/m^3 per year (0.15 in.

H_2O/ft/min per year). Penetration characteristics under the above conditions show a slight tendency to improve once preliminary fabric conditioning takes place.

The success of the model, based upon limited field confirmations summarized in Table 65, dictates very strongly that it be further evaluated. In that the required data inputs have been identified, it is believed that a field oriented program with limited laboratory back-up would satisfy the final validation needs. Minor changes in existing compliance type sampling methods and apparatus should provide the key data for resistance fabric loading relationships that are fundamental to the application of the model. Additionally, such measurements should help to confirm the present observation that electrical charge and/or humidity factors do not play an important role in fly ash filtration with glass fabrics.

Extending the above program to other dust/fabric combinations will provide a rational basis for treating heretofore unresolved problems in many field filtration applications.

Table 65. SUMMARY TABLE SHOWING MEASURED AND PREDICTED VALUE FOR FILTER SYSTEM PENETRATION AND RESISTANCE, COAL FLY ASH FILTRATION WITH WOVEN GLASS FABRICS

PENETRATION

Data source				Percent penetration				
				Measured[a]	Predicted			
					Linear model		Nonlinear model	
Test case	Description	Testing period	Bag service life	Average[b]	Average	Cleaning[c]	Average	Cleaning
A	Nucla, CO Table 11B, Run No. 1	9/21/74	6 months	0.21	0.19	1.52	-	-
B	Sunbury, PA Table 11A, Run No. 1	1/08/75	2 years	0.06	0.20	-	0.27	-
C	Table 11A, Runs 22, 23, 24	3/20/75 to 3/22/75	1.5 days	0.15	0.20	-	0.27	-

RESISTANCE

	Measured				Predicted				Predicted			
					Linear model				Nonlinear model			
Test case	Average	Maximum cleaning	Maximum	Minimum	Average	Maximum cleaning	Maximum	Minimum	Average	Maximum cleaning	Maximum	Minimum
A	1030	1700	1160[d]	850[d]	972	1521	1160[d]	720[d]	-	-	-	-
B	635	710	710[e]	560[e]	620	663	663[e]	567[e]	560	609	609[e]	489[e]

[a] Based on field measurements. See references 8 and 9.

[b] All values listed as average depict overall system performance (penetration and resistance) for combined cleaning and filtering cycles.

[c] All values listed under cleaning describe performance parameter during cleaning only.

[d] Maximum-minimum with Nucla tests indicate resistance immediately before and after cleaning.

[e] Maximum-minimum with Sunbury tests indicate values for envelope curve.

REFERENCES

1. Billings, C. E. and J. E. Wilder. Handbook of Fabric Filter Technology, Volume I, Fabric Filter Systems Study: GCA/Technology Division. EPA No. APTD 0690 (NTIS No. PB-200-648). December 1970.

2. Symposium on the Use of Fabric Filters for the Control of Submicron Particulates - April 8-10, 1974, Boston, Massachusetts. Proceedings published in JAPCA, December 1974. 1140-1197 pp. See also: EPA-650/2-74-043 (NTIS No. PB237-629/AS). May 1974.

3. Draemel, D. C. Relationship Between Fabric Structure and Filtration Performance in Dust Filtration. Control Systems Laboratory. U.S. Environmental Protection Agency, Research Triangle Park, N.C. Report Number EPA-R2-73-288 (NTIS No. PB222-237). July 1973.

4. Turner, J. H. Performance of Nonwoven Nylong Filter Bags. EPA-600/2-76-168a (NTIS No. PB 266-271/AS). December 1976.

5. Harris, D. B. and D. C. Drehmel. Fractional Effluency of Metal Fume Control as Determined by Brink Impactor. (Presented at the 66th Annual APCA Meeting. Chicago. June 1973).

6. McKenna, J. D. Applying Fabric Filtration to Coal-Fired Industrial Boilers. Enviro-Systems and Research, Inc. Roanoke, Va. Control Systems Laboratory, U.S. Environmental Protection Agency, Research Triangle Park, N.C. Report No. EPA-650/2-74-058 (NTIS No. PB237-117/AS). July 1974.

7. Hall, R. R. and R. Dennis. Mobile Fabric Filter System. Design and Field Test Results. GCA/Technology Division, Bedford, Mass. Control Systems Laboratory, U.S. Environmental Protection Agency, Research Triangel Park, N.C. Report No. EPA-650/2-75-059 (NTIS No. PB246-287/AS). July 1975.

8. Bradway, R. M. and R. W. Cass. Fractional Efficiency of a Utility Boiler Baghouse - Nucla Generating Plant. GCA/Technology Division, Bedford, Mass. Control Systems Laboratory, U.S. Environmental Protection Agency, Research Triangle Park, N.C. Report No. EPA-600/12-75-013a (NTIS No. PB246-641/AS). August 1975.

9. Cass, R. W. and R. M. Bradway. Fractional Efficiency of a Utility Boiler Baghouse: Sunbury Steam-Electric Station. GCA/Technology Division, Bedford, Massachusetts. Control Systems, Laboratory, U.S. Environmental Protection Agency, Research Triangle Park, N.C. Report No. EPA-600/2-76-077a (NTIS No. PB253-943/AS). March 1976.

10. Dennis, R. and J. E. Wilder. Fabric Filter Cleaning Studies. GCA/Technology Division, Bedford, Mass. Control Systems Laboratory, Research Triangle Park, N.C. Report No. EPA-650/2-75-009. January 1975.

11. Jorgensen, R., (ed.). Fan Engineering, 7th Edition. Buffalo, N.Y., Buffalo Forge Co., 1970. 729 p.

12. Snyder, C. A. and R. T. Pring. Design Considerations in Filtration of Hot Gases. Ind Eng Chem Process Des Dev. 47:960. 1955.

13. Robinson, J. W., R. E. Harrington, and P. W. Spaite. A New Method for Analysis of Multicompartment Fabric Filtration. Atmos Environ. 1:499-508, 1967.

14. Spaite, P. W., G. W. Walsh. Effect of Fabric Structure on Filter Performance. Amer Ind Hyg Assoc J. 24:357-365. 1963.

15. Solbach, W. Derivation of a Computational Method for Multichamber Cloth Filters on the Basis of Experimental Results. Staub (English). 29(1):28-33, 1969.

16. Noll, K. E., W. T. Davis, S. P. Shelton. New Criteria for the Selection of Fabric Filters for Industrial Application. (Presented at 66th Annual APCA Meeting. Chicago. 1973.)

17. Williams, C. E., T. Hatch, L. Greenberg. Determination of Cloth Area for In-ustrial Air Filters. Heat/Piping/Air Cond. 12:259-263, April 1940.

18. Durham, J. R. Filtration Characteristics of Fabric Filter Media. U.S. Department of Health, Education and Welfare, Public Health Service, National Air Pollution Control Administration. Interim Report. 1969.

19. Anonymous. Dust Collection With Fabrics of Nomex Aramid Fiber. DuPont Corp., Textile Fiber Department. Information Memo No. 336. 1974.

20. Noll, K. E., W. T. Davis, P. J. LaRosa. The Generation and Evaluation of Fabric Filter Performance Curves from Pilot Plant Data. (Presented at 68th Annual APCA Meeting. Boston. 1975.)

21. LaRosa, P. J. Private Communication. 1975.

22. Stinessen, K. O. The Filter Simulator - A Research Backed Method for Filter Fabric Evaluation. (Original source uncertain. Personal Communication, 1976.)

23. Fraser, D. and G. J. Foley. A Predictive Performance Model for Fabric Filter Systems. I. Intermittently Cleaned Single-Compartment Systems. (Presented at 67th Annual APCA Meeting. Denver. 1974.)

24. Leith, D. and M. W. First. Particle Collection by Pulse-Jet Fabric Filter. (Presented at 68th Annual APCA Meeting. Boston. 1975.)

25. Dill, R. S. A Test Method for Air Filters. Trans ASHVE. 44:379.

26. Butterworth, G. A. M. and M. Platt. Filter Fabric Selection and Design: Consideration of Air Permeability and Fiber Characteristics. Fabric Research Laboratories, Inc. Dedham, Mass. (Presented at EPA Fabric Filter Symposium. Charleston, S.C. March 1971).

27. Pedersen, G. C. Fluid Flow Through Monofilament Fabrics. Filtration and Separation. 11(5):586. 1974.

28. Zimon, A. D. Adhesion of Dust and Powder, p. 112. Plenum Press, New York. 1969.

29. Fuchs, N. A. The Mechanism of Aerosols. The MacMillan Company, New York. 1964.

30. Dennis, R. (Ed.) Handbook on Aerosols. U.S. Energy and Development Corporation. TID-26608, NTIS, Springfield, Va. 1976.

31. Dennis, R. Collection Efficiency as a Function of Particle Size, Shape and Density: Theory and Experience. JAPCA. 24(12)1156. December 1974.

32. Borgwardt, R. H. and J. F. Durham. Factors Affecting the Performance of Fabric Filters. (Presented at 60th Annual Meeting of the American Institute of Chemical Engineers. New York. 1967.)

33. Dalla Valle, J. M. Micromeritics. Second edition. Pitman Publishing Corp. New York. 1948.

34. Löffler, F. Investigating Adhesive Forces Between Solid Particles and Fiber Surfaces, Staub, (English Translation), 26, 10. June 1966.

35. Löffler, F. The Adhesion of Dust Particles to Fibrous and Particulate Surface, Staub, (English Translation), 28, 32. November 1968.

36. Boehme, G., et al. Adhesion Measurements Involving Small Particles, Trans Instr Chem Engrs., London. 40, 252. 1962.

37. Corn, M. The Adhesion of Solid Particles to Solid Surfaces, 11. J Air Pol Cont Assoc., 11, 566. 1961.

38. Corn, M. The Adhesion of Solid Particles to Solid Surfaces, 1. A Review, J Air Pol Contr Assoc., 11, 523. 1961.

APPENDIX A

EFFECT OF SEQUENTIAL PORE CLOSURE ON SHAPE OF RESISTANCE VERSUS FABRIC LOADING CURVE

Asssume that a sequential pore bridging or closure process follows an exponential decay pattern in which the rate of pore closure, - dN/dt, at any time is proportional to the number of remaining open pores, N.

$$dN/dt = -kN \qquad (98)$$

If the bridging process is instantaneous, the total pore area, at any time, t, determines the instantaneous pore velocity for a constant volume flow rate, Q, i.e.;

$$V = Q/N A_p$$

where A_p is the individual pore cross section.

Since the number of open pores, N, at any time also determines the total pore area, the integration of Equation (98) following substitution of $N A_p$ for N leads to the expression

$$N A_p = (N A_p)_o \exp(-kt) \qquad (99)$$

or alternately as

$$V = Q/(A'_p)_o \exp(kt)$$

where A'_p refers to total pore area.

If the pore area and depth for the open pores remain unchanged and laminar flow persists, the instantaneous resistance, P, will then depend only on the instantaneous velocity, i.e.;

$$P = f(V) = Q/(A'_p)_o \exp (kt) \qquad (100)$$

If both volume flow rate and inlet dust concentration are assumed to be constant, the dust loading, W, upon the fabric is at all times proportional to the filter operating time. Hence, Equation (100) in derivative form appears as

$$dP/dW = k\, Q/(A'_p)_o \exp (kW) \qquad (101)$$

in which the slope is always increasing.

APPENDIX B

INPUT PARAMETERS FOR ESTIMATING FIBER EFFICIENCY IN SUBSTRATE LAYER

In the following section, the rationale for the input parameter values given in Table 44 is presented in more detail.

- Given a fabric areal density of 312 g/m^2 and a nominal fabric thickness of 0.04 cm (400 μm), the fabric bulk density is 0.78 g/cm^3.

- Assuming the glass fiber density to be 2.2 g/cm^3, the porosity of the fabric becomes

  $$\epsilon = 1 - \beta = 1 - 0.78/2.2 = 0.646$$

- Because 25 percent of the pores are lost in both the warp and fill directions due to yarn contact, the effective pore volume is reduced roughly by a factor of 2.

  $$(0.646)(0.5) = 0.323$$

- If 10 percent of the total fabric weight is assumed to be distributed within the effective pore volume, 0.323 cm^3 per cm^3 of fabric, the following estimate of the fiber volume fraction in the filter is made:

  $$(0.78\ g/cm^3)\ 0.1/0.323 = 0.241\ g/cm^3\ \text{(bulk density)}$$

  $$\beta = 0.241/2.2 = 0.11$$
  $$\epsilon = 1 - \beta = 0.89$$

- Based upon microscopic examination of the fabric structure, the yarn shape and the fabric thickness, the minimum pore dimension appeared to be about 100 μm as shown in Figures 28 and 30. Examination of Figure 140 (an excerpted section of Figure 28 with added dimensional notations) indicates that the dimension characterizing average pore cross section at the surface of the fiber substrate is roughly 0.67 times that of the superficial dimension. In conjunction with the adjustment for corrected porosity, the average gas velocity within the substrate will be approximately 6.3 times greater than the superficial value, i.e.;

$$(1.01/0.363)(1.5)^2 = 6.3$$

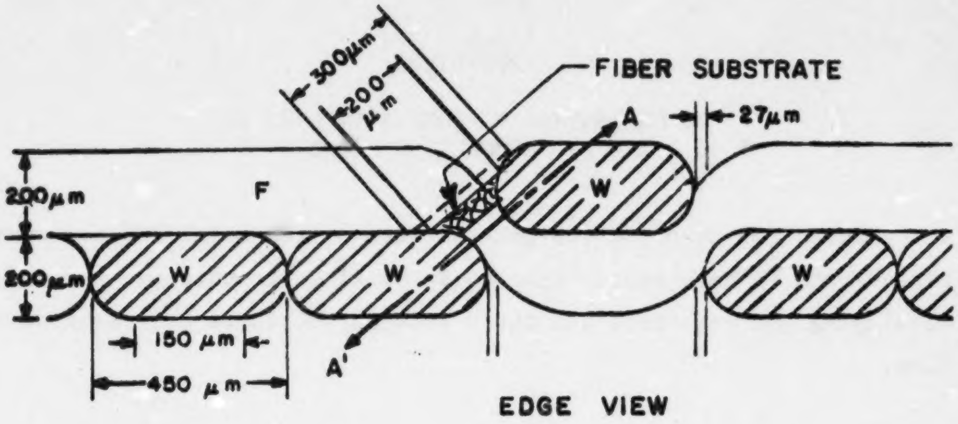

Figure 140. Estimation of pore cross section in fiber substrate region

According to a previous analysis of fabric structure, Figure 9, the dimension characterizing the surface of the substrate was also assumed to be 0.67 times that of the superficial layer. In the former instance, it was shown that the development of a dust layer starting at the substrate surface and continuing until the superficial fabric surface was reached, provided a rational explanation for the curvalinear filtration range for drag versus loading curves. Hence, the estimated gas velocity of 6.3 cm/sec at the surface of the fiber substrate appears as a reasonable value.

APPENDIX C

DETERMINATION OF CONSTANTS USED IN DUST PENETRATION MODEL

The reasons for choosing the general form of the model and the constraints placed upon it have been discussed in Section X. Only the mechanics of developing the equations and their related constants will be discussed here.

The general form chosen to model dust penetration was:

$$Pn = Pn_s + (Pn_o - Pn_s) \exp(-aW') \tag{102}$$

where Pn = actual penetration

Pn_s = steady-state penetration

Pn_o = penetration at $W = W_R$ (residual loading or $W' = 0$)

W' = absolute cake loading, W, minus the residual, W_R

$-a$ = initial slope of the penetration versus loading curves

The original outlet concentration versus loading curves obtained from the bench scale tests were first replotted as penetration versus fabric loading, see Figure 141. Penetration here is defined as the outlet concentration minus the residual concentration, 0.5 mg/m^3, divided by the inlet concentration:

$$Pn = \frac{C_o - C_s}{C_i} \tag{103}$$

Steady-state penetration values were determined at the points where the curves assumed nearly horizontal paths. Extrapolation of the curves in

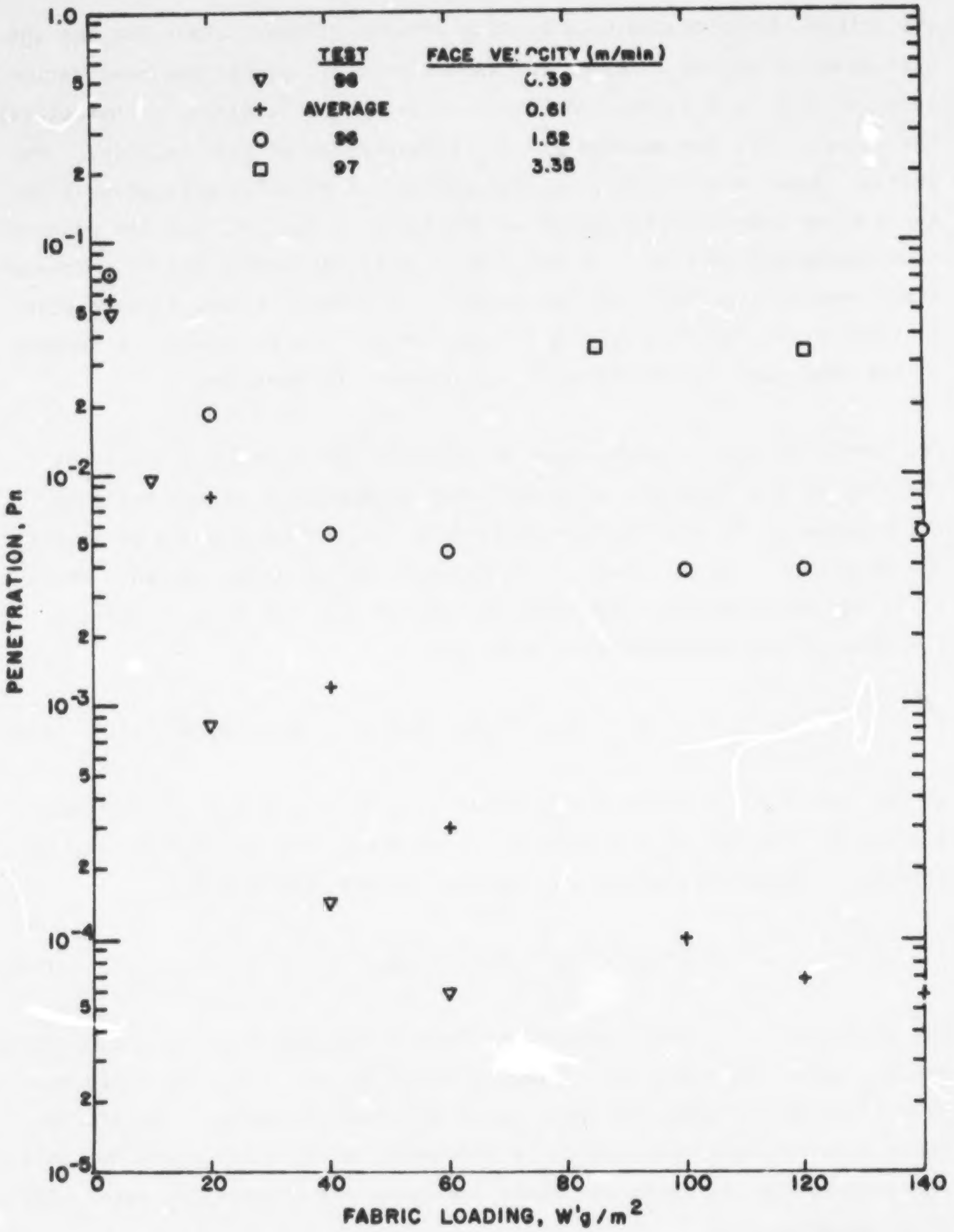

Figure 141. Penetration versus loading for bench scale tests

the initial decay region to a loading of zero yielded values for the initial penetration, Pn_o. Since Pn_o values were all within the penetration range of 0.09 to 0.11 for velocities of 0.39 to 1.52 m/min, a characteristic value of 0.1 was assumed for Pn_o irrespective of face velocity. The initial slope of the curve, -a, was determined by solving Equation (102) for a after substituting proper values for Pn_o, Pn_s, W', and the penetration corresponding to W'. A value of 20 g/m^2 was chosen for W'. Steady-state penetration, Pn_s, and the negative of initial slope, a, were then plotted versus velocity in Figures 142 and 143, respectively. A summary of the data used in the analysis is presented in Table 66.

The choice of the equations used to describe the curves was arbitrary. The plot of the logarithm of steady-state penetration versus velocity curve appeared to have the same form as a drag versus loading curve with one exception. Since steady-state penetration can never exceed a value of 1, any mathematical relationships must account for this constraint. The form of the nonlinear drag model is:

$$S = S_R + K_2 W' + (K_R - K_2)W^* \exp (1 - \exp - W'/W^* \qquad (28)$$

If the term K_2W' is dropped from Equation (28), the curve will actually level off. Therefore, the form of the equation used to describe the relationship between steady-state penetration and velocity was

$$\ln (Pn_s) = \ln X + Y (1 - \exp \; -V/Z) \qquad (104)$$

The constants X, Y, and Z were determined by substituting the actual values for Pn_s and V for three velocities, 0.61, 1.52, and 3.35 m/min into Equation (104) and solving the three equations simultaneously. The steady-state penetration corresponding to a velocity of 0.39 m/min was not used for determining the constants since its value was essentially zero. The final equation is:

$$Pn_s = 1.5 \times 10^{-7} \exp \left\{ 12.7 \left[1 - \exp (-1.03 \, V) \right] \right\} \qquad (105)$$

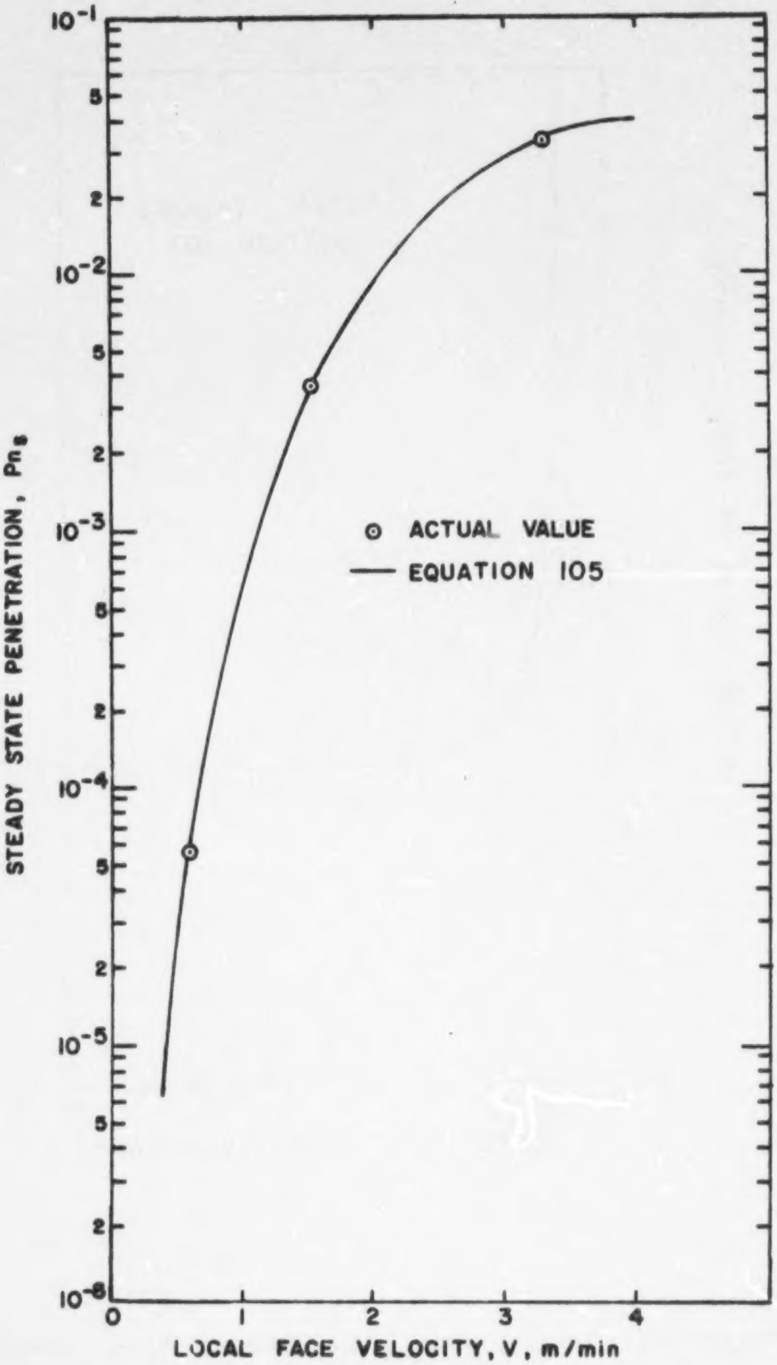

Figure 142. Steady state penetration as a function of velocity

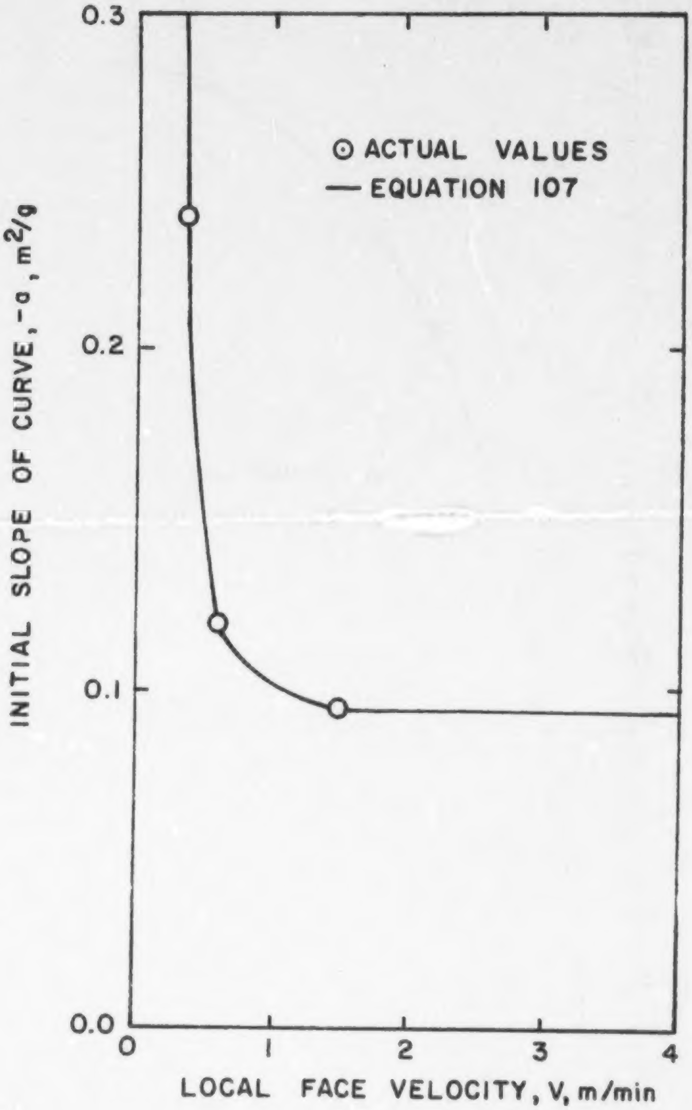

Figure 143. Initial slope of penetration versus loading curve as a function of velocity

Table 66. DATA USED TO DETERMINE CONSTANTS IN DUST PENETRATION MODEL

Test	98	Average[a]	96	97
Face velocity, V, m/min	0.4	0.61	1.52	3.35
Inlet concentration, C_o, g/m^3	8.09	7.01	5.37	4.60
Steady-state penetration, Pn_s	0	$5.7x10^{-5}$	$3.6x10^{-3}$	$3.25x10^{-2}$
Pn at $W' = 20\ g/m^2$	$8.3x10^{-4}$	$8.5x10^{-3}$	$1.9x10^{-2}$	-
a	0.24	0.125	0.094	-
Pn_o	0.11	0.087	0.098	-

[a] Average for test numbers 65, 68, 69, 70, and 99.

The equation that describes the relationship between the initial slope, -a, and velocity was determined in the same manner except that the form of the equation chosen was:

$$a = r/V_s + t \qquad (106)$$

The constants r, s, and t were determined by substituting values of a and V for velocities of 0.39, 0.61, and 1.52 m/min into Equation (106) and solving the three resultant equations simultaneously. Insufficient data were available to determine the variation in penetration with loading at low loadings for the highest velocity and, therefore, a slope was not determined for that test. The resultant equation for the slope is:

$$a = 3.59 \times 10^{-3}/V^4 + 0.094 \ (g/m^2)^{-1} \qquad (107)$$

where V is in m/min.

Equation 107 and the actual slopes for the three velocities are plotted in Figure 143.

APPENDIX D

BAGHOUSE COMPUTER PROGRAM DESCRIPTION

SPECIFICATION OF OPERATING TIMES FOR BAGHOUSE COMPUTER PROGRAM

The pressure drop versus time curve for a three compartment system shown in Figure 144 will be used here to illustrate the various times associated with cleaning and filtering cycles in the program. Vertical (step) increases and decreases in pressure drop represent compartments being removed from service and returned to service, respectively. A complete cycle is represented by the cleaning cycle and the period when all compartments are filtering, the latter designated as total area run time. The cleaning cycle in this example is composed of three individual compartment cleaning cycles. Each cycle consists of one period where all compartments are filtering between individual compartment cleanings and a second period where one compartment is taken off-line for cleaning. The time increment used in the program is determined from the individual compartment cleaning cycle time and the number of increments per compartment specified in the input data. Thus, if five increments are specified, an individual compartment cleaning cycle is split up into five equal time increments.

Required inputs, regardless of the type of cycle employed, are (1) the cleaning cycle time, (2) the individual compartment cleaning time, and (3) the number of time increments desired per individual compartment cleaning cycle. These three values will define the cleaning cycle.

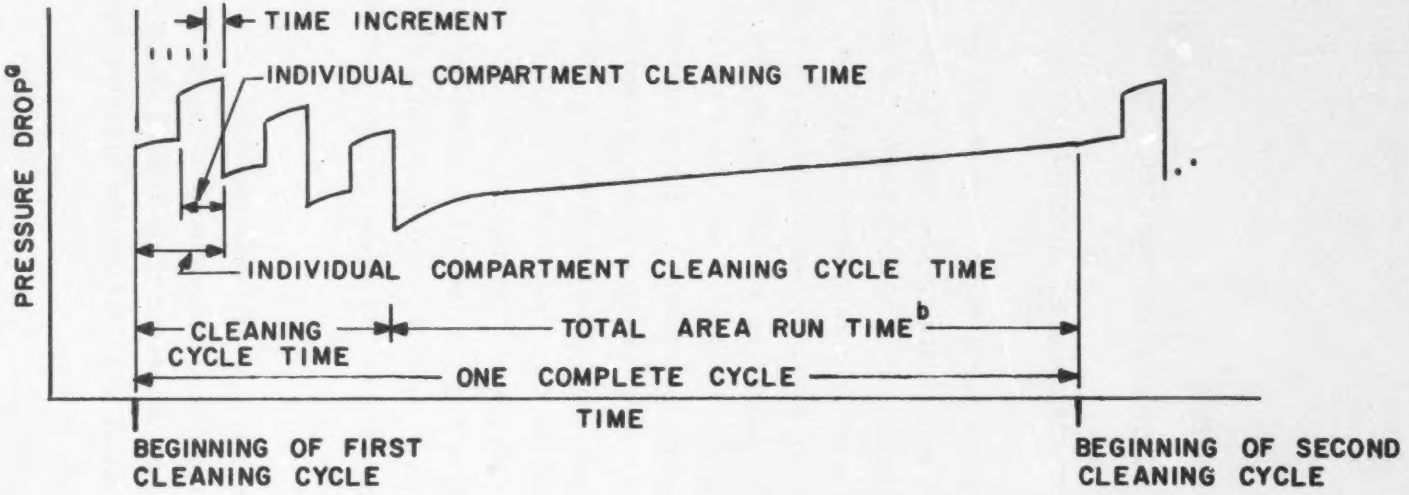
TIME INCREMENT
INDIVIDUAL COMPARTMENT CLEANING TIME
PRESSURE DROP[a]
INDIVIDUAL COMPARTMENT CLEANING CYCLE TIME
CLEANING CYCLE TIME
TOTAL AREA RUN TIME[b]
ONE COMPLETE CYCLE
TIME
BEGINNING OF FIRST CLEANING CYCLE
BEGINNING OF SECOND CLEANING CYCLE

NOTES:

[a] VERTICAL INCREASES AND DECREASES INDICATE A COMPARTMENT BEING TAKEN OFF OR PUT ON LINE, RESPECTIVELY.

[b] ALL COMPARTMENTS ON LINE. FOR TIMED CLEANING CYCLE INITIATION, THIS MUST BE INPUT. FOR A PRESSURE INITIATED CLEANING CYCLE, THIS VALUE IS INDETERMINATE. FOR CONTINOUS CLEANING CYCLES, THIS VALUE IS ZERO.

[c] EXAMPLE OF A THREE COMPARTMENT SYSTEM.

Figure 144. Description of time specifications for baghouse computer program[c]

How the cleaning cycle is initiated is determined by the total area run time and the maximum pressure drop specification, see Table 67. If cleaning is to be continuous (i.e., back-to-back cleaning cycles), total area run time and maximum pressure drop should be specified as zero. If the cleaning cycles is to be initiated on a time basis, a value should be input for the total area run time and the maximum pressure drop should be specified as zero. For pressure-controlled cleaning cycles, the maximum pressure drop should be specified and a value of zero should be entered for the total area run time.

Table 67. INPUT SPECIFICATIONS FOR VARIOUS TYPES OF CLEANING CYCLES

Type of cleaning cycle initiation	Maximum pressure drop	Total area run time
Continuous	zero	zero
Time	zero	Specify value
Pressure drop	Specify value	zero

PROGRAM DESCRIPTION

A listing of the baghouse computer program is presented in Table 68. The variables and arrays used within the program and their definitions are given in Table 69. Finally, the format for input data is shown in Table 70.

Table 68. BAGHOUSE SIMULATION PROGRAM LISTING

```
//*  BAGHUUSE PROGRAM  IHM 370 WITH CALCOMP PLOTTER
//*  1976 GCA TECHNOLOGY    ROGER STERN - DOUG COOPER
//*   BAGHOUSE SIMULATION PROGRAM- IHM 370- ZETA PLOTTER
//*   1977 GCA TECHNOLOGY DIVISION  HANS KLEMM- RICHARD DENNIS
// EXEC FORTG1CG,ACCT=COST,PARM.GO='SIZE=175K'
//FORT.SYSIN DD *

      CALL MODEL
  100 DO 500 I=8,15
      END FILE I
  500 REWIND I
      CALL SCRIBE
      STOP
      END


      SUBROUTINE CAKDRG(SZERO,WDEL,WR,WSTAR,ZKZERO,ZK2,VEL,CDRAG)
C           SUBROUTINE OF BAGHOUSE  4/77/HAK-RD GCA TECHNOLOGY  DIVISION
C-CALCULATES CAKE DRAG
C-ZK2=SPECIFIC CAKE RESISTANCE OF CAKE AT 0.61 M/MIN, N-MIN/G-M
C-WDEL=TOTAL FABRIC LOADING ON AN AREA OF FABRIC, G/M2
C-WR=RESIDUAL FABRIC LOADING ON AN AREA OF FABRIC, G/M2
C-WSTAR= CONSTANT CHARACTERISTIC OF DUST AND FABRIC, G/M2
C-ZKZERO= INITIAL SLOPE OF DRAG VS. LOADING CURVE, N-MIN/G-M
C-VEL=VELOCITY,M/MIN
C-CDRAG=CAKE DRAG,S,  N-MIN/M3
      ZK2V=ZK2*SQRT(VEL*3.281/2.)
      IF(WSTAR.GT.1.E-20) GO TO 10
C-LINEAR MODEL
      CDRAG=ZK2V*WDEL
      GO TO 20
   10 WPRIME=WDEL-WR
      EXPO=-WPRIME/WSTAR
      IF(EXPO.LT.-30.) EXPO=-30.
C-NON-LINEAR MODEL
      CDRAG=ZK2V*WPRIME+(ZKZERO-ZK2V)*WSTAR*(1.-EXP(EXPO))
   20 RETURN
      END


      SUBROUTINE PENET(CZERO,WEIGHT,VEL,WR,PEN)
C           SUBROUTINE OF BAGHOUSE  4/77/HAK-RD GCA TECHNOLOGY  DIVISION
C-CALCULATES TOTAL PENETRATION
C-CZERO=INLET CONCENTRATION, G/M3
C-WEIGHT=TOTAL FABRIC LOADING ON AN AREA OF FABRIC, G/M2
C-VEL=VELOCITY, M/MIN
C-WR=RESIDUAL FABRIC LOADING ON AN AREA OF FABRIC, G/M2
C-PEN=PENETRATION
      CS=0.0005
      A=400.
      IF(VEL.GT.1.E-9) A=0.416/(VEL*3.281)**4+0.094
      IF(VEL.LT.1.E-9) VEL=0.0
      XF=1.5E-7
      IF(VEL.GT.1.E-9) XF=1.5E-7*EXP(12.7*(1.-EXP(-VEL/3.2*3.281)))
      EXPO=(WEIGHT-WR)*A
      PEN=0.0
      IF(EXPO.LT.40.) PEN=(0.1-XF)*EXP(-EXPO)
      PEN=PEN+XF+CS/CZERO
      RETURN
      END
```

Reproduced from
best available copy.

Table 68 (continued). BAGHOUSE SIMULATION PROGRAM LISTING

```
      SUBROUTINE MODEL
C           SUBHOUTINE OF BAGHOUSE 12/1/RWS-DC GCA TECHNOLOGY  DIVISION
C           SUBROUTINE OF BAGHOUSE  4/77/HAK-RD GCA TECHNOLOGY  DIVISION
C-MAIN DRIVER SUBPROGRAM
C-ALL T'S ARE TIMES,MIN
C-ALL W'S ARE CAKE LOADINGS,G/M2
C-ALL S'S ARF DRAGS,N-MIN/M3
C-ALL P'S ARE PENETRATIUNS
C-ALL C'S ARE CONCENTRATIONS
C-A BAG IS A COMPARTMENT
C-ZK2=SPECIFIC CAKE RESISTANCE OF CAKE AT 0.61 M/MIN, N-MIN/G-M
C-WR=RESIDUAL FABRIC LOADING ON AN AREA OF FABRIC, G/M2
C-WSTAR= CONSTANT CHARACTERISTIC OF DUST AND FABRIC, G/M2
C-ZKZERO= INITIAL SLOPE OF DRAG VS. LOADING CURVE, N-MIN/G-M
C-SZERO=RESIDUAL DRAG, N-MIN/M3
C-TEMPK=GAS TEMPERATURE,DEGRESS KELVIN
C-ACAKE=CAKED AREA,THAT PORTION OF A BAG WHICH IS NOT CLEANED
C-ZK2MU=VISCOSITY CORRECTION FOR SPECIFIC CAKE RESISTANCE
C-N=NUMBER OF COMPARTMENTS OR BAGS
C-T=CLEANING CYCLE TIME,MIN
C-NT=TOTAL NUMBER OF CYCLES TO BE MODELED
C-M=NUMBER OF TIME INCREMENTS PER BAG
C-SMALQ=AVERAGE SYSTEM VELOCITY,IF OPERATING AT CONSTANT TOTAL FLOW, M/M
C-CZERO=INLET CONCENTRATION,G/M3
C-LDIAG=PRINT DIAGNOSTICS
C-TLAG=TIME PERIOD FOR WHICH ALL BAGS ARE ON LINE AFTER  ENTIRE CLEANING
C-CYCLE
C-CONSP=PRESSURE DROP IF OPERATING AT CONSTANT TOTAL PRESSURE,N/M2
C-DPSTOP=PRESSURE DROP AT WHICH CLEANING IS INITIATED, N/M2
C-WS=CAKE LOADING AT ZERO TIME, G/M2
C-VRFLO=REVERSE AIR VELOCITY FOR ONE BAG, M/MIN
C-SE=EFFECTIVE CAKE DRAG, N-MIN/M3
      COMMON/INPUT1/N,T,NT,M,SMALQ,CZFRO,TCLEAN,LDIAG,CONSP,TLAG,DPSTOP
      COMMON/INPUT2/ZKZERO,SZERO,TEMPK,ACAKE
      COMMON/RESIS/SE,ZK2
      COMMON/INPUT3/WR,WSTAR,WS,VRFLO
      COMMON ZK2MU
      DIMENSION IDUM(10),PDP(3),PDQ(3),PT(3),PPS(3),PQ(3,5)
      DIMENSION TIME(100),OLDTIM(100),CAKE(100)
      DIMENSION WD(10,100),SBAG(100),QBAG(100),S(10,100),QAREA(10),P(10)
      LOGICAL LCONP,LDIAG
      DATA DRAG,BAG1,BAG2/'AREA','SBAG','QBAG'/
C  READ INPUT DATA
      CALL READIT
      CALL READIM
C-INITIALIZE DATA
      ZK2=ZK2*ZK2MU
      LCONP=.FALSE.
      IF(CONSP.GT.1.E-6) LCONP=.TRUE.
      IREPT=N/10 + 1
C-DETERMINE TOTAL NUMBER OF AREAS ON A BAG(IAREA) AND
C-NUMBER TO BE CLEANED(NAREA)
      ERR=0.01
    7 I=1./(1.-ACAKE)+0.5
      J=1
      IF(ERR.GT.0.06)GO TO 9
      DO 8 I=1,10
      DO 8 J=1,I
      ATEST=FLOAT(J)/FLOAT(I)
      IF(ATEST.LE.(1.-ACAKE+ERR).AND.ATEST.GE.(1.-ACAKE-ERR)) GO TO 9
    8 CONTINUE
```

Table 68 (continued). BAGHOUSE SIMULATION PROGRAM LISTING

```
      ERR=ERR+0.01
      GO TO 7
    9 NAREA=J
      IAREA=I
      AREA=1./IAREA
      CLAREA=AREA*NAREA
      WRITE(6,210) CLAREA
  210 FORMAT(1X,'CLEANED AREA=',T40,E10.4)
      WRITE(6,220)
  220 FORMAT(1H1)
      DO 5 I=1,IAREA
      QAREA(I)=SMALQ
      IF(SMALQ.EQ.0.)QAREA(I)=DELP/SZERO
      IF(WSTAR.EQ.0..AND.SMALQ.EQ.0.)QAREA(I)=DELP/SE
      DO 5 IBAG=1,N
      ULDTIM(IBAG)=-2
      TIME(IBAG)=-1
    5 WD(I,IBAG)=WS
      IFBAG=0
      PAVR=0.0
      TCONT=0.0
      DTLAST=0.0
      PENTOT=0.0
      PAVTOT=0.0
      CZEROE=CZERO
      DPAVG=0.0
      QAVG=0.0
      TCORR=T+TLAG-T/M/N*(M*N+IFIX(TLAG/T*M*N+0.9999))
      IF(TLAG.LT.1.E-9) TCORR=0.0
      TMOD=TLAG+T
      IF(DPSTOP.GT.0.)TMOD=1.E+20
      IF(DPSTOP.GT.0.) TCORR=0.0
      K3=0
      MAXJ=NT*(M*N+IFIX(TLAG/T*M*N+0.9999))+1
C  DETERMINE DRAG THROUGH FABRIC
      SFAB=SZERO
      IF(WSTAR.LT.1.E-20) SFAB=SE
C  LOOP ON TIME
      DO 300 JLOOP=1,MAXJ
      DELT=T/M/N
      TTEST=AMOD(TCONT+0.01,TMOD)-0.01
      IF(TCONT.LT.1.E-9.OR.TTEST.LE.-0.01.OR.TTEST.GE.0.01) GO TO 12
      QAVGN=(QAVG-QSYSTM*DTLAST)/2./TCONT
      PAVNOW=(PAVTOT-PENTOT*DTLAST)/2./TCONT
      DPAVGN=(DPAVG-DELP*DTLAST)/2./TCONT
C-WRITE AVERAGE PRESSURE DROP,FLOW AND PENETRATION UP TO TIME=TCONT
      WRITE(6,230) TCONT,PAVNOW,DPAVGN,QAVGN
   12 CONTINUE
      IF(TTEST.GT.T) GO TO 11
C  EXTRA PASS FOR CLEANED BAG
C-BAG LOOP        1
      DO 13 IBAG=1,N
      IF(OLDTIM(IBAG).LE.TIME(IBAG)) GO TO 13
      IFBAG=IBAG
      TCONT=TCONT+.01
      GO TO 14
   13 CONTINUE
C-END OF BAG LOOP      I
   11 IFBAG=0
      DELT=T/M/N
      JTIME=JLOOP-1
C-DETERMINE TIME
```

Table 68 (continued). BAGHOUSE SIMULATION PROGRAM LISTING

```
      TCONT=JTIME*DELT+TCORR*IFIX((TCONT+DELT)/(T+TLAG))
   14 TTEST=AMOD(TCONT+0.01,TMOD)-0.01
      IF(TTEST.GT.T.AND.TTEST.GE.(T+TLAG-DELT)) DELT=DELT+TCORR
      SSYSTM=0.0
      DELTT=DELT
      VRFLOW=0.0
      IF(LDIAG)WRITE(6,16)(DRAG,I,I=1,IAREA),BAG1
   16 FORMAT(1X,'BAG-DRAG=',1X,11(3X,A4,1X,I2))
C-BAG LOOP    2
      DO 20 IBAG=1,N
      SBAG(IBAG)=0.0
C-AREA LOOP       1
      DO 6 I=1,IAREA
C-IF BAG WAS JUST CLEANED ESTIMATE FLOW VELOCITY FROM LINEAR MODEL
      IF(S(IAREA,IBAG).GT.1.E+19) S(I,IBAG)=SE+WD(I,IBAG)*ZK2
      IF(TCONT.GT.1.E-9)QAREA(I)=DELP/S(I,IBAG)
C-DETERMINE DRAG ON EACH AREA
      CALL CAKDRG(SZERO,WD(I,IBAG),WR,WSTAR,ZKZERO,ZK2,QAREA(I),
     *  S(I,IBAG))
      S(I,IBAG)=S(I,IBAG)+SFAB
    6 SBAG(IBAG)=SBAG(IBAG)+AREA/S(I,IBAG)
C-END OF AREA LOOP       1
      SBAG(IBAG)=1./SBAG(IBAG)
C  DETERMINE TIME IN CYCLE
      IF(TTEST.GT.(T+0.005)) GO TO 21
      OLDTIM(IBAG)=TIME(IBAG)
      TIME(IBAG)=AMOD(TTEST+0.01+IBAG*T/N,T)-0.01
   21 IF(TTEST.GT.T) GO TO 19
C-TEST FOR AN OFF LINE BAG
      IF(TCONT.LT.1.E-9.AND.TIME(IBAG).LT.(T-TCLEAN-.001)) GO TO 19
      IF(TIME(IBAG).LT.(T-TCLEAN-.001).AND.TIME(IBAG).GT.0.005) GO TO 19
      IF(TIME(IBAG).LT.(T-TCLEAN-.001).AND.TTEST.LE.0.01.AND.TLAG.GT.1.E
     *-9) GO TO 19
      DO 22 I=1,IAREA
   22 S(I,IBAG)=1.E+20
      SBAG(IBAG)=1.E+20
      VRFLOW=VRFLO
C-OUTPUT INTERMEDIATE RESULTS
   19 IF(LDIAG)WRITE(6,15)IBAG,(S(I,IBAG),I=1,IAREA),SBAG(IBAG)
   15 FORMAT(1X,I3,7X,11(1X,1PE9.2))
      SSYSTM=SSYSTM+1./SBAG(IBAG)
      IF(OLDTIM(IBAG).GT.TIME(IBAG).AND.TTEST.LT.(T+0.005)) DELTT=0.01
   20 CONTINUE
C-END OF BAG LOOP 2
C-CALCULATE SYSTEM DRAG,PRESSURE DROP AND FLOW VELOCITY
      CZERO=CZEROE
      SSYSTM=1./SSYSTM
      DELP=SMALQ*SSYSTM*N+VRFLOW*SSYSTM
      IF(LCONP) DELP=CONSP
      QSYSTM=SMALQ+VRFLOW/N
      IF(LCONP) QSYSTM=CONSP/SSYSTM/N
C-CORRECT INLET CONCENTRATION FOR REVERSE FLOW AIR
      CZERO=CZEROE*(QSYSTM-VRFLOW/N)/QSYSTM
      IF(LDIAG) WRITE(6,30)(DRAG,I,I=1,IAREA),BAG2
   30 FORMAT(1X,'BAG-FLOW=',1X,11(3X,A4,1X,I2))
      PENTOT=0.0
      WDUMP=0.0
C-BAG LOOP    3
      DO 60 IBAG=1,N
      IF(TTEST.GT.T) GO TO 26
      DELT=DELTT
      IF((TIME(IBAG)+T/M/N).GT.(T-TCLEAN))DELT=T-TCLEAN-TIME(IBAG)
```

Reproduced from
best available copy.

Table 68 (continued). BAGHOUSE SIMULATION PROGRAM LISTING

```
   26 WCOMP=0.0
      CAKE(IBAG)=0.0
C-AREA LOOP   2
      DO 28 I=1,IAREA
      QAREA(I)=DELP/S(I,IBAG)
C-DETERMINE PENETRATION
      CALL PENET(CZERO,WD(I,IBAG),QAREA(I),WR,P(I))
      WAREA=QAREA(I)*(1.-P(I))*DELT*CZERO
      CAKE(IBAG)=CAKE(IBAG)+WD(I,IBAG)*AREA
   27 PENTOT=PENTOT+P(I)*AREA*QAREA(I)/QSYSTM/N
   28 WD(I,IBAG)=WD(I,IBAG)+WAREA
C-END OF AREA LOOP   2
      QBAG(IBAG)=DELP/SBAG(IBAG)
C-OUTPUT INTERMEDIATE RESULTS
      IF(LDIAG)WRITE(6,15)IBAG,(QAREA(I),I=1,IAREA),QBAG(IBAG)
      IF(TTEST.GT.T) GO TO 60
      IF(OLDTIM(IBAG).LE.TIME(IBAG))GO TO 60
C-CLEAN  NAREA AREAS ON A BAG IF NECESSARY
      WDUMP=0.0
      DO 36 II=1,NAREA
      WCOMP=0.0
C-AREA LOUP      3
      DO 35 I=1,IAREA
      IF(WD(I,IBAG).LT.WCOMP) GO TO 35
      WCOMP=WD(I,IBAG)
      IFAREA=I
   35 CONTINUE
C-END OF AREA LOOP       3
      WDUMP=WDUMP+(WD(IFAREA,IBAG)-WR)*AREA
   36 WD(IFAREA,IBAG)=WR
   60 CONTINUE
C-END OF BAG LOOP          3
      DELT=DELTT
      DPAVG=DPAVG+(DTLAST+DELT)*DELP
      QAVG=QAVG+(DTLAST+DELT)*QSYSTM
      PAVTOT=PAVTOT+PENTOT*(DELT+DTLAST)
      PAVR=PAVR+PENTOT*(DELT+DTLAST)
      DTLAST=DELT
      K3=K3+1
      PT(K3)=TCONT
      PDP(K3)=DELP
      PDQ(K3)=QSYSTM
      PPS(K3)=PENTOT
      CONTOT=PENTOT*CZERO
      LMAX=MIN0(5,N)
      DO 100 L=1,LMAX
  100 PQ(K3,L)=QBAG(L)
      IF(K3.LT.3) GO TO 120
      K3=0
C
C  PUNCH PLOT
C
  110 FORMAT(6G10.5)
      WRITE(8,110)  ((PT(K),PDP(K)),K=1,3)
      WRITE(9,110)  ((PT(K),PDQ(K)),K=1,3)
      DO 115 L=1,LMAX
      IUNIT=L+9
  115 WRITE(IUNIT,110) ((PT(K),PQ(K,L)),K=1,3)
      WRITE(15,110)(PT(K),PPS(K),K=1,3)
  120 IF(.NOT.LDIAG) GO TO 290
C
C  PRINT DIAGNOSTICS
```

Table 68 (continued). BAGHOUSE SIMULATION PROGRAM LISTING

```
C
      WRITE(6,130) TCONT,DELP,QSYSTM,CONTOT,WDUMP
  130 FORMAT(1X/' T=',G10.4,10X,'DELP=',G10.4,10X,'DELQ=',G10.4,
     &          10X,'CONCENTRATION=',G10.4,10X,'WEIGHT DUMPED=',G10.4)
      IDUM(10)=0
      DO 250 L=1,IREPT
  140 DO 150 K=1,10
      MAXK=MIN0(K,(N-10*(L-1)))
  150 IDUM(K)=IDUM(10)+K
      WRITE(6,160) (IDUM(K),K=1,MAXK)
  160 FORMAT(5X,10(6X,'BAG ',I2))
      WRITE(6,170) (TIME(IDUM(I)),I=1,MAXK)
  170 FORMAT(' T=',T6,10(F9.2,3X))
      WRITE(6,180) (CAKE(IDUM(I)),I=1,MAXK)
  180 FORMAT(' CAKE=',T6,1PE12.4,9E12.4)
      WRITE(6,190) (SBAG(IDUM(I)),I=1,MAXK)
  190 FORMAT(' SBAG',T6,10E12.4)
      WRITE(6,200) (QBAG(IDUM(I)),I=1,MAXK)
  200 FORMAT(' QBAG',T6,10E12.4,0PF2.0)
  250 CONTINUE
      IF(TTEST.GT.T) GO TO 270
      IF(OLDTIM(N).LT.TIME(N)) GO TO 270
      PAVR=PAVR/2./T
      WRITE(6,260) PAVR
  260 FORMAT(1X,'AVERAGE PENETRATION=',1PG10.3)
      PAVR=0.0
  270 CONTINUE
      WRITE(6,500)
  500 FORMAT(///)
  290 IF(IFBAG.NE.0) GO TO 11
      IF(DPSTOP.LT.1.E-9) GO TO 300
      IF(TMOD.LT.1.E+19.AND.TTEST.GT.(T+T/M/N)) TMOD=TCONT-T-T/M/N
      IF(TTEST.LE.T.OR.DELP.LT.DFSTOP) GO TO 300
      TMOD=TCONT
      TCORR=0.0
  300 CONTINUE
C     *END OF TIME LOOP
C
C FINISH PUNCHING
C
      WRITE(8,400) PT(3),PDP(3)
      WRITE(9,400) PT(3),PDQ(3)
      IUNIT=9+LMAX
      WRITE(IUNIT,400) PT(3),PQ(3,LMAX)
  400 FORMAT(2G10.5,T75,'NEW')
      IF(LMAX.EQ.1) GO TO 425
      LMAX=LMAX-1
      DO 410 L=1,LMAX
      IUNIT=L+9
  410 WRITE(IUNIT,420) PT(3),PQ(3,L)
  420 FORMAT(2G10.5,T75,'SAME')
  425 WRITE(15,400)PT(3),PPS(3)
      QAVGN=(QAVG-QSYSTM*DTLAST)/2./TCONT
      PAVNOW=(PAVTOT-PENTOT*DTLAST)/2./TCONT
      DPAVGN=(DPAVG-DELP*DTLAST)/2./TCONT
      WRITE(6,230) TCONT,PAVNOW,DPAVGN,QAVGN
  230 FORMAT(/1X,'FOR',F10.2,' MINUTES OPERATION,',
     *T50,'AVERAGE PENETRATION=',T80,1PE9.2/
     *T50,'AVERAGE PRESSURE DROP=',T80,0PF10.2,' N/M2'/
     *T50,'AVERAGE SYSTEM FLOW=',T80,0PF10.4,' M/MIN')
      RETURN
      END
```

Table 68 (continued). BAGHOUSE SIMULATION PROGRAM LISTING

```
      SUBROUTINE PLOTIN
C     SUBROUTINE TO INITIALIZE PLOTTER   11/11/75/RWS-DC
C          SUBROUTINE OF BAGHOUSE  4/77/HAK-RD GCA TECHNOLOGY  DIVISION
      COMMON/INPUT1/N,T,NT,M,SMALQ,CZERO,TCLEAN,DIAG,CONSP,TLAG,DPSTOP
      DIMENSION HEAD(19)
      DATA AMP/'&'/
      READ(5,10) HEAD
   10 FORMAT(1X,19A4,T80,A1)
      WRITE(6,15) HEAD
   15 FORMAT(1X,19A4)
      DO 20 IUNIT=8,10
   20 WRITE(IUNIT,25) HEAD,AMP
   25 FORMAT(19A4,T80,A1)
      READ(5,200)XLENTH,YLENTH
  200 FORMAT(2(10X,F10.7))
C-DEFAULT VALUES FOR X&Y AXIS LENGTHS
      IF(XLENTH.LT.1.E-9) XLENTH=6.
      IF(YLENTH.LT.1.E-9) YLENTH=5.
      IF(XLENTH.GT.24.) XLENTH=24.
      IF(YLENTH.GT.12.) YLENTH=12.
      TIME=IFIX(NT*(T+TLAG)/15.+0.05)*15./XLENTH
C-PRESSURE DROP VS. TIME
      WRITE(8,30)TIME,XLENTH,YLENTH
   30 FORMAT(
     &'PRESSURE VS TIME GRAPH',T80,'&'//
     &T28,'TIME (MINUTES)',T75,F5.0/
     &T23,'PRESSURE (N/M2)'/
     &'SEMISEMI',T55,F6.2,T65,F6.2,T80,'1')
C-FLOW VS TIME
      WRITE(9,40)TIME,XLENTH,YLENTH
   40 FORMAT(
     &'FLOWRATE VS TIME GRAPH',T80,'&'//
     &T28,'TIME (MINUTES)',T75,F5.0/
     &T23,'FLOW RATE (M/MIN)'/
     &'SEMISEMI',T55,F6.2,T65,F6.2,T80,'1')
C-INDIVIDUAL FLOW VS TIME
      WRITE(10,50) TIME,XLENTH,YLENTH
   50 FORMAT(
     &'INDIVIDUAL FLOW RATE GRAPH',T80,'&'/
     &'BAG # 1'/
     &T28,'TIME (MINUTES)',T75,F5.0/
     &T23,'FLOW RATE (M/MIN)'/
     &'SEMISEMI',T55,F6.2,T65,F6.2,T80,'1')
      IMAX=MINO(N,5)
      IF(IMAX.EQ.1) GO TO 75
      DO 60 I=2,IMAX
      IUNIT=I+9
   60 WRITE(IUNIT,70) I
   70 FORMAT('BAG # ',I1)
   75 WRITE(15,25) HEAD,AMP
C-PENETRATION VS TIME
      WRITE(15,80)TIME,XLENTH,YLENTH
   80 FORMAT(
     &'PENETRATION VS TIME GRAPH',T80,'&'/
     &/
     &T28,'TIME (MINUTES)',T75,F5.0/
     &T23,'PENETRATION',T70,'1.E-5  1.0'/
     &'LOG-SEMI',T55,F6.2,T65,F6.2,T80,'1')
      DO 100 IUNIT=8,10
  100 WRITE(IUNIT,110)
      WRITE(15,110)
  110 FORMAT(T8,'0.0',T18,'0.0')
      RETURN
      END
```

Reproduced from best available copy.

Table 68 (continued). BAGHOUSE SIMULATION PROGRAM LISTING

```
      SUBROUTINE READIM
C                  SUBROUTINE BAGHOUSE    11/20/75/RWS-DC  GCA
C           SUBROUTINE OF BAGHOUSE  4/77/HAK-RD GCA TECHNOLOGY  DIVISION
C-READS INPUT INFORMATION
C-ZKZERO=INITIAL SLOPE OF DRAG VS LOADING CURVE, N-MIN/G-M
C-SZERO=RESIDUAL DRAG, N-MIN/M3
C-TEMPK=GAS TEMPERATURE,DEGRESS KELVIN
C-ACAKE=CAKED AREA,THAT PORTION OF A BAG WHICH IS NOT CLEANED
C-ZK2MU=VISCOSITY CORRECTION FOR SPECIFIC CAKE RESISTANCE
C-ZMUE=VISCOSITY OF GAS
      COMMON/INPUT2/ZKZERO,SZERO,TEMPK,ACAKE
      COMMON ZK2MU
      ZMUE=1.8E-2
      READ(5,12)ZKZERO,SZERO,TEMPK
   12 FORMAT(4(10X,F10.5))
      READ(5,15)ACAKE
   15 FORMAT(10X,F10.5)
      IF(TEMPK.EQ.298.) GO TO 18
      IF(TEMPK.GT.1.) GO TO 150
      TEMPK=298.
      GO TO 18
  150 ZMUE=1.46E-3*TEMPK**1.5/(TEMPK+110.)
   18 WRITE(6,20)ZKZERO,ZMUE
      WRITE(6,30)SZERO,TEMPK,ACAKE
   20 FORMAT(
     7' KO=',T40,E10.4,' N-MIN/G-M'/
     8' MU=GAS VISCOSITY=',T40,E10.4,' CP')
   30 FORMAT(' SR=RESIDUAL DRAG=', T40,1PE10.4,' N-MIN/M3'/
     1' TEMPERATURE=          ',             T40,E10.4,' DEGREES KELVIN'/
     2' CAKFD AREA=',                        T40,E10.4/
     7)
      ZK2MU=ZMUE/1.8E-2
      RETURN
      END
```

Table 68 (continued). BAGHOUSE SIMULATION PROGRAM LISTING

```
      SUBROUTINE READIT
C                   SUBROUTINE OF BAGHOUSE  11/24/75/RWS-DC  GCA
C          SUBROUTINE OF BAGHOUSE  4/77/HAK-RD GCA TECHNOLOGY  DIVISION
C  READS AND INITIALIZES
C-N=NUMBER OF COMPARTMENTS OR BAGS
C-T=CLEANING CYCLE TIME,MIN
C-NT=TOTAL NUMBER OF CYCLES TO BE MODELED
C-M=NUMBER OF TIME INCREMENTS PER BAG
C-SMALQ=AVERAGE SYSTEM VELOCITY,IF OPERATING AT CONSTANT TOTAL FLOW, M/M
C-CZERO=INLET CONCENTRATION,G/M3
C-TCLEAN=TIME IT TAKES TO CLEAN ONE BAG
C-TCLEAN=TIME IT TAKES TO CLEAN ONE BAG
C- DIAG=PRINT DIAGNOSTICS
C-CONSP=PRESSURE DROP IF OPERATING AT CONSTANT TOTAL PRESSURE,N/M2
C-TLAG=TIME PERIOD FOR WHICH ALL BAGS ARE ON LINE AFTER  ENTIRE CLEANING
C-CYCLE
C-DPSTOP=PRESSURE DROP AT WHICH CLEANING IS INITIATED, N/M2
C-WS=CAKE LOADING AT ZERO TIME, G/M2
C-VRFLO=REVERSE AIR VELOCITY FOR ONE BAG, M/MIN
C-SE=EFFECTIVE CAKE DRAG, N-MIN/M3
C-R2=SPECIFIC RESISTANCE OF CAKE AT 0.61 M/MIN AND 25 C,N-MIN/G-M
C     *SET UP COMMON VARIABLE AREAS FOR SUBROUTINES
      COMMON/INPUT1/N,T,NT,M,SMALQ,CZERO,TCLEAN,DIAG,CONSP,TLAG,DPSTOP
      COMMON/INPUT3/WR,WSTAR,WS,VRFLO
      COMMON/RESIS/SE,R2
      COMMON EPSLON
      LOGICAL DIAG
C     *READ INPUT DATA
      READ(5,10)N,T,TCLEAN,NT,TLAG,M,SMALQ,CZERO,SE,R2,DIAG,CONSP,WR
   10 FORMAT(T15,I6,2(10X,G10.0),T75,I6/T11,G10.0/
     2        T15,I6,3(10X,G10.0)/
     3        T11,G10.5,T35,L6,2(10X,G10.0))
      READ(5,40) WSTAR,DPSTOP,VRFLO
      READ(5,40) WS
C     *INITIALIZE PLOTTER
      WRITE(6,13)
   13 FORMAT('1')
      CALL PLOTIN
C     *WRITE INPUT DATA
      WRITE(6,15)
   15 FORMAT(40X,'PRINTOUT OF INPUT DATA FOR BAGHOUSE ANALYSIS'//)
      WRITE(6,20)N,T,TCLEAN,TLAG,NT,M,SMALQ,CZERO,SE,R2,VRFLO
   20 FORMAT(1X,'NUMBER OF COMPARTMENTS=',T40,I6/
     2        1X,'CYCLE TIME=',    T40,0PF10.5,' MINUTES'/
     3        1X,'CLEAN TIME=',    T40,F10.5,' MINUTES'/
     3        1X,'TOTAL AREA RUN TIME=',T40,F10.5,'MINUTES'/
     4        1X,'NUMBER OF CYCLES MODELED=',T40,I6,' CYCLES'/
     5     1X,'NUMBER OF INCREMENTS PER BAG=',T40,I6,' INCREMENTS'/
     6     1X,'Q/A=VELOCITY=',T40,F10.5,' M/MIN'/
     7     1X,'CONCENTRATION=',T40,1PE10.3,' G/M3'/
     9        1X,'SE=EFFECTIVE BAG DRAG=',T40,E10.3,' N-MIN/M3'/
     9        1X,'K2=CAKE RESISTANCE AT .61 M/MIN=',T40,E10.3,' N-MIN/G-M
     &'/1X,'REVERSE FLOW VELOCITY=',T40,0PF10.4,' M/MIN'/
     &)
      WRITE(6,25) WR,WS
   25 FORMAT(1X,'WR=RESIDUAL LOADING=',T40,1PG10.3,' G/M2'/
     1  1X,'INITIAL CAKE LOADING=',T40,G10.3,' G/M2'/)
      WRITE(6,30)DIAG,CONSP,DPSTOP
   30 FORMAT(1X,'PRINT DIAGNOSTICS=',T40,L6/
     1        1X,'CONSTANT PRESSURE=',T40,1PE10.3,' N/M2'/
     2        1X,'MAXIMUM PRESSURE=',T40,E10.3,' N/M2'/)
```

Table 68 (continued). BAGHOUSE SIMULATION PROGRAM LISTING

```
40 FORMAT(4(10X,G10.5))
   WRITE(6,50) WSTAR
50 FORMAT(' W*=',T40,1PG10.4,' G/M2'/)
   RETURN
   END
```

Table 68 (continued). BAGHOUSE SIMULATION PROGRAM LISTING

```
      SUBROUTINE SCRIBE
C GRAPH LIBRARY  7/16/75/HWS  GCA TECHNOLOGY
C  VERSION 8/1/76
C CARDS-
C TITLE(1-64)       OPTIONS: XPOS(65-69) YPOS(70-74) HEIGHT(75-79)  &(80)
C XAXIS LABEL(1-64)OPTIONS: BEGIN(69-74) UNITS OR LOGS/INCH(75-80)
C YAXIS (SAME)
C TYPE (YAXIS-XAXIS)(SEMI,LOG-,PROB,BAR-)(1-8)
C       OPTIONS: LOG-(9-12) FOR A LOGRITHMIC BAR GRAPH
C                NEW GRAPH DIST(35-40) DEFAULT=6
C                X-AXIS HEIGHT(45-50)  DEFAULT=2
C                X AXIS LENGTH(55-60)  DEFAULT=6
C                Y-AXIS LENGTH(65-70)  DEFAULT=5
C                DUUBLE AXIS(74)  1 FOR X, 2 FOR Y, 3 FOR BOTH
C                SYMBOL(75-80)  POINTS BETWEEN PLOT SYMBOLS
C                               NEGATIVE FOR SYMBOLS BUT NO LINES
C DATA  X(1-10) Y(11-20)
C        OPTION: X(21-30) Y(31-40)  X(41-50) Y(51-60)
C OPTION (END,NEW,SAME)(75-78) (NEW MAKES NEW GRAPH-REPEAT ALL CARDS)
C                               (SAME PLOTS ON OLD GRAPH-NO X-Y AXIS)
C                      (79-80) (CHANGE 'SYMBOL' FOR NEXT PLOT)
      DIMENSION IBUF(4000),XAR(1002),YAR(1002),PRN(50),PRB(100)
      DIMENSION XPLAB(26),YPLAB(26),XPROB(38),YPLAS(26)
      REAL LOG,NEW,NEXT,NEX
      REAL*8 TAR(8),XLAB(8),YLAB(8),SPLAB(12),SPLAT(12)
      DATA XPLAB/.00,.30,.48,.65,.91,1.10,1.32,1.65,1.95,2.30,2.56,2.78,
     &3.00,3.22,3.44,3.70,4.05,4.35,4.68,4.90,5.09,5.35,5.52,6.00,0.,1./
      DATA YPLAB/25*0.0,1./
      DATA YPLAS/24*5.0,.0,1./
      DATA SPLAB/'.01 .05 ','.1.2  .5',' 1  2   ',' 5   10 ','  20  30',
     2           ' 40 50 6','0 70  80','   90   ','95   98 ','99 99.5 ',
     3           ' 99.9  9','9.99    '/
      DATA SPLAT/' 99.99 9','9.9  99.','5 99 98 ','  95  90','   80  7',
     2           '0 60 50 ',' 40 30  ','20   10 ',' 5    2 ',' 1  .5  ',
     3           '.2 .1   ','.01     '/
      DATA XPROB/.0,.16,.45,.65,.91,1.10,1.42,1.68,1.94,2.17,2.43,2.82,
     &3.04,3.33,3.63,3.88,4.24,4.53,4.92,5.21,5.57,5.89,6.28,6.63,
     &7.06,7.51,7.90,8.32,8.84,9.29,9.81,10.36,10.91,11.55,12.27,
     &13.09,13.95,15.00/
      DATA BLA,SEMI,LOG,PROB,BAR/'    ','SEMI','LOG-','PROB','BAR-'/
      DATA SAME,NEW,ENDD/'SAME','NEW ','END '/
      CALL PLOTS(IBUF,4000)
      INUNIT=3
      IOUTUN=4
      NEXT=NEW
   10 ISYM=0
      CALL PLOT(0.,-36.,-3)
      CALL PLOT(0.0,2.,-3)
      IPOS=0
      BARX=0.
      BARY=0.
      PROBX=0.
      LTYP=0
   20 ISYM=ISYM+1
      NEX=NEXT
      IF(NEXT.NE.SAME) GO TO 30
      XBEG=XAR(IMAX+1)
      XINC=XAR(IMAX+2)
      YBEG=YAR(IMAX+1)
      YINC=YAR(IMAX+2)
C   TITLE
```

Table 68 (continued). BAGHOUSE SIMULATION PROGRAM LISTING

```
   30 READ(INUNIT,40,END=1000) TAR,XPOS,YPOS,CHIT,CONT
   40 FORMAT(8A8,3G5.2,A1)
      IF(ABS(XPOS).LT.1.E-20) XPOS=.5
      IF(ABS(YPOS).LT.1.E-20) YPOS=8.0-(.25*IPOS)
      IF(CHIT.LT.1.E-20.AND.ISYM.EQ.1.AND.CONT.NE.BLA) CHIT=.21
      IF(CHIT.LT.1.E-20.AND.CONT.EQ.BLA) CHIT=.14
      WRITE(IOUTUN,41) TAR,XPOS,YPOS,CHIT,CONT
   41 FORMAT(1X,8A8,3X,'XPOS=',F7.3,3X,'YPOS=',F7.3,3X,'HEIGHT=',F7.3,
     &       3X,'CONT=',A1)
      IF(CONT.NE.BLA.OR.IPOS.EQ.0) GO TO 45
      XPOS=XPOS+.2
      DO 42 I=1,7
      IF(TAR(8).EQ.TAR(I)) GO TO 42
      CALL SYMBOL(XPOS-.1,YPOS,CHIT,ISYM,0.,-1)
      GO TO 45
   42 CONTINUE
   45 CALL SYMBOL(XPOS,YPOS,CHIT,TAR,0.,64)
      IPOS=IPOS+1
      IF(CONT.NE.BLA) GO TO 30
C LABELS
      IF(ISYM.GT.1.AND.NEXT.EQ.SAME) GO TO 70
      READ(INUNIT,50) XLAB,XBEG,XINC
   50 FORMAT(8A8,T69,2G6.2)
      WRITE(IOUTUN,55) XLAB,XBEG,XINC
   55 FORMAT(1X,8A8,3X,'XBEG=',G10.3,3X,'XINC=',G10.3)
      READ(INUNIT,50) YLAB,YBEG,YINC
      WRITE(IOUTUN,58) YLAB,YBEG,YINC
   58 FORMAT(1X,8A8,3X,'YBEG=',G10.3,3X,'YINC=',G10.3)
C TYPE
      READ(INUNIT,60) YTYP,XTYP,ZTYP,XOVER,YUP,XAXL,YAXL,IDOUB,LTYP
   60 FORMAT(3A4,T31,4(4X,G6.2),T74,I1,I6)
      IF(XTYP.EQ.BLA) XTYP=SEMI
      IF(YTYP.EQ.BLA) YTYP=SEMI
      IF(YUP.LT.1.E-5) YUP=2.
      YUP=YUP-2.
      CALL PLOT(0.,YUP,-3)
      IF(XAXL.LT..5) XAXL=6.
      IF(ABS(XOVER).LT.1.E-20) XOVER=6.
      PMUVE=XAXL+XOVER
      IF(YAXL.LT..5) YAXL=5.
      WRITE(IOUTUN,65) YTYP,XTYP,ZTYP,XOVER,YUP,XAXL,YAXL,IDOUB,LTYP
   65 FORMAT(1X,3A4,3X,'XOVER=',F6.2,3X,
     2       'XAXIS HT=',F6.2,5X,'XAXIS L=',F6.2,5X,
     3       'YAXIS L=',F6.2,5X,
     4                 '#AXIS=',I1,10X,'POINTS PER TICK=',I6)
      IF(ZTYP.EQ.BLA) ZTYP=SEMI
C DATA
   70 J=1
      WRITE(IOUTUN,75)
   75 FORMAT(T40,'DATA'/
     &       T5,'X1',T15,'Y1',T25,'X2',T35,'Y2',T45,'X3',T55,'Y3',T72,
     &       'NEXT GRAPH TYPE     NEW SYMBOL'/)
      DO 100 I=1,1000
      K=J+2
      READ(INUNIT,80,END=90)  ((XAR(M),YAR(M)),M=J,K),NEXT,NEWSYM
   80 FORMAT(6G10.5,T75,A4,I2)
      WRITE(IOUTUN,85)        ((XAR(M),YAR(M)),M=J,K),NEXT,NEWSYM
   85 FORMAT(1X,6(1PE10.3),T74,A4,T93,I3)
      IF(XAR(J+1).LT.1.E-20.AND.YAR(J+1).LT.1.E-20.AND.XAR(K).LT.1.E-20
     &.AND.YAR(K).LT.1.E-20) J=J-1
      IF(XAR(K).LT.1.E-20.AND.YAR(K).LT.1.E-20) J=J-1
      J=J+3
```

Table 68 (continued). BAGHOUSE SIMULATION PROGRAM LISTING

```
      IF(J.GT.1000) GO TO 90
      IF(NEXT.EQ.BLA) GO TO 100
      IF(XAR(J-1).LT.1.E-20.AND.YAR(J-1).LT.1.E-20) J=J-1
      IF(NEWSYM.NE.0) LTYP=NEWSYM
   90 IMAX=J-1
      IF(NEXT.EQ.BLA) NEXT=ENDD
      GO TO 102
  100 CONTINUE
C SCALES AND AXIS
  102 XAR(IMAX+1)=XBEG
      XAR(IMAX+2)=XINC
      YAR(IMAX+1)=YBEG
      YAR(IMAX+2)=YINC
C  CUT OFF VALUES OUT OF RANGE
      IF(ABS(XINC).LT.1.E-20) GO TO 106
      IF(XTYP.EQ.PROB) GO TO 106
      XBYG=XBEG+XINC*XAXL
      IF(XTYP.EQ.LOG) XBYG=XBEG*10**(XINC*XAXL)
      DO 104 IMLOOP=1,IMAX
      IF(XBYG.GT.XBEG.AND.XAR(IMLOOP).GT.XBYG) XAR(IMLOOP)=XBYG
      IF(XBYG.GT.XBEG.AND.XAR(IMLOOP).LT.XBEG) XAR(IMLOOP)=XBEG
      IF(XBYG.LT.XBEG.AND.XAR(IMLOOP).LT.XBYG) XAR(IMLOOP)=XBYG
      IF(XBYG.LT.XBEG.AND.XAR(IMLOOP).GT.XBEG) XAR(IMLOOP)=XBEG
  104 CONTINUE
  106 IF(ABS(YINC).LT.1.E-20) GO TO 110
      YBYG=YBEG+YINC*YAXL
      IF(YTYP.EQ.LOG) YBYG=YBEG*10**(YINC*YAXL)
      DO 108 IMLOOP=1,IMAX
      IF(YBYG.GT.YBEG.AND.YAR(IMLOOP).GT.YBYG) YAR(IMLOOP)=YBYG
      IF(YBYG.GT.YBEG.AND.YAR(IMLOOP).LT.YBEG) YAR(IMLOOP)=YBEG
      IF(YBYG.LT.YBEG.AND.YAR(IMLOOP).LT.YBYG) YAR(IMLOOP)=YBYG
      IF(YBYG.LT.YBEG.AND.YAR(IMLOOP).GT.YBEG) YAR(IMLOOP)=YBEG
  108 CONTINUE
C  CUT OFF LOW VALUES
  110 XBYG=1.E-20
      YBYG=1.E-20
      IF(XTYP.NE.LOG) GO TO 113
      DO 112 IMLOOP=1,IMAX
      IF(XAR(IMLOOP).LT.XBYG) XAR(IMLOOP)=XBYG
  112 CONTINUE
  113 IF(YTYP.NE.LOG) GO TO 115
      DO 114 IMLOOP=1,IMAX
      IF(YAR(IMLOOP).LT.YBYG) YAR(IMLOOP)=YBYG
  114 CONTINUE
  115 IF(NEX.EQ.SAME) GO TO 147
      IF(XTYP.EQ.BAR.OR.YTYP.EQ.BAR) GO TO 200
      IF(XTYP.NE.SEMI) GO TO 120
      IF(XINC.LT.1.E-20) CALL SCALE(XAR,XAXL,IMAX,1)
  116 CALL AXIS(0.0,0.0,XLAB,-64,XAXL,0.0,XAR(IMAX+1),XAR(IMAX+2))
      IF(IDOUB.EQ.1.OR.IDOUB.EQ.3)
     &CALL AXIS(0.0,YAXL,XLAB,+64,XAXL,0.0,XAR(IMAX+1),XAR(IMAX+2))
  120 IF(YTYP.NE.SEMI) GO TO 130
      IF(YINC.LT.1.E-20) CALL SCALE(YAR,YAXL,IMAX,1)
  126 CALL AXIS(0.0,0.0,YLAB,64,YAXL,90.0,YAR(IMAX+1),YAR(IMAX+2))
      IF(IDOUB.GE.2)
     &CALL AXIS(XAXL,0.0,YLAB,-64,YAXL,90.0,YAR(IMAX+1),YAR(IMAX+2))
  130 IF(XTYP.NE.LOG) GO TO 140
      IF(XINC.LT.1.E-20) GO TO 135
      IF(XBEG.GT.1.E-20) GO TO 133
      XBEG=1.
      XAR(IMAX+1)=1.
  133 CONTINUE
```

Table 68 (continued). BAGHOUSE SIMULATION PROGRAM LISTING

```
      GO TO 136
  135 CALL SCALG(XAR,XAXL,IMAX,1)
  136 CALL LGAXS(0.0,0.0,XLAB,-64,XAXL,0.0,XAR(IMAX+1),XAR(IMAX+2))
      IF(IDOUB.EQ.1.OR.IDOUB.EQ.3)
     &CALL LGAXS(0.0,5.0,XLAB,64,XAXL,0.0,XAR(IMAX+1),XAR(IMAX+2))
  140 IF(YTYP.NE.LOG) GO TO 147
      IF(YINC.LT.1.E-20) GO TO 145
      IF(YBEG.GT.1.E-20) GO TO 143
      YBEG=1.
      YAR(IMAX+1)=1.
  143 CONTINUE
      GO TO 146
  145 CALL SCALG(YAR,YAXL,IMAX,1)
  146 CALL LGAXS(0.0,0.0,YLAB,64,YAXL,90.0,YAR(IMAX+1),YAR(IMAX+2))
      IF(IDOUB.GE.2)
     &CALL LGAXS(6.0,0.0,YLAB,-64,YAXL,90.0,YAR(IMAX+1),YAR(IMAX+2))
  147 IF(XTYP.NE.SEMI.OR.YTYP.NE.SEMI) GO TO 150
      CALL LINE(XAR,YAR,IMAX,1,LTYP,ISYM)
      GO TO 500
  150 IF(XTYP.NE.SEMI.OR.YTYP.NE.LOG) GO TO 160
      LOGT=1
      GO TO 180
  160 IF(XTYP.NE.LOG.OR.YTYP.NE.SEMI) GO TO 170
      LOGT=-1
      GO TO 180
  170 IF(XTYP.NE.LOG.OR.YTYP.NE.LOG) GO TO 200
      LOGT=0
  180 CALL LGLIN(XAR,YAR,IMAX,1,LTYP,ISYM,LOGT)
      GO TO 500
C  BAR GRAPH
  200 IF(XTYP.NE.BAR) GO TO 220
      YAR(IMAX+1)=YAR(IMAX)
      DO 210 I=1,IMAX
      J=IMAX-I+1
      XAR(3*J+1)=XAR(J)
      XAR(3*J)=XAR(J)
      XAR(3*J-1)=XAR(J)
      YAR(3*J+1)=YAR(J+1)
      YAR(3*J)=YBEG
      YAR(3*J-1)=YAR(J)
  210 CONTINUE
      XAR(1)=XBEG
      IMAX=3*IMAX+1
      XAR(IMAX+1)=XBEG
      XAR(IMAX+2)=XINC
      YAR(IMAX+1)=YBEG
      YAR(IMAX+2)=YINC
      BARX=1.
      XTYP=ZTYP
      GO TO 110
  220 IF(YTYP.NE.BAR) GO TO 250
      XAR(IMAX+1)=XAR(IMAX)
      DO 230 I=1,IMAX
      J=IMAX-I+1
      YAR(2*J)=YAR(J)
      YAR(2*J-1)=YAR(J)
      XAR(2*J)=XAR(J+1)
  230 XAR(2*J-1)=XAR(J)
      IMAX=2*IMAX
      BARY=1.
      YTYP=ZTYP
      XAR(IMAX+1)=XBEG
```

Table 68 (continued). BAGHOUSE SIMULATION PROGRAM LISTING

```
      XAR(IMAX+2)=XINC
      YAR(IMAX+1)=YBEG
      YAR(IMAX+2)=YINC
      GO TO 110
C PROB GRAPH
  250 IF(XTYP.NE.PROB) GO TO 300
      IF(NEX.EQ.SAME) GO TO 255
      XPLAB(26)=6.0/XAXL
      CALL LINE(XPLAB,YPLAB,24,1,1,13)
      CHXP=XAXL/6.*.0681
      PSYMS=-CHXP
      PSYT=-.17*(XAXL/6.)
      CALL SYMBOL(PSYMS,PSYT,CHXP,SPLAB,0.,96)
      CALL SYMBOL(0.,-.35,.14,XLAB,0.,69)
      IF(IDOUB.NE.1.AND.IDOUB.NE.3) GO TO 255
      DO 251 IDUMII=1,24
  251 YPLAS(IDUMII)=YAXL
      CALL LINE(XPLAB,YPLAS,24,1,1,13)
      PSYMS=2.*(-CHXP)
      PSYT=YAXL-PSYT
      CALL SYMBOL(PSYMS,PSYT,CHXP,SPLAT,0.,96)
      CALL SYMBOL(0.,5.35,.14,XLAB,0.,69)
  255 DO 270 I=1,IMAX
      LEFT=1
      IF(XAR(I).LT..01) XAR(I)=.01
      IF(XAR(I).LT.50.) GO TO 260
      LEFT=0
      IF(XAR(I).GT.99.99) XAR(I)=99.99
      XAR(I)=100.-XAR(I)
  260 RLP=ALOG10(XAR(I)*100.)*10.+1.
      IF(RLP.LT.1.) RLP=1.
      IF(RLP.GT.38.) RLP=38.
      LP=IFIX(RLP)
      XAR(I)=(XPROB(LP)+(RLP-LP)*(XPROB(LP+1)-XPROB(LP)))/5.
      IF(LEFT.EQ.0) XAR(I)=6.-XAR(I)
  270 CONTINUE
      XAR(IMAX+1)=0.
      XAR(IMAX+2)=XAXL/6.
      PROBX=1.
      XTYP=SEMI
      GO TO 147
  300 IF(YTYP.NE.PROB) GO TO 450
  450 WRITE(6,460) XTYP,YTYP
  460 FORMAT(' NO SUCH GRAPH TYPE AS ',2A4)
      GO TO 1000
C AGAIN
  500 CONTINUE
      IF(BARX.GT..5) XTYP=BAR
      IF(BARY.GT..5) YTYP=BAR
      IF(PROBX.GT..5) XTYP=PROB
      IF(NEXT.NE.NEW) GO TO 510
      CALL PLOT(PMOVE,0.,-3)
      GO TO 10
  510 IF(NEXT.EQ.SAME) GO TO 20
 1000 WRITE(IOUTUN,1010) NEXT
 1010 FORMAT(' END    NEXT= ',A4)
      CALL PLOT(PMOVE,0.,999)
      RETURN
      END

//*                  INSERT SOURCE DECK MODIFICATIONS HERE
```

Table 68 (continued). BAGHOUSE SIMULATION PROGRAM LISTING

```
//GO.SYSLIN DD
//  DD *
//*  INSERT OBJECT DECKS HERE    TAKE OUT SOURCE DECKS ABOVE
//GO.SYSLIB DD DISP=SHR
// DD DSN=SYS1.CALCOMP,DISP=SHR
//GO.FT08F001 DD UNIT=SYSDA,DISP=(NEW,PASS),DSN=&&BAG1,
//   DCB=(RECFM=FB,LRECL=80,BLKSIZE=1600),SPACE=(TRK,(1,1),RLSE)
//GO.FT09F001 DD UNIT=SYSDA,DISP=(NEW,PASS),DSN=&&BAG2,
//   DCB=(RECFM=FB,LRECL=80,BLKSIZE=1600),SPACE=(TRK,(1,1),RLSE)
//GO.FT10F001 DD UNIT=SYSDA,DISP=(NEW,PASS),DSN=&&BAG3,
//   DCB=(RECFM=FB,LRECL=80,BLKSIZE=1600),SPACE=(TRK,(1,1),RLSE)
//GO.FT11F001 DD UNIT=SYSDA,DISP=(NEW,PASS),DSN=&&BAG4,
//   DCB=(RECFM=FB,LRECL=80,BLKSIZE=1600),SPACE=(TRK,(1,1),RLSE)
//GO.FT12F001 DD UNIT=SYSDA,DISP=(NEW,PASS),DSN=&&BAG5,
//   DCB=(RECFM=FB,LRECL=80,BLKSIZE=1600),SPACE=(TRK,(1,1),RLSE)
//GO.FT13F001 DD UNIT=SYSDA,DISP=(NEW,PASS),DSN=&&BAG6,
//   DCB=(RECFM=FB,LRECL=80,BLKSIZE=1600),SPACE=(TRK,(1,1),RLSE)
//GO.FT14F001 DD UNIT=SYSDA,DISP=(NEW,PASS),DSN=&&BAG7,
//   DCB=(RECFM=FB,LRECL=80,BLKSIZE=1600),SPACE=(TRK,(1,1),RLSE)
//GO.FT15F001 DD UNIT=SYSDA,DISP=(NEW,PASS),DSN=&&BAG8,
//   DCB=(RECFM=FB,LRECL=80,BLKSIZE=1600),SPACE=(TRK,(1,1),RLSE)
//GO.FT03F001 DD DISP=(OLD,PASS),DSN=&&BAG1,UNIT=SYSDA,
//  VOL=REF=*.FT08F001
//         DD DISP=(OLD,PASS),DSN=&&BAG2,UNIT=SYSDA,VOL=REF=*.FT09F001
//         DD DISP=(OLD,PASS),DSN=&&BAG3,UNIT=SYSDA,VOL=REF=*.FT10F001
//         DD DISP=(OLD,PASS),DSN=&&BAG4,UNIT=SYSDA,VOL=REF=*.FT11F001
//         DD DISP=(OLD,PASS),DSN=&&BAG5,UNIT=SYSDA,VOL=REF=*.FT12F001
//         DD DISP=(OLD,PASS),DSN=&&BAG6,UNIT=SYSDA,VOL=REF=*.FT13F001
//         DD DISP=(OLD,PASS),DSN=&&BAG7,UNIT=SYSDA,VOL=REF=*.FT14F001
//         DD DISP=(OLD,PASS),DSN=&&BAG8,UNIT=SYSDA,VOL=REF=*.FT15F001
//GO.FT04F001 DD SYSOUT=A,DCB=(LRECL=133,RECFM=FB,BLKSIZE=133)
//GO.PLOTTAPE DD DSN=PLOT3656,
// DISP=(,KEEP),UNIT=(TAPE7,,DEFER),
// DCB=DEN=1,LABEL=(,NL),
// VOL=SER=PL0044
//GO.SYSIN DD *
//*                 INSERT INPUT DATA HERE
```

```
1NUMB OF BAGS=      **CYCLE T=          **CLEAN T=          *****# CYCLES=
2****TLAG=          ***
3NUMB OF INCS=      *******Q/A=         ***CONCEN=          **MIN RSE=
4******K2=          **DIAGNOSTICS=      ***CONS P=          *******WR=
5***WSTAR=          ***DPSTOP=          **REVFLOW=          ********************
6**WSTART=          ***
7TEST RUN #       BAGHOUSE SIMULATION                                        ***
8***XAXIS=          ****YAXIS=          **
9*******KR=         *******SR=          ****TEMPK=          ********************
10**ACAKE=          **
```

Table 69. VARIABLES AND ARRAYS USED IN BAGHOUSE SIMULATION PROGRAM

VARIABLES

ACAKE - fractional area on a bag that is not cleaned, input.

AREA - fractional area on a bag. The product of AREA and the number of areas cleaned gives the fractional area cleaned.

ATEST - intermediate calculation in determining AREA.

BAG1 - heading, 'SBAG'.

BAG2 - heading, 'QBAG'.

CLAREA - fractional area cleaned on a bag, calculated.

CONSP - system pressure, if the system operates at constant pressure, N/m^2.

CONTOT - total outlet concentration from the system, g/m^3.

CZERO - inlet concentration, calculated, g/m^3.

CZEROE - inlet concentration, input, g/m^3.

DELP - system pressure drop, N/m^2.

DELT - time increment, min.

DELTT - intermediate in determining time increment, min.

DPAVG - intermediate in calculating average pressure drop, N/m^2.

DPAVGN - average pressure drop at the end of a cycle, N/m^2.

DPSTOP - maximum system pressure, if exceeded cleaning begins, N/m^2.

DRAG - heading, 'AREA'.

DTLAST - time increment of last loop, min.

ERR - error used in determining cleaned area.

I - index.

IAREA - number of areas on a bag.

IBAG - bag index.

IFAREA - number of the area to be cleaned.

IFBAG - number of the bag just cleaned.

II - index.

IREPT - line counter for output of intermediate calculations.

IUNIT - output file number.

J - index.

JLOOP - index in time loop.

Table 69 (continued). VARIABLES AND ARRAYS USED IN BAGHOUSE SIMULATION PROGRAM

JTIME - JLOOP - 1.
K - index.
K3 - index in determining when to write on a file, data points for graphs are written three at a time.
L - index.
LCONP - constant pressure diagnostics; if true, operation is at constant pressure.
LDIAG - print diagnostics; if true, intermediate calculations are output, input.
LMAX - maximum number of individual flow rate graphs, limit = 5.
M - number of increments per bag, input.
MAXJ - total number of increments used in time loop.
MAXK - maximum number of bags for which calculations are output per line.
N - number of bags (compartments), input.
NAREA - number of areas to be cleaned.
NT - number of cycles modeled, input.
PAVNOW - average penetration of the end of a cycle, referenced to time = 0.
PAVR - average penetration at the end of a cleaning cycle.
PAVTOT - intermediate in calculating average penetration.
PENTOT - total system penetration at any time.
QAVG - intermediate in calculating average system flow, m/min.
QAVGN - average system flow at the end of a cycle, m/min.
QSYSTM - total system flow, m/min.
SE - effective drag, input, N-min/m^3.
SFAB - fabric drag, N-min/m3.
SMALQ - specified constant total flow, input, m/min.
SSYSTM - total system drag, N-min/m^3.
SZERO - residual drag, S_R, input, N-min/m^3.
T - cleaning cycle time, input, min.
TCLEAN - single bag cleaning time, input, min.
TCONT - actual simulated time, min.

Table 69 (continued). VARIABLES AND ARRAYS USED IN BAGHOUSE SIMULATION PROGRAM

TCORR - correction for time interval splitting at the end of a cycle, min.

TEMPK - gas temperature, input, ^{o}K.

TLAG - total area run time, input, min.

TMOD - total cycle time = T+TLAG, reference time for cleaning cycle, min.

TTEST - TCONT in a modulo TMOD system, it is normally the time since cleaning cycle started, min.

VRFLO - reverse flow velocity based on a single compartment, input, m/min.

VRFLOW - reverse flow used in calculations; zero if not cleaning, VRFLO if cleaning, m/min.

WAREA - weight permit area added to an area in one time increment, g/m^2.

WCOMP - intermediate in determining areas of highest loading, g/m^2.

WR - residual fabric loading, input, g/m^2.

WS - absolute fabric loading at time zero, input, g/m^2.

WSTAR - constant for nonlinear drag model, input, g/m^2.

ZK2 - specific cake resistance, K_2, input, N-min/g-m.

ZK2MU - viscosity correction for K_2.

ZKZERO - initial slope of drag versus loading curve, K_R, input, N-min/g-m.

ARRAYS

CAKE(IBAG) - average fabric loading on bag # IBAG, g/m^2.

IDUM(I) - variable array index for output of intermediate results.

OLDTIM(IBAG) - previous time for bag # IBAG, min.

P(IAREA) - penetration for area # IAREA.

PDP(K3)^a - system pressure drop, N/m^2.

PDQ(K3)^a - system flow, m/min.

PPS(K3)^a - system penetration.

PQ(K3,LMAX)^a - individual compartment flow, m/min.

PT(K3)^a - simulated time, min.

Table 69 (continued). VARIABLES AND ARRAYS USED IN BAGHOUSE SIMULATION PROGRAM

QAREA(IAREA) - face velocity on area # IAREA, m/min.

QBAG(IBAG) - average face velocity for bag # IBAG, m/min.

S(IAREA,IBAG) - drag of area # IAREA on bag # IBAG.

SBAG(IBAG) - total drag of bag # IBAG.

TIME(IBAG) - time after cleaning for bag # IBAG.

WD(IAREA,IBAG) - dust cake loading on ares # IAREA on bag # IBAG.

---

[a] These arrays contain only 3 entires. When data is output for subsequent processing by the plot routine SCRIBE, they are output in groups of 3.

Table 70. DATA INPUT FORMAT

Parameter	Units	Record	Columns	Format
Number of bags	-	1	15-20	I6
Cleaning cycle time	Minutes	1	31-40	G10.0
Single bag cleaning time	Minutes	1	51-60	G10.0
Number of cycles modeled	-	1	75-80	I6
Total area run time	Minutes	2	11-20	G10.0
Number of increments per bag	-	3	15-20	I6
Constant flow velocity	m/min	3	31-40	G10.0
Inlet concentration	g/m^3	3	51-60	G10.0
Effective drag, S_E	$N\text{-}min/m^3$	3	71-80	G10.0
Specific cake resistance, K_2	N-min/g-m	4	11-20	G10.5
Print diagnostics	-	4	35-40	L6
Constant pressure drop	N/m^2	4	51-60	G10.0
Residual fabric loading, W_R	g/m^2	4	71-80	G10.0
W*	g/m^2	5	11-20	G10.5
Maximum pressure drop	N/m^2	5	31-40	G10.5
Reverse flow velocity	m/min	5	51-60	G10.5
Initial cake loading	g/m^2	6	11-20	G10.5
TITLE	-	7	2-77	19A4
X-axis length	inches	8	11-20	F10.7
Y-axis length	inches	8	31-40	F10.7
Initial slope, K_R	N-min/g-m	9	11-20	F10.5
Residual drag, S_R	$N\text{-}min/m^3$	9	31-40	F10.5
Gas temperature	^oK	9	51-60	F10.5
Caked area	-	10	11-20	F10.5

INDEX

- Adhesion, dust cake
  - fabrics tested, 296
  - general discussion, 300-305
- Adhesive forces, interfacial
  - cleaned fabric surface (a_c), relation to, 295-299
  - range of, 300, 302
- Aerosol size properties
  - (See particle size properties)
- Air flow
  - pore structure, 77-81
- Atmospheric dust
  - fabric rating tests, 199, 203-205
- Atmospheric dust concentration
  - optical versus gravimetric measurements, 50, 51, 190
  - sateen weave cotton, 204, 205
  - woven glass fabrics, 204, 205
- Bench scale tests
  - apparatus, 31-33, 38
  - data summaries, 169-172
- Capillary flow
  - see Hagen Poiseuille flow, 77-79
- Carman-Kozeny equations
  - K_2 determinations, 164
- Computer printouts
  - input data for Nucla and Sunbury modeling, 379, 384, 385
- Condensation nuclei counter
  - detection sensitivity, 177, 202
- Condensation nuclei measurements, 175, 176
- Dacron fabrics
  - fly ash collection, 171
  - humidity effects, 166
  - physical properties, 63
- Diffusion parameter (η'_{DI})
  - (See particle collection)
- Direct interception parameter (η_{DI})
  - (See particle collection)
- Drag (resistance) model
  - bilinear, single bag, 288, 289
  - linear, critique, 230
  - linear, single bag
    - applications, 285-287
    - critique, 230
  - nonlinear, empirical, 236-242
  - nonlinear, predicted versus experimental results, 244
  - nonlinear, theoretical, 233, 234, 236
- Dust cake density
  - fly ash, 145, 146, 265, 266, 270
- Dust dislodgment
  - (See also fabric cleaning)

INDEX (Continued)

- adhesion, 272
- appearance of cleaned fabric, 282
- bag collapse, 153, 155
- bag tensioning effect, 218, 219
- cleaned area, 290-306
- fabric loading effect, 153, 209, 272
- interfacial adhesive forces, distribution, 209, 213, 214
- interfacial separation, 153, 155, 230
- number of cleaning cycles to attain maximum removal, 218, 219
- repeated cleaning and filtering cycles, 214, 215, 218, 219
- shearing forces, 272
- tensile forces, 153, 272

Dusts/fabrics
- test combinations, 130

Dust/fabric photomicrographs
- before and after cleaning, 148
- cake cracking by flexing, 146
- cleaned and uncleaned areas, 151, 154
- discussion, 130-167
- dust cake at 20X magnification, 147
- pinhole leaks, 137, 138

Dust generator
- NBS design, 37

Dust removal
- (See dust dislodgment)

Effluent concentrations
- fabric loading effect, 202
- face velocity effect, 199, 201 336-339

Fabric acceleration
- calculation for mechanical shaking, 295

Fabric cleaning
- (See also dust dislodgment)
- acceleration, 272
- average residual dust holding versus number of shakes, 293, 294
- cleaned area (a_c) estimation, 290, 291
- cleaned area (a_c) versus dust separation force, 292
- cleaning force calculation, mechanical shaking, 306
- dust dislodgment forces, 272
- dust spallation, 230, 272
- filter performance, 271-289
- partially cleaned filter photograph, 154
- pressure controlled, 307-310
- pulse jet systems, 272
- sequential cleaning schematic, 357
- surface loadings, 271
- time cycle control, 311-314

Fabric collection
- pore cross section, effect of, 332

Fabric drag (resistance)
- clean (S_o), 231, 233, 245, 253
- clean (S_o) versus effective (S_E), 247-249
- effective (S_E), 245, 247
- experimental values, 249

  fabric loading effect, bag tests, 128, 129, 131, 132, 220, 222
  partial cleaning, 273-275, 279
  pore plugging, blinding, 127
  pore velocity, clean Sunbury fabric, 64
  previous dust loading, effect of, 250, 251
  residual (S_R) for miscellaneous dust/fabric combinations, 155-157
  structure effects, 247
  tensioning, effect of at constant velocity, 88, 91, 92
Fabric loading, W,
  residual (W_R) for various dust/fabric combinations, 156, 157
Fabric permeability
  new and cleaned woven glass fabrics, 118-124
Fabric photomicrographs
  Nucla fabric, unused, 69
  Sunbury fabric unused, 68, 75
  yarn appearance, warp and fill, 70, 71
Fabric properties
  acrylic, spun 2/2 twill, 23
  ASTM ratings, 82
  cotton, sateen weave, 63
  Dacron, crowfoot, 63
  general, 81-94
  Nomex fabrics, 23
  Nucla (W. W. Criswell), 60, 61
  rigidity and flexing, 84
  Sunbury (Menardi Southern), 60, 61
  tensile modulus, 84-90
Fabric weave
  pore cross section, schematic, 76
  pore density versus yarn proximity, 72, 74
  Sunbury, textile schematic, 65
  yarn and pore structure, schematic, 74
Fabrics, woven glass
  manufacturers, 63
Filter capacity
  number of shakes, 277
  shaker acceleration, 277
Fly ash collection
  cotton fabric, sateen weave, 171
  Dacron fabric (crowfoot weave), 171
  glass fabric, 3/1 twill, 169-172
  partially cleaned filters, 158-160, 169, 171, 172
Frasier permeability
  (See fabric permeability)
    clean fabrics, 63

Glass bag
  partially cleaned, photomicrograph, 282
Glass fabrics
  fiber size, 320
  field performance, 101-117
  fly ash deposition, initial, 94-96
  thickness measurements, 93, 94
Hagen-Poiseuille flow
  pressure loss, pore, 77-79

INDEX (Continued)

Humidity effects
  Dacron fabric/fly ash, 166

Impaction parameter (η_I)
  (See particle collection)

K_R, nonlinear modeling parameter
  drag/loading relationships, 236-242
  experimentally derived values, 243, 249

Lignite fly ash collection
  glass fabric, 3/1 twill, 170, 171

Models
  (See drag (resistance) and penetration)

Model, filter system
  basic drag equation, 351
  basic modeling process, discussion, 352-361
  capability, 352, 353
  computational procedure for baghouse, 360
  data inputs required, 353
  drag computations, 363-366
  input data summary, 368-371
  Nucla cleaning schedule, simplified, 377
  penetration calculations, 366, 367
  program (computer) description, 361-363
  program flow diagram, 362
  program output, sample, 372
  Summary, design highlights, 406
  Sunbury cleaning schedule, simplified, 383
  validation, 373-405
  validation, Nucla installation, 386-394
  validation, Nucla and Sunbury data inputs, 375
  validation, summaries of predicted and observed performance, 406-408
  validation, Sunbury installation, 394-405
  working equations and relationships, 348-351

Modeling concepts
  full scale applications, resistance, 306-315

Modeling, general
  variables controlling performance, 5, 6

Modeling (Historical)
  Fraser and Foley, 25
  Leith and First, 25-27
  Noll, Davis and LaRosa, 23, 24
  Robinson, Harrington and Spaite, 14-17
  Solbach, 18-20
  Stinessen, 24

Monofilament screens
  fly ash deposition, 97, 99
  pore bridging, 100

Nucla fabric
  field performance, 101-117

Nucla field tests
  data summaries, 112, 114, 117

normal cleaning procedure, 376

Nuclei concentrations (effluent)

  fly ash/glass fabrics, 176-182

  instrumentation for measurement, 49

  mass concentration, relation to, 191, 194-199

  partially loaded glass fabrics, 182

  pinhole effect, severe leakage, 176

  velocity and fabric loading effect, 186

Nuclei concentrations (influent)

  estimation from effluent concentration and filter penetration, 186

Nuclei concentration measurements

  optical (B&L) measurement, comparison, 175-193

Nuclei versus mass concentrations

  calibration curve, 195

  discussion, 191, 194-199

  summary of bench scale measurements, 197, 198

Optical counter measurements (effluent)

  coal fly ash, size and concentration versus fabric loading, 187-189, 193

  lignite fly ash, size and concentration versus fabric loading, 183, 192

Particle collection

  bulked fiber substrate theory, 319, 324

  dust cake, collection theory, 327

  dust cake, granular bed, 325-331

  fiber substrate with dust deposits, 322-325

  impaction and direct interception, 321

  pore bridging, 315

  pore capture, discussion, 315-319

  pore penetration, estimation, 318, 319, 331

Particle size properties

  atmospheric (laboratory) dust, 51

  dust slough-off from clean side of filter, 227, 228

  fly ash, GCA, 34, 42, 44

  lignite fly ash, 48

  logarithmic-normal, surface and volume mean diameters, 165

  Rhyolite (granite), 47

  Sunbury fly ash, 44, 45

Peclet number

  calculation of diffusion parameter, 328, 329

Penetration

  (See also effluent concentrations)

  inlet dust concentration, 334, 335

  model, single bag, 338-343

  pinhole leaks, 136, 138-144

  pore structure effects, 174, 175

  rear (clean) face slough-off of agglomerates, 224-228

  residual outlet concentration, 338, 340, 342

  surface dust load distribution, 337

  variables controlling, single bag, 338

  velocity effects, 220, 224, 335, 336

INDEX (Continued)

Photomicrographs
  (See fabric, dust)
Pilot plant baghouse
  bag illumination, 207
  schematic drawing, 40
  test facility, schematic, 36-40
  testing procedures, 206, 207
  vibration problems, 207
Pinhole velocity, 142
Pinhole leaks,
  leak velocity estimates, 139, 142
  pinhole area estimates, 139
Pore dimensions
  equivalent circular diamter, 78
  hydraulic radius, 77-80
  tabular summary, 78
Pore structure (type)
  Sunbury fabric, schematic, 76, 78
Pore type
  cross section versus type, 73, 74, 76
  hydraulic radius, 78
Pore velocity
  maximum, 80
Porosity (dust cake)
  bulk density (dust cake), 262
  effect on K_2, 254, 263
Program (computer)
  (See model, filter system)
Resistance (drag) models
  see drag (resistance) models
Rhyolite (granite) collection
  glass fabric, 3/1 twill, 170
Sateen weave cotton
  fly ash collection, 191, 193
Specific resistance coefficient (K_2)
  dust cake porosity, 254-263
  experimentally derived values, 249
  fabric permeability, 256
  fabric surface effects, 256
  face velocity effect, 161-163, 259-261
  particle shape effect, 256
  particle size effect, 164, 165
  predicted and/or measured values, 220, 222, 266-269
  specific surface parameter, 164, 165, 261-271
  viscosity effects, 254, 266-269
Specific surface parameter (S_o)
  calculation for polydisperse distribution, 261, 262
  coal fly ash, 267
  granite dust, 268
  lignite fly ash, 267
  Nucla fly ash, 264
  talc dust, 268
Sunbury fabric
  field performance, 101-117

INDEX (Continued)

Sunbury field tests
  data summaries, 102, 103, 105-107, 109, 111, 113, 115
  fabric loading (average) after cleaning, 102, 103
  normal cleaning procedure, 382

Tensile modulus, 84-88
  stress/strain factors, 88
Tensile properties
  apparatus for measurement, 56
  Sunbury fabric, 85
Test aerosols
  discussion, 43-46
Test aerosol size properties
  (See particle size properties)

Yarn shape (dimensions)
  schematic drawing, 61, 74
Yarn shape
  photomicrographs, 70, 71